MONASH University

HUDSON INSTITUTE OF MEDICAL RESEARCH

Investigating DPP4 as a therapeutic target in epithelial ovarian cancer

Laura Rose Moffitt

BBioTech, BSc(Hons)

A thesis submitted for the degree of Doctor of Philosophy at Monash University in 2021

Faculty of Medicine, Nursing and Health Sciences

Department of Molecular and Translational Sciences

Hudson Institute of Medical Research

Copyright notice

Abstract

Epithelial ovarian cancer has the highest mortality rate of all gynaecological malignancies. Clinical management has remained mostly unchanged over time, and patients have ~80% recurrence rate and a five-year survival rate below 45%. There is an urgent need to develop new therapeutic strategies to improve survival rates in women, particularly those with recurrent, chemoresistant disease.

Dipeptidyl peptidase 4 (DPP4) is a serine protease with diverse biological roles, including the ability to regulate the bioactivity of numerous effector molecules involved in immune response. Our laboratory previously demonstrated the overexpression of DPP4 in ovarian cancers, linking DPP4 activity to immune suppression in tumours. This finding suggested that DPP4 inhibition in ovarian cancer may act in an immuno-stimulatory manner, to restore effector function and enhance anti-tumour immunity. Interestingly, the activity and function of DPP4 are also regulated by hypoxia in a cell- and tissue-specific manner. The presence of hypoxic regions within solid tumours further suggests dysfunction of DPP4 in ovarian cancers; however, the influence of hypoxic growth conditions in the tumour microenvironment on DPP4 function have never been explored.

We examined DPP4 expression and activity in human ovarian cancer cell lines OVCAR4, SKOV3 and CaOV3, grown under hypoxic conditions. Chronic hypoxic growth resulted in the upregulation of DPP4; unexpectedly, whilst DPP4 release from the cell surface also increased, the shed enzyme was inactive suggesting uncoupling of DPP4 expression and activity. Concurrently we identified an increase in the expression and protein abundance of matrix metalloproteinases MMP-1, -10 and -13, suggesting these proteases may be involved in the uncoupling process. This data is the first evidence showing the hypoxic regulation of DPP4 in ovarian cancer cells and suggests a new mechanism by which tumour proteases may alter DPP4 function – and thus the activity of its downstream targets – in the tumour microenvironment.

We then explored the use of sitagliptin, a clinically approved DPP4 inhibitor, to alter tumour progression and anti-tumour immune responses *in vivo.* We also tested the hypothesis that the

immunomodulatory effects of sitagliptin would synergise with immune checkpoint inhibition to improve anti-tumour immune response and overall survival in a syngeneic, metastatic ovarian cancer model. Sitagliptin monotherapy prolonged survival in tumour-bearing mice and increased the level of several circulating chemokines involved in T cell recruitment including CXCL10, CXCL11 and CCL3. Concurrently there was an increase in CD8+ T cell activation and proliferation, whilst the infiltration and activity of immunosuppressive Tregs was decreased. In addition, there was a direct increase in the intratumoural localisation of PD-1+CD4+ T cells, and increased tumour expression of PD-L1. Accordingly, combination therapy with sitagliptin + anti-PD-1 further enhanced T effector cell responses via the upregulation of activated CD8+ T cells and Th1 cells in the tumour microenvironment; whilst the combination of sitagliptin + anti-PD-L1 exhibited more subtle effects via enhancement of CD8+ T effector response.

This thesis provides novel insight into the role of DPP4 in ovarian cancer and suggests some potential clinical benefits of DPP4 inhibition as an adjunct therapy in ovarian cancer patients. Moreover, proteolytic shedding of DPP4 by tumours may have potential as a biomarker for the detection or monitoring of disease progression, recurrence or response to therapy. Future clinical trials could implement this treatment strategy as a novel approach for improved disease management.

Declaration

This thesis is an original work of my research and contains no material which has been accepted for the award of any other degree or diploma at any university or equivalent institution and that, to the best of my knowledge and belief, this thesis contains no material previously published or written by another person, except where due reference is made in the text of the thesis.

Signature: ……

Print Name: LAURA MOFFITT

Date: 13th February 2021

Publications during enrolment

1. Wilson, A. L.*, **Moffitt, L. R**.*, Duffield, N., Rainczuk, A., Jobling, T. W., Plebanski, M., & Stephens, A. N. (2018). Autoantibodies against HSF1 and CCDC155 as Biomarkers of Early-Stage, High-Grade Serous Ovarian Cancer. *Cancer epidemiology, biomarkers & prevention, 27*(2), 183–192.
*Authors contributed equally

2. Wilson, A. L., Wilson, K. L., Bilandzic, M., **Moffitt, L. R**., Makanji, M., Gorrell, M. D., Oehler, M. K., Rainczuk, A., Stephens, A. N., & Plebanski, M. (2018). Non-Invasive Fluorescent Monitoring of Ovarian Cancer in an Immunocompetent Mouse Model. *Cancers, 11*(1), 32.

3. **Moffitt, L.**, Karimnia, N., Stephens, A., & Bilandzic, M. (2019). Therapeutic Targeting of Collective Invasion in Ovarian Cancer. *International journal of molecular sciences, 20*(6), 1466.

4. **Moffitt, L. R**., Bilandzic, M., Wilson, A. L., Chen, Y., Gorrell, M. D., Oehler, M. K., Plebanski, M., & Stephens, A. N. (2020). Hypoxia Regulates DPP4 Expression, Proteolytic Inactivation, and Shedding from Ovarian Cancer Cells. *International journal of molecular sciences, 21*(21), 8110.

5. Wilson, A. L., **Moffitt, L. R.**, Wilson, K. L., Bilandzic, M., Wright, M. D., Gorrell, M. D., Oehler, M. K., Plebanski, M., & Stephens, A. N. (2021). DPP4 Inhibitor Sitagliptin Enhances Lymphocyte Recruitment and Prolongs Survival in a Syngeneic Ovarian Cancer Mouse Model. *Cancers*, *13*(3), 487.

Publications 1, 2, 3, and 5 are attached as appendices to this thesis.

Thesis including published works declaration

I hereby declare that this thesis contains no material which has been accepted for the award of any other degree or diploma at any university or equivalent institution and that, to the best of my knowledge and belief, this thesis contains no material previously published or written by another person, except where due reference is made in the text of the thesis.

This thesis includes 1 original paper published in peer reviewed journals. The core theme of the thesis is understanding the role of DPP4 as a potential therapeutic target in epithelial ovarian cancer. The ideas, development and writing up of all the papers in the thesis were the principal responsibility of myself, the student, working within the Faculty of Medicine, Nursing and Health Sciences under the supervision of Dr Andrew Stephens and Professor Magdalena Plebanski.

The inclusion of co-authors reflects the fact that the work came from active collaboration between researchers and acknowledges input into team-based research.

In the case of Chapter 3 my contribution to the work involved the following:

Thesis Chapter	Publication Title	Status	Nature and % of student contribution	Co-author name(s) Nature and % of Co-author's contribution*	Co-author(s), Monash student Y/N*
3	*Hypoxia regulates DPP4 expression, Proteolytic Inactivation, and Shedding from Ovarian Cancer Cells*	*Published*	*Concept design, planning and completion of experiments, data analysis, manuscript writing and editing – 90%*	*1) Maree Bilandzic: technical assistance, manuscript editing – 1%* *2) Amy L Wilson: technical assistance, manuscript editing – 1%* *3) Yiqian Chen: technical assistance, manuscript editing – 1%* *4) Mark D Gorrell: funding acquisition, manuscript editing – 0.5%* *5) Martin K Oehler: funding acquisition, manuscript editing – 0.5%* *6) Magdalena Plebanski: funding acquisition, manuscript editing, supervision – 2%* *7) Andrew N Stephens: concept design, funding acquisition, data analysis, manuscript planning and editing, supervision – 4%*	*No*

I have not renumbered sections of submitted or published papers in order to generate a consistent presentation within the thesis.

Student name: Laura R Moffitt

Student signature: **Date:** 13/02/21

I hereby certify that the above declaration correctly reflects the nature and extent of the student's and co-authors' contributions to this work. In instances where I am not the responsible author I have consulted with the responsible author to agree on the respective contributions of the authors.

Main Supervisor name: Dr Andrew N Stephens

Main Supervisor signature: **Date:** 13/02/2021

COVID-19 Disclosure

The COVID-19 pandemic had a severe impact on the progress and completion of this thesis. In January 2020, I commenced an animal study encompassing aim 2 and 3 of this project at RMIT University, Bundoora (associate supervisor location). The study involved 204 mice and in March 2020, all animals had established tumours and begun various treatments. At this time stage 3 state restrictions were imposed due to the COVID-19 pandemic and RMIT advised to shut down all research. Fortunately, our research group obtained an exemption for a small proportion of 'short-term, essential' research, and I was able to continue my study with limited animal numbers. Unfortunately, this resulted in the immediate culling of a substantial number of mice and significantly decreased the anticipated data resulting from the study. For example, in chapter 4 of this thesis, data was collected and presented for mice culled at week 4 and week 6 of the experiment. Similarly, in chapter 5, data was presented from mice culled at week 6. The original plan for this study was to also collect data at week 8 of the experiment to ascertain an additional time point for immunological analysis and tumour collection. I believe that this time point was important to understand the long-term effects of the treatments described in chapters 4 and 5. The animal study was recommenced 6 months later on a much smaller scale to obtain data for survival analysis. Furthermore, the reduced capacity of core facilities at the institute due to workplace shutdowns resulted in a significant delay in the production of tissue micro arrays for analysis. All of these factors hindered the progress of my thesis and limited the time available for in-depth analysis of final experiments.

Acknowledgements

First and foremost, I wish to express my heartfelt gratitude to my main supervisor, Dr Andrew Stephens. From the outset of my time in the Ovarian Cancer Biomarkers (OCB) laboratory, you have been a wealth of information and support. Your genuine care for your students is something I admire and your assistance especially throughout the final and most challenging year of my PhD did not go unnoticed. I am truly grateful for the belief that you showed in me, even when I didn't have it in myself. Your success in multiple areas of research are a testament to your dedication to the field and inspire me to achieve greatness in my future career in science.

I also wish to sincerely thank my co-supervisor, Professor Magdalena Plebanksi and the Translational Immunology and Nanotechnology (TIN) laboratory at RMIT University, Bundoora. Magda, I am in awe of your abundance of knowledge and your passion for research. I feel extremely lucky to have been given the opportunity to work alongside your group. I especially wish to extend my appreciation to Dr Kirsty Wilson from the TIN research group, who was always willing to give up her time to assist me with technical or theory-related immunology. Kirsty, your expertise in this field and ability to teach was extremely valuable throughout my PhD, and I hope that we will be able to work together in the future.

To the other members of the OCB laboratory, thank you for being such a fantastic group of people to work with. In particular, I wish to thank Dr. Amy Wilson, Dr. Maree Bilandzic and Bashirah Basri. Amy, I feel privileged to have grown as students together and am excited to be future colleagues. We seem to be of one mind and manage to have a lot of fun when we work together. I am lucky to have gained a great friend throughout my PhD journey and hope that it will continue into the future. Maree, you will never realise how much you taught me before and during my PhD, both professionally and personally. I am so grateful to have met someone as passionate about their research as you. Bashirah, thank you so much for going above and beyond to help throughout all of those long days in the lab. I value every little thing that you helped me with during my PhD and genuinely enjoyed working with you.

I am eternally grateful for my family – mum Evelyne, dad Les, and brother Tom. My family have been my biggest advocates throughout my entire education and have always provided me with the most loving and supportive environment. I could not have done my PhD without them and feel the happiest in hoping that I made them proud. Likewise, I am so thankful to

my friends for their constant encouragement throughout my studies, especially two of my oldest friends, Kate and Nicole.

I would particularly like to thank my partner, Shaun, for his continued support throughout my PhD. Shaun, you have always had confidence that I can achieve anything I set my mind to, and your reassurance was exactly what I needed to complete my PhD, especially in the midst of the COVID-19 pandemic. I never felt alone in my journey when you were there.

Finally, I wish to dedicate this thesis to two of my uncles, Trevor Moffitt and Rob Reeve, who both sadly passed away in 2015. Uncle Trevor, your attitude towards life gave me the courage and perspective to overcome the biggest challenges that I faced throughout my PhD. Uncle Rob, your fight with brain cancer gave me the passion to pursue a career in cancer research. Although it couldn't help with your battle, I truly hope that one day research can change and save the lives of people like you.

This research was supported by an Australian Government Research Training Program (RTP) Scholarship and the Monash Graduate Research Completion Award (GRCA).

List of Abbreviations

2YT	2 Yeast Tryptone
3D	3-dimensional
AAb	Autoantibody
ACK	Ammonium-Chloride-Potassium
ACT	Adoptive cell therapy
ADA	Adenosine deaminase
AgCXCL10	Antagonistic CXCL10
ALDOA	Aldolase, Fructose-Bisphosphate A (gene)
ANOVA	Analysis of variance
APC	Antigen presenting cell
bFGF	Basic fibroblast growth factor
bp	Base pair
BRAF	B-Raf Proto-Oncogene, Serine/Threonine Kinase (gene)
BRCA1	Breast cancer susceptibility gene 1
BRCA2	Breast cancer susceptibility gene 2
BSA	Bovine serum albumin
CA-125	Cancer antigen-125
CAF	Cancer associated fibroblast
CAR	Chimeric antigen receptor
CARMA1	Caspase recruitment domain-containing membrane-associated guanylate kinase protein-1
CCL	C-C Motif Chemokine Ligand
cDNA	Copy DNA
CIC	Cortical inclusion cyst
CIIK	Cytokine-induced killer
$CoCl_2$	Cobalt Chloride
CRISPR	Clustered regularly interspaced short palindromic repeats
CRC	Colorectal cancer
CTL	Cytotoxic lymphocyte
CTLA-4	Cytotoxic T-lymphocyte-associated protein 4
CXC	CXC-Motif Chemokine
CXCL	C-X-C Motif Chemokine Ligand
CXCR	C-X-C Chemokine Receptor
DASH	DPP4 activity and/or structure homologue
DC	Dendritic cell
ddH2O	Double-distilled water
DMEM	Dulbecco's modified Eagle's medium

DMSO	Dimethyl sulphoxide
DNA	Deoxyribonucleic acid
DPP4	Dipeptidyl peptidase 4; CD26
DPP4i	DPP4 inhibitor
DPP8	Dipeptidyl peptidase 8
DPP9	Dipeptidyl peptidase 9
E. coli	Esherichia coli
ECM	Extracellular matrix
EDTA	Ethylenediaminetetraacetic acid
EGF	Epidermal growth factor
ELISpot	Enzyme-linked immunosorbent spot
EMT	Epithelial-mesenchymal transition
EOC	Epithelial ovarian cancer
EtOH	Ethanol
FAP	Fibroblast activation protein; seprase
FBS	Fetal bovine serum
FDA	Food and Drug Administration
FFPE	Formalin fixed paraffin embedded
FIGO	Federation of Gynecology and Obstetrics
FMO	Fluorescence minus one
Foxp3	Forkhead box P3
G	Gauge
GBM	Glioblastoma multiforme
GLP-1	Glucagon-like peptide 1
GM-CSF	Granulocyte-macrophage colony-stimulating factor
GR	Glucocorticoid receptor
HCC	Hepatocellular carcinoma
HE4	Human epididymis protein 4
HER2	Human epidermal growth factor receptor 2
HGSOC	High-grade serous ovarian carcinoma
HI-FBS	Heat inactivated-FBS
HIF	Hypoxia-inducible factor
HIF-1α	Hypoxia-inducible factor-1 alpha
HIF-1β	Hypoxia-inducible factor-1 beta
HNSCC	Head and neck squamous cell carcinoma
HRD	Homologous recombination deficiency
HRP	Horseradish peroxidase
IB	Intrabursal

ICI	Immune checkpoint inhibitor
IFN	Interferon
IFN-γ	Interferon-gamma
IgG	Immunoglobulin G
IL-	Interleukin
IP	Intraperitoneal
irAE	Immune-related adverse event
iRFP	Near-infrared fluorescent protein
ITS	Insulin-transferrin-selenium
kDa	Kilodalton
kg	Kilogram
KRAS	KRAS Proto-Oncogene, GTPase (gene)
LDHA	Lactate dehydrogenase A (gene)
M	Molar
M-MDSC	Monocytic myeloid-derived suppressor cell
MAPK	Mitogen-activated protein kinase
MDSC	Myeloid-derived suppressor cell
MET	Mesenchymal-epithelial transition
mg	Milligram
MHC	Major histocompatibility complex
µg	Microgram
µl	Microlitre
ml	Millilitre
MMP	Matrix metalloproteinase
MOSEC	Mouse ovarian surface epithelial cells
mPBS	Mouse phosphate buffered saline
mRNA	Messenger RNA
MUC-1	Mucin-1
MYC	MYC Proto-Oncogene, BHLH Transcription Factor (gene)
NCBI	National Centre for Biotechnology Information
Nf1	Neurofibromatosis type 1 (gene)
NF-κB	Nuclear factor-kappa-light-chain-enhancer of activated B cells
ng	Nanogram
NK	Natural killer
NKT	Natural killer T
nm	Nanometre
ns	Not significant
NSCLC	Non-small-cell lung carcinoma
NY-ESO-1	New York esophageal squamous cell carcinoma 1

O_2	Oxygen
ORR	Objective response rate
OS	Overall survival
OSE	Ovarian surface epithelium
P/S	Penicillin/streptomycin
p53	Tumour protein 53
PARP	Poly ADP-ribose polymerase
PARPi	PARP inhibitor
PBS	Phosphate buffered saline
PCR	Polymerase chain reaction
PD-1	Programmed death-1
PD-L1	Programmed death-ligand 1
PFS	Progression free survival
pg	Picogram
PLD	Pegylated liposomal doxorubicin
PMN-MDSC	Polymorphonuclear myeloid-derived suppressor cell
pmol	Picomole
Pten	Phosphatase and tensin homolog (gene)
qPCR	Quantitative PCR
RCC	Renal cell carcinoma
RIPA	Radioimmunoprecipitation assay
RMI	Risk malignancy index
RNA	Ribonucleic acid
ROMA	Risk ovarian malignancy algorithm
RORɣt	Retinoic acid receptor-related orphan receptor gamma
ROS	Reactive oxygen species
RPM	Rotations per minute
SCC	Squamous cell carcinoma
SD	Standard deviation
sDPP4	Soluble DPP4
SFM	Serum free media
shRNA	Short hairpin RNA
SLC2A1	Solute Carrier Family 2 Member 1 (gene)
SMAD	SMA and Mothers against decapentaplegic homolog
STAT	Signal transducer and activator of transcription
STIC	Serous tubal intraepithelial carcinoma
T-bet	T-box protein expressed in T cells

TAA	Tumour associated antigen
TAE	Tris-acetate-EDTA
TAM	Tumour-associated macrophage
TDLN	Tumour-draining lymph nodes
TE	Trypsin-EDTA
TGF-β	Transforming growth factor-beta
Th	T helper
Th1	T helper type 1
Th17	T helper type 17
Th2	T helper type 2
TIL	Tumour infiltrating lymphocyte
Tim-3	T cell immunoglobulin mucin-3
TIMP	Tissue inhibitor of metalloproteinase
T_m	Melting temperature
TMA	Tissue microarray
TMB	Tetramethylbenzidine
TME	Tumour microenvironment
TNF	Tumour necrosis factor
TNF-α	Tumour necrosis factor-alpha
Treg	Regulatory T cell
Trm	Tissue-resident memory T
UV	Ultraviolet
V	Volts
VEGF	Vascular endothelial growth factor
VEGFR	Vascular endothelial growth factor receptor
vs	Versus
WT	Wild-type

Table of Contents

Copyright notice ii
Abstract ..... iii-iv
Declaration v
Publications during enrolment vi
Thesis including published works declaration ..... vii-viii
COVID-19 Disclosure ix
Acknowledgements ..... x-xi
List of Abbreviations ..... xii-xvi
Table of Contents ..... xvii-xxi
List of Figures ..... xxii-xxiv
List of Tables ..... xxv-xxvi

Chapter 1: Introduction 27-65
Literature Review 28-63
1.1 Ovarian cancer background 28-36
1.1.1 Overview 28
1.1.2 Risk factors 29
1.1.3 Classification 32
1.1.4 Pathogenesis 33
1.1.5 Conventional and emerging treatment strategies 35
1.2 Ovarian cancer tumour environment 37-41
1.2.1 The unique mode of ovarian cancer metastasis 37
1.2.2 The role of hypoxia in the cancer microenvironment 39
1.2.3 Hypoxic mediators in ovarian cancer 40
1.3 The immunological scope of ovarian cancer 42-51
1.3.1 Overview of the immune system in ovarian cancer 42
1.3.2 The T cell response in ovarian cancer 43
1.3.3 Immunosuppression in ovarian cancer 46
1.3.4 Cytokine networks in the ovarian cancer tumour microenvironment 46
1.3.5 The role of hypoxia on the immune system in ovarian cancer 48
1.3.6 Immunotherapies in ovarian cancer 48
1.4 Uncovering the role of DPP4 in ovarian cancer 52-62
1.4.1 Overview of DPP4 function 52
1.4.2 DPP4 in the tumour microenvironment 53
1.4.3 DPP4 in anti-tumour immunity 57
1.4.4 Evidence of an association between DPP4 and hypoxia 59
1.4.5 Current knowledge of DPP4 in ovarian cancer 59
1.4.6 DPP4 as a novel therapeutic target 62
1.5 Conclusions 63

Project rationale 64-65
1.6 Hypothesis 65
1.7 Aims 65

Chapter 2: Materials & Methods 67-107

2.1 Molecular biology 68-73
2.1.1 Plasmids 68
2.1.2 Plasmid linearisation 68
2.1.3 Phosphorylation/annealing of oligonucleotides 69
2.1.4 Ligation 69
2.1.5 Transformation of TOP10 Chemically Competent *E. coli* cells 70
2.1.6 Plasmid extraction 70
2.1.6.1 Mini prep 70
2.1.6.2 Maxi prep 71
2.1.7 Preparation of glycerol stocks 73
2.2 DNA analysis 74-77
2.2.1 Polymerase chain reaction 74
2.2.2 Gel electrophoresis 75
2.2.3 Colony PCR screening 75
2.2.4 Gel purification 76
2.2.5 Nucleic acid quantification 77
2.2.6 DNA sequencing 77
2.3 *In vitro* methods 78-80
2.3.1 Cell culture and passaging 78
2.3.2 Cell counts 79
2.3.3 Freezing and recovering cell stocks 79
2.3.4 Hypoxic incubation 79
2.3.5 Cell viability 80
2.3.6 Stable transfection 80
2.4 RNA analysis 81-84
2.4.1 shRNA design 81
2.4.2 Real-time PCR primer design 81
2.4.3 RNA extraction 82
2.4.4 cDNA synthesis 82
2.4.5 Real-time quantitative PCR 83
2.4.6 Absolute quantification of gene expression 84
2.5 Protein analysis 85-93
2.5.1 Protein extraction 85
2.5.2 Protein estimation by BCA assay 85
2.5.3 DPP4 enzyme activity assays 86
2.5.3.1 DPP4 activity in cell lysate 86
2.5.3.2 DPP4 activity in cell culture supernatant 87
2.5.4 Enzyme linked immunosorbent assays (ELISAs) 87
2.5.4.1 DPP4 ELISA 87
2.5.4.2 HIF-1α ELISA 88
2.5.5 Protease assays 90
2.5.5.1 MMP array 90
2.5.5.2 Proteome profiler array 91
2.5.6 Chemokine assay 92
2.6 Tissue staining 94-96
2.6.1 Immunofluorescence 94
2.7 *In vivo* methods 97-98
2.7.1 Mice 97

2.7.2 Monitoring 97
2.7.3 Intraperitoneal injection 97
2.7.4 Implantation of ovarian cancer cells 97
2.7.5 Sitagliptin administration 98
2.7.6 Monoclonal antibody administration 98
2.7.7 Euthanasia 98
2.8 *Ex vivo* methods 99-101
2.8.1 Cardiac blood collection and processing 99
2.8.2 Peritoneal wash collection and processing 99
2.8.3 Organ collection 100
2.8.4 Spleen processing 100
2.8.5 Cell count of processed organs 101
2.8.6 Serum preparation 101
2.9 Flow cytometry 102-104
2.9.1 Preparation of compensation beads 102
2.9.2 Cell staining 102
2.9.3 Data acquisition 104
2.10 Statistical analysis 107

Chapter 3: The role of DPP4 expression and activity in ovarian cancer cells in vitro 109-127
Preface 110-112
Published: Moffitt *et al*., (2020). IJMS, 21(21) 113-126
3.1 Conclusions 127

Chapter 4: Inhibition of DPP4 activity in a metastatic ovarian cancer mouse model..... 129-176
Preface 130-131
4.1 Introduction 132-138
4.2 Results 139-158
4.2.1 Sitagliptin prolonged survival in mice with metastatic ovarian disease 139
4.2.2 Sitagliptin altered the cytokine landscape in metastatic ovarian disease 141
4.2.3 Sitagliptin altered CD4+ and CD8+ T effector cell abundance throughout metastatic ovarian disease 142
4.2.4 Sitagliptin enhanced the T effector response in metastatic disease 145
4.2.5 Sitagliptin decreased regulatory T cells during the early stages of metastatic disease 149
4.2.6 Sitagliptin modulated systemic immunosuppressive effects of regulatory T cells over time 151
4.2.7 Sitagliptin altered peripheral immune suppression by myeloid-derived suppressor cells throughout disease progression 155
4.2.8 Sitagliptin sustained effective innate immunity throughout disease progression 157
4.3 Discussion 159-171
4.3.1 Sitagliptin as a novel immunotherapeutic to improve survival in metastatic ovarian cancer 159
4.3.2 Sitagliptin modulates DPP4-specific cytokines and influences multiple chemotactic-dependent T effector responses 163

4.3.3 Sitagliptin may indirectly mediate immune responses via modification of non DPP4-specific cytokine pathways 165
4.3.4 Sitagliptin influences innate immunity 167
4.3.5 Sitagliptin sustains anti-tumour immunity throughout metastatic disease 168
4.3.6 The potential of sitagliptin to increase susceptibility of ovarian tumours to PD-1 blockade 170
4.4 Conclusions 172
4.5 Acknowledgements 172
4.6 Supplementary Figures 173-176

Chapter 5: Investigating the combination of sitagliptin with immune checkpoint inhibitors as a novel immunotherapy in ovarian cancer 177-224
Preface 178
5.1 Introduction 179-184
5.2 Results 185-209
5.2.1 Defining a treatment strategy for combination therapy 185
5.2.2 Clinical outcomes of sitagliptin + anti-PD-1/PD-L1 combination therapy 186
5.2.2.1 Sitagliptin + anti-PD-1/PD-L1 prolonged survival 186
5.2.2.2 Sitagliptin + anti-PD-1 may decrease overall metastatic burden 188
5.2.3 Immune parameters with the combination of sitagliptin + anti-PD-1 190
5.2.3.1 Sitagliptin + anti-PD-1 altered T cell populations in the spleen, peritoneal cavity and tumour infiltrates 190
5.2.3.2 Combination therapy using Sitagliptin + anti-PD-1 enhanced the functional potential of T effector cells 193
5.2.3.3 Sitagliptin + anti-PD-1 polarised the adaptive immune response towards Th1 immunity 196
5.2.3.4 Sitagliptin + anti-PD-1 decreased T-regulatory cell populations and mitigated immunosuppressive effects induced by anti-PD-1 alone 198
5.2.3.5 Combination therapy altered circulating cytokines in tumour bearing mice 200
5.2.4 Immune parameters with the combination of sitagliptin + anti-PD-L1 203
5.2.4.1 Sitagliptin increased intratumoural PD-L1 expression in metastatic ID8 tumours 203
5.2.4.2 Sitagliptin + anti-PD-L1 enhanced the functional potential of CD8+ T effector cells 204
5.2.4.3 Sitagliptin + anti-PD-L1 increased peripheral NKT cells 206
5.2.4.4 Sitagliptin + anti-PD-L1 altered the cytokine landscape in a sitagliptin-dependent manner 207
5.2.5 Summary of significant features of sitagliptin + combination therapies 208
5.3 Discussion 210-221
5.3.1 Combination therapy may improve clinical parameters associated with ovarian cancer 210
5.3.2 Combination therapy enhances T effector cell responses in the TME 212
5.3.3 Sitagliptin anti-PD-1 promotes Th1 immunity by upregulation of CXCR3 216
5.3.4 Combination therapy may promote immunological memory 217
5.3.5 Cytokine expression reveals similar mechanisms of anti-tumour immunity from both combination therapies 218
5.3.6 Insight into potential mechanisms of immunosuppression induced by PD-1/PD-L1 blockade 220

5.4 Conclusions **222**
5.5 Acknowledgements **222**
5.6 Supplementary Figures **223**

Chapter 6: Discussion ***225-247***
Preface **226**
6.1 New insights into DPP4 as a biomarker and therapeutic target in ovarian cancer **227-230**
6.1.1 Mechanisms of regulation that impact the status of DPP4 as a biomarker 227
6.1.2 Uncovering sources and functional diversity of DPP4 229
6.2 Sitagliptin as an immune modulator in metastatic ovarian cancer **231-236**
6.2.1 Sitagliptin amplifies the T effector response 231
6.2.2 Sitagliptin influences cytokines in the TNF network 233
6.2.3 Considering spatial and phenotypic diversity in the immune response 236
6.3 The effect of sitagliptin in primary versus metastatic disease **237-238**
6.3.1 Similar mechanisms of sitagliptin-mediated anti-tumour immunity in primary and metastatic disease 237
6.3.2 Distinct anti-tumour responses in mice treated with sitagliptin in different disease models 237
6.4 Feasibility and challenges associated with clinical translation of sitagliptin combined with immune checkpoint inhibition to treat ovarian cancer **239-244**
6.4.1 Clinical safety and efficacy of sitagliptin + anti-PD-1/PD-L1 239
6.4.2 Overcoming mechanisms of resistance to PD-1/PD-L1 blockade 240
6.4.3 Biomarkers to identify susceptible cohorts of patients to PD-1/PD-L1 blockade 242
6.4.4 Additional opportunities for combination therapy 243
6.5 Study limitations and technical challenges **245-246**
6.6 Future directions **247**

Concluding remarks **248**

References **249-273**

Appendix A: Methods **274-282**
A.1 General solutions and buffers **274-277**
A.2 Oligonucleotides **278-279**
A.3 Proteins **280-281**
A.4 Flow cytometry **282**

Appendix B: Moffitt *et al.*, (2019). IJMS, 20(6) **283-299**
Appendix C: Wilson & Moffitt *et al.*, (2018). Cancer Epidemiol. Biomarkers Prev., 27(2) **301-310**
Appendix D: Wilson *et al.*, (2021). Cancers, 13(3) **311-328**
Appendix E: Wilson *et al.*, (2018). Cancers, 11(2) **329-347**

List of Figures

Chapter 1

Figure 1.1. The survival rate of ovarian cancer according to FIGO stage at diagnosis..... 29
Figure 1.2. A working model of ovarian cancer metastasis..... 38
Figure 1.3. HIF-1α is a prognostic factor in patients with primary epithelial ovarian cancers 40
Figure 1.4. Overview of selected anti- and pro-tumour immune responses in the ovarian tumour microenvironment..... 45
Figure 1.5. Structure of DPP4 53
Figure 1.6. Schematic diagrams representing the proposed mechanisms of DPP4 as a tumour suppressor and marker of malignancy 55
Figure 1.7. A working model of the effect of DPP4 activity on CXCL10-dependent recruitment of T cells within the tumour microenvironment 58
Figure 1.8. Evidence of DPP4 upregulation in ovarian cancer tissue 61

Chapter 2

Figure 2.1. Schematic diagram representing the main features of the pSIF-H1-Puro shRNA cloning vector 68

Chapter 3

Figure 1. The effect of hypoxia on cell growth, HIF-1α and DPP4 expression in ovarian cancer cells. 115
Figure 2. Hypoxia induces shedding of inactive DPP4 from ovarian cancer cells..... 116
Figure 3. Hypoxia regulates protease expression in ovarian cancer cells 117
Figure 4. Matrix metalloproteinases (MMP) activity influences DPP4 expression and release in ovarian cancer cells..... 118
Figure 5. MMP10 and MMP13 affect DPP4 expression and release from ovarian cancer cells 118

Chapter 4

Figure 4.1. DPP4 inhibition alters leukocyte populations and prolongs survival in a primary ovarian cancer mouse model 137
Figure 4.2. Schematic representation of the experimental timeline for sitagliptin treatment in a metastatic ovarian cancer mouse model..... 139
Figure 4.3. Survival for mice treated with sitagliptin compared to untreated controls 140
Figure 4.4. Sitagliptin alters cytokine levels in ID8 metastatic tumour bearing mice..... 141
Figure 4.5. Circulating T cells and CD8+ T cells and tumour infiltrating T lymphocytes in mice treated with sitagliptin at week 4 143
Figure 4.6. Splenic, peritoneal and intratumoural T lymphocyte populations in mice treated with sitagliptin at week 6..... 144
Figure 4.7. Proliferating and activated CD8+ T cells and infiltrating lymphocyte activation status in mice treated with sitagliptin at week 4 146
Figure 4.8. Activated CD8+ and CD4+ T cells and infiltrating lymphocyte activation in mice treated with sitagliptin at week 6 148
Figure 4.9. Regulatory T cells and CD8+ T cell: Regulatory T cell ratio in mice treated with sitagliptin at week 4 150

Figure 4.10. Proliferating and tumour infiltrating regulatory T cells in mice treated with sitagliptin at week 6 151
Figure 4.11. PD-1+ and CCR4+ regulatory T cells in mice treated with sitagliptin at week 4 153
Figure 4.12. PD-1+ and CCR4+ regulatory T cells in mice treated with sitagliptin at week 6 154
Figure 4.13. Myeloid-derived suppressor cells in in mice treated with sitagliptin at week 4 156
Figure 4.14. Myeloid-derived suppressor cells in in mice treated with sitagliptin at week 6 157
Figure 4.15. Activated macrophages in mice treated with sitagliptin at week 4 and week 6 158
Figure 4.16. Schematic representation of proposed sitagliptin-mediated immune responses in a metastatic ovarian cancer model 161
Supplementary Figure S4.1. Weight and circumference of mice treated with sitagliptin 173
Supplementary Figure S4.2. Flow cytometry gating strategy 174
Supplementary Figure S4.3. Concentration of differentially expressed circulating cytokines in mice treated with sitagliptin at week 6 176

Chapter 5

Figure 5.1. Schematic representation of the experimental timeline for sitagliptin + anti-PD-1/PD-L1 antibody treatment in a metastatic ovarian cancer mouse model 185
Figure 5.2. Weight, circumference and overall survival of mice treated with sitagliptin + anti-PD-1 antibody 187
Figure 5.3. Weight, circumference and overall survival of mice treated with sitagliptin + anti-PD-L1 antibody 188
Figure 5.4. T cells, CD8+ T cells and CD4+ T cells in mice treated with sitagliptin + anti-PD-1 antibody 191
Figure 5.5. Tumour-infiltrating T cells, CD8+ T cells and CD4+ T cells from mice treated with sitagliptin + anti-PD-1 antibody 192
Figure 5.6. Activated and proliferating CD8+ and CD4+ T cells in mice treated with sitagliptin + anti-PD-1 antibody 194
Figure 5.7. Activation and inhibitory status of tumour-infiltrating CD8+ T cells in mice treated with sitagliptin + anti-PD-1 antibody 195
Figure 5.8. CXCR3 expression on T cells in mice treated with sitagliptin + anti-PD-1 antibody 197
Figure 5.9. T regulatory cells and PD1+ T regulatory cells in mice treated with sitagliptin + anti-PD-1 antibody 199
Figure 5.10. Activated and CCR4+ T regulatory cells in mice treated with sitagliptin + anti-PD-1 antibody 200
Figure 5.11. Differential expression of cytokines in mice treated with sitagliptin + anti-PD-1 antibody 202
Figure 5.12. Intratumoural PD-L1 expression in mice treated with sitagliptin 203
Figure 5.13. Overall CD8+ T effector cell response in mice treated with sitagliptin + anti-PD-L1 205
Figure 5.14. NKT cells in mice treated with sitagliptin + anti-PD-L1 antibody 206
Figure 5.15. Differential expression of cytokines in mice treated with sitagliptin + anti-PD-L1 207
Figure 5.16. Schematic representation of proposed immune responses in mice bearing ID8 metastatic tumours treated with the combination of sitagliptin + PD-1/PD-L1 blockade 214

Supplementary Figure S5.1. Flow cytometry gating strategy 223

Appendix A

Figure A.1. FMO controls for flow cytometry 282

Appendix B

Figure 1. Metastasis model in ovarian cancer 284
Figure 2. Collective invasion in epithelial ovarian cancer 286

Appendix C

Figure 1. A - Autoantigen discovery and validation strategy; B - Identification of antigens discriminating between groups 304
Figure 2. Ig type and gene ontology localisation of antigens associated with benign or malignant disease 305
Figure 3. Antigen reactivity networks linking early- with late-stage disease 306
Figure 4. Validation of autoantibodies against CCDC155 and HSF1 in the independent validation cohort by ELISA 307

Appendix D

Figure 1. Circulating soluble and tumour-specific DPP4 expression and enzyme activity in mice treated with sitagliptin 316
Figure 2. Tumour burden and metastatic spread in ID8 pROSA-iRFP720 tumour-bearing mice following sitagliptin treatment 318
Figure 3. Gross lymphocyte populations and circulating cytokines in mice treated with sitagliptin 317
Figure 4. Lymphocyte activation and proliferation in ID8 tumour-bearing mice treated with sitagliptin 321
Figure 5. Chemokine receptor expression in ID8 tumour-bearing mice treated with sitagliptin 322
Figure 6. Chemokine receptor expression in ID8 tumour-bearing mice treated with sitagliptin and paclitaxel 323

Appendix E

Figure 1. Strategy for pROSA-puro-iRFP720 vector generation and genomic screening ... 331
Figure 2. iRFP720 fluorescence and characterisation of pROSA-iRFP720-expressing ID8 cells 332
Figure 3. In vivo tracking of iRFP720 fluorescence in real time 334
Figure 4. Expression of serous tumour markers by immunofluorescence 336
Figure 5. Circulating endogenous iRFP720-specific IgG antibodies in mice bearing pROSA-iRFP720 ID8 tumours 337
Figure 6. Changes in immune populations over time in mice bearing pROSA-iRFP720 ID8 tumours 338

List of Tables

Chapter 2
Table 2.1. Reagents required for restriction enzyme digest of pSIF-H1-Puro vector 69
Table 2.2. Reagents required for phosphorylation/annealing of shRNA template oligonucleotides 69
Table 2.3. Reagents required for ligation of shRNA templates into the pSIF-H1-Puro vector 70
Table 2.4. Reagents required in a standard PCR for primer amplification of DNA 74
Table 2.5. Standard PCR cycling conditions 74
Table 2.6. Reagents required in colony PCR screen for primer amplification of plasmid DNA 76
Table 2.7. Bacterial colony PCR screen cycling conditions 76
Table 2.8. Preparation of DNA sequencing reactions 77
Table 2.9. Reaction components required for cDNA synthesis from total RNA 83
Table 2.10. Master mix preparation for real-time PCR reactions 83
Table 2.11. Real-time PCR cycling conditions 84
Table 2.12. Working concentrations for protein standards for the BCA assay 86
Table 2.13. Preparation of DPP4 protein standards 88
Table 2.14. Preparation of HIF-1α protein standards 89
Table 2.15. Preparation of MMP array standards 90
Table 2.16. Preparation of standard series for 31-plex chemokine assay 93
Table 2.17. Antibodies used for immunofluorescence staining of mouse tissue 96
Table 2.18. Monoclonal antibodies administered to mice during in vivo experiments 98
Table 2.19. Antibodies used in flow cytometry experiments 105

Chapter 3
Table 1. Human primer sequences for real-time PCR 121

Chapter 4
Table 4.1. Summary of immune response to sitagliptin treatment over time in a metastatic ovarian cancer model 160

Chapter 5
Table 5.1. Post-mortem observations in mice treated with sitagliptin + anti-PD-1 antibody 189
Table 5.2. Key changes in selected immune parameters between treatment groups 208

Appendix A
Table A.1. Bacterial screening primer sequences 278
Table A.2. shRNA template sequences 278
Table A.3. Forward and reverse sequences for primer pairs used in real-time PCR 278
Table A.4. Working concentrations of DNA standards for real-time PCR 279
Table A.5. List of human protease targets analysed in the cell lysates and culture media of OVCAR4 cells 280
Table A.6. MMP array 10-target standard values 280
Table A.7. Bio-Plex Pro™ Mouse 31-plex chemokine panel normalised standard values, expected control ranges and bead regions 281

Appendix B

Table 1. Selected targeted drugs in clinical trials for the treatment of metastatic ovarian cancer 290

Appendix C

Table 1. Summary of sample cohort characteristics 304
Table 2. Identified antigens common to both early- and late-stage cancers 305

Chapter One

Introduction

Literature Review

1.1 Ovarian cancer background

1.1.1 Overview

Ovarian cancer is the most lethal gynaecological malignancy that comprises three distinct disease types based on their cell type of origin – epithelial, sex cord-stromal and germ cell tumours[1]. Tumours arising from epithelial cells account for approximately 90% of all ovarian cancers[2], therefore epithelial ovarian cancer (EOC) is the focus of most research and available literature. In 2018 there were an estimated 295,414 new cases of ovarian cancer and 184,799 deaths worldwide[3]. In Australia, ovarian cancer has an incidence rate of 10.8 cases per 100,000 women[4] and accounts for approximately 28% of all gynaecological cancers[5]. In 2019, the Australian Institute of Health and Welfare (AIHW) estimated the diagnosis of 1510 new cases and 1046 deaths from ovarian cancer[6], making ovarian cancer the tenth most commonly diagnosed cancer and the sixth most common cause of death from cancer in Australian women[5].

Ovarian cancer is managed according to the International Federation of Gynecology and Obstetrics (FIGO) staging system which provides diagnostic and prognostic information based on the extent of disease spread[7]**.** Stage I and II ovarian cancers are generally localised to the ovaries/fallopian tubes and within the pelvic region, whilst diagnosis at stages III and IV indicates extensive macroscopic tumour metastasis within the peritoneal cavity and other organs including the liver, spleen and lungs[7]. Ovarian cancer typically presents with non-specific and vague symptoms – particularly during early stages – which often delays clinical diagnosis to late-stage disease[8-10]. Whilst cases diagnosed at stage I or II have a 5-year survival rate of 92% and 70% respectively; when the disease is detected at stage III or IV the 5-year survival rate is only 39% and 17% respectively (Figure 1.1)[11]. Unfortunately, these late-stage diagnoses account for over 60% of all ovarian cancer cases, which contributes to the abnormally high mortality rate for this relatively low-incidence disease[12]. There are currently

no early detection methods for ovarian cancer due to a lack of predictive biomarkers, and despite advances in surgical techniques and chemotherapeutics most women diagnosed with ovarian cancer will receive a poor prognosis[13]. In addition, the development of chemoresistance following primary treatment options is common especially amongst patients diagnosed with late-stage disease[14]. Presently the 5-year relative overall survival of ovarian cancer is only 43%[15], which has not improved significantly in the past 30 years since platinum-based therapies became available.

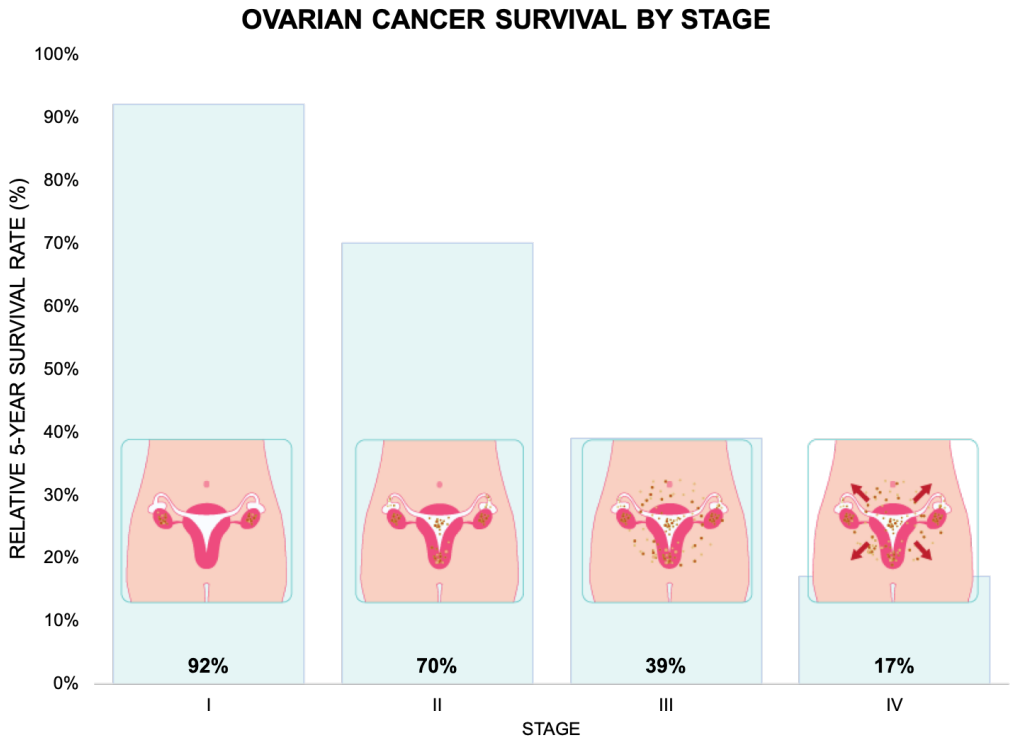

Figure 1.1. The survival rate of ovarian cancer according to FIGO stage at diagnosis. *The relative 5-year survival rate is highest for patients diagnosed at stage I (92%), and progressively decreases to 17% for patients diagnosed with stage IV disease[11]. Schematic images obtained from <https://www.roche.co.th/en/disease-areas/ovarian-cancer.html>.*

1.1.2 Risk factors

An important approach into developing screening methods and treatment strategies for ovarian cancer involves considering the risk factors that contribute to the development of the disease. Presently, genetic predisposition is the strongest basis for determining whether a woman is at risk of developing ovarian cancer. Germline mutations in the DNA repair genes

BRCA1 or *BRCA2* account for approximately 10% of all EOC cases[1,16]. The lifetime risk of developing ovarian cancer by age 70 is higher for carriers of mutations in *BRCA1* than *BRCA2*, and penetrance differs between populations, likely due to the effects of other risk factors and the type of mutation[17-20]. *BRCA1* and *BRCA2* mutation carriers also have approximately 50% chance of developing breast cancer by age 70[21]. However, compared to non-carriers, patients that are diagnosed with hereditary ovarian cancer are usually associated with a more favourable outcome including increased chemosensitivity and improved 5-year overall survival[22,23]. Women with a known *BRCA1* or *BRCA2* mutation can elect to undergo risk-reducing surgery which usually involves the complete removal of both ovaries and fallopian tubes (bilateral salpingo-opherectomy) with or without a total hysterectomy[24]. This prophylactic surgery can reduce the risk of developing ovarian cancer by up to 80%[25-27]; however, the physiological costs are extensive, including the early onset of menopause symptoms in pre-menopausal women[28]. Evidently, the development of biomarkers to further identify the predisposition to ovarian cancer amongst high-risk cohorts – such as *BRCA1/2* mutation carriers – will improve decision making and quality of life for these women.

Aside from genetic factors, several epidemiological studies have suggested that there is a positive correlation between lifetime ovulation events and the risk of developing ovarian cancer; as it has been proposed that cancer may arise in the ovarian epithelium via damage obtained from repeated ovulation cycles[14]. Many retrospective studies have reported that factors resulting in inhibition of ovulation, including pregnancy, tubal ligation and oral contraceptive use are associated with a reduced risk of ovarian cancer[29-31]. Moreover, such studies suggested that these factors may also have a prolonged protective effect on the development of disease[32,33]. Conversely, events that increase lifetime ovulation occurrence such as early age at menarche, late age at menopause and hormone replacement therapies are linked to an increased risk of developing ovarian cancer[34]. As most risks for ovarian cancer are positively associated with increasing age, prognosis is also poor for older women. In Australia, 60% of new diagnoses occur in women above 60 years[12]. Women aged 80 and over

only have a 16% 5-year relative survival rate compared to 87% for women who are aged less than 30 years at the time of diagnosis[5].

Other factors such as obesity are not associated with an increased risk of the most common type of ovarian cancer[35]; however, there is evidence of a moderately increased risk amongst patients with diabetes mellitus[36]. Inflammatory conditions including endometriosis, pelvic inflammatory disease and polycystic ovaries may also be associated with the development of ovarian cancer[14,37,38]. Pro-inflammatory mediators related to these conditions are elevated in epithelial ovarian cancers[14]. Whilst it is well established that chronic inflammation contributes to many cancers, the mechanism by which these conditions may be involved in ovarian carcinogenesis is not yet fully understood.

One of the challenges facing researchers is the need to improve methods for identification of risk factors and associated biomarkers implicated in ovarian cancer. Currently, the most useful screening methods to determine the risk for the development of ovarian cancer in addition to a pelvic ultrasound includes analysis of the tumour markers cancer antigen-125 (CA-125) and human epididymis protein 4 (HE4), and calculation of the risk ovarian malignancy algorithm (ROMA) and risk malignancy index (RMI). All of these methods demonstrate similar sensitivities at differentiating benign vs malignant tumours in women with pre-existing pelvic masses[39,40], however, there is no evidence to suggest that they reduce disease mortality[41]. Unravelling the molecular profile and obtaining stronger evidence on the origin and early events of ovarian cancer (see Section 1.1.4*)* will greatly improve the chances of developing practical early detection screens that would see the earlier diagnosis and therefore improved prognosis of the disease.

1.1.3 Classification

The traditional understanding of ovarian cancer has changed from what was once considered a single disease with many subtypes to the concept that it is in fact several related but distinct diseases with specific pathological, genetic and behavioural profiles[42,43]. Advances in molecular and histopathological techniques have allowed a greater insight into the characteristics of epithelial ovarian tumours. We have come to understand that the initial genetic changes that occur in ovarian carcinomas involve 'signature' mutation(s) that tend to be representative of the different histological subtypes, whilst secondary genetic aberrations accumulate during tumour progression[44]. A proposed and later revised 'dualistic model' of ovarian carcinogenesis designates epithelial ovarian tumours as either Type I or Type II[45,46]. Type I tumours include low-grade serous, mucinous, clear cell and endometrioid carcinomas[46]. These tumours are typically considered low-grade; they are slow growing, well-differentiated and frequently harbour mutations in genes for protein kinase signalling pathways such as *KRAS* and *BRAF* but are otherwise genetically stable[1]. Due to the low proliferative state of Type I tumours, they are often diagnosed at early-stage and are associated with good prognosis and overall clinical outcome[46].

Type II tumours include high-grade serous ovarian carcinoma (HGSOC), carcinosarcoma and undifferentiated carcinosarcoma[46]. HGSOCs are highly heterogeneous, account for the vast majority of EOC diagnoses (~75%) and are responsible for the highest proportion of deaths from ovarian cancer (90%)[21]. These tumours usually present at an advanced stage, are highly aggressive and characterised by a universal *p53* mutation[44]. This genetic change likely occurs early in pathogenesis and causes significant chromosomal instability and loss of tumour suppression capability, via the loss of DNA repair mechanisms and increased cell proliferation[21]. Further sporadic genetic abnormalities quickly accumulate following *p53* disruption, which contributes to the extensive heterogeneity observed in most HGSOCs[47]. Genomic instability in HGSOC also often involves an increase in copy number of *MYC*, which

is heavily involved in regulation of growth and metabolism[21]. Moreover, most HGSOCs have abnormalities of *BRCA1* or *BRCA2,* which may be hereditary or acquired[48].

HGSOCs have been further classified into four molecular subtypes (differentiated, proliferative, mesenchymal and immunoreactive) based on widespread gene expression cluster analysis[49]. These subtypes are likely to reflect different patterns of oncogene activation and the degree of intratumoural lymphocytic infiltration[49]. Immunoreactive tumours possess a distinct immune signature including overexpression of genes involved in an adaptive immune response (discussed in Section 1.3.1) and are linked to the most favourable prognosis of all HGSOCs[17]. Evidently, as our understanding of the complex genetic and pathological characteristics of ovarian cancer and HGSOCs in particular improves, so will the ability to develop screening measures and molecularly targeted treatments for each disease subtype.

1.1.4 Pathogenesis

Unlike many other malignancies, the origin and pathogenesis of ovarian cancer is not completely understood. Due to the fact that most ovarian cancers are incredibly morphologically and genetically diverse, the process of tumorigenesis is likely to be dependent upon their biological origin and therefore reflect the distinct nature of each subtype[50]. The traditionally hypothesised view of ovarian cancer pathogenesis was that all subtypes arose via the ovarian surface epithelium (OSE). According to this model, over the course of a woman's lifetime, numerous invaginations into the cortical stroma developed on the ovarian surface, which frequently pinched off within the stroma to form cortical inclusion cysts (CICs)[50,51]. It was thought that inflammatory cytokines and oxidative stress inflicted by repeated ovulation cycles contributed to the plasticity and accumulation of DNA damage within the cells of the CICs[52]. In addition, the hormone-rich ovarian environment would induce proliferation and differentiation of the epithelial cells within the CICs into Müllerian-type tissue, making them more susceptible to neoplastic transformation[51]. This theory however, does not

adequately explain the origin and morphology of type II tumours, particularly HGSOCs, and is largely flawed by the fact that precursor lesions are very rarely found on the ovaries[53].

A recently explored and now generally accepted interpretation of type II tumour pathogenesis was founded by pathological examination of tissue removed from *BRCA1/2* mutation carriers in risk reduction surgery, which identified that in fact most precursor lesions were found in epithelium of the fallopian tubes[53,54]. These precursor tubal lesions are termed serous tubal intraepithelial carcinomas (STICs) and their molecular profile is highly similar to that of HGSOCs, including an identical signature *p53* mutation in the majority of concurrent samples[47,54,55]. Ovulatory cytokines and reactive oxygen species are likely to contribute to the carcinogenic environment that instigate DNA damage and cell plasticity, allowing precursor cells to acquire a proliferative phenotype[50,56]. This model of pathogenesis implies that as STICs develop into invasive carcinomas, malignant cells are shed or 'exfoliated' from the fallopian tube fimbria and implant on the ovaries where 'primary' tumours develop[46,50].

For many years ovarian cancer research was based upon the OSE model, where perhaps important evidence regarding early tumorigenic events was overlooked. Furthermore, whilst precursor lesions in the fallopian tube have been suggested to be responsible for up to 70% of HGSOCs[54] there remains a proportion of tumours which are apparently unaccounted for by the STIC theory. It is likely that some high-grade serous tumours arise from low-grade serous carcinomas derived from the OSE[51]. Nonetheless, expanding our understanding of the pathogenesis of ovarian tumours is crucial for (1) developing early detection methods by knowledge of the origin and initial events of tumorigenesis and (2) providing pathways/checkpoints by which prevention and treatment strategies can be modelled upon; which are both likely to be specific for each tumour subtype.

1.1.5 Conventional and emerging treatment strategies

The management of ovarian cancer requires multidisciplinary expertise in order to achieve an optimal overall outcome for the patient. Currently, the first-line treatment of ovarian cancer is generally standard across all histological subtypes, owing to the fact that most women present with advanced stage disease[57]. For these patients, primary debulking surgery to remove the tumour mass and any macroscopic metastatic nodules throughout the peritoneal cavity provides initial histopathological diagnosis and staging information[58]. One important prognostic factor at all stages of ovarian cancer is the extent of residual disease following surgery. Compared to the presence of any residual tumour, complete surgical debulking (no residual tumour) is associated with a hazard reduction for progression free survival of 66%[59]. Therefore, further developments in surgical techniques which achieve complete cytoreduction will greatly improve outcomes for ovarian cancer patients.

Following primary cytoreductive surgery, most women receive systemic treatment involving adjuvant chemotherapy with a combination of platinum- and taxane-based agents (usually carboplatin and paclitaxel) for at least 6 cycles[2,60]. Alternatively, for patients diagnosed at late stages of disease, neoadjuvant chemotherapy may be administered to reduce tumour burden prior to surgery[59]. In this case, women receive 3 cycles of chemotherapy, followed by interval cytoreductive surgery, followed by at least 3 more cycles of chemotherapy[61,62]. More recently there has been a focus on strategies to improve chemotherapy regimens and outcomes for women diagnosed with advanced stages of ovarian cancer. Clinical trials have investigated the use of different doses and combinations of chemotherapy[63,64], including intravenous vs intraperitoneal routes of administration[65,66] and hyperthermic intraperitoneal chemotherapy[67]; with varying outcomes likely to be reflective of the level of surgical reduction and individual patient's disease/tumour characteristics[2,68]. Despite the fact that most patients initially respond well to chemotherapy following surgery, relapse occurs in about 85% of ovarian cancer cases[69,70]. Disease recurrence is biologically aggressive and usually accompanied with acquired chemoresistance, leading to a poor prognosis[1,47].

More recent advances in the understanding of ovarian tumour biology has allowed for the development of novel, molecularly targeted therapies. In many ovarian cancers, tumour growth and vascular metastasis is promoted by dysregulation in the angiogenic pathway[13,58]. An important mediator in this pathway is vascular endothelial growth factor (VEGF), which is upregulated in HGSOCs and is associated with decreased overall survival[71]. Clinical trials have investigated inhibition of the angiogenic pathway by targeting VEGF using the monoclonal anti-VEGF antibody, bevacizumab[60,72]. Data from several of these trials suggest that maintenance treatment with bevacizumab in addition to chemotherapy may increase progression free survival (PFS) time[73,74]. Other clinical trials have targeted the poly ADP-ribose polymerase (PARP) pathway of DNA repair by exploiting synthetic lethality in patients with *BRCA1/2* mutations and defects in other homologous combination repair pathways, which occurs in up to 50% of HGSOCs[44,75,76]. PARP inhibitors such as olaparib have shown promise in clinical trials, where significant improvement in PFS was observed in patients with *BRCA*-mutated tumours[77,78]. However, the effect of anti-angiogenic drugs and PARP inhibitors on overall survival (OS) is still unclear and their widespread use is hindered by uncertainties surrounding the development of resistance[60,73,76,79].

Tumour heterogeneity is a significant factor contributing to the lack of long-term efficacy of many current therapies for ovarian cancer[52]. Other than some predominant genetic mutations in HGSOC, including *p53* and *BRCA1/2*, subsequent somatic mutations are generally unpredictable[44], which is exacerbated by regions of global DNA hypomethylation leading to overall genomic disarray[80]. As a result, ovarian cancers exhibit widespread inter- and intra-tumoural heterogeneity, where there is variation in the genomic and phenotypic characteristics of tumour foci between and within tumours of the same patient[81,82]. Therefore, treating the tumour itself may require a personalised approach to target several pathways involved in its growth and metastasis**.** In other areas of research, therapies which modulate the immune system may be effective to overcome some of the complexities of ovarian tumour heterogeneity (see Section 1.3.6).

1.2 Ovarian cancer tumour environment

1.2.1 The unique mode of ovarian cancer metastasis

One of the many challenging features of ovarian cancer is the way in which the disease metastasises. Whilst many other malignancies spread via the lymphatic or circulatory system, ovarian cancer metastasises passively within the peritoneal cavity via the ascites fluid and is driven by a process termed collective invasion[83]. During ovarian cancer metastasis, malignant cells are shed from the primary ovarian tumour to form highly invasive multicellular aggregates known as spheroids in the abdominal cavity[84]. Spheroid formation occurs from the cellular acquisition of a unique expression profile resulting in epithelial-mesenchymal transition (EMT)-like phenotypic changes involving the upregulation of E-cadherin and activation of N-cadherin and Vimentin[85-87]. The spheroids disseminate, settle, attach and spread on the peritoneal surface and infiltrate the mesothelial lining, invading surrounding tissue and forming secondary tumour nodules[84] (Figure 1.2).

Once attached at distant sites within the peritoneal cavity, tumour cells undergo mesenchymal-epithelial transition (MET) for colonisation and invasion into surrounding tissue[85,88]. The complex cellular changes that occur to these tumour cells are facilitated by pro-inflammatory and tumour-promoting factors including VEGF, interleukin-6 (IL-6) and tumour necrosis factor-alpha (TNF-α) that are contained within the ascites fluid in the peritoneal cavity of patients with metastatic ovarian cancer[88,89,85]. The critical point of attachment and infiltration is characterised by the presence of a specialised population of highly invasive cells termed ‘leader’ cells[90]. Leader cells drive collective invasion by cellular cytoskeletal rearrangement to form protrusive invadopodia; and penetrate the mesothelial lining though expression of cell-surface proteolytic enzymes to degrade the ECM and physically invade surrounding tissue[91]. Leader cells have recently been shown to be an

absolute requirement for the process of invasion in ovarian cancer[92] and are therefore a promising target for therapeutic intervention (see Appendix B)[91].

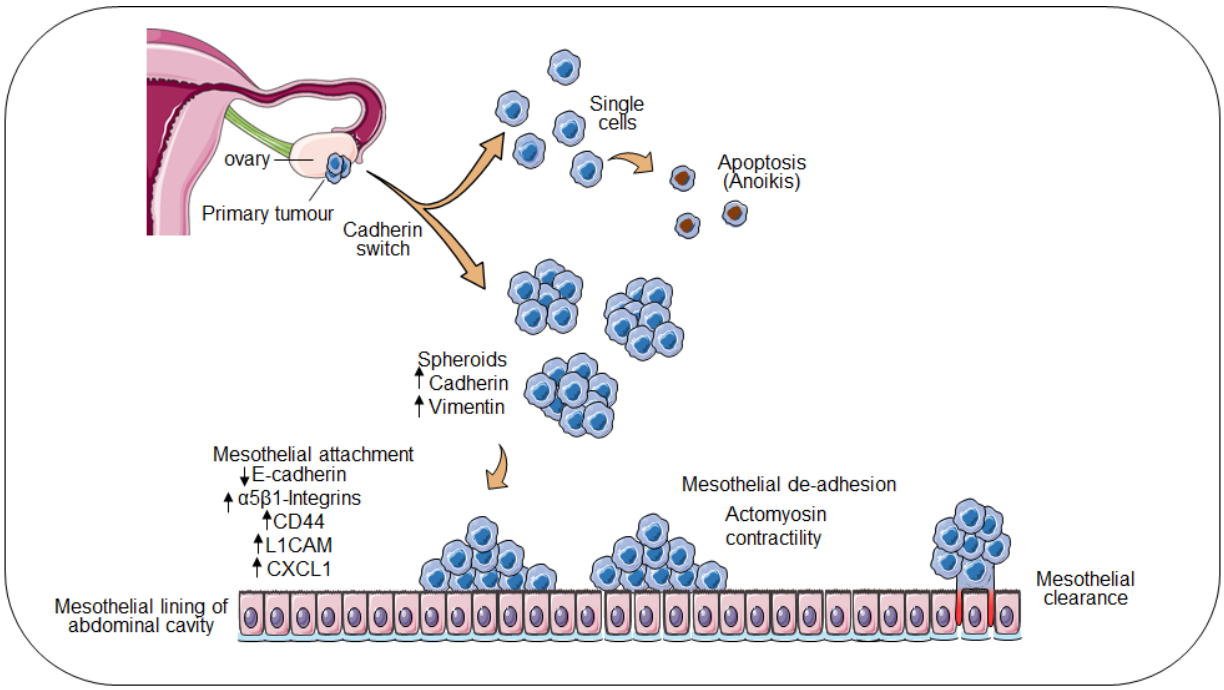

Figure 1.2. A working model of ovarian cancer metastasis. *According to this model, malignant cells from the primary ovarian tumour are shed into the surrounding peritoneal cavity. The cells undergo a phenotypic epithelial-mesenchymal transition (EMT) and form cellular aggregates termed spheroids, which exist as intermediate structures in the ascites fluid. Spheroids can settle and attach on secondary sites on the peritoneum where their phenotype is reverted to an epithelial state, allowing invasion and proliferation into the mesothelial layer and surrounding tissue. Figure from Moffitt et al., 2019[91].*

Invasive spheroids present in malignant ascites have increased proliferative and migration potential, high tumour forming capabilities *in vitro* and contribute to tumorigenesis *in vivo* in mice[69,84]. The ascites fluid from which spheroids are collected has an O_2 concentration of 1-3%[93], and cells within spheroids are found to utilise glucose mainly for anaerobic glycolysis, indicating their metabolic resistance to hypoxia[69]. Accordingly, spheroids isolated from ovarian cancer patients have demonstrated resistance to platinum-based chemotherapies and taxane-based therapies via protection from apoptosis[69]. Gene profiling of sphere-forming cells has also identified that their expression pattern is similar to that of stem cells[69]. This includes

significant upregulation of genes implicated in many developmental processes involving embryogenesis, neurogenesis and stem cell expansion in spheroid cells compared to their parent cells[69].

1.2.2 The role of hypoxia in the cancer microenvironment

Within rapidly growing solid tumours, such as HGSOCs, oxygen is unable to diffuse freely into the tumour core resulting in reduced cellular oxygen availability and creation of a hypoxic microenvironment[94]. Although inadequate oxygenation can induce necrosis of cancer cells, it is well recognised that hypoxia and the downstream factors induced under such conditions play an important role in promoting the pathogenesis of various cancers[94-96]. Malignant cells can survive hypoxic stress by undergoing several metabolic adaptions, many of which are subject to the transcriptional control of hypoxia-inducible factors (HIFs). HIFs regulate oxygen homeostasis and HIF-1 is the main contributor to the cellular response to reduced O_2 concentration. HIF-1 is a heterodimer that comprises a constitutively expressed HIF-1β subunit and a HIF-1α subunit which is the primary mediator of hypoxia via direct regulation by oxygen levels[94]. Under normal physiological conditions (i.e., adequate oxygen) HIF-1α is easily degraded by hydroxylation, however a lack of oxygen (i.e., in solid tumours) initiates stabilisation and accumulation of the HIF-1α protein where it heterodimerises with HIF-1β[94,97]. Therefore, HIF-1α is considered an appropriate marker of hypoxia[98]. In addition to decreased oxygen concentration; increased reactive oxygen and nitrogen species and loss of function of some tumour suppressor genes can contribute to increased levels of HIF-1α in many cancers[99].

The stabilised HIF-1 protein complex binds to hypoxia response elements of DNA, which can have numerous downstream oncogenic signalling effects to promote processes involved in the hallmarks of cancer[100]. Cellular and physiological responses to hypoxia include the switch to glycolytic metabolism, promotion of cell proliferation, resistance to apoptosis, immune

evasion, angiogenesis and metastasis[100]. The increased expression of HIF-1α has been described in various human cancers including premalignant lesions, lung, prostate, breast and colon carcinomas[95]. Hypoxia also contributes to chemoresistance and is associated with disease aggression of many cancers[101].

1.2.3 Hypoxic mediators in ovarian cancer

In epithelial ovarian cancers, HIF-1α may be a useful prognostic marker as its overexpression is associated with poor overall survival (Figure 1.3)[102,103]. Other studies suggest that HIF-1α expression is also related to relative 5-year survival rate, the degree of malignancy, metastatic capability and histological grade[104].

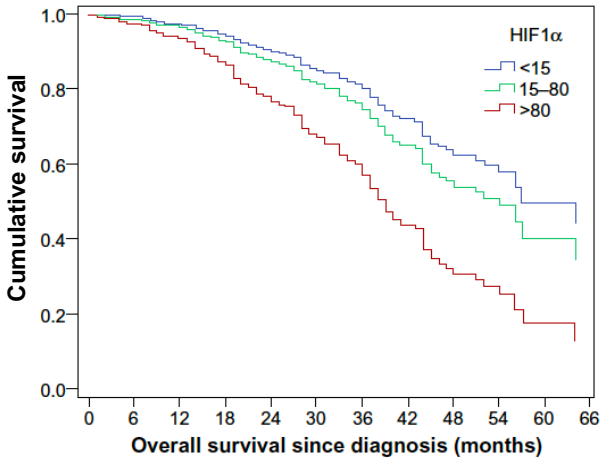

Figure 1.3. HIF-1α is a prognostic factor in patients with primary epithelial ovarian cancers. *Increased tissue concentration of HIF-1α (>80pg/mg protein) is correlated with decreased overall survival. Figure from Braicu et al. (2014)[102].*

A recent study validated the hypoxia inducible expression of 9 different genes of interest in primary and metastatic ovarian cancer samples[105]. Several genes involved in glycolytic pathways such as *SLC2A1, LDHA* and *ALDOA* were upregulated in response to hypoxia[105]. In particular, *VEGF* was consistently elevated amongst most samples[105]. VEGF has a well-documented role in cell growth and migration, angiogenesis and inhibition of apoptosis[106] and HIF1-α is a primary transcription factor in the angiogenic process in cancer. This correlation

provides further evidence of the role of hypoxia and HIF1-α specifically in the growth and spread of ovarian tumours. In addition to metabolic changes induced by hypoxia, evidence has suggested that hypoxic stress regulates mediators that trigger pathways involved in EMT which is a central event in cancer metastasis[107]. Activation of genes involved in this phenotypic transition allow the infiltration of malignant cells through endothelial barriers and invasion to secondary sites. HIF1-α has been shown to regulate several genes involved in EMT including E-cadherin, vimentin and Twist1[108]. In addition, HIF-1α may contribute to the invasiveness of human ovarian cancer cells by epidermal growth factor (EGF)-mediated downregulation of E-cadherin[109]. Evidently, targeting genes under the transcriptional control of HIF1-α is a promising strategy for treating ovarian cancer. Indeed, VEGF inhibitors such as bevacizumab (see Section 1.1.5) have shown promise in the clinic.

1.3 The immunological scope of ovarian cancer

1.3.1 Overview of the immune system in ovarian cancer

The immune system is a crucial factor in the progression and prognosis of epithelial ovarian cancer[110,111]. There are several components of the host immune response, including the production of tumour-associated autoantibodies (AAbs), which are generated against tumour-associated antigens (TAAs) during early stages of disease[112] (see Appendix C). The immune cell repertoire located within ovarian tumours and the surrounding microenvironment consists of adaptive immune cells including CD4+ and CD8+ T lymphocytes and B cells; and innate immune cells such as natural killer (NK) cells, macrophages, neutrophils, myeloid-derived suppressor cells (MDSCs) and dendritic cells (DCs)[89,113,114]. Neutrophils promote the formation of a premetastatic niche during the early stages of ovarian cancer tumorigenesis[115] and are considered biomarkers of disease and potential therapeutic targets[116]. Macrophages are also key regulators of ovarian cancer tumorigenesis[117,118]. The classically activated M1 macrophage phenotype exhibits anti-tumour activity[119], whilst alternatively activated M2 macrophages promote tumour progression via secretion of chemokines that induce immunosuppressive responses[120]. Innate immune cells clearly define a crucial component of the anti-tumour response, however; this review will mainly focus on the T cell response in ovarian cancer, as most clinical therapies target this subset of adaptive cells. Ovarian cancer cell growth is also directly influenced by the milieu of soluble factors that are present in malignant ascites fluid[121]. These molecules, including cytokines, chemokines and growth factors are secreted by tumour cells, leukocytes, fibroblasts and mesothelial cells[89] and play a complex role in modulating the nature of the immune response[113,122]. Although multiple immune surveillance pathways are activated during ovarian cancer progression, mechanisms of immune evasion dominate the ovarian cancer landscape, including upregulation of immunosuppressive/regulatory pathways, impaired antigen recognition and immune tolerance, which ultimately promotes tumour progression[123].

1.3.2 The T cell response in ovarian cancer

An overview of the anti-tumour and pro-tumour immune responses in epithelial ovarian cancer is depicted in Figure 1.4**.** At the forefront of the anti-tumour response are antigen presenting cells (APCs) including DCs, which are responsible for the uptake and display of antigenic peptides in the context of major histocompatibility complex (MHC) molecules and subsequent activation of CD8+ and CD4+ T lymphocytes[124,125]. In ovarian cancer, one of the most important prognostic factors is the presence of tumour infiltrating lymphocytes (TILs). Multiple independent studies have demonstrated that increased levels of TILs in ovarian tumours are correlated with a significant increase in median survival time and overall outcome[126-130]. Upon their activation, CD8+ cytotoxic T lymphocytes (CLTs) become potent eliminators of cancer cells via antigen-specific, perforin/granzyme-mediated apoptosis[131,132]**.** CTLs are powerful effector cells and are generally accepted as the primary mediators of the anti-tumour response in ovarian cancer. Regulatory T cells (Tregs) conversely mediate immunosuppression. Evidence suggests that increased intraepithelial CD8+/Treg cell ratio is associated with improved overall patient survival in ovarian cancer, emphasising the importance of this type of T effector response on clinical outcome[126].

Antigen presenting cells activate naïve CD4+ T lymphocytes into distinct subtypes of T helper (Th) cells; Th1, Th2 or Th17[89]. Other T helper subtypes also exist in lower abundance[133], however for the purpose of this review they will not be discussed. The Th1 cells drive the cell-mediated effector response via secretion of pro-inflammatory cytokines such as IL-2, interferon-gamma (IFN-γ) and TNF-α to promote tumour-specific accumulation and activation of CTLs[134-136]. Conversely, Th2 cells are defined by secretion of IL-4, IL-5, IL-10 and IL-13[137] and are important as a defence against extracellular pathogens, but also negatively regulate the Th1 response by inhibition of inflammatory responses[137-139]. The expression of Th2-derived cytokines is associated with the activation of M2 tumour-associated macrophages[140] which correlate with poor clinical outcome in ovarian cancer patients[141]. The balance between the Th1 and Th2 response in terms of relative expression of cytokines may also be important

for diagnosis and prognosis in ovarian cancer[142]. The more recently discovered Th17 subset are characterised by secretion of the pro-inflammatory cytokine IL-17 and promote a Th1-type response by recruitment of tumour-infiltrating CD8+ T cells[143]. Although Th17 cells are not the only source of IL-17[144], increased levels of tumour infiltrating Th17 cells and tumour-associated IL-17 are correlated with significantly improved survival in ovarian cancer patients[143], validating their role in anti-tumour immunity.

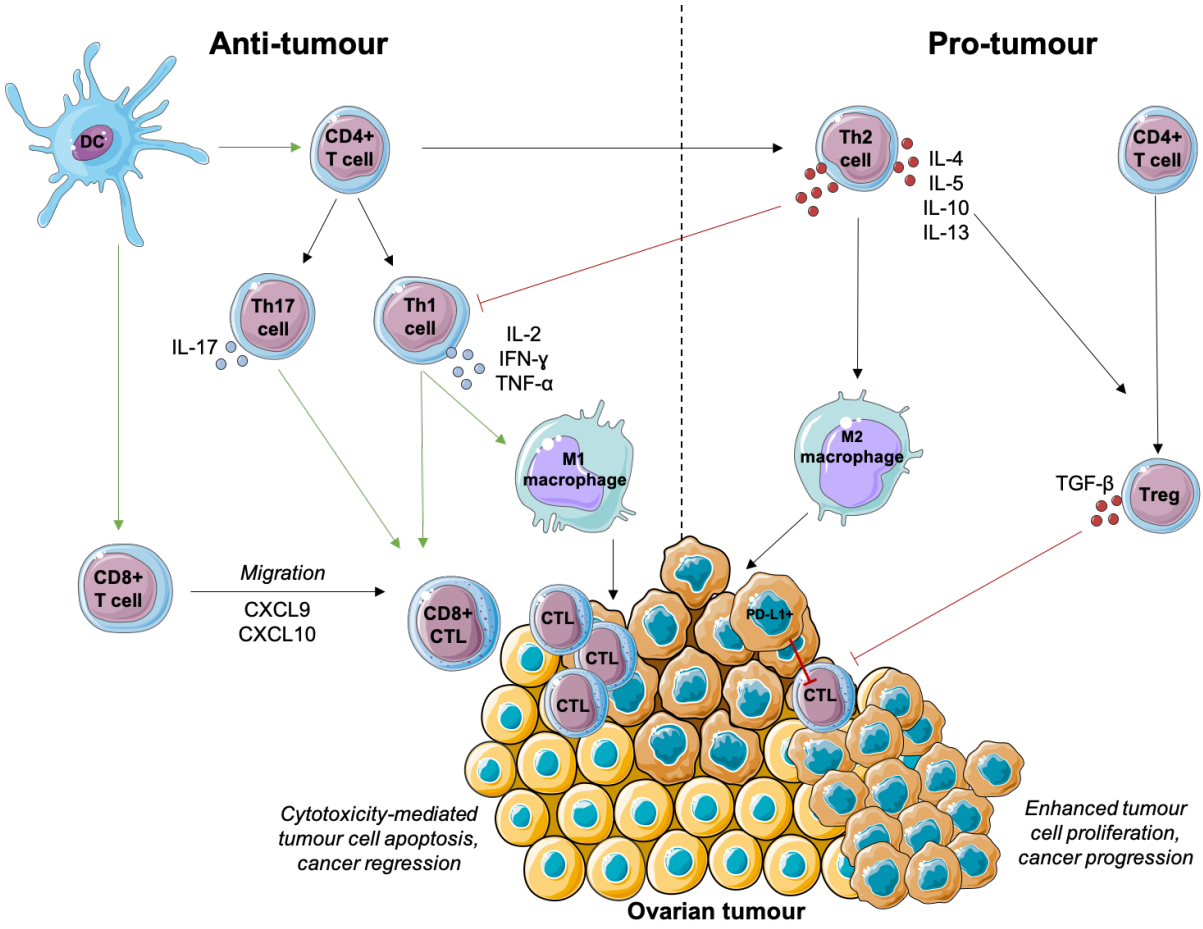

Figure 1.4. Overview of selected anti- and pro-tumour immune responses in the ovarian tumour microenvironment. *Dendritic cells activate CD8+ T cells into CTLs, which are recruited to the tumour site via chemotactic migration involving CXCL9 and CXCL10. DCs also activate naïve CD4+ T cells into Th1, Th2 or Th17 subtypes. Th1 cells secrete pro-inflammatory cytokines including IL-2, IFN-ɣ and TNF-α to activate M1 macrophages, and, together with IL-17 secretion by Th17 cells, induce the accumulation of CTLs in the TME. Tumour cells undergo cytotoxicity-mediated apoptosis via the actions of infiltrating CTLs, which promotes cancer regression. On the other hand, Th2 cells secrete immunosuppressive cytokines including IL-4, IL-5, IL-10 and IL-13 which inhibits the anti-tumour actions of Th1 cells. Th2 cells also induce differentiation of M2 macrophages and Tregs. Release of immunosuppressive factors including TGF-β by Tregs inhibits the activity of CTLs in the tumour. Expression of PD-L1 on the surface of tumour cells also blocks CTL activation and induces T cell exhaustion, contributing to enhanced tumour cell proliferation and cancer progression. Green arrow = activation, Red bar = inhibition. CTL: cytotoxic T lymphocyte, CXCL: C-X-C motif chemokine ligand, DC: dendritic cell, IFN-ɣ: interferon-gamma, IL: interleukin, PD-L1: programmed death-ligand 1, TGF-β: transforming growth factor-beta, Th1: T helper type 1, Th2: T helper type 2, Th17: T helper type 17, Treg: regulatory T cell, TME: tumour microenvironment, TNF-α: tumour necrosis factor-alpha.*

1.3.3 Immunosuppression in ovarian cancer

Although ovarian tumours are immunogenic even at late stages, there is widespread evidence of immunosuppression in EOCs, such as the overexpression of programmed death-ligand 1 (PD-L1)[145]. PD-L1 is an inhibitory ligand expressed on the surface of multiple immune cell types and other non-haematopoietic cells[146] and is correlated with poor prognosis in ovarian, gastric and breast cancers[145,147,148]. PD-L1 interacts with its cognate receptor, programmed death-1 (PD-1), which is induced on activated T cells, B cells and macrophages[149]. The PD-1/PD-L1 pathway plays a significant role in maintaining a balance between T cell activation and immune tolerance via inhibition of antigen receptor signalling[149]. Overstimulation of this inhibitory pathway in various cancers induces immune escape via a significant reduction of T cell activity and an increase in T cell exhaustion and apoptosis[150,151], therefore decreasing tumour clearance by the host's immune system[152]. PD-1 expression is also upregulated on regulatory T cells (Tregs) and increases their suppressive activity[153]. The Tregs are a subpopulation of CD4+ T cells that downregulate effector mechanisms of activated immune cells and mediate immune tolerance in order to prevent autoimmunity[154,155]. In ovarian cancer, Tregs disrupt local antigen-specific CTL function by decreasing their tumour killing capacity and secreting immunosuppressive factors including IL-10 and transforming growth factor beta (TGF-β), which promotes immune escape and tumour progression[136,156,157]. Analyses of T lymphocyte infiltration in ovarian cancers have revealed that Tregs detected by the presence of Foxp3[158] are increased in T cell infiltrates and are associated with reduced survival and advanced disease stages[126,155,159,160].

1.3.4 Cytokine networks in the ovarian cancer tumour microenvironment

As previously mentioned, cytokine and chemokine networks are a crucial element of the immune response via regulation of inflammatory pathways, lymphocyte migration and trafficking[161]. Within the highly heterogenous ovarian tumour microenvironment (TME), there is strong evidence of significant disruptions to multiple cytokine networks affecting autocrine

and paracrine signalling pathways, which impacts tumour cell behaviour, angiogenesis, lymphocyte infiltration and supports metastatic growth[162]. For example, TNF, CXCL12 and IL-6 – which comprise the 'TNF network' – and the related signalling pathways have an established role in ovarian cancer pathogenesis[113]. Kulbe and colleagues reported that genes involved in these signalling pathways were significantly overexpressed and interrelated in ovarian cancer patient biopsies[163]. The TNF network was correlated with enrichment for genes involved in important pathways and processes in tumour growth including angiogenesis, adhesion, cell cycle and immune cell signatures[163].

Levels of various signalling cytokines including IL-6 and IL-8 are elevated in ovarian cancer patient ascites[164], are associated with increased cancer cell growth and metastasis and are a poor indicator of overall survival[165-167]. Increased IL-6 concentration is also correlated with chemoresistance in ovarian cancer patients[168,169]. Secretion of other immunosuppressive factors including IL-10 by ovarian cancer cells and immune cells within the TME alters the differentiation of dendritic cells[170] and contributes to the polarisation of macrophages towards an immunosuppressive, tumour-associated phenotype[171]. Other important chemokines involved in EOC progression including CXCL9, CXCL10 and their receptor CXCR3 are upregulated in ovarian tumours[172,173]. Expression of CXCL9 and CXCL10 in HGSOCs was correlated with T cell infiltration and a more favourable prognosis[172]. These chemokine ligands have a primary role in the migration and recruitment of T cells towards tumours[174] and may increase tumour recognition by antigen presenting cells[175]. Evidently, the influence of the ovarian TME on the expression and function of cytokine networks can have a significant effect on the pro- or anti-tumour response and therefore on tumour progression. There is now considerable interest in cytokines and their networks as candidates for targeted therapy.

1.3.5 The role of hypoxia on the immune system in ovarian cancer

Hypoxia has been identified as a likely factor in the immunosuppressive behaviour of ovarian tumours[176,177]. Townsend and colleagues recently described how the positive correlation between angiogenic markers, oxygen supply and patient survival outcomes could be linked to favourable T cell responses in HGSOCs[178]. Their studies revealed that highly vascularised tumours contained higher levels of markers of immune cytotoxicity than those of low vascularisation (i.e., under hypoxia)[178]. This research also established that a hypoxic tumour environment significantly impaired CD8+ T cell effector function *in vitro*, possibly via the downregulation of IFN-γ and TNF-α[178]. Hypoxia also appeared to stimulate autophagy in these T cells, which may be attributed to the changes in cell cycle regulation under the transcriptional control of HIF-1α. The type of anti-tumour response in relation to the ratio of effector:regulatory cells was also associated with vascularity and oxygenation, where the presence of Foxp3 positive lymphocytes was only beneficial for patient survival with highly vascularised tumours[178] and their presence in low oxygenated tumours was disadvantageous. Tumour hypoxia also influences other immune populations in the TME. For example, MDSCs are recruited to areas of hypoxia and decrease the anti-tumour immune response by inhibiting the activity of T cells and NK cells[179]. The role of hypoxia in ovarian tumours appears to be influential on both the differentiation and function of T lymphocytes, and the cellular changes that occur in response to hypoxia may be partially responsible for evasion of the immune system by ovarian tumours.

1.3.6 Immunotherapies in ovarian cancer

Given the significant role of the immune system in ovarian cancer, substantial research efforts have focused on harnessing the host immune system to enhance the anti-tumour response. As previously mentioned, the PD-1/PD-L1 interaction regulates the threshold of the immune response in the periphery to prevent excessive inflammation and autoimmunity and is therefore considered an immune 'checkpoint'. In ovarian cancer and many other malignancies,

this critical point of control is dysregulated and the overexpression of PD-1/PD-L1 encourages immune evasion[180]. Another important immune checkpoint in various cancers is the cytotoxic T lymphocyte-associated antigen (CTLA-4)/B7 axis. The coinhibitory receptor CTLA-4 is expressed on activated T cells and competes with the costimulatory molecule CD28 to binds its ligands, B7-1 and B7-2[181]. The CTLA-4/B7 interaction reduces early stages of T cell activation and impairs the priming ability of APCs[182,183]. These targetable pathways have led to the development of immune checkpoint inhibitors (ICIs) to restore T cell anti-tumour immunity, and have demonstrated impressive results in various tumour types[184]. For example, antibodies targeting anti-CTLA-4 (ipilimumab) and anti-PD-1 (pembrolizumab) both showed substantial efficacy in phase 3 trials in patients with metastatic melanoma[185,186]; however, long-term follow up studies revealed that pembrolizumab was superior to ipilimumab in terms of improvement to PFS and OS[187]. Furthermore, outcomes from the phase III KEYNOTE 010 study demonstrated that pembrolizumab treatment in non-small-cell lung carcinoma (NSCLC) patients significantly prolonged median survival time and increased the 1-year survival rate from 35% to 43% compared to patients receiving the chemotherapy docetaxel[188]. As a result of their success in clinical trials, various anti-PD-1, anti-PD-L1 and anti-CTLA-4 antibodies have been approved for the management of these cancers and other solid tumours[184,189,190].

Unfortunately, immune checkpoint inhibition as a monotherapy has not seen the same success in with ovarian cancer patients than other malignancies, most likely due to the highly heterogenous intra- and extra-tumoural environment. In 2015, Hamanishi and colleagues reported the findings of a phase II clinical trial where 20 women with platinum-resistant ovarian cancer were treated with up to 6 cycles of the anti-PD-1 antibody nivolumab at a dose of 1mg/kg or 3mg/kg[191]. Across both cohorts, the best objective response rate (ORR) was only 15% (3 out of 20 patients)[191]. Similarly, the phase Ib JAVELIN solid tumour trial where patients with recurrent or refractory ovarian cancer received the anti-PD-L1 antibody avelumab at 10mg/kg every 2 weeks demonstrated an ORR of 9.6% (12 out of 125 patients)[192]. In the phase II KEYNOTE-100 study, women with recurrent ovarian cancer treated with

pembrolizumab 200mg every 3 weeks exhibited an 8% ORR (30 out of 376 patients)[193]. These clinical trials suggest that anti-PD-1 or anti-PD-L1 inhibition alone is unlikely to be effective for the majority of ovarian cancer patients, and that inhibition of only the PD-1/PD-L1 interaction may be insufficient to restore active anti-tumour immunity due to other immune evasion mechanisms initiated by the tumour and TME in ovarian cancer.

More recently the focus of immunotherapy in ovarian cancer has evolved and strategies aimed at improving their efficacy in ovarian cancer have involved optimising dosing schedules and combining immune checkpoint inhibitors with other existing therapeutics. The combination of avelumab to standard chemotherapy demonstrated a lack of efficacy as a frontline treatment and was terminated prematurely (NTC02718417)[194]; and the combination of avelumab with pegylated liposomal doxorubicin (PLD) in patients with platinum-resistant disease in the phase III JAVELIN Ovarian 200 trial did not prolong PFS or OS[195]. A recent phase II trial using a combination of nivolumab (anti-PD-1) and bevacizumab (anti-VEGF) in women with relapsed ovarian cancer reported an ORR of 40% in platinum-sensitive patients and 16.7% in platinum-resistant patients[196], demonstrating a potential therapeutic window for this combination treatment in chemo-naïve or -sensitive patients. The combination of PARP inhibitors with ICIs is also being investigated in several clinical trials, however the efficacy in BRCA-mutated vs BRCA-wild-type disease remains uncertain. In the phase II MEDIOLA study, the combination of durvalumab (anti-PD-L1) with olaparib (PARPi) in 32 patients with BRCA-mutated platinum-sensitive relapsed ovarian cancer resulted in an ORR of 71.9% and complete response in 7 patients[197], whilst the same combination in a phase I trial in a smaller cohort of previously treated women with BRCA wild-type recurrent tumours demonstrated an ORR of only 17%[198].

Other promising novel therapeutics for ovarian cancer include those that stimulate the innate immune response. Inhibition of CD47 – which is overexpressed in ovarian cancer – was shown to enhance macrophage phagocytosis of tumour cells[199]. A recent phase I clinical trial in a small cohort of patients revealed that CD47 blockade using the monoclonal antibody

magrolimab resulted in an objective response and reduced target tumour size by up to 50% in participants with ovarian cancer[200], with ongoing studies to determine its efficacy in combination with anti-PD-L1 therapies[201]. Furthermore, immunotherapies that target cytokine networks are also under investigation but are yet to demonstrate substantial efficacy in ovarian disease. For example, a phase I/II clinical trial with the anti-IL-6 monoclonal antibody siltuximab reported that the treatment was well tolerated but no objective responses occurred in patients with chemoresistant EOC[202]. Additionally, treatment with the TNF-α blocker etanercept in a phase I trial in women with advanced ovarian cancer revealed that 6 out of 18 patients achieved stable disease with otherwise minimal clinical benefit[203].

Evidently, the complexities of the immune response to ovarian tumours require a combination approach for first- and subsequent lines of treatment. Importantly, issues such as toxicity and resistance must also be considered for all new immunotherapy regimens. Additional clinical trials involving combination therapies are ongoing and are likely to provide further insight into the potential therapeutic benefit of targeting immune pathways in ovarian cancer.

1.4 Uncovering the role of DPP4 in ovarian cancer

1.4.1 Overview of DPP4 function

Dipeptidyl peptidase 4 (DPP4, also known as CD26) is a type II transmembrane glycoprotein that comprises 766 amino acids, and is active as a homodimer[204]. A soluble form of active DPP4 (sDPP4) also exists in extracellular fluid following its proteolytic cleavage from the cell surface[205,206]. DPP4 is the archetypal member of the DPP4 activity and/or structure homologue (DASH) family of serine proteases, which also includes fibroblast activation protein (FAP/seprase), DPP8 and DPP9[207-209]. DPP4 is ubiquitously expressed on the cell surface of many epithelial cell types, including the liver, lung, kidney, intestine, prostate, endothelial capillaries, immune organs such as the thymus and spleen and specific populations of immune cells including activated lymphocytes and monocytes[210-214].

The structural properties of DPP4 are responsible for its multifunctionality as a binding molecule and bioactive enzyme, and has been implicated in metabolism, immunity, endocrinology and cancer[205,213]. DPP4 contains a short cytoplasmic extension, whilst the extracellular portion includes a highly glycosylated and cysteine rich N-terminal β-propeller and a C-terminal α/β-hydrolase domain, which comprises the active site with a highly conserved catalytic triad (Figure 1.5)[205,213,215,216].

DPP4 exhibits highly specific and unique enzymatic activity by cleavage of the dipeptide at the N-terminal position of a peptide with proline or alanine at the penultimate position[207,217]. The enzymatic role of DPP4 involves modulation of the bioactivity of several regulatory chemokines, neuropeptides and peptide hormones, and is most well-known for its role in type 2 diabetes via degradation of glucagon-like peptide 1 (GLP1)[218]. Independent of its enzymatic activity, DPP4 is well documented for its role to enhance cellular responses to external stimuli, particularly as an immune signalling molecule in T cell co-stimulation and activation, via its association/binding with adenosine deaminase (ADA), cavelolin-1, CD45 and CARMA1[219-221].

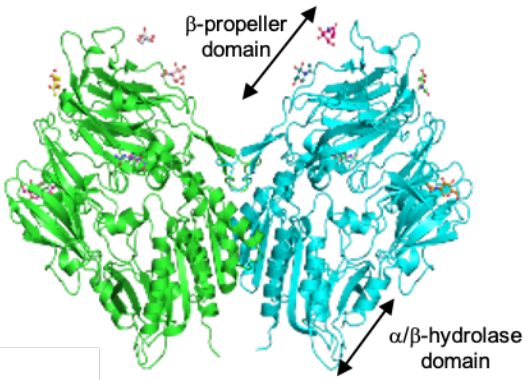

Figure 1.5. Structure of DPP4. *The crystal structure of human DPP4 as an enzymatically active homodimer bound to ligand NAG (PDB entry: 1 j2e; <https://www.ebi.ac.uk/pdbe/entry/pdb/1j2e/analysis>). Each monomer is composed of a β-propeller domain and α/β-hydrolase domain. Figure adapted from Hiramatsu et al. (2003)[216].*

1.4.2 DPP4 in the tumour microenvironment

As a cell surface protease, DPP4 is considered important in tumour progression and invasion. DPP4 is a pleiotropic protein, and its role within a cancer context is influenced by the complexities of the TME; including components of the extracellular matrix (ECM) such as matrix metalloproteinases (MMPs) and tissue inhibitors of metalloproteinases (TIMPs), external and cellular stimuli, the immune system, organ/tissue specific behaviour and cell and differentiation dependent responses[222]. DPP4 has been implicated in several malignancies including renal cell carcinoma, lung adenocarcinoma, prostate cancer, melanoma, thyroid cancer and T cell malignancies[223]; however, its specific role varies between different cancers, and the widespread functions of DPP4 endorse its status as both a tumour suppressor and a marker of malignancy (Figure 1.6).

DPP4 has been associated with tumour suppressive functions in prostate cancer, melanoma, lung cancer and ovarian carcinoma[223], although the latter is under debate (see Section 1.4.5). In melanocytes, loss of function of DPP4 at the RNA level is correlated with early melanoma tumorigenesis[224]. In addition, serum DPP4 activity and the percentage of CD26 (DPP4) expressing white blood cells in melanoma patients is significantly decreased compared to

healthy controls[225]. Rescue of a malignant phenotype has been achieved by transfecting DPP4 in melanoma cell lines, suggesting its possible use as a therapeutic target[226]. Similarly, DPP4 expression is also downregulated in NSCLC cells[227]. Its role as a tumour suppressor in NSCLC was found to be mediated independent of its enzymatic activity and may be related to increased levels of FAP-α and CD44, which are correlated with poor prognosis in NSCLC patients[228]. In prostate cancer cells, the loss of DPP4 has been associated with increased expression of basic fibroblast growth factor (bFGF), which contributes to increased cell proliferation, migration and invasion[229]. Other studies have also suggested that DPP4 activity is reduced in patients with metastatic prostate cancer compared to controls; as a result, signalling via CXCR4 is decreased leading to increased invasion and metastasis[230,231].

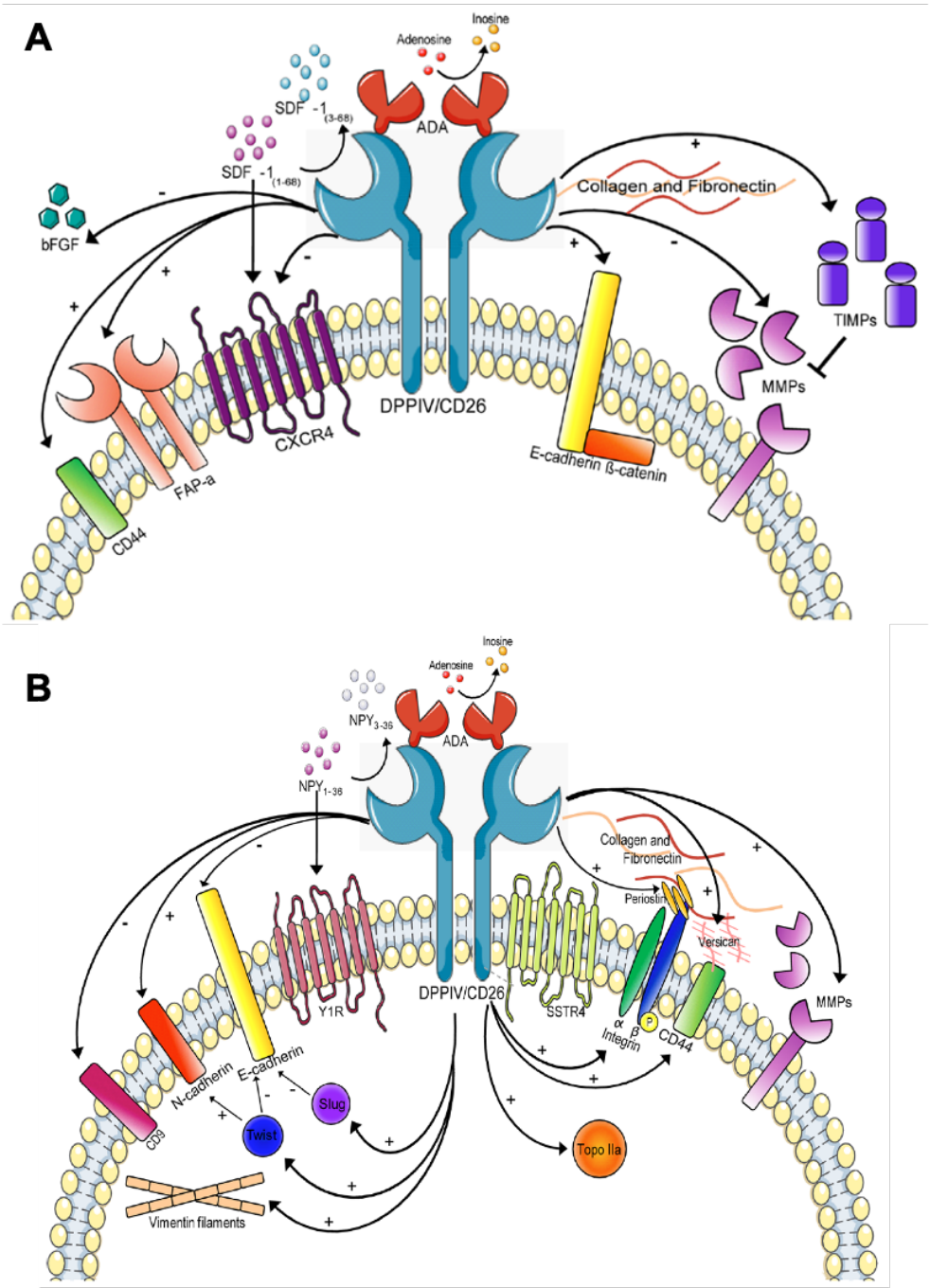

Figure 1.6. Schematic diagrams representing the proposed mechanisms of DPP4 as a tumour suppressor and marker of malignancy. *DPP4/CD26 interacts with proteins involved in adhesion, extracellular matrix (ECM) remodelling and cell signalling. The downstream effects of DPP4 expression or enzymatic activity can modulate cancer progression, invasion and metastasis by either (A) tumour suppressive or (B) tumour promoting functions, dependent on the physiological context. See text for more details. Figures from Beckenkamp et al. (2016)*[228].

Research has suggested DPP4 as a potential 'tumour promoter' or marker of malignancy in colorectal cancer, haematological malignancies, breast cancer and prostate cancer (despite also being reported as a tumour suppressor as described above). For example, lung endothelial DPP4 binds fibronectin to promote metastasis and colonisation of breast cancer cells[232]. In addition, DPP4 binds plasminogen 2 and enhances invasiveness of cells via MMP-9 upregulation in prostate cancer cells[233]. In colorectal cancer cells, overexpression of DPP4 and its association with integrin β1 is correlated with increased migration, invasion and adhesion to fibronectin and collagen[234]. Furthermore, subpopulations of CD26 $(DPP4)^+$ cells isolated from the tumours of colorectal cancer patients displayed EMT-like expression profiles, including the downregulation of E-cadherin and upregulation of N-cadherin, Twist and vimetin[234], suggesting a possible role of DPP4 in EMT.

Soluble DPP4 (sDPP4) is readily measurable in serum[235] and has been extensively investigated as a clinically relevant protein in colorectal cancer (CRC). Several studies have identified decreased levels of serum DPP4 in CRC patients compared to healthy controls[236,237], and the use of sDPP4 as a biomarker in combination with current screening measures may be a more specific and sensitive early diagnostic tool[237]. Numerous reports have identified expression profiles of DPP4 in CRC patients, however some of this is yet to be consolidated or have produced conflicting results[238].

Complexities surrounds the fact that sDPP4 measured in serum may not be directly reflective of DPP4 activity, and its use as a biomarker should consider both expression and enzyme activity. Evidently, it is important to explore the role of DPP4 in different pathological contexts. It is likely that as further research is performed to examine DPP4 in various cancers, its prognostic potential will become more apparent.

1.4.3 DPP4 in anti-tumour immunity

As previously discussed, the immune system plays an elaborate role on the progression of ovarian cancer, however for the purpose of this review we will only describe the proposed impact of DPP4 upon anti-tumour immunity.

The significant influence of CXC-motif chemokines (CXC) and their G-protein coupled receptors is becoming more apparent in cancers[239]. In an immune context, some CXC chemokines are potent chemo-attractants and are gaining interest for their potential role within the inflammatory environment of ovarian tumours[240]. In ovarian cancer, the secretion of IFN and IL-17 from Th17 cells at the tumour site stimulates the release of CXCL9 and CXCL10 from tumour cells[241]. These chemokines play an important role in the Th1-type response by recruiting activated T lymphocytes, macrophages, NK, NKT and dendritic cells and promoting their effector mechanisms at sites of inflammation and tumours[239].

DPP4 has the enzymatic ability to inactivate or alter the biochemical specificity of several chemokines by cleavage of the dipeptide at their N-terminus[242]. As a substrate of DPP4, cleavage of CXCL10 occurs rapidly to produce an antagonistic form of the protein (AgCXCL10) that retains binding affinity to its cognate receptor CXCR3 whilst competitively inhibiting the binding of agonist CXCL10; thereby abolishing its signalling effects involved in leukocyte recruitment and trafficking[242,243]. Reported recently as a possible mechanism of in the pathogenesis of liver cancer, AgCXCL10 was identified as a potential factor in poor treatment outcomes[243].

It is well established that the degree of CD8+ TILs is positively associated with increased overall survival in ovarian cancer[178], and interest surrounds the possible involvement of DPP4 and CXCL10 in this paradigm in EOC[244]. Recent research published by Rainczuk and colleagues investigated whether the cleaved form of CXCL10 was present in serous epithelial ovarian tumour samples. Expression profiling identified high mRNA levels of AgCXCL10 in

these tumours, compared to that in controls and benign carcinomas[244]. Furthermore, DPP4 was also significantly associated with the presence of CXCL10, and the data suggested that DPP4 may be responsible for contributing to CXCL10 cleavage within ovarian tumours[244]. The cleaved form of CXCL10 may prevent chemotaxis and leukocyte recruitment into the ovarian tumour epithelium (Figure 1.7)[245]. The data also suggested that CXCL10-dependent T cell infiltration was significantly less in serous tumours than in other tissue subtypes[244]. An important observation was that in some high CXCL10 expressing tissue samples with low levels of TILs, there were antagonistic CXCL10 and DPP4 found to be present. This provides an important correlation between DPP4 expression, antagonistic CXCL10 and decreased leukocyte recruitment in serous ovarian cancers[244], and suggests there may be prognostic potential in the antagonistic form of CXCL10.

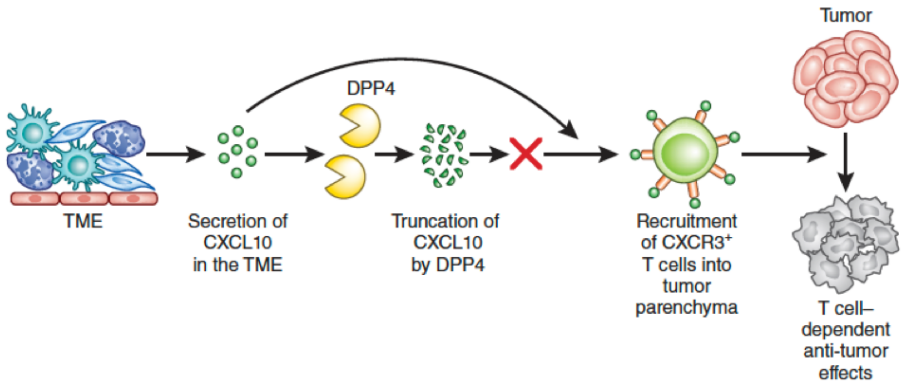

Figure 1.7. A working model of the effect of DPP4 activity on CXCL10-dependent recruitment of T cells within the tumour microenvironment. *Tumour cells secrete CXCL10 into the surrounding environment. CXCL10 is a chemokine involved in T effector cell recruitment and contributes to T cell dependent anti-tumour effects. DPP4 overexpression within the TME stimulates DPP4-mediated enzymatic cleavage of CXCL10 into a truncated, inactive form of CXCL10. Cleaved CXCL10 is unable to recruit T cells to the tumour site, resulting in less T lymphocyte infiltration. Figure adapted from Ohnuma et al. (2015)[245].*

Modification by DPP4 of important chemokines that result in altered biochemical activity in relation to tumour growth and progression highlights the need for further characterisation of

DPP4 in ovarian tumours. Considering the intrinsic function of DPP4 in T cell immunity, exploring the link between the two may certainly provide important insights into mechanisms of tumour progression and potential treatment opportunities by harnessing the immune system.

1.4.4 Evidence of an association between DPP4 and hypoxia

The first suggestion of DPP4 as a novel HIF-1 target gene was proposed by Dang and colleagues, where they identified that the induction of hypoxia in *VEGF* knockout colon cancer xenografts was associated with significant upregulation of DPP4 mRNA and protein[246]. Subsequently, the loss of HIF-1α caused downregulation of DPP4. These changes were dependent upon the stabilisation of HIF-1α, suggesting the transcriptional regulation of DPP4 by HIF-1[246]. Low oxygen conditions contribute to increased shedding of DPP4 by up to 50% in smooth muscle cells[247], whilst apparently contradictory results have found that relative DPP4 expression and protease activity of sDPP4 in human preadipocytes is decreased in response to hypoxia[248]. Pharmacological inhibition of DPP4 activity by treatment with sitagliptin was shown to decrease reactive oxygen species (ROS) and protect against ROS-mediated renal damage induced by hypoxic conditions[249,250]. Despite the well-established role of hypoxia and the widespread function of DPP4 within tumours and their metastases, the likely relationship between hypoxia (and its mediators) and DPP4 in cancer remains largely unknown.

1.4.5 Current knowledge of DPP4 in ovarian cancer

There are conflicting opinions surrounding the role of DPP4 in ovarian tumours. Much of the research on DPP4 in ovarian cancer was reported by Kajiyama and colleagues approximately 15 years ago. The authors suggested that ovarian cancer cell lines which overexpressed DPP4 *in vitro* had reduced invasive capacity, lower migration potential and exhibited significant morphological changes[251]. The same study indicated an *in vivo* correlation between

DPP4 overexpression and the reduction of intraperitoneal dissemination of cancer cells leading to prolonged survival in mice, and similar findings suggested that DPP4 overexpression was associated with enhanced chemosensitivity to paclitaxel[251-253]. The decrease in invasive potential of these cells was thought to be attributable in part to reduced pro-MMP-2 activity (the precursor for MMP-2). MMP-2 is a protease that degrades constituents of the ECM and its activity has been linked to carcinoma invasion[251]. In further reports of ovarian cancer cell lines overexpressing DPP4, MMP-2 expression levels were reduced, which correlated with morphologic changes and suppressed invasive ability[252]. However, this combination of results tended to focus on the function of DPP4 as an adhesion molecule and *in vivo* studies used nude mice, which are immunocompromised[254]. Considering the crucial role of the immune system in ovarian cancer and, in turn, the function of DPP4 in modulating the effects of many immune mediators as previously described, it is difficult to draw conclusions about the true effect of DPP4 in an ovarian tumour environment based on these findings. Furthermore, recent research of DPP4 in clinical samples have produced contradicting data to that explained above. Immunohistochemical analysis of ovarian tumour sections found that DPP4 protein expression was significantly higher in cancer tissue compared to borderline or benign tumours (Figure 1.8A)[255]. This study also analysed the expression of the DPP4 relative – seprase; and identified that together their abundance was associated with tumour stage and lymph node metastasis and may be useful as a prognostic indicator[255].

Similar findings were also reported by Rainczuk and colleagues where serial section analysis identified that DPP4 protein was elevated in serous and endometrioid ovarian tumours together with cancer-adjacent tissues compared to normal tissue (Figure 1.8B)[244]. By contrast, benign tumours exhibited significantly decreased DPP4 levels relative to normal. Considering the role of DPP4 as a potential modulator of leukocyte infiltration (see Section 1.4.3), its

overexpression in ovarian tumours warrants further investigation in both a functional and physiological context to understand its influence on EOC growth and metastasis.

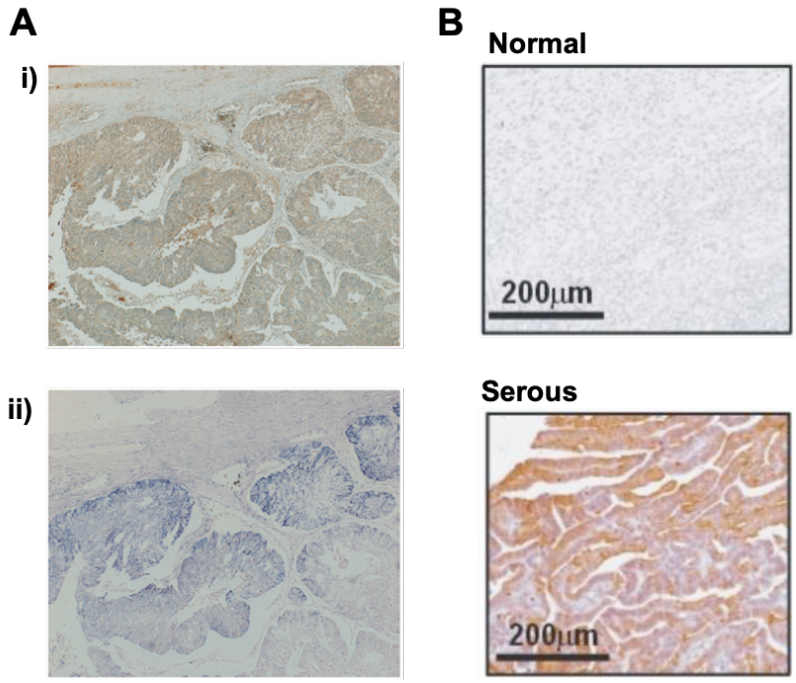

Figure 1.8. Evidence of DPP4 upregulation in ovarian cancer tissue. *(A) Zhang et al. (2015) investigated ovarian tumour tissue for the presence of DPP4 by i) immunohistochemistry and ii) in-situ hybridisation. (B) Rainczuk et al. (2013) analysed DPP4 expression by immunohistochemical analysis in serial ovarian tissue sections. Both reports demonstrated the upregulation of DPP4 in the majority of ovarian tumour samples*[244,255]*.*

It is entirely plausible that there are several, independent mechanisms by which DPP4 contributes to ovarian cancer. For example, DPP4 may have roles within cell differentiation, attachment and dissemination of spheroids, ECM degradation at the cellular invasion front, or immune suppression via cleavage of chemokines such as CXCL10 to inhibit leukocyte recruitment. Any or all of these possibilities are important in determining the specific function of DPP4 in ovarian tumours. By further understanding the molecular mechanisms of DPP4 we can achieve a greater understanding of the pathogenesis of ovarian cancer and investigate strategies to overcome potential DPP4-mediated tumour progression.

1.4.6 DPP4 as a novel therapeutic target

Until recently, the perception of DPP4 as a therapeutic target was based on its role in insulin regulation and therefore the potential for diabetes treatment. Indeed, several clinically approved small molecule DPP4 enzyme inhibitors ('gliptins') are indicated for the treatment of type 2 diabetes[256]**.** However, more comprehensive knowledge about the role of DPP4 in malignancies as an adhesion molecule and a mediator of chemokine activity emphasises its potential as a novel therapeutic target in these diseases. Multiple meta-analyses have provided evidence of the clinical efficacy of DPP4 inhibition in various cancer types. Bishnoi and colleagues found that diabetic patients with CRC or lung cancer who were receiving DPP4 inhibitors (DPP4i) had a significant survival advantage compared to patients not treated with DPP4i, although the advantage was not significant when patients were separated according to cancer type[257]**.** Similarly, a more recently published retrospective trial involving over 15,000 patients with prostate cancer determined that patients who were treated with DPP4 inhibitors for type 2 diabetes had a significant survival advantage compared to those not on DPP4i[258]. However, the same survival advantage with DPP4i was not observed in patients with pancreatic or breast cancer[258].

A pre-clinical study using the DPP4 inhibitor sitagliptin in hepatocellular carcinoma (HCC) demonstrated that inhibition of DPP4 activity upregulates levels of the C-C motif chemokine ligand 11 (CCL11) and increases migration of eosinophils into tumours[259], highlighting the efficacy of DPP4 inhibition as a moderator of immune cell trafficking. Furthermore, treatment of ovarian cancer cells lines *in vitro* with sitagliptin reduced cell migration and invasiveness and maintained paclitaxel sensitivity[260]. In a model of polycystic ovary syndrome in rats, DPP4 inhibition significantly decreased the protein and mRNA levels of the cytokine TGF-β1 in the ovaries[261], which is an important mediator of the immunosuppressive properties of Tregs in the ovarian cancer environment [157]. Together these studies suggest targeting DPP4 in the ovarian TME has the potential to influence important pathways of the immune response and may synergise with other, existing therapies to increase their efficacy.

1.5 Conclusions

Ovarian cancer is a particularly challenging disease to manage due to the late stage of diagnosis and recurrence in the majority of patients. Substantial amounts of research have highlighted several genetic, environmental and lifestyle-associated risk factors correlated with the development of ovarian cancer; however, our understanding of the pathological context of the disease is key to uncovering novel treatment solutions, with a common goal to provide women diagnosed with ovarian cancer a greater chance of survival. It is clear that in order to provide a better standard of care for ovarian cancer patients requires a more comprehensive understanding of i) novel markers of malignancy, recurrence or factors indicative of response to treatment, ii) the key drivers/events that leads to extensive metastatic spread and iii) the complexities of the host immune system that play such a crucial role in overall outcome. In particular, it must be acknowledged that the dynamic nature of the immune system can tip the balance from pro- to anti-tumour immunity over time – for example before, during or after treatment with chemotherapy – and have a significant effect on overall outcome. Similarly, large amounts of evidence including that described in this literature review highlights the need for a dynamic approach to the treatment of ovarian cancer, including the identification of common pathways involved in the anti-tumour immune response, in combination with other targeted therapies which have the potential to influence the way in which ovarian cancer is treated in the future.

Project rationale

The overall survival for epithelial ovarian cancer patients has not significantly improved in the last 30 years and the 5-year mortality remains at approximately 70%[58]. The deadliest subtype, high-grade serous carcinoma, accounts for the majority of cases and is difficult to treat based on the extensive heterogeneity observed in these tumours[21]. The standard of care for women diagnosed with ovarian cancer is debulking surgery followed by several cycles of platinum-based chemotherapy[2]. Unfortunately, many patients eventually develop recurrent, platinum-resistant disease and will succumb to the disease after the limited treatment options are exhausted[70]. Recent advances in the understanding of the pathogenic and morphologic characteristics of ovarian tumours have encouraged the development of novel, molecularly targeted therapies. However, clinical trials for these new therapies such as anti-VEGF antibodies and PARP inhibitors have delivered mixed results and require further research to identify patients who are most likely to achieve a clinical benefit[76,262]. There is an urgent need not only to develop new therapies to improve survival of patients diagnosed with EOCs; but to gain a better understanding of the biology of ovarian cancer so that treatment efficacy can be optimised.

Our laboratory is investigating dipeptidyl peptidase 4 (DPP4/CD26) in ovarian cancers. DPP4 is a type II transmembrane glycoprotein that comprises 766 amino acids, and is active as a homodimer[204]. DPP4 can mediate cell-cell and cell-matrix adhesion, therefore possessing roles in diverse cellular processes, particularly in the regulation of metabolism, immune function and cellular invasion[263]. Previous work on the role of DPP4 in ovarian cancer is limited, and some important factors discussed below have been overlooked. The ovarian TME *in vivo* is highly heteromorphic, with discrete regions undergoing chronic hypoxic stress at any time[95]. The main regulator of hypoxia, HIF-1α, is correlated with both the development of chemoresistance and decreased survival for ovarian cancer patients, suggesting that genes associated with the hypoxic response may contribute to overall prognosis[102,105]. DPP4

expression in some cell types is regulated in a hypoxia-dependent manner *in vitro* and *in vivo*[247,248,264]; however, the effects of hypoxia on DPP4 expression, activity and function have never been examined in ovarian cancer.

1.6 Hypothesis

DPP4 is an active determinant in the growth and metastasis of high-grade serous ovarian carcinomas and inhibition of DPP4 activity in ovarian tumours slows their progression and improves the anti-tumour immune response; thereby providing a rationale to potentially improve treatments via the use of an FDA approved DPP4 inhibitor.

1.7 Aims

1. To determine the role/s of DPP4 expression and activity in ovarian cancer cells *in vitro*.
2. To understand how inhibition of DPP4 activity influences metastatic tumour progression and anti-tumour immune responses *in vivo*.
3. To evaluate the potential synergistic action of DPP4 inhibition with immune checkpoint inhibitors as a novel therapy for ovarian cancer.

Chapter Two

Materials & Methods

2.1 Molecular biology

2.1.1 Plasmids

The pSIF-H1-Puro shRNA cloning and expression vector (#SI100C-1) was purchased from System Biosciences (CA, USA). shRNA template strands (see Appendix A for sequences) were purchased from Bioneer Pacific (Kew East, VIC, Australia).

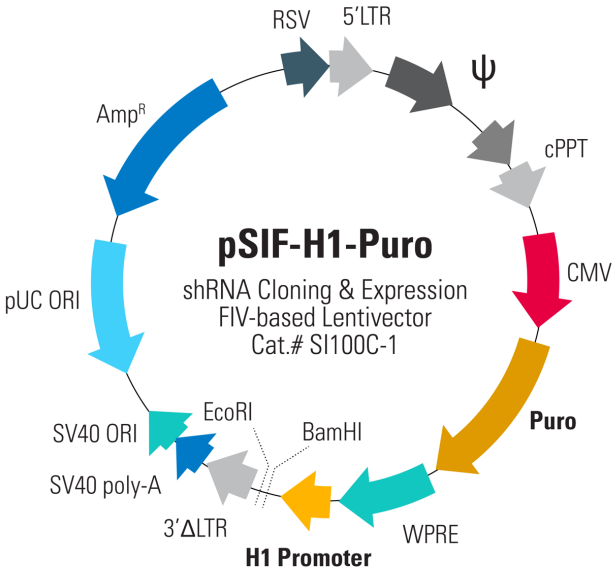

Figure 2.1. Schematic diagram representing the main features of the pSIF-H1-Puro shRNA cloning vector. *The pSIF-H1-Puro vector contains EcoRI and BamHI restriction enzyme sites for the directed insertion of a DNA sequence. The DNA insert is preceded by a 5` H1 promoter and contains a 3` ΔLTR. Ampicillin and puromycin resistance genes are present for antibiotic selection in bacterial and mammalian cells, respectively.*

2.1.2 Plasmid linearisation

Plasmids were linearised via restriction enzyme digest. For linearisation of the pSIF-H1-Puro vector, a restriction digest was prepared in a tube according to Table 2.1 and incubated overnight at 37°C.

Table 2.1. Reagents required for restriction enzyme digest of pSIF-H1-Puro vector.

	Volume (ul)
10X NEBuffer™ 3.1 (NEB #B7203S)	5
*Bam*HI (NEB #R0136S)	0.5
*Eco*RI (NEB #R0101S)	0.5
pSIF-H1-Puro	Volume for 2µg
ddH_2O	Up to 50µl
Total volume (µl)	**50**

2.1.3 Phosphorylation/annealing of oligonucleotides

To phosphorylate and anneal short hairpin RNA (shRNA) template oligonucleotides, a reaction was prepared in a tube according to Table 2.2. The reaction was incubated for 30 minutes at 37°C, and then for 2 minutes at 95°C. The reaction was allowed to cool to room temperature.

Table 2.2. Reagents required for phosphorylation/annealing of shRNA template oligonucleotides.

	Volume (µl)
Top strand shRNA template oligo (20µM)	1
Bottom strand shRNA template oligo (20µM)	1
10x T4 polynucleotide kinase buffer (NEB #B0201S)	2
ddH_2O	14
T4 polynucleotide kinase (NEB #M0201S)	2
Total volume (µl)	***20***

2.1.4 Ligation

To ligate double stranded oligos with the vector backbone, quick ligation reactions were prepared in tubes according to Table 2.3. The reactions were incubated for 15 minutes at room temperature.

Table 2.3. Reagents required for ligation of shRNA templates into the pSIF-H1-Puro vector.

	Volume (ul)
Linearised pSIF-H1-Puro vector	Volume for 50ng
Double stranded shRNA template (1uM)	0.5
2x T4 quick ligase reaction buffer (NEB #M2200S)	10
ddH_2O	Up to 20µl
T4 quick ligase (NEB #M2200S)	1
Total volume (µl)	***20***

2.1.5 Transformation of TOP10 Chemically Competent *E. coli* cells

To facilitate the uptake of plasmid DNA into bacterial cells, one tube of TOP10 Chemically Competent Escherichia coli (*E. coli)* cells for each transformation reaction was briefly thawed on ice. 10µl of ligation mixture (see Section 2.1.4) was added directly to the tube of competent cells. The tube was mixed by gently tapping and incubated on ice for 30 minutes. The cells were heat-shocked for 90 seconds in a 42°C water bath. The tube was then incubated on ice for 2 minutes. 250µl of 2YT media (see Appendix A) was aseptically transferred to the tube and the cells were incubated for 1 hour at 37°C in a shaking incubator set to 225RPM. 125µl of the cell suspension was aseptically transferred onto a pre-warmed 2YT agar plate supplemented with ampicillin 100µg/ml (see Appendix A) and spread across the entire plate. The plate was allowed to dry for 1-2 minutes before being inverted and incubated at 37°C for 16 hours.

2.1.6 Plasmid extraction

2.1.6.1 Mini prep

A single *E. coli* colony from a fresh cultured agar plate was picked and inoculated into 3ml of 2YT media supplemented with ampicillin 100µg/ml (see Appendix A) and incubated at 37°C for 16 hours (or overnight) with gentle agitation. The cells were collected by centrifugation at 8000RPM for 2 minutes and resuspended in 1ml of sterile water. 600µl of cell suspension was

transferred to a new microcentrifuge tube for plasmid extraction, and the remaining 400µl was used for glycerol stock preparation (see Section 2.1.7).

Extraction of plasmid DNA by mini prep was performed using the *AccuPrep*® Plasmid Mini Extraction Kit (Bioneer, #K-3030). The 600µl bacterial cell suspension (see above) was centrifuged at 8000RPM for 2 minutes and the supernatant was removed. The cell pellet was completely resuspended in 250µl of Buffer 1 (containing RNase A). Cells were lysed by the addition of 250µl of Buffer 2 and the tube was mixed by gentle inversion 4 times. 350µl of Buffer 3 was added to the lysate to neutralise the solution. The tube was mixed immediately by gentle inversion 4 times. The tube was centrifuged at 13,000RPM for 10 minutes at 4°C to pellet cellular debris. The cleared lysate was transferred to a DNA binding column assembled with a 2ml collection tube and centrifuged at 13,000RPM for 1 minute. The flow-through was discarded and the DNA binding column was re-assembled with the collection tube. To remove salts and soluble debris, 700µl of Buffer 4 (containing 80% ethanol (EtOH)) was added to the DNA binding column and centrifuged at 13,000RPM for 1 minute. The flow-through was discarded and the DNA binding column re-assembled with the collection tube. Residual EtOH was removed by additional centrifugation of the DNA binding column at 13,000RPM for 1 minute. The DNA binding column was transferred to a new microcentrifuge tube and 50µl of pre-warmed (60°C) sterile water was added to the column and incubated at room temperature for 5 minutes. The plasmid DNA was eluted into the microcentrifuge tube by centrifugation at 13,000RPM for 1 minute. Plasmid DNA was quantified (see Section 2.2.5) and stored at -20°C.

2.1.6.2 Maxi prep

To generate a starter culture, a single *E. coli* colony from a fresh cultured agar plate was picked and inoculated into 3ml of 2YT media supplemented with ampicillin 100µg/ml and incubated at 37°C for 8 hours with gentle agitation. The entire starter culture was transferred to 200ml of 2YT media supplemented with ampicillin 100µg/ml and incubated at 37°C for 16

hours (overnight) with gentle agitation. The following day, 5ml of the cell culture was transferred to a 50ml tube and used for glycerol stock preparation (see Section 2.1.7).

Extraction of plasmid DNA by maxi prep was performed using the QIAGEN Plasmid Maxi Kit (Qiagen, #12165). The bacterial cell culture (see above) was transferred into a large plastic centrifuge bottle (Beckman Coulter, IN, USA) and centrifuged at 6000RPM for 15 minutes at 4°C. The supernatant was discarded, and the cell pellet was resuspended in 8ml of Buffer P1. The cell suspension was transferred to a plastic centrifuge tube (Beckman Coulter, IN, USA). Cells were lysed by the addition of 8ml of Buffer P2 and the tube was mixed by gentle inversion 6 times and incubated at room temperature for 5 minutes. 8ml of Buffer P3 was added to neutralise the lysate. The tube was mixed by gentle inversion 6 times and incubated on ice for 20 minutes. Samples were centrifuged at 15,000 x g for 20 minutes at 4°C to pellet cellular debris. The cleared lysate was filtered into a 50ml tube using filter paper and a funnel to remove any excess debris. A QIAGEN tip was assembled with a new 50ml tube and equilibrated by adding 8ml of Buffer QBT, allowing the flow-through to empty into the tube by gravity flow. The filtered lysate was applied to the equilibrated QIAGEN tip and allowed to empty into the 50ml tube by gravity flow. The QIAGEN tip was washed twice with 10ml of Buffer QC, allowing the flow-through to enter the tube by gravity flow. The tube was emptied at appropriate intervals to ensure the tip was never covered with resin. The QIAGEN tip was assembled with a new 50ml tube and the DNA was eluted by adding 5ml of Buffer QF and allowing the flow-through to empty into the tube by gravity flow. To precipitate the DNA, 3.5ml of isopropanol (Sigma, #190764) was added to the 5ml of eluted DNA. 1.1ml of the precipitated DNA solution was aliquoted into 8 new microcentrifuge tubes. The tubes were centrifuged at 15,000 x g for 30 minutes at 4°C. The supernatant was discarded and 300µl of 70% EtOH was added to each tube to wash the DNA pellet. The tubes were centrifuged at 15,000 x g for 10 minutes at 4°C. The supernatant was carefully discarded, and the tubes were inverted on paper towel for 20 minutes to air dry the pellet. The samples were pooled by resuspending all

DNA pellets in a total volume of 200µl of sterile water. Plasmid DNA was quantified (see Section 2.2.5) and stored at -20°C

2.1.7 Preparation of glycerol stocks

The bacterial culture to be used to prepare the glycerol stock was centrifuged at 5000RPM for 5 minutes to create a cell pellet. The supernatant was completely discarded, and the pellet was resuspended in 750µl of 2YT/50%glycerol solution (see Appendix A). The glycerol stock was aseptically transferred to a labelled cryovial and stored at -80C.

2.2 DNA analysis

2.2.1 Polymerase chain reaction

All primers used are listed in Appendix A. Lyophilised primers were reconstituted in ddH_2O to make a stock concentration of 100uM. The stock was diluted 1:2 in ddH_2O for use in polymerase chain reaction (PCR) experiments at 50µM. In general, each PCR was prepared in duplicate in 200µl strip tubes according to Table 2.4 and amplified according to the conditions in Table 2.5 using a ProFlex™ PCR System (Applied Biosystems, CA, USA).

Table 2.4. Reagents required in a standard PCR for primer amplification of DNA.

	Per reaction (µl)
Forward primer (50uM)	1
Reverse primer (50µM)	1
2X GoTaq® Green Master Mix (Promega, #M7123)	25
ddH_2O	18
Sample template cDNA (final amount 50ng)	5
Total	***50***

Table 2.5. Standard PCR cycling conditions.

Stage		***Temperature***	***Time***	***Cycles***
1	Initialisation	95°C	5 mins	1
	Denature	95°C	30 sec	
2	Anneal	55°C	30 sec	35
	Extend	72°C	30 sec	
3	Final elongation	72°C	10 mins	1

2.2.2 Gel electrophoresis

A 1% agarose gel was placed into a gel tank filled with 1x TAE buffer (see Appendix A) ensuring the surface of the gel was covered. Samples were prepared by combining 5µl of sample DNA, 2µl 6X DNA Loading Dye (Thermo Fisher, #R0611) and 5µl ddH2O in a tube. 5µl of GeneRuler DNA Ladder Mix (Thermo Fisher, #SM0333) was loaded into the first well of the gel and samples were loaded to subsequent wells. The gel was run at 90-100V for 1-2 hours depending on the size of the expected product. The gel was imaged using the FluorChem E imaging system (ProteinSimple, CA, USA) to identify DNA bands. If necessary, DNA bands were excised under UV light.

2.2.3 Colony PCR screening

Bacterial colonies arising from transformation of chemically competent *E. coli* cells (see Section 2.1.5) were screened for correct template integration into the pSIF-H1-Puro vector backbone by PCR using primers to amplify the inserted template. A master mix was prepared to screen each bacterial clone according to Table 2.6. Using aseptic technique, up to 10 well-separated colonies per plate were carefully picked using a pipette tip. The tip was placed in a tube containing the PCR master mix and gently swirled. DNA was amplified according to the conditions in Table 2.7 using a ProFlex™ PCR System (Applied Biosystems, CA, USA). Each PCR product was separated by gel electrophoresis (see Section 2.2.2) to confirm that the size of the insert was as expected. Positive clones were inoculated into 3ml of 2YT media supplemented with ampicillin 100µg/ml and cultured for plasmid DNA extraction by mini- or maxi-prep (see Section 2.1.6.1/2.1.6.2). The identity of the template insert was confirmed by sequence analysis (see Section 2.2.6) using the pSIF-H1-Puro ForwardF primer (see Appendix A).

Table 2.6. Reagents required in colony PCR screen for primer amplification of plasmid DNA.

	Per reaction (ul)
pSIF-H1-Puro ForwardF + ReverseF (10uM)	1
2X GoTaq® Green Master Mix (Promega, #M7123)	12.5
ddH_2O	11.5
DNA (from colonies)	-
Total volume (ul)	**25**

Table 2.7. Bacterial colony PCR screen cycling conditions.

Stage		***Temperature***	***Time***	***Cycles***
1	Initialisation	94°C	4 mins	1
2	Denature	94°C	30 sec	
	Anneal	60°C	30 sec	30
	Extend	72°C	30 sec	
3	Final elongation	72°C	7 mins	1

2.2.4 Gel purification

DNA bands excised from agarose gel were purified using the *AccuPrep*® Gel Purification Kit (Bioneer, #K-3035). Briefly, the gel slice was weighed, and 3 volumes of gel binding Buffer 1 were added to 1 volume of the gel slice (e.g., 300µl of Buffer 1 for 100µg of gel slice). The gel mixture was incubated on a heat block at 60°C for 10 minutes and was vortexed every 2 minutes to allow for complete dissolving. The mixture was transferred to a DNA binding column assembled with a 2ml collection tube and centrifuged at 13,000RPM for 1 minute. The flow-through was discarded and the DNA binding column was reassembled with the collection tube. To remove salts and impurities, 500µl of Buffer 2 (containing 80% EtOH) was added to the DNA binding column and centrifuged at 13,000RPM for 1 minute. The flow-through was discarded and the wash step was repeated. Residual EtOH was removed by additional centrifugation at 13,000RPM for 1 minute. The DNA binding column was transferred to a new microcentrifuge tube and 30µl of pre-warmed (60°C) sterile water was added to the column

and incubated at room temperature for 5 minutes. The DNA was eluted by centrifugation at 13,000RPM for 1 minute. DNA was quantified (see Section 2.2.5) and stored at -20°C.

2.2.5 Nucleic acid quantification

DNA and RNA were quantified and assessed for purity using the NanoDrop™ 2000 spectrophotometer (Thermo Scientific, DE, USA).

2.2.6 DNA sequencing

DNA samples were prepared for Sanger Sequencing according to Table 2.8**.** Samples were sequenced by the Monash Health Translational Precinct (MHTP) Medical Genomics Facility.

Table 2.8. Preparation of DNA sequencing reactions.

Template	***Quantity***
Primer	3.2pmol
DNA:	
- Plasmid	300ng
- PCR product	10ng
ddH_2O	To 16µl

2.3 *In vitro* methods

All methods in this section were performed aseptically in a Euroclone Safemate Class II Biological Safety Cabinet.

2.3.1 Cell culture and passaging

The ovarian cancer cell lines: murine ID8 (RRID:CVCL_IU14) was a kind gift from Dr. Kathy Roby (University of Kansas Medical Center, USA)[265]; human OVCAR4 (RRID:CVCL_1627) was a kind gift from Professor David Bowtell (Peter MacCallum Cancer Centre, Melbourne, Australia); and human SKOV3 (RRID:CVCL_0532) and CaOV3 (RRID:CVCL_0201) were purchased from the American Type Culture Collection (ATCC). All cell lines were authenticated using STR profiling within the last three years. ID8 cells were cultured in Dulbecco's modified Eagle's medium (DMEM) (High glucose; Sigma-Aldrich, #D5796) supplemented with 4% heat-inactivated fetal bovine serum (HI-FBS – see Appendix A; Thermo Fisher, #16000044), 1% penicillin/streptomycin (P/S) (Thermo Fisher, #15240062) and 1x Insulin-transferrin-selenium (ITS) selenite media supplement (see Appendix A; Sigma-Aldrich, #I3146). OVCAR4 cells were cultured in RPMI-1640 (with sodium bicarbonate; Sigma-Aldrich, #R0883), supplemented with 10% FBS and 1% P/S. SKOV3 cells were cultured in DMEM/Nutrient Mix F-12 (Thermo Fisher, #11320082) supplemented with 10% FBS and 1% P/S. CaOV3 cells were cultured in DMEM (High glucose; Sigma, #D5796), supplemented with 10% FBS and 1% P/S. All cell lines were routinely incubated at 37°C and 5% CO_2. Cells reaching 80% confluence were washed once with Dulbecco's Phosphate Buffered Saline (PBS) (Sigma-Aldrich, #D8537) and then once with 2x Trypsin-EDTA (TE) (Thermo Fisher, #1540054). Cells were trypsinised by the addition of an appropriate amount of 2x TE to cover the surface of the flask. Cells were incubated at 37°C and 5% CO_2 for up to 5 minutes or until cells were detached. Using a sterile pipette, the trypsin was neutralised using an equal or greater volume of fresh, complete growth medium. Cells were centrifuged at 1000RPM for 5 minutes to obtain a pellet and the supernatant was discarded. For routine passaging, cells

were resuspended in complete growth medium and transferred into sterile culture flasks at an appropriate dilution factor with fresh medium added.

2.3.2 Cell counts

To obtain a cell count, 10µl of cell suspension was combined with 10µl of Trypan Blue Solution (0.4%) (Thermo Fisher, #15250061). 10µl of the diluted sample was pipetted into a Countess® Cell Counting Chamber Slide (Thermo Fisher, #C10228) and total cell amounts including viability were determined using a Countess™ II FL Automated Cell Counter (Thermo Fisher, CA, USA).

2.3.3 Freezing and recovering cell stocks

Cells to be stored as stocks were trypsinised and pelleted as per Section 2.3.1. Cells were gently resuspended in 1ml of FBS containing 10% dimethyl sulphoxide (DMSO) (Sigma-Aldrich, #D2650), transferred into a cryogen vial and frozen at -80°C. To recover frozen cell stocks, the cryogen vial was thawed in a 37°C water bath and transferred into a falcon tube containing 9ml of fresh complete growth medium. The cell suspension was centrifuged at 1000RPM for 5 minutes to form a pellet. The supernatant was discarded to remove all traces of DMSO, and cells were resuspended in fresh complete growth media. The entire volume of cell suspension was transferred into a sterile flask and incubated at 37°C and 5% CO_2 for at least 7 days to allow for recovery of the cells.

2.3.4 Hypoxic incubation

Cells were counted as per Section 2.3.2 and seeded at a density indicated in figure legends into an appropriate culture dish with complete media and allowed to adhere for at least 6 hours. Following cell adhesion, the complete media was replaced with media supplemented with 150µM $CoCl_2$ (Sigma-Aldrich, #232696-5G). Cells were incubated in the Biospherix hypoxia suite at 37°C, 2% O_2 and 5% CO_2 for the desired experimental duration.

2.3.5 Cell viability

To measure viability of cultured cells, AlamarBlue® Cell Viability Reagent (Thermo Fisher, #DAL1100) was added to the wells of a 96-well plate at a final concentration of 10% (10µl in 100µl). The plate was incubated for at least 6 hours (or overnight) and the fluorescence with excitation wavelength 530-560nm and emission wavelength 590nm was measured by a FLUOstar® Omega microplate reader (BMG Labtech, Victoria, Australia).

2.3.6 Stable transfection

OVCAR4 cells were seeded in 6-well plates at a density of 1.5 x 10^5 cells/well to achieve an overnight confluency of ~80%. Transfection reagents were prepared in two separate tubes. Solution one contained 3ug of plasmid DNA and was made up to 100µl with serum free media (SFM). Solution two contained 10µl of Lipofectamine® 2000 Transfection Reagent (Invitrogen, #11668019) and 90µl of SFM per transfection reaction. Solutions one and two were combined and incubated at room temperature for 45 minutes. 800µl of SFM was added to the transfection mixture and was mixed gently by pipetting. Culture media was removed, and cells were washed twice with SFM to remove all traces of FBS. The 1ml final transfection solution was added to each well and cells were incubated at 37°C with 5% CO_2 for 8 hours. Following the incubation period, the transfection media was removed, cells were washed twice with SFM to remove all traces of lipofectamine and growth medium was replaced with complete media. Cells were allowed to recover for 24 hours. Cells were harvested and seeded into new wells and positive transfectants were selected using 1µg/ml puromycin (Sigma, #P8833) and allowed to grow for approximately two weeks to achieve stable gene expression.

2.4 RNA analysis

2.4.1 shRNA design

To inhibit human *MMP10 and MMP13* expression *in vitro*, fold-back stem-loop shRNA structures were designed for cloning into the pSIF-H1-Puro vector according to manufacturer's guidelines (System Biosciences, CA, USA). Briefly, inhibitory stem-loops comprised a 21-bp sense strand (obtained from the Sigma MISSION® shRNA database) identical to the coding region of the target gene, a 12-bp loop (CTTCCTGTCAGA) and a 21-bp antisense strand followed by an RNA polymerase III terminator sequence (TTTTT). Restriction sites for *Bam*HI and *Eco*RI were incorporated at the 5′ and 3′ end of the shRNA, respectively, for cloning into the pSIF-H1-Puro vector. shRNA sequences are listed in Appendix A. The following primers were designed to flank the shRNA target region to screen for successful knockdown of the target gene; *MMP10* F: 5′-CACAGTTTGGCTCATGCCTA-3′, *MMP10* R: 5′-TGCCATTCACATCATCTTGC-3′; *MMP13* F: 5′-TTGAGCTGGACTCATTGTCG-3′, MMP13 R: 5′-CTCAGTCATGGAGCTTGCTG-3′.

2.4.2 Real-time PCR primer design

Quantitative Real time PCR using the absolute method was completed as previously published by our laboratory[266]. Briefly, to design primers the gene of interest was searched in the National Centre for Biotechnology Information (NCBI) database (http://www.ncbi.nlm.nih.gov/gene). The Reference Sequence was selected from the UCSC Genome browser (https://genome.ucsc.edu/). The complete sequence was obtained, and intron/exon boundaries were identified. The sequence was copied to Primer3 (http://biotools.umassmed.edu/bioapps/primer3) and primers were designed to surround intron boundaries, to create a product of approximately 100 base pairs and a T_m range 60-64°C. Primer pairs were copied into the Blast function of the NCBI website to check for specificity. The sequence alignment was checked to ensure it matched the gene of interest

and did not share significant coverage with other targets. Primers were purchased from Bioneer Pacific and are listed in Appendix A.

2.4.3 RNA extraction

To harvest cells for RNA extraction from a T25cm^2 flask, cell culture media was removed and 1ml of TRIzol™ Reagent (Invitrogen, #15596026) was directly added to homogenise cells. Cells were scraped from the surface of the flask, transferred into a microcentrifuge tube and incubated on ice for 5 minutes to allow dissociation of nucleoprotein complexes. To extract RNA, 200µl of chloroform (Sigma, #1024452500) was added to the tube and vortexed briefly. Samples were incubated at room temperature for 5 minutes and then centrifuged at 12,000 x g for 15 minutes at 4°C. The upper, aqueous phase separated during centrifugation was transferred into a fresh microcentrifuge tube. RNA was precipitated from the aqueous phase by adding 500µl isopropanol (Sigma, #190764). Tubes were vortexed and incubated on ice for 15 minutes. Samples were centrifuged at 12,000 x g for 10 minutes at 4°C and the supernatant was carefully removed. The RNA pellet was washed by adding 1ml of 75% EtOH and tapping the tube to dislodge the pellet. Samples were centrifuged at 8000 x g for 5 minutes at 4°C. The supernatant was carefully removed, and the 75% ethanol wash was repeated with 500µl. The supernatant was completely removed using a pipette and the tube was inverted onto paper towel to air dry the pellet for 10 minutes at room temperature. The RNA pellet was resuspended in 30µl of sterile water and total RNA was quantified (see Section 2.2.5).

2.4.4 cDNA synthesis

cDNA was synthesised from total RNA using the Tetro cDNA Synthesis Kit (Bioline, #BIO-65043). Briefly, for each RNA sample, a priming premix was prepared in a microcentrifuge tube on ice according to Table 2.9. The reverse transcriptase enzyme was added last, and the reaction was mixed gently by pipetting. Samples were incubated at 45°C for 30 minutes,

followed by incubation at 85°C for 5 minutes to terminate the reaction. Samples were chilled on ice and cDNA was quantified (see Section 2.2.5) and stored at -20°C.

Table 2.9. Reaction components required for cDNA synthesis from total RNA.

	Per reaction (µl)
RNA	Volume for 1µg
Oligo $(dT)_{18}$ primer mix	1
10mM dNTP mix	1
5x RT buffer	4
Tetro Reverse Transcriptase (200u/µl)	1
ddH_2O	Up to 20µl
Total volume (µl)	***20***

2.4.5 Real-time quantitative PCR

PCR standards for each target gene were prepared via dilution of a 100pg/µl stock to create a series of standards at appropriate working concentrations (see Appendix A). For each target, a master mix was prepared for DNA standards and samples according to Table 2.10.

Table 2.10. Master mix preparation for real-time PCR reactions.

Master mix	***Volume per reaction (µl)***	
	1µl template	**4µl template**
Power SYBR® Green (ThermoFisher, #4367659)	5	5
Forward Primer (50µM)	0.2	0.2
Reverse Primer (50µM)	0.2	0.2
ddH_2O	3.6	0.6
Total volume (µl)	***9***	***6***

A range of 5 standards was chosen for each target gene depending on the expected level of gene expression. For low levels of expression, 1µl of standard DNA was added to 9µl of master mix. For high levels of expression, 4µl of standard DNA was added to 6µl of master mix. cDNA samples were diluted 1:20 in ddH_2O and 4µl of each sample was added to 6µl of

master mix. All reactions were performed in triplicate wells of a MicroAmp® Optical 384-Well Reaction Plate (Applied Biosystems, #4343814). Real-time quantitative PCR (qPCR) was performed using the QuantStudio™ 6 Flex Real-Time PCR System (Applied Biosystems, CA, USA) as per the cycling conditions in Table 2.11.

Table 2.11. Real-time PCR cycling conditions.

Stage		*Temperature*	*Time*	*Cycles*
1	Enzyme Activation (denaturation)	95 °C	10 mins	1
2	Denature Anneal/Extend	95 °C 60 °C	15 sec 60 sec	40
3	Melt Curve/Dissociation	95 °C 60 °C 95 °C 60 °C	10 sec 60 sec 15 sec 15 sec	1

2.4.6 Absolute quantification of gene expression

The raw data generated from qPCR was analysed using the QuantStudio™ 6 Flex Real-Time PCR System software (version 1.3, Applied Biosystems, CA, USA). The software calculated unknown sample values through interpolation from the standard curve using the absolute ΔCT (cycle threshold) method. The determined sample value was normalised to the corresponding ribosomal 18S value (averaged over three replicates).

2.5 Protein analysis

2.5.1 Protein extraction

To collect cells for protein extraction from a T25cm^2 flask, cell culture media was removed, and cells were washed twice with cold PBS. 1ml of cold RIPA lysis buffer (see Appendix A) was added to the flask and kept on ice for 5 minutes to allow lysis of cells. Cells were scraped from the surface of the flask and collected into a microcentrifuge tube. Samples were centrifuged at 14,000 x g for 15 minutes at 4°C to pellet the cell debris. The supernatant containing the protein lysate was transferred to a fresh tube for further analysis.

2.5.2 Protein estimation by BCA assay

Protein concentration was estimated using the Pierce™ BCA Protein Assay Kit (Thermo Scientific, #23225). A 1mg/ml bovine serum albumin (BSA) solution was prepared by diluting the 2mg/ml BSA stock solution 1:2 in ddH_2O. Protein standards were then prepared according to Table 2.12**.** Protein samples were diluted 1:50 and 1:100 in ddH_2O. The BCA solution was prepared by adding 1-part reagent B to 50 parts reagent A. 10µl of each standard and 10µl of each diluted sample were added in triplicate to wells of a 96 well plate. 200µl of BCA solution was added to each well and the plate was incubated at 37°C for 1 hour. Absorbance in each well was measured at 595nm using a FLUOstar® Omega microplate reader (BMG Labtech, Victoria, Australia). A standard curve was generated to determine concentration of the protein samples**.**

Table 2.12. Working concentrations for protein standards for the BCA assay.

Standard #	Volume 1mg/ml BSA (µl)	Volume ddH_2O (µl)	Final BSA concentration (µg/ml)
1	0	500	0
2	5	495	10
3	10	490	20
4	25	475	50
5	50	450	100
6	75	425	150
7	100	400	200
8	125	375	250

2.5.3 DPP4 enzyme activity assays

2.5.3.1 DPP4 activity in cell lysate

DPP4 enzymatic activity in cell lysates was measured using a colorimetric assay as previously described[267]. Briefly, samples were prepared by diluting 5µg total protein up to 50µl in assay buffer. Recombinant DPP4 (Abcam, #79138) was used as a positive control for DPP4 activity, and recombinant DPP4 + 1µM sitagliptin (see Appendix A) was used as a negative control for DPP4 activity inhibition. 50µl of each sample and controls were added in triplicate to wells of a clear 96-well microplate (Interpath, #655101). 50µl of the DPP4 substrate H-Gly-Pro-pNA (Sigma, #G0513) (see Appendix A) was added to each well. Substrate hydrolysis was measured by reading absorbance at 405nm and 570nm every 10 minutes for 3 hours using a Cytation™ 3 Multi-Mode Reader (BioTek, VT, USA) at 37°C. Absorbance readings at 570nm were subtracted from readings at 405nm to account for the optical interference from cell culture media.

2.5.3.2 DPP4 activity in cell culture supernatant

DPP4 enzymatic activity in cell culture supernatant samples was measured using a fluorometric assay as previously described[207]. Briefly, cell culture supernatant samples were concentrated by centrifugation at 4000RPM for 15 minutes at 4°C using a 10kDa filter spin column (Sigma, #Z722065). The recovered protein concentrate made up to 50µl in assay buffer. Recombinant DPP4 (Abcam, #79659) was used as a positive control for DPP4 activity, and recombinant DPP4 + 1µM sitagliptin (see Appendix A) was used as a negative control for DPP4 activity. A 'gain well' was set up by incubating 50µl of positive control and 50µl of DPP4 substrate H-Gly-Pro-AMC (Sigma, #G2761) (see Appendix A) in one well of a black 96-well microplate (Interpath, #655090) at 37°C for 1 hour. 50µl of each sample and controls were then added in triplicate to the appropriate wells and 50µl of H-Gly-Pro-AMC was added to each well**.** The gain was set using the 'gain well' and substrate hydrolysis was measured by reading fluorescence at 355_{ex}/450_{em} every 2 minutes for 3 hours using a Cytation™ 3 Multi-Mode Reader (BioTek, VT, USA) at 37°C.

2.5.4 Enzyme-linked immunosorbent assays (ELISAs)

2.5.4.1 DPP4 ELISA

DPP4 protein concentration in cell culture media and whole cell lysate was determined using a Human CD26 (DPP4) ELISA kit (Abcam, #ab119513) according to the manufacturer's protocol. Briefly, all reagents were prepared to 1x concentration and a series of DPP4 protein standards were prepared according to Table 2.13. Cell culture supernatant samples were concentrated by centrifugation at 4000RPM for 15 minutes at 4°C using a 10kDa filter spin column (Sigma, #Z722065). The recovered protein concentrate was diluted 1:5 in sample diluent. Whole cell protein samples were prepared by combining 10µg of total protein with sample diluent up to 100µl.

Table 2.13. Preparation of DPP4 protein standards.

Standard #	*Sample to dilute*	*Volume to dilute (µl)*	*Volume of sample diluent (µl)*	*Final DPP4 concentration (ng/ml)*
1	Stock	-	-	500
2	Standard 1	225	255	250
3	Standard 2	225	225	125
4	Standard 3	225	225	62.5
5	Standard 4	225	225	31.3
6	Standard 5	225	225	15.6
7	None (blank)	-	225	0

Wells of the coated ELISA plate were carefully washed twice with 400µl of wash buffer and the plate was gently tapped on paper towel to remove excess wash buffer after the last wash. 100µl of prepared standards and samples were added in duplicate to appropriate wells. 50µl of biotin-conjugate was added to all wells. The plate was covered with an adhesive film and incubated on a plate shaker at 400RPM for 3 hours at room temperature. The plate contents were emptied, and all wells were washed 4 times with 400µl of wash buffer as above. 100µl of streptavidin-HRP was immediately added to all wells. The plate was covered with an adhesive film and incubated on a plate shaker at 400RPM for 1 hour at room temperature. The plate contents were emptied, and all wells were washed 4 times with 400µl of wash buffer as above. 100µl of TMB substrate solution was added to all wells. The plate was incubated on a plate shaker at 400RPM for 15 minutes at room temperature protected from light. The reaction was stopped by adding 100µl of stop solution quickly and uniformly to each well. Absorbance was measured at 450nm using the FLUOstar® Omega microplate reader (BMG Labtech, Victoria, Australia). A standard curve was generated to determine sample concentrations of DPP4.

2.5.4.2 HIF-1α ELISA

HIF-1α protein concentration in whole cell lysate was determined using a HIF1a Human SimpleStep ELISA® Kit (Abcam, #ab171577) according to the manufacturer's protocol.

Briefly, all reagents were prepared to 1x concentration and a series of HIF-1α protein standards were prepared according to Table 2.14. Samples were prepared by combining 5µg of total protein with cell extraction buffer PTR up to 50µl.

Table 2.14. Preparation of HIF-1α protein standards.

Standard #	*Sample to dilute*	*Volume to dilute (µl)*	*Volume of extraction buffer PTR (µl)*	*Final HIF-1α concentration (ng/ml)*
1	Stock	300	200	15
2	Standard 1	150	150	7.5
3	Standard 2	150	150	3.75
4	Standard 3	150	150	1.88
5	Standard 4	150	150	0.94
6	Standard 5	150	150	0.47
7	Standard 6	150	150	0.23
8	None (blank)	-	150	0

50µl of all prepared standards and samples were added in duplicate to appropriate wells of the coated ELISA plate. 50µl of the antibody cocktail was added to each well and the plate was covered with an adhesive film and incubated on a plate shaker at 400RPM for 1 hour at room temperature. The plate contents were emptied, and each well was washed 3 times with 350µl of wash buffer PT. The plate was gently tapped on paper towel to remove excess wash buffer after the last wash. 100µl of TMB substrate was added to each well and the plate was covered with an adhesive film and incubated at 400RPM for 10 minutes at room temperature protected from light. The reaction was stopped by adding 100µl of stop solution quickly and uniformly to each well. The plate was shaken on a plate shaker for 1 minute to mix the well contents. Absorbance was measured at 450nm using the FLUOstar® Omega microplate reader (BMG Labtech, Victoria, Australia). A standard curve was generated to determine sample concentrations of HIF-1α.

2.5.5 Protease arrays

Quantitative measurement of 40 unique proteases in cell lysates and cell culture media was performed using the following antibody arrays: Human MMP antibody array (Abcam, #ab197453); and Proteome Profiler™ Array (R&D Systems, #ARY021) as per the manufacturer's instructions. Proteins analysed are listed in Appendix A.

2.5.5.1 MMP array

The Human MMP antibody array (Abcam, #ab197453) was used for analysis of 10 MMP-targets. All reagents were prepared to 1x concentration and a standard dilution series containing all analytes was prepared according to Table 2.15. Standard values of each analyte are listed in Appendix A. Cell culture supernatant samples were concentrated by centrifugation at 4000RPM for 15 minutes at 4°C using a 10kDa filter spin column (Sigma, #Z722065). The recovered protein concentrate was made up to 100µl in sample diluent. Whole cell protein samples were prepared by combining 50µg of total protein with sample diluent up to 100µl.

Table 2.15. Preparation of MMP array standards.

Standard #	*Sample to dilute*	*Volume to dilute (µl)*	*Volume of sample diluent (µl)*
1	Stock	-	-
2	Standard 1	100	200
3	Standard 2	100	200
4	Standard 3	100	200
5	Standard 4	100	200
6	Standard 5	100	200
7	Standard 6	100	200
8	None (blank)	-	100

100µl of sample diluent was added to each well of the array chamber and incubated at room temperature for 30 minutes to block slides. Buffer was removed and 100µl of each standard and samples was added to the appropriate wells. The array was incubated overnight at 4°C.

Samples were removed and each well was washed 5 times for 5 minutes each with 150µl of wash buffer I at room temperature with gentle shaking. Buffer was removed and each well was washed twice with 150µl of wash buffer II as above. The array chamber was gently tapped on paper towel to remove excess wash buffer between each wash step. 80µl of detection antibody cocktail was added to each well and the array was incubated for 2 hours at room temperature with gentle shaking. Samples were removed and each well was washed 5 times with 150µl of wash buffer I and twice with 150µl of wash buffer II as above. 80µl of Cy3 equivalent dye-conjugated streptavidin was added to each well and the array was incubated for 1 hour at room temperature protected from light. Samples were removed and each well was washed 5 times with 150µl of wash buffer I as above. The slide was removed from the incubation device and carefully placed in the slide washer/dryer tube. 30ml of wash buffer I was added to cover the entire slide and the tube was incubated for 15 minutes at room temperature with gentle shaking. The buffer was removed, 30ml of wash buffer II was added and the tube was incubated for 5 minutes at room temperature with gentle shaking. The array slide was dried by centrifuging the slide washer/dryer tube at 1000RPM for 3 minutes without the cap. The array was visualised using a Typhoon 9410 Variable Mode Imager (GE Healthcare, CA, USA) equipped with a Cy3 wavelength filter. Signal intensities were determined using ImageJ v1.4 software (National Institute of Health, MD, USA)[268] and standard curves were generated for each analyte to determine sample concentrations.

2.5.5.2 Proteome profiler array

The Proteome Profiler™ Array (R&D Systems, #ARY021) was used for analysis of 34 protease targets. All reagents were prepared to 1x concentration. Cell culture supernatant samples were concentrated by centrifugation at 4000RPM for 15 minutes at 4°C using a 10kDa filter spin column (Sigma, #Z722065). The recovered protein concentrate was made up to 1.5ml with array buffer 6. Whole cell protein samples were prepared by combining 200µg of total protein with array buffer 6 up to 1.5ml.

2ml of array buffer 6 was added to wells of the 4-well multi-dish. Each of the 4 membranes were placed in a separate well of the multi-dish. The membranes were blocked in array buffer 6 for 1 hour at room temperature with gentle shaking. 15µl of detection antibody cocktail was added to each sample and incubated at room temperature for 1 hour. Buffer was aspirated from each well of the multi-dish and the sample/antibody mixture was added. The membranes were incubated overnight at 4°C with gentle shaking. Membranes were placed in separate wash containers and washed 3 times with 20ml wash buffer for 10 minutes at room temperature with gentle shaking. 2ml of streptavidin-HRP was added to each well of the multi-dish. Membranes were placed in the multi-dish and incubated for 30 minutes at room temperature with gentle shaking. Membranes were washed 3 times with 20ml wash buffer as above. Membranes were removed from wash buffer, placed on a plastic sheet protector and incubated with 1ml of Chemi reagent for 1 minute. The reagent mix was removed by gently blotting each membrane with an absorbent wipe. The membranes were visualised using the ChemiDoc™ XRS+ System **(**Bio-Rad Laboratories, CA, USA) to detect chemiluminescence. Signal intensities were determined using ImageJ v1.4 software (National Institute of Health, MD, USA)[268] and replicate values were individually normalised against a reference array to determine relative sample expression of each analyte.

2.5.6 Chemokine assay

Detection and quantification of 31 different chemokines (listed in Appendix A) in mouse serum was performed using the Bio-Plex Pro™ Mouse Chemokine Panel, 31-plex (Bio-Rad, #12009159), according to the manufacturer's protocol. Briefly, all reagents were prepared to 1x concentration and a standard fourfold dilution series containing all analytes was prepared according to Table 2.16. Lot-specific standard values of each analyte are listed in Appendix A. Samples were prepared by diluting mouse serum 1:5 in sample diluent.

Table 2.16. Preparation of standard series for 31-plex chemokine assay.

Standard #	*Sample to dilute*	*Volume to dilute (µl)*	*Volume of standard diluent (µl)*
1	Stock	250	
2	Standard 1	50	150
3	Standard 2	50	150
4	Standard 3	50	150
5	Standard 4	50	150
6	Standard 5	50	150
7	Standard 6	50	150
8	None (blank)	-	150

50µl of the coupled magnetic beads were added to each well of the assay plate. The plate was washed twice with 100µl of wash buffer using the Bio-Plex Pro™ Wash Station (Bio-Rad Laboratories, CA, USA); MAG x2 program. 50µl of all standards, controls and samples were added in duplicate to appropriate wells of the plate. The plate was covered with sealing tape and incubated at 850RPM for 30 minutes at room temperature. The plate was washed 3 times as above using the MAG x3 program. 25µl of detection antibodies was added to each well and the plate was covered with sealing tape and incubated at 850RPM for 30 minutes at room temperature. The plate was washed 3 times as above using the MAG x3 program. 50µl of streptavidin-PE was added to each well and incubated at 850RPM for 10 minutes at room temperature. The plate was washed 3 times as above using the MAG x3 program. To resuspend the beads, 125µl of assay buffer was added to each well. The plate was covered with sealing tape and incubated at 850RPM for 5 minutes at room temperature. The plate was immediately read using the Bio-Plex® MAGPIX™ Multiplex Reader **(**Bio-Rad Laboratories, CA, USA)**.** Standard curves were generated for each analyte, and data was processed using the Bio-Plex Manager™ software to determine sample analyte concentrations.

2.6 Tissue staining

2.6.1 Immunofluorescence

Tissue micro arrays (TMAs) were constructed by the Victoria Cancer Biobank (Monash Health, VIC, Australia) from formalin fixed, paraffin embedded (FFPE) tissues. Each TMA block contained duplicate tumour tissue cores from the ID8 ovarian cancer mouse model as described in figure texts and was sectioned to produce TMA slides. Slides were baked in an oven at 60°C for 30 minutes and sections were dewaxed in xylene (2 min x 3). Slides were rehydrated by immersing in 100% ethanol (1 min x 3). Slides were then washed in dH_2O for 5 minutes and then in 1 x Dako EnVision FLEX Wash Buffer (Agilent, #K8007) for 5 minutes at room temperature. Antigen retrieval was performed by boiling slides in Dako PT link in 1 x Dako Target Retrieval Solution, (pH 6.1; Agilent, #S1699) for 30 minutes. Slides were cooled at room temperature and washed in 1 x Dako EnVision FLEX Wash Buffer for 5 minutes at room temperature. Blocking was performed using the Dako Protein Block, Serum Free (Agilent, #X0909) for 30 minutes at room temperature. Slides were washed in 1 x Dako EnVision FLEX Wash Buffer for 5 minutes at room temperature. Slides were incubated with the appropriate primary antibody (see Table 2.17) diluted in Dako Antibody Diluent (Agilent, #S0809) overnight at 4°C protected from light. Slides were washed in 1 x Dako EnVision FLEX Wash Buffer (10 min x 3). For indirect immunofluorescence, sections were incubated with secondary antibody diluted in Dako Antibody Diluent for 1 hour at room temperature protected from light. Following secondary antibody incubation, slides were washed in 1 x Dako EnVision FLEX Wash Buffer (10 min x 3). Sections were counterstained with DAPI solution for 15 minutes at room temperature and slides were washed in dH_2O for 5 minutes Coverslips were mounted into slides using Prolong Gold Antifade reagent (Invitrogen, #P36934) and allowed to dry overnight protected from light. Fluorescence images were captured using the VS120 Virtual Slide Microscope (Olympus Life Science, Tokyo, Japan). Immunofluorescence staining of TMAs and image capture was performed by Angela Vais, Senior Histology Officer at the

Monash Histology Platform (MHP), Monash Health Translational Precinct (MHTP) node (VIC, Australia)

Fluorescence images were then processed using the Olympus OlyVIA software v2.9.1. Fluorescence data were analysed by ImageJ v1.4 software (National Institute of Health, MD, USA)[268] by calculating the percentage area of CD3+, CD4+, CD8+ or PD-L1+ and colocalisation of CD8+CD69+, CD4+CXCR3+ or CD4+PD-1+ of total tissue area using a consistent binary threshold.

Table 2.17. Antibodies used for immunofluorescence staining of mouse tissue.

Antibody		*Clone*	*Host species*	*Isotype*	*Species reactivity*	*Conjugate*	*Concentration*	*Incubation conditions*	*Supplier*	*Catalogue number*
Primary	CD3 molecular complex	17A2	Rat	IgG2b, κ	Mouse	Alexa Fluor® 647	30µg/ml	4˚C overnight	BD Biosciences	557869
	CD4	4SM95	Rat	IgG1, κ	Mouse	eFluor® 660	10µg/ml	4˚C overnight	Invitrogen	50-9766-82
	CD8a	53-6-7	Rat	IgG2a, κ	Mouse	eFluor® 615	20µg/ml	4˚C overnight	Invitrogen	42-0081-82
	CD69	H1.2F3	Armenian Hamster	IgG	Mouse	Alexa Fluor® 488	30µg/ml	4˚C overnight	BioLegend	104516
	CXCR3		Rabbit	IgG	Human, mouse, rat	-	5µg/ml	4˚C overnight or 1h at 37˚C	GeneTex	GTX31566
	PD-1		Goat	IgG	Mouse	-	2µg/ml	4˚C overnight	R&D Systems	AF1021
	PD-L1		Goat	IgG	Mouse	-	20µg/ml	4˚C overnight	R&D Systems	AF1019
Secondary	Rabbit IgG		Goat	IgG		Alexa Fluor® 488	1.5ug/ml	1h at room temperature	Jackson ImmunoResearch	711-545-152
	Goat IgG		Donkey	IgG		Alexa Fluor® 488	1µg/ml	1h at room temperature	Abcam	ab150129

2.7 *In vivo* methods

2.7.1 Mice

Female 6-8-week-old C57BL/6J mice were purchased from the Animal Resources Centre (WA, Australia) and housed in the PC2 area of the RMIT Animal Facility (RAF) at RMIT University, Bundoora, Australia. All protocols involving the use of mice were approved by the RMIT Animal Ethics Committee (ethics approval #1926). All research activities including procedures, treatments and routine care of animals were in compliance with institutional guidelines and Australian regulations for the responsible conduct of research.

2.7.2 Monitoring

Mice were monitored in accordance with approved ethics conditions. Tumour bearing mice were monitored twice weekly for standard parameters including i) general appearance, both undisturbed and upon handling, ii) changes in food/water intake and iii) behaviour or other signs of distress. Weight and circumference were measured weekly.

2.7.3 Intraperitoneal injection

Mice were manually restrained using the scruffing technique, with their head tilted down at a 45° angle to expose the abdomen. The injection site was swabbed with 70% ethanol and a 29G needle (insulin syringe) with the bevel facing upwards was inserted into the lower right quadrant of the abdomen, avoiding the abdominal midline. No more than 200µl of volume was injected.

2.7.4 Implantation of ovarian cancer cells

For ID8 tumour inoculation, 5 x 10^6 viable ID8 cells were resuspended in 150µl sterile PBS and injected into the peritoneal cavity (see Section 2.7.3) of female C57BL/6J mice.

2.7.5 Sitagliptin administration

Two to three weeks following tumour inoculation, mice commenced daily oral sitagliptin treatment (DPP4 inhibition). Tablets of sitagliptin phosphate monohydrate 100mg (Januvia®, Merck Sharp & Dohme Corp., NJ, USA) were crushed, combined with SF-AIN-93M rodent diet (Specialty Feeds, WA, Australia) and fed to mice daily at a dose of 50mg/kg body weight/day until endpoint. DPP4 inhibition in serum was confirmed by DPP4 enzyme activity assay (see Section 2.5.3).

2.7.6 Monoclonal antibody administration

Two weeks following commencement of sitagliptin treatment, mice were administered monoclonal antibody (Table 2.18) once every 2 days, for a total of 5 injections per mouse. Antibodies were diluted to 10mg/kg in a maximum volume of 200µl sterile PBS and injected into the peritoneal cavity (see Section 2.7.3).

Table 2.18. Monoclonal antibodies administered to mice during in vivo experiments.

Antibody	*Clone*	*Supplier*	*Catalogue number*
InVivoPlus anti-mouse PD-1	29F.1A12	BioXCell	BP0273
InVivoPlus anti-mouse PD-L1	10F.9G2	BioXCell	BP0101
InVivoPlus rat IgG2a isotype control, anti-trinitrophenol	2A3	BioXCell	BP0089
InVivoPlus rat IgG2b isotype control, anti-keyhole limpet hemocyanin	LTF-2	BioXCell	BP0090

2.7.7 Euthanasia

At specific cull points, mice were humanely euthanised via CO_2 asphyxiation. Mice were placed in a sealed induction chamber which was subsequently filled with CO_2 at a 20% displacement rate. Mice were closely observed for complete cessation of respiration for at least 1 minute, and death was confirmed by lack of the pedal reflex and loss of the corneal reflex. A terminal cardiac bleed (see Section 2.8.1) was immediately performed following CO_2 euthanasia.

2.8 *Ex vivo* methods

2.8.1 Cardiac blood collection and processing

To collect cardiac blood from euthanised mice, a 25G needle was inserted through the thoracic cavity with the needle pointing in the dorsal position. Blood was drawn into a 1ml syringe, and half of the volume was ejected into an Eppendorf tube for serum (see Section 2.8.6), and the other half of the volume was ejected into a 50ml tube containing 100ul 0.1M EDTA (Sigma, #ED2SS) solution for leukocyte isolation. Blood collected for leukocyte isolation was processed to remove red blood cells. 5ml of 1 x ACK lysis buffer (see Appendix A) was added to the blood and incubated at room temperature for 5 minutes. mPBS (see Appendix A) was added up to 10ml to neutralise the lysis buffer, and the blood was centrifuged at 1400RPM for 4 minutes. The supernatant was carefully aspirated using a pipette and a second lysis was performed if red blood cells remained. The remaining cell pellet was resuspended in 1ml PBS/1%FBS, filtered through a 40µm cell strainer (Corning, #CLS431750) into a fresh tube and a cell count was performed (see Section 2.8.5).

2.8.2 Peritoneal wash collection and processing

To collect cells within the peritoneal cavity, the skin was gently retracted to expose the abdominal wall and 3ml of mPBS/1%FBS was injected directly into the peritoneal cavity using a 21G needle. Wash contents was aspirated and collected into a 50ml tube. The wash contents were centrifuged at 1400RPM for 4 minutes and the supernatant was removed using a pipette. If red blood cells were present, a lysis was performed in the same manner described above (see Section 2.8.1). The remaining cell pellet was resuspended in 500µl of mPBS/1%FBS, filtered through a 40µm cell strainer into a fresh tube and a cell count was performed (see Section 2.8.1).

2.8.3 Organ collection

A medial incision was made through the abdominal wall of the mouse, followed by additional lateral incisions to expose the organs within the peritoneal cavity. The spleen was resected and placed in a 10ml tube containing 3ml mPBS/2%FBS for immediate processing (see Section 2.8.4). Both ovaries, fallopian tubes and uterus were carefully removed in their entirety. The cavity was explored for evidence of macroscopic tumours, and organs/tissue containing tumours were dissected; most commonly the small intestine, omentum, liver and sections of the peritoneal wall. All organs collected post-mortem except the spleen were placed in histological cassettes (Thermo Scientific, #1001058) and fixed in 10% neutral buffered formalin (Sigma, #HT501320) at room temperature for up to 30 days, after which they were transferred to 70% EtOH and stored at 4°C until further processing.

2.8.4 Spleen processing

A sterile 100µm cell strainer (Corning, #CLS431752) was placed in a small petri dish and the tube containing the spleen tissue in mPBS/2%FBS was emptied into the strainer. A sterile 3ml syringe was removed from the packet and the flat end was used to gently homogenise the tissue through the strainer. Excess cells were washed off from the syringe end into the strainer using 1ml mPBS/2%FBS. Homogenised cells were gently resuspended in the petri dish using a pipette, and the cell suspension was transferred back into the same 10ml tube used for tissue collection. The same cell strainer was used for each group of mice and was rinsed with mPBS between each use to remove any large tissue. The cell suspension was centrifuged at 1400RPM for 4 minutes to pellet all spleen cells. To lyse red blood cells, 3ml of 1x ACK lysis buffer was added to the cell pellet and incubated at room temperature for 5 minutes. The buffer was neutralised by adding mPBS up to 10ml. The solution was centrifuged at 1400RPM for 4 minutes and the supernatant was carefully removed. The remaining cell pellet was resuspended in 2ml mPBS/1%FBS**,** filtered through a 40µm cell strainer into a new tube and a cell count was performed (see Section 2.8.5).

2.8.5 Cell count of processed organs

Cells isolated from blood, peritoneal wash and spleen (described above) were diluted 1:1000 by adding 10µl of cell suspension to 10ml mPBS in an Accuvette Cup (#A35473, Beckman Coulter, CA, USA). Cell counts were performed using a Z-Series Particle Counter Cell Analyser (Beckman Coulter, CA, USA), with the instrument background count < 200 and the aperture flushed three times in between cell types.

2.8.6 Serum preparation

Blood collected for serum was kept at room temperature in the dark for 45 minutes – 1 hour. Blood was then centrifuged at 14,800RPM for 20 minutes to separate the serum as the top layer. Serum was carefully transferred to a new tube using a pipette and stored at -20°C until required for analysis.

2.9 Flow cytometry

2.9.1 Preparation of compensation beads

Fluorescently conjugated antibody compensation beads were prepared using the AbC™ Total Antibody Compensation Bead Kit (ThermoFisher Scientific, #A10497 and #A10513). Components A and B were vortexed for approximately 10 seconds. A 5ml round bottom polystyrene tube (Falcon, #352235) was labelled for each antibody. One drop of component A was added to each tube. A pre-titrated amount of each mouse antibody was added to the appropriate tube and vortexed briefly. Tubes were incubated for 15 minutes at room temperature protected from light. 3ml of mPBS was added to each tube and centrifuged for 5 minutes at 300 x g. The supernatant was carefully removed, and the bead pellet was resuspended in 500µl of mPBS. One drop of component B was added to each tube and vortexed briefly. LIVE/DEAD viability dye compensation beads were prepared using the ArC™ Amine Reactive Compensation Bead Kit (ThermoFisher Scientific, #A10346 and #A10628). One drop of component A was added to a labelled 5ml polystyrene round bottom tube and incubated at room temperature for 15 minutes. 3µl of LIVE/DEAD™ Fixable Blue Dead Cell Stain (Invitrogen, #L23105) was added directly to the tube and incubated for 30 minutes at room temperature protected from light. 3ml of mPBS was added to the tube and centrifuged for 5 minutes at 300 x g. The supernatant was carefully removed, and the bead pellet was resuspended in 500µl of mPBS. One drop of component B was added, and the tube was vortexed briefly. All compensation beads were stored at 4°C protected from light and vortexed prior to use.

2.9.2 Cell staining

Leukocytes from the blood, peritoneal cavity and spleen were isolated as previously described (see Section 2.8.1, 2.8.2 & 2.8.4). 1-2 x 10^6 cells from each sample were added to wells of a 96-well V-bottom plate (Sigma, #CLS3363). A primary stain master mix was prepared in PBS/1%FBS containing all extracellular antibodies at the appropriate dilution (Table 2.19).

Anti-mouse CD16/CD32 (clone 2.4G2; BD Biosciences, #553141) diluted 1:50 was added to the primary stain to block non-specific Fc receptor binding. A master mix was prepared similarly for each fluorescence minus one (FMO) control. All samples and FMOs were resuspended in 30µl of the primary stain or FMO master mix. Unstained cells were resuspended in 30µl of mPBS/1%FBS. Cells were incubated for 10 minutes at room temperature protected from light. Each well was flooded with 200µl of PBS/1%FBS, cells were centrifuged at 1400RPM for 4 minutes and the supernatant was discarded. A secondary stain master mix was prepared containing LIVE/DEAD™ Fixable Blue Dead Cell Stain diluted 1:1000 in mPBS/1%FBS. All full stain cells were resuspended in 30µl of the secondary stain. FMO and unstained cells were resuspended in 30µl of mPBS/1%FBS. Cells were incubated for 10 minutes at room temperature protected from light. Each well was flooded with 200µl of mPBS/1%FBS, cells were centrifuged at 1400RPM for 4 minutes and the supernatant was discarded. A fixation/permeabilisation solution was prepared by diluting eBioscience™ Fixation/Permeabilisation Concentrate (Invitrogen, #00-5123) 1:4 in eBioscience™ Fixation/Permeabilisation Diluent (Invitrogen, #00-5223). A fixation/permeabilisation wash buffer was prepared by diluting eBioscience™ Permeabilisation Buffer (10X) (Invitrogen, #00-8333) 1:10 in ddH_2O. All cells including unstained controls and FMOs were resuspended in 50µl of fixation/permeabilisation solution and incubated for 25 minutes at 4°C protected from light**.** Each well was flooded with 150µl fixation/permeabilisation wash buffer, cells were centrifuged at 1400RPM for 4 minutes and the supernatant was discarded. An intracellular stain master mix was prepared in fixation/permeabilisation wash buffer containing all intracellular antibodies at the appropriate dilution (Table 2.19). Anti-mouse CD16/CD32 diluted 1:50 was added to the intracellular stain to block non-specific Fc receptor binding. A master mix was prepared similarly for necessary FMO controls. All full stain and appropriate FMO cells were resuspended in 30µl of the intracellular master mix. Remaining FMO and unstained cells were resuspended in 30µl of fixation/permeabilisation wash buffer. Cells were incubated for 15 minutes at room temperature protected from light. Each well was flooded with 100µl of fixation/permeabilisation wash buffer and cells were centrifuged at 1400RPM for 4 minutes.

The supernatant was discarded, and the wash was repeated. All cells were resuspended in 60µl of PBS/1% paraformaldehyde (Sigma-Aldrich, #100496) and transferred to a 96-well round bottom plate (Falcon, #353077) for analysis by flow cytometry.

2.9.3 Data acquisition

Fluorescently stained blood, peritoneal cavity and spleen leukocyte samples described above were analysed using the ZE5 Cell Analyzer (Bio-Rad Laboratories, CA, USA) equipped with a 5-laser, 27 colour detection system. Sample collection and data acquisition was set up using the Everest software (version 2.3, Bio-Rad Laboratories, CA, USA). Voltages were determined for each fluorochrome using untreated, fully stained control cells and were maintained throughout sample collection. For each sample, 400,000 events were analysed at a rate of 6000-8000 events/second. Data compensation and gating was performed using FlowJo software v10.6.2 (Beckton Dickinson, OR, USA). Gates for immune cell populations were set using FMO controls (see Appendix A).

Table 2.19. Antibodies used in flow cytometry experiments.

Antibody	*Clone*	*Working dilution*	*Fluorochrome*	*Detector channel*	*Supplier*	*Catalogue number*
CD4	RM4-5	100	BUV395	[UV] 387/11	BD Biosciences	740208
Live/dead	N/A	1000	LIVE/DEAD® Fixable Blue	[UV] 447/60	Invitrogen	L23105
NK1.1	PK136	100	BUV661	[UV] 670/30	BD Biosciences	741477
CD69	H1.2F3	100	BUV737	[UV] 700/LP	BD Biosciences	564684
CD11c	HL3	100	BV421	[V] 410/10	BD Biosciences	562782
F4/80	T45-2342	100	BV510	[V] 525/50	BD Biosciences	743280
CXCR3	CXCR3-173	100	BV605	[V] 615/24	Biolegend	126523
CD8a	53-6.7	100	BV650	[V] 670/30	Biolegend	100742
CD103	2E7	100	BV711	[V] 720/60	Biolegend	121435

Ki67*	B56	200	BV786	[V] 750/LP	BD Biosciences	563756
MHC II (I-A/I-E)	29G	200	BB515	[B] 525/35	BD Biosciences	565254
GR-1 (Ly-6G/Ly-6C)	RB6-8C5	100	PerCP Cy5.5	[B] 692/80	BD Biosciences	552093
PD-1	RMP1-30	100	PE	[G] 577/15	Biolegend	109103
CD25	PC61	100	PE-CF594	[G] 615/24	BD Biosciences	562694
CD11b	M1/70	100	PE-Cy5	[G] 670/30	Biolegend	101210
CCR4	2G12	100	PE-Cy7	[G] 750/LP	Biolegend	131213
FoxP3*	FJK-16s	50	APC	[R] 670/30	Invitrogen	17-5773-82
CD3	500A2	200	AF 700	[R] 720/60	BD Biosciences	557984

* Intracellular antibodies

2.10 Statistical analysis

Results were graphed and statistical analyses were performed using GraphPad Prism 8 v8.4.2 (GraphPad Software, CA, USA) except where otherwise stated in the figure text. All data was assessed for normality and log transformed to approximate normality where required. Significance between more than two groups was determined by one-way analysis of variance (ANOVA) and Bonferroni's multiple comparisons test. Pairwise comparisons were performed by unpaired *t*-test; where variances were significantly different between groups, Welch's correction was applied. For non-normally distributed data, Mann-Whitney *u*-test was used for pairwise comparisons. Spearman's correlation was used to measure the strength of relationships between variables. Cytokine data (Chapter 4 and Chapter 5) was analysed using Qlucore Omics Explorer software v3.6 (Qlucore AB, Lund, Sweden) to perform multivariate analysis and generate heatmaps of differentially expressed cytokines. All data are presented as mean ± SD and results with a p-value ≤ 0.05 were considered significant except where otherwise stated in the figure text.

Chapter Three

The role of DPP4 expression and activity in ovarian cancer cells in vitro

Preface

The majority of women diagnosed with epithelial ovarian cancer will initially respond positively to first-line treatment, however; resistance to conventional therapies commonly occurs, where additional treatment options and overall survival rates are significantly reduced[269]. The pathology of ovarian disease is complex, and recent advances surrounding its origin has enabled a greater understanding of the multiple molecular pathways that contribute to ovarian cancer tumorigenesis and metastasis. Moreover, significant evidence supports the fact that in addition to the intrinsic malignant capacity of ovarian cancer cells, a critical biological aspect of invasive ovarian cancer is the external tumour microenvironment (TME) contained within malignant ascites fluid[270]. In ovarian disease, the TME encompasses the entire peritoneal cavity and consists of stromal cells including immune cells, cancer-associated fibroblasts (CAFs) and endothelial cells; and components of the extracellular matrix (ECM) including cytokines, chemokines and adhesion molecules, all of which can influence the heterogeneity, tumorigenicity and metastatic capacity of ovarian tumours[271]. One of the hallmarks of the ovarian TME is the reduced oxygen supply, which creates hypoxic regions within tumours and the surrounding ascites fluid. Hypoxia and the accompanied oxidative stress contribute to tumour aggression, chemoresistance and poor prognosis[103,272].

Cellular adaptations to hypoxia include the disruption of several metabolic pathways including those involved in cell proliferation, survival, angiogenesis, invasion and the immune response[99,100]. Additionally, the hypoxic TME upregulates the expression of various suppressive factors including VEGF, IL-10 and TGF-β[105,273]. In ovarian cancer patients, upregulation of IL-6 in the ascites fluid is indicative of poor patient outcome and is correlated with resistance to common chemotherapeutics[169,274]. Multiple studies have aimed to target these hypoxia-inducible pathways in ovarian cancer**,** some of which have been implemented in the clinic, including inhibition of VEGF using the monoclonal antibody bevacizumab. Bevacizumab combined with chemotherapy in patients with platinum-resistant recurrent

ovarian cancer was shown to improve PFS compared to chemotherapy alone but did not improve overall survival[275], and is currently only recommended as a maintenance therapy for patients with late-stage disease[276]. Evidently, there is much to be discovered about the impact of hypoxia in the tumour microenvironment. As additional data emerges of the influence of the TME on ovarian cancer cells, so does our understanding of ovarian cancer pathogenesis and potential therapeutic targets or biomarkers. However, despite the clear effect of hypoxic conditions on cancer cell behaviour, it is often overlooked during *in vitro* experimentation, which may explain some of the uncertainties regarding various molecular pathways in ovarian cancer.

Dipeptidyl peptidase 4 (DPP4), also known as CD26, is a highly specific transmembrane serine protease that is expressed on multiple endothelial and epithelial cell types, and immune cells[263]. DPP4 possesses distinct structural domains which are responsible for its various roles as an adhesion molecule and an enzyme, and is involved in multiple physiological pathways including insulin regulation, inflammation, ECM and immune cell recruitment[263]. DPP4 has been implicated in several cancer types, however its specific function is highly dependent on the microenvironment in which it is expressed and has therefore been attributed both tumour-suppressing and tumour-promoting roles (reviewed in[277]). Furthermore, DPP4 can be cleaved from the cell surface to produce an enzymatically active, soluble form of the protein (sDPP4)[278], which has been proposed as a biomarker in other malignancies including colorectal cancer, melanoma and lung cancer[225,279,280].

There is conflicting evidence of the role of DPP4 in ovarian cancer, likely due to its functional versatility and differences between cell lines. For example, some studies report that the overexpression of DPP4 is associated with decreased invasion of ovarian cancer cells *in vitro*[251,252], whilst investigation of human tumour tissue demonstrated that DPP4 expression was correlated with poor prognosis[281]. As yet, no studies have analysed the potential role of sDPP4 in ovarian cancer, either as an enzymatically active moderator of circulating

substrates, or as a potential biomarker. Our laboratory previously identified the overexpression of DPP4 in epithelial ovarian tumours[282] and its expression is altered under hypoxic conditions in other cell types[247,248,264]. Although there is evidence to suggest that the hypoxic tumour microenvironment may affect DPP4 function and regulation in ovarian cancer cells, there have been no studies to investigate this hypothesis. Furthermore, many previous studies of DPP4 have failed to assess DPP4 activity in relation to its expression, emphasising a potential gap in research which may be important to correctly interpret the role of DPP4 in different pathologies.

This chapter is focused on investigating the role of DPP4 in ovarian tumour cells under conditions which more closely reflect the tumour microenvironment by exploring how DPP4 function is influenced by the hypoxic response *in vitro.* All work in this chapter was completed using human ovarian cancer cell lines. To mimic the *in vivo* hypoxic conditions in the ovarian TME, cells were grown at an O_2 concentration of 2%. Methods to measure gene expression, protein abundance and specific activity were optimised in each case. We assessed DPP4 expression and specific activity under chronic hypoxia, and analysed potential proteolytic mechanisms of its regulation under these growth conditions. This chapter aims to build a more comprehensive depiction of the role and regulation of DPP4 activity in ovarian tumour cells and provide a novel insight into the potential influence of DPP4 expression (i.e., as an adhesion molecule) and/or enzymatic activity on the characteristics of ovarian cancer cells.

The work in this chapter aligns with Aim 1 of my PhD project - *To investigate the role/s of DPP4 expression and activity in ovarian cancer cells in vitro*, and has been published as follows: Moffitt, L. R. *et al.* (2020). Hypoxia Regulates DPP4 Expression, Proteolytic Inactivation, and Shedding from Ovarian Cancer Cells. *International journal of molecular sciences, 21*(21), 8110.

International Journal of
Molecular Sciences

MDPI

Article

Hypoxia Regulates DPP4 Expression, Proteolytic Inactivation, and Shedding from Ovarian Cancer Cells

Laura R. Moffitt [1,2], Maree Bilandzic [1,2], Amy L. Wilson [1,2], Yiqian Chen [1,2], Mark D. Gorrell [3], Martin K. Oehler [4,5], Magdalena Plebanski [6] and Andrew N. Stephens [1,2,*]

1 Department of Molecular and Translational Sciences, Monash University, Clayton, VIC 3168, Australia; laura.moffitt@monash.edu (L.R.M.); maree.bilandzic@hudson.org.au (M.B.); amy.wilson@hudson.org.au (A.L.W.); yiqian.chen@hudson.org.au (Y.C.)
2 Centre for Cancer Research, Hudson Institute of Medical Research, Clayton, VIC 3168, Australia
3 Centenary Institute, Faculty of Medicine and Health, University of Sydney, Camperdown NSW 2006, Australia; m.gorrell@centenary.org.au
4 Department of Gynaecological Oncology, Royal Adelaide Hospital, Adelaide, SA 5000, Australia; martin.oehler@adelaide.edu.au
5 Robinson Institute, University of Adelaide, Adelaide, SA 5000, Australia
6 School of Health and Biomedical Sciences, RMIT University, Bundoora, VIC 3082, Australia; magdalena.plebanski@rmit.edu.au
* Correspondence: andrew.n.stephens@hudson.org.au; Tel.: +61-3-8572-2686

Received: 9 October 2020; Accepted: 28 October 2020; Published: 30 October 2020

Abstract: The treatment of ovarian cancer has not significantly changed in decades and it remains one of the most lethal malignancies in women. The serine protease dipeptidyl peptidase 4 (DPP4) plays key roles in metabolism and immunity, and its expression has been associated with either pro- or anti-tumour effects in multiple tumour types. In this study, we provide the first evidence that DPP4 expression and enzyme activity are uncoupled under hypoxic conditions in ovarian cancer cells. Whilst we identified strong up-regulation of *DPP4* mRNA expression under hypoxic growth, the specific activity of secreted DPP4 was paradoxically decreased. Further investigation revealed matrix metalloproteinases (MMP)-dependent inactivation and proteolytic shedding of DPP4 from the cell surface, mediated by at least MMP10 and MMP13. This is the first report of uncoupled DPP4 expression and activity in ovarian cancer cells, and suggests a previously unrecognized, cell- and tissue-type-dependent mechanism for the regulation of DPP4 in solid tumours. Further studies are necessary to identify the functional consequences of DPP4 processing and its potential prognostic or therapeutic value.

Keywords: ovarian cancer; DPP4; hypoxia; MMP; tumour microenvironment

1. Introduction

Epithelial ovarian cancers (EOCs) remain the most lethal of gynaecological malignancies, and account for >80% of ovarian tumour diagnoses [1]. A lack of screening or early detection modalities means that most patients are diagnosed with advanced disease, and the majority of these relapse with chemoresistant disease within 18 months [2]. Despite efforts to develop targeted therapies, 5-year survival has remained at approximately 40% for the past 30 years [2]. There is an urgent and unmet need for improved diagnostic, prognostic and therapeutic tools to reduce mortality for ovarian cancer patients.

Dipeptidyl peptidase 4 (DPP4; CD26) is a member of the prolyl oligopeptidase serine protease family, which includes the related enzymes fibroblast activated protein (FAP), DPP8, and DPP9 [3]. Expressed by multiple cell types, DPP4 catalyses the cleavage of N-terminal *X-Pro* and *X-Ala* dipeptides from a variety of substrates to directly modify their bioactivities [4,5]. Indeed, a number of inflammatory mediators with central roles in immune suppression and tumour progression (e.g., CCL5, 11, 22; CXCL2, 6, 9–12) are potential targets for DPP4-directed cleavage [3–5]. DPP4 also non-enzymatically regulates adhesion via interaction with extracellular matrix (ECM) proteins (e.g., collagen, fibronectin), and is involved in signalling pathways through association with FAP and CXCR4 [6]. Accordingly, DPP4 expression is linked with tumorigenic behaviour in a variety of cancer types (reviewed in [6]).

Whilst DPP4 over-expression in ovarian cancer tissues is well established [5,7], both pro- and anti-tumour effects have been attributed to DPP4 [6] and in vitro analyses have generated significant conflict surrounding its functional significance. High DPP4 expression in ovarian cancer cells is correlated with an epithelial phenotype and reduced invasiveness [8,9]; conversely, DPP4 expression has also been associated with the enhanced migratory capacity and tumorigenic potential of ascites-derived cancer cells [9]. Similarly, whilst DPP4 expression in ovarian cancer cells varies according to cell type [10], studies disagree regarding in which cell types, and to what degree, DPP4 is expressed [9,10]. The functional role and prognostic significance of DPP4 expression in ovarian cancer thus remains unclear [6,10].

Within hypoxic tumour "nests" and poorly oxygenated ascites fluid [11], malignant ovarian cancer cells thrive and form multicellular aggregates (spheroids) that metastasize throughout the peritoneal cavity [11]. Hypoxia-inducible factor 1-alpha (HIF-1α), a master regulator of hypoxic response, is upregulated in ovarian tumour tissues and is correlated with chemo-resistance and decreased overall survival for ovarian cancer patients [12,13]. Some studies have demonstrated hypoxia-induced DPP4 expression in diverse cell types including smooth muscle cells and adipocytes [14–16]. Indeed, recent work in human preadipocytes showed that HIF-1α strongly induced DPP4 expression and potentially regulated its proteolytic release from the cell surface [15]. The strong expression of DPP4 in cancer tissues, together with high expression in cancer cells derived from poorly oxygenated ascites fluid [10,11], suggests that the tumour microenvironment can exert a distinct influence on DPP4 expression and function in vivo. However, the role of hypoxia on DPP4 expression in ovarian cancer has never been evaluated.

In this study we have investigated the role of hypoxic conditions on DPP4 expression and function in ovarian cancer cells in vitro. We provide evidence for the hypoxic regulation of DPP4 in ovarian cancer cells and identify a potential matrix metalloproteinase-mediated mechanism of DPP4 proteolysis from the cell surface. Importantly, whilst the mechanism of hypoxia-induced DPP4 regulation also occurs in non-malignant cells, our data shows that the enzymes regulating DPP4 function differ in malignancy and suggest complex regulation of DPP4 in tumour versus non-tumour tissues.

2. Results

2.1. DPP4 Expression Is Upregulated by Hypoxia in Ovarian Cancer Cells

Several studies suggest that the in vitro and in vivo expression of DPP4 may be affected by hypoxia in a cell- and tissue-dependent manner [14,16,17]. To assess the effect of hypoxic growth on DPP4 expression and abundance in ovarian cancer, cell lines OVCAR4, CaOV3, and SKOV3 were cultured under either normoxic (20% O_2) or hypoxic (2% O_2) conditions for 48 h. Cells cultured under prolonged hypoxia reached a lower overall cell density, however, cell viability was unaffected (Figure 1A).

Samples were collected following 4, 8, 24, and 48 h of incubation and assessed for HIF-1α (to confirm induction of hypoxia) and DPP4 expression. In high grade serous cancer (HGSC) cell lines OVCAR4 and CaOV3 [18], *HIF-1α* mRNA expression was rapidly induced under hypoxia and remained elevated compared to normoxic levels over the incubation period (Figure 1B). Adenocarcinoma- derived SKOV3 line which forms clear cell tumours in vivo [18–20] displayed acute induction of *HIF-1α*

mRNA after 4 h, which returned rapidly to a similar level to cells grown under normoxic conditions (Figure 1B). *HIF-1α* was notably more abundant in SKOV3 than OVCAR4 or CaOV3 cells, consistent with higher HIF-1α expression reported in clear cell ovarian tumours compared to other histotypes [21]. Corresponding protein analysis by ELISA demonstrated parallel increases over time of HIF-1α protein in all cell types (Figure 1C).

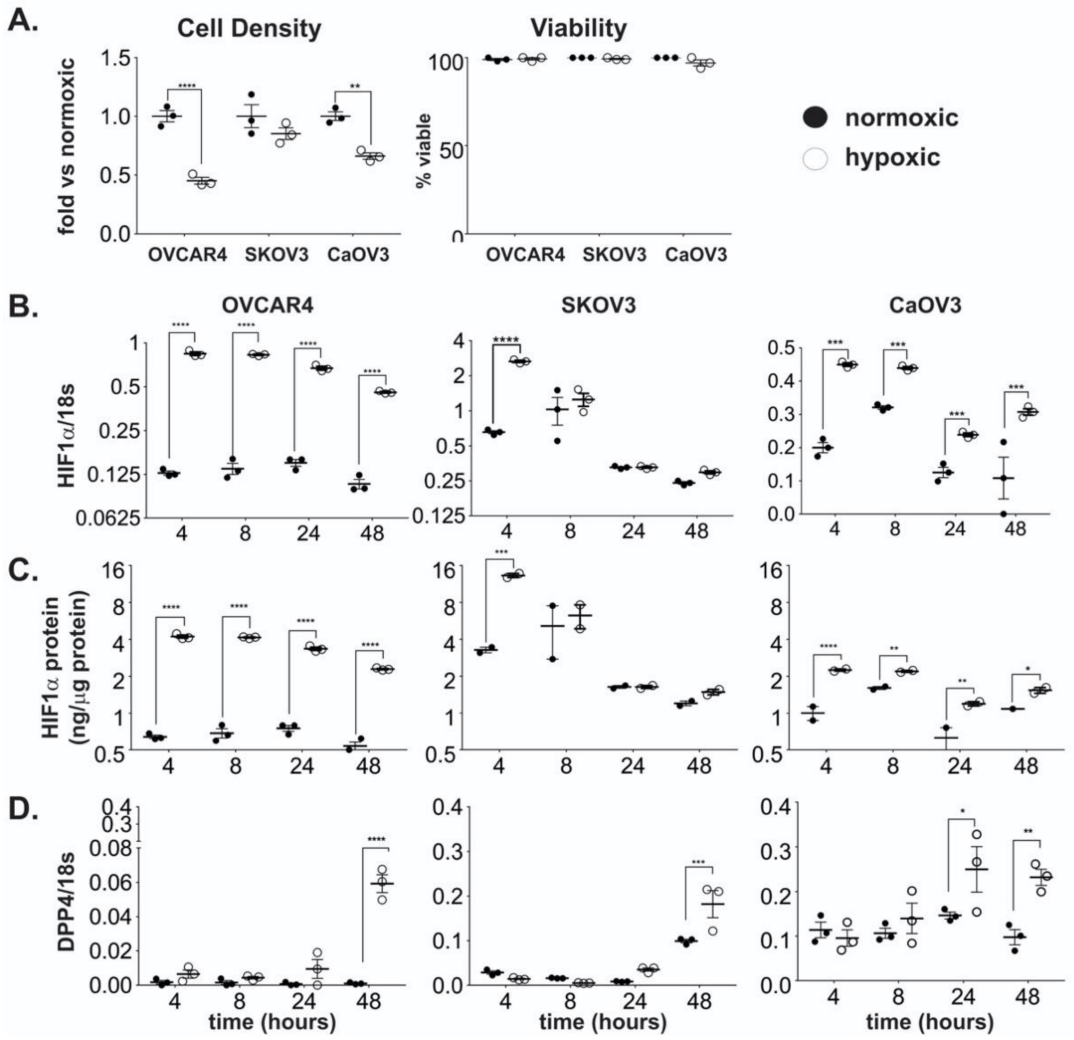

Figure 1. The effect of hypoxia on cell growth, HIF-1α and DPP4 expression in ovarian cancer cells. Ovarian cancer cell lines OVCAR4, SKOV3, and CaOV3 were seeded at ~10^6 cells/25 cm^2 flask and cultured under normoxic or hypoxic conditions for up to 48 h. (**A**) Cell density and viability at 48 h. (**B**) HIF-1α mRNA expression and (**C**) protein abundance were measured by qRT-PCR and ELISA respectively. (**D**) DPP4 mRNA expression was measured by qRT-PCR. Data represent the mean ± SD, n = 3/group. * $p < 0.05$; ** $p < 0.01$; *** $p < 0.001$; **** $p < 0.0001$.

Each cell line was assessed for the induction of *DPP4* expression. In every case, *DPP4* mRNA increased in a time-dependent manner in cells grown under hypoxic conditions compared to those grown under normoxia (Figure 1D). By 48 h, all cells grown under hypoxia showed significantly elevated *DPP4* mRNA expression. Whilst lower cell densities were observed under hypoxic versus normoxic growth, the increase in *DPP4* expression was not associated with changes in cell viability after 48 h (Figure 1A). This incubation period was selected as cells that were cultured under hypoxia for longer than 48 h demonstrated decreased cell viability (data not shown). Together these results

show *DPP4* mRNA expression is consistently upregulated under conditions of chronic hypoxic growth in ovarian cancer cell lines.

2.2. Chronic Hypoxia Induces DPP4 Shedding from the Surface of Ovarian Cancer Cells

Since OVCAR4 cells displayed the most robust hypoxic response amongst the three cell lines examined, they were used as a model to measure changes in DPP4 abundance and activity under hypoxia. Unexpectedly, despite the induction of *DPP4* mRNA expression there was no significant difference in DPP4 protein abundance in cells grown under hypoxic conditions (Figure 2A). Moreover, cellular DPP4 enzyme activity remained unchanged (Figure 2A) suggesting DPP4 abundance and enzyme activity in cells were maintained in a relatively steady state under hypoxic conditions.

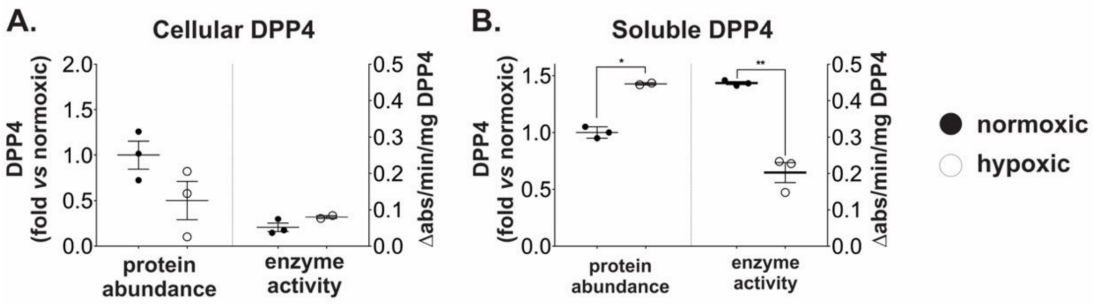

Figure 2. Hypoxia induces shedding of inactive DPP4 from ovarian cancer cells. OVCAR4 cells were cultured under normoxia or hypoxia for 48 h. ELISA for quantitation of DPP4 protein abundance and enzyme assays for DPP4 activity were performed on (**A**) cell lysates and (**B**) conditioned media. Enzyme activity is expressed as specific activity relative to the measured abundance of DPP4. The data represent the mean ± SD, $n = 3$/group. * $p < 0.05$; ** $p < 0.01$.

DPP4 can exist in both cellular and secreted (sDPP4) forms, and it has been suggested that hypoxia may stimulate sDPP4 release from the cell surface [15]. We therefore also assessed DPP4 abundance and enzyme activity in conditioned media from cells grown under hypoxia. By contrast to cell lysates, conditioned media contained ~50% more sDPP4 protein following hypoxic growth (Figure 2B). Paradoxically, sDPP4 specific enzyme activity decreased under these conditions (Figure 2B). Western blotting was unable to confirm proteolysis of sDPP4 in the Fetal Bovine Serum (FBS)-supplemented media (see Supplementary Figure S1A); however, detection by ELISA argued against extensive degradation of sDPP4 following secretion. Together, these data indicate that cellular DPP4 abundance and activity is maintained in a steady state during hypoxia by the release of sDPP4 into the surrounding milieu. However, it also demonstrates that sDPP4 is likely inactivated either during or soon after release from ovarian cancer cells in vitro.

2.3. Chronic Hypoxic Growth Stimulates Matrix Metalloproteinase Expression and Alters DPP4 Release from Cells

Matrix metalloproteinases (MMPs) are well-characterized for their roles in ECM remodelling and are strongly associated with tumour invasion [22]. Based on recent data suggesting that MMPs may mediate shedding of DPP4 from smooth muscle cells [15], we hypothesized that MMPs may play a similar role in ovarian cancer cells. Cell lysates and conditioned media from OVCAR4 cells grown under normoxic or hypoxic conditions, were analysed for changes in the abundance of selected proteases (Figure 3A, Supplementary Table S1). Under hypoxic growth conditions, we observed significant increases in the cellular abundance of MMPs 1, 10, and 13, and substantially increased secreted levels of these MMPs (Figure 3A and Supplementary Figure S1B). Likewise, the cellular abundance of cathepsins CTSB, CTSD, CTSV, and CTSZ was also increased under hypoxia; however, extracellular CTSV and CTSZ were unaltered, and only moderate changes in extracellular CTSB and CTSD were detected (Figure 3A).

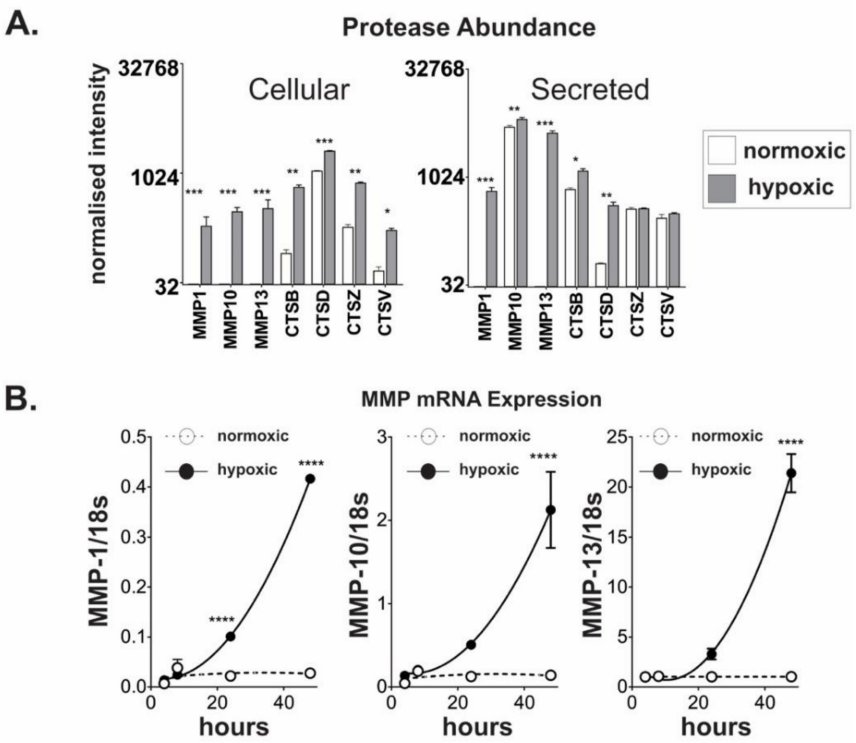

Figure 3. Hypoxia regulates protease expression in ovarian cancer cells. Cell lysates and conditioned media from OVCAR4 cells grown under normoxia and hypoxia were analysed for abundance of 27 different human proteases (Supplementary Table S1) using antibody arrays. (**A**) Normalized detection intensities for cellular and secreted proteases (MMP1, MMP10, MMP13, CTSB, CTSD, CTSZ, and CTSV) that were significantly different following hypoxic incubation of OVCAR4 cells. (**B**) Expression levels of *MMP1*, *MMP10*, and *MMP13* were validated by qRT-PCR. The data represent the mean ± SD, $n = 3$/group. *$p < 0.05$; **$p < 0.01$; ***$p < 0.001$; ****$p < 0.0001$.

The changes in MMPs 1, 10, and 13 were further explored by qRT-PCR. In each case, the gene expression of *MMP1, MMP10*, and *MMP13* was substantially increased following prolonged exposure to hypoxia (Figure 3B). In addition, *DPP4* expression was strongly correlated (Pearson correlation) with *MMP1* ($r = 0.99$, $p = 0.007$), *MMP10* ($r = 0.99$, $p = 0.011$), and *MMP13* ($r = 0.98$, $p = 0.024$) expression in cells grown under hypoxic, but not normoxic, conditions.

We next used the pan-MMP inhibitor GM6001 [23] to broadly assess the role of MMP enzyme activity in sDPP4 release from OVCAR4 cells. Cells treated with GM6001 remained sensitive to hypoxia and showed an increase of *DPP4* mRNA expression at 48 h (Figure 4A). Global MMP activity was therefore not required for DPP4 expression. However, compared to untreated cells, hypoxia failed to induce sDPP4 secretion from GM6001 treated cells or stimulate the previously observed reduction in sDPP4 activity (Figure 4C), confirming that sDPP4 release from cells was influenced by MMP activity in vitro.

2.4. MMP10 and MMP13 Mediate DPP4 Expression and Release from Cancer Cells

To more deeply explore the relationship between DPP4 and MMPs, shRNA was used to individually knock down the expression of *MMP1, MMP10*, and *MMP13* in OVCAR4 cells. Efficient knock down of both *MMP10* and *MMP13* was confirmed by qRT-PCR (Figure 5A); *MMP1* knock down (KD) was unsuccessful (not shown) and was not examined further. When challenged with hypoxia, *MMP10* mRNA expression was reduced by ~60% in *MMP10*-KD cells (Figure 5A); whilst knock-down of *MMP13* resulted in complete inhibition of *MMP13* expression under both normoxic and hypoxic conditions (Figure 5A).

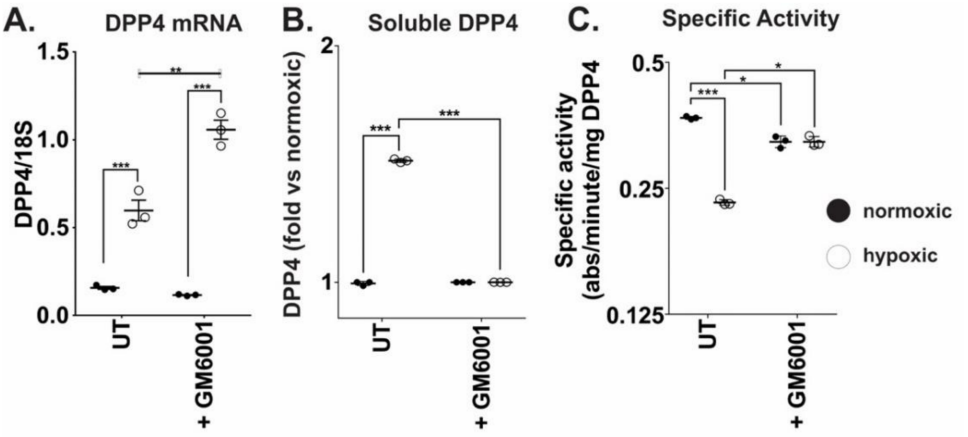

Figure 4. Matrix metalloproteinases (MMP) activity influences DPP4 expression and release in ovarian cancer cells. OVCAR4 cells were treated with the pan-MMP inhibitor GM6001 (25 μM) and cultured under normoxia or hypoxia for 48 h. Cells were harvested and analysed for (**A**) DPP4 mRNA expression; and conditioned media were collected and analysed for (**B**) soluble DPP4 protein abundance and (**C**) DPP4 enzyme activity. The data represent the mean ± SD, n = 3/group. * $p < 0.05$; ** $p < 0.01$; *** $p < 0.001$.

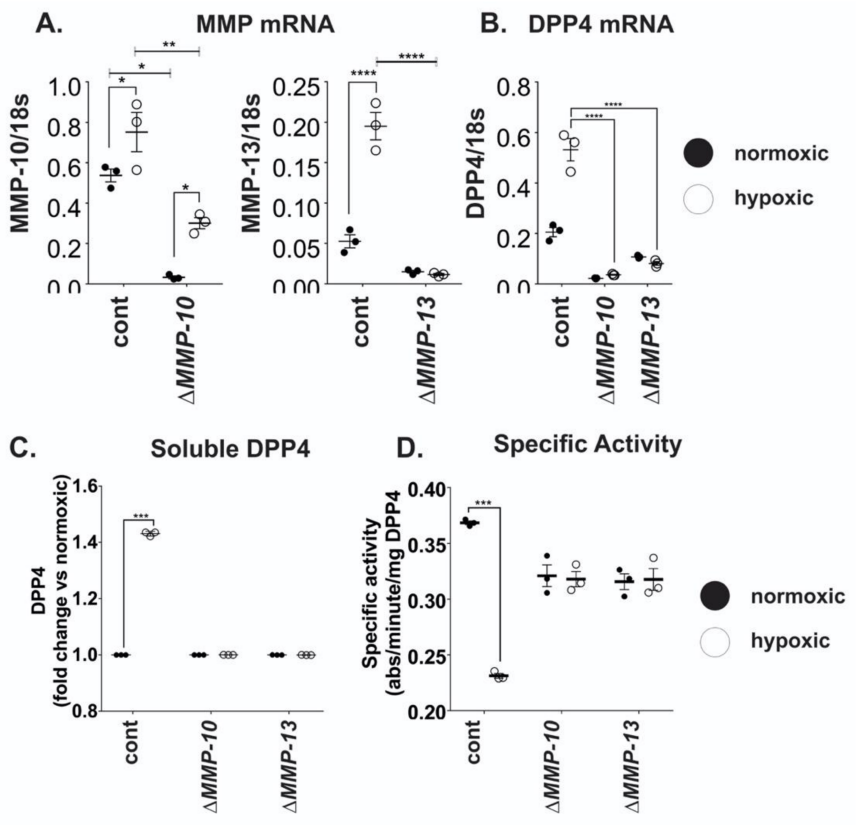

Figure 5. MMP10 and MMP13 affect DPP4 expression and release from ovarian cancer cells. OVCAR4 cells with stable shRNA knockdown of *MMP10* or *MMP13* were cultured under normoxia or hypoxia for 48 h. Total RNA was extracted, and qRT-PCR performed to confirm (**A**) knockdown of *MMP10* and *MMP13* relative to controls, and (**B**) examine the effects of MMP10 and MMP13 on *DPP4* mRNA expression. DPP4 ELISA and enzyme assay were performed on conditioned media of cells to assess changes in (**C**) sDPP4 release and (**D**) specific activity induced by the downregulation of *MMP10* and *MMP13*. The data represent the mean ± SD, n = 3/group. * $p < 0.05$; ** $p < 0.01$; *** $p < 0.001$; **** $p < 0.0001$.

Compared to control cells, hypoxia failed to induce DPP4 expression in either *MMP10*-KD or *MMP13*-KD cells (Figure 5B). Consistent with the lack of *DPP4* induction following MMP knock-down, neither *MMP10*-KD nor *MMP13*-KD cells displayed any difference in DPP4 abundance or activity under hypoxia (Figure 5C,D). Control cells expressing the scrambled shRNA control responded as previously observed. Together with the results of pan-MMP inhibition (above), these data suggest that DPP4 shedding from the ovarian cancer cell surface is mediated by MMP activity, whilst DPP4 mRNA expression is influenced by both MMP10 and MMP13 at the transcriptional level, suggesting the involvement of a more complex regulatory mechanism.

3. Discussion

A key factor contributing to ovarian cancer progression is the hypoxic environment within the tumour mass and peritoneal ascites fluid. The expression of HIF-1α as a marker of hypoxic response is strongly correlated with chemo-resistance and is an independent predictor of poor prognosis for EOC patients [12,13]. Several studies have linked the induction of DPP4 in response to hypoxia in vitro and in vivo [15,24]. However, DPP4 abundance and activity vary between different cancer types, and exhibit complex patterns of regulation [25]. Neither the expression nor function of DPP4 in ovarian cancer cells have previously been examined under conditions of hypoxic growth that mimic the tumour microenvironment.

When cultured under conditions of low atmospheric oxygen for prolonged periods, we identified a significant and sustained increase in *DPP4* expression in all ovarian cancer cell lines examined. Whilst there is evidence proposing DPP4 as a marker of HIF-1α induction [14], our data suggested that DPP4 expression was largely independent of HIF-1α status; however, all cell lines tested constitutively expressed HIF-1α, potentially masking any specific or HIF-1α dependent effects. Typical of a housekeeping gene, DPP4 can be regulated in a cell-type-specific manner [26–28] by transcription factors including Stat1α and hepatocyte nuclear factor-1 (HNF-1), specific physiological stimuli (e.g., secreted cytokines) and post-translational modifications (e.g., glycosylation [29]), all of which can be affected by the hypoxic tumour microenvironment [28]. Our data evidences a previously undescribed mechanism of DPP4 regulation in ovarian cancer cells mediated according to oxygen status, either directly via HIF-1α modulation or indirectly via its downstream targets.

An unexpected and novel finding was the active shedding of inactivated DPP4 from cancer cells under hypoxic growth, which was mediated in part by an increase in MMP activity. There is conflicting evidence across multiple cancer types regarding the regulation of DPP4 expression and activity, however, prior studies have failed to consider the hypoxic tumour microenvironment that is common to many solid cancers. Our discovery of the uncoupling of DPP4 expression from enzyme activity in cancer cells provides a plausible explanation for this previously unclear role of DPP4 in various tumours, including ovarian, colorectal, and potentially other cancers. In non-malignant cells such as smooth muscle and adipocytes, hypoxia-induced DPP4 shedding is mediated by increased activity of MMPs 1, −2, and −14 [15]. Our data suggests that the mechanism of DPP4 release from cancer cells is likely to be different, involving proteolytic release and inactivation mediated by at least MMP10 and MMP13, which directly supports recent evidence that hypoxia promotes ovarian cancer cell invasion via an MMP-13 mediated mechanism [30]. By analogy, DPP4 is shed from the surface of CD4+ T cells by kallikrein-related peptidase 5 (KLK5) [31], and in hepatoma cells Serpin B3 induces overexpression of inactive DPP4 [32]. The regulation of DPP4 shedding from the cell surface, and the activation status of sDPP4, is thus a cell-type dependent phenomenon. Whether DPP4 shedding in ovarian cancer cells is directly mediated by MMP activity, via MMP-dependent activation of pro-enzymes, or by a more complex interrelationship with other protease systems [33] requires further investigation. In addition, the possibility of other mechanisms of sDPP4 release including vesicle-mediated trafficking and factors which influence surface expression such as genetic heterogeneity should also be considered in future studies.

Elevated levels of circulating sDPP4 have been suggested as a prognostic biomarker in colorectal cancer, where they are associated with reduced overall and progression free survival [34]. Interestingly, decreased sDPP4 enzyme activity in colorectal cancer relative to healthy controls is also associated with poor prognosis [35], and a similar decrease in activity occurs in patients with melanoma [36]. These findings are consistent with our data, where increased extracellular DPP4 abundance was accompanied by decreased activity. Whilst altered DPP4 glycosylation or phosphorylation [37] could also influence the reliability of sDPP4 measurement, it is likely that enzymatic processing and inactivation of DPP4 plays a role in at least some solid tumour types to influence both abundance and activity status. The measurement of specific, proteolytic DPP4 fragments shed by cancer cells may thus be more relevant as a biomarker of disease status.

Although DPP4 has important functions in metabolism, recent data also support its key roles in immunity and inflammation [4,7,38]. DPP4 can regulate the bioactivity of several chemokines to influence immune and inflammatory responses critical to cancer progression [7,25,39]. For example, suppression or down-regulation of DPP4 promotes prostate cancer progression via reduced degradation of its substrate CXCL12, leading to enhanced signalling via CXCR4 and increased invasion and metastatic spread to peripheral organs in vivo [40,41]. Similarly, reduced DPP4 activity in poorly differentiated gliomas [42] and an associated decrease in Substance P processing is linked to the loss of cell growth inhibition via reduced calcium signalling [43]. Altered DPP4 function is also postulated as an underlying mechanism in the poor response of some high grade ovarian cancers [7], and the in vitro and in vivo interactions between DPP4 and specific cytokines are established as an important mechanistic contribution in different cancer types [7,38]. The apparent cancer-specific incidence of DPP4 inactivation thus suggests the potential of inhibiting DPP4 in tailored therapeutic interventions to improve anti-tumour immunity. Indeed, DPP4 inhibition using the anti-diabetes drug Sitagliptin has been associated with reduced incidence of breast cancer in diabetes patients [44], and has an immune-mediated protective effect in several preclinical models [38,45,46]. For example, Sitagliptin treatment improves anti-tumour responses via enhanced CCL11-mediated eosinophil migration in hepatocellular carcinoma mouse models [45], and promotes CXCL9- and CXCL10-mediated dendritic cell trafficking to melanoma tumours [46].

Cell migration and invasion are accompanied by proteolytic degradation of the ECM, in which MMPs, Kallikreins, Cathepsins, and DPP4 all have established roles. In particular, the DPP4-FAP heterodimer localizes at the cell surface as an enzymatically active complex and is correlated with the upregulation of MMPs [3,47]. DPP4 enzyme activity also promotes cell migration and adhesion in cervical cancer lines [48], and its inhibition is associated with decreased invasion, migration, and colony formation capacity in thyroid cancer cells [49]. It is unclear, however, how DPP4 inactivation might influence invasion in the poorly oxygenated peritoneal environment and ascites fluid present in metastatic ovarian cancers [11]. DPP4 expression has been associated with tumour initiating cell populations in several tumour types [50,51], and ovarian cancer spheroids (free-floating organoids with a hypoxic core) found in ascites fluid contain putative ovarian cancer stem cells [52]. The alterations in DPP4 abundance and activity observed under hypoxic conditions may therefore be related to a transition state between transcriptionally plastic cell phenotypes, required to preserve or maintain cancer cell populations during hypoxic stress.

4. Materials and Methods

4.1. Cell Culture

The human ovarian cancer cell lines SKOV3 (RRID: CVCL_0532) and CaOV3 (RRID: CVCL_0201) were purchased from the ATCC. The OVCAR4 (RRID: CVCL_1627) cell line was a kind gift from Professor David Bowtell (Peter MacCallum Cancer Centre, Melbourne). All cell lines have been authenticated using STR profiling within the last three years. SKOV3, CaOV3, and OVCAR4 cells were maintained in Dulbecco's Modified Eagle's Medium (DMEM)/Nutrient Mixture F-12

Ham (Sigma-Aldrich, St. Louis, MO, USA), DMEM (Sigma-Aldrich, St. Louis, MO, USA) or RPMI-1640 Medium (Sigma-Aldrich, St. Louis, MO, USA), respectively; supplemented with 10% Fetal Bovine Serum (FBS) (Thermo Fisher Scientific, Waltham, MA, USA) and 1% penicillin/streptomycin (p/s; Thermo Fisher Scientific, Waltham, MA, USA). Cells were incubated at 37 °C under either normoxia (20% O_2, 5% CO_2) or hypoxia (2% O_2, 5% CO_2, 150 μM $CoCl_2$; BioSpherix hypoxia suite) as indicated in the text. Cell counts and viability were determined using Trypan Blue cell viability dye and the Countess II FL automated cell counter (Thermo Fisher Scientific, Waltham, MA, USA). All lines were validated mycoplasma-negative.

4.2. Quantitative Real-Time PCR (qRT-PCR)

Total RNA was extracted from cells using Ultraspec® RNA reagent (Fisher Biotec Australia, Wembley, Australia) according to the manufacturer's instructions. cDNA was synthesized by reverse transcription from 1 μg RNA using the Tetro cDNA synthesis kit (Bioline, London, UK). For quantitative real-time PCR (qRT-PCR) analysis of specific genes, sense and antisense oligonucleotide primers were designed against published human sequences and verified as previously described [53]. Primer pairs for each gene are listed in Table 1. Real-time PCR samples were prepared to a final volume of 10 μl using the Applied Biosystems *Power* SYBR™ Green PCR Master Mix. Quantitative real-time PCR was completed as previously described [53] using the QuantStudio™ 6 Flex Real-Time PCR System (Applied Biosystems, Foster City, CA, USA) with all reactions performed in triplicate. Yields were converted to femtograms based on the standard curve for each PCR product, and the resultant mRNA levels were normalized to the *18S* mRNA level per sample (averaged over 3 replicates).

Table 1. Human primer sequences for real-time PCR.

Gene	Accession Number	Primer Sequences 5′–3′	
		Forward	Reverse
18S	NR_003286.4	GTAACCCGTTGAACCCCATT	CCATCCAATCGGTAGTAGCG
HIF-1α	NM_001530	CAGCTATTTGCGTGTGAGGA	CCTCATGGTCACATGGATGA
DPP4	NM_001935	ATGCCAGGAGGAAGGAATCT	TATAGAGGGGCAGACCAGGA
MMP1	NM_002421	GGACAACTCTCCTTTTGATGGA	CAAAGCCCCGATATCAGTAGAA
MMP10	NM_002425	CACAGTTTGGCTCATGCCTA	TGCCATTCACATCATCTTGC
MMP13	NM_002427	GACCCTGGAGCACTCATGTT	TCCTCGGAGACTGGTAATGG

4.3. Enzyme Linked Immunosorbent Assay (ELISA)

Protein quantitation in total cell lysate or cell culture supernatant were performed using commercially available ELISA kits (Human HIF-1-alpha; ab171577 and Human CD26; ab11951, Abcam, Cambridge, UK) as per the manufacturer's instructions. CD26 ELISA was performed using 10 μg of protein from cell lysate or concentrated cell culture supernatant. HIF-1-alpha ELISA was performed using 5 μg of protein lysate. Absorbance was measured using a FLUOstar® Omega microplate reader (BMG Labtech, Mornington, Australia).

4.4. DPP4 Enzyme Activity Assays

DPP4 enzymatic activity in cell lysates was measured as described [5] using 15 μg of total protein lysate per well. Substrate hydrolysis was measured every 10 min for 3 h using a Cytation™ 3 Multi-Mode Reader (BioTek, Winooksi, VT, USA) at 37 °C. Absorbance readings at 570 nm were subtracted from readings at 405 nm to account for the optical interference from cell culture media. All samples were measured in triplicate.

For secreted DPP4 enzymatic activity, a more sensitive fluorogenic assay was used. In each case a 2 mM solution of the fluorogenic DPP4 substrate Gly-Pro-7-amido-4-methylcoumarin (Sigma-Aldrich, St. Louis, MO, USA) in Tris-EDTA buffer with 10% methanol was added to each well of a black 96-well plate containing 15 μg of concentrated cell culture supernatant from an initial volume of 1 mL.

Each sample was assayed in triplicate and substrate hydrolysis was determined by measuring fluorescence at $355_{ex}/450_{em}$ every 10 min for 3 h using the Cytation™ 3 Multi-Mode Reader at 37 °C.

4.5. Protease Arrays

Relative quantitative measurement of 40 unique proteases in cell lysates and cell culture media was determined using commercially available antibody arrays (Human MMP antibody array, ab197453 Abcam, Cambridge, UK; and Proteome Profiler™ Array, ARY021 R&D Systems, Minneapolis, MN, USA) as per the manufacturer's instructions. Each array was probed using 50 µg of total protein from either cell lysate or concentrated cell culture supernatant. Arrays were visualized using either a Typhoon Variable Mode Imager (Molecular Dynamics, Sunnyvale, CA, USA) equipped with a Cy3 wavelength filter (Human MMP array) or a ChemiDoc™ XRS+ System (BioRad, Hercules, CA, USA) to detect chemiluminescence (Proteome Profiler array). Signal intensities were determined using Fiji software v1.0 [54,55], and replicate values were individually normalized against a reference array.

4.6. Targeted Knockdown of Selected MMPs Using shRNA

To inhibit human *MMP10* and *MMP13* expression in vitro, we designed fold-back stem-loop shRNA structures using the design recommendations by System Biosciences (Palo Alto, CA, USA). Inhibitory stem-loops comprised a 21-bp sense strand (obtained from the Sigma MISSION® shRNA database) identical to the coding region of the target gene, a 12-bp loop (CTTCCTGTCAGA) and a 21-bp antisense strand followed by an RNA polymerase III terminator sequence (TTTTT). Restriction sites for *Bam*HI and *Eco*RI were incorporated at the 5′ and 3′ end of the shRNA, respectively, for cloning into the pSIF-H1-Puro vector (System Biosciences, Palo Alto, CA, USA). Construct identity was confirmed by sequencing analysis. For MMP knockdown pSIF-H1-Puro-*MMP10* or -*MMP13* vectors were transfected into the OVCAR4 cell line using Lipofectamine® 2000 (Invitrogen, Carlsbad, CA, USA) according to the manufacturer's instructions. Positive transfectants were selected using Puromycin (1 µg/mL; Sigma-Aldrich, St. Louis, MO, USA). Total cellular RNA was extracted and MMP expression was assessed by qRT-PCR (as above) using the following primers; *MMP10* F: 5′-CACAGTTTGGCTCATGCCTA-3′, *MMP10* R: 5′-TGCCATTCACATCATCTTGC-3′; *MMP13* F: 5′-TTGAGCTGGACTCATTGTCG-3′, MMP13 R: 5′-CTCAGTCATGGAGCTTGCTG-3′.

4.7. Statistical Analysis

All statistical analyses were performed using GraphPad Prismv7.0b (GraphPad Software Inc., San Diego, CA, USA). Significance between groups was determined by two-way ANOVA and Bonferroni's multiple comparisons test, or by paired *t*-test. Spearman's correlation was used to measure the strength of relationships between variables. All data are presented as mean ± SD. Results with a p-value ≤ 0.05 were considered significant.

5. Conclusions

The current study provides the first insights into the potential influence of the hypoxic microenvironment on DPP4 expression and function in ovarian cancers, and we have shown for the first time that MMP enzyme activity is necessary for DPP4 shedding from ovarian cancer cells, suggesting similar mechanisms may exist in other cancers where DPP4 plays a role. The discovery of a link between hypoxia, DPP4 expression and MMP-dependent shedding offers a much-needed new mechanistic understanding into potentially contradictory findings in the literature on DPP4 expression and its prognostic utility in ovarian cancer. Our data demonstrates a highly regulated relationship between DPP4 function and expression and hypoxia-induced proteases in the tumour microenvironment and suggests further studies are needed to elucidate the complex role of DPP4 in epithelial ovarian cancers and other solid tumours.

Supplementary Materials: The following are available online at http://www.mdpi.com/1422-0067/21/21/8110/s1.

Author Contributions: Conceptualization, L.R.M. and A.N.S.; Data curation, L.R.M. and A.N.S.; Formal analysis, L.R.M. and A.N.S.; Funding acquisition, M.D.G., M.K.O., M.P. and A.N.S.; Investigation, L.R.M.; Methodology, L.R.M., M.B., A.L.W., Y.C. and A.N.S.; Project administration, A.N.S.; Supervision, M.P. and A.N.S.; Validation, L.R.M.; Visualization, L.R.M. and A.N.S.; Writing—Original draft, L.R.M. and A.N.S.; Writing—Review & editing, L.R.M., M.B., A.L.W., Y.C., M.D.G., M.K.O., M.P. and A.N.S. All authors have read and agreed to the published version of the manuscript.

Funding: This work was supported by NHMRC grant #1099375 and the Victorian Government's Operational Infrastructure Support Program. M.P. is supported by an NHMRC Senior Fellowship. A.S. is supported by a fellowship from the Ovarian Cancer Research Foundation (OCRF.com.au).

Acknowledgments: We acknowledge the facilities, scientific and technical assistance of FlowCore, Monash Micro Imaging and MHTP Medical Genomics of Monash University and Monash Health Translation Precinct. Internal audit #11868188.

Conflicts of Interest: The authors declare no conflict of interest.

References

1. Siegel, R.L.; Miller, K.D.; Jemal, A. Cancer statistics, 2018. *CA Cancer J. Clin.* **2018**, *68*, 7–30. [CrossRef] [PubMed]
2. Jayson, G.C.; Kohn, E.C.; Kitchener, H.C.; Ledermann, J.A. Ovarian cancer. *Lancet* **2014**, *384*, 1376–1388. [CrossRef]
3. Gorrell, Mark D. Dipeptidyl peptidase IV and related enzymes in cell biology and liver disorders. *Clin. Sci.* **2005**, *108*, 277–292. [CrossRef] [PubMed]
4. Yu, D.M.; Yao, T.W.; Chowdhury, S.; Nadvi, N.A.; Osborne, B.; Church, W.B.; McCaughan, G.W.; Gorrell, M.D. The dipeptidyl peptidase IV family in cancer and cell biology. *FEBS J.* **2010**, *277*, 1126–1144. [CrossRef] [PubMed]
5. Zhang, H.; Maqsudi, S.; Rainczuk, A.; Duffield, N.; Lawrence, J.; Keane, F.M.; Justa-Schuch, D.; Geiss-Friedlander, R.; Gorrell, M.D.; Stephens, A.N. Identification of novel dipeptidyl peptidase 9 substrates by two-dimensional differential in-gel electrophoresis. *FEBS J.* **2015**, *282*, 3737–3757. [CrossRef]
6. Beckenkamp, A.; Davies, S.; Willig, J.B.; Buffon, A. DPPIV/CD26: A tumor suppressor or a marker of malignancy? *Tumour Biol.* **2016**, *37*, 7059–7073. [CrossRef]
7. Rainczuk, A.; Rao, J.R.; Gathercole, J.L.; Fairweather, N.J.; Chu, S.; Masadah, R.; Jobling, T.W.; Deb-Choudhury, S.; Dyer, J.; Stephens, A.N. Evidence for the antagonistic form of CXC-motif chemokine CXCL10 in serous epithelial ovarian tumours. *Int. J. Cancer* **2014**, *134*, 530–541. [CrossRef]
8. Kajiyama, H.; Shibata, K.; Terauchi, M.; Ino, K.; Nawa, A.; Kikkawa, F. Involvement of DPPIV/CD26 in epithelial morphology and suppressed invasive ability in ovarian carcinoma cells. *Ann. N. Y. Acad. Sci.* **2006**, *1086*, 233–240. [CrossRef]
9. Kajiyama, H.; Kikkawa, F.; Maeda, O.; Suzuki, T.; Ino, K.; Mizutani, S. Increased expression of dipeptidyl peptidase IV in human mesothelial cells by malignant ascites from ovarian carcinoma patients. *Oncology* **2002**, *63*, 158–165. [CrossRef]
10. Kikkawa, F.; Kajiyama, H.; Shibata, K.; Ino, K.; Nomura, S.; Mizutani, S. Dipeptidyl peptidase IV in tumor progression. *Biochim. Biophys. Acta-Proteins Proteom.* **2005**, *1751*, 45–51. [CrossRef]
11. Kim, K.S.; Sengupta, S.; Berk, M.; Kwak, Y.G.; Escobar, P.F.; Belinson, J.; Mok, S.C.; Xu, Y. Hypoxia enhances lysophosphatidic acid responsiveness in ovarian cancer cells and lysophosphatidic acid induces ovarian tumor metastasis in vivo. *Cancer Res.* **2006**, *66*, 7983–7990. [CrossRef] [PubMed]
12. McEvoy, L.M.; O'Toole, S.A.; Spillane, C.D.; Martin, C.M.; Gallagher, M.F.; Stordal, B.; Blackshields, G.; Sheils, O.; O'Leary, J.J. Identifying novel hypoxia-associated markers of chemoresistance in ovarian cancer. *BMC Cancer* **2015**, *15*, 547. [CrossRef] [PubMed]
13. Braicu, E.I.; Luketina, H.; Richter, R.; Castillo-Tong, D.C.; Lambrechts, S.; Mahner, S.; Concin, N.; Mentze, M.; Zeillinger, R.; Vergote, I.; et al. HIFI α is an independent prognostic factor for overall survival in advanced primary epithelial ovarian cancer–A study of the OVCAD consortium. *Onco Targets Ther.* **2014**, *7*, 1563–1569. [CrossRef] [PubMed]
14. Dang, D.T.; Chun, S.Y.; Burkitt, K.; Abe, M.; Chen, S.; Havre, P.; Mabjeesh, N.J.; Heath, E.I.; Vogelzang, N.J.; Cruz-Correa, M.; et al. Hypoxia-inducible factor-1 target genes as indicators of tumor vessel response to vascular endothelial growth factor inhibition. *Cancer Res.* **2008**, *68*, 1872–1880. [CrossRef]

15. Röhrborn, D.; Eckel, J.; Sell, H. Shedding of dipeptidyl peptidase 4 is mediated by metalloproteases and up-regulated by hypoxia in human adipocytes and smooth muscle cells. *FEBS Lett.* **2014**, *588*, 3870–3877. [CrossRef]
16. Chowdhury, H.H.; Velebit, J.; Radic, N.; Francic, V.; Kreft, M.; Zorec, R. Hypoxia Alters the Expression of Dipeptidyl Peptidase 4 and Induces Developmental Remodeling of Human Preadipocytes. *J. Diabetes Res.* **2016**, *2016*, 7481470. [CrossRef] [PubMed]
17. Tilan, J.U.; Lu, C.; Galli, S.; Izycka-Swieszewska, E.; Earnest, J.P.; Shabbir, A.; Everhart, L.M.; Wang, S.; Martin, S.; Horton, M.; et al. Hypoxia shifts activity of neuropeptide Y in Ewing sarcoma from growth-inhibitory to growth-promoting effects. *Oncotarget* **2013**, *4*, 2487–2501. [CrossRef] [PubMed]
18. Domcke, S.; Sinha, R.; Levine, D.A.; Sander, C.; Schultz, N. Evaluating cell lines as tumour models by comparison of genomic profiles. *Nat. Commun.* **2013**, *4*, 2126. [CrossRef] [PubMed]
19. Beaufort, C.M.; Helmijr, J.C.A.; Piskorz, A.M.; Hoogstraat, M.; Ruigrok-Ritstier, K.; Besselink, N.; Murtaza, M.; van IJcken, W.F.J.; Heine, A.A.J.; Smid, M.; et al. Ovarian cancer cell line panel (OCCP): Clinical importance of in vitro morphological subtypes. *PLoS ONE* **2014**, *9*, e103988. [CrossRef]
20. Shaw, T.J.; Senterman, M.K.; Dawson, K.; Crane, C.A.; Vanderhyden, B.C. Characterization of intraperitoneal, orthotopic, and metastatic xenograft models of human ovarian cancer. *Mol. Ther.* **2004**, *10*, 1032–1042. [CrossRef]
21. Lee, S.; Garner, E.I.; Welch, W.R.; Berkowitz, R.S.; Mok, S.C. Over-expression of hypoxia-inducible factor 1 alpha in ovarian clear cell carcinoma. *Gynecol. Oncol.* **2007**, *106*, 311–317. [CrossRef] [PubMed]
22. Page-McCaw, A.; Ewald, A.J.; Werb, Z. Matrix metalloproteinases and the regulation of tissue remodelling. *Nat. Rev. Mol. Cell Biol.* **2007**, *8*, 221–233. [CrossRef] [PubMed]
23. Filatova, N.A.; Kirpichnikova, K.M.; Vakhromova, E.A.; Gamalei, I.A. [Effect of alpha-lipoic acid on the sensitivity of transformed fibroblasts to lysis by natural killer cells. Comparison with NAC action]. *Tsitologiia* **2009**, *51*, 398–402. [PubMed]
24. Chowdhury, H.H.; Velebit, J.; Mekjavic, I.B.; Eiken, O.; Kreft, M.; Zorec, R. Systemic Hypoxia Increases the Expression of DPP4 in Preadipocytes of Healthy Human Participants. *Exp. Clin. Endocrinol. Diabetes* **2018**, *126*, 91–95. [CrossRef] [PubMed]
25. Lambeir, A.M.; Durinx, C.; Scharpé, S.; De Meester, I. Dipeptidyl-peptidase IV from bench to bedside: An update on structural properties, functions, and clinical aspects of the enzyme DPP IV. *Crit. Rev. Clin. Lab. Sci.* **2003**, *40*, 209–294. [CrossRef] [PubMed]
26. Bauvois, B.; Djavaheri-Mergny, M.; Rouillard, D.; Dumont, J.; Wietzerbin, J. Regulation of CD26/DPPIV gene expression by interferons and retinoic acid in tumor B cells. *Oncogene* **2000**, *19*, 265–272. [CrossRef]
27. Erickson, R.H.; Lai, R.S.; Kim, Y.S. Role of hepatocyte nuclear factor 1alpha and 1beta in the transcriptional regulation of human dipeptidyl peptidase IV during differentiation of Caco-2 cells. *Biochem. Biophys. Res. Commun.* **2000**, *270*, 235. [CrossRef] [PubMed]
28. Kumar, G.K.; Klein, J.B. Analysis of expression and posttranslational modification of proteins during hypoxia. *J. Appl. Physiol.* **2004**, *96*, 1178–1186. [CrossRef]
29. Zhong, J.; Gong, Q.; Goud, A.; Srinivasamaharaj, S.; Rajagopalan, S. Recent Advances in Dipeptidyl-Peptidase-4 Inhibition Therapy: Lessons from the Bench and Clinical Trials. *J. Diabetes Res.* **2015**, *2015*. [CrossRef]
30. Zhang, H.; Yang, Q.; Lian, X.; Jiang, P.; Cui, J. Hypoxia-Inducible Factor-1alpha (HIF-1alpha) Promotes Hypoxia-Induced Invasion and Metastasis in Ovarian Cancer by Targeting Matrix Metallopeptidase 13 (MMP13). *Med. Sci. Monit.* **2019**, *25*, 7202–7208. [CrossRef]
31. Nargis, T.; Kumar, K.; Ghosh, A.R.; Sharma, A.; Rudra, D.; Sen, D.; Chakrabarti, S.; Mukhopadhyay, S.; Ganguly, D.; Chakrabarti, P. KLK5 induces shedding of DPP4 from circulatory Th17 cells in type 2 diabetes. *Mol. Metab.* **2017**, *6*, 1529–1539. [CrossRef] [PubMed]
32. Fasolato, S.; Trevellin, E.; Ruvoletto, M.; Granzotto, M.; Zanus, G.; Boscaro, E.; Babetto, E.; Terrin, L.; Battocchio, M.A.; Ciscato, F.; et al. SerpinB3 induces dipeptidyl-peptidase IV/CD26 expression and its metabolic effects in hepatocellular carcinoma. *Life Sci.* **2018**, *200*, 134. [CrossRef] [PubMed]
33. Fortelny, N.; Cox, J.H.; Kappelhoff, R.; Starr, A.E.; Lange, P.F.; Pavlidis, P.; Overall, C.M. Network Analyses Reveal Pervasive Functional Regulation Between Proteases in the Human Protease Web (Analysis of the Interconnected Human Protease Web). *PLoS Biol.* **2014**, *12*, e1001869. [CrossRef] [PubMed]

34. Lam, C.S.-C.; Cheung, A.H.-K.; Wong, S.K.-M.; Wan, T.M.-H.; Ng, L.; Chow, A.K.-M.; Cheng, N.S.-M.; Pak, R.C.-H.; Li, H.-S.; Man, J.H.-W.; et al. Prognostic significance of CD26 in patients with colorectal cancer. *PLoS ONE* **2014**, *9*, e98582. [CrossRef] [PubMed]
35. Larrinaga, G.; Perez, I.; Sanz, B.; Beitia, M.; Errarte, P.; Fernandez, A.; Blanco, L.; Etxezarraga, M.C.; Gil, J.; Lopez, J.I. Dipeptidyl-Peptidase IV Activity Is Correlated with Colorectal Cancer Prognosis. *PLoS ONE* **2015**, *10*, e0119436. [CrossRef] [PubMed]
36. Matić, I.Z.; Đorđić, M.; Grozdanić, N.; Damjanović, A.; Kolundžija, B.; Erić-Nikolić, A.; Džodić, R.; Šašić, M.; Nikolić, S.; Dobrosavljević, D.; et al. Serum activity of DPPIV and its expression on lymphocytes in patients with melanoma and in people with vitiligo. *BMC Immunol.* **2012**, *13*, 48. [CrossRef] [PubMed]
37. Cordero, O.J.; Salgado, F.J.; Nogueira, M. On the origin of serum CD26 and its altered concentration in cancer patients. *Cancer Immunol. Immunother.* **2009**, *58*, 1723. [CrossRef]
38. Barreira da Silva, R.; Laird, M.E.; Yatim, N.; Fiette, L.; Ingersoll, M.A.; Albert, M.L. Dipeptidylpeptidase 4 inhibition enhances lymphocyte trafficking, improving both naturally occurring tumor immunity and immunotherapy. *Nat. Immunol.* **2015**, *16*, 850–858. [CrossRef]
39. Rainczuk, A.; Rao, J.; Gathercole, J.; Stephens, A.N. The emerging role of CXC chemokines in epithelial ovarian cancer. *Reproduction* **2012**, *144*, 303–317. [CrossRef]
40. Sun, Y.-X.; Pedersen, E.; Shiozawa, Y.; Havens, A.; Jung, Y.; Wang, J.; Pienta, K.; Taichman, R. CD26/dipeptidyl peptidase IV regulates prostate cancer metastasis by degrading SDF-1/CXCL12. *Off. J. Metastasis Res. Soc.* **2008**, *25*, 765–776. [CrossRef]
41. Russo, J.W.; Gao, C.; Bhasin, S.S.; Voznesensky, O.S.; Calagua, C.; Arai, S.; Nelson, P.S.; Montgomery, B.; Mostaghel, E.A.; Corey, E.; et al. Downregulation of Dipeptidyl Peptidase 4 Accelerates Progression to Castration-Resistant Prostate Cancer. *Cancer Res.* **2018**, *78*, 6354. [CrossRef] [PubMed]
42. Busek, P.; Stremenova, J.; Sromova, L.; Hilser, M.; Balaziova, E.; Kosek, D.; Trylcova, J.; Strnad, H.; Krepela, E.; Sedo, A. Dipeptidyl peptidase-IV inhibits glioma cell growth independent of its enzymatic activity. *Int. J. Biochem. Cell Biol.* **2012**, *44*, 738–747. [CrossRef] [PubMed]
43. Busek, P.; Stremenova, J.; Krepela, E.; Sedo, A. Modulation of substance P signaling by dipeptidyl peptidase-IV enzymatic activity in human glioma cell lines. *Physiol. Res.* **2008**, *57*, 443–449. [PubMed]
44. Tseng, C.-H. Sitagliptin May Reduce Breast Cancer Risk in Women With Type 2 Diabetes. *Clin. Breast Cancer* **2017**, *17*, 211–218. [CrossRef] [PubMed]
45. Hollande, C.; Boussier, J.; Ziai, J.; Nozawa, T.; Bondet, V.; Phung, W.; Lu, B. Inhibition of the dipeptidyl peptidase DPP4 (CD26) reveals IL-33-dependent eosinophil-mediated control of tumor growth. *Nat. Immunol.* **2019**, *20*, 257. [CrossRef] [PubMed]
46. Cook, S.J.; Lee, Q.; Wong, A.C.; Spann, B.C.; Vincent, J.N.; Wong, J.J.; Schlitzer, A.; Gorrell, M.D.; Weninger, W.; Roediger, B. Differential chemokine receptor expression and usage by pre-cDC1 and pre-cDC2. *Immunol. Cell Biol.* **2018**, *96*, 1131–1139. [CrossRef] [PubMed]
47. Augoff, K.; Hryniewicz-Jankowska, A.; Tabola, R.; Czapla, L.; Szelachowski, P.; Wierzbicki, J.; Grabowski, K.; Sikorski, A.F. Upregulated expression and activation of membrane-associated proteases in esophageal squamous cell carcinoma. *Oncol. Rep.* **2014**, *31*, 2820–2826. [CrossRef]
48. Beckenkamp, A.; Willig, J.B.; Santana, D.B.; Nascimento, J.; Paccez, J.D.; Zerbini, L.F.; Bruno, A.N.; Pilger, D.A.; Wink, M.R.; Buffon, A. Differential Expression and Enzymatic Activity of DPPIV/CD26 Affects Migration Ability of Cervical Carcinoma Cells. *PLoS ONE* **2015**, *10*, e0134305. [CrossRef] [PubMed]
49. Lee, J.J.; Wang, T.Y.; Liu, C.L.; Chien, M.N.; Chen, M.J.; Hsu, Y.C.; Leung, C.H.; Cheng, S.P. Dipeptidyl Peptidase IV as a Prognostic Marker and Therapeutic Target in Papillary Thyroid Carcinoma. *J. Clin. Endocrinol. Metab.* **2017**, *102*, 2930–2940. [CrossRef] [PubMed]
50. Cheung, A.H.; Iyer, D.N.; Lam, C.S.; Ng, L.; Wong, S.K.M.; Lee, H.S.; Wan, T.; Man, J.; Chow, A.K.M.; Poon, R.T.; et al. Emergence of CD26+ Cancer Stem Cells with Metastatic Properties in Colorectal Carcinogenesis. *Int. J. Mol. Sci.* **2017**, *18*, 1106. [CrossRef] [PubMed]
51. Raspadori, D.; Pacelli, P.; Sicuranza, A.; Abruzzese, E.; Iurlo, A.; Cattaneo, D.; Gozzini, A.; Galimberti, S.; Barate, C.; Pregno, P.; et al. Flow Cytometry Assessment of CD26(+) Leukemic Stem Cells in Peripheral Blood: A Simple and Rapid New Diagnostic Tool for Chronic Myeloid Leukemia. *Cytom. B Clin. Cytom.* **2019**, 294–299. [CrossRef] [PubMed]

52. Shishido, A.; Mori, S.; Yokoyama, Y.; Hamada, Y.; Minami, K.; Qian, Y.; Wang, J.; Hirose, H.; Wu, X.; Kawaguchi, N.; et al. Mesothelial cells facilitate cancer stemlike properties in spheroids of ovarian cancer cells. *Oncol. Rep.* **2018**, *40*, 2105–2114. [CrossRef] [PubMed]
53. Sarraj, M.A.; Chua, H.K.; Umbers, A.; Loveland, K.L.; Findlay, J.K.; Stenvers, K.L. Differential expression of TGFBR3 (betaglycan) in mouse ovary and testis during gonadogenesis. *Growth Factors* **2007**, *25*, 334–345. [CrossRef]
54. Schindelin, J.; Arganda-Carreras, I.; Frise, E.; Kaynig, V.; Longair, M.; Pietzsch, T.; Preibisch, S.; Rueden, C.; Saalfeld, S.; Schmid, B. Fiji: An open-source platform for biological-image analysis. *Nat. Methods* **2012**, *9*, 676–682. [CrossRef] [PubMed]
55. Rueden, C.T.; Schindelin, J.; Hiner, M.C.; DeZonia, B.E.; Walter, A.E.; Arena, E.T.; Eliceiri, K.W. ImageJ2: ImageJ for the next generation of scientific image data. *BMC Bioinform.* **2017**, *18*, 529. [CrossRef]

3.1 Conclusions

Our publication in the *International Journal of Medical Sciences (IJMS)* reports a previously undescribed influence of hypoxic conditions on the function and regulation of the cell surface protease DPP4 in ovarian cancer cells. As a hallmark of many solid malignancies, hypoxia represents an opportunity to mimic *in vitro* some of the conditions that are observed in ovarian cancers *in vivo.* Our research identified an inverse correlation between sDPP4 expression and DPP4 activity under conditions of chronic hypoxia, where specific activity was a more accurate functional output than expression or activity alone. This study highlights that DPP4 expression should be assessed concurrently with enzyme activity in order to gain a greater understanding of the functional status, and therefore potential role of DPP4 in any pathological context. There is much to be discovered surrounding the intricacies of ovarian disease in relation to diagnosis, treatment and management. We propose that DPP4 regulation, expression and activity are closely linked to the hypoxic conditions in the ovarian TME, and that future research may benefit from investigating sDPP4 as a potential biomarker in disease. The research methods employed in this chapter utilise the basic biological features of ovarian cancer cells and enable *in vitro* tools to identify the functional consequences of specific growth conditions. This research will be useful to inform further studies investigating the role of DPP4 in ovarian cancer and other solid tumour types. Future research should focus on understanding the underlying molecular basis of how DPP4 influences ovarian tumour growth via the use of DPP4 variant cell lines *in vivo*. Unfortunately, these studies could not be completed during this PhD due to time constraints; however, mouse cell lines including DPP4 knockout, DPP4 enzyme inactive and DPP4 overexpressing have been generated in our laboratory for prospective *in vivo* experiments.

Chapter Four

Inhibition of DPP4 activity in a metastatic ovarian cancer mouse model

Preface

The data collected from Aim 1 of this project suggests that DPP4 expression and activity may be altered in the ovarian cancer microenvironment[283]. We showed that hypoxia significantly alters DPP4 expression and activity in ovarian cancer cells, and specific changes to DPP4 abundance and activity occurs under these conditions. Therefore, we were interested in further investigating the functional consequences of changes to DPP4 activity *in vivo.* The current understanding of the multifaceted role of DPP4 in ovarian cancer was discussed in Chapter 1, where we highlighted potential gaps in knowledge relating to DPP4 expression and activity.

The work presented in this chapter directly aligns with Aim 2 of my PhD project - To understand how inhibition of DPP4 activity influences metastatic tumour progression and anti-tumour immune responses *in vivo.* Recent work in our lab demonstrated that DPP4 inhibition via the clinically approved, orally available inhibitor sitagliptin[284] in a primary ovarian cancer mouse model prolonged survival and enhances the anti-tumour immune response (see Appendix D)[285]. Experiments performed in this chapter build further on these previous studies using a metastatic ovarian cancer mouse model, which accurately represents the more common clinical scenario of diagnosis with late-stage disease.

Using the syngeneic ID8 model of ovarian cancer also allowed us to investigate the immunological effects of DPP4 inhibition in mice with a functional immune system. Data provided in this chapter provides further evidence of the role of DPP4 activity in ovarian tumours and directly demonstrates the effects of DPP4 inhibition on metastatic tumour development and anti-tumour immune responses *in vivo.* We found that treatment with sitagliptin in the context of metastatic disease prolonged survival time and altered various immune parameters including the peripheral cytokine landscape, percentages of lymphocyte populations in the blood, spleen and peritoneal cavity, and infiltrating T cells within ID8

tumours. Data from this chapter provides evidence of the efficacy of sitagliptin as an immunomodulatory therapy and its potential to re-sensitise tumours to other immunotherapies.

4.1 Introduction

The leading cause of death from ovarian cancer is recurrence accompanied by metastatic disease, where tumours invade healthy tissue within the peritoneal cavity and surrounding organs[84]. Unfortunately, most recurrent ovarian tumours are resistant to conventional therapies. Treatment of metastatic ovarian cancer remains the most challenging aspect of disease management due to the highly heterogenous nature of most ovarian tumours and the tumour microenvironment (TME)[1,286,287]. The complexities of the ovarian cancer TME provides optimal conditions for metastatic disease and therefore represents an opportunity for therapeutic intervention[288]. Targetable pro-tumorigenic pathways include those that facilitate the initiation, progression and invasion of ovarian cancer, and others that promote resistance to existing therapies or immune evasion[289]. The recent emergence of targeted therapies including PARP inhibitors such as olaparib and anti-angiogenic treatments such as bevacizumab only provide a modest improvement to overall survival in some patients[1]. As a result, recent research has focused on various other approaches to treat ovarian cancer, including those that target the immune system.

Although the ovarian cancer TME is highly intrinsically immunosuppressive, epithelial ovarian cancers remain immunogenic even at late stages[290,291]. Therefore, the host immune system plays a critical role in patient outcome[127,155,290,292]. The ovarian cancer TME consists of a complex network of several lymphocytic populations including resident and infiltrating T cells, regulatory T cells, myeloid-derived suppressor cells (MDSCs), macrophages, natural killer (NK) cells and dendritic cells (DCs) which are regulated by an abundance of cytokines and chemokines[111,293]. Although multiple aspects of the immune system contribute to the overall response, evidence suggests that a major contributor to prolonged survival in ovarian cancer is the presence of immune responsive T cells[129]. Indeed, several studies have demonstrated that increased levels tumour infiltrating lymphocytes (TILs) is correlated with improved clinical outcome[126,127,129]. This is also supported by the fact that ‘immunoreactive’ ovarian cancers are

associated with a more favourable prognosis[49]. These tumours exhibit a high abundance of intratumoural T cells and have a distinct genetic immune signature including increased expression of markers which are associated with a positive T effector cell response (e.g. granzyme B) and T cell trafficking (e.g. CXCL9)[49]. Components of the local TME including stromal cell interactions, cytokine/chemokine signalling and ECM remodelling also significantly contributes to the immune response and tumour behaviour. Consequently, various strategies aimed at targeting the immunosuppressive TME and/or harnessing the immune system in ovarian cancer are under development[294].

In response to their remarkable efficacy in other malignancies, a significant area of immunotherapy research in EOC is focused on immune checkpoint inhibitors (ICIs). ICIs are monoclonal antibodies which block immune checkpoints such as those that limit the activity of cytotoxic T lymphocytes, for example cytotoxic T lymphocyte associated protein 4 (CTLA-4), the programmed death 1 (PD-1) receptor or its ligand (PD-L1). Unfortunately, clinical trials using ICIs as a single agent have obtained minimal response rates of 10-15% in patients with ovarian cancer[295], and have failed to progress to further trials as a monotherapy. ICIs and combination therapies are discussed in further detail in Chapter 5. There is also evidence that women with ovarian cancer may benefit from Adoptive Cell Therapy (ACT), where peripheral or tumour-associated leukocytes are isolated from the patient, activated, modified and amplified *in vitro* and then reinfused to mount an anti-tumour response[296]. Several variations of this technique have been trialled in ovarian cancer, including Cytokine-Induced Killer (CIK) ACT, which was shown to improve PFS in a phase II study[297]. Similarly, ACT with infusion of autologous TILs in women with platinum-resistant, recurrent ovarian cancer have exhibited promise in some small cohorts[298,299]. More recent improvements to ACT involve the expression of a chimeric antigen receptor (CAR) and have demonstrated tumour clearance in pre-clinical models; however, this technology still requires extensive additional research. Other immunotherapeutic agents include cancer vaccines, which is usually a tumour-associated antigen (TAA) designed to stimulate an antigen-specific, effector and memory T cell anti-

tumour immune response. Some potential cancer vaccine targets include NY-ESO-1, mucin-1 (MUC-1), mesothelin, p53 and human epidermal growth factor receptor (HER2). A phase II clinical trial evaluating the NY-ESO-1 based vaccine demonstrated clinical benefit via improved OS in newly diagnosed ovarian cancer patients[300]. Although numerous of the immunotherapies described above are involved in clinical trials, there are no current immunotherapies approved for standard-of-care therapy for ovarian cancer patients. Therefore, widespread research continues to enhance current methods and to identify novel mechanisms and targetable pathways to modulate the immune microenvironment, increase the anti-tumour immune response and ultimately improve the clinical outcome for women with ovarian cancer.

In order to develop novel immune-based therapies, appropriate experimental models must be utilised. Various strategies exist to model the ovarian TME *in vitro*, including 3D matrices, spheroids, co-culture of malignant cells with mesothelial cells, organoids and explants[301]. However, a key aspect of investigating new treatments and understanding the immune response is to accurately recapitulate the human form of disease in pre-clinical models. There are several well-established experimental murine models of ovarian cancer, however, an important consideration is the method of implantation of cancer cells. Shaw and colleagues investigated xenograft models with several different ovarian cancer cell lines and reported that tumours resulting from intraperitoneal (IP) injection of cells demonstrated a similar pattern of dissemination to human disease, where tumour deposits were observed around the liver, spleen and peritoneal wall[302]. In 2000, Roby and colleagues identified that late passage mouse ovarian surface epithelial cells (MOSECs) formed tumours *in vivo* in immunocompetent mice[265]. Their model demonstrated that syngeneic C57BL/6 mice which received IP injection of MOSECs formed ascites fluid after 22-48 days and macroscopic tumours were observed in sites analogous to that of late-stage human ovarian disease, such as the omentum, bowel, diaphragm, kidneys, pancreas, stomach and peritoneal wall[265]. The clonal ID8 cell line exhibited the highest tumour load of all late passage MOSECs[265], and was further shown to

accurately depict the peritoneal metastasis observed in high-grade serous ovarian cancer (HGSOC), evidenced by functional vasculature to tumour deposits and the presence of infiltrating leukocytes including T cells and macrophages[303]. The ID8 cell line is therefore commonly used as a syngeneic immunocompetent mouse model of human ovarian cancer for the development of immunotherapies and to investigate immune interactions in the TME[294].

Dipeptidyl peptidase 4 (DPP4; CD26) is highly specific serine protease that is expressed on the surface of several cell types and is enzymatically capable of cleaving the two N-terminal amino acids from a protein with proline or alanine in the penultimate position[277,304]. DPP4 has various roles in adhesion/co-stimulation and immune modulation via its independent abilities as a protein-binding molecule and enzyme[263]. DPP4 is active in multiple pathologies but has been extensively studied for its role in type 2 diabetes. DPP4-mediated cleavage and inactivation of the incretin hormone glucagon-like peptide-1 (GLP-1) contributes to insulin resistance[305] and has prompted the development of various DPP4 inhibitors to control glucose levels[306]. Through its proteolytic function, DPP4 also cleaves pro-inflammatory chemokines to modulate leukocyte migration and chemotaxis[307]. For example, N-terminal truncation of CXCL10 by DPP4 produces an antagonistic form of the chemokine, which impairs CXCR3-mediated chemotaxis[242] and lymphocyte migration in mice[308]. There are conflicting reports of the specific role(s) of DPP4 in ovarian cancer, likely due to its functional versatility. Overexpression of DPP4 has been reported in epithelial ovarian tumours[244] and data from our laboratory suggests that DPP4 activity may be altered in the ovarian cancer microenvironment[283]. In addition, reports show that the truncated, antagonistic form of CXCL10 is present in high abundance in the ovarian cancer tumour epithelium[244], implicating DPP4 as a potential moderator of the immune response in ovarian tumours and suggesting its potential as a therapeutic target. Prospective studies have demonstrated that DPP4 inhibition *in vivo* preserves the full-length, bioactive form of CXCL10[309], highlighting the opportunity to exploit DPP4 inhibition as a potential treatment strategy to restore immune function in cancers where DPP4 is overexpressed. Retrospective analyses have found that

sitagliptin use for at least 1 year may significantly reduce the risk of breast and prostate cancer in patients with type 2 diabetes[310,311].

More recently, the effect of DPP4 inhibition in pre-clinical models of malignancies has been explored. DPP4 inhibition via sitagliptin in rats with liver cancer demonstrated anti-cancer activity and improved liver pathology by inhibition of inflammation and NF-κB activation[312]. Similarly, sitagliptin treatment in an induced colon cancer rat model significantly reduced the number of precancerous lesions and reduced reactive oxygen species (ROS) in the blood compared to controls, suggesting a potential protective effect of sitagliptin against colon carcinogenesis[249]. Sitagliptin also significantly reduced tumour growth in a melanoma mouse model[308]. The authors showed that sitagliptin increased the concentration of CXCL10 in tumours, which correlated with a significant increase in tumour infiltrating CD4+ and CD8+ T cells[308]. A similar phenomenon was demonstrated in hepatocellular carcinoma mouse models, where preservation of the full-length CXCL10 protein promoted CXCR3-mediated chemotaxis of T cells and NK cells towards tumours[313]. Hollande and colleagues demonstrated a distinct mechanism of DPP4 inhibition whereby sitagliptin exhibited eosinophil-dependent anti-tumour activity in models of hepatocellular carcinoma and breast cancer[259]. Together this research signifies an important role of DPP4 activity in the immunoregulation of various malignancies but highlights the fact the functional consequences of DPP4 inhibition are likely to be cancer-specific and result in complex changes to multiple immune parameters.

Previous research by our laboratory demonstrated that DPP4 inhibition in a primary, syngeneic ovarian cancer mouse model significantly enhanced the anti-tumour immune response (Figure 4.1**;** data from Wilson *et al.*, (2021) - see Appendix D)[285]. Briefly, sitagliptin caused a significant increase in the percentage of activated (CD69+) CD8+ T cells in the peritoneal cavity (Figure 4.1A). An increased abundance of activated CD8+ T cells was also localised to the primary tumour (Figure 4.1B). Furthermore, proliferative CD8+ and CD4+ T cells were increased in the spleen and peritoneal cavity in sitagliptin-treated mice (Figure

4.1C, D). Sitagliptin also prolonged survival in tumour-bearing mice, where treated mice had a median survival of 138 days compared to 108 days in the untreated controls (Figure 4.1E). In this study, intrabursal implantation of cancer cells was utilised to accurately recapitulate the early stages of ovarian tumorigenesis.

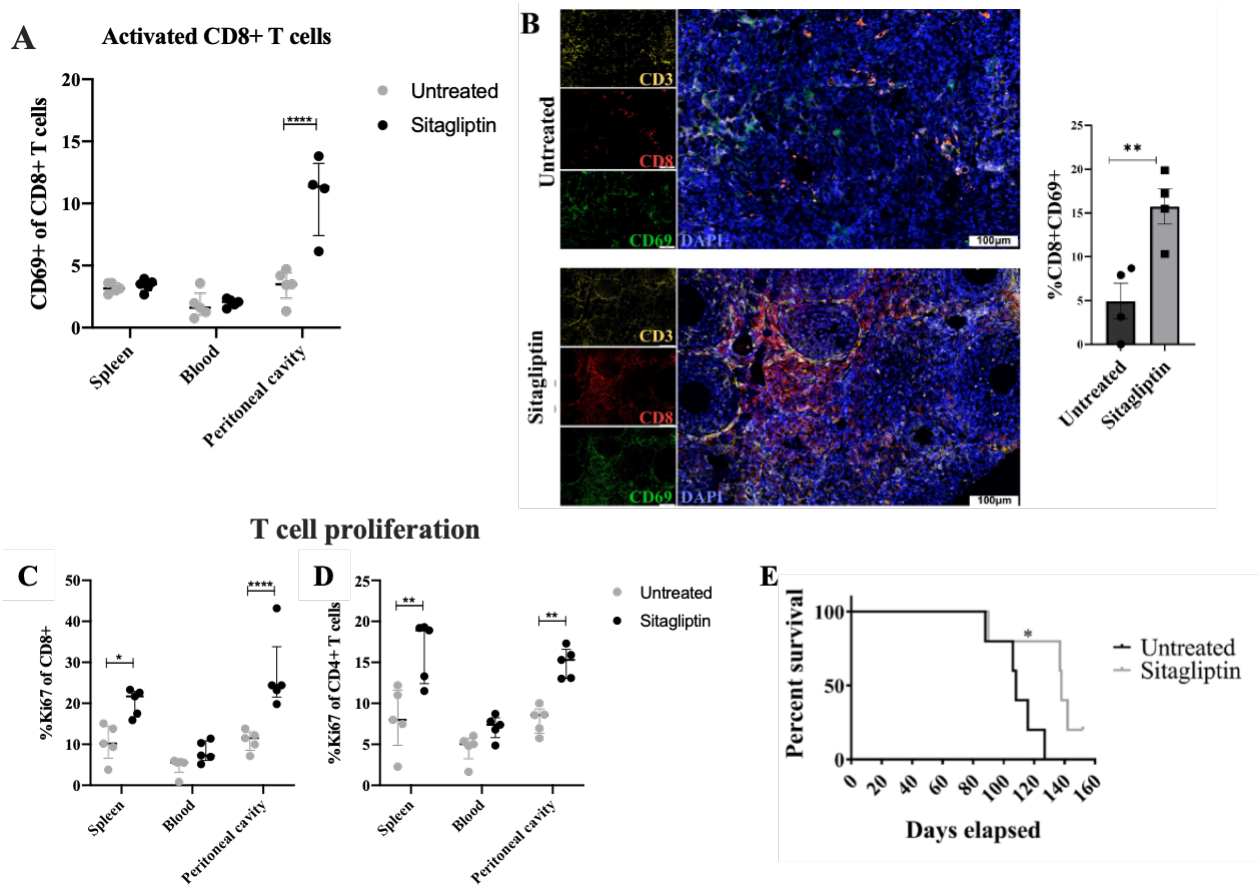

Figure 4.1. DPP4 inhibition alters leukocyte populations and prolongs survival in a primary ovarian cancer mouse model. *ID8 cells were implanted into the ovarian bursa of female C57BL/6 mice and daily oral sitagliptin treatment (50mg/kg) was commenced two weeks post-tumour-inoculation. Leukocytes were isolated from the spleen, blood and peritoneal cavity of ID8 tumour-bearing mice at week 4 post-inoculation and examined by flow cytometry. Activated T cells demonstrated by (A) percentage of CD69+ CD8+ T cells and (B) representative images of ovarian tumour sections stained with CD3 (yellow), CD8 (red) and CD69 (green). Nuclei are stained with DAPI (blue). Bar graphs show the percentage area of ovarian tumour sections stained with CD8+CD69+. Percentages of proliferating (Ki67+) (C) CD8+ T cells and (D) CD4+ T cells. (E) Kaplan-Meier curve and log-rank test of overall survival analysis. Data are presented as mean ± SD, n=5. * = p<0.05; ** = p<0.01; *** = p<0.001; **** = p<0.0001. Figures from Wilson et al., (2021)*[281].

However, as mentioned earlier, ovarian cancer mouse models involving intraperitoneal implantation of cancer cells are widely acknowledged as metastatic disease models and can provide effective pre-clinical evidence of drug efficacy during late-stage disease. Therefore, in the current study we sought to investigate the immune response to DPP4 inhibition in a metastatic, syngeneic ovarian cancer mouse model via treatment with the clinically approved inhibitor sitagliptin. We hypothesised that DPP4 inhibition would improve the anti-tumour immune response in late-stage disease via enhanced lymphocyte trafficking *in vivo*.

4.2 Results

Female 6-8-week-old C57BL/6J mice were inoculated with 5.0 x 10^6 ID8 cells by intraperitoneal (IP) injection. Tumours were allowed to develop for 2 weeks, after which mice commenced daily oral sitagliptin treatment (DPP4 inhibition) at a dose of 50mg/kg body weight/day until endpoint. Mice were humanely culled at week 4 and week 6 post-tumour-inoculation and at humane endpoint (Figure 4.2). These time points were chosen based on previous work in our laboratory indicating their suitability to monitor disease progression and immune status. Sitagliptin had no significant effect on body weight or circumference (Supplementary Figure S4.1). Inhibition of DPP4 activity by sitagliptin *in vivo* was previously confirmed by our laboratory[285]. At week 4 and week 6, serum was collected and analysed for circulating levels of various cytokines, tumours were harvested for infiltrating leukocyte analysis and leukocytes from the blood, spleen and peritoneal cavity were isolated and evaluated by flow cytometry for specific immune cell populations including CD8+ T cells, CD4+ T cells, proliferating and activated T cells, regulatory T cells (Tregs), CD103+, CCR4+ and PD-1+ Tregs, myeloid-derived suppressor cells (MDSCs) and activated macrophages (Supplementary Figure S4.2).

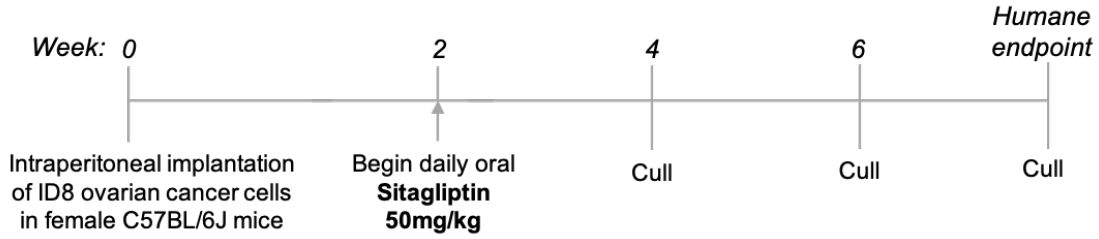

Figure 4.2. Schematic representation of the experimental timeline for sitagliptin treatment in a metastatic ovarian cancer mouse model.

4.2.1 Sitagliptin prolonged survival in mice with metastatic ovarian disease

One of the most important parameters to evaluate the clinical efficacy of an ovarian cancer treatment is overall survival. The median overall survival for the most commonly diagnosed subtype, HGSOC, is less than 4 years[314]. As previously mentioned, one of the most positive

predictors of overall survival in ovarian cancer is the presence of infiltrating T cells[315]**.** Recently published data in our laboratory suggested that sitagliptin improves T cell-mediated immunity and lymphocyte infiltration in primary ovarian tumours[285]. Therefore, we also evaluated the effect of sitagliptin on the time taken to reach humane endpoint in a metastatic ovarian cancer model, which was used as a measurement for overall survival.

Kaplan-Meier curves indicated that sitagliptin significantly increased survival in metastatic ID8 tumour-bearing mice, where the median survival time of mice treated with sitagliptin was 67 days, compared to 63 days in untreated controls (Figure 4.3; n=6, p-value = 0.0255). This small (~11%) but significant increase in survival time is similar to what we observed in primary disease[285] and suggests that treatment with sitagliptin can potentially increase overall survival in patients at all stages of disease.

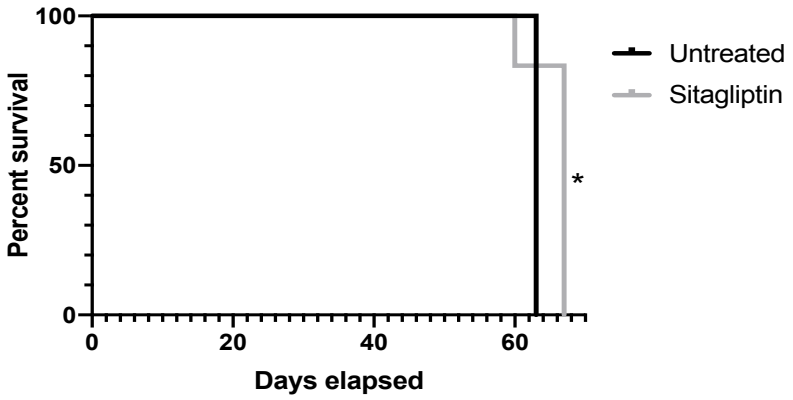

Figure 4.3. Survival for mice treated with sitagliptin compared to untreated controls. *Mice bearing metastatic ID8 tumours commenced daily sitagliptin treatment 2 weeks-post-inoculation and were culled at humane endpoint. The days elapsed until humane endpoint was recorded. Survival represented by Kaplan-Meier curves and log-rank test of overall survival analysis between treatment groups; n=6, *p<0.05.*

4.2.2 Sitagliptin altered the cytokine landscape in metastatic ovarian disease

We next assessed the effect of sitagliptin on the extent of the overall immune response *in vivo* by comparing the abundance of circulating cytokines between untreated and sitagliptin-treated mice. Analysis of serum from mice culled at week 6 that were treated with sitagliptin revealed a panel of 20 differentially expressed cytokines (Figure 4.4A). Amongst the significantly upregulated cytokines were IFN-ɣ, CXCL12 and IL-6 (Supplementary Figure S4.3). Upon STRING network analysis[316] of all differentially expressed cytokines, the data indicated enrichment of networks involved in chemokine signalling, IL-17 signalling and TNF signalling pathways (Figure 4.4B).

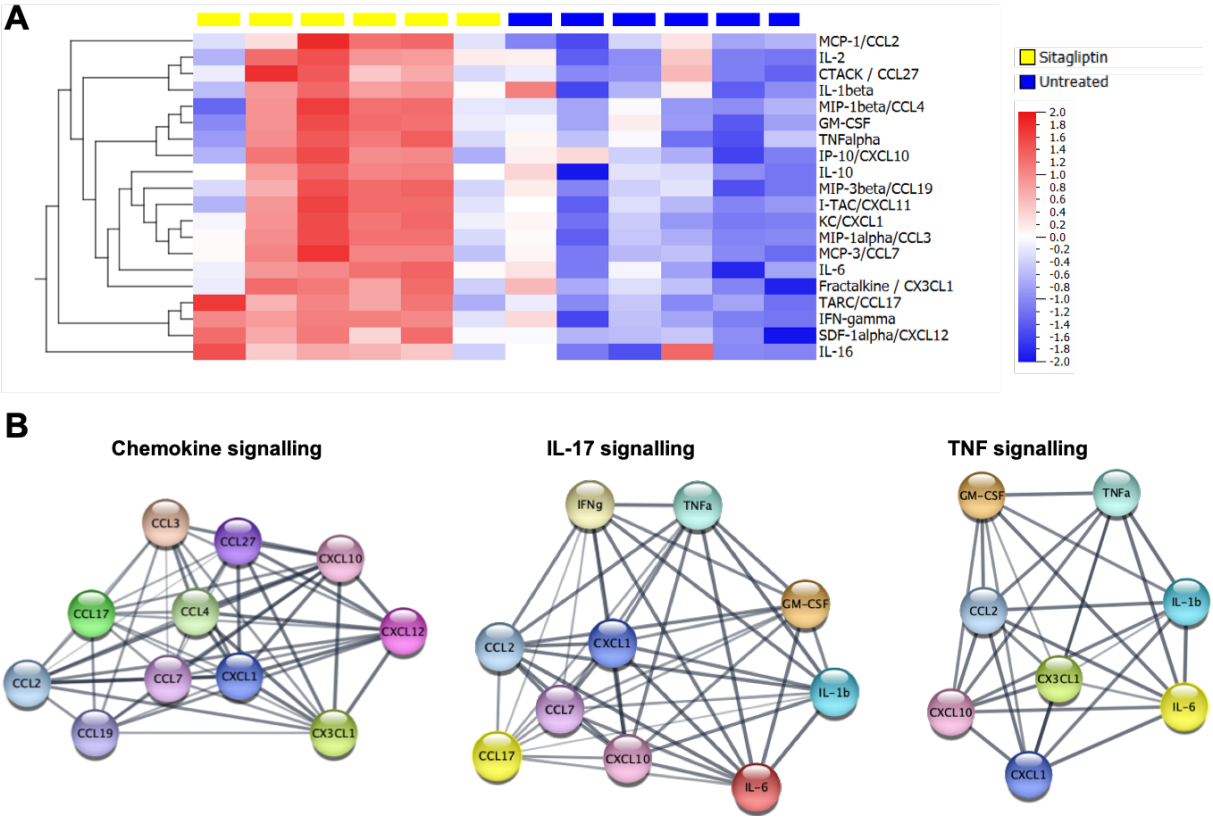

Figure 4.4. Sitagliptin alters cytokine levels in ID8 metastatic tumour bearing mice. *Mice bearing metastatic ID8 tumours commenced daily sitagliptin treatment 2 weeks-post-inoculation and were culled 6-weeks post-tumour-inoculation. Cytokine levels in serum were measured using the Bio-Plex Pro™ Mouse Chemokine Panel, 31-plex (Bio-Rad, #12009159) and analysed using Qlucore Omics Explorer software 3.6 (Qlucore AB, Lund, Sweden) (A) Heatmap representing differentially expressed cytokines between sitagliptin and untreated mice determined by two-group comparison with p-value = 0.05. (B) STRING network analysis representing enrichment in functional networks amongst the differentially expressed cytokines.*

4.2.3 Sitagliptin altered CD4+ and CD8+ T effector cell abundance throughout metastatic ovarian disease

The considerable changes observed in the circulating cytokine levels suggested a strong immune-mediated response to sitagliptin. In ovarian cancer, T lymphocytes are a robust indicator of the immune response; therefore, more specific changes in immune cell populations were investigated by analysing the abundance of T cells, CD8+ and CD4+ (CD25-FoxP3-) T effector cells over time. Sitagliptin significantly increased the percentages of T cells and CD8+ T cells in the blood at week 4-post-tumour-inoculation (Figure 4.5A, B), indicating that sitagliptin evokes a CD8+ T cell specific immune response at the outset of metastatic disease. CD8+ T cells are the major immune cell population responsible for killing of malignant cells and are a positive prognostic indicator in ovarian cancer[127,317]. Further analysis of infiltrating T lymphocyte populations demonstrated a significant increase in CD8+ T cells and a trending increase in CD3+ and CD4+ T cells in the metastatic tumours of mice treated with sitagliptin compared to untreated controls at week 4-post-tumour-inoculation (Figure 4.5C, D. E), suggesting the rapid accumulation of T effector cells to malignant sites following treatment with sitagliptin.

Furthermore, at week-6-post-tumour inoculation, mice treated with sitagliptin had significantly increased percentages of T cells in the peritoneal cavity (Figure 4.6A) and CD4+ T cells in the spleen and peritoneal cavity (Figure 4.6B, C). Corresponding analysis of lymphocyte infiltration show a trending increase in percentages of CD8+ and CD4+ T cells in the tumours of mice treated with sitagliptin compared to the untreated controls at this time point (Figure 4.6D, E).

These data suggest that sitagliptin promotes differentiation of T cells in peripheral circulation and recruitment into the local tumour microenvironment, which is usually indicative of a more

favourable clinical outcome in ovarian cancer[127]. Together, these results demonstrate that sitagliptin improves the overall immune landscape throughout metastatic disease progression.

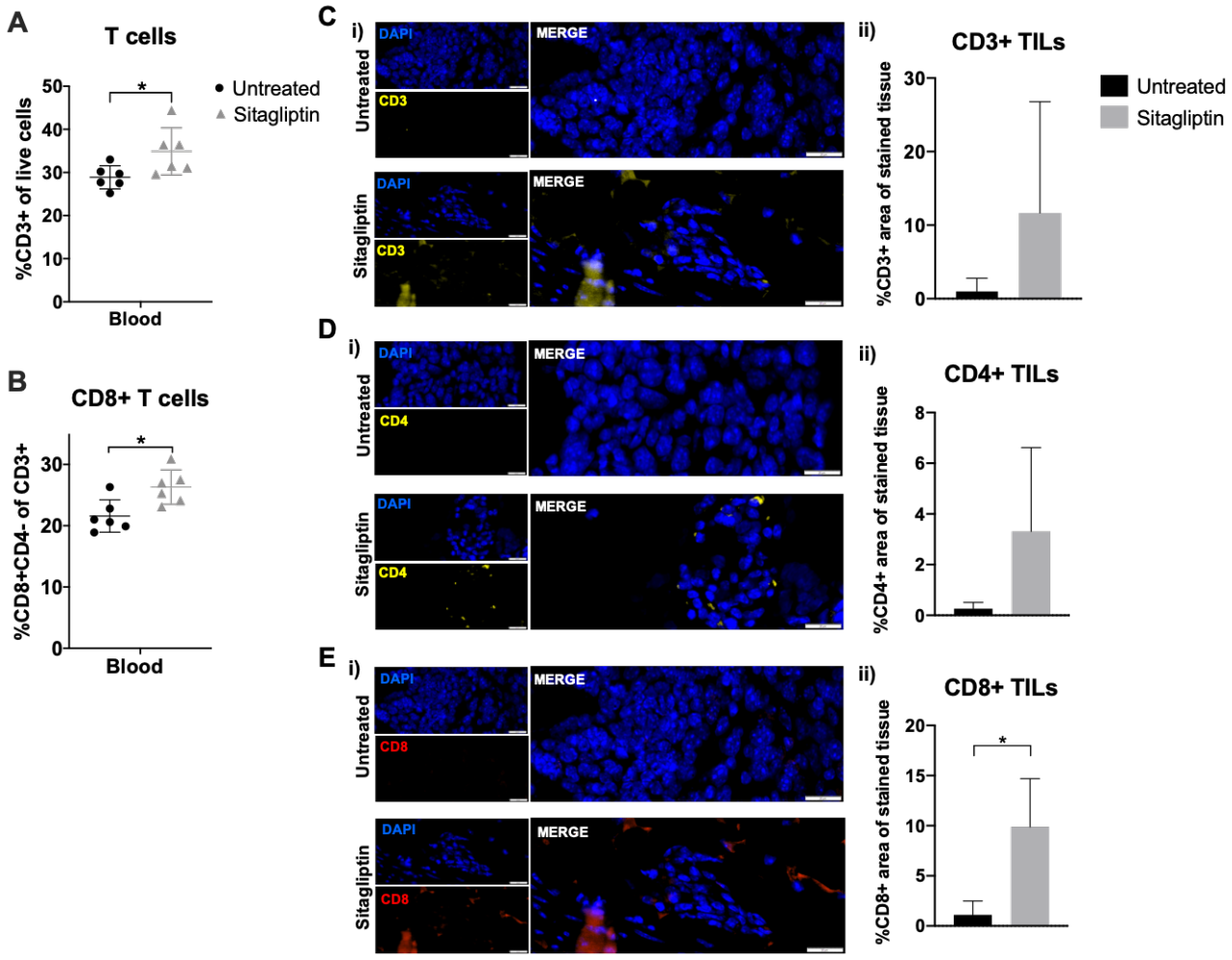

Figure 4.5. Circulating T cells and CD8+ T cells and tumour infiltrating T lymphocytes in mice treated with sitagliptin at week 4*. Mice bearing metastatic ID8 tumours commenced daily sitagliptin treatment 2 weeks-post-inoculation and were culled 4-weeks post-tumour-inoculation. Leukocytes from the blood were isolated and analysed for the abundance of T cells and CD8+ T cells by flow cytometry. Percentages of (A) T cells (%CD3+ of live) and (B) CD8+ T cells (%CD8+CD4- of T cells) in the blood. Tumours were harvested to examine leukocyte infiltration by immunofluorescence. Metastatic ID8 tumour sections were stained with primary antibodies against (C) CD3, (D) CD4 or (E) CD8 in untreated vs sitagliptin treated mice. Representative images (i) and corresponding percentage area (ii) of infiltrating CD3+, CD4+ and CD8+ T cells, respectively, are shown. Scale bar = 20μm. Data are represented as mean ± SD, n=3-6. Differences between groups were determined by an unpaired t-test; *p<0.05.*

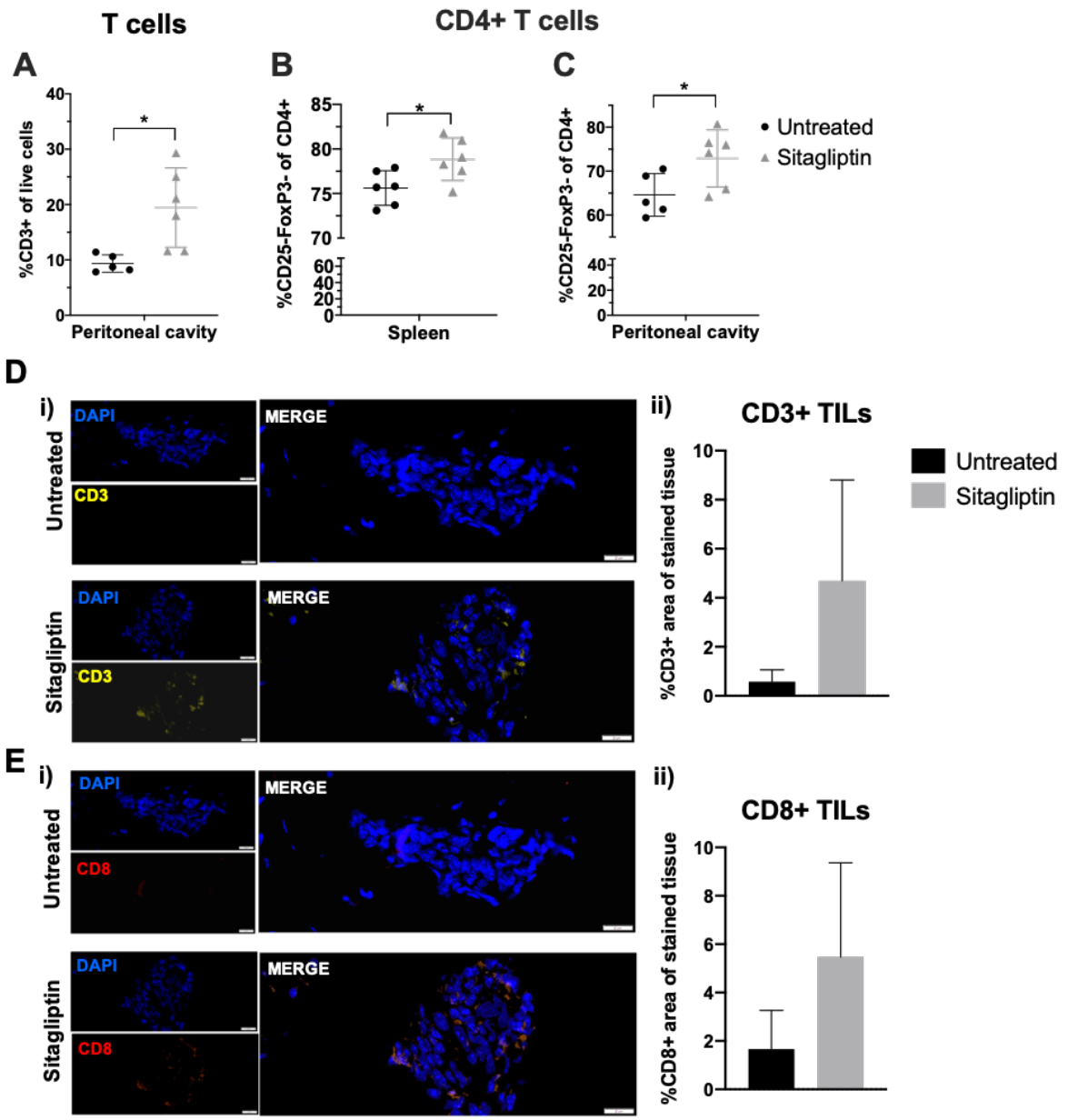

Figure 4.6. Splenic, peritoneal and intratumoural T lymphocyte populations in mice treated with sitagliptin at week 6. *Mice bearing metastatic ID8 tumours commenced daily sitagliptin treatment 2 weeks-post-inoculation and were culled 6-weeks post-tumour-inoculation. Leukocytes from the spleen and peritoneal cavity were isolated and analysed for the abundance of T cells and CD4+ T cells by flow cytometry. Percentages of (A) T cells (%CD3+ of live) in the peritoneal cavity and CD4+ T cells (%CD25-FoxP3- of CD4+ (CD4+CD8-) cells) in the (B) spleen and (C) peritoneal cavity. Tumours were harvested to examine leukocyte infiltration by immunofluorescence. Metastatic ID8 tumour sections were stained with primary antibodies against (D) CD3 or (E) CD8 in untreated vs sitagliptin treated mice. Representative images (i) and corresponding percentage area (ii) of infiltrating CD3+ and CD8+ T cells, respectively, are shown. Scale bar = 20μm. Data are represented as mean ± SD, n=3-6. Differences between groups were determined by an unpaired t-test, *p<0.05.*

4.2.4 Sitagliptin enhanced the T cell effector response in metastatic disease

CD8+ T effector cells are responsible for antigen-specific, granzyme-mediated killing of malignant cells[317] and are associated with prolonged survival in ovarian cancer[110,129]. CD4+ T cells (T helper cells) are responsible for mediating antigen-specific responses, including the activation of cytotoxic T cells, B cells and interaction with dendritic cells[318]. Proliferation and activation of CD8+ and CD4+ T cells occurs rapidly upon antigen recognition and co-stimulation via antigen presenting cells (APCs)[319]. Due to the observed shift from increased CD8+ T cell abundance at week 4 to increased CD4+ T cells at week 6 (see Section 4.2.3), we were interested to assess the effect of sitagliptin on the functional status of both T cell subsets over time. Proliferating T cells were identified by the intracellular marker Ki67[320]; CD69 was used as a marker for activated T cells[321], and PD-1 was used as a marker for T cell inhibition/exhaustion[322].

Consistent with our earlier findings, our results demonstrate that at week 4-post-tumour inoculation, sitagliptin treatment in mice caused a significant increase in the percentages of proliferating CD8+ T cells in the spleen (Figure 4.7A), and activated CD8+ T cells in the peritoneal cavity (Figure 4.7B) indicating a heightened functional CD8+ T cell response at the site of antigen cross-presentation and in the TME at this time point. Furthermore, a trending increase in activated CD8+ T cells was detected by activation marker CD69 in the lymphocytic infiltrates of tumours from sitagliptin treated mice compared to controls at week 4 (Figure 4.7C), suggesting the potential migration of activated T effector cells into the tumour site. CD8+ T cells destroy their target cells efficiently upon their activation, and their infiltration into tumours indicates a likely cytotoxic effect. Additionally, mice treated with sitagliptin exhibited a trending increase in PD-1+ CD4+ TILs (Figure 4.7D), suggesting a potential mechanism of immunoregulation in these tumours.

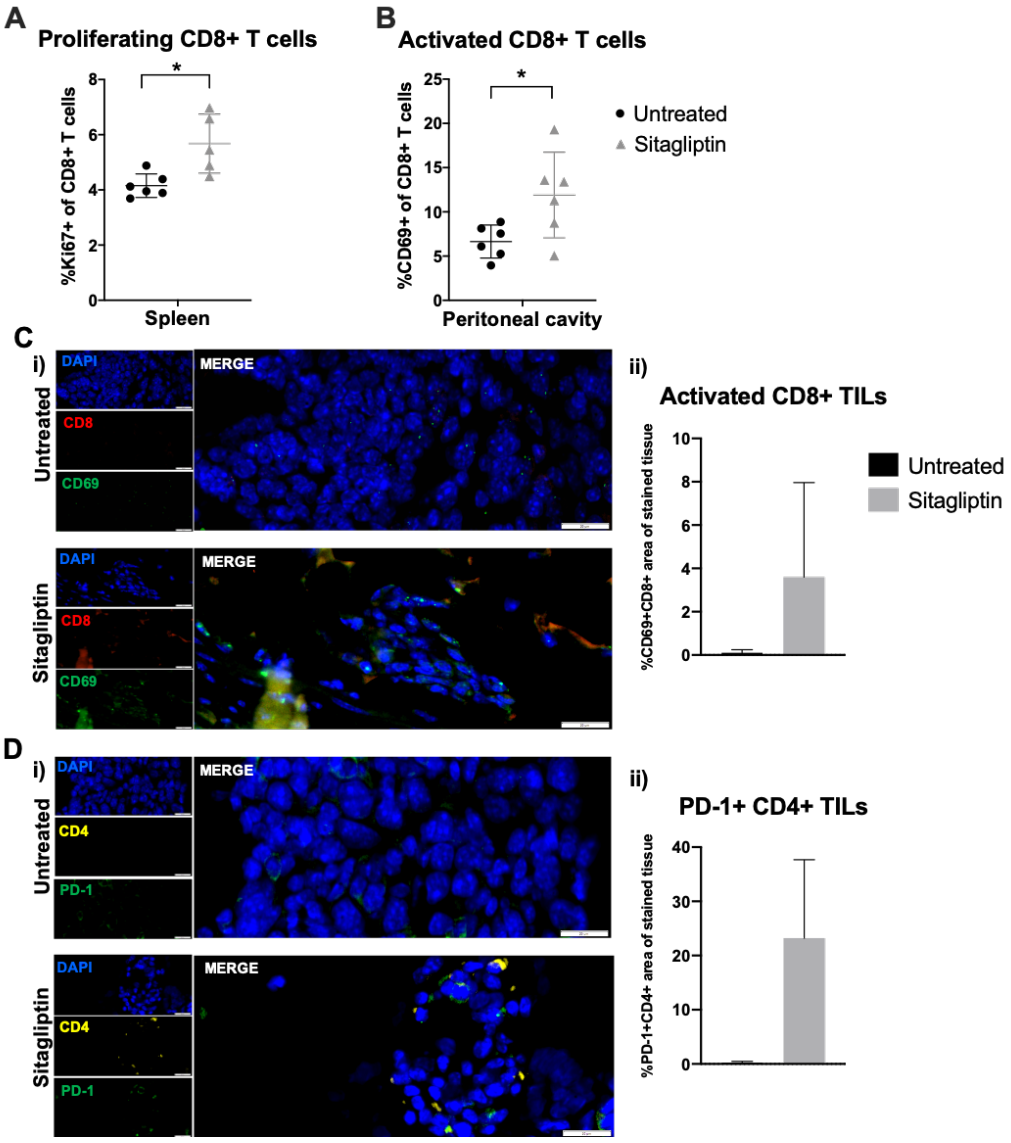

Figure 4.7. Proliferating and activated CD8+ T cells and infiltrating lymphocyte activation status in mice treated with sitagliptin at week 4. *Mice bearing metastatic ID8 tumours commenced daily sitagliptin treatment 2 weeks-post-inoculation and were culled 4-weeks post-tumour-inoculation. Leukocytes from the spleen and peritoneal cavity were isolated and analysed for the abundance of proliferating CD8+ T cells and activated CD8+ T cells by flow cytometry. Percentages of (A) proliferating CD8+ T cells (%Ki67 of CD8+ T cells) in the spleen and (B) activated CD8+ T cells (%CD69+ of CD8+ T cells) in the peritoneal cavity. Tumours were harvested to examine leukocyte infiltration by immunofluorescence. Metastatic ID8 tumour sections were stained with primary antibodies against (C) CD8 (red) and CD69 (green) or (D) CD4 (yellow) and PD-1 (green) in untreated vs sitagliptin treated mice. Representative images (i) and corresponding percentage area (ii) of infiltrating CD69+CD8+ and PD-1+CD4+ T cells, respectively, are shown. Scale bar = 20μm. Data are represented as mean ± SD, n=3-6. Differences between groups were determined by an unpaired t-test, *p<0.05.*

Conversely, at week-6-post-tumour inoculation, percentages of circulating CD8+ T cells in mice treated with sitagliptin were significantly decreased (Figure 4.8A), and activated CD4+ T cells were increased in the spleen (Figure 4.8B). Notably, there was no difference observed in the abundance of activated CD8+ TILs or PD-1+CD4+ TILs in sitagliptin treated mice compared to controls at week 6 (Figure 4.8C, D). The abundance of infiltrating PD-1+ CD8+ T cells were also evaluated, however there was no difference between treatment groups (data not shown).

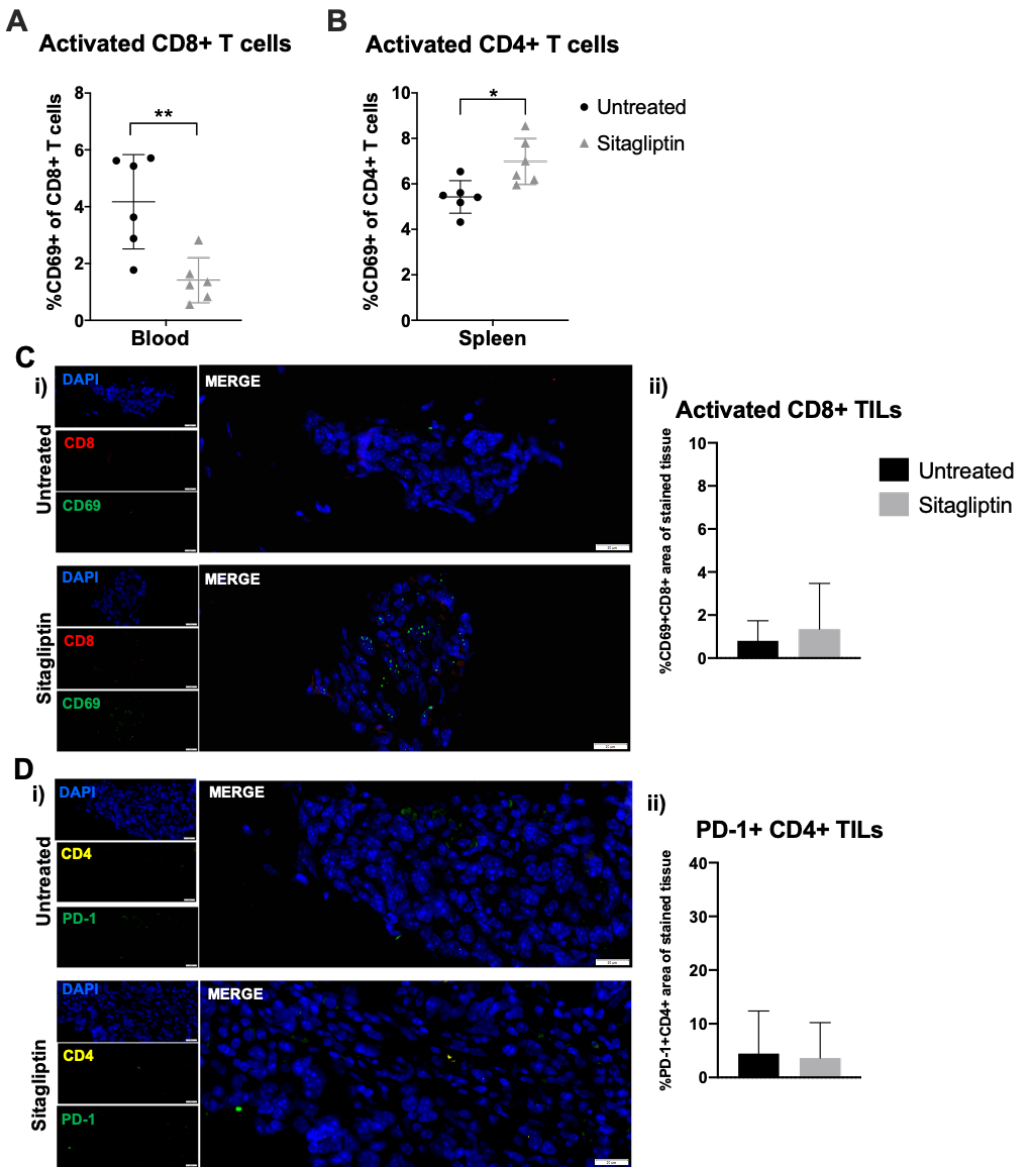

Figure 4.8. Activated CD8+ and CD4+ T cells and infiltrating lymphocyte activation in mice treated with sitagliptin at week 6. *Mice bearing metastatic ID8 tumours commenced daily sitagliptin treatment 2 weeks-post-inoculation and were culled 6-weeks post-tumour-inoculation. Leukocytes from the spleen and blood were isolated and analysed for the abundance of activated CD8+ T cells and activated CD4+ T cells by flow cytometry. Percentages of (A) activated CD8+ T cells (%CD69+ of CD8+ T cells) in the blood and (B) activated CD4+ T cells (%CD69+ of CD4+ T cells) in the spleen. Tumours were harvested to examine leukocyte infiltration by immunofluorescence. Metastatic ID8 tumour sections were stained with primary antibodies against (C) CD8 (red) and CD69 (green) or (D) CD4 (yellow) and PD-1 (green) in untreated vs sitagliptin treated mice. Representative images (i) and corresponding percentage area (ii) of infiltrating CD69+CD8+ and PD-1+CD4+ T cells, respectively, are shown. Scale bar = 20μm. Data are represented as mean ± SD, n=3-6. Differences between groups were determined by an unpaired t-test; *p<0.05, **p<0.01.*

4.2.5 Sitagliptin decreased regulatory T cells during the early stages of metastatic disease

The ovarian cancer TME is intrinsically immunosuppressive and immune evasion mechanisms are correlated with poor prognosis and overall survival[111,155]. The balance between the effector response and regulation by suppressive cells is crucial in determining the success of the overall immune response. Tregs are a suppressive subset of T cells that are responsible for maintaining immune homeostasis; however, in a malignant environment, Tregs diminish the effects of the anti-tumour immune response and promote tumour progression[154]. In ovarian cancer, increased levels of Tregs are correlated with poor survival[155], whilst an increased ratio of CD8+ T cells : Tregs is usually indicative of a more favourable prognosis[126]. Therefore, we were interested in evaluating the effect of sitagliptin on Tregs and their function, including proliferation and tumour infiltrating ability. Tregs were defined as (CD25+FoxP3+) CD4+ cells; and proliferating and tumour homing Tregs were defined as those cells expressing Ki67[320] or CD103[323], respectively.

At week-4-post-tumour inoculation, mice treated with sitagliptin had significantly decreased percentages of Tregs cells in the spleen and blood (Figure 4.9A, B) suggesting a systemic decrease in immunosuppression at this time point. Furthermore, the CD8+ T cell: Treg ratio was concomitantly increased in the blood and peritoneal cavity (Figure 4.9C, D), indicative of a more favourable effector response in these compartments.

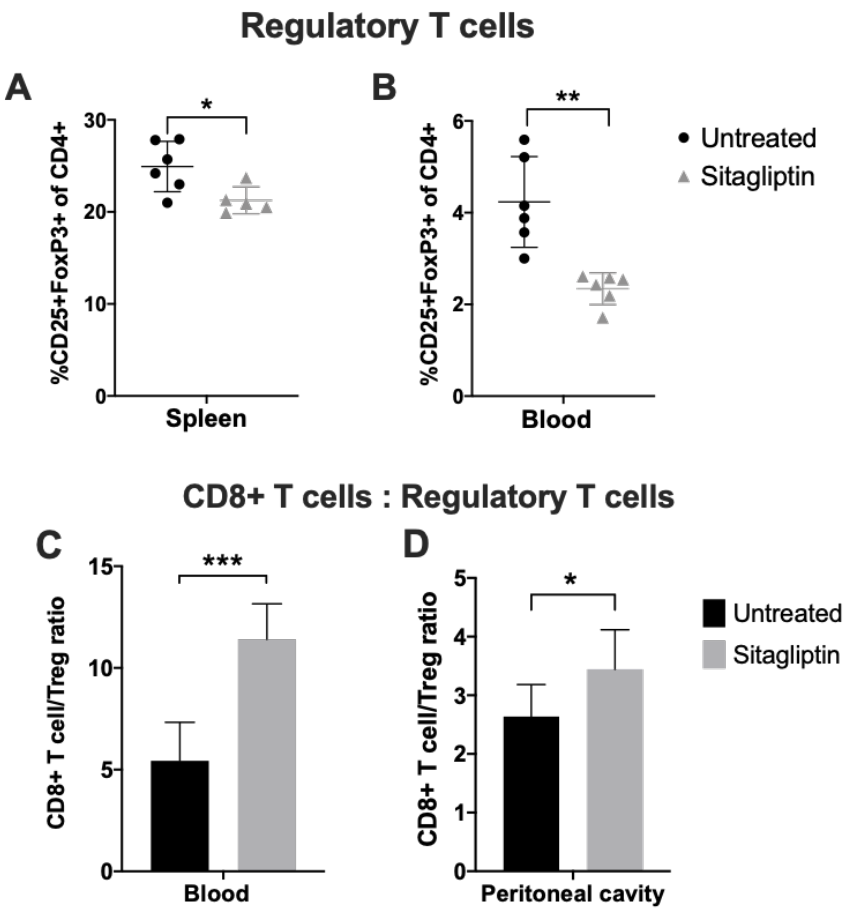

Figure 4.9. Regulatory T cells and CD8+ T cell: Regulatory T cell ratio in mice treated with sitagliptin at week 4. *Mice bearing metastatic ID8 tumours commenced daily sitagliptin treatment 2 weeks-post-inoculation and were culled 4-weeks post-tumour-inoculation. Leukocytes from the spleen, blood and peritoneal cavity were isolated and analysed for the abundance of CD8+ T cells and regulatory T cells (Tregs) by flow cytometry. Percentages of Tregs (%CD25+FoxP3+ of CD4+ (CD4+CD8-) cells) in the (A) spleen and (B) blood. The ratio of CD8+ T cells (%CD8+CD4- of T cells): Tregs (%CD25+FoxP3+ of CD4+ (CD4+CD8-) cells) in the (C) blood and (D) peritoneal cavity. Data are represented as mean ± SD, n=6. Differences between groups were determined by an unpaired t-test; *p<0.05, **p<0.01.*

Conversely, at week 6-post-tumour inoculation, mice treated with sitagliptin exhibited increased percentages of proliferating and tumour homing Tregs in the peritoneal cavity (Figure 4.10). Consistent with the migration and accumulation of CD4+ T cells in the peritoneal cavity, these Tregs may be differentiated in the TME due to long-term exposure to tumour antigens.

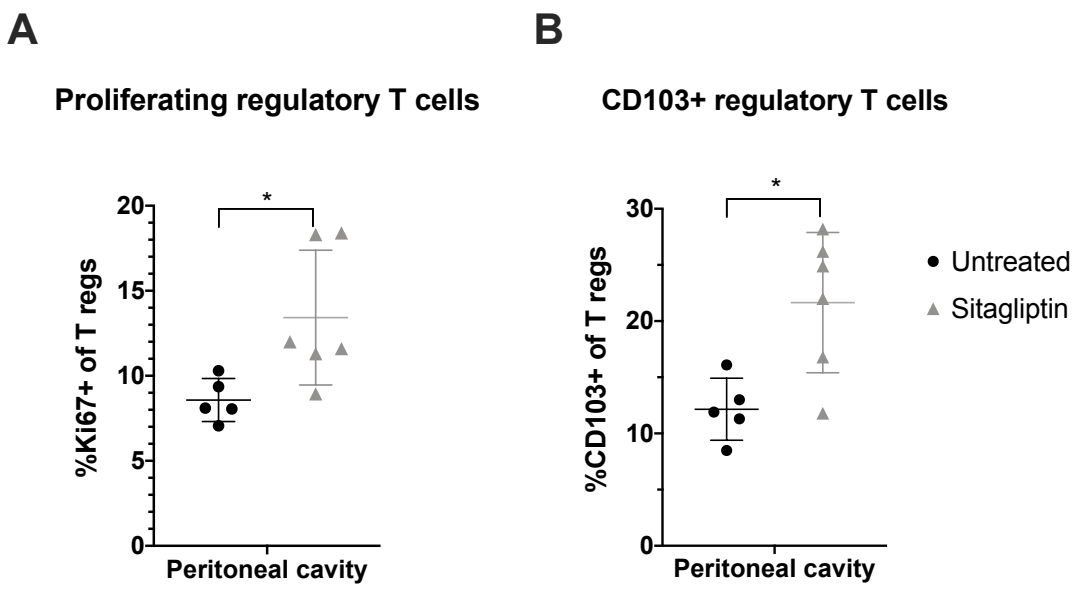

Figure 4.10. Proliferating and tumour infiltrating regulatory T cells in mice treated with sitagliptin at week 6. *Mice bearing metastatic ID8 tumours commenced daily sitagliptin treatment 2 weeks-post-inoculation and were culled 6-weeks post-tumour-inoculation. Leukocytes from the peritoneal cavity were isolated and analysed for the abundance of proliferating and tumour homing regulatory T cells (Tregs) by flow cytometry. Percentages of (A) proliferating Tregs (%Ki67+ of Tregs) and (B) tumour infiltrating Tregs (%CD103+ of Tregs) in the peritoneal cavity. Data are represented as mean ± SD, n=6. Differences between groups were determined by an unpaired t-test; *p<0.05.*

4.2.6 Sitagliptin modulated systemic immunosuppressive effects of regulatory T cells over time

We next sought to further investigate how sitagliptin modulates the functional state of Tregs throughout metastatic disease. Tregs express specific receptors that enhance their ability to diminish the anti-tumour response in the TME. For example, in ovarian tumours intratumoural PD-1+ Tregs represent a distinct subset of highly suppressive cells[324]. In addition, CCR4+ Tregs are essential in chemokine-mediated migration to ovarian tumours[155] and evidence suggests that they may contribute to poor outcomes in other malignancies including breast and lung cancer[325,326]. We therefore assessed the effect of sitagliptin on the abundance of PD-1+ and CCR4+ Tregs in our ovarian cancer disease model over time.

At week-4-post-tumour inoculation, PD-1+ Tregs were significantly increased in the spleen and peritoneal cavity (Figure 4.11A, C) but decreased in the blood (Figure 4.11B) of mice treated with sitagliptin. Similarly, CCR4+ Tregs were significantly increased in the peritoneal cavity (Figure 4.11E) but decreased in the blood (Figure 4.11D), indicating that sitagliptin heightened the presence of potentially immune suppressive Tregs in the peritoneal cavity at this time point. Moreover, the decreased circulating levels of these subsets of Tregs suggests their migration from the blood to peripheral sites of inflammation.

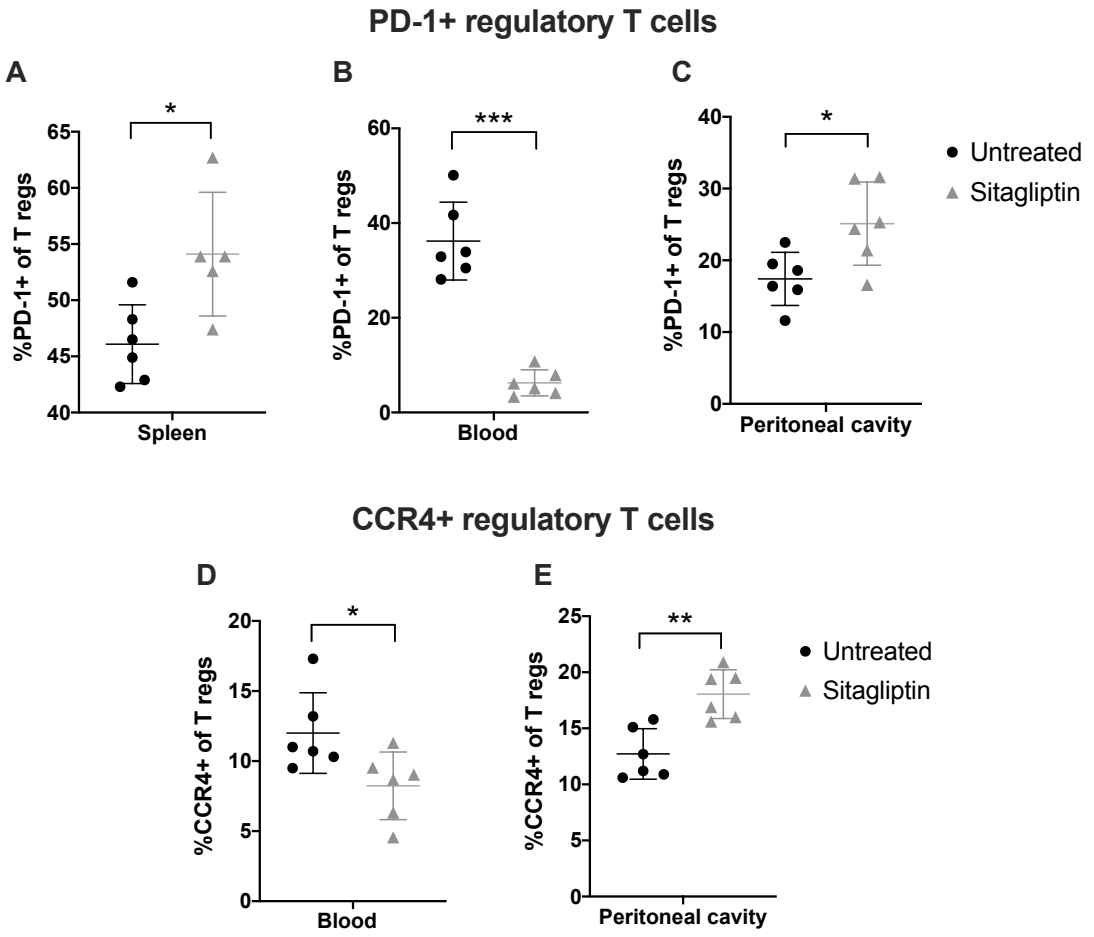

Figure 4.11. PD-1+ and CCR4+ regulatory T cells in mice treated with sitagliptin at week 4. *Mice bearing metastatic ID8 tumours commenced daily sitagliptin treatment 2 weeks-post-inoculation and were culled 4-weeks post-tumour-inoculation. Leukocytes from the spleen, blood and peritoneal cavity were isolated and analysed for the abundance of PD-1+ and CCR4+ regulatory T cells (Tregs) by flow cytometry. Percentages of PD-1+ Tregs (%PD1+ of Tregs) in the (A) spleen, (B) blood and (C) peritoneal cavity; and CCR4+ Tregs (%CCR4+ of Tregs) in the (D) blood and (E) peritoneal cavity. Data are represented as mean ± SD, n=6. Differences between groups were determined by an unpaired t-test; *p<0.05, **p<0.01, ***p<0.005.*

This hypothesis is supported by data at week-6-post-tumour inoculation, where mice treated with sitagliptin demonstrated a significant decrease in percentages of PD-1+ Tregs in the spleen and blood (Figure 4.12A, B); alongside a decrease in CCR4+ Tregs in the spleen and peritoneal cavity (Figure 4.12C, D). These results suggest that long-term treatment with sitagliptin potentially decreases systemic immunosuppression from Tregs in metastatic ovarian disease.

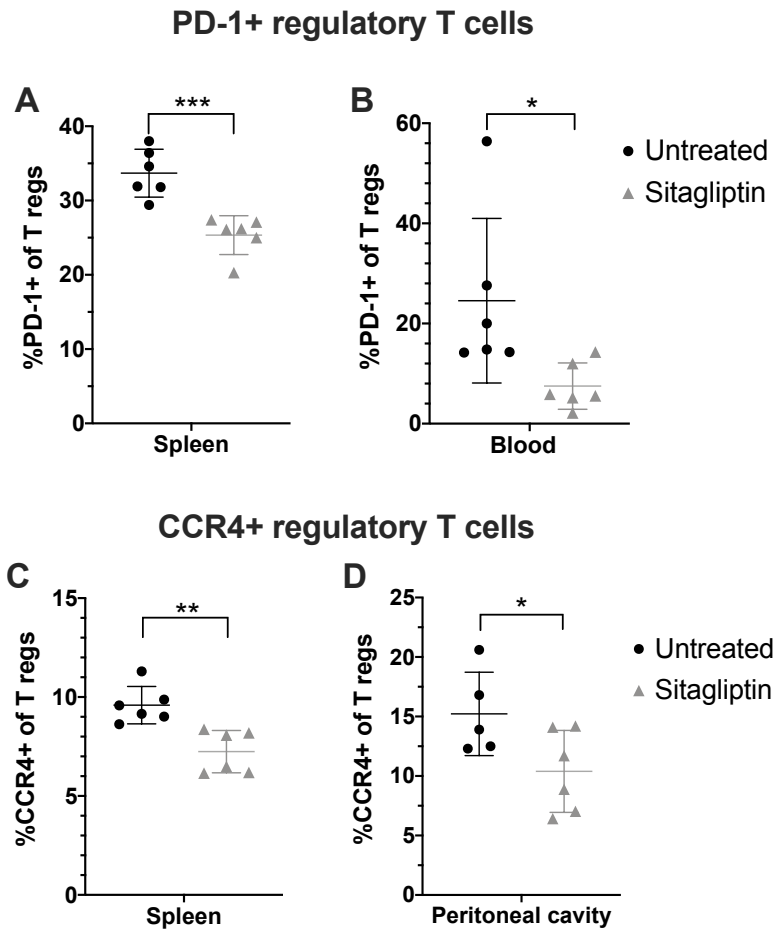

Figure 4.12. PD-1+ and CCR4+ regulatory T cells in mice treated with sitagliptin at week 6. *Mice bearing metastatic ID8 tumours commenced daily sitagliptin treatment 2 weeks-post-inoculation and were culled 6-weeks post-tumour-inoculation. Leukocytes from the spleen, blood and peritoneal cavity were isolated and analysed for the abundance of PD-1+ and CCR4+ regulatory T cells (Tregs) by flow cytometry. Percentages of PD-1+ Tregs (%PD1+ of Tregs) in the (A) spleen and (B) blood; and CCR4+ Tregs (%CCR4+ of Tregs) in the (C) spleen and (D) peritoneal cavity. Data are represented as mean ± SD, n=6. Differences between groups were determined by an unpaired t-test; *p<0.05, **p<0.01, ***p<0.005.*

Taken together with the results from Section 4.2.5, our data shows that sitagliptin decreases the overall suppressive effect of Tregs in early-stage metastatic disease by decreasing their abundance, and regulates the suppressive behaviour of Tregs at later stages of disease progression. This indicates that sitagliptin may exert a sustained influence on the regulatory component of the adaptive immune system.

4.2.7 Sitagliptin altered peripheral immune suppression by myeloid-derived suppressor cells throughout disease progression

In addition to Tregs, myeloid-derived suppressor cells (MDSCs) contribute to the negative regulation of the immune response. MDSCs are a uniquely heterogeneous population of immature myeloid-cell progenitors that are highly potent suppressors of antigen-specific T cell functions[179]. MDSCs are upregulated in the peripheral blood of ovarian cancer patients and enhance stem cell-like behaviour of tumour cells[327]. In this study we investigated the abundance of the two major subsets of MDSCs in mice: monocytic and granulocytic/polymorphonuclear. Monocytic MDSCs (M-MDSCs) share similarities to monocytes and rapidly differentiate into tumour-associated macrophages (TAMs) at the tumour site where they contribute to non-specific T cell suppression[179,328]. Polymorphonuclear MDSCS (PMN-MDSCs) share similarities to neutrophils and are the more potent subset, possibly via the increased production of reactive oxygen species (ROS), and have been shown to suppress T cell activity through antigen-specific mechanisms[328]. In this study, M-MDSCs were defined as (CD11c-CD11b+Gr1^{int}) CD3- cells and PMN-MDSCs were defined as (CD11c-CD11b+Gr1^{hi}) CD3- cells.

At week-4-post-tumour inoculation, mice treated with sitagliptin had significantly decreased percentages of PMN-MDSCs in the spleen and blood compared to controls (Figure 4.13), suggesting a decrease in peripheral and circulating immunosuppression at this time point. This reduction was sustained, where at week-6-post-tumour inoculation, the percentages of M-MDSCs and PMN-MDSCs in the spleen were significantly decreased in sitagliptin-treated mice (Figure 4.14). Although MDSCs were unchanged in the peritoneal cavity between sitagliptin and untreated mice (data not shown), our results suggest that sitagliptin is effective at moderating peripheral immune suppression from MDSCs throughout metastatic disease progression.

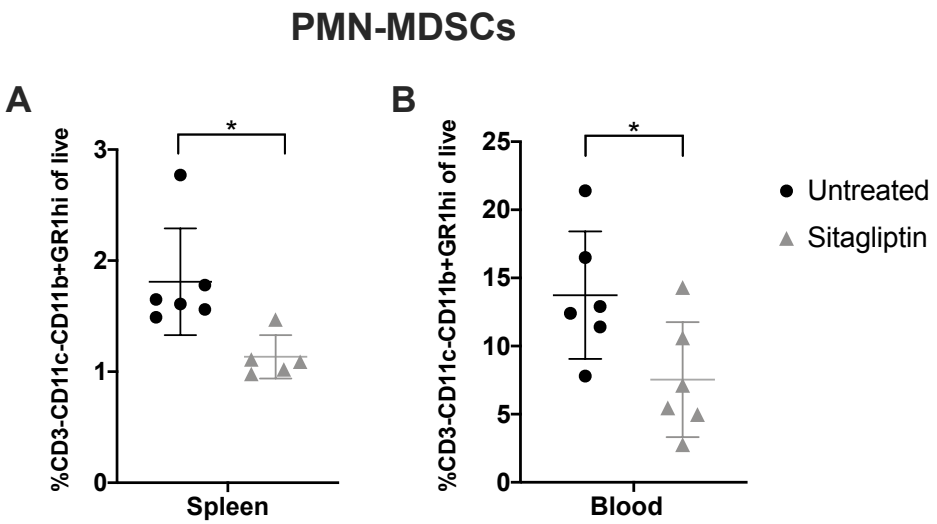

Figure 4.13. Myeloid-derived suppressor cells in in mice treated with sitagliptin at week 4. *Mice bearing metastatic ID8 tumours commenced daily sitagliptin treatment 2 weeks-post-inoculation and were culled 4-weeks post-tumour-inoculation. Leukocytes from the spleen and blood were isolated and analysed for the abundance of polymorphonuclear myeloid-derived suppressor cells (PMN-MDSCs) by flow cytometry. Percentages of PMN-MDSCs (%CD3-CD11c-CD11b+Gr1^{hi} of live cells) in the (A) spleen and (B) blood. Data are represented as mean ± SD, n=6. Differences between groups were determined by an unpaired t-test; *p<0.05.*

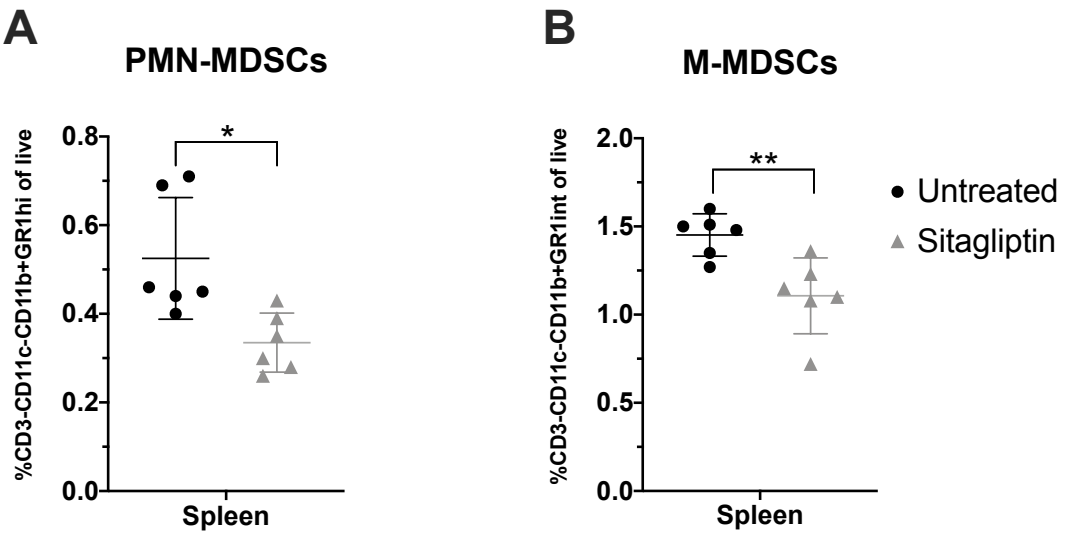

Figure 4.14. Myeloid-derived suppressor cells in in mice treated with sitagliptin at week 6. *Mice bearing metastatic ID8 tumours commenced daily sitagliptin treatment 2 weeks-post-inoculation and were culled 6-weeks post-tumour-inoculation. Leukocytes from the spleen, blood and peritoneal cavity were isolated and analysed for the abundance of polymorphonuclear myeloid-derived suppressor cells (PMN-MDSCs) and monocytic MDSCs (M-MDSCs) by flow cytometry. Percentages of (A) PMN-MDSCs (%CD3-CD11c-CD11b+Gr1^{hi} of live cells) and (B) monocytic MDSCs (%CD3-CD11c-CD11b+Gr1^{int} of live cells) in the spleen. Data are represented as mean ± SD, n=6. Differences between groups were determined by an unpaired t-test; *p<0.05, **p<0.01.*

4.2.8 Sitagliptin sustained effective innate immunity throughout disease progression

In ovarian cancer, innate immune cells such as macrophages, natural killer cells and dendritic cells are essential components of the anti-tumour immune response. Tumour associated macrophages (TAMs) comprise the majority of infiltrating immune cells within the TME[329]. In ovarian cancer, most TAMs are the suppressive, M2-polarised subtype, which contribute to tumour cell proliferation and metastasis[330,331]. Classically activated M1-polarised TAMs, however, are correlated with a more favourable prognosis[332,333]. M1 macrophages are activated by inflammatory cytokines such as IFN-ɣ and other stimuli within the tumour environment and exert anti-tumour effects via phagocytosis and antigen/MHC class II presentation to T cells[334]. Although MHC class II molecules are also expressed across other

activated macrophage subsets, high MHC II expression is considered a marker of M1-polarised cells[333]. In this study we identified activated macrophages as (CD11c-CD11b+F4/80+MHC-II^{hi}) CD3- cells.

Mice treated with sitagliptin had significantly increased percentages of activated macrophages in the spleen compared to untreated controls at week-4-post-tumour inoculation (Figure 4.15A). Conversely, at week-6-post-tumour inoculation we observed decreased percentages of activated macrophages in the spleen of sitagliptin-treated mice (Figure 4.15B), but those percentages in the peritoneal cavity were significantly increased (Figure 4.15C). These data suggest that sitagliptin enhanced macrophage activation in peripheral lymphoid organs during the early stages of metastatic spread, whereas at advanced stages of disease the activated macrophages migrate from the spleen to the peritoneal cavity to influence the tumour microenvironment.

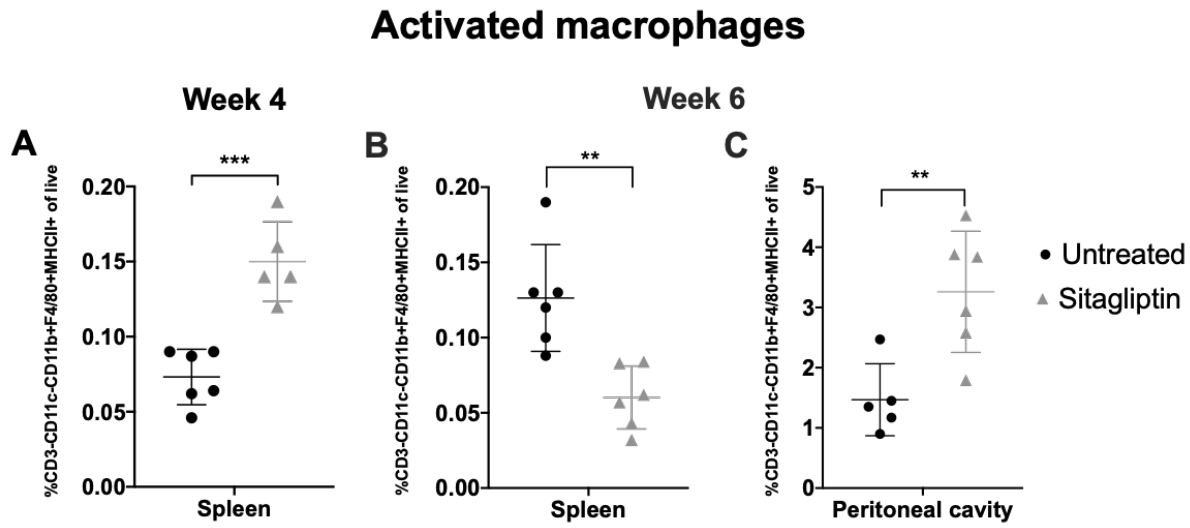

Figure 4.15. Activated macrophages in mice treated with sitagliptin at week 4 and week 6. *Mice bearing metastatic ID8 tumours commenced daily sitagliptin treatment 2 weeks-post-inoculation and were culled 4- and 6-weeks post-tumour-inoculation. Leukocytes from the spleen and peritoneal cavity were isolated and analysed for the abundance of activated macrophages by flow cytometry. Percentages of activated macrophages (%CD3-CD11c-CD11b+F4/80+MHCII+ of live cells) in the (A) spleen at week 4; and (B) spleen and (C) peritoneal cavity at week 6. Data are represented as mean ± SD, n=6. Differences between groups were determined by an unpaired t-test; **p<0.01, ***p<0.005.*

4.3 Discussion

4.3.1 Sitagliptin as a novel immunotherapeutic to improve survival in metastatic ovarian cancer

The intrinsic immunogenicity exhibited by ovarian tumours is insufficient to circumvent the multiple mechanisms of immune evasion and immunosuppression that exist within the tumour and the surrounding TME. Unfortunately, many monotherapies that suppress inhibitory pathways such as immune checkpoint inhibitors have failed to significantly enhance the anti-tumour immune response or clinical outcomes related to ovarian cancer. It is possible that blockade of a single inhibitory pathway is inadequate to overcome multiple other mechanisms of resistance, and that targeted treatments may induce activation of other suppressive pathways. The presence of infiltrating lymphocytes in 'immunoreactive' ovarian tumours correlates with enhanced responses to treatment and overall survival[127], and is a promising approach to restore anti-tumour immunity in ovarian cancers. In this study we investigated how treatment with the DPP4 inhibitor sitagliptin in a syngeneic, metastatic ovarian cancer mouse model influenced immune cell populations and overall survival. Sitagliptin significantly altered multiple immune parameters, including cytokine expression, lymphocyte proportions, and proliferation, activation and infiltration of T cells in late-stage, metastatic disease, which is summarised in Table 4.1 and Figure 4.16.

Sitagliptin treatment significantly prolonged survival in mice bearing metastatic ID8 tumours compared to untreated controls. However, the relatively small cohort size and short survival period makes it difficult to draw definite conclusions about how sitagliptin may impact the overall survival of women with ovarian cancer. Indeed, other studies have shown that patients receiving sitagliptin treatment for type 2 diabetes have decreased cancer incidence and that sitagliptin may be protective against some malignancies[310,311]; although this has not yet been demonstrated for ovarian cancer. Additional retrospective or clinical trials may delineate the survival advantage, if any, of sitagliptin treatment in women with advanced ovarian cancer.

Table 4.1. Summary of immune response to sitagliptin treatment over time in a metastatic ovarian cancer model. *Table representing changes in the abundance of various immune cell populations from leukocytes isolated from the spleen, blood and peritoneal cavity, and tumour sections from tumour-bearing mice treated with sitagliptin vs untreated controls at week 4 and week 6. Upwards arrows represent an increased change and downwards arrows represent a decreased change.*

Immune cell population	**Week 4**				**Week 6**			
	Spleen	*Blood*	*Peritoneal cavity*	*Tumour*	*Spleen*	*Blood*	*Peritoneal cavity*	*Tumour*
T cells		↑		↑			↑	↑
CD4+ T cells				↑	↑		↑	
CD8+ T cells		↑		↑				↑
Proliferating CD8+ T cells	↑							
Activated CD8+ T cells			↑	↑		↑		↑
Activated CD4+ T cells					↑			
PD-1+ CD4+ T cells				↑				
Regulatory T cells	↓		↓					
CD8+ T cells: Tregs		↑	↑					
Proliferating regulatory T cells							↑	
CD103+ regulatory T cells							↑	
PD-1+ regulatory T cells	↑	↓	↑		↓	↓		
CCR4+ regulatory T cells		↓	↑		↓		↓	
PMN-MDSCs	↓	↓			↓			
M-MDSCs					↓			
Activated macrophages	↑				↓		↑	

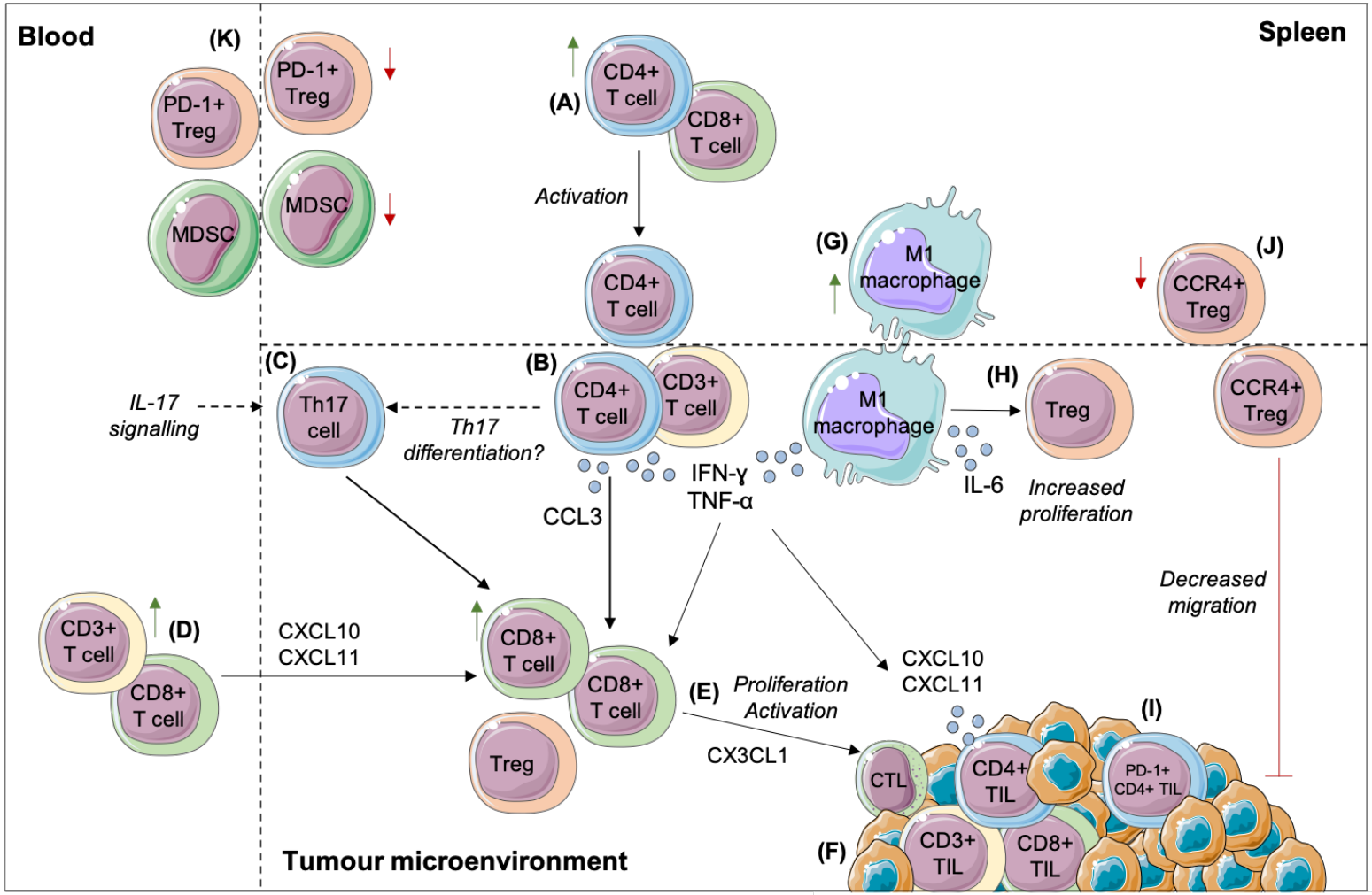
Blood
Spleen
(K)
PD-1+ Treg
PD-1+ Treg
MDSC
MDSC
(A)
CD4+ T cell
CD8+ T cell
Activation
CD4+ T cell
(G)
M1 macrophage
(J)
CCR4+ Treg
(C)
Th17 cell
IL-17 signalling
Th17 differentiation?
(B)
CD4+ T cell
CD3+ T cell
M1 macrophage
(H)
Treg
CCR4+ Treg
IFN-γ
TNF-α
IL-6
Increased proliferation
CCL3
Decreased migration
CD3+ T cell
(D)
CD8+ T cell
CXCL10
CXCL11
CD8+ T cell
CD8+ T cell
Treg
(E)
Proliferation
Activation
CX3CL1
CXCL10
CXCL11
(I)
CTL
CD4+ TIL
PD-1+ CD4+ TIL
CD3+ TIL
CD8+ TIL
(F)
Tumour microenvironment

Figure 4.16. Schematic representation of proposed sitagliptin-mediated immune responses in a metastatic ovarian cancer model. *(A) Throughout metastatic tumour progression, sitagliptin increased the abundance of CD4+ T cells in the spleen which was accompanied by their increased activation. (B) Sitagliptin increased the percentages of CD3+ and CD4+ T cells in the peritoneal cavity, where CD4+ T cells may be responsible for the accumulation of CD8+ T cells via CCL3-mediated cell recruitment. (C) Enrichment for cytokines involved in IL-17 signalling may induce the differentiation of Th17 cells, which could account for the increased abundance of CD4+ T cells in the peritoneal cavity. (D) Increased levels of circulating CD3+ and CD8+ T cells. CD8+ T cells are likely recruited to the peritoneal cavity by chemotactic migration via upregulation of CXCL10 and CXCL11. (C) As a result, the CD8+:Treg ratio in the peritoneal cavity was increased. (E) Sitagliptin induced proliferation and activation of CD8+ T cells in the TME and may increase infiltration of activated CD8+ T cells. The activity of CTLs in the TME could be enhanced by increased expression of CX3CL1. (F) Increased CD3+, CD4+ and CD8+ TILs via sitagliptin treatment may be associated with increased survival and improved overall prognosis. (G) Elevated levels of activated M1-like macrophages in the spleen at week 4, and then the peritoneal cavity at week 6 is indicative of their migration to the TME, where the potential secretion of cytokines such as IFN-ɣ and TNF-α, which are also secreted by CD4+ T cells, enhances the CD8+ T cell response in the local TME. (H) M1 macrophages in the TME secrete IL-6, which was elevated in the serum of sitagliptin-treated mice and may be responsible for the increased proliferation of Tregs in the TME. (I) Sitagliptin may cause an increase in PD-1+ CD4+ TILs, which could be beneficial to enhance susceptibility to PD-1 blockade. Sitagliptin also managed immunosuppression in the long-term, where at week 6, CCR4+ Tregs were decreased in the spleen and peritoneal cavity (J), which may prevent their migration to the tumour and therefore augment immunosuppression by Tregs. (K) In addition, at week 6, sitagliptin decreased percentages of PD-1+ Tregs and MDSCs in the spleen and blood. Green arrow = upregulation, Red arrow = downregulation, Red bar = inhibition. CTL: cytotoxic T lymphocyte, CCL3: C-C motif chemokine ligand 3, CX3CL1: C-X3-C motif chemokine ligand 1, CXCL: C-X-C motif chemokine ligand, IFN-ɣ: interferon-gamma, IL: interleukin, MDSC: myeloid derived suppressor cell, PD-1: programmed death-1 receptor, Th17: T helper type 17, TIL: tumour infiltrating lymphocyte, Treg: regulatory T cell, TME: tumour microenvironment, TNF-α: tumour necrosis factor-alpha.*

4.3.2 Sitagliptin modulates DPP4-specific cytokines and influences multiple chemotactic-dependent T effector responses

The proteolytic post-translational modification of chemokines within the TME plays a significant role in regulation of the immune response, as it either activates or abolishes their chemotactic function. Modulation of the bioactivity of chemokines represents an effective mechanism of immune evasion or escape in solid tumours and provides novel targets for therapeutic intervention to restore the anti-tumour immune response[335] (discussed in Chapter 3). The functional consequences of DPP4-mediated truncation of chemokines are tissue-dependent, substrate-specific and can positively or negatively influence chemotaxis and immune cell differentiation.

We showed that DPP4 inhibition enriched for cytokines involved in chemokine signalling networks. Unsurprisingly, sitagliptin treatment correlated with an increase in circulating levels of DPP4 specific substrates including CCL3, CXCL10, CXCL11, CXCL12 and GM-CSF[336,337]. CCL3 secretion by T helper cells in the TME is important for recruitment of CCR5+ CD8+ T effector cells[338], which could explain the increased abundance of activated CD4+ T cells in the peritoneal cavity alongside elevated CD8+ TILs in mice treated with sitagliptin. Moreover, CXCL10 and CXCL11 are integral members of the CXCL9, -10, -11/CXCR3 axis as regulators of leukocyte migration, differentiation and activation[339]. Binding to their receptor CXCR3 induces chemotaxis, Ca^{2+} influx, and can result in phosphorylation of the STAT transcription factor family. DPP4-mediated truncation of CXCL10 and CXCL11 results in decreased CXCR3 activation, loss of calcium-signalling and reduced chemotactic capacity[242]. Therefore, DPP4 inhibition by sitagliptin in this study is likely to restore the original function of these fundamental chemokines, as others have previously shown[308]. Consistent with what Barreira da Silva and colleagues demonstrated in melanoma mouse models[308], it is also likely that the increased expression of CXCL10 in our study is responsible for the enhanced recruitment of TILs, which is associated with improved overall survival in ovarian cancer[172].

CXCL10 mediated activation of CXCR3 signalling leads to phosphorylation of STAT1, STAT4 and STAT5. Favourable outcome and improved response to chemotherapy in HGSOC patients has been associated with high levels of STAT1 and increased expression of CXCL10 and CXCL11[340]. However, in CD8+ T cells, STAT3 downregulates the CXCR3/CXCL10 axis and prevents CD8+ T cell accumulation[341], indicating an important role of the correct balance of the STAT family of transcription factors in CXCR3-mediated T cell recruitment. Therefore, it may be beneficial in future research to investigate whether sitagliptin increases STAT expression in tumour tissues to further define the mechanism of T cell infiltration.

CXCR3 signalling also activates the immune cell regulators T-bet and RORyt and promotes differentiation of CD4+ T cells towards the Th1 and Th17 effector subtypes[342]. Indeed, our analysis revealed enrichment of cytokines involved in IL-17 signalling, which regulates the Th17 response[144]. Therefore, the upregulation of CD4+ T cells in the peritoneal cavity in sitagliptin-treated mice may signify their differentiation into a Th17 effector phenotype, which will be discussed further in Chapter 6.

Incidentally, C57BL/6 mice are natural null mutants of CXCL11[343]. A 2bp insertion in the coding sequence causes a frameshift mutation and the generation of a premature stop codon. The translated protein contains the first 13 amino acids of CXCL11, followed by 23 additional irrelevant amino acids, but lacks the critical CXC motif for receptor binding. However, the mutated protein still contains the N-terminus DPP4 cleavage site. Therefore, although the CXCL11 protein in these mice is non-functional and could not influence signalling through CXCR3, its upregulation is still relevant in the overall context of this study.

Consistent with what was observed in primary disease[285], our data also indicated that sitagliptin treatment correlated with increased circulating levels of the DPP4 substrate, CXCL12. However, others have shown that CXCL12 was undetectable in melanoma tumours

of sitagliptin- and untreated mice[308], suggesting that intratumoural vs peripheral expression of chemokines varies and that the effect of sitagliptin on the cytokine landscape may be dependent on cancer type. Increased levels of CXCL12 are associated with enhanced proliferation and invasive capacity of ovarian cancer cells[344] via interaction with its cognate receptor, CXCR4[345]. Thus, alternate mechanisms of immune evasion may be induced upon the rescue of other pathways by sitagliptin.

When interpreting this data, it must be considered that sitagliptin treatment prevents truncation of DPP4-specific substrates, thereby permitting expression of the full-length variant. In 2016, Decalf and colleagues validated that sitagliptin treatment in healthy individuals resulted in a rapid decrease in the levels of truncated CXCL10; however, overall levels of CXCL10 were not significantly affected, suggesting that DPP4 inhibition does not necessarily alter production of CXCL10, instead it selectively alters its processing[309]. Therefore, additional studies should also test the levels of truncated vs full-length DPP4 substrates in sitagliptin treated mice to further distinguish their bioactivity.

4.3.3 Sitagliptin may indirectly mediate immune responses via modification of non DPP4-specific cytokine pathways

Multiple non DPP4-specific substrates were also upregulated in response to treatment with sitagliptin, including IFN-ɣ**,** TNF-α and IL-6. This contradicts outcomes from an induced liver cancer model in rats, where sitagliptin treatment suppressed concentrations of IL-6 and TNF-α[312]; however, the time point used to measure cytokine levels was earlier than our study. DPP4 expression and activity is cell type specific, thus both results validate the ability of DPP4 to influence these pathways and highlights the potential tumour-specific, off-target effects of sitagliptin. IFN-ɣ is predominantly produced by T cells and NK cells and is a master regulator of immunosurveillance and the Type I immune response[346]. In ovarian tumours production of IFN-ɣ has been shown to correlate with CXCR3 expression in CD4+ T cells[342] and is

associated with increased TILs[127]. TNF-alpha is commonly overexpressed in HGSOCs[347] and induces the expression of chemoattractant cytokines[348]. In ovarian cancer cell lines, TNF-α and IFN-ɣ synergise to stimulate secretion of chemotactic molecules including CXCL10 and CXCL11[349], which substantiates our data and further defines a role of TNF-α and IFN-ɣ in anti-tumour immunity in ovarian tumours.

IL-6 is secreted by multiple cell types including TAMs, CD4+ T cells, MDSCs, fibroblasts and tumour cells[350]. In general, IL-6 is understood to have an important function in inflammation-associated tumour progression, where chronic IL-6 signalling supports tumorigenesis and metastatic growth by promoting tumour cell proliferation, angiogenesis and immunosuppression[351]. However, the role of IL-6 in inflammation is complex and may contribute to tumour suppression in some contexts[350]. For example, IL-6 is involved in the transition from innate to acquired immunity via regulation of the expression of various cytokines including CCL4, CCL5, CCL17 and CXCL10 to influence leukocyte trafficking and activation[352,353]. Therefore, the role of IL-6 in our study may be associated with the increase in CCL4, CCL17 and CXCL10 and increased percentages of intratumoural T lymphocytes.

Ikeda and colleagues reported that sDPP4 enhances the transcription of IL-6 and TNF-α in THP-1 cells[354]. Previous studies by our laboratory have shown that sitagliptin increases levels of sDPP4 in the blood, and that hypoxia increases shedding of sDPP4 from the ovarian cancer cell surface[283,285]**.** Thus, sDPP4 may be responsible for the observed upregulation in IL-6 and TNF-α. However, altered sDPP4 expression may also induce compensatory mechanisms by related enzymes, which should be considered in future studies. Secretion of TNF-α**,** IFN-ɣ and IL-6 by tumour-associated macrophages (TAMs) induces expression of the inhibitory ligand PD-L1 on the ovarian cancer cell surface[355]. Although the exact source of upregulation of TNF-α**,** IFN-ɣ and IL-6 in this study cannot be elucidated, their expression may explain the observed increase in PD-L1+ cells in the tumours of sitagliptin-treated mice. As a target of immune

checkpoint inhibition, the increased expression of PD-L1 in ovarian tumours provides further therapeutic opportunity for checkpoint blockade via anti-PD-L1 antibodies.

Sitagliptin treatment also correlated with increased abundance of circulating CX3CL1, otherwise known as fractalkine. Membrane-bound CX3CL1 is expressed by tumour cells and has been associated with increased proliferation and malignant potential in EOC[356]. Contrarily, the soluble form of CX3CL1 stimulates chemotaxis and promotes anti-tumour immunity by inducing NK and Th1 cells[357,358], and may act cooperatively with CXCL10 to enhance the cytotoxic response[359]. Therefore, the sitagliptin-mediated upregulation of soluble CX3CL1 may enhance tumour suppression. However, the differing roles of membrane bound vs soluble CX3CL1 highlights the complexities of the response to signals in the TME and future studies should also investigate expression of membrane bound CX3CL1 to understand the mechanism of its upregulation in response to treatment with sitagliptin.

This study measured circulating levels of cytokines from mouse serum, which provides a robust overview of the peripheral immune response; however, additional research should consider investigating intratumoural cytokine abundance and their expression in the ascites fluid, which is more representative of the local tumour microenvironment and where cytokines are likely to have differing roles. Overall, we demonstrated that sitagliptin altered the chemokine landscape to stimulate expression of several factors involved in recruitment of effector cells and Th-1 mediated immunity.

4.3.4 Sitagliptin influences innate immunity

Despite the upregulation of various factors involved in the expansion and activity of MDSCs, including IL-6, IL-10, IFN-ɣ, and GM-CSF[360,361], we observed a general reduction in percentages of MDSCs throughout sitagliptin treatment in mice bearing metastatic ID8 tumours compared to untreated controls. Our data indicates the most significant differences

in MDSC percentages in the spleen; however, blood-circulating and tumour-infiltrating M-MDSCs have the highest clinical relevance in EOC[362]. Therefore, our results may not be representative of a clinically significant difference to the immune contexture in metastatic ovarian cancer.

The upregulation of IFN-ɣ in sitagliptin-treated mice is likely to be responsible for the polarisation of M1-like macrophages in the peritoneal cavity, which could theoretically lead to increased phagocytosis of tumour cells in the TME to enhance anti-tumour responses. In general, M1 polarised macrophages are more prevalent in primary tumours of HGSOC than other histotypes and their enrichment may cause increased chemosensitivity in tumours[332]. IFN-ɣ polarised macrophages are responsive to inflammatory stimuli such as TNF-α and resistant to immunosuppressive factors like IL-10[363], both of which were also upregulated by sitagliptin. Moreover, M1 macrophages produce IL-1β, TNF-α and IL-6, and also exert anti-tumour activity via increasing cytotoxic T cell recruitment to tumours[364], which may be responsible, at least in part, for the observed increase in tumour-infiltrating CD8+ T cells. With innate immune cells gaining interest as targets for immunomodulatory therapy[118], sitagliptin may provide a novel therapeutic pathway to promote M1 polarisation, although the exact mechanism cannot be clarified from this study.

4.3.5 Sitagliptin sustains anti-tumour immunity throughout metastatic disease

An important outcome of this research was the identification of a sustained immune response, which is a key aspect of successfully harnessing the immune system. Initially we observed a clear, positive anti-tumour immune response early during sitagliptin treatment, where the percentages of proliferating, activated and total CD8+ T cells were increased and Tregs were decreased at week 4. As sDPP4 levels increase in response to treatment with sitagliptin[285] and may be secreted in the hypoxic TME[283], the observed initial increase in CD8+ T cell proliferation could be due to the ability of sDPP4 to enhance lymphocyte proliferation,

independent of its enzyme activity and ADA-binding capacity[365]. A similar phenomenon may explain the increase in T cell activation, as sDPP4 has also been shown to enhance the antigen specific lymphocyte response[366]. However, this is speculative and requires further investigation to determine the functional consequences of sDPP4 on T cell functionality.

A decrease in activated CD8+ T cells in the blood was observed at week 6 in sitagliptin-treated mice, with a corresponding increase in activated CD4+ T cells in spleen. Tumour cell infiltrates indicated an increase in activated CD4+ and CD8+ T cells, suggesting that the decrease in circulating levels of activated CD8+ T cells at this time point could be indicative of their migration and infiltration into the tumour, which may be facilitated by the restoration of full-length CXCL10. This is also supported by previous evidence which shows that sitagliptin enhances leukocyte migration to improve the DPP4-mediated anti-tumour response and controls tumour growth in pre-clinical models of melanoma, hepatocellular carcinoma (HCC) and breast cancer[259,308,313]. In this regard, sitagliptin may promote the conversion from an immunologically 'cold' to a 'hot' tumour by increasing tumour lymphocyte infiltration, which is discussed further in Chapter 5.

The sustained anti-tumour immune response also gives rise to the possibility that sitagliptin interferes with immunoediting throughout metastatic ovarian disease. The dynamic process of 'cancer immunoediting' is a developing concept that is currently understood to be a three-phase process; elimination, equilibrium and escape[367]. There is evidence to suggest that immunoediting occurs in human cancers in response to immunotherapies, where T-cell dependent immunoselection causes elimination of 'immunodominant' tumour cells and the outgrowth of clones that display reduced immunogenicity[368,369]. The sitagliptin-mediated upregulation of effector cytokines including IFN-ɣ and TNF-α may be partially responsible for prolonging the inflammatory signals in the local TME and enhancing the elimination phase of the immune response**.** However, the corresponding upregulation of IL-6 and IL-10 in sitagliptin-treated mice may also be indicative of tumour dormancy, or the equilibrium phase

of immunoediting; where rather than elimination, occult tumour growth is managed by the immune system[367,368]. To test these hypotheses, an enzyme-linked immunosorbent spot (ELISpot) assay could be performed on isolated leukocytes to quantify cell-specific cytokine secretion.

4.3.6 The potential of sitagliptin to increase susceptibility of ovarian tumours to PD-1 blockade

We identified a novel role for sitagliptin as a mediator of the PD-1/L1 axis, which contributes to the immunosuppressive TME in ovarian cancer[370]. The increased abundance of infiltrating PD1+ CD4+ T cells in metastatic ovarian tumours highlights a potential mechanism by which sitagliptin treatment may stimulate immunosuppression, as prolonged expression of PD-1 can contribute to T cell exhaustion and eventual immune escape[371]. After 2 weeks of treatment with sitagliptin, percentages of PD-1+ Tregs were decreased in the blood but increased in the peritoneal cavity compared to untreated controls. PD-L1+ APCs can convert naïve CD4+ T cells in the periphery to Tregs[372]; therefore, the upregulation of PD-1 on Tregs in the peritoneal cavity may be indicative of their recent differentiation in the TME, potentially making them more susceptible to PD-1 blockade at this time point.

An unexpected result in this study was the long-term effect of DPP4 inhibition on PD-1 expression on Tregs. After 4 weeks of treatment with sitagliptin, percentages of PD-1+ Tregs decreased in the spleen and blood, suggesting that sitagliptin managed the apparent immunosuppression initiated earlier in disease progression by the tumour/TME. TILs collected from patients with NSCLC show that high expression of PD-1 on activated Tregs is correlated with nonresponse to PD-1 blockade therapy and is associated with a shorter PFS time, signifying its potential use as a predictive marker of resistance[373]. Therefore, sitagliptin may be effective at countering the mechanisms of suppression in the tumour microenvironment and improving the status of predictive biomarkers in the long-term.

There is also evidence to suggest that the balance between PD-1 expression on Tregs and T effector cells is an important predictor of PD-1 blockade therapy[373,374]. When PD-1 is highly expressed on Tregs, PD-1 blockade amplifies their activation and suppressor function, leading to tumour progression[375]. Therefore, the decrease in percentage of PD-1+ Tregs proposes that PD-1 blockade would not exacerbate their function. In addition, the sitagliptin-mediated decrease in PD-1+ Tregs and concurrent increase in tumour-infiltrating PD-1+ CD8+ T effector cells may increase tumour susceptibility to PD-1/PD-L1 blockade to further improve the anti-tumour immune response.

Conversely the role of PD-1+ Tregs in malignancy is unclear. Tumour-infiltrating PD-1+ Tregs isolated from glioblastoma multiforme (GBM) patients exhibited significantly reduced suppressive capacity and were enriched in gene signatures associated with exhaustion; however, Tregs isolated from the blood retained their suppressive activity[376]. Therefore, the detected decrease in PD-1+ Tregs may in fact be indicative of an exhausted phenotype. As we did not measure infiltrating PD-1+ Tregs in tumours, it is difficult to correlate our findings with that observed in previous studies. The function of PD-1+ Tregs should be considered in future studies by analysing their infiltration into tumours and examining their suppressive and proliferative activity to deduce whether sitagliptin enhances Treg capacity or promotes their exhaustion in the ovarian cancer TME. The intricacies of pro- and anti-tumour activity exhibited by a combination of different cell types in the TME also highlights the fact that developing new treatment regimens requires a comprehensive understanding of the phenotype of targetable cells.

4.4 Conclusions

We have shown that sitagliptin has a significant capacity to alter the immune contexture via restoration of the bioactivity of DPP4 substrates including CXCL10 and improvement of T cell activation and infiltration in an immunocompetent, metastatic ovarian cancer mouse model. However, it appears that the effects of sitagliptin goes beyond direct mediation of DPP4 substrates and effectively influences multiple aspects of the immune response, including various immunosuppressive pathways and innate immunity, suggesting a multifaceted and complex role of DPP4 in the TME. As a clinically approved therapy for the treatment of type 2 diabetes, sitagliptin can be easily translated to the clinic and is shown to exhibit minimal side effects, even at the high doses used in this study[377]. Together with our previous data on sitagliptin treatment in a primary ovarian cancer mouse model[285] there is now substantial evidence to support the re-purpose of sitagliptin as an immunomodulatory therapy for women with ovarian cancer. Moreover, this study provided several points of data to suggest that sitagliptin treatment in metastatic ovarian cancer may provide a more optimal TME to improve the response other immunotherapies such as immune checkpoint inhibition via anti-PD-1 or anti-PD-L1. Therefore, additional research should assess the combination of sitagliptin with PD-1/L1 blockade to determine its potential efficacy as a novel therapeutic strategy in ovarian cancer.

4.5 Acknowledgements

I wish to acknowledge the use of the facilities and technical assistance of Monash Histology Platform, Department of Anatomy and Developmental Biology, Monash University; in particular Angela Vais for her assistance with immunofluorescence staining of mouse tissue.

4.6 Supplementary Figures

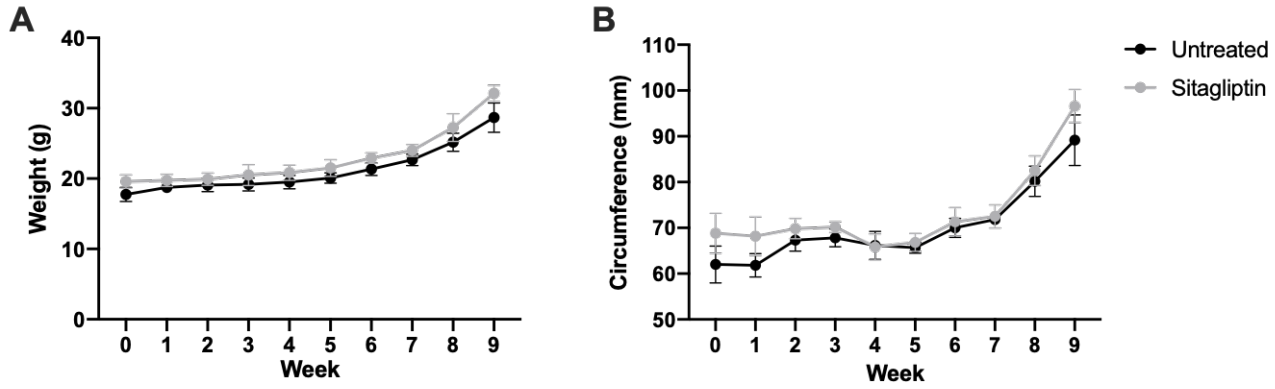

Figure S4.1. Weight and circumference of mice treated with sitagliptin. *Mice bearing metastatic ID8 tumours commenced sitagliptin treatment 2 weeks-post-inoculation and were culled at humane endpoint. (A) Weight and (B) circumference were measured weekly. Data are represented as mean ± SD, n=6.*

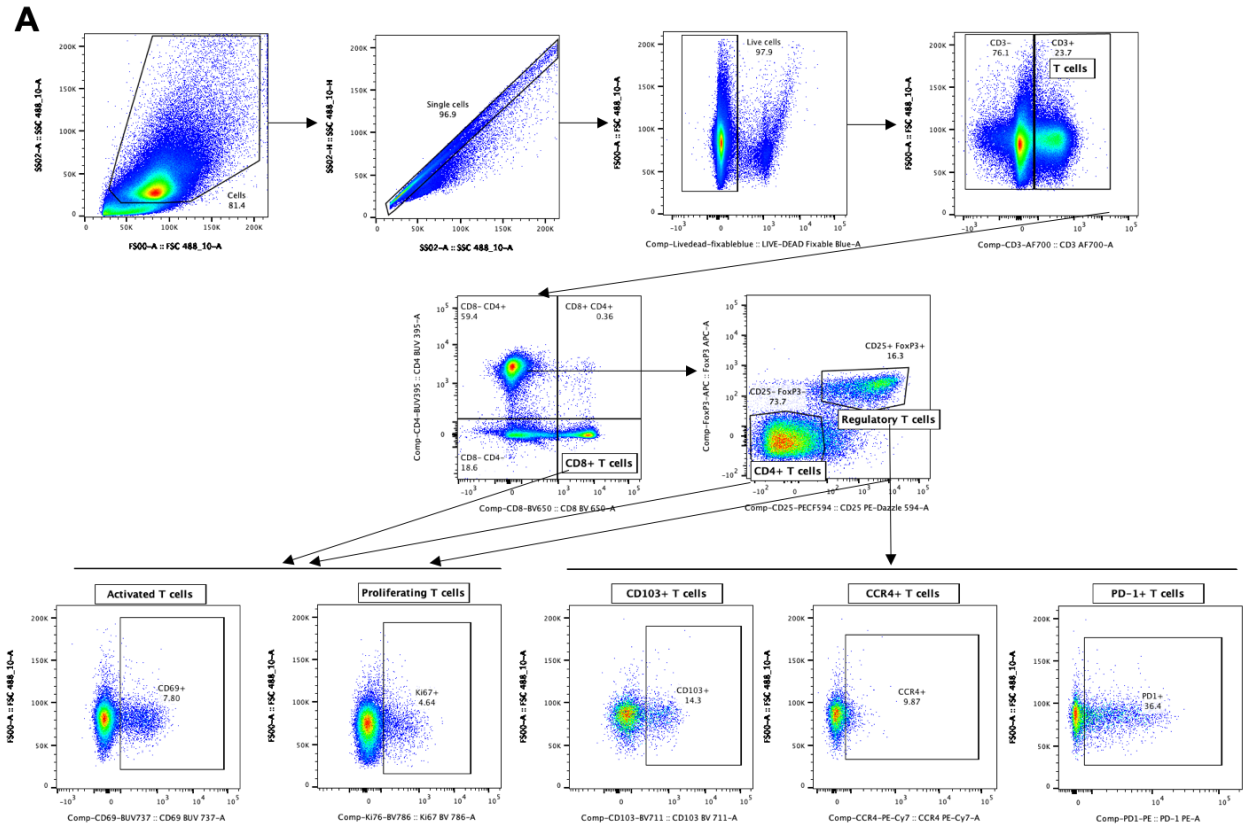
A
Cells
81.4
Single cells
96.9
Live cells
97.9
CD3-
76.1
CD3+
23.7
T cells
CD8- CD4+
59.4
CD8+ CD4+
0.36
CD8- CD4-
18.6
CD8+ T cells
CD25+ FoxP3+
16.3
CD25- FoxP3-
73.7
Regulatory T cells
CD4+ T cells
Activated T cells
CD69+
7.80
Proliferating T cells
Ki67+
4.64
CD103+ T cells
CD103+
14.3
CCR4+ T cells
CCR4+
9.87
PD-1+ T cells
PD1+
36.4

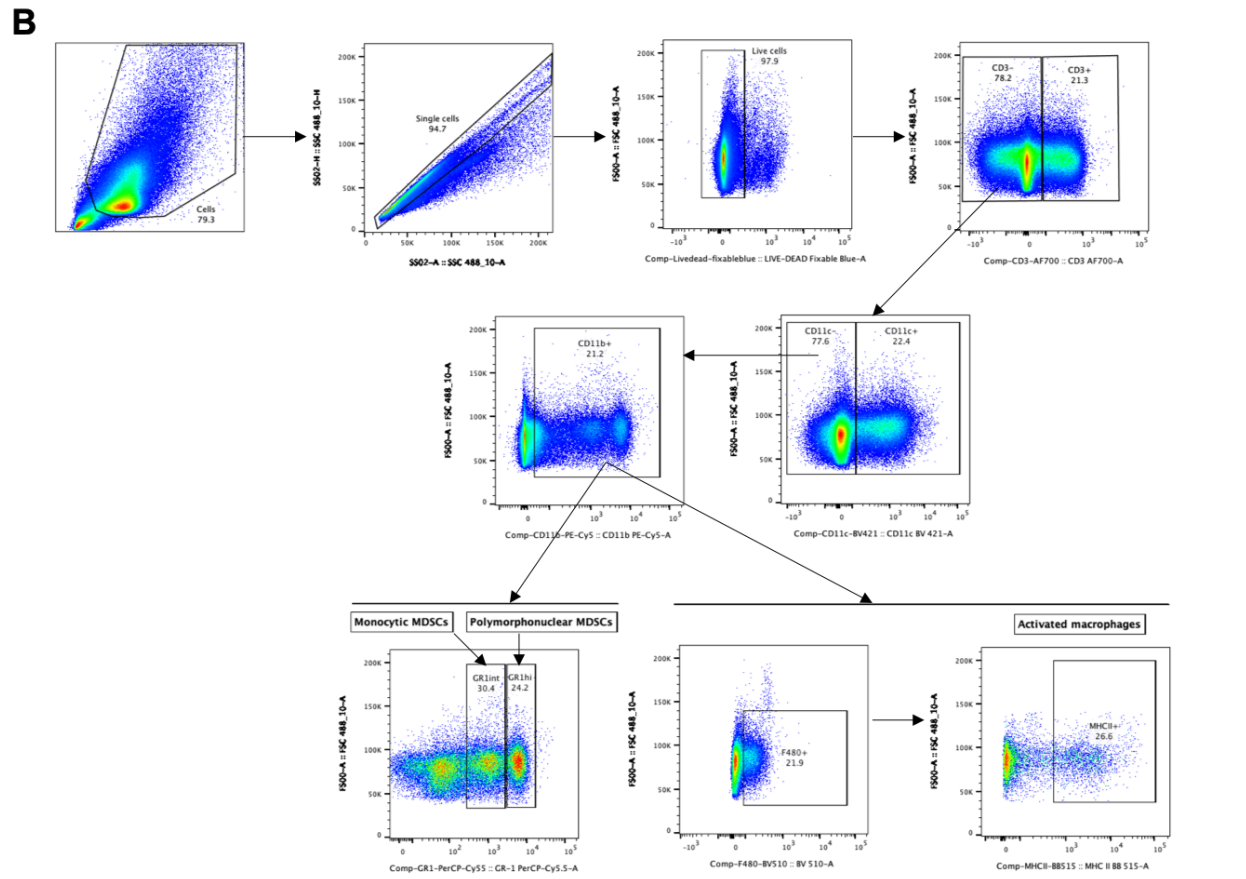
B
Cells
79.3
Single cells
94.7
Live cells
97.9
CD3-
78.2
CD3+
21.3
CD11b+
21.2
CD11c-
77.6
CD11c+
22.4
Monocytic MDSCs
Polymorphonuclear MDSCs
GR1int
30.4
GR1hi
24.2
Activated macrophages
F480+
21.9
MHCII+
26.6

Supplementary Figure S4.2. Flow cytometry gating strategy. *Fluorescence density plots representing sequential gating used to identify specific subsets of immune cells as shown by the arrows. All cells were defined on the FSC-A vs SSC-A axes and single cells were defined on the SSC-A vs SSC-H axes. Dead cells were excluded using the LIVE/DEAD™ Fixable Blue Stain. (A) T cells were defined as CD3+; CD8+ T cells were defined as CD3+CD8+CD4-; CD4 T cells were defined as CD3+CD8-CD4+CD25-FoxP3-; regulatory T cells were defined as CD3+CD8-CD4+CD25+FoxP3+; activated T cells were defined as CD69+; proliferating T cells were defined as Ki67+; infiltrating T cells were defined as CD103+, migrating T cells were defined as CCR4+; inhibitory/exhausted T cells were defined as PD-1+. (B) Monocytic myeloid derived suppressor cells (M-MDSCs) were defined as CD3-CD11c-CD11b+Gr1int; polymorphonuclear myeloid derived suppressor cells (PMN-MDSCs) were defined as CD3-CD11c-CD11b+Gr1hi; macrophages were defined as CD3-CD11c-Cd11b+F4/80+; activated macrophages were defined as MHCII+. All gates were determined using fluorescence minus one (FMO) controls.*

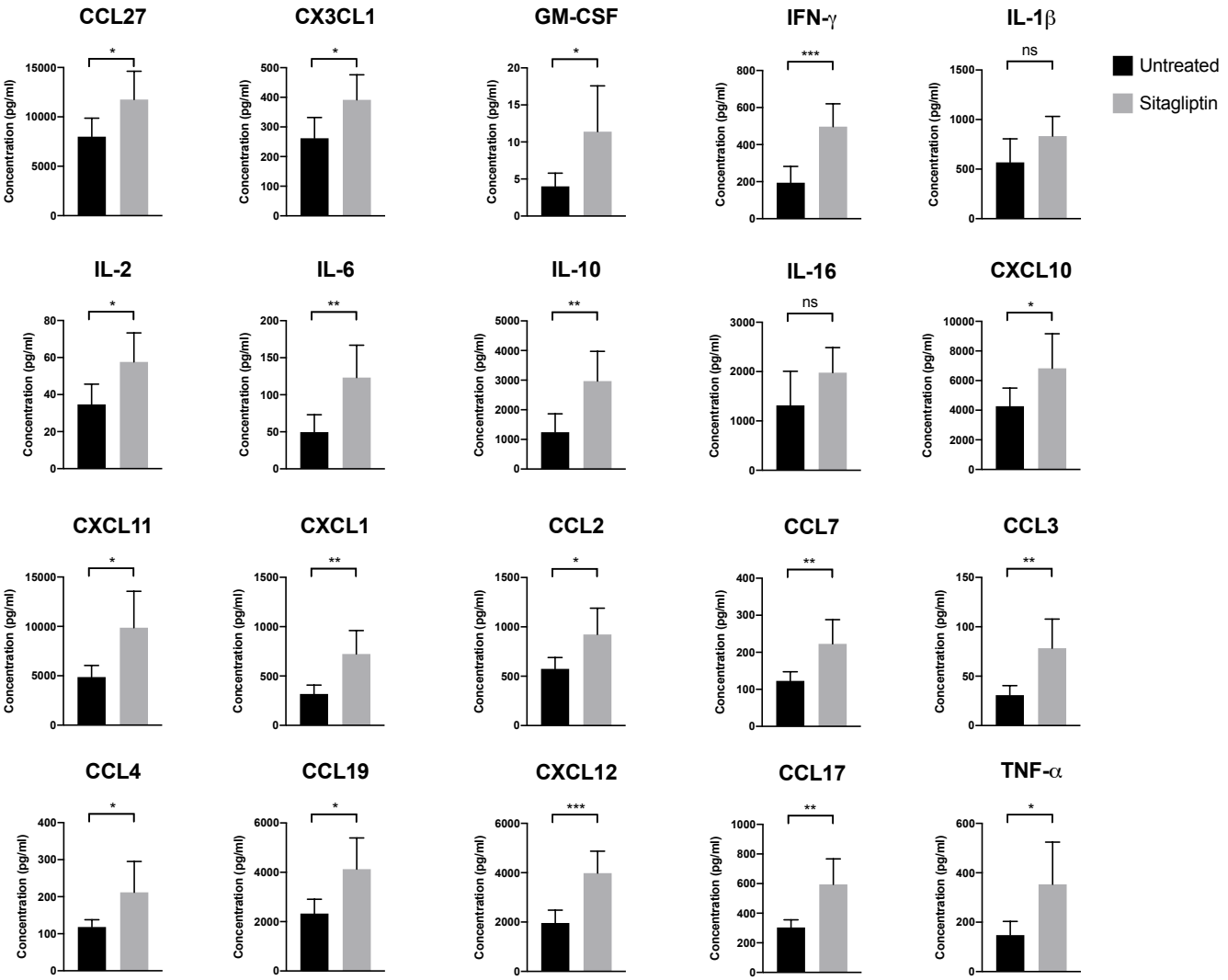

Supplementary Figure S4.3. Concentration of differentially expressed circulating cytokines in mice treated with sitagliptin at week 6. *Mice bearing metastatic ID8 tumours commenced daily sitagliptin treatment 2 weeks-post-inoculation and were culled 6-weeks post-tumour-inoculation. Chemokine levels in serum were measured using the Bio-Plex Pro™ Mouse Chemokine Panel, 31-plex (Bio-Rad, #12009159) and 20 differentially expressed cytokines between sitagliptin vs untreated mice were identified. Differences in the concentration of individual cytokines between groups were determined by an unpaired t-test. Data are represented as mean ± SD, n=6; *p<0.05, **p<0.01, ***p<0.005.*

Chapter Five

Investigating the combination of sitagliptin with immune checkpoint inhibitors as a novel immunotherapy in ovarian cancer

Preface

The data gathered from Aim 2 of this study highlights that targeting DPP4 using the enzyme inhibitor sitagliptin significantly alters multiple immune parameters throughout disease progression in a syngeneic ovarian cancer mouse model. Immune checkpoint inhibitors have recently gained attention for their ability to reduce immunosuppression and improve overall response in multiple solid tumour types[378]**.** However, immune checkpoint inhibition including anti-PD-1 or anti-PD-L1 antibodies have only shown modest improvement to survival in ovarian cancer patients when used as a single agent[1,379]. Recent evidence suggests that effective anti-PD-1 therapy requires a functional intratumoural CXCR3 pathway, and that sensitivity to anti-PD-1 can be restored by inducing CXCR3 ligands[380]. Previous work by our lab demonstrated that DPP4 inhibition with sitagliptin treatment *in vivo* significantly increased the percentage of CXCR3+ tumour infiltrating lymphocytes in a primary ovarian cancer mouse model[285]. The results from Chapter 4 suggested that, similar to primary disease, sitagliptin enhanced T effector cell activation and infiltration of lymphocytes into tumours in a pre-clinical model of metastatic disease. Moreover, sitagliptin increased percentages of PD-1+ CD4+ TILs, revealing a potential mechanism by which sitagliptin may restore sensitivity of metastatic ovarian tumours to blockade of the PD-1/PD-L1 axis. Based on this evidence we investigated whether a combination of sitagliptin with immune checkpoint inhibitors anti PD-1 or anti-PD-L1 could synergise to provide therapeutic benefit *in vivo.*

The work presented in this chapter directly aligns with Aim 3 of my PhD project – To evaluate the potential synergistic action of DPP4 inhibition with immune checkpoint inhibitors as a novel therapy for ovarian cancer. The data provides evidence for a synergistic effect of sitagliptin + PD-1/PD-L1 blockade on anti-tumour immune responses in a metastatic ovarian cancer mouse model. We show that these novel combination therapies enhanced multiple components of the T effector response and alleviated some of the mechanisms of suppression induced by immune checkpoint inhibition therapy.

5.1 Introduction

The host immune system is a crucial factor in the progression and prognosis of ovarian cancer. The repertoire of immune cells located within ovarian tumours and the surrounding tumour microenvironment (TME) consists of a heterogenous network of adaptive immune cells including CD4+ and CD8+ T cells and B cells; and innate immune cells such as natural killer (NK) cells, macrophages, neutrophils and dendritic cells (DCs)[242]. Tumour infiltrating T effector cells are associated with a significant improvement in survival rate in ovarian cancer patients[127]. However, despite the fact that ovarian cancers are immunogenic at advanced stages of disease, there is widespread evidence of heightened immunosuppression throughout disease progression.

Programmed death-1 (PD-1) is an inhibitory co-receptor that is widely expressed on T cells, B cells and macrophages[149]. PD-1 is a key regulator of the threshold of the immune response via interaction with programmed death ligand 1 (PD-L1), which is expressed on the surface of target cells. Signalling through the PD-1/PD-L1 axis inhibits T cell activity and downregulates the effector response[149]. Upregulation of PD-L1 is observed in a high proportion of ovarian cancer patients, which is inversely correlated with CD8+ T cell infiltration in tumours and is indicative of a poor prognosis[145]. The interaction of the PD-1 receptor on T cells in the TME with PD-L1 on tumour cells inhibits T cell activation and weakens the immune response to effectively promote tumour survival[145,381]. The PD-1/PD-L1 axis and other immune checkpoint pathways involving the cytotoxic T lymphocyte-associated protein 4 (CTLA-4) receptor are implicated in various cancer types and as a result, much research has focused on blockade of the receptor-ligand interaction via the development of antagonistic antibodies known as immune checkpoint inhibitors[382].

Immune checkpoint inhibitors (ICIs) have demonstrated a significant ability to reduce immunosuppression and improve long-term survival rates in multiple solid tumour types[378]. In

particular, anti-PD-1 antibodies such as pembrolizumab and nivolumab have revolutionised the treatment of metastatic melanoma and non-small cell lung carcinoma (NSCLC)[383-385]. However, such therapies have only shown modest improvement to survival in ovarian cancer patients[1,379]. A large phase II clinical trial of pembrolizumab in patients with recurrent ovarian cancer (KEYNOTE-100) achieved an objective response rate (ORR) of 8.0% with a progression free survival (PFS) of 1.9 months[193]. As a result of underwhelming efficacy in clinical trials, neither anti-PD-1 nor anti-PD-L1 have gained approval as a monotherapy for the treatment of ovarian cancer. Combination therapies however, combining ICIs with chemotherapy have delivered more promising results[180]. The standard first-line chemotherapy for ovarian cancer involves the combination of carboplatin and paclitaxel. In a phase I trial from the KEYNOTE-021 study combining pembrolizumab (anti-PD-1) plus carboplatin and paclitaxel in 25 treatment-naïve advanced NSCLC patients, the ORR was 48%, which is greater than that observed by treatment with chemotherapy alone[386]. The more recent phase III KEYNOTE-407 trial in 559 untreated NSCLC patients receiving pembrolizumab plus carboplatin and paclitaxel reported a median OS of 15.9 months compared 11.3 months in the placebo controls, demonstrating the significant survival benefit via the combination of PD-1 blockade and standard chemotherapy[387]. However, the combination of ICIs with chemotherapy as a first-line treatment has yet to be trialled in ovarian cancer patients.

Other targeted combination approaches involving ICIs include the addition of inhibitors of angiogenesis such as vascular endothelial growth factor (VEGF) and its receptor (VEGFR) or poly(ADP-ribose) polymerase (PARP) inhibitors[388]. A phase I study investigating the combination of durvalumab (anti-PD-L1) with the VEGFR inhibitor, cediranib, reported an 75% disease control rate in a small cohort of women with recurrent or advanced stage ovarian cancer[198], whilst a phase II trial of combined nivolumab (anti-PD-1) with bevacizumab (anti-VEGF) in patients with relapsed EOC showed that 11 out of 38 participants experienced a confirmed response[196]. In each trial, the overall response was superior in platinum-sensitive vs platinum-resistant participants. Furthermore, the combination of durvalumab (anti-PD-L1)

with the PARP inhibitor olaparib was effective in women with BRCA-mutated, platinum sensitive ovarian cancer, where the disease control rate was 81% and the ORR was 63%[197] . Although PARP inhibitors were initially developed to target the mutated *BRCA* pathway of DNA repair, pre-clinical data indicates that PARP inhibitors may also increase the efficacy of ICIs independently of *BRCA* status by stimulating interferon signalling to induce anti-tumour immunity[389,390]. This was supported by a recent clinical trial with pembrolizumab (anti-PD-1) in combination with niraparib (PARPi) in a cohort of 62 women with recurrent ovarian cancer, which demonstrated anti-tumour activity and similar disease control rates irrespective of platinum-sensitivity, *BRCA*-mutation and homologous recombination deficiency (HRD) status[391]. Evidently, the combination of ICIs with PARP inhibitors appears to be more effective than with VEGF/VEGFR inhibitors in women with chemoresistant disease. These trials have emphasised the need to better understand the TME and identify functional biomarkers to predict response to anti-PD-1/L1 in ovarian cancer.

PD-L1 expression is likely to have a prognostic role in predicting the efficacy of PD-1/PD-L1 blockade, however the exact mechanisms that determine the clinical response to these immunotherapies are still under investigation. Indeed, clinical trials in some cancer types including melanoma, NSCLC, renal cell carcinoma (RCC), colorectal carcinoma (CRC) and lymphoma have provided evidence of an association with pre-treatment tumour expression of PD-L1 and response to blockade of the PD-1/PD-L1 pathway[392,393]. However, multiple other trials have refuted this hypothesis, where investigators reported that patient response rate to anti-PD-1/PD-L therapy was independent of PD-L1 expression in clinical trials in NSCLC[394] and ovarian cancer[196,198] patients. In a pre-clinical ovarian cancer model, Lin and colleagues showed that PD-L1 blockade in ID8 tumour-bearing, PD-L1 deficient mice was ineffective at reducing tumour volume, whilst PD-L1 blockade in PD-L1$^{-/-}$ ID8 tumour-bearing, wild-type (WT) mice decreased tumour growth compared to controls, indicating the role of host PD-L1 expression in determining the tumour response to anti-PD-L1 therapy[395]. The authors also demonstrated the upregulation of T effector cell cytokines IFN-ɣ and TNF-α in T cells from

tumour-draining lymph nodes (TDLN) and in the ascites of ID8 tumour-bearing mice following treatment with anti-PD-L1 antibody[395], suggesting that the PD-L1 blockade-mediated reduction in tumour growth may be attributed to stimulation of the T effector response. Furthermore, PD-L1 expression on tumour infiltrating DCs and macrophages, but not on tumour cells, was correlated with clinical response to PD-L1 therapy in patients with ovarian carcinoma[395]. Additional research has revealed more specific parameters that may predict the response to immune checkpoint inhibitors. A clinical trial investigating the combination of durvalumab (anti-PD-L1) with olaparib (PARPi) or cediranib (VEGFRi) showed that the percentage of tumour infiltrating lymphocytes (TILs) and PD-L1+ TILs may be a more effective indicator of response durability to durvalumab than PD-L1 expression in tumour tissues[198].

Therefore, whilst host- and tumour-expression of PD-L1 may be a useful predictive biomarker in some malignancies, there are issues with the reliability of PD-L1 as a prognostic indicator of response to PD-1/PD-L1 blockade, possibly due to its inducible pattern of expression, and in contexts where PD-L1 expression is driven by non-immune related mechanisms[396]. This highlights the need to further understand the clinical efficacy of PD-1/PD-L1 blockade in the context of more complex host-tumour interactions and other immune populations in the TME.

T cell infiltration and immunologically 'hot' tumours provide a therapeutic opportunity to improve the efficacy of immune checkpoint inhibition[397]. The presence of TILs is a significant prognostic factor in ovarian cancer[315], despite some uncertainty regarding which of CD3+, CD4+ or CD8+ T cells provide the greatest survival benefit[126-128,398]. Evidence in other solid cancers also suggests that 'priming' of the tumour to enhance infiltrating T cells may improve the response to PD-1 blockade[399,400]. For example, higher CD8+ T cell densities at the invasive margin in pre-treatment tumour samples from patients with metastatic melanoma predicted a positive response to pembrolizumab (anti-PD-1)[400]. Moreover, patients that responded to pembrolizumab exhibited a further increase in CD8+ T cells at the invasive margin and in the tumour parenchyma during treatment, compared to patients whose cancer progressed[400].

The CXCR3 receptor and corresponding ligands, CXCL9 and CXCL10, directly influences T effector cell infiltration[31]. Recent data suggests an important role of the CXCR3 axis in the response to anti-PD-1 therapy and is now gaining interest as an opportunity for therapeutic intervention[339,401,402]. For example, anti-PD-1 treatment was ineffective at reducing tumour growth in CXCR3 knockout mouse models[380,403], demonstrating the requirement for a functional CXCR3 pathway to mediate the anti-PD-1 anti-tumour immune response. In the MC38 tumour model, the authors showed that CXCR3 expression on CD8+ T cells was essential for activation of CD8+ T cells in response to anti-PD1 therapy, and that host derived CXCL9 was required for complete therapeutic benefit[380]. This was supported by another study in a melanoma mouse model which showed that blockade of CXCR3 significantly amplified tumour growth, which was rescued by the intratumoural injection of recombinant CXCL9 and CXCL10[404]. Moreover, treatment with CXCL9 and CXCL10 increased tumour-associated CD8+, CD4+ and CXCR3+ T cells and synergised with anti-PD-1 to significantly reduce tumour volume. Furthermore, in an orthotopic hepatocellular carcinoma (HCC) model, elevated expression of the CXCR3 ligand, CXCL10, by treatment with a vascular endothelial growth factor receptor (VEGFR) inhibitor synergised with anti-PD-1 therapy to inhibit growth and increase survival via CXCR3-mediated CD8+ T cell infiltration[405].

We have discussed the multiple roles of the serine protease DPP4 in cancer (see Chapter 1). Previous work by our lab demonstrated that DPP4 inhibition using sitagliptin, an FDA approved inhibitor, significantly increased the percentage of CXCR3+ tumour infiltrating lymphocytes in a primary ovarian cancer mouse model[285]. In addition, other reports have shown that inhibition of DPP4 *in vivo* increases activated T cell infiltration and restores the functional CXCR3 ligand, CXCL10[309,313]. In Chapter 4, we investigated DPP4 inhibition with sitagliptin in a syngeneic, metastatic ovarian cancer mouse model. We determined that sitagliptin-treated mice had elevated circulating levels of CXCL10 and a corresponding increase in tumour-specific leukocyte infiltration compared to untreated mice. This data suggested that sitagliptin may facilitate conversion from an immunologically ‘cold’ to ‘hot’

tumour, where the increase in infiltrating PD-1+ CD4+ T cells could provide enhanced susceptibility to PD-1/L1 blockade. The potential therapeutic benefit of combining sitagliptin with immune checkpoint inhibitors targeting the PD-1/PD-L1 axis has not previously been investigated.

We hypothesised that simultaneous inhibition of DPP4 and PD-1/PD-L1 would synergise *in vivo* to enhance the anti-tumour immune response, reduce tumour burden and prolong survival. We investigated this hypothesis via treatment with a combination of sitagliptin + anti-PD-1 or anti-PD-L1 antibody in a metastatic, syngeneic ovarian cancer mouse model to assess the therapeutic effect of these novel therapies in an immunocompetent model that recapitulates late-stage ovarian disease.

5.2 Results

5.2.1 Defining a treatment strategy for combination therapy

In order to investigate the potential synergistic action of sitagliptin and anti-PD-1 or anti-PD-L1 antibody therapy, metastatic tumours were established in female C57BL/6J mice over two weeks as previously described in chapter 4; at which point mice commenced daily oral sitagliptin treatment (50mg/kg body weight/day) until endpoint. This time point was chosen to initiate antibody therapy due to the fact that a significant proportion of sitagliptin-mediated intratumoural responses occurred two weeks following commencement of sitagliptin treatment (see Chapter 4). Mice received IP injections of either (i) anti-PD-1 (clone 29F.1A12) or IgG2a control antibody; or (ii) anti-PD-L1 (clone 10F.9G2) or IgG2b control antibody every second day for a total of 5 injections. We tested these two different approaches of blocking the PD-1/PD-L1 pathway to assess any differences that may arise via targeting PD-1 on T cells or PD-L1 on tumour cells. Mice were humanely culled at week 6 post-tumour-inoculation and at humane endpoint (Figure 5.1). At week 6, serum was collected for cytokine analysis, tumours were harvested for immunofluorescence staining and leukocytes from the blood, spleen and peritoneal cavity were isolated and analysed by flow cytometry for specific immune cell populations including T cells (CD3+), CD8+ T cells, CD4+ T cells, regulatory T cells (Tregs), migrating, inhibitory, proliferating and activated T cells and natural killer T (NKT) cells (Supplementary Figure S5.1).

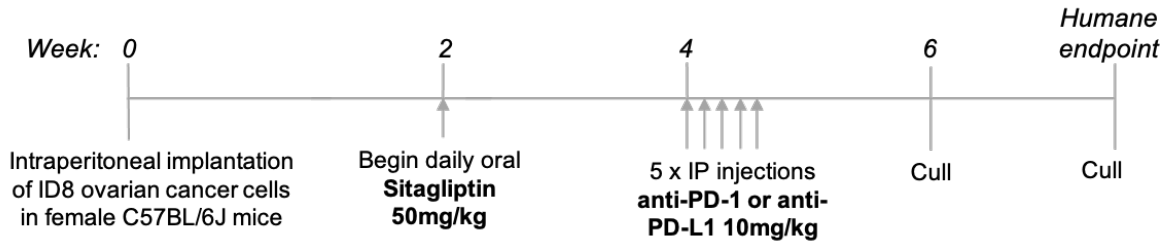

Figure 5.1. Schematic representation of the experimental timeline for sitagliptin + anti-PD-1/PD-L1 antibody treatment in a metastatic ovarian cancer mouse model.

5.2.2 Clinical outcomes of sitagliptin + anti-PD-1/L1 combination therapy

5.2.2.1 Sitagliptin + anti-PD-1/PD-L1 prolonged survival

We previously showed that sitagliptin prolonged survival in mice with metastatic ovarian cancer (see Chapter 4), therefore we were interested to understand if combining sitagliptin with anti-PD-1/PD-L1 therapy maintained or further improved this survival advantage. Weight and circumference were used to monitor overall body condition[406] and time taken for mice to reach humane endpoint was used to quantify overall survival.

Sitagliptin plus anti-PD-1: No significant differences were observed in either weight or abdominal circumference across all treatment groups for mice treated with sitagliptin + anti-PD-1 (Figure 5.2A, B). Kaplan-Meier curves and log-rank analysis indicated that sitagliptin + anti-PD-1 significantly prolonged survival compared to untreated controls (p-value = 0.0051) (Figure 5.2C). However, there was no significant difference in survival between mice that received sitagliptin + anti-PD-1 compared to either treatment alone (median survival: sitagliptin alone, 67 days; anti-PD-1 alone, 65 days; sitagliptin + anti-PD-1, 71 days), indicating that there may not be an overall survival advantage for the combination treatment (Figure 5.2C).

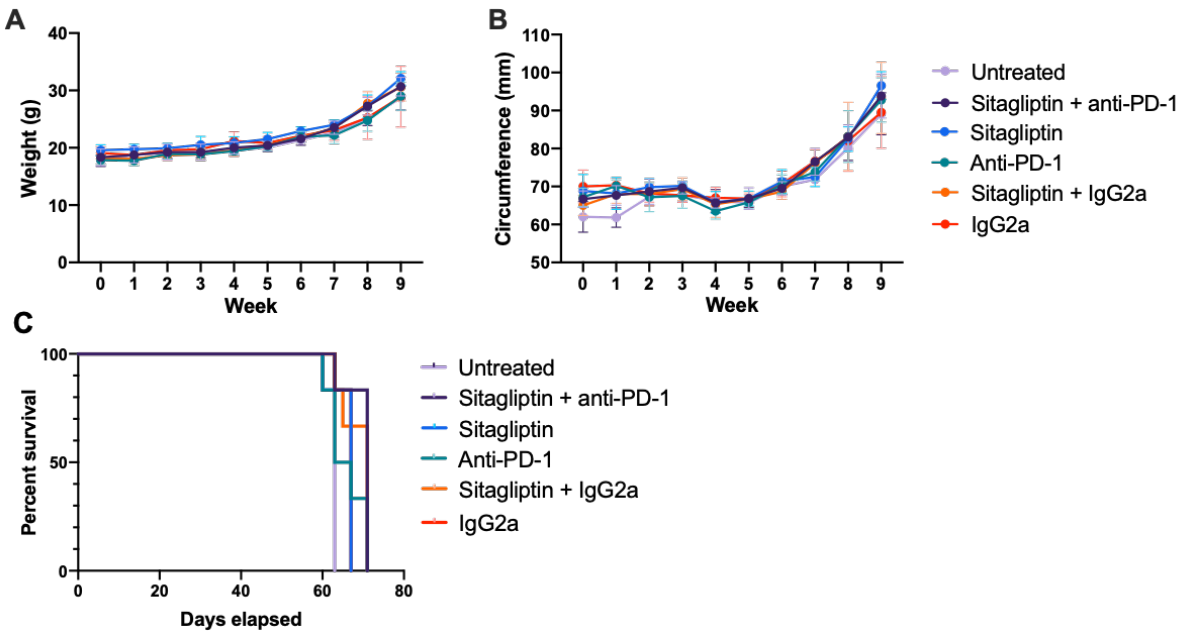

Figure 5.2. Weight, circumference and overall survival of mice treated with sitagliptin + anti-PD-1 antibody. *Mice bearing metastatic ID8 tumours commenced sitagliptin treatment and antibody therapy at 2- and 4 weeks-post-tumour-inoculation, respectively, and were culled at humane endpoint. (A) Weight and (B) circumference were measured weekly. (C) Kaplan-Meier curves and log-rank test of overall survival analysis between treatment groups. Data are represented as mean ± SD, n=6.*

Sitagliptin plus anti-PD-L1: Similar to sitagliptin + anti-PD-1, there was no difference in weight or circumference in mice receiving combination therapy or either therapy alone compared to controls (Figure 5.3A, B), demonstrating that sitagliptin + PD-L1 did not impact body condition according to these parameters. Kaplan-Meier curves and log-rank analyses identified that treatment with sitagliptin + anti-PD-L1 significantly prolonged the survival of mice compared to untreated controls (p-value = 0.0051). There was no significant difference in percent survival between mice that received combination therapy vs either treatment alone (median survival; sitagliptin alone 67 days, PD-L1 alone 66 days, sitagliptin + anti-PD-L1 69 days, indicating that there was no overall survival advantage for the combination treatment (Figure 5.3C).

Overall, sitagliptin + anti-PD-L1/L1 were both equally as effective at prolonging survival in mice bearing metastatic ID8 tumours, suggesting that these novel combination therapies may provide a potential clinical benefit by delaying disease progression.

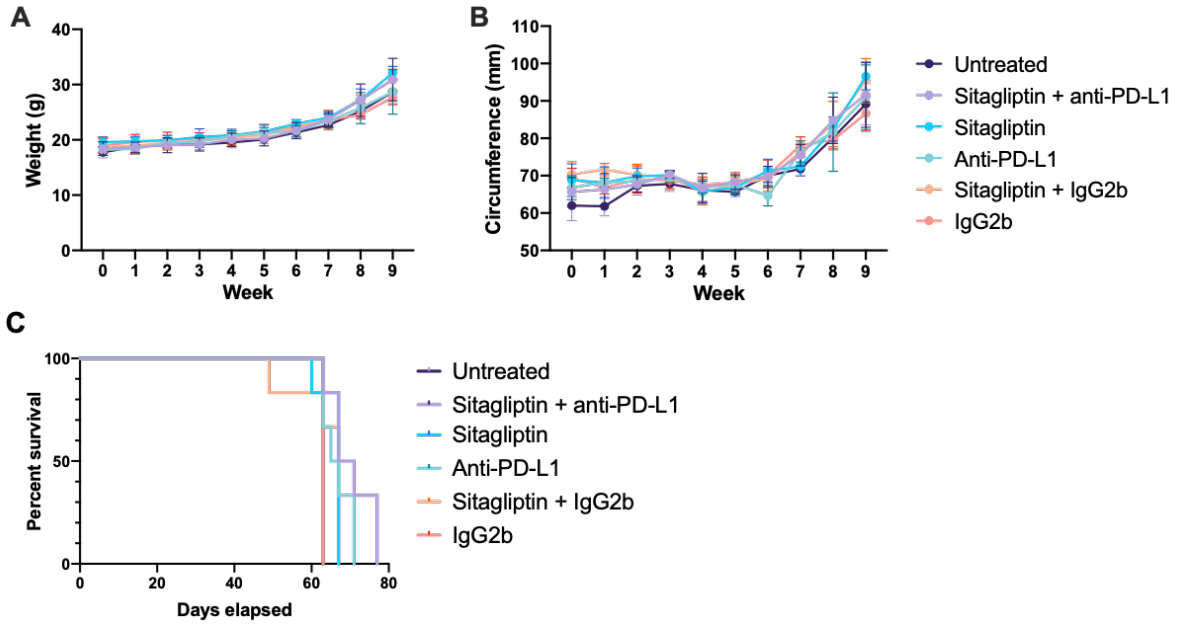

Figure 5.3. Weight, circumference and overall survival of mice treated with sitagliptin + anti-PD-L1 antibody. *Mice bearing metastatic ID8 tumours commenced sitagliptin treatment and antibody therapy at 2- and 4 weeks-post-tumour-inoculation, respectively, and were culled at humane endpoint. (A) Weight and (B) circumference were measured weekly. (C) Kaplan-Meier curves and log-rank test of overall survival analysis between treatment groups. Data are represented as mean ± SD, n=6.*

5.2.2.2 Sitagliptin + anti-PD-1 may decrease overall metastatic burden

To obtain a more accurate snapshot of tumour burden, the abdominal cavity was exposed post-mortem and macroscopic tumour nodules within the peritoneal space and surrounding organs directly counted. Similar to our previous study using sitagliptin in mice with primary ovarian cancer[285], mice that received combination sitagliptin + anti-PD-1 therapy had an overall reduction in visible metastases compared to single therapy or untreated control groups (Table 5.1). A reduction in omental metastases was associated with anti-PD-1 treatment alone; conversely, peritoneal wall metastases were increased in the anti-PD-1 alone group whilst combination with sitagliptin prevented this increase (Table 5.1). Overall, the combination

of sitagliptin with anti-PD-1 reduced total tumour burden in mice with advanced metastatic disease.

Table 5.1. Post-mortem observations in mice treated with sitagliptin + anti-PD-1 antibody. *Mice bearing metastatic ID8 tumours commenced sitagliptin treatment and antibody therapy at 2- and 4 weeks-post-tumour-inoculation, respectively, and were culled 6-weeks post-tumour-inoculation. Observations were made post-mortem to assess for the extent of disease including liver anaemia, and liver, omental, peritoneal wall and small intestine metastases. Each '+' represents the presence of the observation in one mouse. n = 6.*

	Untreated	*Sitagliptin*	*Anti-PD-1*	*Sitagliptin + anti-PD-1*
Liver anaemia	-	+	+	-
Liver metastases	+	-	-	-
Omental metastases	+++	++++	++	++
Peritoneal wall metastases	+	+	+++	+
Small intestine metastases	++++++	++++++	++++++	+++++
Overall metastasis score	**11**	**11**	**11**	**8**

5.2.3 Immune parameters with the combination of sitagliptin + anti-PD-1

5.2.3.1 Sitagliptin + anti-PD-1 altered T cell populations in the spleen, peritoneal cavity and tumour infiltrates

The presence of T cells in the TME and their infiltration in tumours is a positive prognostic indicator in ovarian cancer[126,127]. CD8+ T cells, or cytotoxic lymphocytes (CTLs), are critical in killing of malignant cells, whilst the CD4+ T cell response supports the activation of B cells, CD8+ T cells and innate immune cells. In order to gain a general understanding of the immune landscape following treatment with sitagliptin + anti-PD-1, percentages of all T cells, CD8+ T cells and CD4+ (CD25-FoxP3-) T cells in the spleen, blood and peritoneal cavity were assessed.

The combination of sitagliptin + anti-PD-1 reduced CD8+ and CD4+ T cell populations in the spleen, which was anti-PD-1 specific in both cases (Figure 5.4Bi, Ci). These changes were associated with a concomitant overall increase in CD3+ T cells in the peritoneal cavity (Figure 5.4Aiii), which was specifically induced by sitagliptin. There was a supporting trend of increasing CD8+ T cells in the peritoneal cavity, which did not reach significance, and no changes were observed in CD4+ T cells in the peritoneal cavity (Figure 5.4Biii, Ciii). CD8+ T cells were also increased in the blood of mice treated with sitagliptin alone (Figure 5.4Bii) which was discussed in chapter 4; otherwise, there were no overall changes to T cell populations in combination treated mice.

Overall, other than some subtle changes to T cell populations, the combination of sitagliptin + anti-PD-1 did not affect circulating CD3+, CD8+ or CD4+ T cells, or T cells resident in the spleen and peritoneal cavity compared to either treatment alone or untreated mice, indicating the combination treatment does not significantly alter the overall peripheral immune landscape.

Tumour infiltrating lymphocyte (TIL) populations were also directly examined in tumour tissues by immunofluorescence staining. Similar to observations in mice treated with sitagliptin alone, infiltrating CD8+ T cells were significantly increased in tumours from mice treated with sitagliptin + anti-PD-1 compared to untreated controls (Figure 5.5B). There was no significant difference in abundance of infiltrating T cells or CD4+ T cells in tumours from combination treated mice compared to controls (Figure 5.5C, D; images not shown).

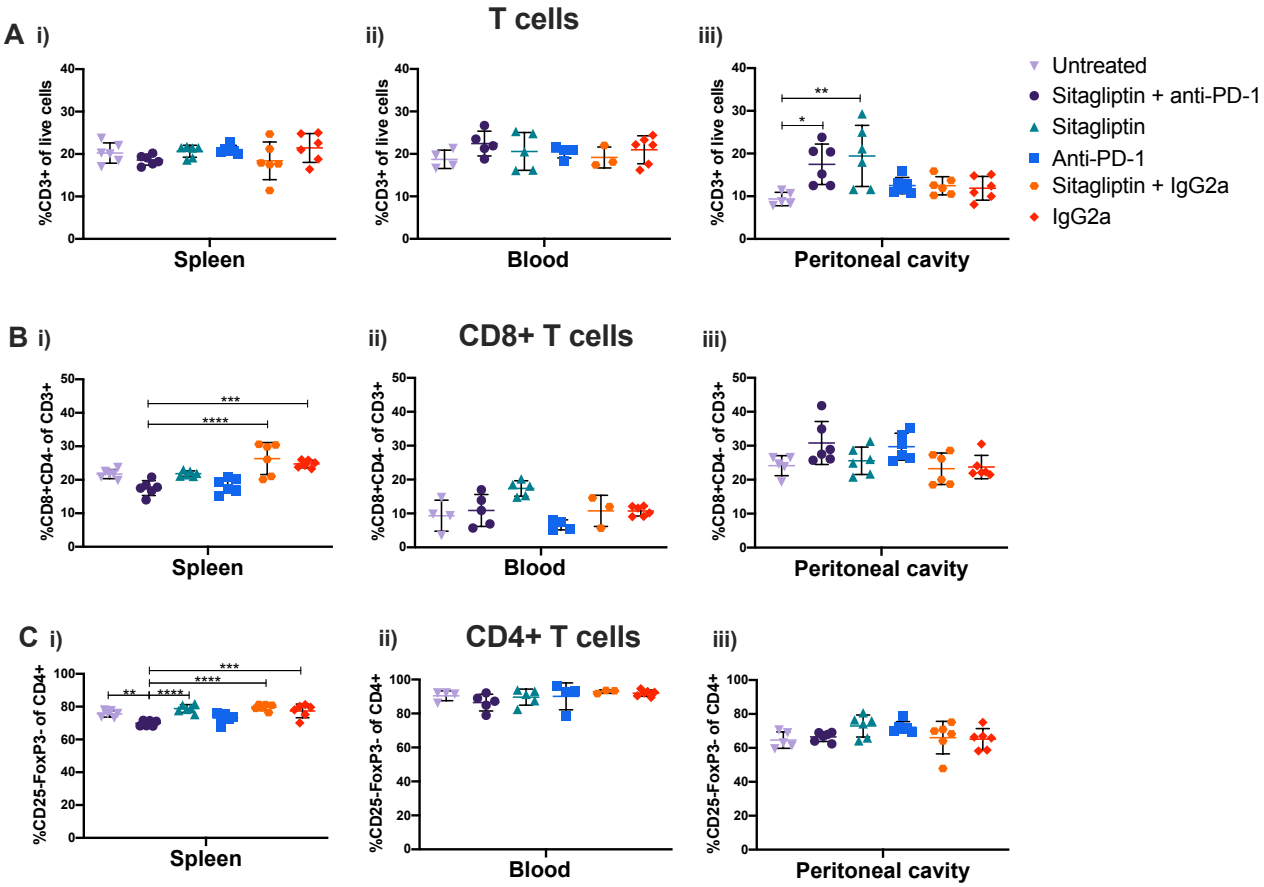

Figure 5.4. T cells, CD8+ T cells and CD4+ T cells in mice treated with sitagliptin + anti-PD-1 antibody. *Mice bearing metastatic ID8 tumours commenced sitagliptin treatment and antibody therapy at 2- and 4 weeks-post-tumour-inoculation, respectively, and were culled 6-weeks post-tumour-inoculation. Leukocytes from the spleen, blood and peritoneal cavity were isolated and analysed for the abundance of T cells, CD8+ T cells and CD4+ T cells by flow cytometry. Percentages of (A) T cells (%CD3+ of live), (B) CD8+ T cells (%CD8+CD4- of T cells) and (C) CD4+ T cells (%CD25-FoxP3- of CD4+ (CD4+CD8-) cells) in the i) spleen, ii) blood and iii) peritoneal cavity. Data are represented as mean ± SD, n=6. Differences between groups were determined by one-way ANOVA; *p<0.05, **p<0.01, ***p<0.005, ****p<0.001.*

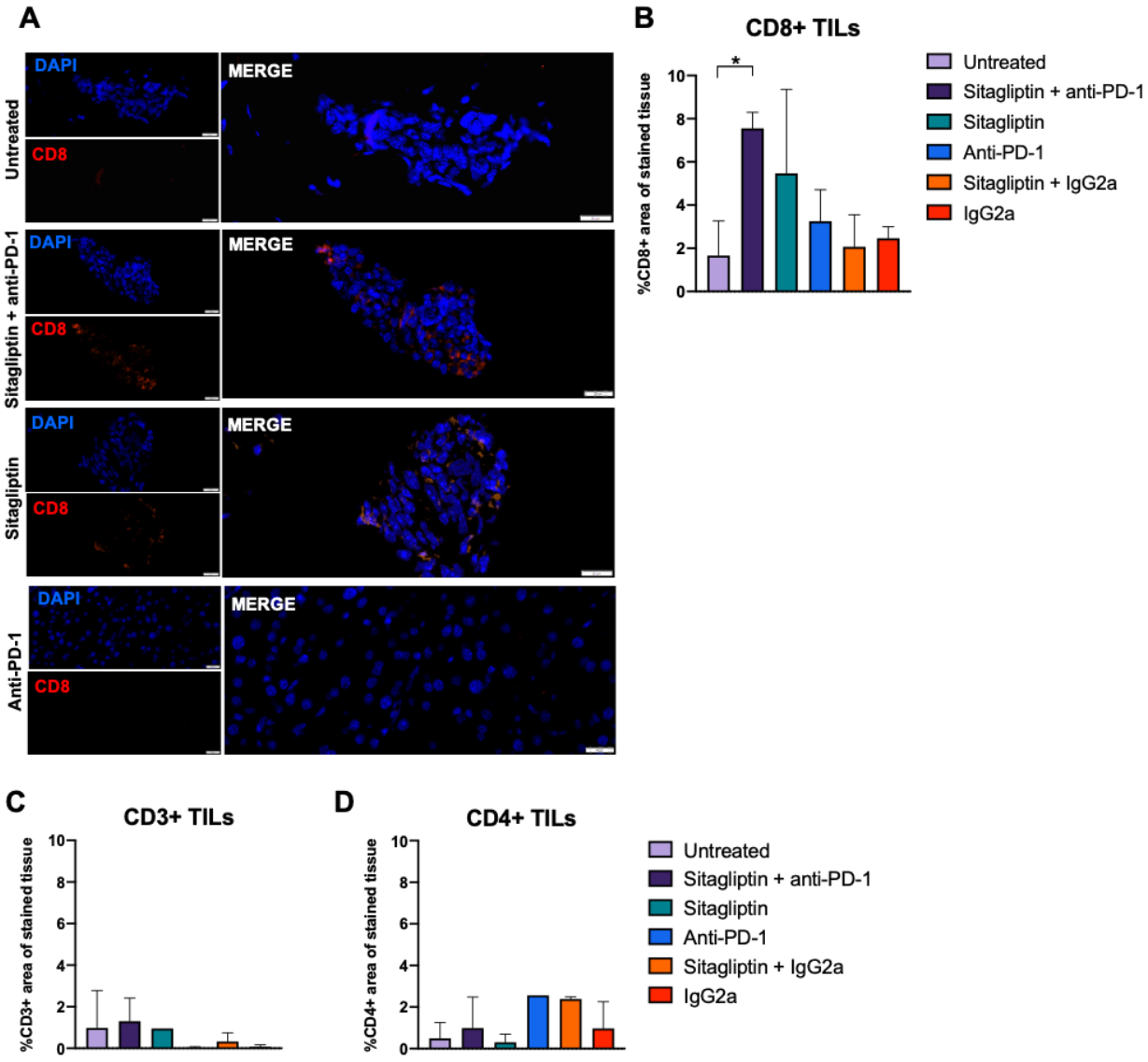

Figure 5.5. Tumour-infiltrating T cells, CD8+ T cells and CD4+ T cells from mice treated with sitagliptin + anti-PD-1 antibody. *Mice bearing metastatic ID8 tumours commenced sitagliptin treatment and antibody therapy at 2- and 4 weeks-post-tumour-inoculation, respectively, and were culled 6-weeks post-tumour-inoculation. Tumours were harvested to examine leukocyte infiltration by immunofluorescence. Metastatic ID8 tumour sections were stained with primary antibodies against CD8 (red). (A) Representative images of CD8+ expression in tumour sections and (B) corresponding percentage area of infiltrating CD8+ T cells. Percentage area of infiltrating (C) CD4+ and (D) CD3+ T cells. Scale bar = 20μm. Data are presented as mean ± SD, n=3-6. Differences between groups were determined by one-way ANOVA; *p<0.05.*

5.2.3.2 Combination therapy using Sitagliptin + anti-PD-1 enhanced the functional potential of T effector cells

The proliferation and activation status of T effector cells influences their ability to exert an anti-tumour response and may provide a more accurate depiction of their functional efficacy in the TME than percentages of CD8+ and CD4+ T cells alone. In chapter 4, we demonstrated that sitagliptin treatment increased tumour-infiltrating PD-1+ CD4+ T cells at week 4, thereby potentially increasing sensitivity to anti-PD1 therapy at this time point. Therefore, we were interested in evaluating the functional status of T effector cells in response to combination therapy by using Ki67 as a marker of proliferation[320], CD69 as a marker of activation[321] and PD-1 as a marker of inhibition/exhaustion[322].

Mice that received combination sitagliptin + anti-PD-1 therapy had significantly increased percentages of proliferating Ki67+CD8+ (p-value = 0.0072 vs untreated) and Ki67+CD4+ (p-value <0.0001 vs untreated) T cells resident in spleen (Figure 5.6A), which was also accompanied by an increase in the percentage of activated CD69+ CD8+ T cells (Figure 5.6B). Similarly, activated CD69+ CD8+ T cells were also increased in the peritoneal cavity (Figure 5.6C) suggesting the expansion of CD8+ T effector cells in the spleen and recruitment to the peritoneal cavity in response to the combination therapy. The activation status of CD4+ T cells resident in spleen or peritoneal cavity was unaffected. Overall, the combination of sitagliptin + anti-PD-1 synergised to induce the activation and proliferation of T effector cells in the spleen and was suggestive of migration from spleen to the peritoneal cavity.

The activation status of TILs was further explored by immunofluorescence staining. Mice that received sitagliptin + anti-PD-1 combination therapy exhibited an increasing trend in infiltrating activated CD69+ CD8+ T cells, which was mediated by sitagliptin (Figure 5.7A). There was also a decreasing trend in PD-1+ CD4+ T cells in the tumours of mice that received combination therapy compared to anti-PD-1 alone (Figure 5.6B), demonstrating a synergistic

effect of sitagliptin + anti-PD-1 at decreasing potential T cell exhaustion and simultaneously increasing T cell activation.

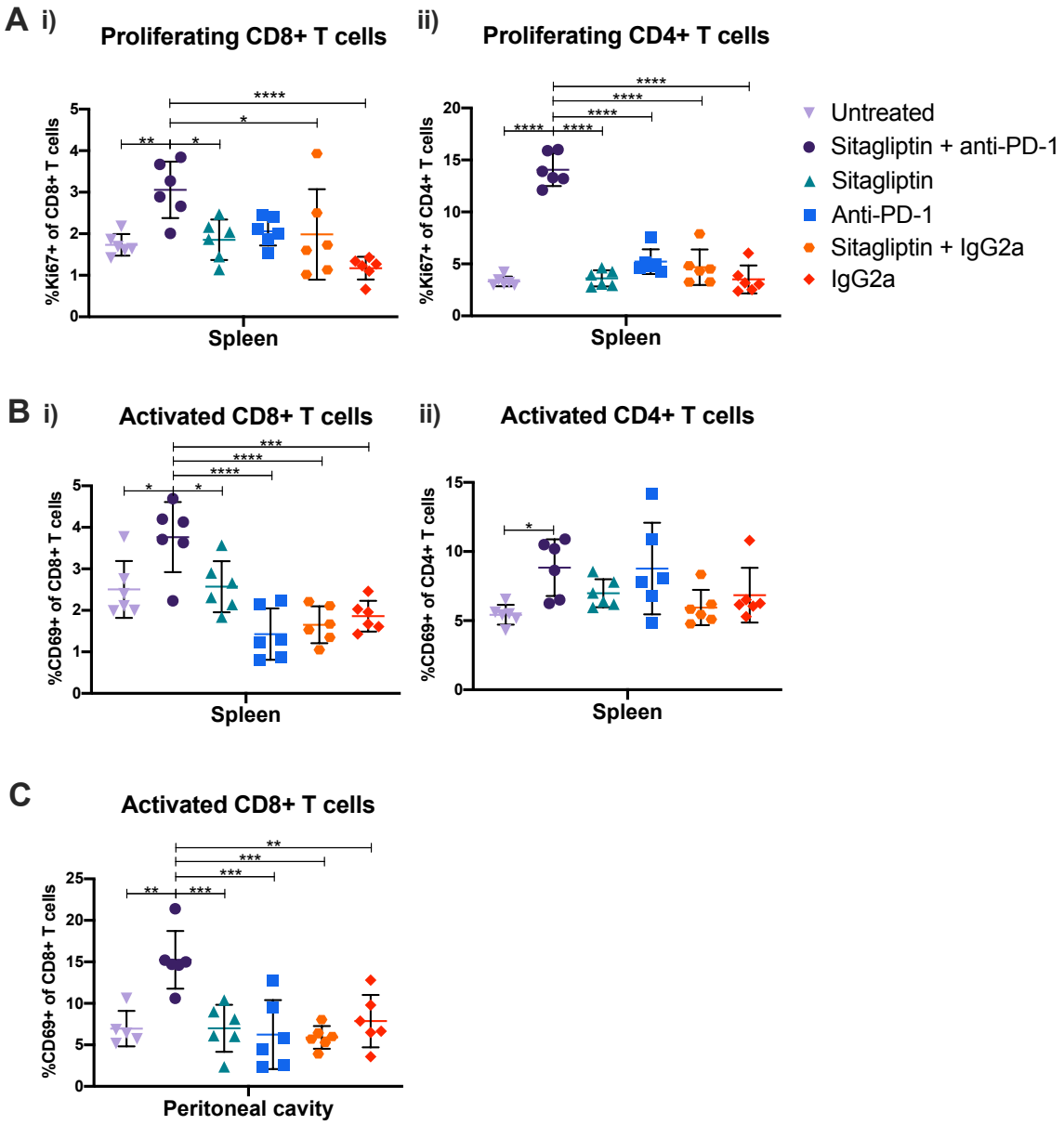

Figure 5.6. Activated and proliferating CD8+ and CD4+ T cells in mice treated with sitagliptin + anti-PD-1 antibody. *Mice bearing metastatic ID8 tumours commenced sitagliptin treatment and antibody therapy at 2- and 4 weeks-post-tumour-inoculation, respectively, and were culled 6-weeks post-tumour-inoculation. Leukocytes from the spleen and peritoneal cavity were isolated and analysed for the abundance of activated and proliferating CD8+ T cells and CD4+ T cells by flow cytometry. (A) Percentages of proliferating i) CD8+ T cells (%Ki67+ of CD8+ T cells) and ii) CD4+ T cells (%Ki67+ of CD4+ T cells) in the spleen. (B) Percentages of activated i) CD8+ T cells (%CD69+ of CD8+ T cells) and ii) CD4+ T cells (%CD69+ of CD4+ T cells) in the spleen. (C) Percentages of activated CD8+ T cells in the peritoneal cavity. Data are represented as mean ± SD, n=6. Differences between groups were determined by one-way ANOVA; *p<0.05, **p<0.01, ***p<0.005, ****p<0.001.*

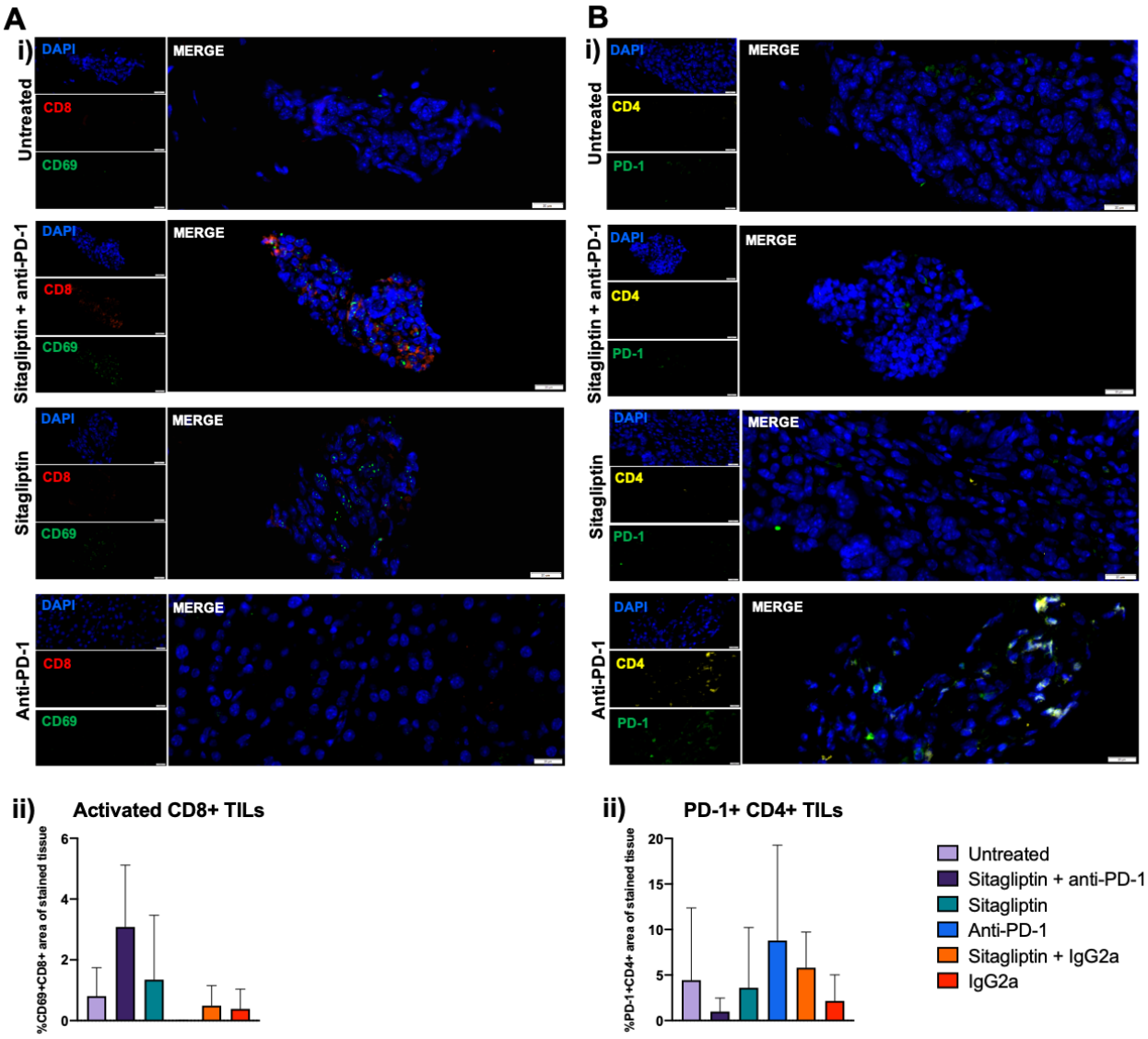

Figure 5.7. Activation and inhibitory status of tumour-infiltrating CD8+ T cells in mice treated with sitagliptin + anti-PD-1 antibody. *Mice bearing metastatic ID8 tumours commenced sitagliptin treatment and antibody therapy at 2- and 4 weeks-post-tumour-inoculation, respectively, and were culled 6-weeks post-tumour-inoculation. Tumours were harvested to examine leukocyte infiltration by immunofluorescence. Metastatic ID8 tumour sections were stained with primary antibodies against (A) CD8 (red) and CD69 (green) and (B) CD4 (yellow) and PD-1 (green). Representative images (i) and corresponding percentage area (ii) of infiltrating CD69+CD8+ and PD-1+CD4+ T cells, respectively, are shown. Scale bar = 20μm. Data are presented as mean ± SD, n=3-6. Differences between groups were determined by one-way ANOVA.*

5.2.3.3 Sitagliptin + anti-PD-1 polarised the adaptive immune response towards Th1 immunity

Activated CD4+ T helper (Th) cells can be broadly divided into Th1 and Th2 subsets. In a cancer context, Th1 related immune cells drive anti-tumoural immune responses including enhancing the killing capacity of some innate cells and increasing the activation of CD8+ T cells, whilst the Th2 response is implicated in tumour cell proliferation and survival[111]. Therefore, Th1 driven responses are associated with a more favourable prognosis in epithelial ovarian cancers.

To investigate whether increased activation of CD8+ T cells (see Section 5.2.3.2) may be driven by the Th1 response, we examined the proportions of CXCR3+ CD4+ (CD25-FoxP3-) T cells[175]**.** Compared to controls, mice treated with combination therapy had an increased percentage of Th1 cells in the blood (Figure 5.8A; p-value = 0.0052 vs untreated) and in the peritoneal cavity (Figure 5.8B; p-value = 0.0237 vs untreated). There were no changes noted in spleen (not shown). This increase in CXCR3+ CD4+ T cells suggests polarisation of cells towards a Th1 phenotype in response to the combination therapy, which was most marked in circulation. Th1 polarisation in the peritoneal cavity was largely due to Sitagliptin alone, with a small additive effect induced by the combination (Figure 5.8B).

The tumour infiltrating Th1 T cell subset was also evaluated in tumour tissue by immunofluorescence staining. Compared to untreated controls, tumours from mice treated with sitagliptin exhibited a trending increase in infiltrating CXCR3+ CD4+ T cells (Figure 5.8C). This trend was also observed to a lesser extent in tumours from mice treated with the combination therapy. Our data indicates that sitagliptin may facilitate the increase in intratumoural Th1 cells by mediating their migration from the blood into the TME.

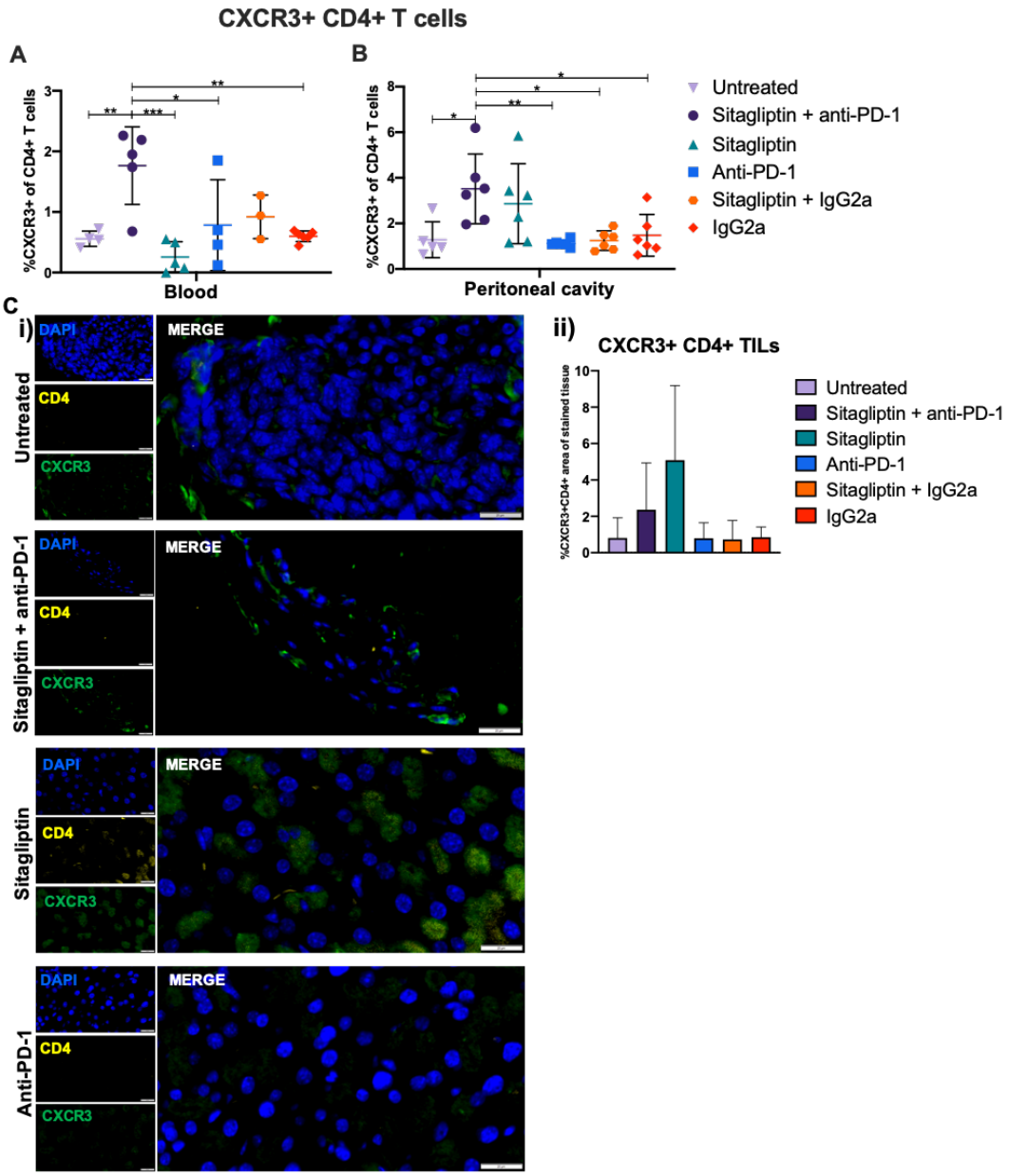

Figure 5.8. CXCR3 expression on T cells in mice treated with sitagliptin + anti-PD-1 antibody. *Mice bearing metastatic ID8 tumours commenced sitagliptin treatment and antibody therapy at 2- and 4 weeks-post-tumour-inoculation, respectively, and were culled 6-weeks post-tumour-inoculation. Leukocytes from the blood and peritoneal cavity were isolated and analysed for the abundance CXCR3+ CD4+ T cells by flow cytometry. Percentages of CXCR3+ CD4+ T cells (%CXCR3+ of CD4+ T cells) in the (A) blood and (B) peritoneal cavity. Tumours were harvested to examine leukocyte infiltration by immunofluorescence. Metastatic ID8 tumour sections were stained with primary antibodies against (C) CD4 (yellow) and CXCR3 (green). Representative images (i) and corresponding percentage area (ii) of infiltrating CXCR3+CD4+ T cells. Scale bar = 20μm. Data are represented as mean ± SD, n=3-6. Differences between groups were determined by one-way ANOVA; *p<0.05, **p<0.01, ***p<0.005.*

5.2.3.4 Sitagliptin + anti-PD-1 decreased T-regulatory cell populations and mitigated immunosuppressive effects induced by anti-PD-1 alone

Regulatory T cells (Tregs) are one of the key drivers of immune tolerance and pro-tumour immune responses. Tregs suppress activation, proliferation and cytokine production of T effector cells and produce suppressive cytokines within the TME[113]. Importantly, an increased population of tumour infiltrating Tregs in ovarian tumours is strongly associated with reduced survival[126,155]. Specific subsets of Tregs can be characterised according to their cell surface receptor expression. Of particular interest for this study was the expression of PD-1 on Tregs, which represents a distinct subset of highly suppressive cells[324].

We analysed the effect of sitagliptin + anti-PD-1 on the proportion of Tregs, with particular emphasis on the suppressive PD-1+ subset. Tregs were defined as CD4+(CD25+FoxP3+) cells. Interestingly, there was a significant increase in the percentages of Tregs resident in the spleen of mice treated with sitagliptin + anti-PD-1 compared to controls (p-value = 0.0002 vs untreated) which was not significant when compared to anti-PD-1 alone (p-value = 0.2180). A similar non-significant trend was observed in mice treated with anti-PD-1 alone (p-value = 0.0630), suggesting that the spleen-specific increase in Tregs was partially mediated by anti-PD-1.

By contrast treatment with either sitagliptin + anti-PD-1 or anti-PD-1 alone was associated with a significant decrease in PD-1+ Tregs in the peritoneal cavity (Figure 5.9B). Thus, combination therapy with anti PD-1 may have decreased the differentiation of adaptive Tregs, or their retention in – or migration from – the spleen to the peritoneal microenvironment.

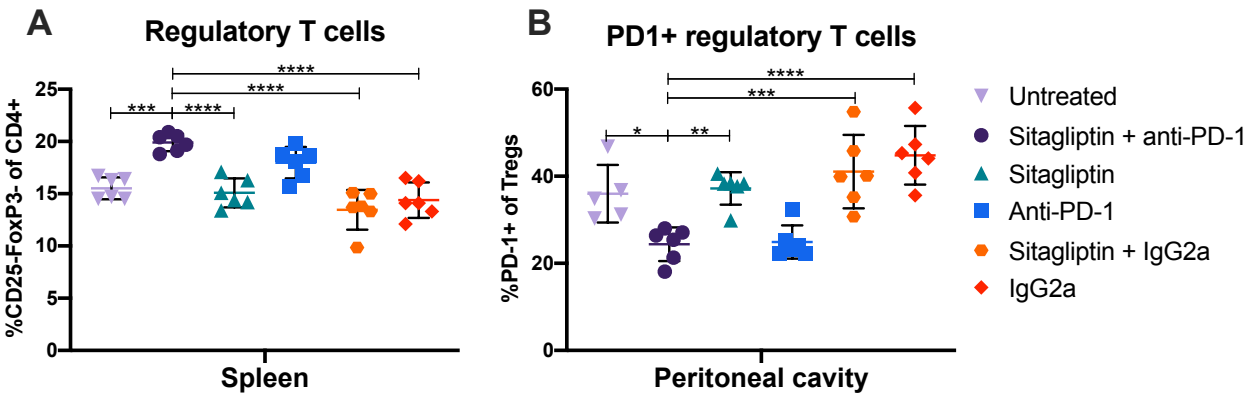

Figure 5.9. T regulatory cells and PD1+ T regulatory cells in mice treated with sitagliptin + anti-PD-1 antibody. *Mice bearing metastatic ID8 tumours commenced sitagliptin treatment and antibody therapy at 2- and 4 weeks-post-tumour-inoculation, respectively, and were culled 6-weeks post-tumour-inoculation. Leukocytes from the spleen and peritoneal cavity were isolated and analysed for the abundance of T regulatory cells and PD-1+ T regulatory cells by flow cytometry. Percentages of (A) T regulatory cells (%CD25+FoxP3+ of CD4+(CD4+CD8-) cells) in the spleen and (B) PD-1+ T regulatory cells (%PD-1+ of Tregs) in the peritoneal cavity. Data are represented as mean ± SD, n=6. Differences between groups were determined by one-way ANOVA; *p<0.05, **p<0.01, ***p<0.005, ****p<0.001.*

To investigate this phenomenon further we assessed Treg populations for activation status (CD69+) and migratory potential (CCR4+). Expression of CCR4+ on Tregs has been shown to be important for their chemokine-mediated migration to ovarian tumours and inhibition of the host anti-tumour response[155]. Mice treated with anti-PD-1 alone had significantly increased percentages of circulating activated and migratory Tregs compared to controls (Figure 5.10), suggesting that anti-PD-1 may increase their suppressive behaviour. This increase was prevented in mice treated with sitagliptin + PD-1 (Figure 5.10), suggesting that sitagliptin mitigated the anti-PD-1-mediated increase in these cell subsets. There was no difference in the percentages of CD69+ or CCR4+ Tregs in the spleen or peritoneal cavity (not shown).

The data suggest that anti-PD-1 therapy may in fact enhance the suppressive capacity of Tregs through increased migratory capacity, and therefore contribute to tumour survival rather

than tumour ablation. Combining sitagliptin with anti-PD-1 thus abrogated some of the negative anti-PD-1-specific effects on the anti-tumour response.

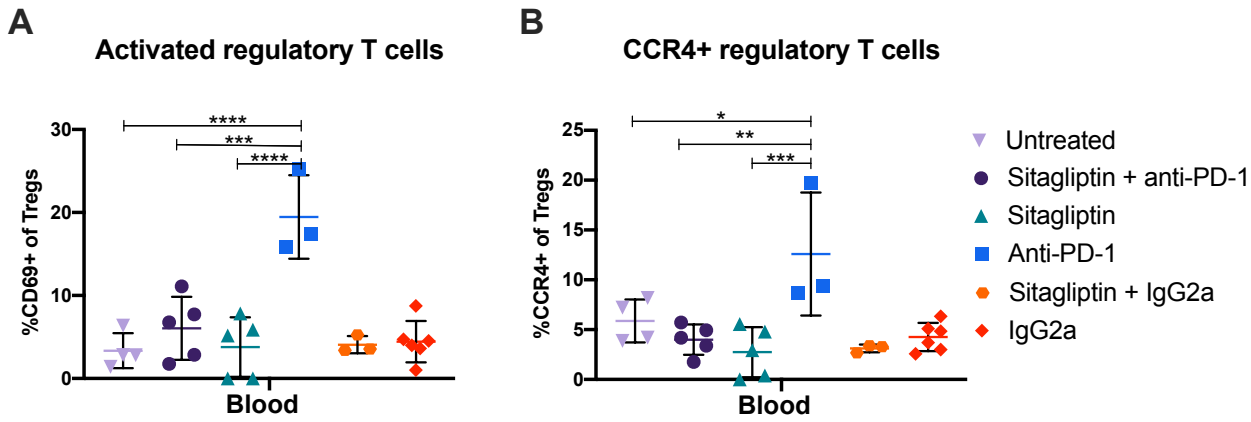

Figure 5.10. Activated and CCR4+ T regulatory cells in mice treated with sitagliptin + anti-PD-1 antibody. *Mice bearing metastatic ID8 tumours commenced sitagliptin treatment and antibody therapy at 2- and 4 weeks-post-tumour-inoculation, respectively, and were culled 6-weeks post-tumour-inoculation. Leukocytes from the spleen, blood and peritoneal cavity were isolated and analysed by flow cytometry and immune cell markers were used to identify activated and CCR4+ T regulatory cells. Percentages of (A) activated T regulatory cells (%CD69+ of Tregs) and (B) CCR4+ T regulatory cells (%CCR4+ of Tregs) in blood. Data are represented as mean ± SD, n=6. Differences between groups were determined by one-way ANOVA; *p<0.05, **p<0.01, ***p<0.005, ****p<0.001.*

5.2.3.5 Combination therapy altered circulating cytokines in tumour bearing mice

Soluble factors such as cytokines are a key element of the immune response in the ovarian TME and are crucial to regulate the differentiation, trafficking and activity of immune cells. In Chapter 4 we established that sitagliptin significantly influenced the abundance of multiple circulating chemokines and signalling molecules to alter the cytokine landscape and discussed the implications of these changes in the context of anti-tumour immunity. As DPP4 has the capacity to enzymatically modify multiple bioactive substrates, the immunomodulatory effects of its inhibition are unsurprising. We were therefore interested to assess how the addition of PD-1 blockade affected the cytokine landscape.

Multivariate analysis identified the differential expression of several effector molecules across the treatment groups, including CCL12, CCL1, TNF-α, CCL20, IL-10, GM-CSF, CXCL12 and CXCL16 (Figure 5.11A). The relative lack of clustering of each treatment shows that mice could not be grouped on an unsupervised basis, which may be due to the fact in almost all cases, the control IgG antibody affected cytokine levels potentially via a minor inflammatory response. The concentration of each differentially expressed cytokine was analysed individually, and we found that some of the significant differences in cytokine levels were exclusively sitagliptin-mediated, such as the upregulation of CXCL12, whilst others were augmented by the addition of anti-PD-1.

For example, GM-CSF, CXCL12, IL-6 and, to a lesser extent, CCL20, were all increased in response to sitagliptin alone, but not in the combination therapy. The concentration of CCL1 was not significantly different between groups when analysed by ANOVA (Figure 5.11B). Combination therapy decreased circulating levels of CXCL16, whilst some of the effects on cytokine abundance appeared to be exclusively mediated only PD-1 blockade, such as the increased concentration of CCL12 (Figure 5.11B).

Primarily, we showed that treatment with sitagliptin alone, anti-PD-1 alone and the combination treatment each has a unique effect on the cytokine landscape in ovarian cancer.

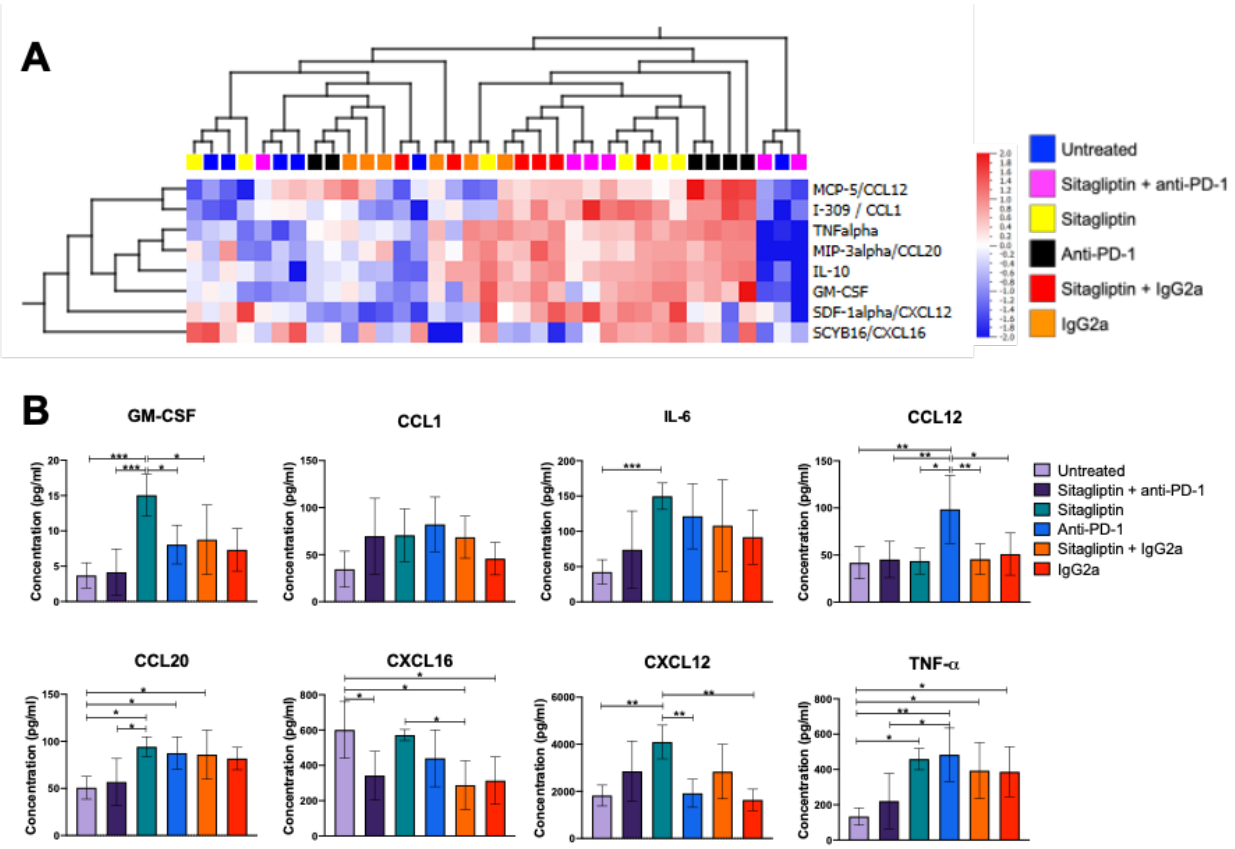

Figure 5.11. Differential expression of cytokines in mice treated with sitagliptin + anti-PD-1 antibody. *Mice bearing metastatic ID8 tumours commenced sitagliptin treatment and antibody therapy at 2- and 4 weeks-post-tumour-inoculation, respectively, and were culled 6-weeks post-tumour-inoculation. Cytokine levels in serum were measured using the Bio-Plex Pro™ Mouse Chemokine Panel, 31-plex (Bio-Rad, #12009159) and analysed using Qlucore Omics Explorer software 3.6 (Qlucore AB, Lund, Sweden). (A) Heatmap representing differentially expressed cytokines between groups was determined by multi-group comparison with p-value = 0.05. (B) Individual concentrations of differentially expressed cytokines. Data are represented as mean ± SD, n=6. Differences between groups were determined by one-way ANOVA; *p<0.05, **p<0.01, ***p<0.005.*

5.2.4 Immune parameters with the combination of sitagliptin + anti-PD-L1

5.2.4.1 Sitagliptin increased intratumoural PD-L1 expression in metastatic ID8 tumours

Similar to PD-1, there is evidence to suggest that PD-L1 may be a useful prognostic factor to predict response to immune checkpoint inhibition[395]. Despite this, clinical trials have reported modest efficacy with sub-clinical utility. When combined with anti PD-1, sitagliptin induced changes in specific T-cell subsets and immune effector molecules which provided some enhancement to the effects of immune checkpoint blockade (see Section 5.2.3 above). Based on this, we sought to further investigate the potential synergies between sitagliptin and ICIs targeting PD-L1.

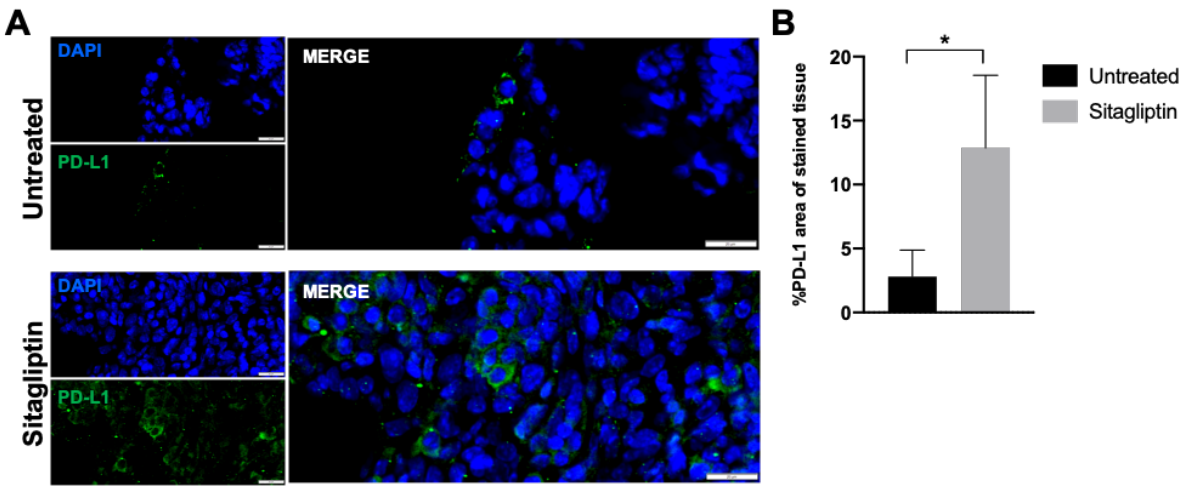

Figure 5.12. Intratumoural PD-L1 expression in mice treated with sitagliptin. *Mice bearing metastatic ID8 tumours commenced sitagliptin treatment at week 2-post-inoculation and were culled at week 6-post-tumour inoculation. Tumours were harvested and immunofluorescence was performed on tumour sections using primary antibody against PD-L1 (green). Representative images (i) and corresponding percentage area (ii) of intratumoural PD-L1 expression in tumours of untreated vs sitagliptin treated mice. Scale bar = 20μm. Data are presented as mean ± SD, n=3-6. Differences between groups were determined by unpaired t-test; *p<0.05, **p<0.01, ***p<0.005, ****p<0.001.*

We first evaluated the abundance of PD-L1 in tumour tissue in response to sitagliptin treatment. ID8 tumours express basal of PD-L1[407], however, tumours from mice treated with sitagliptin had significantly increased intratumoural PD-L1 staining compared to the untreated controls (Figure 5.12). This increase in intratumoural PD-L1 in response to sitagliptin suggests the potential to enhance response to anti-PD-L1 treatment in ovarian tumours.

5.2.4.2 Sitagliptin + anti-PD-L1 enhanced the functional potential of CD8+ T effector cells

Similar to the observed effects of sitagliptin + anti-PD-1 on T effector activation and proliferation (see Section 5.2.3.2), we assessed changes in CD69+ and Ki67+ CD8+ T cell subsets in mice treated with sitagliptin + anti-PD-L1. Both sitagliptin alone and anti-PD-L1 combination therapy significantly increased the percentage of circulating CD8+ T cells compared to controls (Figure 5.13A). Interestingly, treatment with anti-PD-L1 decreased the proportion of proliferating Ki67+ CD8+ T cells in the peritoneal cavity whilst the inclusion of sitagliptin abrogated this change (Figure 5.13B).

Similarly, the presence of activated (CD69+) CD8+ T cells in harvested tumours was undetectable in mice treated with PD-L1 alone (Figure 5.13C). However, sitagliptin + anti-PD-1 caused a trending increase in the percentage of tumour-infiltrating activated (CD69+) CD8+ T cells (Figure 5.13C). Taken together, the data indicates that combination therapy simultaneously improved the proliferation of CD8+ T cells in the peritoneal cavity and infiltration of activated CD8+ T effector cells. Thus, the apparent negative influence of anti PD-L1 on the proliferative capacity of circulating CD8+ T cells could be negated when combined with sitagliptin. Unlike treatments with PD-1 (see Section 5.2.3), there were no other changes noted in any samples tested.

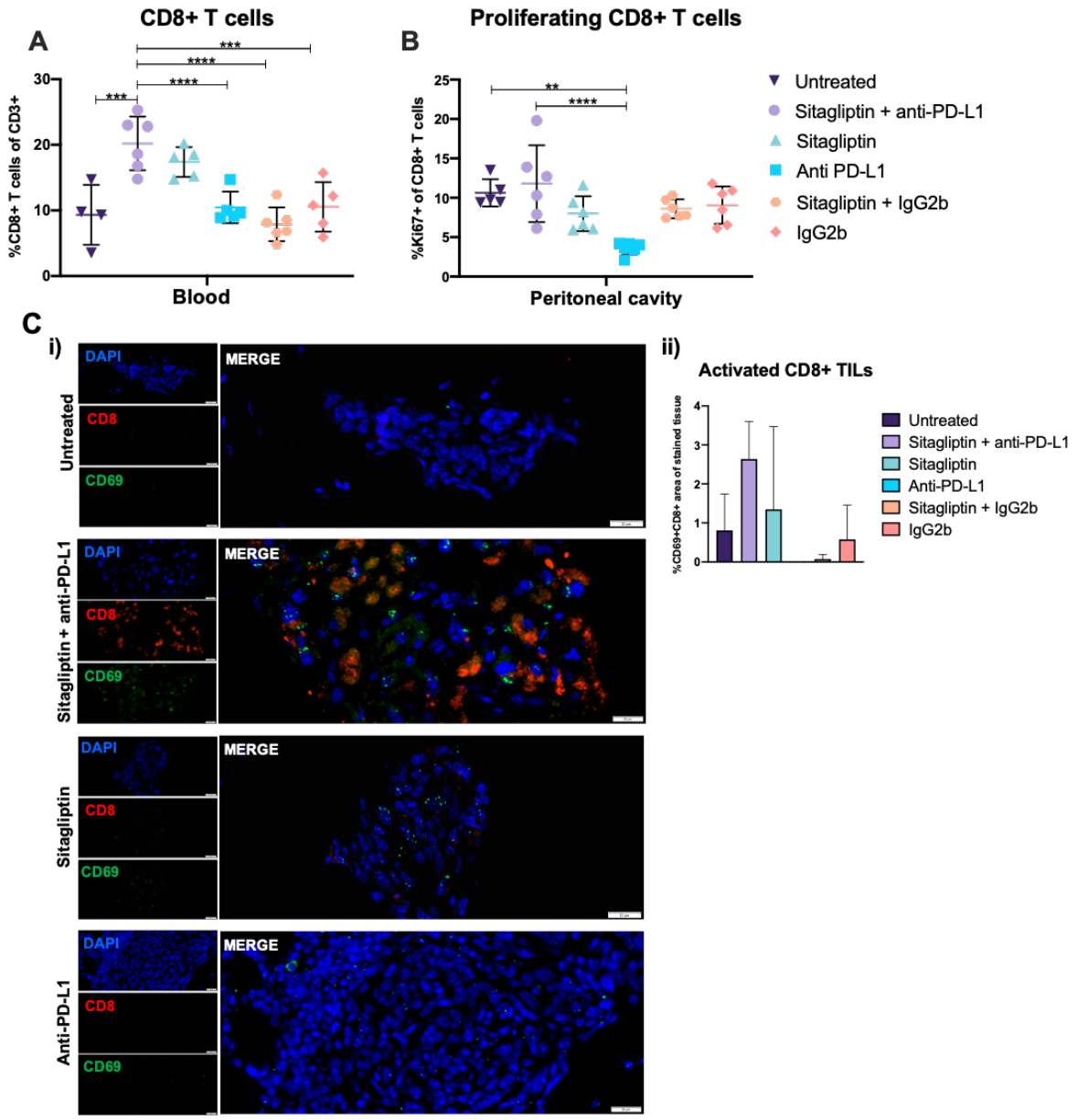

Figure 5.13. Overall CD8+ T effector cell response in mice treated with sitagliptin + anti-PD-L1. *Mice bearing metastatic ID8 tumours commenced sitagliptin treatment and antibody therapy at 2- and 4 weeks-post-tumour-inoculation, respectively, and were culled 6-weeks post-tumour-inoculation. Leukocytes from the blood and peritoneal cavity were isolated and analysed for the abundance of CD8+ T cells and proliferating CD8+ T cells by flow cytometry. Percentages of (A) CD8+ T cells (%CD8+CD4- of T cells) in the blood and (B) proliferating CD8+ T cells (%Ki67+ of CD8+ T cells) in the peritoneal cavity. Tumours were harvested to examine leukocyte infiltration by immunofluorescence. (C) Metastatic ID8 tumour sections were stained with primary antibodies against CD8 (red) and CD69 (green). Representative images (i) and corresponding percentage area (ii) of infiltrating CD69+CD8+ T cells. Data are represented as mean ± SD, n=3-6. Differences between groups were determined by one-way ANOVA; *p<0.05, **p<0.01, ***p<0.005, ****p<0.001.*

5.2.4.3 Sitagliptin + anti-PD-L1 increased peripheral NKT cells

Whilst CD8+ T effector cells are the primary cell type responsible for tumour cell destruction in ovarian cancer, NKT cells display characteristics of both T- and NK- cells and are also key regulators of tumour immunosurveillance[408]. There is evidence to suggest that PD-1/PD-L1 blockade may enhance the activity of NKT cells via stimulation of Th1 cytokine secretion[409] Low levels of NKT cells have been reported in other solid cancers including CRC, melanoma, breast and renal cell cancer[410] and are associated with poor clinical outcome in patients with head and neck squamous cell carcinoma (HNSCC)[411].

To further understand anti-tumour responses in mice treated with sitagliptin + anti-PD-L1, we examined the abundance of NKT cells (defined as %NK1.1+ of T cells). In mice treated with sitagliptin + anti-PD-L1, percentages of NKT cells in the spleen were significantly increased compared to anti-PD-L1 alone (p-value <0.0001) and all control groups (Figure 5.14A). Percentages of NKT cells in the blood were also significantly increased by anti-PD-L1 combination therapy compared to anti-PD-L1 alone (p-value = 0.0239), suggesting that sitagliptin + anti-PD-L1 may enhance the anti-tumour effector response via differentiation of NKT cells (Figure 5.14B).

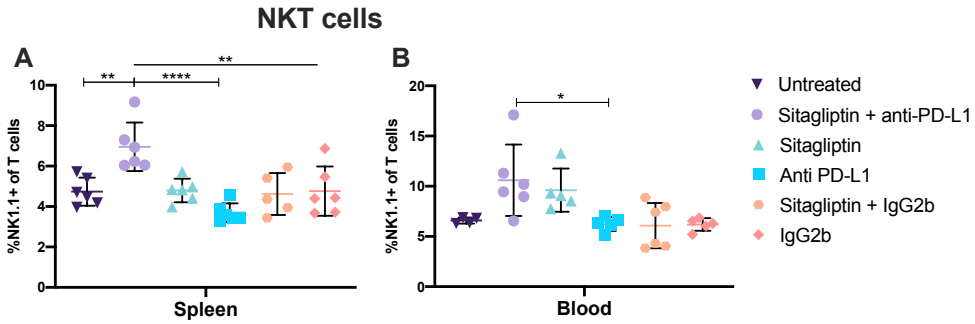

Figure 5.14. NKT cells in mice treated with sitagliptin + anti-PD-L1 antibody. *Mice bearing metastatic ID8 tumours commenced sitagliptin treatment and antibody therapy at 2- and 4 weeks-post-tumour-inoculation, respectively, and were culled 6-weeks post-tumour-inoculation. Leukocytes from the spleen and blood were isolated and analysed for the abundance of natural killer T (NKT) cells by flow cytometry. Percentages of NKT cells (%NK1.1+ of T cells) in the (A) spleen and (B) blood. Data are represented as mean ± SD, n=6. Differences between groups were determined by one-way ANOVA; *p<0.05, **p<0.01, ****p<0.001.*

5.2.4.4 Sitagliptin + anti-PD-L1 altered the cytokine landscape in a sitagliptin-dependent manner

As performed for anti PD-1 treated mice (above), serum cytokine levels were measured in all treatment groups (Figure 5.15). Multivariate analysis identified 4 differentially expressed cytokines between treatment groups – CCL12, CXCL12, CCL7 and TNF-α (Figure 5.15A). Hierarchical clustering was much more distinct with this combination of sitagliptin + anti-PD-L1 than anti-PD-1. Once again, CXCL12 was significantly increased (Figure 5.15B) in response to sitagliptin treatment alone (see Section 5.2.3.5). TNF-α and CCL7 were also significantly increased by sitagliptin alone compared to untreated controls (Figure 5.15B). By contrast CCL12 abundance increased in an anti-PD-L1 dependent manner, which was largely abrogated by the addition of sitagliptin (Figure 5.15B).

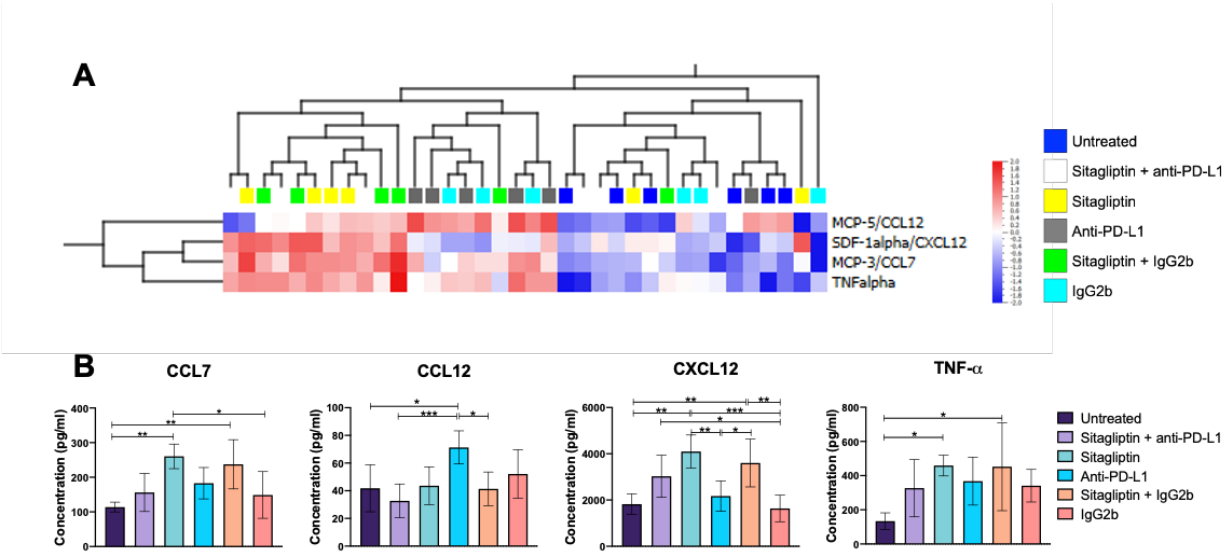

Figure 5.15. Differential expression of cytokines in mice treated with sitagliptin + anti-PD-L1. *Mice bearing metastatic ID8 tumours commenced sitagliptin treatment and antibody therapy at 2- and 4 weeks-post-tumour-inoculation, respectively, and were culled 6-weeks post-tumour-inoculation. Cytokine levels in serum were measured using the Bio-Plex Pro™ Mouse Chemokine Panel, 31-plex (Bio-Rad, #12009159) and analysed using Qlucore Omics Explorer software 3.6 (Qlucore AB, Lund, Sweden). (A) Heatmap representing differentially expressed cytokines between groups was determined by multi-group comparison with p-value = 0.05. (B) Individual concentrations of differentially expressed cytokines. Data are represented as mean ± SD, n=6. Differences between groups were determined by one-way ANOVA; *p<0.05, **p<0.01, ***p<0.005.*

5.2.5 Summary of significant features of sitagliptin + combination therapies

Comparison of the observed effects of each combination therapy revealed features in the anti-tumour immune response between sitagliptin + anti-PD-1 vs anti-PD-L1 *in vivo*. These predominantly involved changes in T effector response (Table 5.2).

Table 5.2. Key changes in selected immune parameters between treatment groups. *Differences and similarities in the immune responses between tumour-bearing mice treated with sitagliptin alone, sitagliptin + anti-PD-1 or sitagliptin + anti-PD-L1. The effect of each treatment is denoted by arrows to represent the strength of the response, where 1 arrow represents a small effect, and 3 arrows represents a major effect on the parameter. Upwards arrows represent an increased change and downwards arrows represent a decreased change.*

Immune parameter	**Treatment group**		
	Sitagliptin alone	*Sitagliptin + anti-PD-1*	*Sitagliptin + anti-PD-L1*
Circulating CXCL12	↑↑↑	-	-
T cell abundance	↑↑	↑↑	↑
T cell activation	↑↑↑	↑↑↑	↑
T cell proliferation	↑↑	↑↑	↑
Th1 cells	↑	↑↑↑	-
Tregs	↓↓	↓↓↓	-
NKT cells	-	-	↑↑

Sitagliptin alone upregulated the expression of circulating CXCL12, whilst the same effect was not observed in either of the combination therapies. T cell abundance was generally mediated by sitagliptin in both combination therapies, where small differences between sitagliptin alone and combination therapies may be indicative of a synergistic effect, and differences were less widespread in mice treated with sitagliptin + anti-PD-L1. T cell activation was also universally increased by sitagliptin and both combination therapies, however to a lesser extent in mice treated with sitagliptin + anti-PD-L1. Similarly, all 3 treatments increased T cell proliferation;

in the case of sitagliptin + anti-PD-L1 this only occurred in the context of CD8+ T cells in the peritoneal cavity. A distinguishing feature of the sitagliptin + anti-PD-1 treatment was the effect on CXCR3+ CD4+ (Th1) T cells, which were increased in the spleen, peritoneal cavity and to a lesser degree in tumours. In addition, it appeared that sitagliptin mediated the intratumoural infiltration of Th1 cells, as there was a trending increase in Th1 cells in the tumours of mice treated with sitagliptin alone. Sitagliptin alone and in combination with anti-PD-1 had a significant influence on functional capacity of Tregs, which was not observed in mice treated with sitagliptin + anti-PD-L1. However. only sitagliptin + anti-PD-L1 increased percentages of NKT cells, which remained unaffected by sitagliptin alone and the other combination therapy.

5.3 Discussion

5.3.1 Combination therapy may improve clinical parameters associated with ovarian cancer

The ovarian cancer immune landscape is a highly dynamic environment that is influenced by crosstalk between tumour cells, stromal cells, immune cells, multiple components of the extracellular matrix (ECM) and soluble factors such as chemokines and signalling molecules. Our knowledge of the interactions that take place in the TME are crucial to understanding the potential therapeutic benefit of novel immunotherapies. Our previous work identified that sitagliptin alone could substantially extend survival and reduce metastatic spread in mice with primary ovarian cancers[285]; and data presented in chapter 4 suggested this effect may be partially applicable in the context of metastatic disease, which is more relevant to the majority of clinical ovarian cancer cases. Accordingly, in this chapter I investigated whether DPP4 inhibition using sitagliptin may synergise with ICIs to influence or improve immune function and overall survival in a syngeneic, metastatic ovarian cancer mouse model.

Combination therapy with sitagliptin + anti-PD-1 reduced total metastatic tumour burden in mice with disseminated ovarian cancer. This is in contrast to a prior study using a CT26 colon carcinoma tumour model, where sitagliptin + anti-PD-1 did not reduce tumour volume or alter anti-tumour immunity without the further inclusion of anti-CTLA-4[308]. Differences in DPP4 activation status may underlie response to sitagliptin; for example, DPP4 is shed from the ovarian cancer cell surface as an inactive form by an as-yet undefined proteolytic mechanism[283]. It is thus likely that the influence of sitagliptin over tumour- and immune-specific processes will operate in a tumour-specific manner. Both combination therapies (sitagliptin + anti-PD-1 and sitagliptin + anti-PD-1) significantly improved survival compared to untreated controls and either antibody alone, but not compared to sitagliptin alone, suggesting a sitagliptin mediated effect on survival. However, endpoint was dictated by the accumulation of ascites and resulted in mice being culled at the same or similar time as other groups. This is

relevant in a clinical context as women with malignant ascites frequently undergo paracentesis, involving the needle drainage of peritoneal fluid[412]. This technique is common in the management of patients with late-stage ovarian cancer and assists with the short-term alleviation of symptoms to improve quality of life[413,414]. Repeated ascites drainage significantly prolongs survival in the ID8 ovarian cancer mouse model[415], therefore the presence of ascites may not necessarily be reflective of true 'endpoint' in this study and it is possible that our data underestimated survival outcomes. Furthermore, although malignant ascites is correlated with extent of metastases and late-stage diagnoses[416], gene expression profiling of women with HGSOC has revealed a subgroup of patients with low-volume ascites that is associated with an anti-tumour immune signature, higher abundance of TILs and longer overall survival[417]. Future pre-clinical studies should consider using the ascites drainage method to understand the true effect of sitagliptin combination therapies on overall survival and may benefit from analysing ascites-derived levels of cytokines, signalling molecules and phenotypic characteristics of immune cells[418].

In addition, post-mortem macroscopic inspection of tumour metastases in specific organs may not be an accurate reflection of tumour burden as it is unlikely to detect smaller metastatic nodules and seeding of tumours; and relies on consistency and investigator objectivity between animals. Research recently published by our laboratory proposed that tumour burden can be monitored in real-time in an immunocompetent mouse model of ovarian cancer using a non-invasive technique that involves expression of a near-infrared fluorescent protein (iRFP) by implanted cancer cells (see Appendix E)[419]. This technique was not implemented in the current study as the presence of non-endogenous antigen, and the corresponding potential for a confounding immune response, could have skewed the results. However, this approach should be considered for future research after elucidating the potential immunogenic effects of the iRFP protein in the context of PD-1/PD-L1 blockade.

5.3.2 Combination therapy enhances T effector cell responses in the TME

An overview of the immune responses potentiated by sitagliptin + anti-PD-1/PD-L1 combination therapy is shown in Figure 5.16. The presence of CD8+ TILs are a positive prognostic indicator for women with HGSOC. A recent meta-analysis reported the median survival of patients with high levels of CD8+ TILs was 5.1 years compared to 2.8 years for women negative for CD8+ TILs[420]. Other studies have demonstrated the sitagliptin-mediated trafficking of T cells into tumours[308,313], and there is evidence to suggest that blockade of the PD-1/PD-L1 axis is associated with an increase in CD8+ TIL density[421]. Therefore, sitagliptin may synergise with anti-PD-1/PD-L1 therapy to increase infiltration of T cells. Consistent with this hypothesis, sitagliptin alone increased the percentage of infiltrating CD8+ T cells in metastatic ovarian tumours (see Chapter 4) and the combination of sitagliptin + anti-PD-1/PD-L1 exhibited a similar trend.

In the ID8 model tumour infiltrating DCs maintain an immature phenotype and contribute to immunosuppression by impeding T cell proliferation. Blockade of the PD-1/PD-L1 axis may induce maturation of tumour-infiltrating DCs via upregulation of CD86, CD80 and CD40[422] and therefore promote T cell activation and proliferation in the TME. Our data supports these findings, where the combination of sitagliptin + anti-PD-1 synergistically increased the percentage of activated CD8+ T cells in the peritoneal cavity and in tumour cell infiltrates compared to untreated controls, suggesting the sitagliptin-mediated infiltration of CD8+ T cells and subsequent activation via PD-1 blockade. Similarly, the combination of sitagliptin + anti-PD-L1 increased percentages of proliferating CD8+ T cells in the peritoneal cavity and showed an increasing trend in tumour infiltration of activated CD8+ T cells. At the tumour site, activated CD8+ T cells exert potent cytotoxic activity via granule exocytosis and Fas ligand (FasL) mediated apoptosis[423]. Therefore, sitagliptin + anti-PD-1/PD-L1 therapy may induce tumour cell ablation by sitagliptin mediated trafficking and tumour infiltration of CD8+ cytotoxic T lymphocytes (CTLs), where checkpoint blockade restores a functional T effector response.

The enhanced CD8+ T effector cell response in mice treated with sitagliptin + anti-PD-L1 may be influenced by the observed increase in percentages of NKT cells, which was not seen with the combination of sitagliptin + anti-PD-1. NKT cells represent a unique phenotype that bridges innate and adaptive immunity[424] but are usually suppressed in the ovarian TME[425]. Splenic NKT cells signify a 'helper' cell type by their ability to induce downstream activation of adaptive immune responses including B cells, CD4+ and CD8+ T cells, whilst NKT cells in the TME can directly mediate tumour cell killing[424]. We observed increased NKT cell percentages in the spleen and blood, which correlated with increased proliferating CD8+ T cells in the peritoneal cavity and activated TILs. As the changes to NKT cells and CD8+ T cell activity were observed in different physiological sites; the mechanism of NKT cell regulation is likely to be indirect activation via the secretion of Th1-type cytokines that contribute to activation of other sources of anti-tumour immunity or via interaction with APCs in the periphery[408]. In addition, the fact that only the combination of sitagliptin + anti-PD-L1, but not anti-PD-1, influenced NKT cells suggests that anti-PD-L1 may potentiate anti-tumour immunity via a PD-1-independent mechanism.

In the ID8 model percentages of tumour-infiltrating CD8+ T cells and T helper cells increase throughout tumour development but decline over time[422], which is consistent with the development of immunosuppression and mechanisms of immune evasion, including those induced by the PD-1/PD-L1 axis. Therefore, in order to better understand changes in T cell abundance over time it may be advantageous in future studies to measure levels of TILs at additional time points to gain a greater insight into the long-term benefit of the combination of sitagliptin + PD-1/PD-L1.

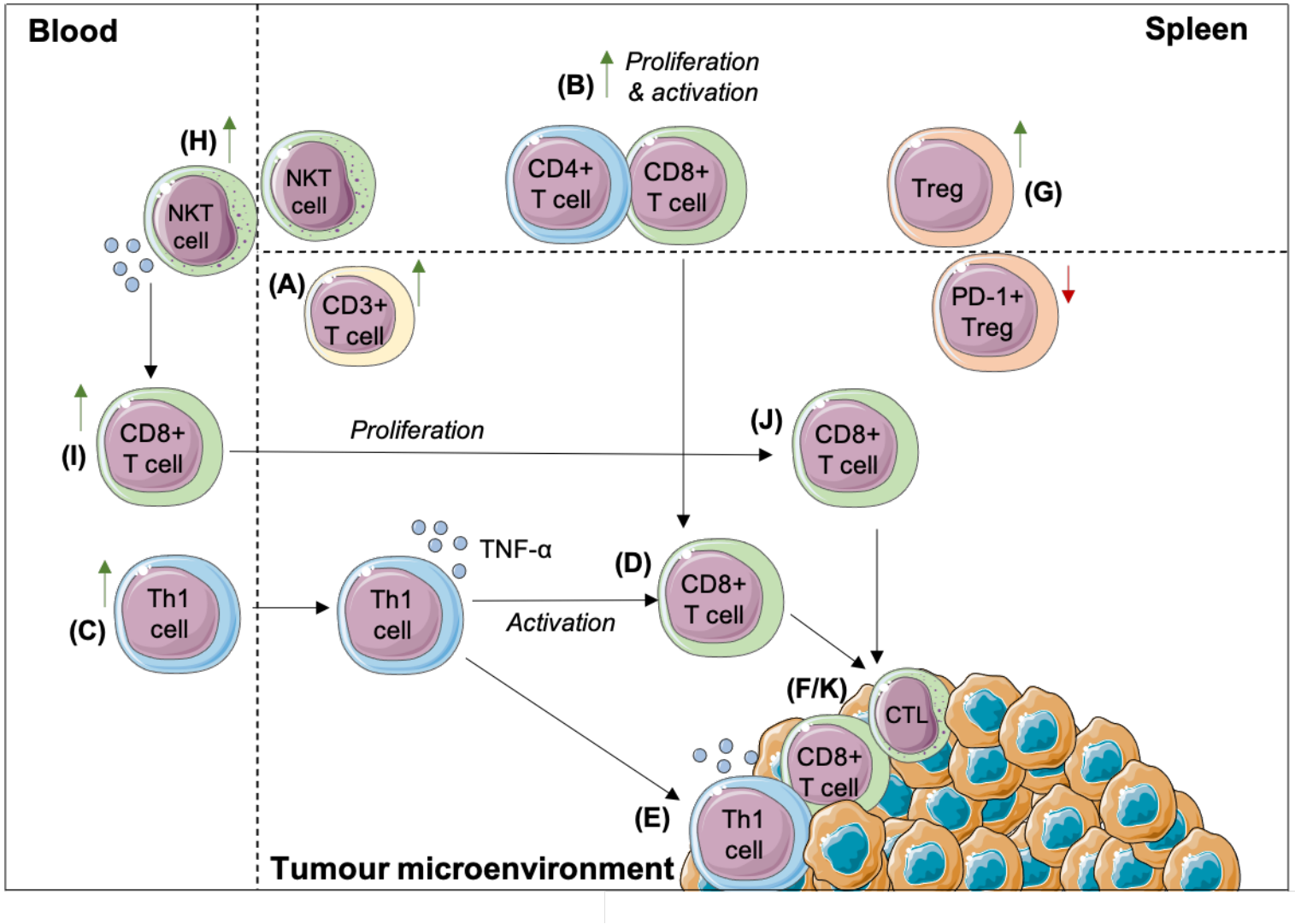
Blood
Spleen
(B)
Proliferation & activation
(H)
NKT cell
NKT cell
CD4+ T cell
CD8+ T cell
Treg
(G)
(A)
CD3+ T cell
PD-1+ Treg
(I)
CD8+ T cell
Proliferation
(J)
CD8+ T cell
TNF-α
(C)
Th1 cell
Th1 cell
(D)
CD8+ T cell
Activation
(F/K)
CTL
CD8+ T cell
(E)
Th1 cell
Tumour microenvironment

Figure 5.16. Schematic representation of proposed immune responses in mice bearing ID8 metastatic tumours treated with the combination of sitagliptin + PD-1/PD-L1 blockade. *Immune responses prompted by sitagliptin + anti-PD-1 antibody (A-G) and sitagliptin + anti-PD-L1 antibody (H-K). (A) Sitagliptin + anti-PD-1 caused an increase in percentages of CD3+ T cells in the peritoneal cavity, indicating an elevated T cell presence in the TME. (B) In the spleen, sitagliptin + anti-PD-1 increased CD4+ and CD8+ T cell proliferation and activation. (C) The Th1 T cell subtype was increased in the circulation and peritoneal cavity of sitagliptin + anti-PD-1-treated mice. (D) TNF-α secretion by Th1 cells may mediate the subsequent activation of CD8+ T cells in the peritoneal cavity; alternatively, activated CD8+ T cells may migrate from the spleen. (E) The increased infiltration of Th1 cells in tumours from mice treated with sitagliptin + anti-PD-1 is likely to promote the simultaneous accumulation of (F) tumour associated CD8+ T cells and activated CD8+ T cells via secretion of inflammatory molecules. (G) Tregs were increased in the spleen of mice treated with sitagliptin + anti-PD-1, but the immunosuppression of the Tregs may be mitigated by the decrease in PD-1+ Tregs that were present in the peritoneal cavity. (H) Sitagliptin + anti-PD-L1 increased the abundance of NKT cells in the spleen and blood, which may provide peripheral Th1-type signalling leading to the (I) increased percentages of CD8+ T cells in the blood. (J) The concurrent increase in proliferating CD8+ T cells in the peritoneal cavity suggests the potential migration of CD8+ T cells from the blood into the TME. (K) Similar to the PD-1 combination therapy, sitagliptin + anti-PD-L1 increased tumour infiltration of activated CD8+ T cells, which in both cases may be representative of a CTL effector subtype and are likely to potentiate anti-tumour immunity. Green arrow = upregulation, Red arrow = downregulation. CTL: cytotoxic T lymphocyte, PD-1: programmed death-1, Th1: T helper type 1, Treg: regulatory T cell, TME: tumour microenvironment, TNF-α: tumour necrosis factor-alpha.*

5.3.3 Sitagliptin anti-PD-1 promotes Th1 immunity by upregulation of CXCR3

Our study supports recent research which suggests that effective anti-PD-1 therapy requires a functional intratumoural CXCR3 pathway (discussed in Section 5.1)[380]. We observed an increase in percentages of Th1 cells (CXCR3+ CD4+ T cells) in the blood, peritoneal cavity and tumour infiltrates of mice treated with sitagliptin + anti-PD-1. Mice treated with sitagliptin alone also exhibited increased infiltration of CXCR3+ CD4+ T cells, suggesting that the infiltration of CXCR3+ T cells was due to sitagliptin treatment, which is likely to be mediated by the upregulation of CXCL10 as we previously demonstrated (see Chapter 4). Interestingly, a study by Han and colleagues reported that higher percentages of CXCR3+ T cells in the blood was associated with resistance to pembrolizumab (anti-PD-1) treatment[404]. However, in these patients there was a simultaneous decrease in circulating CXCR3 ligands, CXCL9 and CXCL10[404], which is likely to be responsible for the lack of tumour infiltration of CXCR3+ T cells. Overall, our data supports previous findings of the requirement for CXCR3 for a positive response to PD-1 blockade, where we found that the intratumoural expression of CXCR3+ T cells in mice treated with sitagliptin + anti-PD-1 was associated with a significant improvement to anti-tumour immunity.

The functional consequences of CXCR3+ T cells in the TME are widespread. CXCR3 expression is strongly associated with the induction of Th1 cells and CTLs which are recruited to tumour sites via CXCR3 ligand-dependent chemotaxis. In the periphery, CXCR3-dependent responses drive secretion of CXCR3 ligands such as CXCL9 and CXCL10 and a stimulate a feedback loop leading to further recruitment of CXCR3+ T effector cells and amplification of the immune response[175]. Therefore, the infiltration of Th1 cells may be responsible for the observed increase in activated CD8+ T cells, which was exacerbated by blockade of the inhibitory PD-1 receptor. The presence of CXCR3+ CD4+ TILs is indicative of CXCR3-dependent chemotactic recruitment of T cells into the TME, which has been previously shown as a sitagliptin-mediated mechanism of anti-tumour immunity in pre-clinical cancer

models[308,313]. CXCR3 expression is a prognostic factor in patients with gastric and renal cancers and osteosarcoma[426-428]. Our data provides evidence of the upregulation of a crucial pathway required for functional PD-1 blockade, which is likely to occur by 'priming' of the TME by sitagliptin treatment prior to the administration of anti-PD-1 antibody in ovarian cancer tumours.

5.3.4 Combination therapy may promote immunological memory

Our data shows that sitagliptin + anti-PD-1 therapy increased percentages of activated and proliferating CD8+ and CD4+ T cells in the spleen. Similarly, sitagliptin + anti-PD-L1 increased levels of circulating CD8+ T cells. This could be indicative of clonal expansion of short-lived effector cells but may also be reflective of the generation of memory T cells. The ongoing effector T cell response and generation of memory T cells is key to providing long-term anti-cancer immunity[429]. In multiple cancer types, the production of memory T cells is associated with a more favourable outcome[430] and is one of the objectives for improving cancer vaccine strategies[431] and immunotherapies[432]. Although the generation and maintenance of memory T cells predominantly occurs in the bone marrow[433], memory CD8+ T cells in the spleen are maintained by proliferation[434]. Distinct proliferative behaviours of CD8+ T cells directs their cell fate towards memory precursor or terminal effectors, which can be distinguished by measuring the durations of cell cycle phases[435]**.** Therefore, it may be beneficial to interrogate markers of memory T cells such as CD45RO and CD62L[432,436,437] to further understand the effect of sitagliptin + anti-PD-1 on the generation of T cell memory and the longevity of the anti-tumour immune response. In addition, investigation of tissue-resident memory T (Trm) cells via expression of CD103 in tumour infiltrates may provide a greater prognostic indicator for combination therapy. There is evidence to suggest that CD103+ TILs are upregulated during anti-PD-1 treatment[438] and are associated with improved overall survival in HGSOC patients[439-441].

It should also be considered that expression of CD69 on CD8+ T cells in the TME, which was observed in both combination treatments, may be indicative of a Trm cell phenotype[442]. Trm cells develop from effector cells in the periphery and as described above, can be detected by CD103 expression; however, upregulation of CD69 is induced prior to CD103 to promote retention of memory precursors in the local TME[443]. Functional Trm cells depend on Th1-type cytokines including IFN-ɣ and TNF-α[444], which were upregulated by sitagliptin alone (see Chapter 4) and have been identified in several solid malignancies including melanoma, colorectal, breast and ovarian cancers[442]. CD69+CD103+CD8+ TILs may therefore be a better prognostic indicator for overall survival and should be investigated in future studies to assess the impact of sitagliptin combined with PD-1/PD-L1 blockade on the generation of a memory T cell response and long-term anti-tumour immunity.

5.3.5 Cytokine expression reveals similar mechanisms of anti-tumour immunity from both combination therapies

The increased expression of circulating CCL12, CXCL12 and TNF-α was common to both combination therapies, suggesting a shared role in their regulation. Interestingly, these cytokines have been reported as contributors to a tumour-promoting network in ovarian cancer[445]. However, in our study their upregulation correlates with an anti-tumour immune response, suggesting a potential alternative function. CCL12 has only been described in mice and is a human homolog of CCL2[446], which is a potent chemoattractant for monocytes, T cells and NK cells[447]. The specific role of CCL2 in ovarian cancer is unclear. Some evidence suggests that CCL2 may increase migration and adhesive capacity of ovarian cancer cells[448]. Conversely, others have shown that expression of CCL2 in ovarian tumours is associated with increased response to chemotherapy and favourable overall survival[449] and that CCL2 overexpression may contribute to *in vivo* tumour latency[450], potentially via the accumulation of cytotoxic neutrophils in premetastatic niches[451]. The role of neutrophils was not explored in this study, however other factors which were upregulated by sitagliptin + anti-PD-1 therapy

including CXCL16 may also be involved in their cytotoxicity[451], suggesting a potential function of these innate cells in the anti-tumour response to treatment with sitagliptin + anti-PD-1/PD-L1.

Higher serum CXCL12 concentration correlates with the presence of distant metastases in gastric carcinoma patients[452] and evidence supports a role of the CXCL12/CXCR4 axis in ovarian cancer invasion[344]. However, we observed less extensive metastases in mice treated with sitagliptin + anti-PD-1, indicating that the mechanism of action of CXCL12 may be different. Furthermore, the significance of the upregulation of circulating CXCL12 is difficult to interpret due to several mechanisms of processing that occur in the blood which alters its activity[453]. This phenomenon and its impact on the current data is discussed in further detail in Chapter 6.

Due to the pleiotropic nature of TNF-α[454], the consequences of its upregulation across both combination treatment groups is paradoxical in ovarian cancer. TNF-α is involved in various anti-tumour immune responses in cancer, including T effector cell activation, conversion of M2 macrophages to the M1 phenotype and recruitment of neutrophils and monocytes[455], which is consistent with the observed increase in T effector responses in mice treated with sitagliptin + anti-PD-1/PD-L1. Equally, there is evidence of TNF-α involvement in the pathogenesis and progression of ovarian cancer. Kulbe and colleagues showed endogenous expression of TNF-α by ovarian cancer cell lines was associated with increased peritoneal metastases in nude mice[445]. As nude mice lack the ability to generate mature T cells[456], it is difficult to interpret this data in the context of the immune response. We show that increased TNF-α concentration correlates with several improvements to anti-tumour immunity; however, additional data is required to understand the downstream effects of circulating TNF-α on cytokine networks and the sitagliptin + ICI-mediated anti-tumour immune response in ovarian tumours.

Our data suggests that the combination of sitagliptin with anti-PD-1 induced a greater cytokine response than when combined with anti-PD-L1, where circulating levels of GM-CSF, IL-6, CCL1, CCL20 and CXCL16 were also upregulated in mice treated with sitagliptin + -anti-PD-1 in addition to those described above. Although the exact mechanism responsible for the differences in immune responses and cytokine expression between the combination therapies could not be ascertained throughout this study, it is likely to involve different binding partners of PD-1 and PD-L1[149,457,458]. Gene profiling may assist with identifying functional pathways activated in response to these cytokines in ovarian cancer in the context of sitagliptin + ICI therapy. Future research would also benefit from measuring intratumoural expression of cytokines to get an overall indication of local signals in the TME and to decipher some of the complexities that arise from analysing circulating levels of cytokines.

5.3.6 Insight into potential mechanisms of immunosuppression induced by PD-1/PD-L1 blockade

This study revealed some unexpected, novel consequences of anti-PD-1 and anti-PD-L1 therapy alone and highlighted some of the mechanisms by which PD-1/PD-L1 blockade may contribute to mechanisms of resistance[370]. We showed that anti-PD-1 alone and in combination with sitagliptin was associated with increased percentages of Tregs in the spleen, which is consistent with evidence from a mouse model of squamous cell carcinoma (SCC), where anti-PD-1 therapy increased the ratio of Tregs:CD4+ T effector cells that was mediated by the immunosuppressive cytokine TGF-β[459]**.** However, our data shows also shows that anti-PD-1 mediated a decrease in PD-1+ Tregs in the peritoneal cavity. As high expression of PD-1 on Tregs may be associated with non-response to PD-1 blockade (discussed in Chapter 4)[373], its downregulation may enhance susceptibility to anti-PD-1 therapy. Anti-PD-1 alone also significantly increased percentages of circulating activated and migrating (CCR4+) T regs. Krempski and colleagues showed *in vitro* blockade of PD-1 in tumour-associated DCs increased the release of immunoregulatory cytokines IL-10, IL-6 and G-CSF[422]**,** which may be

responsible for the anti-PD-1 mediated increase in abundance and activation of Tregs in this study. TGF-β is also an important factor in the differentiation of Tregs[460], and its expression by activated Tregs promotes immunosuppressive functions by maintaining their survival in the periphery and inhibiting T cell proliferation and effector responses[461,462]. TGF-β reduces CXCR3 expression on CD8+ T cells and suppresses CXCR3+ mediated trafficking of T effector cells into tumours[463]. The sitagliptin-mediated increase in CXCR3+ T effector cells may decrease Treg differentiation and activation via a feedback mechanism involving the downregulation of TGF-β and therefore ameliorate some of the suppressive effects of PD-1 blockade on Tregs.

Furthermore, our results demonstrated that anti-PD-1 alone reduced proliferating T cells in the peritoneal cavity, which may be due to the decreased expression of PD-1+ on Tregs, thereby enhancing their suppressive capacity. This data could also indicate the insufficient capacity of PD-1 blockade to reduce T cell inhibition due to other mechanisms of suppression such as expression of CTLA-4[464]. A similar phenomenon may also be responsible for the significant decrease in proliferating CD8+ T cells in the peritoneal cavity of mice treated with anti-PD-L1 alone compared to untreated controls, which was ameliorated by the addition of sitagliptin. Our data provides evidence of some previously undescribed mechanisms of potential immunosuppression induced by PD-1 and PD-L1 blockade. The complex function of PD-1 on T cells in response to PD-1 blockade and in combination with sitagliptin, including the effect of transient vs sustained expression, should be explored in future studies. Additional research is also warranted to identify the source and pathways involved in these suppressive phenotypes and how sitagliptin counteracts these mechanisms by analysing the functional status of tumour infiltrating DCs and suppressive TILs.

5.4 Conclusions

This study uncovers novel mechanisms by which sitagliptin may synergise with ICIs in ovarian cancer to promote anti-tumour immunity. The combination of sitagliptin with anti-PD-1 antibody significantly enhanced multiple parameters of the peripheral and local T effector response to drive anti-tumour immunity, where we identified a substantial expansion of the T effector cell response and induction of a CXCR3-mediated Th1 type response. We also provide evidence that sitagliptin + PD-1 blockade may promote generation of a memory T cell response, which is beneficial for long-term treatment efficacy, but requires further investigation. Conversely, the combination of sitagliptin + anti-PD-L1 antibody was associated with more subtle changes via the stimulation of cytotoxicity driven responses, including enhancement of the CD8+ T cell response and increase in peripheral NKT cells. Both combination therapies were also associated with significant alterations to cytokine expression but did not impact overall survival compared to either treatment alone. We highlight some of the potential immunosuppressive consequences of anti-PD-1 and anti-PD-L1 therapy and show that the addition of sitagliptin attenuates these effects in some contexts, but not in others. This study provides the first evidence of the potential effect of sitagliptin to optimise the efficacy of ICIs to improve anti-tumour immunity in ovarian cancer and may serve as a rationale to further investigate this novel combination immunotherapy in clinical trials.

5.5 Acknowledgements

I wish to acknowledge use of the facilities and technical assistance of Monash Histology Platform, Department of Anatomy and Developmental Biology, Monash University; in particular Angela Vais for her assistance with immunofluorescence staining of mouse tissue.

5.6 Supplementary Figures

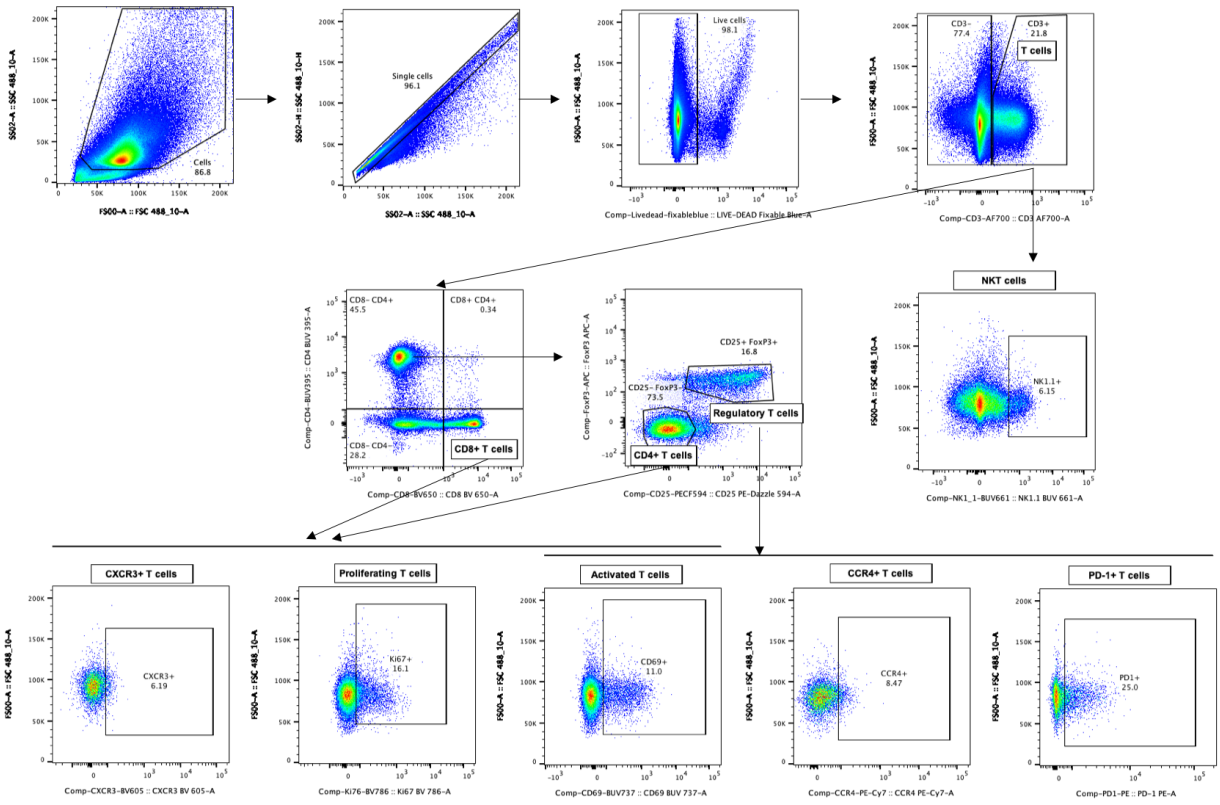

Supplementary Figure S5.1. Flow cytometry gating strategy. *Fluorescence density plots representing sequential gating used to identify specific subsets of immune cells as shown by the arrows. All cells were defined on the FSC-A vs SSC-A axes and single cells were defined on the SSC-A vs SSC-H axes. Dead cells were excluded using the LIVE/DEAD™ Fixable Blue Stain. T cells were defined as CD3+; CD8+ T cells were defined as CD3+CD8+CD4-; CD4 T cells were defined as CD3+CD8-CD4+CD25-FoxP3-; regulatory T cells were defined as CD3+CD8-CD4+CD25+FoxP3+; migrating T cells were defined as CXCR3+ or CCR4+; activated T cells were defined as CD69+; proliferating T cells were defined as Ki67+; inhibitory/exhausted T cells were defined as PD-1+. All gates were determined using fluorescence minus one (FMO) controls.*

Chapter Six

Discussion

Preface

DPP4 represents a unique therapeutic target in ovarian cancer due to its multifaceted roles in various physiological pathways including glucose metabolism, immune cell trafficking and inflammation. We utilised the ID8 syngeneic model of ovarian cancer to investigate the immune landscape in the context of DPP4 inhibition to understand the functional effects of DPP4 activity *in vivo* in a model of metastatic disease. This thesis has provided substantial evidence for the role of DPP4 in ovarian cancer, including mechanisms of regulation *in vitro,* immune-related consequences of inhibition of DPP4 activity *in vivo* and its clinical application in the context of immune checkpoint inhibition.

Here we explain the broader implications of the research outcomes that have been described in this thesis, including novel insights into the role of DPP4 expression and activity in ovarian cancer and the TME. Briefly, we discuss factors which may influence the role of DPP4 as a biomarker and a therapeutic target in ovarian cancer, and how understanding the source of DPP4 and sDPP4 may better define its functional consequences. The implications of how DPP4 inhibition by sitagliptin treatment may be useful to improve immune status and clinical outcomes as a monotherapy are investigated in the context of primary and metastatic disease. We further describe the clinical applicability and translatability of the combination of sitagliptin with immune checkpoint inhibitors (ICIs) to enhance anti-tumour immunity and evaluate how to overcome mechanisms of resistance to traditional ICIs. We discuss the challenges and limitations associated with these studies and how future research should address some of the remaining gaps in knowledge regarding the role of DPP4 in ovarian cancer.

6.1 New insights into DPP4 as a biomarker and therapeutic target in ovarian cancer

6.1.1 Mechanisms of regulation that impact the status of DPP4 as a biomarker

The concept of DPP4 as a biomarker in cancer is not novel; however, the reliability of DPP4 as either a pro- or anti-tumour marker in different cancer types remains controversial[228]. For example, DPP4 has been associated with tumour suppression in lung cancer[227] and melanoma[226]; but has been correlated with mechanisms of tumour progression in colorectal[234] and breast cancer[232]. Evidence in prostate cancer reports DPP4 as a marker of malignancy[233], whilst others suggest its role as a tumour suppressor[229]. These variations in the literature may be due to i) the pleiotropic nature of membrane bound and soluble DPP4, ii) diverse tissue and cellular distribution, which is differentially altered throughout various pathologies and iii) complex patterns of regulation at the transcriptional level, via responses to external stimuli and post-translational processing (reviewed in[263,465-468]), meaning that the specific function of DPP4 is highly contextually dependent.

Here, we propose a novel mechanism of DPP4 regulation in epithelial ovarian cancer, where DPP4 expression and activity are altered under conditions of low oxygenation, which may be reflected in the hypoxic TME in ovarian cancers. We describe an MMP-mediated mechanism of sDPP4 release by HGSOC cells, which is consistent with what others have shown in smooth muscle cells and adipocytes[247,248,469]. Distinct from the active form of sDPP4 released by adipocytes[247], we showed that sDPP4 released by cancer cells is enzymatically inactive. MMP-mediated cleavage of DPP4 may therefore be responsible for increased levels of sDPP4 in the TME. Future research could focus on interrogation of the DPP4 protein sequence and structure to determine whether DPP4 has a putative MMP cleavage site. However, as DPP4 can be expressed on multiple other cell types in the TME, other mechanisms affecting total DPP4 abundance and activity *in vivo* are also to be expected.

Earlier studies of DPP4 expression in ovarian cancer cells have failed to substantiate its involvement in ovarian cancer progression, perhaps due to specific patterns of regulation being overlooked or that remain unknown, or the limitations of *in vitro* experiments. Previous research found that overexpression of DPP4 in the SKOV3 ovarian cancer cell line was associated with decreased capacity for invasion and migration *in vitro* and less extensive peritoneal metastases in nude mice[251,252,470]. However, recent reassessment of multiple ovarian cancer cell lines that are commonly used in ovarian cancer research, including SKOV3, were found to be unsuitable models of HGSOC[471,472]. Moreover, it is important to consider that expression of DPP4 is likely to vary between cancer subtypes[473], where DPP4 expression in non-serous histotypes such as the SKOV3 cell line may not be reflective of HGSOC[472,474], which is the focus of our research.

It is likely that multiple mechanisms of DPP4 regulation remain unknown. For example, recent research by Diaz-Jimenez and colleagues reported a novel mechanism of DPP4 regulation, where they showed that glucocorticoid receptor (GR) directly transcriptionally increases DPP4 expression during the differentiation of monocyte-to-macrophage-like THP-1 cells[475]. Furthermore, the upregulation of DPP4 mediated glucocorticoid-induced migration of M1 macrophages in an enzyme activity-dependent manner[475]. Ovarian cancer patients are often treated with glucocorticoids such as dexamethasone as an adjuvant to chemotherapy[476]. Despite concerns surrounding immunosuppression induced by glucocorticoids[476], this new insight into the regulation of DPP4 provides evidence of a potential benefit of DPP4 expression in ovarian cancer, which may be partially responsible for the increased leukocyte count observed in patients that receive glucocorticoid treatment prior to chemotherapy[477]. Therefore, strategical approaches surrounding when to use DPP4 inhibition as a potential treatment should consider the balance of the pro- vs anti-tumour effect of DPP4 and the source of DPP4 expression.

6.1.2 Uncovering sources and functional diversity of DPP4

Current evidence suggests that, under various pathophysiological conditions, circulating sDPP4 may be derived from T cells[478,479], endothelial cells[480], adipocytes[247,248], smooth muscle cells[469] and/or hepatocytes[481]. We demonstrated that DPP4 is cleaved from ovarian cancer cells, therefore, ovarian tumours may be an additional source of sDPP4 in serum. Lettau and colleagues recently showed that sDPP4 co-localises with granzymes, perforin and granulysin in cytotoxic lymphocytes and is released upon cytotoxic degranulation[482]. Thus, the presence of sDPP4 in serum may also be reflective of an active anti-tumour response. Our laboratory and others have shown that sitagliptin treatment *in vivo* effectively inhibits DPP4 activity but is associated with increased levels of circulating sDPP4[285,483]. In mice, sDPP4 in serum following DPP4 inhibition was derived predominantly from bone-marrow derived haematopoietic cells[484]. The source(s) of sDPP4 in our ovarian cancer mouse model is yet to be determined, however due to the sitagliptin-mediated enhancement of the T effector response, elevated sDPP4 may be representative of a recently activated cytotoxic response. Additional experiments with tumour-specific knockout of DPP4 may clarify whether tumour-associated DPP4 also contributes to circulating sDPP4 levels.

The different roles of DPP4 must also be considered when assessing the use of DPP4 as a biomarker in epithelial ovarian cancer, including how sDPP4 may differ functionally compared to cell surface expressed DPP4, and the conditions under which sDPP4 remains enzymatically active. In addition, sDPP4 is likely to exert different effects the local TME than in the periphery, therefore, the source and activity of sDPP4 is important. For example, sDPP4 activity upregulates mRNA expression of IL-6, IL-8 and MCP-1, directly activates the MAPK and NF-kB pathways and induces inflammation and proliferation of vascular smooth muscle cells[469]. Kosowska and colleagues recently showed that a similar phenomenon may occur in ovarian cancer, where DPP4 inhibition with sitagliptin in SKOV3 and OVCAR3 cells inhibited ERK phosphorylation[260], thereby disrupting MAPK signalling. sDPP4 has also been shown to enhance weakly responsive antigen-specific activation in peripheral lymphocytes,

independent of its enzymatic and ADA-binding capacity, suggesting that circulating sDPP4 may stimulate the T memory response[365,485]. In ovarian cancer, fibroblasts play a key role in tumour cell metastasis to the omentum[486]. Lee and colleagues found that sDPP4 stimulated fibroblast activation via NF-κB and SMAD signalling, which was prevented by inhibition of DPP4 activity[487]. Therefore, sDPP4 in the ovarian TME may have a role in facilitating metastases to the omentum, which is supported by our findings in a primary model of ovarian cancer, where sitagliptin increased sDPP4 expression but decreased metastases in the peritoneal cavity[285].

Consistent with our data which revealed that DPP4 expression and activity may be 'uncoupled' in ovarian cancer, a study on oral squamous cell carcinoma (SCC) showed that sDPP4 secreted from T cells had decreased enzyme activity compared to controls, which was mediated by cell-derived inhibitory factors including TGF-β[478]. We provide evidence that hypoxia, which upregulates TGF-β in cancer cells[488], may contribute to the uncoupling of DPP4 activity and expression in ovarian cancer cells. Therefore, future studies should consider investigating TGF-β *in vitro* to determine whether it is responsible for DPP4 cleavage from ovarian cancer cells and the subsequent decrease in sDPP4 activity.

Overall, there is substantial evidence to support a role of DPP4, particularly sDPP4, in ovarian cancer. We provide the first evidence of sDPP4 release by ovarian cancer cells and propose that specific DPP4 activity, rather than overall DPP4 activity, may offer a more informative measurement of DPP4 as a biomarker. Further examination of the source and function of sDPP4 in circulation and in the ovarian TME (i.e., ascites), and their respective relevance as biomarkers of disease status or prognosis may enhance our understanding of the pathogenesis of disease. Moreover, additional research should aim to determine whether sitagliptin-mediated inhibition of sDPP4 activity impacts tumour progression or the anti-tumour response to validate its potential as a therapeutic target.

6.2 Sitagliptin as an immune modulator in metastatic ovarian cancer

6.2.1 Sitagliptin amplifies the T effector response

Although the immunomodulatory effect of DPP4 is not fully defined, several substrates of DPP4 are key mediators of the immune response. However, in patients receiving sitagliptin for type 2 diabetes, there is no difference to circulating levels of inflammatory markers after 12 months of treatment[484]. Similarly, short-term treatment with sitagliptin did not induce any significant alteration to systemic immune function in healthy individuals[489]. The recommended dose of sitagliptin indicated for type 2 diabetes treatment (100mg/day; equivalent to mouse 2mg/kg)[377] is much less than that administered in this study (50mg/kg) and in other pre-clinical cancer models[259,308]. Consistent with the use of sitagliptin in other cancer models studies, we observed significant changes to the chemokine landscape and immune cell populations involved in the T cell response in metastatic ovarian tumour-bearing mice, which was discussed in Chapter 4. Here, we explain further details of some potential additional mechanisms of sitagliptin-mediated anti-tumour immunity.

As described throughout this thesis, T cell infiltration is a key aspect relating to favourable prognosis in ovarian cancer. We demonstrated that sitagliptin treatment in mice bearing metastatic ovarian tumours significantly upregulated CD8+ T cells in the peritoneal cavity and may improve intratumoural infiltration of T cells, including CD4+ T cells, CD8+ T cells and activated CD8+ T cells. In the presence of appropriate inflammatory stimuli, activated CD8+ T cells are potent effector CTLs which are capable of rapid tumour cell killing[490]. As the CD8+ T cell response requires CD4+ T cell help, we showed that the sitagliptin-mediated activation of CTLs may be induced by activated CD4+ T cells in the TME via the enrichment of cytokines secreted by Th1 cells including TNF-α, IFN-ɣ and IL-2[491]. TNF-α and IFN-ɣ can i) have direct anti-tumour activity in the TME, ii) stimulate the response of other effector cells and iii) regulate the development of the T helper response via a feedback loop[492]. The role of TNF-alpha will be further discussed in Section 6.2.2. IL-2 is a pleiotropic cytokine that is essential for CD8+

T effector cell terminal differentiation during clonal expansion, is required for the expression of functional effector molecules such as granzyme B and perforin[493], and may have a role in converting Tregs into Th17 cells[494]. Consistent with additional mechanisms required to activate CD8+ T cells in the TME, our studies identified the enrichment of cytokines in the IL-17 signalling network which suggests the potential induction of Th17 cells[495]. Indicative of their Th1-like phenotype in ovarian cancers, Th17 cells express high levels of TNF-α, IFN-ɣ and IL-2 and stimulate secretion of CXCL9 and CXCL10 by tumour cells[143]. In ovarian tumours, Th17 cells have a strong positive correlation with CD4+ and CD8+ T effector cells but are inversely correlated with Tregs[143]. The potential upregulation of Th17 cells by sitagliptin should be further investigated in future studies by analysing more specific markers and cytokine profiles of these cell subsets.

Amplification of the CTL response is critical for overcoming immunosuppression and mechanisms of tolerance in the TME and is therefore an important element in defining the efficacy of immunotherapies[423]. The co-ordinated migration and amplification of the CTL response is regulated by chemokine gradients in the TME. We showed that sitagliptin modulates CTL trafficking via enrichment for cytokines involved in chemokine signalling, including the DPP4 substrates CXCL10, CXCL11 and CCL3. Other than the important role of the CXCL10/CXR3 axis, which was discussed in detail in Chapter 4, the upregulation of CCL3 and CCL4 was recently shown to facilitate rapid migration of infiltrating CTLs *in vivo* via homotypic recruitment that induces T cell 'swarming'[496]. Therefore, sitagliptin may enhance mechanisms of T effector cell trafficking in ovarian cancer via restoration of the bioactivity of chemokines involved in T cell migration and recruitment.

Interestingly, the sitagliptin-mediated increase in T cell abundance and activation in the peritoneal cavity also indicates expansion of the immune response in the hypoxic ovarian TME. As discussed in Chapter 1, hypoxia plays an important role in the metabolic adaptations of cancer cells to survive in the TME and is generally associated with cancer progression,

immune escape and resistance to anti-cancer therapies[96,497]. Although hypoxic conditions have been shown to decrease the proliferative capacity of CD8+ T cells[498], recent evidence has revealed more complex functions of hypoxia that may be immunostimulatory, such as increasing immunogenicity of tumour cells[499]. Doedens and colleagues reported that enhanced HIF activity in CTLs improved tumour control in a mouse B16 melanoma model[500]. Thus, in the context of our study, sitagliptin treatment may partially counteract the hypoxic-mediated prevention in CD8+ T cell expansion and allow for improved T effector cell function in the TME. Additional research should confirm hypoxia in the metastatic ovarian cancer model by analysing intratumoural expression of HIF-1α.

6.2.2 Sitagliptin influences cytokines in the TNF network

Sitagliptin consistently upregulated levels of circulating CXCL12, TNF-α and IL-6. As mediators of the 'TNF network'[163,445] – which is generally associated with poor anti-tumour response – their upregulation in this study is interesting and warrants further investigation. Here, we discuss further evidence that may explain some of these ambiguous results. CXCL12 is a potent chemokine for the recruitment of resting T cells and its N-terminal truncation via DPP4 abolishes its chemotactic capacity[501,502]. There is conflicting data surrounding the prognostic value of CXCL12 in malignancy which is likely to be cancer- and subtype-dependent[503]. Multiple studies have suggested that CXCL12 is a pro-tumour chemokine and promotes invasion and metastasis via the CXCR4/CXCL12 axis (reviewed in [504,505]). For example, CXCL12 secretion by fibroblasts and signalling through CXCR4 promoted angiogenesis, vascularisation and invasive tumour growth in a breast cancer xenograft model[506]. Others have shown that CXCL12 increases proliferation and invasion of CXCR4-expressing ovarian cancer cell lines[345].

However, there is also evidence to suggest that CXCL12 has anti-tumour roles[507]. In pancreatic ductal adenocarcinoma tissue low levels of CXCL12 expression was found in

malignant cells, with a reciprocal increase in its receptor, CXCR4[507]. A recently published study revealed that high CD8+ T cell density and expression of CXCL12 was a favourable prognostic marker in patients with late stage CRC[508]. Meta-analysis also identified that CXCL12 was a marker of reduced overall survival in oesophogastric, pancreatic and lung cancer patients, but predicted better survival in breast cancer[509]. The same study reported no significant association with CXCL12 and overall survival in ovarian cancer[509]. In a syngeneic mouse model of breast cancer, high expression of tumour specific CXCL12 inhibited primary tumour growth and spontaneous metastases. In addition, the anti-tumour effect of CXCL12 was associated with enhanced T effector cell cytotoxicity and decreased accumulation of splenic MDSCs[510], which is consistent with our findings. The upregulation of CXCL12 in response to sitagliptin may therefore be reflective of the heightened immune response.

There are 6 known isoforms of CXCL12 in humans[511], which makes interpretation of its role even more complex. The multi-plex assay used in this study detected the predominant α-isoform. CXCL-12α activity is post-translationally regulated in the blood by processing of the NH_2 and COOH terminus, impacting its ability to bind heparin and significantly altering biological function[453]. CXCL12 is also induced by hypoxia[512], which is a hallmark of ovarian tumours. Thus, the source of CXCL12 in circulation may be related to tumour-specific secretion. In addition, it is possible that the effects of CXCL12 may be masked by other cytokines such as CXCL10 and CXCL11. Based on this evidence, it is difficult to ascertain the exact mechanism of CXCL12 signalling in this study. It would be useful to look at intratumoural CXCL12 and cognate receptor expression in ovarian tumours to further understand the role of CXCL12 in the periphery and in the ovarian TME in the context of our studies.

TNF-α and IL-6 are upregulated in HGSOC tissue[347], however, circulating levels of these cytokines are not associated with an increased risk of ovarian cancer[513]. IL-6 is elevated in the serum of pre-operative HGSOC patients and may be a useful biomarker in combination with other diagnostic techniques to identify cancer in patients with suspected malignant

ovarian mass[514]. Despite studies suggesting the potential involvement of TNF-α and IL-6 in ovarian tumorigenesis[515,516], both of these cytokines are also important mediators in several anti-tumour pathways. TNF-α is a critical regulatory molecule of CD8+ T cell-mediated effector responses[517] and has been shown to increase tumour susceptibility to chemotherapeutic agents[518]. Moreover, IL-6 has been implicated in the differentiation of Th17 cells[519], which may partially explain the sitagliptin-mediated enrichment in cytokines involved in the IL-17 signalling network. Therefore, in this study the upregulation of TNF-α and IL-6 may be a direct consequence of the inflammatory response that is initiated by sitagliptin to enhance the T effector response; however, this requires further investigation.

It should also be considered whether the simultaneous upregulation of CXCL12, TNF-α and IL-6 in the peripheral circulation of sitagliptin-treated mice actually correlates with their involvement in the TNF network. Evidence of this cytokine network in the ovarian TME was provided via analysis of tumour biopsies which demonstrated co-localised expression of CXCL12, TNF-α and IL-6[163]. Therefore, to confirm whether this network is relevant in the context of our studies, tumour sections should be analysed for expression of relevant cytokines and downstream pathways.

Our research provides compelling evidence of sitagliptin as an immunomodulator in metastatic ovarian cancer by alteration of cytokine expression and induction of T cell responses. These studies measured circulating levels of cytokines from mouse serum taken at week-6-post-tumour inoculation. This time point was chosen as all mice had extensive peritoneal metastases and was therefore an appropriate snapshot of late-stage immune responses. Whilst the data provides a robust overview of the peripheral immune response at this time point, it does not take into account patterns of cytokine expression that fluctuate over time during cancer progression and in response to treatment[520,521]. Therefore, the changes to cytokine levels observed in this study are a transient depiction of the circulating immune landscape and the results cannot be overinterpreted in the context of disease progression.

Furthermore, additional research should consider investigating intratumoural cytokine abundance and their expression in the ascites fluid, which is more representative of the local tumour microenvironment and where cytokines are likely to have differing roles. We also acknowledge the complexities of the immune landscape and that determining the specific role of each of the affected cytokines and their downstream pathways in the anti-tumour response would provide further insight into the mechanism of action of sitagliptin; however, this was beyond the scope of this PhD project.

6.2.3 Considering spatial and phenotypic diversity in the immune response

This research also highlights the need to consider the spatiotemporal diversity of the immune response in cancer models by examining the abundance and phenotype of cells in different compartments including the spleen, peritoneal cavity and in peripheral blood. For example, whilst TILs reveal a snapshot of the intratumoural immune response, peripheral blood immune cell subsets are likely to reflect patient responsiveness to immunotherapy[522]. Analysis of discrete physiological regions is important for providing an overall depiction of the anti-tumour response. We showed that sitagliptin increased percentages of CD8+ T cells in the spleen, blood and peritoneal cavity, all of which are key sources of immune regulation. Splenic CD8+ T cell abundance may denote T cell expansion at the site of antigen presentation, whilst CD8+ T cells in the peritoneal cavity represents an effective mechanism of tumour destruction and circulating CD8+ T cells may signify positive host response to therapy. The data presented in this thesis also emphasises that analysis of specific subsets of TILs may allow for improved stratification of patients that are likely to respond to therapy. For example, total CD3+ cells do not discriminate between regulatory T cells or exhausted T cells (i.e., PD-1+), which contribute to immunosuppression rather than tumour elimination.

6.3 The effect of sitagliptin in primary versus metastatic disease

6.3.1 Similar mechanisms of sitagliptin-mediated anti-tumour immunity in primary and metastatic disease

Our data highlights some significant similarities in the immune response to sitagliptin between the primary disease model as described recently by our laboratory[285] and the metastatic disease model discussed throughout this thesis. For example, in both the early- and late-stage disease models of ovarian cancer, sitagliptin treated mice exhibited an increase in percentages of circulating CD8+ T cells, which may be a positive prognostic factor[522] of response to sitagliptin. Furthermore, sitagliptin increased the ratio of CD8+ T cells:Tregs in the blood, proliferating CD8+ T cells in the spleen and activated CD8+ T cells in the peritoneal cavity in both models of disease, which is substantial evidence that sitagliptin promotes expansion of the anti-tumour response and the accumulation of effector cells the TME throughout disease progression. Sitagliptin treatment enhanced the percentage of activated CD8+ TILs, which may be an important factor in the significantly prolonged survival time in both models. Levels of circulating CXC12 were also consistently elevated by sitagliptin treatment in mouse models of early- and late-stage disease. The potential consequences of CXCL12 upregulation were described in Section 6.2.2. Notably, many of the observed similarities are associated with anti-tumour immunity, suggesting an overall protective effect of sitagliptin throughout all stages of ovarian cancer, and therefore its potential clinical application at various stages of clinical diagnosis.

6.3.2 Distinct anti-tumour responses in mice treated with sitagliptin in different disease models

In the primary model of early-stage ovarian cancer, which is achieved via intrabursal (IB) implantation of ID8 cells, metastases were observed throughout the peritoneum, with macroscopic tumour deposits on the small intestine and liver[285]. However, in the IP model of late-stage disease, we observed more extensive metastatic tumour clusters on the peritoneal

wall, large tumours in the omentum and metastatic nodules on the small intestine, diaphragm, ovaries, kidneys and liver. Differences between the tumour burden of these disease models is difficult to quantify but should consider that DPP4 expression is likely to have a different role in primary vs metastatic disease, including the influence of DPP4 as an adhesion molecule on tissue remodelling in the ECM. In prostate cancer cells, DPP4 binds and activates plasminogen-2, which stimulates expression of MMP-9 to promote degradation of the ECM and facilitate invasion[233]. DPP4 may play a similar role in metastasis in ovarian cancer. However, as sitagliptin only inhibits DPP4 enzymatic activity and not binding capacity, sitagliptin is unlikely to impact this pathway of tumorigenesis. Nonetheless, future studies should investigate the potential role of DPP4 on ECM remodelling in ovarian cancer.

In mice with primary disease, circulating levels of IL-10, IL-16, CCL2 and CCL17 were all decreased by treatment with sitagliptin. By contrast these cytokines were significantly elevated in the serum of sitagliptin-treated mice with metastatic disease. Furthermore, the differential expression of 7 cytokines in primary vs 20 cytokines in metastatic disease indicates that sitagliptin has a more widespread effect on signalling pathways in later stages of disease, possibly due to complex patterns of ECM remodelling in the TME and the heightened systemic inflammatory response involved in metastatic progression[523]. Therefore, many of the variations in cytokine expression may be representative of pathways involved in the spread of ovarian cancer. The changes in cytokine expression between primary and metastatic disease may also reflect the difference in immune status, where sitagliptin stimulates an otherwise exhausted immune phenotype that is observed in metastatic disease.

These subtle differences in immune response between models of primary and metastatic ovarian cancer warrants further investigation to ascertain the preferred therapeutic window (i.e., as a first- or second-line therapy) to optimise the anti-tumour effects of sitagliptin throughout disease progression.

6.4 Feasibility and challenges associated with clinical translation of sitagliptin combined with immune checkpoint inhibition to treat ovarian cancer

6.4.1 Clinical safety and efficacy of sitagliptin + anti-PD-1/PD-L1

The clinical translatability of sitagliptin combined with PD-1/PD-L1 blockade is relatively straightforward given that clinical trials have already determined the risk of adverse events, where in most cases side effects are manageable. DPP4 inhibitors have an excellent tolerability profile and are not associated with significantly increased incidence of adverse events, including those related to gastrointestinal and cardiovascular safety[524,525]. Toxicity studies found that the highest non-lethal repeat-dose of sitagliptin was 750mg/kg in mice, indicating that long-term use is particularly well tolerated even at high concentrations[377]. Renal and liver toxicity was only associated with systemic doses equivalent to >50 times the human exposure levels[377]. Despite some concerns that DPP4 inhibition may be associated with a risk of pancreatitis and pancreatic cancer[526], these claims were unsupported from a recent large meta-analysis of 165 randomised controlled trials[527].

For PD-1/PD-L1 inhibitors, immune-related adverse events (irAEs) are more widespread and are reported in up to 37% of patients receiving these therapies, which occasionally leads to treatment interruption or withdrawal[528]. The most common irAEs associated with PD-1/PD-L1 blockade include gastrointestinal and endocrinological disturbances, skin rash, mild arthralgia and myalgia[528,529]. Understanding patients at risk of experiencing adverse events is therefore important in managing the toxicity and side effects of PD-1/PD-L1 blockade and required for determining the optimal therapeutic strategy for combination with sitagliptin.

As an anti-diabetes drug, sitagliptin has a well-established effect on metabolism, however the dose of sitagliptin administered to mice in our studies is ~25 times higher than the human equivalent dose indicated for type 2 diabetes. Therefore, it may be informative to analyse

basal metabolic parameters in response to sitagliptin in future studies, including blood glucose, fat deposit and fat distribution to gain a more comprehensive insight into its potential side effects if used as a cancer drug. Additionally, investigations should also pursue the potential for sitagliptin administered at higher doses to mitigate some of the toxicities associated with PD-1/PD-L1 inhibitors.

6.4.2 Overcoming mechanisms of resistance to PD-1/PD-L1 blockade

Non-response to anti-PD-1 antibody therapy is correlated with hypoxia and hypoxic gene signatures in metastatic melanoma[530,531], indicating that hypoxia plays a role in resistance to immune checkpoint therapy. Scharping and colleagues reported that treatment with the anti-diabetic drug metformin in B16 tumour-bearing mice inhibited the oxygen consumption rate for tumour cells but increased oxygen consumption in TILs[532]. In the same study, the combination of metformin + PD-1 blockade synergised to significantly improve T cell function *in vivo*, highlighting a therapeutic opportunity to increase the efficacy of anti-PD-1 therapy via remodelling of the hypoxic TME[532]. Research by our laboratory and others have shown that DPP4 is regulated by hypoxia in various metabolic contexts[247,248,283,533]. Similar to the findings described above, there is evidence that DPP4 inhibition protects against oxidative stress associated with hypoxia. In cardiac H9C2 cells, the DPP4 inhibitor anagliptin decreased intracellular ROS[533]. Therefore, it is possible that DPP4 inhibition by sitagliptin plays a role in remodelling the hypoxic TME in ovarian cancer, thereby increasing susceptibility of cancer cells to PD-1/PD-L1 blockade.

Our research provides insight into potential mechanisms of immune escape to PD-1 blockade and therefore their relative lack of efficacy in ovarian cancer. We showed that anti-PD-1 alone increased levels of Tregs in the spleen and levels of activated and migrating Tregs in the circulation of mice bearing metastatic ovarian tumours. Activity of PD-1 blockade therapy relies on recognition of neoantigens, which are generated as a consequence of somatic

mutations. Accordingly, low mutational burden and therefore decreased neoantigen presentation is a factor leading to ICI resistance. Indeed, studies in NSCLC patients found that high mutational and neoantigen burden was strongly correlated with clinical benefit of anti-PD-1 therapy[534]. Compared to hypermutated malignancies such as lung cancer and melanoma[535], HGSOC has a relatively low mutational burden and has far less chance of harbouring neoantigens[536]. Therefore, the induction of splenic and circulating Tregs by anti-PD-1 alone in our study may occur due to low neoantigen presentation in the TME. We were able to demonstrate that the combination therapy mitigated the immunosuppressive effects of anti-PD-1 alone, suggesting that sitagliptin may increase neoantigen expression and therefore partially overcome mechanisms of resistance to PD1-/PD-1 blockade as a standalone therapy.

In ovarian cancer the standard of care remains a combination of cytoreductive surgery and chemotherapy. Therefore, the clinical application of the combination of sitagliptin + PD-1/PD-L1 blockade must be considered in the context of prior exposure to chemotherapy. Several studies suggest that chemotherapy may increase the immunogenicity of various cancer types. For example, in the E.G7-OVA tumour-bearing mouse model, chemotherapy increased expression of CXCL9 and CXCL10 in tumour homogenates and increased the percentages of PD-1+ T cells[537]. In support of this finding, a recent pre-clinical study demonstrated that chemotherapy enhanced radiotherapy induced anti-tumour effects in combination with anti-PD-1 via a CXCR3/CXCL10 mediated mechanism of T cell recruitment[538], thereby implicating the CXCR3/CXCL10 axis in response to anti-PD-1 therapy.

In ovarian cancer cell lines, *in vitro* treatment with chemotherapy induces the expression of PD-L1[539]. Moreover, in the ascites of a stage III ovarian cancer patient, PD-L1 expression was increased 5-fold after 4 days of chemotherapy but returned to pre-treatment levels at day 11[539]. There is also some evidence to suggest that chemotherapy may increase expression of neoantigens in relapsed tumours in patients with HGSOC[540]. Together these data suggest that chemotherapy may increase susceptibility to anti-PD-1 therapy via upregulation of tumour-

associated PD-L1 and enhance mechanisms associated with T cell recruitment that could be beneficial in conjunction with sitagliptin treatment. Therefore, chemotherapy may in fact enhance the efficacy of this novel combination therapy by increasing the immunogenicity of tumours and neoantigen burden. Further investigation would be required to determine the potential clinical benefits of different treatment schedules, including whether the combination therapy should be incorporated with adjuvant chemotherapy or should be provided as a second-line treatment.

6.4.3 Biomarkers to identify susceptible cohorts of patients to PD-1/PD-L1 blockade

One of the challenges of implementing a new therapy in a highly heterogenous disease such as ovarian cancer is stratifying patients to optimise dosing schedules and identify those with the greatest chance of clinical benefit. As a potential prognostic indicator, PD-1 expression on lymphocytes was associated with favourable survival in HGSOC patients[541], whilst others demonstrated that expression status of PD-L1 on tumour-associated immune cells in ovarian tumours did not correlate with PFS or OS[542]. Likewise, there are multiple conflicting reports of the role of PD-L1 expression status to predict responses to anti-PD-1/PD-L1 therapies. In the phase II KEYNOTE-100 study, the investigators showed that in a cohort of 376 patients pembrolizumab (anti-PD-1) was more efficacious in patients with higher PD-L1 expression[193]. By contrast, results from 125 patients treated with alevumab (anti-PD-L1) from the phase Ib JAVELIN trial did not correlate with PD-L1 expression[192]. Similar findings were also reported by Hamanishi and colleagues, where PD-L1 expression was not significantly correlated with objective response to nivolumab (anti-PD-1) in a small cohort of 20 patients[191]. All of these open-label clinical trials were in women with recurrent advanced ovarian cancer, highlighting the need to consolidate these findings in subsequent trials. These inconsistencies may be explained by *de novo* PD-L1 expression induced via secretion of pro-inflammatory IFNs by activated T cells[543]. Thus, the presence of PD-L1 is likely to be co-localised to sites of T

effector cell accumulation[544], and current mechanisms of tumour tissue sampling may decrease the likelihood of identifying PD-L1 expression due to its concentrated pattern of expression within tumours[544]. Based on this evidence, investigators should therefore be cautious when stratifying patients according to PD-L1 expression status and should consider the presence of other factors.

As discussed in chapter 1, ovarian cancer patients that carry a *BRCA1/2* mutation have a more favourable prognosis than non-carriers[22,23] which may be due to the increased infiltration of CD3+ and CD8+ T cells compared to tumours without a homologous recombination deficiency[545]. Similarly, *BRCA1/2* mutated tumours exhibit higher expression of PD-1 and PD-L1 in tumour-associated immune cells[545]. Therefore, *BRCA1/2* mutation status in ovarian cancer may be a useful prognostic biomarker to predict response to anti-PD-1/PD-L1 therapy and represents a therapeutic opportunity to develop new treatment strategies for this cohort of patients.

6.4.4 Additional opportunities for combination therapy

Considering the potential for ovarian cancer patients with *BRCA1/2* mutations to have a higher response rate to anti-PD-1/PD-L1 therapies, studies have investigated the combination of PARP inhibitors – which target BRCA-mutated tumours – with immune checkpoint inhibitors. A phase II clinical trial combining the PARP inhibitor olaparib with durvalumab (anti-PD-L1) in 25 women with recurrent ovarian cancer demonstrated modest clinical activity, where the ORR was 14%[546]. However, an interesting outcome of this study was the upregulation of IFN-ɣ signalling, including CXCL9 and CXCL10 expression[546]. As DPP4 has the capacity to enzymatically inactivate CXCL9 and CXCL10, their upregulation in the context of this clinical trial may not be favourable. However, the addition of sitagliptin to this treatment regime could improve clinical outcomes by restoring the bioactivity of CXCL9 and CXCL10 as T cell chemoattractants to further enhance the anti-tumour immune response.

Due to the lack of efficacy of PD-1/PD-L1 blockade as standalone therapies in ovarian cancer, it is likely that other inhibitory mechanisms contribute to loss of T effector cell activity and that targeting multiple pathways may restore anti-tumour immunity. Many studies have implicated the immune regulator T cell immunoglobulin mucin-3 (Tim-3) with PD-1 as a marker of T cell exhaustion[547]. Tim-3 was co-expressed with PD-1 in a large proportion of CD8+ TILs in solid tumour models of colon carcinoma, breast cancer and melanoma[548] and on CD8+ T cells isolated from melanoma patients[549]. In ovarian cancer patients, CD8+ TILs that co-express Tim-3 and PD-1 are indicative of poor prognosis and have a more profoundly impaired cytotoxic capacity than PD-1+ CD8+ TILs[550]. Therefore, co-expression of PD-1 and Tim-3 may be a superior indicator of T cell exhaustion than PD-1 alone and could be a more suitable prognostic indicator of response to checkpoint inhibition therapy. The possibility of combining sitagliptin with other immune checkpoint inhibitors should also be considered as a therapeutic strategy for cancer immunotherapy.

6.5 Study limitations and technical challenges

As a cell surface protease, DPP4 has been associated with adhesion, migration and invasion in multiple cancer types. One aspect of DPP4 that was not explored in our studies was the *in vivo* effect of sitagliptin on DPP4-mediated adhesive properties including migration and invasive capacity via its expression on tumour cells and endothelial cells. Recent examination of the effect of sitagliptin on ovarian cancer cells *in vitro* found that sitagliptin significantly reduced migration of SKOV3 cells through Matrigel[260]. Indeed, further investigations into the adhesive function DPP4 in the context of our study may clarify some of the ambiguity in our data. Similarly, the role of DPP4 expression on T cells was not specifically explored in this study. Cell-surface DPP4 has an important function in T cell co-stimulation[221,551,552]; however, DPP4 activity is non-essential for co-stimulation[553] and has been shown to be unaffected by sitagliptin treatment *in vivo*[489,554].

Analysis of TILs in Chapters 4 and 5 was hindered by issues with construction of the TMA blocks that were used for immunofluorescence staining. Unfortunately, there was significant loss of cores in the TMAs and consequent reduction in statistical power. Therefore, although we were able to identify multiple trends in T cell infiltration in tumour sections, the data did not reach statistical significance as the sample size was reduced. Due to time constraints, additional TMAs could not be constructed for the purpose of these studies; however, extra tumour tissue is available and will be used for ongoing experiments.

The *in vivo* experiments in this thesis were limited in the capacity to measure tumour burden throughout disease progression. In our studies, all mice had metastatic tumour deposits at humane endpoint and were ethically culled following the accumulation of ascites. Mice developed ascites after ~6 weeks, and survival time did not extend beyond ~10 weeks. Roby and colleagues found that in the syngeneic model of ovarian cancer tumour load did not correlate with ascites formation or survival time[265], which was also demonstrated by real-time

monitoring of tumour burden using the iRFP model that was developed by our laboratory (see Appendix E)[419]. Future pre-clinical studies investigating sitagliptin *in vivo,* alone or in combination with other therapies in ovarian cancer should consider the use of the iRFP tumour model[419]. In this study we chose not to utilise the iRFP model to monitor tumour burden due to the presence of exogenous antigen that may be potentially recognised and therefore influence the data. In addition, the suitability of this model for late-stage disease should be further assessed, as fluorescence intensity was shown to be highly elevated prior to peritoneal spread, and decreased upon ascites accumulation[419], suggesting that tumour burden may be difficult to quantify in real-time in late stages of disease. The development of biomarkers of disease progression will also be useful in future studies to provide a more quantitative measurement of tumour load which can be monitored over time.

Research in this thesis utilised the syngeneic ID8 model of ovarian cancer which is widely used as an immunocompetent model of disease[407,555]. Genetic derivatives of the ID8 cell line have been recently generated using CRISPR/Cas9 technology, including single *p53* knockout, with variations including additional knockout of *BRCA1, BRCA2, Pten* and *Nf1*[556,557]. These cell lines may more accurately represent HGSOC tumorigenesis, have distinct immune profiles and exhibit different responses to therapies[556,557]. Furthermore, transgenic mouse models of tumorigenesis which utilise the Cre/Lox system to conditionally knockout genes including *p53*, *cMyc* and *KRAS,* or the spontaneous laying hen model of ovarian cancer may be more suitable to study ovarian cancer in the context of malignant transformation and progression of disease[558]. Therefore, further studies should consider the use of newly characterised models to understand the effect of novel combination immunotherapies in tumour models which better recapitulate the genetic aberrations and biology in HGSOC.

6.6 Future directions

Questions remain regarding the utility of sDPP4 as a biomarker in ovarian cancer; namely, whether sDPP4 is involved in the pathogenesis of ovarian cancer or is a metabolic consequence of disease. Investigation of sDPP4 and its activity as a biomarker of either disease progression or response to therapy will be further explored by analysing ovarian cancer patient samples that are available to our laboratory via a tissue biobank.

There is still much to be discovered about the ovarian TME regarding the role of DPP4 in the anti-tumour response. We intend to conduct additional experiments to determine the mechanism/s by which DPP4 may contribute to ovarian cancer pathogenesis, and subsequently the specific action of sitagliptin in the TME. Multiple DPP4 variant ID8 cell lines have been generated including i) DPP4 overexpression, ii) DPP4 knockout and iii) DPP4 enzyme inactive (substitution of serine at amino acid position 630 to alanine), that will be utilised *in vivo* to investigate tumour-specific expression and activity of DPP4 in the context of primary and metastatic disease. These variants will also be used in combination with anti-PD-1/PD-L1 to investigate whether it is DPP4 activity, expression or a combination of both that synergises with immune checkpoint blockade to enhance the anti-tumour immune response.

The work presented in this thesis provides a solid rationale to therapeutically target DPP4 in ovarian cancer. Moreover, potential synergism of DPP4 inhibition with immune checkpoint inhibitors was demonstrated in Chapter 5, highlighting the opportunity for further clinical translatability to ovarian cancer patients with late-stage disease. Due to the immunomodulatory activity of sitagliptin *in vivo,* the outcomes of these studies may also prompt further investigation into combination therapies of sitagliptin with other ICIs including anti-CTLA-4, PARP inhibitors, VEGF inhibitors or chemotherapy.

Concluding remarks

The role of DPP4 in ovarian cancer remains a complex area of research. It is now clear that DPP4 is likely to have several functions in the pathogenesis and progression of ovarian disease, which is vastly influenced by the heterogenous TME. In particular, the hypoxic environment that induces various metabolic adaptations by tumour cells was shown to regulate tumour-specific expression and activity of DPP4, which may impact local immune responses, influence transcriptional pathways and/or serve as a biomarker of disease progression in its soluble form (sDPP4). The *in vivo* effect of DPP4 inhibition using the FDA approved inhibitor sitagliptin in primary and metastatic ovarian disease further validates its role in the progression of epithelial ovarian cancers. Accordingly, sitagliptin may improve survival of ovarian cancer patients by slowing the growth of tumours via predominantly T effector cell-mediated mechanisms to enhance the anti-tumour response. The clinical translatability of sitagliptin makes its repurposing as an immunomodulatory therapy indicated for ovarian cancer relatively simple and should be intently considered especially in patients with metastatic ovarian disease. The combination of sitagliptin with PD-1/PD-L1 blockade also provides an opportunity to further enhance anti-tumour immunity and provides an insight into non-response to immune checkpoint inhibitors in ovarian cancer.

References

1 Davidson, B. & Tropé, C. G. Ovarian cancer: Diagnostic, biological and prognostic aspects. *Womens Health* **10**, 519-533, doi:10.2217/whe.14.37 (2014).

2 Jelovac, D. & Armstrong, D. K. Recent progress in the diagnosis and treatment of ovarian cancer. *CA Cancer J. Clin.* **61**, 183, doi:10.3322/caac.20113 (2011).

3 Bray, F. *et al.* Global cancer statistics 2018: GLOBOCAN estimates of incidence and mortality worldwide for 36 cancers in 185 countries. *CA Cancer J. Clin.* **68**, 394-424, doi:10.3322/caac.21492 (2018).

4 Australian Institute of Health and Welfare. *Cancer in Australia 2017*. (AIHW, 2017).

5 Australian Institute of Health and Welfare & Cancer Australia. *Gynaecological cancers in Australia: an overview*. (2012).

6 Australian Institute of Health and Welfare. Cancer in Australia 2019. (AIHW, Canberra, 2019).

7 Javadi, S., Ganeshan, D. M., Qayyum, A., Iyer, R. B. & Bhosale, P. Ovarian Cancer, the Revised FIGO Staging System, and the Role of Imaging. *AJR Am. J. Roentgenol.* **206**, 1351-1360, doi:10.2214/ajr.15.15199 (2016).

8 Goff, B. A., Mandel, L., Muntz, H. G. & Melancon, C. H. Ovarian carcinoma diagnosis: results of a national ovarian cancer survey. *Cancer* **89**, 2068, doi:10.1002/1097-0142(20001115)89:103.0.CO2-Z (2000).

9 Goff, B. A., Mandel, L. S., Melancon, C. H. & Muntz, H. G. Frequency of symptoms of ovarian cancer in women presenting to primary care clinics. *JAMA* **291**, 2705, doi:10.1001/jama.291.22.2705 (2004).

10 Badgwell, D. & Bast, R. C., Jr. Early detection of ovarian cancer. *Dis. Markers* **23**, 397-410 (2007).

11 American Cancer Society. *Survival rates for ovarian cancer, by stage*, <https://www.cancer.org/cancer/ovarian-cancer/detection-diagnosis-staging/survival-rates.html> (2016).

12 Australian Institute of Health and Welfare and National Breast and Ovarian Cancer Centre. in *Cancer series: no. 52 Cancer series: no.52* (Canberra: AIHW, 2010).

13 Metzger-Filho, O., Moulin, C. & D'Hondt, V. First-line systemic treatment of ovarian cancer: A critical review of available evidence and expectations for future directions. *Curr. Opin. Oncol.* **22**, 513-520, doi:10.1097/CCO.0b013e32833ae99c (2010).

14 Hunn, J. & Rodriguez, G. C. Ovarian cancer: Etiology, risk factors, and epidemiology. *Clin. Obstet. Gynecol.* **55**, 3-23, doi:10.1097/GRF.0b013e31824b4611 (2012).

15 Australian Institute of Health and Welfare. in *All cancers combined* (2012).

16 Bandera, C. A. Advances in the understanding of risk factors for ovarian cancer. *Journal of Reproductive Medicine for the Obstetrician and Gynecologist* **50**, 399-406 (2005).

17 Leong, H. S. *et al.* Efficient molecular subtype classification of high-grade serous ovarian cancer. *J. Pathol.* **236**, 272-277, doi:10.1002/path.4536 (2015).

18 Antoniou, A. *et al.* Average risks of breast and ovarian cancer associated with BRCA1 or BRCA2 mutations detected in case Series unselected for family history: a combined analysis of 22 studies. *Am. J. Hum. Genet.* **72**, 1117 (2003).

19 Mavaddat, N. *et al.* Cancer Risks for BRCA1 and BRCA2 Mutation Carriers: Results From Prospective Analysis of EMBRACE. *J. Natl. Cancer Inst.* **105**, 812, doi:10.1093/jnci/djt095 (2013).

20 King, M.-C., Marks, J. H. & Mandell, J. B. Breast and ovarian cancer risks due to inherited mutations in BRCA1 and BRCA2. *Science (New York, N.Y.)* **302**, 643, doi:10.1126/science.1088759 (2003).

21 Bowtell, D. D. L. The genesis and evolution of high-grade serous ovarian cancer. *Nature Reviews Cancer* **10**, 803-808, doi:10.1038/nrc2946 (2010).

22 Da, Y. *et al.* Association of BRCA1 and BRCA2 mutations with survival, chemotherapy sensitivity, and gene mutator phenotype in patients with ovarian cancer.(Report). *JAMA, The Journal of the American Medical Association* **306**, 1557 (2011).

23 Bolton, K. L. *et al.* Association between BRCA1 and BRCA2 mutations and survival in women with invasive epithelial ovarian cancer. *JAMA* **307**, 382, doi:10.1001/jama.2012.20 (2012).

24 Lewis, K. E., Lu, K. H., Klimczak, A. M. & Mok, S. C. Recommendations and Choices for BRCA Mutation Carriers at Risk for Ovarian Cancer: A Complicated Decision. *Cancers (Basel)* **10**, doi:10.3390/cancers10020057 (2018).

25 Domchek, S. M. *et al.* Association of risk-reducing surgery in BRCA1 or BRCA2 mutation carriers with cancer risk and mortality. *JAMA* **304**, 967-975, doi:10.1001/jama.2010.1237 (2010).
26 Kauff, N. D. *et al.* Risk-reducing salpingo-oophorectomy for the prevention of BRCA1- and BRCA2-associated breast and gynecologic cancer: a multicenter, prospective study. *Journal of clinical oncology : official journal of the American Society of Clinical Oncology* **26**, 1331-1337, doi:10.1200/JCO.2007.13.9626 (2008).
27 Finch, A. P. *et al.* Impact of oophorectomy on cancer incidence and mortality in women with a BRCA1 or BRCA2 mutation. *J. Clin. Oncol.* **32**, 1547-1553, doi:10.1200/jco.2013.53.2820 (2014).
28 Stewart, M. E., Knisely, A. T., Sullivan, M. W., Ring, K. L. & Modesitt, S. C. Evaluation of screening and risk-reducing surgery for women followed in a high-risk breast/ovarian cancer clinic: it is all about the tubes in BRCA mutation carriers. *Gynecologic oncology reports* **28**, 18-22, doi:10.1016/j.gore.2019.01.010 (2019).
29 Whittemore, S. A., Harris, S. R. & Itnyre, S. J. Characteristics Relating to Ovarian Cancer Risk: Collaborative Analysis of 12 U.S. Case-Control Studies: II. Invasive Epithelial Ovarian Cancer in White Women. *Obstet. Gynecol. Surv.* **48**, 486-488 (1993).
30 Tsilidis, K. K. *et al.* Oral contraceptive use and reproductive factors and risk of ovarian cancer in the European Prospective Investigation into Cancer and Nutrition. *Br. J. Cancer* **105**, 1436, doi:10.1038/bjc.2011.371 (2011).
31 Sieh, W. *et al.* Tubal ligation and risk of ovarian cancer subtypes: a pooled analysis of case-control studies. *Int. J. Epidemiol.* **42**, 579-589, doi:10.1093/ije/dyt042 (2013).
32 Collaborative Group on Epidemiological Studies of Ovarian Cancer. Ovarian cancer and oral contraceptives: collaborative reanalysis of data from 45 epidemiological studies including 23 257 women with ovarian cancer and 87 303 controls. *The Lancet* **371**, 303-314, doi:10.1016/S0140-6736(08)60167-1 (2008).
33 Cooper, G., Schildkraut, J., Whittemore, A. & Marchbanks, P. Pregnancy recency and risk of ovarian cancer. *Cancer Causes Control* **10**, 397-402, doi:10.1023/A:1008960520316 (1999).
34 Tavani, A. *et al.* Influence of menstrual and reproductive factors on ovarian cancer risk in women with and without family history of breast or ovarian cancer. *Int. J. Epidemiol.* **29**, 799-802 (2000).
35 Olsen, C. M. *et al.* Obesity and risk of ovarian cancer subtypes: evidence from the Ovarian Cancer Association Consortium. *Endocr. Relat. Cancer* **20**, 251-262, doi:10.1530/erc-12-0395 (2013).
36 Zhang, D., Li, N., Xi, Y., Zhao, Y. & Wang, T. Diabetes mellitus and risk of ovarian cancer. A systematic review and meta-analysis of 15 cohort studies. *Diabetes Res. Clin. Pract.* **130**, 43-52, doi:10.1016/j.diabres.2017.04.005 (2017).
37 Chittenden, B. G., Fullerton, G., Maheshwari, A. & Bhattacharya, S. Polycystic ovary syndrome and the risk of gynaecological cancer: a systematic review. *Reprod. Biomed. Online* **19**, 398, doi:10.1016/S1472-6483(10)60175-7 (2009).
38 Munksgaard, P. S. & Blaakaer, J. The association between endometriosis and ovarian cancer: a review of histological, genetic and molecular alterations. *Gynecol. Oncol.* **124**, 164, doi:10.1016/j.ygyno.2011.10.001 (2012).
39 Anton, C. *et al.* A comparison of CA125, HE4, risk ovarian malignancy algorithm (ROMA), and risk malignancy index (RMI) for the classification of ovarian masses. *Clinics (Sao Paulo)* **67**, 437-441, doi:10.6061/clinics/2012(05)06 (2012).
40 Al Musalhi, K. *et al.* Evaluation of HE4, CA-125, Risk of Ovarian Malignancy Algorithm (ROMA) and Risk of Malignancy Index (RMI) in the Preoperative Assessment of Patients with Adnexal Mass. *Oman Med. J.* **31**, 336-344, doi:10.5001/omj.2016.68 (2016).
41 Buys, S. S. *et al.* Effect of screening on ovarian cancer mortality: the Prostate, Lung, Colorectal and Ovarian (PLCO) Cancer Screening Randomized Controlled Trial. *JAMA* **305**, 2295, doi:10.1001/jama.2011.766 (2011).
42 Köbel, M. *et al.* Ovarian Carcinoma Subtypes Are Different Diseases: Implications for Biomarker Studies (Ovarian Carcinoma Subtypes Are Different). *PLoS Med.* **5**, e232, doi:10.1371/journal.pmed.0050232 (2008).
43 Ayhan, J. A. *et al.* Defining the Cut Point Between Low-grade and High-grade Ovarian Serous Carcinomas: A Clinicopathologic and Molecular Genetic Analysis. *The American Journal of Surgical Pathology* **33**, 1220-1224, doi:10.1097/PAS.0b013e3181a24354 (2009).
44 The Cancer Genome Atlas Research Network. Integrated genomic analyses of ovarian carcinoma. *Nature* **474**, 609, doi:10.1038/nature10166 (2011).

45 Shih, I.-M. & Kurman, R. J. Ovarian tumorigenesis: a proposed model based on morphological and molecular genetic analysis. *The American journal of pathology* **164**, 1511, doi:10.1016/S0002-9440(10)63708-X (2004).
46 Kurman, R. J. & Shih, I.-M. The Dualistic Model of Ovarian Carcinogenesis: Revisited, Revised, and Expanded. *The American journal of pathology* **186**, 733, doi:10.1016/j.ajpath.2015.11.011 (2016).
47 Gilks, C. B. & Prat, J. Ovarian carcinoma pathology and genetics: recent advances. *Hum. Pathol.* **40**, 1213-1223, doi:10.1016/j.humpath.2009.04.017 (2009).
48 Köbel, M., Huntsman, D. & Gilks, C. B. Critical molecular abnormalities in high-grade serous carcinoma of the ovary. *Expert Rev. Mol. Med.* **10**, 14-e22, doi:http://dx.doi.org/10.1017/S146239940800077X (2008).
49 Tothill, R. W. *et al.* Novel molecular subtypes of serous and endometrioid ovarian cancer linked to clinical outcome. *Clinical cancer research : an official journal of the American Association for Cancer Research* **14**, 5198, doi:10.1158/1078-0432.CCR-08-0196 (2008).
50 Karst, A. M. & Drapkin, R. Ovarian Cancer Pathogenesis: A Model in Evolution. *J. Oncol.* **2010**, 13, doi:10.1155/2010/932371 (2010).
51 Kurman, J. R. & Shih, J. I.-M. The Origin and Pathogenesis of Epithelial Ovarian Cancer: A Proposed Unifying Theory. *The American Journal of Surgical Pathology* **34**, 433-443, doi:10.1097/PAS.0b013e3181cf3d79 (2010).
52 Kroeger, T. P. & Drapkin, T. R. Pathogenesis and heterogeneity of ovarian cancer. *Curr. Opin. Obstet. Gynecol.* **29**, 26-34, doi:10.1097/GCO.0000000000000340 (2017).
53 Walker, J. L. *et al.* Society of Gynecologic Oncology recommendations for the prevention of ovarian cancer. *Cancer* **121**, 2108-2120, doi:10.1002/cncr.29321 (2015).
54 Kindelberger, W. D. *et al.* Intraepithelial Carcinoma of the Fimbria and Pelvic Serous Carcinoma: Evidence for a Causal Relationship. *The American Journal of Surgical Pathology* **31**, 161-169, doi:10.1097/01.pas.0000213335.40358.47 (2007).
55 Kuhn, E. *et al.* TP53 mutations in serous tubal intraepithelial carcinoma and concurrent pelvic high-grade serous carcinoma—evidence supporting the clonal relationship of the two lesions. *J. Pathol.* **226**, 421-426, doi:10.1002/path.3023 (2012).
56 Huang, H.-S. *et al.* Mutagenic, surviving and tumorigenic effects of follicular fluid in the context of p53 loss: initiation of fimbria carcinogenesis. *Carcinogenesis* **36**, 1419-1428, doi:10.1093/carcin/bgv132 (2015).
57 Aletti, G. D., Gallenberg, M. M., Cliby, W. A., Jatoi, A. & Hartmann, L. C. Current Management Strategies for Ovarian Cancer. *Mayo Clin. Proc.* **82**, 751-770, doi:10.4065/82.6.751 (2007).
58 Jayson, G. C., Kohn, E. C., Kitchener, H. C. & Ledermann, J. A. Ovarian cancer. *The Lancet* **384**, 1376-1388, doi:10.1016/S0140-6736(13)62146-7 (2014).
59 du Bois, A. *et al.* Role of surgical outcome as prognostic factor in advanced epithelial ovarian cancer: A combined exploratory analysis of 3 prospectively randomized phase 3 multicenter trials. *Cancer* **115**, 1234-1244, doi:10.1002/cncr.24149 (2009).
60 Collinson, F. J., Seligmann, J. & Perren, T. J. Ovarian cancer: Advances in first-line treatment strategies with a particular focus on anti-angiogenic agents. *Curr. Oncol. Rep.* **14**, 509-518, doi:10.1007/s11912-012-0274-4 (2012).
61 Vergote, I. *et al.* Neoadjuvant Chemotherapy or Primary Surgery in Stage IIIC or IV Ovarian Cancer. *The New England Journal of Medicine* **363**, 943-953, doi:10.1056/NEJMoa0908806 (2010).
62 Wright, A. A. *et al.* Neoadjuvant Chemotherapy for Newly Diagnosed, Advanced Ovarian Cancer: Society of Gynecologic Oncology and American Society of Clinical Oncology Clinical Practice Guideline. *J. Clin. Oncol.* **34**, 3460-3473, doi:10.1200/jco.2016.68.6907 (2016).
63 Vasey, P. A. *et al.* Phase III randomized trial of docetaxel-carboplatin versus paclitaxel-carboplatin as first-line chemotherapy for ovarian carcinoma. *J. Natl. Cancer Inst.* **96**, 1682, doi:10.1093/jnci/djh323 (2004).
64 Bookman, M. A. *et al.* Evaluation of new platinum-based treatment regimens in advanced-stage ovarian cancer: a Phase III Trial of the Gynecologic Cancer Intergroup. *Journal of clinical oncology : official journal of the American Society of Clinical Oncology* **27**, 1419, doi:10.1200/JCO.2008.19.1684 (2009).
65 Alberts, D. S. *et al.* Intraperitoneal Cisplatin plus Intravenous Cyclophosphamide versus Intravenous Cisplatin plus Intravenous Cyclophosphamide for Stage III Ovarian Cancer. *The New England Journal of Medicine* **335**, 1950-1955, doi:10.1056/NEJM199612263352603 (1996).

66 Armstrong, D. K. *et al.* Intraperitoneal Cisplatin and Paclitaxel in Ovarian Cancer. *The New England Journal of Medicine* **354**, 34-43, doi:10.1056/NEJMoa052985 (2006).
67 Mahmood, R. D., Morgan, R. D., Edmondson, R. J., Clamp, A. R. & Jayson, G. C. First-Line Management of Advanced High-Grade Serous Ovarian Cancer. *Curr. Oncol. Rep.* **22**, 64, doi:10.1007/s11912-020-00933-8 (2020).
68 Sebastian, V. *et al.* Rethinking ovarian cancer: recommendations for improving outcomes. *Nature Reviews Cancer* **11**, 719, doi:10.1038/nrc3144 (2011).
69 Liao, J. *et al.* Ovarian cancer spheroid cells with stem cell-like properties contribute to tumor generation, metastasis and chemotherapy resistance through hypoxia-resistant metabolism. *PLoS One* **9**, doi:10.1371/journal.pone.0084941 (2014).
70 Corrado, G. *et al.* Optimizing treatment in recurrent epithelial ovarian cancer. *Expert Rev. Anticancer Ther.* **17**, 1147-1158, doi:10.1080/14737140.2017.1398088 (2017).
71 Williams, E., Martin, S., Moss, R., Durrant, L. & Deen, S. Co-expression of VEGF and CA9 in ovarian high-grade serous carcinoma and relationship to survival. *Virchows Arch.* **461**, 33-39, doi:10.1007/s00428-012-1252-9 (2012).
72 Abahssain, H. *et al.* Angiogenesis and anti-angiogenic therapies in epithelial ovarian cancer. *Current Angiogenesis* **3**, 60-65 (2014).
73 Burger, R. A. *et al.* Incorporation of bevacizumab in the primary treatment of ovarian cancer. *N. Engl. J. Med.* **365**, 2473-2483, doi:10.1056/NEJMoa1104390 (2011).
74 Aghajanian, C. *et al.* OCEANS: a randomized, double-blind, placebo-controlled phase III trial of chemotherapy with or without bevacizumab in patients with platinum-sensitive recurrent epithelial ovarian, primary peritoneal, or fallopian tube cancer. *Journal of clinical oncology : official journal of the American Society of Clinical Oncology* **30**, 2039-2045, doi:10.1200/JCO.2012.42.0505 (2012).
75 Banerjee, S. & Kaye, S. B. New strategies in the treatment of ovarian cancer: current clinical perspectives and future potential. *Clinical cancer research : an official journal of the American Association for Cancer Research* **19**, 961, doi:10.1158/1078-0432.CCR-12-2243 (2013).
76 Liu, J. F., Konstantinopoulos, P. A. & Matulonis, U. A. PARP inhibitors in ovarian cancer: current status and future promise. *Gynecol. Oncol.* **133**, 362, doi:10.1016/j.ygyno.2014.02.039 (2014).
77 Fong, P. C. *et al.* Inhibition of Poly(ADP-Ribose) Polymerase in Tumors from BRCA Mutation Carriers. *The New England Journal of Medicine* **361**, 123-134, doi:10.1056/NEJMoa0900212 (2009).
78 Ledermann, J. *et al.* Olaparib Maintenance Therapy in Platinum-Sensitive Relapsed Ovarian Cancer. *The New England Journal of Medicine* **366**, 1382-1392, doi:10.1056/NEJMoa1105535 (2012).
79 Penson, R. T. *et al.* Phase II study of carboplatin, paclitaxel, and bevacizumab with maintenance bevacizumab as first-line chemotherapy for advanced mullerian tumors. *Journal of clinical oncology : official journal of the American Society of Clinical Oncology* **28**, 154, doi:10.1200/JCO.2009.22.7900 (2010).
80 Zhang, W. *et al.* Global DNA Hypomethylation in Epithelial Ovarian Cancer: Passive Demethylation and Association with Genomic Instability. *Cancers (Basel)* **12**, 764 (2020).
81 Geistlinger, L. *et al.* Multiomic Analysis of Subtype Evolution and Heterogeneity in High-Grade Serous Ovarian Carcinoma. *Cancer Res.* **80**, 4335, doi:10.1158/0008-5472.CAN-20-0521 (2020).
82 Roberts, C. M., Cardenas, C. & Tedja, R. The Role of Intra-Tumoral Heterogeneity and Its Clinical Relevance in Epithelial Ovarian Cancer Recurrence and Metastasis. *Cancers (Basel)* **11**, 1083, doi:10.3390/cancers11081083 (2019).
83 Friedl, P. & Gilmour, D. Collective cell migration in morphogenesis, regeneration and cancer. *Nature Reviews Molecular Cell Biology* **10**, 445-457, doi:10.1038/nrm2720 (2009).
84 Shield, K., Ackland, M. L., Ahmed, N. & Rice, G. E. Multicellular spheroids in ovarian cancer metastases: Biology and pathology. *Gynecol. Oncol.* **113**, 143-148, doi:10.1016/j.ygyno.2008.11.032 (2009).
85 Ahmed, N., Thompson, E. W. & Quinn, M. A. Epithelial–mesenchymal interconversions in normal ovarian surface epithelium and ovarian carcinomas: An exception to the norm. **213**, 581-588, doi:10.1002/jcp.21240 (2007).
86 Lengyel, E. Ovarian cancer development and metastasis. *The American journal of pathology* **177**, 1053, doi:10.2353/ajpath.2010.100105 (2010).
87 Patel, I. S., Madan, P., Getsios, S., Bertrand, M. A. & MacCalman, C. D. Cadherin switching in ovarian cancer progression. *Int. J. Cancer* **106**, 172-177, doi:10.1002/ijc.11086 (2003).

88 Ahmed, N. & Stenvers, K. L. Getting to know ovarian cancer ascites: opportunities for targeted therapy-based translational research. *Front. Oncol.* **3**, 256, doi:10.3389/fonc.2013.00256 (2013).
89 Thibault, B., Castells, M., Delord, J.-P. & Couderc, B. Ovarian cancer microenvironment: implications for cancer dissemination and chemoresistance acquisition. *Cancer Metastasis Rev.* **33**, 17-39, doi:10.1007/s10555-013-9456-2 (2014).
90 Khalil, A. A. & Friedl, P. Determinants of leader cells in collective cell migration. *Integr. Biol. (Camb.)* **2**, 568-574, doi:10.1039/c0ib00052c (2010).
91 Moffitt, L., Karimnia, N., Stephens, A. & Bilandzic, M. Therapeutic Targeting of Collective Invasion in Ovarian Cancer. *Int. J. Mol. Sci.* **20**, doi:10.3390/ijms20061466 (2019).
92 Bilandzic, M. *et al.* Keratin-14 (KRT14) Positive Leader Cells Mediate Mesothelial Clearance and Invasion by Ovarian Cancer Cells. *Cancers (Basel)* **11**, 1228 (2019).
93 Kim, K.-S. *et al.* Hypoxia enhances lysophosphatidic acid responsiveness in ovarian cancer cells and lysophosphatidic acid induces ovarian tumor metastasis in vivo. *Cancer Res.* **66**, 7983 (2006).
94 Jessica, A. B., Shetal, A. P. & Simon, M. C. The impact of O2 availability on human cancer. *Nature Reviews Cancer* **8**, 967, doi:10.1038/nrc2540 (2008).
95 Zhong, H. *et al.* Overexpression of hypoxia-inducible factor 1alpha in common human cancers and their metastases. *Cancer Res.* **59**, 5830 (1999).
96 Muz, B., de la Puente, P., Azab, F. & Azab, A. K. The role of hypoxia in cancer progression, angiogenesis, metastasis, and resistance to therapy. *Hypoxia* **3**, 83-92, doi:10.2147/HP.S93413 (2015).
97 Semenza, G. L. Hydroxylation of HIF-1: oxygen sensing at the molecular level. *Physiology (Bethesda)* **19**, 176 (2004).
98 Semenza, G. L. Involvement of hypoxia-inducible factor 1 in human cancer. *Internal medicine (Tokyo, Japan)* **41**, 79, doi:10.2169/internalmedicine.41.79 (2002).
99 Semenza, G. L. Defining the role of hypoxia-inducible factor 1 in cancer biology and therapeutics. *Oncogene* **29**, 625, doi:10.1038/onc.2009.441 (2009).
100 Ruan, K., Song, G. & Ouyang, G. Role of hypoxia in the hallmarks of human cancer. *J. Cell. Biochem.* **107**, 1053-1062, doi:10.1002/jcb.22214 (2009).
101 McEvoy, L. M. *et al.* Identifying novel hypoxia-associated markers of chemoresistance in ovarian cancer. *BMC Cancer* **15**, 547-, doi:10.1186/s12885-015-1539-8 (2015).
102 Braicu, E. I. *et al.* HIFI α is an independent prognostic factor for overall survival in advanced primary epithelial ovarian cancer – A study of the OVCAD consortium. *Onco Targets Ther.* **7**, 1563-1569, doi:10.2147/OTT.S65373 (2014).
103 Birner, P., Schindl, M., Obermair, A., Breitenecker, G. & Oberhuber, G. Expression of Hypoxia-inducible Factor 1α in Epithelial Ovarian Tumors: Its Impact on Prognosis and on Response to Chemotherapy. *Clin. Cancer Res.* **7**, 1661-1668 (2001).
104 Jin, Y., Wang, H., Liang, X., Ma, J. & Wang, Y. Pathological and prognostic significance of hypoxia-inducible factor 1α expression in epithelial ovarian cancer: a meta-analysis. *Tumour Biol.* **35**, 8149-8159, doi:10.1007/s13277-014-2059-x (2014).
105 Baker, A. F. *et al.* Evaluation of a Hypoxia Regulated Gene Panel in Ovarian Cancer. *Cancer Microenviron.* **8**, 45-56, doi:10.1007/s12307-015-0166-x (2015).
106 Semenza, G. L. Regulation of hypoxia-induced angiogenesis: a chaperone escorts VEGF to the dance. *The Journal of clinical investigation* **108**, 39 (2001).
107 Jiang, J., Tang, Y. L. & Liang, X. H. EMT: A new vision of hypoxia promoting cancer progression. *Cancer Biology and Therapy* **11**, 714-723, doi:10.4161/cbt.11.8.15274 (2011).
108 Du, J. *et al.* Hypoxia promotes vasculogenic mimicry formation by inducing epithelial-mesenchymal transition in ovarian carcinoma. *Gynecol. Oncol.* **133**, 575-583, doi:10.1016/j.ygyno.2014.02.034 (2014).
109 Cheng, J. C., Klausen, C. & Leung, P. C. K. Hypoxia-inducible factor 1 alpha mediates epidermal growth factor-induced down-regulation of E-cadherin expression and cell invasion in human ovarian cancer cells. *Cancer Lett.* **329**, 197-206, doi:10.1016/j.canlet.2012.10.029 (2013).
110 Nelson, B. H. The impact of T-cell immunity on ovarian cancer outcomes. *Immunol. Rev.* **222**, 101-116, doi:10.1111/j.1600-065X.2008.00614.x (2008).
111 Gavalas, N. G., Karadimou, A., Dimopoulos, M. A. & Bamias, A. Immune Response in Ovarian Cancer: How Is the Immune System Involved in Prognosis and Therapy: Potential for Treatment Utilization. *Clinical and Developmental Immunology* **2010**, 791603, doi:10.1155/2010/791603 (2010).

112 Wilson, A. L. *et al.* Autoantibodies against HSF1 and CCDC155 as Biomarkers of Early-stage, High Grade Serous Ovarian Cancer. . *Cancer Epidemiol. Biomarkers Prev.*, doi:10.1158/1055-9965.epi-17-0752 (2017).
113 Charbonneau, B., Goode, E. L., Kalli, K. R., Knutson, K. L. & Derycke, M. S. The immune system in the pathogenesis of ovarian cancer. *Crit. Rev. Immunol.* **33**, 137-164, doi:10.1615/critrevimmunol.2013006813 (2013).
114 Baert, T. *et al.* Myeloid Derived Suppressor Cells: Key Drivers of Immunosuppression in Ovarian Cancer. *Front. Immunol.* **10**, 1273-1273, doi:10.3389/fimmu.2019.01273 (2019).
115 Lee, W. *et al.* Neutrophils facilitate ovarian cancer premetastatic niche formation in the omentum. *J. Exp. Med.* **216**, 176-194, doi:10.1084/jem.20181170 (2019).
116 Zhou, Q., Hong, L., Zuo, M.-Z. & He, Z. Prognostic significance of neutrophil to lymphocyte ratio in ovarian cancer: evidence from 4,910 patients. *Oncotarget* **8**, 68938-68949, doi:10.18632/oncotarget.20196 (2017).
117 Allavena, P., Sica, A., Solinas, G., Porta, C. & Mantovani, A. The inflammatory micro-environment in tumor progression: The role of tumor-associated macrophages. *Crit. Rev. Oncol. Hematol.* **66**, 1-9, doi:10.1016/j.critrevonc.2007.07.004 (2007).
118 Baci, D. *et al.* The Ovarian Cancer Tumor Immune Microenvironment (TIME) as Target for Therapy: A Focus on Innate Immunity Cells as Therapeutic Effectors. *Int. J. Mol. Sci.* **21**, doi:10.3390/ijms21093125 (2020).
119 Mantovani, A., Sica, A. & Locati, M. Macrophage Polarization Comes of Age. *Immunity* **23**, 344-346, doi:10.1016/j.immuni.2005.10.001 (2005).
120 Mantovani, A. *et al.* The chemokine system in diverse forms of macrophage activation and polarization. *Trends Immunol.* **25**, 677-686, doi:10.1016/j.it.2004.09.015 (2004).
121 Mills, G. B. *et al.* Ascitic fluid from human ovarian cancer patients contains growth factors necessary for intraperitoneal growth of human ovarian adenocarcinoma cells. *J. Clin. Invest.* **86**, 851-855, doi:10.1172/jci114784 (1990).
122 Krieg, C. & Boyman, O. The role of chemokines in cancer immune surveillance by the adaptive immune system. *Semin. Cancer Biol.* **19**, 76-83, doi:10.1016/j.semcancer.2008.10.011 (2009).
123 Yigit, R., Massuger, L. F., Figdor, C. G. & Torensma, R. Ovarian cancer creates a suppressive microenvironment to escape immune elimination. *Gynecol. Oncol.* **117**, 366-372, doi:10.1016/j.ygyno.2010.01.019 (2010).
124 Ridge, J. P., Di Rosa, F. & Matzinger, P. A conditioned dendritic cell can be a temporal bridge between a CD4+ T-helper and a T-killer cell. *Nature* **393**, 474-478, doi:10.1038/30989 (1998).
125 Embgenbroich, M. & Burgdorf, S. Current Concepts of Antigen Cross-Presentation. *Front. Immunol.* **9**, 1643-1643, doi:10.3389/fimmu.2018.01643 (2018).
126 Sato, E. *et al.* Intraepithelial CD8 + Tumor-Infiltrating Lymphocytes and a High CD8+/regulatory T Cell Ratio Are Associated with Favorable Prognosis in Ovarian Cancer. *Proc. Natl. Acad. Sci. U. S. A.* **102**, 18538-18543 (2005).
127 Zhang, L. *et al.* Intratumoral T Cells, Recurrence, and Survival in Epithelial Ovarian Cancer. *The New England Journal of Medicine* **348**, 203-213, doi:10.1056/NEJMoa020177 (2003).
128 Tomšová, M., Melichar, B., Sedláková, I. & Šteiner, I. Prognostic significance of CD3+ tumor-infiltrating lymphocytes in ovarian carcinoma. *Gynecol. Oncol.* **108**, 415-420, doi:10.1016/j.ygyno.2007.10.016 (2008).
129 Leffers, N. *et al.* Prognostic significance of tumor-infiltrating T-lymphocytes in primary and metastatic lesions of advanced stage ovarian cancer. *Cancer Immunol. Immunother.* **58**, 449-459, doi:10.1007/s00262-008-0583-5 (2009).
130 James, F. R. *et al.* Association between tumour infiltrating lymphocytes, histotype and clinical outcome in epithelial ovarian cancer. *BMC Cancer* **17**, 657-657, doi:10.1186/s12885-017-3585-x (2017).
131 Fan, Z. & Zhang, Q. Molecular mechanisms of lymphocyte-mediated cytotoxicity. *Cell. Mol. Immunol.* **2**, 259-264 (2005).
132 Cullen, S. P. & Martin, S. J. Mechanisms of granule-dependent killing. *Cell Death Differ.* **15**, 251-262, doi:10.1038/sj.cdd.4402244 (2008).
133 Saravia, J., Chapman, N. M. & Chi, H. Helper T cell differentiation. *Cell. Mol. Immunol.* **16**, 634-643, doi:10.1038/s41423-019-0220-6 (2019).
134 Bos, R. & Sherman, L. A. CD4+ T-cell help in the tumor milieu is required for recruitment and cytolytic function of CD8+ T lymphocytes. *Cancer Res.* **70**, 8368, doi:10.1158/0008-5472.CAN-10-1322 (2010).

135 Nishimura, T. *et al.* Distinct role of antigen-specific T helper type 1 (Th1) and Th2 cells in tumor eradication in vivo. *The Journal of experimental medicine* **190**, 617-627, doi:10.1084/jem.190.5.617 (1999).
136 Ahrends, T. *et al.* CD4+ T Cell Help Confers a Cytotoxic T Cell Effector Program Including Coinhibitory Receptor Downregulation and Increased Tissue Invasiveness. *Immunity* **47**, 848-861.e845, doi:10.1016/j.immuni.2017.10.009 (2017).
137 Abbas, A. K., Murphy, K. M. & Sher, A. Functional diversity of helper T lymphocytes. *Nature* **383**, 787-793, doi:10.1038/383787a0 (1996).
138 Kidd, P. Th1/Th2 balance: the hypothesis, its limitations, and implications for health and disease. *Altern. Med. Rev.* **8**, 223-246 (2003).
139 Guenova, E. *et al.* TH2 cytokines from malignant cells suppress TH1 responses and enforce a global TH2 bias in leukemic cutaneous T-cell lymphoma. *Clin. Cancer Res.* **19**, 3755-3763, doi:10.1158/1078-0432.Ccr-12-3488 (2013).
140 DeNardo, D. G. *et al.* CD4+ T Cells Regulate Pulmonary Metastasis of Mammary Carcinomas by Enhancing Protumor Properties of Macrophages. *Cancer Cell* **16**, 91-102, doi:10.1016/j.ccr.2009.06.018 (2009).
141 Zhang, Q.-w. *et al.* Prognostic Significance of Tumor-Associated Macrophages in Solid Tumor: A Meta-Analysis of the Literature. *PLoS One* **7**, e50946, doi:10.1371/journal.pone.0050946 (2012).
142 Hao, C. J. *et al.* Effects of the balance between type 1 and type 2 T helper cells on ovarian cancer. *Genet. Mol. Res.* **15**, doi:10.4238/gmr.15027936 (2016).
143 Kryczek, I. *et al.* Phenotype, distribution, generation, and functional and clinical relevance of Th17 cells in the human tumor environments. *Blood* **114**, 1141, doi:10.1182/blood-2009-03-208249 (2009).
144 Song, Y. & Yang, J. M. Role of interleukin (IL)-17 and T-helper (Th)17 cells in cancer. *Biochem. Biophys. Res. Commun.* **493**, 1-8, doi:10.1016/j.bbrc.2017.08.109 (2017).
145 Hamanishi, J. *et al.* Programmed Cell Death 1 Ligand 1 and Tumor-Infiltrating $CD8^+$ T Lymphocytes Are Prognostic Factors of Human Ovarian Cancer. *Proc. Natl. Acad. Sci. U. S. A.* **104**, 3360-3365, doi:10.1073/pnas.0611533104 (2007).
146 Kamphorst, A. O. *et al.* Rescue of exhausted CD8 T cells by PD-1-targeted therapies is CD28-dependent.(IMMUNOTHERAPY)(Author abstract). *Science* **355**, 1423, doi:10.1126/science.aaf0683 (2017).
147 Wu, C. *et al.* Immunohistochemical localization of programmed death-1 ligand-1 (PD-L1) in gastric carcinoma and its clinical significance. *Acta Histochem.* **108**, 19-24, doi:10.1016/j.acthis.2006.01.003 (2006).
148 Ghebeh, H. *et al.* The B7-H1 (PD-L1) T Lymphocyte-Inhibitory Molecule Is Expressed in Breast Cancer Patients with Infiltrating Ductal Carcinoma: Correlation with Important High-Risk Prognostic Factors. *Neoplasia (New York, N.Y.)* **8**, 190-198, doi:10.1593/neo.05733 (2006).
149 Keir, M. E., Butte, M. J., Freeman, G. J. & Sharpe, A. H. PD-1 and Its Ligands in Tolerance and Immunity. **26**, 677-704, doi:10.1146/annurev.immunol.26.021607.090331 (2008).
150 Yoshiko, I. *et al.* Involvement of PD-L1 on tumor cells in the escape from host immune system and tumor immunotherapy by PD-L1 blockade. *Proc. Natl. Acad. Sci. U. S. A.* **99**, 12293-12297, doi:10.1073/pnas.192461099 (2002).
151 Dong, H. *et al.* Tumor-associated B7-H1 promotes T-cell apoptosis: a potential mechanism of immune evasion. *Nat. Med.* **8**, 793-800, doi:10.1038/nm730 (2002).
152 Okazaki, T., Chikuma, S., Iwai, Y., Fagarasan, S. & Honjo, T. A rheostat for immune responses: the unique properties of PD-1 and their advantages for clinical application. *Nat. Immunol.* **14**, 1212-1218, doi:10.1038/ni.2762 (2013).
153 Keir, M. E., Francisco, L. M. & Sharpe, A. H. PD-1 and its ligands in T-cell immunity. *Curr. Opin. Immunol.* **19**, 309-314, doi:10.1016/j.coi.2007.04.012 (2007).
154 Takeuchi, Y. & Nishikawa, H. Roles of regulatory T cells in cancer immunity. *Int. Immunol.* **28**, 401-409, doi:10.1093/intimm/dxw025 (2016).
155 Curiel, T. J. *et al.* Specific recruitment of regulatory T cells in ovarian carcinoma fosters immune privilege and predicts reduced survival. *Nat. Med.* **10**, 942-949, doi:10.1038/nm1093 (2004).
156 Bauer, C. A. *et al.* Dynamic Treg interactions with intratumoral APCs promote local CTL dysfunction. *The Journal of clinical investigation* **124**, 2425-2440, doi:10.1172/JCI66375 (2014).
157 Tran, D. Q. TGF-β: the sword, the wand, and the shield of FOXP3+ regulatory T cells. *J. Mol. Cell. Biol.* **4**, 29-37, doi:10.1093/jmcb/mjr033 (2011).

158 Fontenot, J. D., Gavin, M. A. & Rudensky, A. Y. Foxp3 programs the development and function of CD4+CD25+ regulatory T cells. *Nat. Immunol.* **4**, 330-336, doi:10.1038/ni904 (2003).
159 Wolf, D. *et al.* The Expression of the Regulatory T Cell–Specific Forkhead Box Transcription Factor FoxP3 Is Associated with Poor Prognosis in Ovarian Cancer. *Clin. Cancer Res.* **11**, 8326, doi:10.1158/1078-0432.CCR-05-1244 (2005).
160 Barnett, J. C. *et al.* Ovarian cancer tumor infiltrating T-regulatory (T reg) cells are associated with a metastatic phenotype. *Gynecol. Oncol.* **116**, 556-562, doi:10.1016/j.ygyno.2009.11.020 (2010).
161 Balkwill, F. Cancer and the chemokine network. *Nat. Rev. Cancer* **4**, 540-550, doi:10.1038/nrc1388 (2004).
162 Barbieri, F., Bajetto, A. & Florio, T. Role of chemokine network in the development and progression of ovarian cancer: a potential novel pharmacological target. *J. Oncol.* **2010**, 426956, doi:10.1155/2010/426956 (2010).
163 Kulbe, H. *et al.* A Dynamic Inflammatory Cytokine Network in the Human Ovarian Cancer Microenvironment. *Cancer Res.* **72**, 66, doi:10.1158/0008-5472.CAN-11-2178 (2012).
164 Milliken, D., Scotton, C., Raju, S., Balkwill, F. & Wilson, J. Analysis of chemokines and chemokine receptor expression in ovarian cancer ascites. *Clin. Cancer Res.* **8**, 1108-1114 (2002).
165 Rodrigues, I. S. S. *et al.* IL-6 and IL-8 as Prognostic Factors in Peritoneal Fluid of Ovarian Cancer. *Immunol. Invest.* **49**, 510-521, doi:10.1080/08820139.2019.1691222 (2020).
166 Chudecka-Głaz, A. M. *et al.* Assessment of selected cytokines, proteins, and growth factors in the peritoneal fluid of patients with ovarian cancer and benign gynecological conditions. *Onco Targets Ther.* **8**, 471-485, doi:10.2147/ott.S73438 (2015).
167 Lo, C.-W. *et al.* IL-6 trans-signaling in formation and progression of malignant ascites in ovarian cancer. *Cancer Res.* **71**, 424, doi:10.1158/0008-5472.CAN-10-1496 (2011).
168 Wang, Y. *et al.* Autocrine production of interleukin-6 confers cisplatin and paclitaxel resistance in ovarian cancer cells. *Cancer Lett.* **295**, 110-123, doi:10.1016/j.canlet.2010.02.019 (2010).
169 Penson, R. T. *et al.* Cytokines IL-1beta, IL-2, IL-6, IL-8, MCP-1, GM-CSF and TNFalpha in patients with epithelial ovarian cancer and their relationship to treatment with paclitaxel. *Int. J. Gynecol. Cancer* **10**, 33-41, doi:10.1046/j.1525-1438.2000.00003.x (2000).
170 Chen, F., Hou, M., Ye, F., Lv, W. & Xie, X. Ovarian Cancer Cells Induce Peripheral Mature Dendritic Cells to Differentiate Into Macrophagelike Cells In Vitro. *Int. J. Gynecol. Cancer* **19**, 1487-1493, doi:10.1111/IGC.0b013e3181bb70c6 (2009).
171 Hagemann, T. *et al.* Ovarian Cancer Cells Polarize Macrophages Toward A Tumor-Associated Phenotype. *J. Immunol.* **176**, 5023-5032, doi:10.4049/jimmunol.176.8.5023 (2006).
172 Bronger, H. *et al.* CXCL9 and CXCL10 predict survival and are regulated by cyclooxygenase inhibition in advanced serous ovarian cancer. *Br. J. Cancer* **115**, 553 (2016).
173 Furuya, M. M. D. P. *et al.* Up-regulation of CXC chemokines and their receptors: implications for proinflammatory microenvironments of ovarian carcinomas and endometriosis. *Hum. Pathol.* **38**, 1676-1687, doi:10.1016/j.humpath.2007.03.023 (2007).
174 Ian, C.-L., Ivan, M., Jiang-Hong, G. & Pius, L. Structure-Function Relationship between the Human Chemokine Receptor CXCR3 and Its Ligands. *J. Biol. Chem.* **278**, 289-295, doi:10.1074/jbc.M209470200 (2003).
175 Groom, J. R. & Luster, A. D. CXCR3 in T cell function. *Exp. Cell Res.* **317**, 620-631, doi:10.1016/j.yexcr.2010.12.017 (2011).
176 Noman, M. Z. *et al.* The cooperative induction of hypoxia-inducible factor-1 alpha and STAT3 during hypoxia induced an impairment of tumor susceptibility to CTL-mediated cell lysis. *Journal of immunology (Baltimore, Md. : 1950)* **182**, 3510, doi:10.4049/jimmunol.0800854 (2009).
177 Duechler, M., Peczek, L., Szubert, M. & Suzin, J. Influence of hypoxia inducible factors on the immune microenvironment in ovarian cancer. *Anticancer Res.* **34**, 2811-2820 (2014).
178 Townsend, K. N. *et al.* Markers of T cell infiltration and function associate with favorable outcome in vascularized high-grade serous ovarian carcinoma. *PLoS One* **8**, e82406-e82406, doi:10.1371/journal.pone.0082406 (2013).
179 Gabrilovich, D. I. & Nagaraj, S. Myeloid-derived suppressor cells as regulators of the immune system. *Nature reviews. Immunology* **9**, 162-174, doi:10.1038/nri2506 (2009).
180 Borella, F. *et al.* Immune Checkpoint Inhibitors in Epithelial Ovarian Cancer: An Overview on Efficacy and Future Perspectives. *Diagnostics (Basel)* **10**, 146, doi:10.3390/diagnostics10030146 (2020).

181 Collins, A. V. *et al.* The Interaction Properties of Costimulatory Molecules Revisited. *Immunity* **17**, 201-210, doi:10.1016/s1074-7613(02)00362-x (2002).
182 Qureshi, O. S. *et al.* Trans-Endocytosis of CD80 and CD86: A Molecular Basis for the Cell-Extrinsic Function of CTLA-4. *Science* **332**, 600-603, doi:10.1126/science.1202947 (2011).
183 Masteller, E. L., Chuang, E., Mullen, A. C., Reiner, S. L. & Thompson, C. B. Structural Analysis of CTLA-4 Function In Vivo. *J. Immunol.* **164**, 5319-5327, doi:10.4049/jimmunol.164.10.5319 (2000).
184 Champiat, S. *et al.* Incorporating Immune-Checkpoint Inhibitors into Systemic Therapy of NSCLC. *J. Thorac. Oncol.* **9**, 144-153, doi:10.1097/JTO.0000000000000074 (2014).
185 Hodi, F. S. *et al.* Improved Survival with Ipilimumab in Patients with Metastatic Melanoma. *N. Engl. J. Med.* **363**, 711-723, doi:10.1056/nejmoa1003466 (2010).
186 Eggermont, A. M. M. *et al.* Adjuvant Pembrolizumab versus Placebo in Resected Stage III Melanoma. *N. Engl. J. Med.* **378**, 1789-1801, doi:10.1056/NEJMoa1802357 (2018).
187 Robert, C. *et al.* Pembrolizumab versus ipilimumab in advanced melanoma (KEYNOTE-006): post-hoc 5-year results from an open-label, multicentre, randomised, controlled, phase 3 study. *Lancet Oncol.* **20**, 1239-1251, doi:10.1016/S1470-2045(19)30388-2 (2019).
188 Herbst, R. S. *et al.* Pembrolizumab versus docetaxel for previously treated, PD-L1-positive, advanced non-small-cell lung cancer (KEYNOTE-010): a randomised controlled trial. *Lancet* **387**, 1540-1550, doi:10.1016/S0140-6736(15)01281-7 (2016).
189 Baumeister, S. H., Freeman, G. J., Dranoff, G. & Sharpe, A. H. Coinhibitory Pathways in Immunotherapy for Cancer. *Annu. Rev. Immunol.* **34**, 539-573, doi:10.1146/annurev-immunol-032414-112049 (2016).
190 Postow, M. A., Callahan, M. K. & Wolchok, J. D. Immune Checkpoint Blockade in Cancer Therapy. *J. Clin. Oncol.* **33**, 1974-1982, doi:10.1200/jco.2014.59.4358 (2015).
191 Hamanishi, J. *et al.* Safety and Antitumor Activity of Anti–PD-1 Antibody, Nivolumab, in Patients With Platinum-Resistant Ovarian Cancer. *J. Clin. Oncol.* **33**, 4015-4022, doi:10.1200/jco.2015.62.3397 (2015).
192 Disis, M. L. *et al.* Efficacy and Safety of Avelumab for Patients With Recurrent or Refractory Ovarian Cancer: Phase 1b Results From the JAVELIN Solid Tumor TrialEfficacy and Safety of Avelumab for Patients With Recurrent or Refractory Ovarian CancerEfficacy and Safety of Avelumab for Patients With Recurrent or Refractory Ovarian Cancer. doi:10.1001/jamaoncol.2018.6258 (2019).
193 Matulonis, U. A. *et al.* Antitumor activity and safety of pembrolizumab in patients with advanced recurrent ovarian cancer: results from the phase II KEYNOTE-100 study. *Ann. Oncol.* **30**, 1080-1087, doi:10.1093/annonc/mdz135 (2019).
194 ClinicalTrials.gov. *NTC02718417. Avelumab in Previously Untreated Patients With Epithelial Ovarian Cancer (JAVELIN OVARIAN 100)*, <https://clinicaltrials.gov/ct2/show/NCT02718417> (
195 Pujade-Lauraine, E. *et al.* Avelumab alone or in combination with pegylated liposomal doxorubicin versus pegylated liposomal doxorubicin alone in platinum-resistant or refractory epithelial ovarian cancer: Primary and biomarker analysis of the phase III JAVELIN Ovarian 200 trial. *Gynecol. Oncol.* **154**, 21-22, doi:10.1016/j.ygyno.2019.04.053 (2019).
196 Liu, J. F. *et al.* Assessment of Combined Nivolumab and Bevacizumab in Relapsed Ovarian Cancer: A Phase 2 Clinical Trial. *JAMA Oncol* **5**, 1731-1738, doi:10.1001/jamaoncol.2019.3343 (2019).
197 Drew, Y. *et al.* Phase II study of olaparib + durvalumab (MEDIOLA): Updated results in germline BRCA-mutated platinum-sensitive relapsed (PSR) ovarian cancer (OC). *Ann. Oncol.* **30**, v485-v486, doi:10.1093/annonc/mdz253.016 (2019).
198 Lee, J.-M. *et al.* Safety and Clinical Activity of the Programmed Death-Ligand 1 Inhibitor Durvalumab in Combination With Poly (ADP-Ribose) Polymerase Inhibitor Olaparib or Vascular Endothelial Growth Factor Receptor 1-3 Inhibitor Cediranib in Women's Cancers: A Dose-Escalation, Phase I Study. *J. Clin. Oncol.* **35**, 2193-2202, doi:10.1200/jco.2016.72.1340 (2017).
199 Liu, R. *et al.* CD47 promotes ovarian cancer progression by inhibiting macrophage phagocytosis. *Oncotarget* **8**, 39021-39032, doi:10.18632/oncotarget.16547 (2017).
200 Sikic, B. I. *et al.* First-in-Human, First-in-Class Phase I Trial of the Anti-CD47 Antibody Hu5F9-G4 in Patients With Advanced Cancers. *J. Clin. Oncol.* **37**, 946-953, doi:10.1200/JCO.18.02018 (2019).
201 Lakhani, N. J. *et al.* A phase Ib study of the anti-CD47 antibody magrolimab with the PD-L1 inhibitor avelumab (A) in solid tumor (ST) and ovarian cancer (OC) patients. *J. Clin. Oncol.* **38**, 18-18, doi:10.1200/JCO.2020.38.5_suppl.18 (2020).

202 Angevin, E. *et al.* A phase I/II, multiple-dose, dose-escalation study of siltuximab, an anti-interleukin-6 monoclonal antibody, in patients with advanced solid tumors. *Clin. Cancer Res.* **20**, 2192-2204, doi:10.1158/1078-0432.Ccr-13-2200 (2014).
203 Madhusudan, S. *et al.* Study of Etanercept, a Tumor Necrosis Factor-Alpha Inhibitor, in Recurrent Ovarian Cancer. *J. Clin. Oncol.* **23**, 5950-5959, doi:10.1200/JCO.2005.04.127 (2005).
204 Wagner, L., Klemann, C., Stephan, M. & von Hörsten, S. Unravelling the immunological roles of dipeptidyl peptidase 4 (DPP4) activity and/or structure homologue (DASH) proteins. *Clin. Exp. Immunol.* **184**, 265-283, doi:10.1111/cei.12757 (2016).
205 Lambeir, A. M., Durinx, C., Scharpé, S. & De Meester, I. Dipeptidyl-peptidase IV from bench to bedside: An update on structural properties, functions, and clinical aspects of the enzyme DPP IV. *Crit. Rev. Clin. Lab. Sci.* **40**, 209-294 (2003).
206 Durinx, C. *et al.* Molecular characterization of dipeptidyl peptidase activity in serum. *Eur. J. Biochem.* **267**, 5608-5613, doi:10.1046/j.1432-1327.2000.01634.x (2000).
207 Leiting, B. *et al.* Catalytic properties and inhibition of proline-specific dipeptidyl peptidases II, IV and VII. *The Biochemical journal* **371**, 525, doi:10.1042/BJ20021643 (2003).
208 Chen, T., Ajami, K., McCaughan, G. W., Gorrell, M. D. & Abbott, C. A. Dipeptidyl peptidase IV gene family. The DPIV family. *Adv. Exp. Med. Biol.* **524**, 79 (2003).
209 Ohnuma, K., Dang, N. H. & Morimoto, C. Revisiting an old acquaintance: CD26 and its molecular mechanisms in T cell function. *Trends Immunol.* **29**, 295-301, doi:10.1016/j.it.2008.02.010 (2008).
210 Gorrell, M. D., Gysbers, V. & McCaughan, G. W. Vol. 54 249-264 (Oxford, UK, 2001).
211 Matheeussen, V. *et al.* Expression and spatial heterogeneity of dipeptidyl peptidases in endothelial cells of conduct vessels and capillaries. *Biol. Chem.* **392**, 189-198, doi:10.1515/bc.2011.002 (2011).
212 Gorrell, M. D. Dipeptidyl peptidase IV and related enzymes in cell biology and liver disorders. *Clinical science (London, England : 1979)* **108**, 277 (2005).
213 Yu, D. M. T. *et al. The dipeptidyl peptidase IV family in cancer and cell biology*. Vol. 277 (2010).
214 Kotani, T. *et al.* Immunohistochemical localization of dipeptidyl aminopeptidase IV in thyroid papillary carcinoma. *Int. J. Exp. Pathol.* **73**, 215-222 (1992).
215 Engel, M. *et al.* The Crystal Structure of Dipeptidyl Peptidase IV (CD26) Reveals Its Functional Regulation and Enzymatic Mechanism. *Proc. Natl. Acad. Sci. U. S. A.* **100**, 5063-5068, doi:10.1073/pnas.0230620100 (2003).
216 Hiramatsu, H. *et al.* The structure and function of human dipeptidyl peptidase IV, possessing a unique eight-bladed β -propeller fold. *Biochem. Biophys. Res. Commun.* **302**, 849-854, doi:10.1016/S0006-291X(03)00258-4 (2003).
217 Hopsu-Havu, V. & Ekfors, T. Distribution of a dipeptide naphthylamidase in rat tissues and its localisation by using diazo coupling and labeled antibody techniques. *Histochemie* **17**, 30-38, doi:10.1007/BF00306327 (1969).
218 Rohrborn, D., Wronkowitz, N. & Eckel, J. DPP4 in Diabetes. *Front. Immunol.* **6**, 386, doi:10.3389/fimmu.2015.00386 (2015).
219 De Meester, I. *et al.* Binding of adenosine deaminase to the lymphocyte surface via CD26. *Eur. J. Immunol.* **24**, 566-570, doi:10.1002/eji.1830240311 (1994).
220 Fleischer, B. CD26: a surface protease involved in T-cell activation. *Immunol. Today* **15**, 180-184, doi:10.1016/0167-5699(94)90316-6 (1994).
221 Ohnuma, K. *et al.* CD26 up-regulates expression of CD86 on antigen-presenting cells by means of caveolin-1. *Proc. Natl. Acad. Sci. U. S. A.* **101**, 14186-14191, doi:10.1073/pnas.0405266101 (2004).
222 Arrebola, Y. M., Gómez, H., Valiente, P. A., Chávez, M. D. L. A. & Pascual, I. Dipeptidyl peptidase IV and its implication in cancer. *Biotecnologia Aplicada* **31**, 93-110 (2014).
223 Zhao, Y., Yang, L. & Zhou, Z. Dipeptidyl peptidase-4 inhibitors: Multitarget drugs, not only antidiabetes drugs. *J. Diabetes* **6**, 21-29, doi:10.1111/1753-0407.12063 (2014).
224 McGuinness, C. & Wesley, U. V. Dipeptidyl peptidase IV (DPPIV), a candidate tumor suppressor gene in melanomas is silenced by promoter methylation. *Front. Biosci.* **13**, 2435-2443 (2008).
225 Matić, I. Z. *et al.* Serum activity of DPPIV and its expression on lymphocytes in patients with melanoma and in people with vitiligo. *BMC Immunol.* **13**, 48, doi:10.1186/1471-2172-13-48 (2012).

226 Pethiyagoda, C. L., Welch, D. R. & Fleming, T. P. Dipeptidyl peptidase IV (DPPIV) inhibits cellular invasion of melanoma cells. *Clin. Exp. Metastasis* **18**, 391-400, doi:10.1023/A:1010930918055 (2000).
227 Wesley, U. V., Tiwari, S. & Houghton, A. N. Role for dipeptidyl peptidase IV in tumor suppression of human non small cell lung carcinoma cells. *Int. J. Cancer* **109**, 855-866, doi:10.1002/ijc.20091 (2004).
228 Beckenkamp, A., Davies, S., Willig, J. B. & Buffon, A. DPPIV/CD26: a tumor suppressor or a marker of malignancy? *Tumour Biol.* **37**, 7059-7073, doi:10.1007/s13277-016-5005-2 (2016).
229 Wesley, U. V., McGroarty, M. & Homoyouni, A. Dipeptidyl Peptidase Inhibits Malignant Phenotype of Prostate Cancer Cells by Blocking Basic Fibroblast Growth Factor Signaling Pathway. *Cancer Res.* **65**, 1325 (2005).
230 Nazarian, A. *et al.* Inhibition of Circulating Dipeptidyl Peptidase 4 Activity in Patients with Metastatic Prostate Cancer. *Mol. Cell. Proteomics* **13**, 3082-3096, doi:10.1074/mcp.M114.038836 (2014).
231 Sun, Y.-X. *et al.* CD26/dipeptidyl peptidase IV regulates prostate cancer metastasis by degrading SDF-1/CXCL12. *Official Journal of the Metastasis Research Society* **25**, 765-776, doi:10.1007/s10585-008-9188-9 (2008).
232 Cheng, H. C., Abdel-Ghany, M., Elble, R. C. & Pauli, B. U. Lung endothelial dipeptidyl peptidase IV promotes adhesion and metastasis of rat breast cancer cells via tumor cell surface-associated fibronectin. *The Journal of biological chemistry* **273**, 24207 (1998).
233 Gonzalez-Gronow, M., Grenett, H. E., Weber, M. R., Gawdi, G. & Pizzo, S. V. Interaction of plasminogen with dipeptidyl peptidase IV initiates a signal transduction mechanism which regulates expression of matrix metalloproteinase-9 by prostate cancer cells. *The Biochemical journal* **355**, 397, doi:10.1042/0264-6021:3550397 (2001).
234 Pang, R. *et al.* A subpopulation of CD26+ cancer stem cells with metastatic capacity in human colorectal cancer. *Cell stem cell* **6**, 603, doi:10.1016/j.stem.2010.04.001 (2010).
235 Iwaki-Egawa, S., Watanabe, Y., Kikuya, Y. & Fujimoto, Y. Dipeptidyl peptidase IV from human serum: purification, characterization, and N-terminal amino acid sequence. *J. Biochem.* **124**, 428-433 (1998).
236 Cordero, O. J., Ayude, D., Nogueira, M., Rodríguez-Berrocal, F. J. & Cadena, M. P. D. L. Preoperative serum CD26 levels: diagnostic efficiency and predictive value for colorectal cancer. *Br. J. Cancer* **83**, 1139, doi:10.1054/bjoc.2000.1410 (2000).
237 De Chiara, L. *et al.* Serum CD26 is related to histopathological polyp traits and behaves as a marker for colorectal cancer and advanced adenomas. *BMC Cancer* **10**, 333, doi:10.1186/1471-2407-10-333 (2010).
238 Yazbeck, R., Jaenisch, S. E. & Abbott, C. A. Potential disease biomarkers: dipeptidyl peptidase 4 and fibroblast activation protein. *Protoplasma* **255**, 375, doi:10.1007/s00709-017-1129-5 (2018).
239 Strieter, R. M. *et al.* Cancer CXC chemokine networks and tumour angiogenesis. *Eur. J. Cancer* **42**, 768-778, doi:10.1016/j.ejca.2006.01.006 (2006).
240 Rainczuk, A., Rao, J., Gathercole, J. & Stephens, A. N. The emerging role of CXC chemokines in epithelial ovarian cancer. *Reproduction* **144**, 303-317, doi:10.1530/REP-12-0153 (2012).
241 Kryczek, I. *et al.* Phenotype, distribution, generation, and functional and clinical relevance of Th17 cells in the human tumor environments. *Blood* **114**, 1141-1149, doi:10.1182/blood-2009-03-208249 (2009).
242 Proost, P. *et al.* Amino-terminal truncation of CXCR3 agonists impairs receptor signaling and lymphocyte chemotaxis, while preserving antiangiogenic properties. *Blood* **98**, 3554 (2001).
243 Casrouge, A. *et al.* Evidence for an antagonist form of the chemokine CXCL10 in patients chronically infected with HCV. *The Journal of clinical investigation* **121**, 308, doi:10.1172/JCI40594 (2011).
244 Rainczuk, A. *et al.* Evidence for the antagonistic form of CXC-motif chemokine CXCL10 in serous epithelial ovarian tumours. *Int. J. Cancer* **134**, 530-541, doi:10.1002/ijc.28393; 10.1002/ijc.28260 (2013).
245 Ohnuma, K., Hatano, R. & Morimoto, C. DPP4 in anti-tumor immunity: going beyond the enzyme. *Nat. Immunol.* **16**, 791, doi:10.1038/ni.3210 (2015).
246 Dang, D. T. *et al.* Hypoxia-inducible factor-1 target genes as indicators of tumor vessel response to vascular endothelial growth factor inhibition. *Cancer Res.* **68**, 1872-1880, doi:10.1158/0008-5472.CAN-07-1589 (2008).

247 Röhrborn, D., Eckel, J. & Sell, H. Shedding of dipeptidyl peptidase 4 is mediated by metalloproteases and up-regulated by hypoxia in human adipocytes and smooth muscle cells. *FEBS Lett.* **588**, 3870-3877, doi:10.1016/j.febslet.2014.08.029 (2014).
248 Chowdhury, H. H. *et al.* Hypoxia Alters the Expression of Dipeptidyl Peptidase 4 and Induces Developmental Remodeling of Human Preadipocytes. *Journal of Diabetes Research* **2016**, doi:10.1155/2016/7481470 (2016).
249 Femia, A. P. *et al.* Long-term treatment with Sitagliptin, a dipeptidyl peptidase-4 inhibitor, reduces colon carcinogenesis and reactive oxygen species in 1,2-dimethylhydrazine-induced rats. *Int. J. Cancer* **133**, 2498 (2013).
250 Vaghasiya, J., Sheth, N., Bhalodia, Y. & Manek, R. Sitagliptin protects renal ischemia reperfusion induced renal damage in diabetes. *Regul. Pept.* **166**, 48, doi:10.1016/j.regpep.2010.08.007 (2011).
251 Kajiyama, H. *et al.* Prolonged survival and decreased invasive activity attributable to dipeptidyl peptidase IV overexpression in ovarian carcinoma. *Cancer Res.* **62**, 2753-2757 (2002).
252 Kajiyama, H. *et al.* Involvement of DPPIV/CD26 in epithelial morphology and suppressed invasive ability in ovarian carcinoma cells. *Ann. N. Y. Acad. Sci.* **1086**, 233-240, doi:10.1196/annals.1377.007 (2006).
253 Kajiyama, H. *et al.* The expression of dipeptidyl peptidase IV (DPPIV/CD26) is associated with enhanced chemosensitivity to paclitaxel in epithelial ovarian carcinoma cells. *Cancer Sci.* **101**, 347-354, doi:10.1111/j.1349-7006.2009.01378.x (2010).
254 Kikkawa, F. *et al.* Dipeptidyl peptidase IV in tumor progression. *Biochimica et Biophysica Acta - Proteins and Proteomics* **1751**, 45-51, doi:10.1016/j.bbapap.2004.09.028 (2005).
255 Zhang, M., Xu, L., Wang, X., Sun, B. & Ding, J. Expression levels of seprase/FAPα and DPPIV/CD26 in epithelial ovarian carcinoma. *Oncol. Lett.* **10**, 34-42, doi:10.3892/ol.2015.3151 (2015).
256 Thrasher, J. Pharmacologic Management of Type 2 Diabetes Mellitus: Available Therapies. *Am. J. Med.* **130**, S4-s17, doi:10.1016/j.amjmed.2017.04.004 (2017).
257 Bishnoi, R. *et al.* Dipeptidyl peptidase 4 inhibitors as novel agents in improving survival in diabetic patients with colorectal cancer and lung cancer: A Surveillance Epidemiology and Endpoint Research Medicare study. *Cancer Medicine* **8**, 3918-3927, doi:https://doi.org/10.1002/cam4.2278 (2019).
258 Shah, C. *et al.* Impact of DPP4 Inhibitors in Survival of Patients With Prostate, Pancreas, and Breast Cancer. *Front. Oncol.* **10**, doi:10.3389/fonc.2020.00405 (2020).
259 Hollande, C. *et al.* Inhibition of the dipeptidyl peptidase DPP4 (CD26) reveals IL-33-dependent eosinophil-mediated control of tumor growth. *Nat. Immunol.* **20**, 257, doi:10.1038/s41590-019-0321-5 (2019).
260 Kosowska, A. *et al.* Sitagliptin Modulates the Response of Ovarian Cancer Cells to Chemotherapeutic Agents. *Int. J. Mol. Sci.* **21**, doi:10.3390/ijms21238976 (2020).
261 Wang, F., Zhang, Z. F., He, Y. R., Wu, H. Y. & Wei, S. S. Effects of dipeptidyl peptidase-4 inhibitors on transforming growth factor-β1 signal transduction pathways in the ovarian fibrosis of polycystic ovary syndrome rats. *J. Obstet. Gynaecol. Res.* **45**, 600-608, doi:10.1111/jog.13847 (2019).
262 Wang, Z. *et al.* Broad targeting of angiogenesis for cancer prevention and therapy. *Semin. Cancer Biol.* **35 Suppl**, S224-s243, doi:10.1016/j.semcancer.2015.01.001 (2015).
263 Yu, D. M. *et al.* The dipeptidyl peptidase IV family in cancer and cell biology. *FEBS J* **277**, 1126-1144, doi:10.1111/j.1742-4658.2009.07526.x (2010).
264 Chowdhury, H. H. *et al.* Systemic Hypoxia Increases the Expression of DPP4 in Preadipocytes of Healthy Human Participants. *Exp. Clin. Endocrinol. Diabetes* **126**, 91-95, doi:10.1055/s-0043-113451 (2018).
265 Roby, K. F. *et al.* Development of a syngeneic mouse model for events related to ovarian cancer. *Carcinogenesis* **21**, 585-591, doi:10.1093/carcin/21.4.585 (2000).
266 Bilandzic, M. *et al.* Betaglycan alters NFkappaB-TGFbeta2 cross talk to reduce survival of human granulosa tumor cells. *Mol. Endocrinol.* **27**, 466-479, doi:10.1210/me.2012-1239 (2013).
267 Zhang, H. *et al.* Identification of novel dipeptidyl peptidase 9 substrates by two-dimensional differential in-gel electrophoresis. *The FEBS journal* **282**, 3737, doi:10.1111/febs.13371 (2015).
268 Schneider, C. A., Rasband, W. S. & Eliceiri, K. W. NIH Image to ImageJ: 25 years of image analysis. *Nature Methods* **9**, 671-675, doi:10.1038/nmeth.2089 (2012).

269 Rojas, V., Hirshfield, K. M., Ganesan, S. & Rodriguez-Rodriguez, L. Molecular Characterization of Epithelial Ovarian Cancer: Implications for Diagnosis and Treatment. *Int. J. Mol. Sci.* **17**, doi:10.3390/ijms17122113 (2016).
270 Kim, S., Kim, B. & Song, Y. S. Ascites modulates cancer cell behavior, contributing to tumor heterogeneity in ovarian cancer. *Cancer Sci.* **107**, 1173-1178, doi:10.1111/cas.12987 (2016).
271 Luo, Z. *et al.* Tumor microenvironment: The culprit for ovarian cancer metastasis? *Cancer Lett.* **377**, 174-182, doi:10.1016/j.canlet.2016.04.038 (2016).
272 Ai, Z., Lu, Y., Qiu, S. & Fan, Z. Overcoming cisplatin resistance of ovarian cancer cells by targeting HIF-1-regulated cancer metabolism. *Cancer Lett.* **373**, 36-44, doi:10.1016/j.canlet.2016.01.009 (2016).
273 Hao, N. B. *et al.* Macrophages in tumor microenvironments and the progression of tumors. *Clin. Dev. Immunol.* **2012**, 948098, doi:10.1155/2012/948098 (2012).
274 Cohen, S. *et al.* Platinum-resistance in ovarian cancer cells is mediated by IL-6 secretion via the increased expression of its target cIAP-2. *J. Mol. Med. (Berl.)* **91**, 357-368, doi:10.1007/s00109-012-0946-4 (2013).
275 Pujade-Lauraine, E. *et al.* Bevacizumab combined with chemotherapy for platinum-resistant recurrent ovarian cancer: The AURELIA open-label randomized phase III trial. *J. Clin. Oncol.* **32**, 1302-1308, doi:10.1200/jco.2013.51.4489 (2014).
276 Deborah, K. A. *et al.* NCCN Guidelines Insights: Ovarian Cancer, Version 1.2019. *Journal of the National Comprehensive Cancer Network J Natl Compr Canc Netw* **17**, 896-909, doi:10.6004/jnccn.2019.0039 (2019).
277 Enz, N., Vliegen, G., De Meester, I. & Jungraithmayr, W. CD26/DPP4 - a potential biomarker and target for cancer therapy. *Pharmacol. Ther.*, doi:10.1016/j.pharmthera.2019.02.015 (2019).
278 Durinx, C. *et al.* Molecular characterization of dipeptidyl peptidase activity in serum. *Eur. J. Biochem.* **267**, 5608-5613, doi:10.1046/j.1432-1327.2000.01634.x (2000).
279 De Chiara, L. *et al.* Postoperative Serum Levels of sCD26 for Surveillance in Colorectal Cancer Patients. *PLoS One* **9**, e107470-e107470, doi:10.1371/journal.pone.0107470 (2014).
280 Blanco-Prieto, S. *et al.* Serum calprotectin, CD26 and EGF to establish a panel for the diagnosis of lung cancer. *PLoS One* **10**, e0127318-e0127318, doi:10.1371/journal.pone.0127318 (2015).
281 Zhang, M. Z., Qiao, Y. H. & Suo, Z. H. Correlation of DPPIV expression with clinicopathological features and prognosis in epithelial ovarian carcinoma. *Zhonghua zhong liu za zhi [Chinese journal of oncology]* **30**, 848-852 (2008).
282 Rainczuk, A. *et al.* Evidence for the antagonistic form of CXC-motif chemokine CXCL10 in serous epithelial ovarian tumours. *Int. J. Cancer* **134**, 530-541, doi:10.1002/ijc.28393 (2014).
283 Moffitt, L. R. *et al.* Hypoxia Regulates DPP4 Expression, Proteolytic Inactivation, and Shedding from Ovarian Cancer Cells. *Int. J. Mol. Sci.* **21**, 8110 (2020).
284 Kim, D. *et al.* (2R)-4-oxo-4-3-(trifluoromethyl)-5,6-dihydro1,2,4triazolo4,3-apyrazin-7(8H)-yl-1-(2,4,5-trifluorophenyl)butan-2-amine: a potent, orally active dipeptidyl peptidase IV inhibitor for the treatment of type 2 diabetes. *J. Med. Chem.* **48**, 141 (2005).
285 Wilson, A. L. *et al.* DPP4 Inhibitor Sitagliptin Enhances Lymphocyte Recruitment and Prolongs Survival in a Syngeneic Ovarian Cancer Mouse Model. *Cancers (Basel)* **13**, 487 (2021).
286 Kurman, R. J. & Shih, I.-M. Molecular pathogenesis and extraovarian origin of epithelial ovarian cancer—Shifting the paradigm. *Hum. Pathol.* **42**, 918-931, doi:https://doi.org/10.1016/j.humpath.2011.03.003 (2011).
287 Jiménez-Sánchez, A. *et al.* Heterogeneous Tumor-Immune Microenvironments among Differentially Growing Metastases in an Ovarian Cancer Patient. *Cell* **170**, 927-938.e920, doi:10.1016/j.cell.2017.07.025 (2017).
288 Quail, D. F. & Joyce, J. A. Microenvironmental regulation of tumor progression and metastasis. *Nat. Med.* **19**, 1423-1437, doi:10.1038/nm.3394 (2013).
289 Jiang, Y., Wang, C. & Zhou, S. Targeting tumor microenvironment in ovarian cancer: Premise and promise. *Biochim Biophys Acta Rev Cancer* **1873**, 188361-188361, doi:10.1016/j.bbcan.2020.188361 (2020).
290 Clarke, B. *et al.* Intraepithelial T cells and prognosis in ovarian carcinoma: novel associations with stage, tumor type, and BRCA1 loss. *Mod. Pathol.* **22**, 393-402, doi:10.1038/modpathol.2008.191 (2009).
291 Mantia-Smaldone, G. M., Corr, B. & Chu, C. S. Immunotherapy in ovarian cancer. *Hum. Vaccin. Immunother.* **8**, 1179-1191, doi:10.4161/hv.20738 (2012).
292 Adams, S. F. *et al.* Intraepithelial T cells and tumor proliferation: impact on the benefit from surgical cytoreduction in advanced serous ovarian cancer. *Cancer* **115**, 2891-2902, doi:10.1002/cncr.24317 (2009).

293 Ghisoni, E., Imbimbo, M., Zimmermann, S. & Valabrega, G. Ovarian Cancer Immunotherapy: Turning up the Heat. *Int. J. Mol. Sci.* **20**, doi:10.3390/ijms20122927 (2019).
294 Martinez, A., Delord, J. P., Ayyoub, M. & Devaud, C. Preclinical and Clinical Immunotherapeutic Strategies in Epithelial Ovarian Cancer. *Cancers (Basel)* **12**, doi:10.3390/cancers12071761 (2020).
295 Palaia, I., Tomao, F., Sassu, C. M., Musacchio, L. & Benedetti Panici, P. Immunotherapy For Ovarian Cancer: Recent Advances And Combination Therapeutic Approaches. *Onco Targets Ther.* **13**, 6109-6129, doi:10.2147/OTT.S205950 (2020).
296 Perica, K., Varela, J. C., Oelke, M. & Schneck, J. Adoptive T cell immunotherapy for cancer. *Rambam Maimonides Med J* **6**, e0004-e0004, doi:10.5041/RMMJ.10179 (2015).
297 Liu, J. *et al.* Maintenance therapy with autologous cytokine-induced killer cells in patients with advanced epithelial ovarian cancer after first-line treatment. *J. Immunother.* **37**, 115-122, doi:10.1097/CJI.0000000000000021 (2014).
298 Fujita, K. *et al.* Prolonged disease-free period in patients with advanced epithelial ovarian cancer after adoptive transfer of tumor-infiltrating lymphocytes. *Clin. Cancer Res.* **1**, 501-507 (1995).
299 Ikarashi, H. *et al.* Immunomodulation in patients with epithelial ovarian cancer after adoptive transfer of tumor-infiltrating lymphocytes. *Cancer Res.* **54**, 190-196 (1994).
300 Kunle, O. *et al.* Efficacy of vaccination with recombinant vaccinia and fowlpox vectors expressing NY-ESO-1 antigen in ovarian cancer and melanoma patients. *Proc. Natl. Acad. Sci. U. S. A.* **109**, 5797-5802, doi:10.1073/pnas.1117208109 (2012).
301 Lengyel, E. *et al.* Epithelial ovarian cancer experimental models. *Oncogene* **33**, 3619-3633, doi:10.1038/onc.2013.321 (2014).
302 Shaw, T. J., Senterman, M. K., Dawson, K., Crane, C. A. & Vanderhyden, B. C. Characterization of intraperitoneal, orthotopic, and metastatic xenograft models of human ovarian cancer. *Mol. Ther.* **10**, 1032-1042, doi:10.1016/j.ymthe.2004.08.013 (2004).
303 Leinster, D. A. *et al.* The peritoneal tumour microenvironment of high-grade serous ovarian cancer. *J. Pathol.* **227**, 136-145, doi:10.1002/path.4002 (2012).
304 Bongers, J., Lambros, T., Ahmad, M. & Heimer, E. P. Kinetics of dipeptidyl peptidase IV proteolysis of growth hormone-releasing factor and analogs. *Biochimica et biophysica acta, Protein structure and molecular enzymology* **1122**, 147-153, doi:10.1016/0167-4838(92)90317-7 (1992).
305 Drucker, D. J. & Nauck, M. A. The incretin system: glucagon-like peptide-1 receptor agonists and dipeptidyl peptidase-4 inhibitors in type 2 diabetes. *Lancet* **368**, 1696-1705, doi:10.1016/S0140-6736(06)69705-5 (2006).
306 Ahrén, B. Clinical results of treating type 2 diabetic patients with sitagliptin, vildagliptin or saxagliptin – diabetes control and potential adverse events. *Best Pract. Res. Clin. Endocrinol. Metab.* **23**, 487-498, doi:10.1016/j.beem.2009.03.003 (2009).
307 Vanheule, V., Metzemaekers, M., Janssens, R., Struyf, S. & Proost, P. How post-translational modifications influence the biological activity of chemokines. *Cytokine* **109**, 29-51, doi:10.1016/j.cyto.2018.02.026 (2018).
308 Barreira da Silva, R. *et al.* Dipeptidylpeptidase 4 inhibition enhances lymphocyte trafficking, improving both naturally occurring tumor immunity and immunotherapy. *Nat. Immunol.*, doi:10.1038/ni.3201 (2015).
309 Decalf, J. *et al.* Inhibition of DPP 4 activity in humans establishes its in vivo role in CXCL 10 post-translational modification: prospective placebo-controlled clinical studies. *EMBO Mol. Med.* **8**, 679-683, doi:10.15252/emmm.201506145 (2016).
310 Tseng, C. H. Sitagliptin may reduce prostate cancer risk in male patients with type 2 diabetes. *Oncotarget*, doi:10.18632/oncotarget.12137 (2016).
311 Tseng, C.-H. Sitagliptin May Reduce Breast Cancer Risk in Women With Type 2 Diabetes. *Clin. Breast Cancer* **17**, 211-218, doi:https://doi.org/10.1016/j.clbc.2016.11.002 (2017).
312 Jiang, W. *et al.* Effect of sitagliptin, a DPP-4 inhibitor, against DENA-induced liver cancer in rats mediated via NF-κB activation and inflammatory cytokines. *J. Biochem. Mol. Toxicol.* **32**, e22220, doi:10.1002/jbt.22220 (2018).
313 Nishina, S. *et al.* Dipeptidyl Peptidase 4 Inhibitors Reduce Hepatocellular Carcinoma by Activating Lymphocyte Chemotaxis in Mice. *Cell. Mol. Gastroenterol. Hepatol.* **7**, 115-134, doi:https://doi.org/10.1016/j.jcmgh.2018.08.008 (2019).
314 Gockley, A. *et al.* Outcomes of Women With High-Grade and Low-Grade Advanced-Stage Serous Epithelial Ovarian Cancer. *Obstet. Gynecol.* **129**, 439-447, doi:10.1097/AOG.0000000000001867 (2017).

315 Santoiemma, P. P. & Powell, D. J. Tumor infiltrating lymphocytes in ovarian cancer. *Cancer Biol. Ther.* **16**, 807-820, doi:10.1080/15384047.2015.1040960 (2015).
316 Szklarczyk, D. *et al.* STRING v10: protein-protein interaction networks, integrated over the tree of life. *Nucleic Acids Res.* **43**, D447-452, doi:10.1093/nar/gku1003 (2015).
317 Zhang, N. & Bevan, M. J. CD8(+) T cells: foot soldiers of the immune system. *Immunity* **35**, 161-168, doi:10.1016/j.immuni.2011.07.010 (2011).
318 Ahrends, T. & Borst, J. The opposing roles of CD4+ T cells in anti-tumour immunity. *Immunology* **154**, 582-592, doi:10.1111/imm.12941 (2018).
319 Chen, L. & Flies, D. B. Molecular mechanisms of T cell co-stimulation and co-inhibition. *Nature reviews. Immunology* **13**, 227-242, doi:10.1038/nri3405 (2013).
320 Gerdes, J. *et al.* Cell cycle analysis of a cell proliferation-associated human nuclear antigen defined by the monoclonal antibody Ki-67. *The Journal of Immunology* **133**, 1710 (1984).
321 Simms, P. E. & Ellis, T. M. Utility of flow cytometric detection of CD69 expression as a rapid method for determining poly- and oligoclonal lymphocyte activation. *Clin. Diagn. Lab. Immunol.* **3**, 301-304 (1996).
322 Cunningham, R. A., Holland, M., McWilliams, E., Hodi, F. S. & Severgnini, M. Detection of clinically relevant immune checkpoint markers by multicolor flow cytometry. *J Biol Methods* **6**, e114-e114, doi:10.14440/jbm.2019.283 (2019).
323 Anz, D. *et al.* CD103 is a hallmark of tumor-infiltrating regulatory T cells. *Int. J. Cancer* **129**, 2417-2426, doi:10.1002/ijc.25902 (2011).
324 Toker, A. *et al.* Regulatory T Cells in Ovarian Cancer Are Characterized by a Highly Activated Phenotype Distinct from that in Melanoma. *Clin. Cancer Res.* **24**, 5685, doi:10.1158/1078-0432.CCR-18-0554 (2018).
325 Gobert, M. *et al.* Regulatory T cells recruited through CCL22/CCR4 are selectively activated in lymphoid infiltrates surrounding primary breast tumors and lead to an adverse clinical outcome. *Cancer Res.* **69**, 2000-2009, doi:10.1158/0008-5472.Can-08-2360 (2009).
326 Qin, X. J. *et al.* CCL22 recruits CD4-positive CD25-positive regulatory T cells into malignant pleural effusion. *Clin. Cancer Res.* **15**, 2231-2237, doi:10.1158/1078-0432.Ccr-08-2641 (2009).
327 Li, X. *et al.* Myeloid-derived suppressor cells promote epithelial ovarian cancer cell stemness by inducing the CSF2/p-STAT3 signalling pathway. *The FEBS Journal* **n/a**, doi:10.1111/febs.15311.
328 Kumar, V., Patel, S., Tcyganov, E. & Gabrilovich, D. I. The Nature of Myeloid-Derived Suppressor Cells in the Tumor Microenvironment. *Trends Immunol.* **37**, 208-220, doi:10.1016/j.it.2016.01.004 (2016).
329 Mantovani, A., Schioppa, T., Porta, C., Allavena, P. & Sica, A. Role of tumor-associated macrophages in tumor progression and invasion. *Cancer Metastasis Rev.* **25**, 315-322, doi:10.1007/s10555-006-9001-7 (2006).
330 Yin, M. *et al.* Tumor-associated macrophages drive spheroid formation during early transcoelomic metastasis of ovarian cancer. *J. Clin. Invest.* **126**, 4157-4173, doi:10.1172/jci87252 (2016).
331 Carroll, M. J., Kapur, A., Felder, M., Patankar, M. S. & Kreeger, P. K. M2 macrophages induce ovarian cancer cell proliferation via a heparin binding epidermal growth factor/matrix metalloproteinase 9 intercellular feedback loop. *Oncotarget* **7**, 86608-86620, doi:10.18632/oncotarget.13474 (2016).
332 Macciò, A. *et al.* Role of M1-polarized tumor-associated macrophages in the prognosis of advanced ovarian cancer patients. *Sci. Rep.* **10**, 6096, doi:10.1038/s41598-020-63276-1 (2020).
333 Cheng, H., Wang, Z., Fu, L. & Xu, T. Macrophage Polarization in the Development and Progression of Ovarian Cancers: An Overview. *Front. Oncol.* **9**, doi:10.3389/fonc.2019.00421 (2019).
334 Chanmee, T., Ontong, P., Konno, K. & Itano, N. Tumor-associated macrophages as major players in the tumor microenvironment. *Cancers (Basel)* **6**, 1670-1690, doi:10.3390/cancers6031670 (2014).
335 Bronger, H., Magdolen, V., Goettig, P. & Dreyer, T. Proteolytic chemokine cleavage as a regulator of lymphocytic infiltration in solid tumors. *Cancer Metastasis Rev.* **38**, 417-430, doi:10.1007/s10555-019-09807-3 (2019).
336 Broxmeyer, H. E. *et al.* Dipeptidylpeptidase 4 negatively regulates colony-stimulating factor activity and stress hematopoiesis. *Nat. Med.* **18**, 1786-1796, doi:10.1038/nm.2991 (2012).

337 Broxmeyer, H. E., Capitano, M., Campbell, T. B., Hangoc, G. & Cooper, S. Modulation of Hematopoietic Chemokine Effects In Vitro and In Vivo by DPP-4/CD26. *Stem Cells Dev.* **25**, 575-585, doi:10.1089/scd.2016.0026 (2016).
338 Castellino, F. *et al.* Chemokines enhance immunity by guiding naive CD8+ T cells to sites of CD4+ T cell–dendritic cell interaction. *Nature* **440**, 890-895, doi:10.1038/nature04651 (2006).
339 Tokunaga, R. *et al.* CXCL9, CXCL10, CXCL11/CXCR3 axis for immune activation – A target for novel cancer therapy. *Cancer Treat. Rev.* **63**, 40-47, doi:10.1016/j.ctrv.2017.11.007 (2018).
340 Au, K. K. *et al.* STAT1-associated intratumoural T(H)1 immunity predicts chemotherapy resistance in high-grade serous ovarian cancer. *J Pathol Clin Res* **2**, 259-270, doi:10.1002/cjp2.55 (2016).
341 Yue, C. *et al.* STAT3 in CD8+ T Cells Inhibits Their Tumor Accumulation by Downregulating CXCR3/CXCL10 Axis. *Cancer Immunol Res* **3**, 864-870, doi:10.1158/2326-6066.Cir-15-0014 (2015).
342 Groom, Joanna R. *et al.* CXCR3 Chemokine Receptor-Ligand Interactions in the Lymph Node Optimize CD4+ T Helper 1 Cell Differentiation. *Immunity* **37**, 1091-1103, doi:10.1016/j.immuni.2012.08.016 (2012).
343 Sierro, F. *et al.* Disrupted cardiac development but normal hematopoiesis in mice deficient in the second CXCL12/SDF-1 receptor, CXCR7. *Proc. Natl. Acad. Sci. U. S. A.* **104**, 14759-14764, doi:10.1073/pnas.0702229104 (2007).
344 Scotton, C. J. *et al.* Multiple Actions of the Chemokine CXCL12 on Epithelial Tumor Cells in Human Ovarian Cancer. *Cancer Res.* **62**, 5930 (2002).
345 Mao, T. L., Fan, K. F. & Liu, C. L. Targeting the CXCR4/CXCL12 axis in treating epithelial ovarian cancer. *Gene Ther.* **24**, 621-629, doi:10.1038/gt.2017.69 (2017).
346 Daniel, H. K. *et al.* Demonstration of an Interferon γ -dependent Tumor Surveillance System in Immunocompetent Mice. *Proc. Natl. Acad. Sci. U. S. A.* **95**, 7556-7561 (1998).
347 Gupta, M., Babic, A., Beck, A. H. & Terry, K. TNF-α expression, risk factors, and inflammatory exposures in ovarian cancer: evidence for an inflammatory pathway of ovarian carcinogenesis? *Hum. Pathol.* **54**, 82-91, doi:10.1016/j.humpath.2016.03.006 (2016).
348 Ohmori, Y. *et al.* Tumor necrosis factor-alpha induces cell type and tissue-specific expression of chemoattractant cytokines in vivo. *Am. J. Pathol.* **142**, 861-870 (1993).
349 Müller, M., Carter, S., Hofer, M. J. & Campbell, I. L. Review: The chemokine receptor CXCR3 and its ligands CXCL9, CXCL10 and CXCL11 in neuroimmunity--a tale of conflict and conundrum. *Neuropathol. Appl. Neurobiol.* **36**, 368-387, doi:10.1111/j.1365-2990.2010.01089.x (2010).
350 Fisher, D. T., Appenheimer, M. M. & Evans, S. S. The two faces of IL-6 in the tumor microenvironment. *Semin. Immunol.* **26**, 38-47, doi:10.1016/j.smim.2014.01.008 (2014).
351 Naugler, W. E. & Karin, M. The wolf in sheep's clothing: the role of interleukin-6 in immunity, inflammation and cancer. *Trends Mol. Med.* **14**, 109-119, doi:10.1016/j.molmed.2007.12.007 (2007).
352 Rachel, M. M. *et al.* IL-6 Trans-Signaling via STAT3 Directs T Cell Infiltration in Acute Inflammation. *Proc. Natl. Acad. Sci. U. S. A.* **102**, 9589-9594, doi:10.1073/pnas.0501794102 (2005).
353 Jones, S. A. Directing transition from innate to acquired immunity: defining a role for IL-6. *J. Immunol.* **175**, 3463-3468, doi:10.4049/jimmunol.175.6.3463 (2005).
354 Ikeda, T., Kumagai, E., Iwata, S. & Yamakawa, A. Soluble CD26/Dipeptidyl Peptidase IV Enhances the Transcription of IL-6 and TNF-α in THP-1 Cells and Monocytes. *PLoS One* **8**, e66520, doi:10.1371/journal.pone.0066520 (2013).
355 Qu, Q. X., Xie, F., Huang, Q. & Zhang, X. G. Membranous and Cytoplasmic Expression of PD-L1 in Ovarian Cancer Cells. *Cell. Physiol. Biochem.* **43**, 1893-1906, doi:10.1159/000484109 (2017).
356 Gaudin, F. *et al.* Identification of the Chemokine CX3CL1 as a New Regulator of Malignant Cell Proliferation in Epithelial Ovarian Cancer. *PLoS One* **6**, e21546, doi:10.1371/journal.pone.0021546 (2011).
357 Robinson, L. A. *et al.* The chemokine CX3CL1 regulates NK cell activity in vivo. *Cell. Immunol.* **225**, 122-130, doi:10.1016/j.cellimm.2003.09.010 (2003).
358 Fraticelli, P. *et al.* Fractalkine (CX3CL1) as an amplification circuit of polarized Th1 responses. *J. Clin. Invest.* **107**, 1173-1181, doi:10.1172/jci11517 (2001).
359 Liu, F. *et al.* IP-10 and fractalkine induce cytotoxic phenotype of murine NK cells. *Science bulletin (Beijing)* **61**, 202-211, doi:10.1007/s11434-015-0961-2 (2016).

360 Mabuchi, S., Yokoi, E., Komura, N. & Kimura, T. Myeloid-derived suppressor cells and their role in gynecological malignancies. *Tumour Biol.* **40**, 1010428318776485, doi:10.1177/1010428318776485 (2018).
361 Yaseen, M. M., Abuharfeil, N. M., Darmani, H. & Daoud, A. Mechanisms of immune suppression by myeloid-derived suppressor cells: the role of interleukin-10 as a key immunoregulatory cytokine. *Open Biol* **10**, 200111, doi:10.1098/rsob.200111 (2020).
362 Okła, K. *et al.* Clinical Relevance and Immunosuppressive Pattern of Circulating and Infiltrating Subsets of Myeloid-Derived Suppressor Cells (MDSCs) in Epithelial Ovarian Cancer. *Front. Immunol.* **10**, 691-691, doi:10.3389/fimmu.2019.00691 (2019).
363 Ivashkiv, L. B. IFNγ: signalling, epigenetics and roles in immunity, metabolism, disease and cancer immunotherapy. *Nat. Rev. Immunol.* **18**, 545-558, doi:10.1038/s41577-018-0029-z (2018).
364 Mantovani, A. & Locati, M. Tumor-Associated Macrophages as a Paradigm of Macrophage Plasticity, Diversity, and Polarization: Lessons and Open Questions. *Arterioscler. Thromb. Vasc. Biol.* **33**, 1478-1483, doi:10.1161/ATVBAHA.113.300168 (2013).
365 Yu, D. M. T. *et al.* Soluble CD26/dipeptidyl peptidase IV enhances human lymphocyte proliferation in vitro independent of dipeptidyl peptidase enzyme activity and adenosine deaminase binding. *Scand. J. Immunol.* **73**, 102, doi:10.1111/j.1365-3083.2010.02488.x (2011).
366 Schmitz, T., Underwood, R., Khiroya, R., Bachovchin, W. W. & Huber, B. T. Potentiation of the immune response in HIV-1+ individuals. *J. Clin. Invest.* **97**, 1545-1549, doi:10.1172/jci118577 (1996).
367 Schreiber, R. D., Old, L. J. & Smyth, M. J. Cancer Immunoediting: Integrating Immunity's Roles in Cancer Suppression and Promotion. *Science* **331**, 1565-1570, doi:10.1126/science.1203486 (2011).
368 Mittal, D., Gubin, M. M., Schreiber, R. D. & Smyth, M. J. New insights into cancer immunoediting and its three component phases — elimination, equilibrium and escape. *Curr. Opin. Immunol.* **27**, 16-25, doi:10.1016/j.coi.2014.01.004 (2014).
369 von Boehmer, L. *et al.* NY-ESO-1-specific immunological pressure and escape in a patient with metastatic melanoma. *Cancer Immun.* **13**, 12-12 (2013).
370 Cai, J., Wang, D., Zhang, G. & Guo, X. The Role Of PD-1/PD-L1 Axis In Treg Development And Function: Implications For Cancer Immunotherapy. *Onco Targets Ther.* **12**, 8437-8445, doi:10.2147/ott.S221340 (2019).
371 Wherry, E. J. T cell exhaustion. *Nat. Immunol.* **12**, 492-499, doi:10.1038/ni.2035 (2011).
372 Francisco, L. M. *et al.* PD-L1 regulates the development, maintenance, and function of induced regulatory T cells. *J. Exp. Med.* **206**, 3015-3029, doi:10.1084/jem.20090847 (2009).
373 Kumagai, S. *et al.* The PD-1 expression balance between effector and regulatory T cells predicts the clinical efficacy of PD-1 blockade therapies. *Nat. Immunol.* **21**, 1346-1358, doi:10.1038/s41590-020-0769-3 (2020).
374 Aksoylar, H.-I. & Boussiotis, V. A. PD-1+ Treg cells: a foe in cancer immunotherapy? *Nat. Immunol.* **21**, 1311-1312, doi:10.1038/s41590-020-0801-7 (2020).
375 Kamada, T. *et al.* PD-1+ regulatory T cells amplified by PD-1 blockade promote hyperprogression of cancer. *Proceedings of the National Academy of Sciences* **116**, 9999-10008, doi:10.1073/pnas.1822001116 (2019).
376 Lowther, D. E. *et al.* PD-1 marks dysfunctional regulatory T cells in malignant gliomas. *JCI Insight* **1**, doi:10.1172/jci.insight.85935 (2019).
377 European Medicines Agency (EMA). *Sitagliptin (Januvia) Scientific Discussion*, <https://www.ema.europa.eu/en/documents/scientific-discussion/januvia-epar-scientific-discussion_en.pdf> (2007).
378 Darvin, P., Toor, S. M., Sasidharan Nair, V. & Elkord, E. Immune checkpoint inhibitors: recent progress and potential biomarkers. *Exp. Mol. Med.* **50**, 1-11, doi:10.1038/s12276-018-0191-1 (2018).
379 Pietzner, K. *et al.* Checkpoint-inhibition in ovarian cancer: rising star or just a dream? *J. Gynecol. Oncol.* **29**, e93-e93, doi:10.3802/jgo.2018.29.e93 (2018).
380 Chow, M. T. *et al.* Intratumoral Activity of the CXCR3 Chemokine System Is Required for the Efficacy of Anti-PD-1 Therapy. *Immunity* **50**, 1498-1512.e1495, doi:10.1016/j.immuni.2019.04.010 (2019).
381 Gatalica, Z. *et al.* Programmed Cell Death 1 (PD-1) and Its Ligand (PD-L1) in Common Cancers and Their Correlation with Molecular Cancer Type. *Cancer Epidemiology Biomarkers & Prevention* **23**, 2965, doi:10.1158/1055-9965.EPI-14-0654 (2014).

382 Sznol, M. & Chen, L. Antagonist antibodies to PD-1 and B7-H1 (PD-L1) in the treatment of advanced human cancer. *Clinical cancer research : an official journal of the American Association for Cancer Research* **19**, 1021-1034, doi:10.1158/1078-0432.CCR-12-2063 (2013).
383 Champiat, S. *et al.* Incorporating immune-checkpoint inhibitors into systemic therapy of NSCLC. *J. Thorac. Oncol.* **9**, 144-153, doi:10.1097/jto.0000000000000074 (2014).
384 Robert, C. *et al.* Pembrolizumab versus Ipilimumab in Advanced Melanoma. *N. Engl. J. Med.* **372**, 2521-2532, doi:10.1056/NEJMoa1503093 (2015).
385 Borghaei, H. *et al.* Nivolumab versus Docetaxel in Advanced Nonsquamous Non–Small-Cell Lung Cancer. *N. Engl. J. Med.* **373**, 1627-1639, doi:10.1056/NEJMoa1507643 (2015).
386 Gadgeel, S. M. *et al.* Pembrolizumab (pembro) plus chemotherapy as front-line therapy for advanced NSCLC: KEYNOTE-021 cohorts A-C. *J. Clin. Oncol.* **34**, 9016-9016, doi:10.1200/JCO.2016.34.15_suppl.9016 (2016).
387 Paz-Ares, L. *et al.* Pembrolizumab plus Chemotherapy for Squamous Non-Small-Cell Lung Cancer. *N. Engl. J. Med.* **379**, 2040-2051, doi:10.1056/NEJMoa1810865 (2018).
388 Li, X. *et al.* Strategic Combination Therapies for Ovarian Cancer. *Curr. Cancer Drug Targets* **20**, 573-585, doi:http://dx.doi.org.ezproxy.lib.monash.edu.au/10.2174/1568009620666200511084007 (2020).
389 Shen, J. *et al.* PARPi Triggers the STING-Dependent Immune Response and Enhances the Therapeutic Efficacy of Immune Checkpoint Blockade Independent of BRCAness. *Cancer Res.* **79**, 311-319, doi:10.1158/0008-5472.CAN-18-1003 (2019).
390 Wang, Z. *et al.* Niraparib activates interferon signaling and potentiates anti-PD-1 antibody efficacy in tumor models. *Sci. Rep.* **9**, 1853, doi:10.1038/s41598-019-38534-6 (2019).
391 Konstantinopoulos, P. A. *et al.* Single-Arm Phases 1 and 2 Trial of Niraparib in Combination With Pembrolizumab in Patients With Recurrent Platinum-Resistant Ovarian Carcinoma. *JAMA Oncol* **5**, 1141-1149, doi:10.1001/jamaoncol.2019.1048 (2019).
392 Taube, J. M. *et al.* Association of PD-1, PD-1 ligands, and other features of the tumor immune microenvironment with response to anti-PD-1 therapy. *Clin. Cancer Res.* **20**, 5064-5074, doi:10.1158/1078-0432.CCR-13-3271 (2014).
393 Ansell, S. M. *et al.* PD-1 Blockade with Nivolumab in Relapsed or Refractory Hodgkin's Lymphoma. *N. Engl. J. Med.* **372**, 311-319, doi:10.1056/NEJMoa1411087 (2015).
394 Brahmer, J. *et al.* Nivolumab versus Docetaxel in Advanced Squamous-Cell Non–Small-Cell Lung Cancer. *N. Engl. J. Med.* **373**, 123-135, doi:10.1056/NEJMoa1504627 (2015).
395 Lin, H. *et al.* Host expression of PD-L1 determines efficacy of PD-L1 pathway blockade-mediated tumor regression. *The Journal of clinical investigation* **128**, 805-815, doi:10.1172/JCI96113 (2018).
396 Sun, C., Mezzadra, R. & Schumacher, T. N. Regulation and Function of the PD-L1 Checkpoint. *Immunity* **48**, 434-452, doi:10.1016/j.immuni.2018.03.014 (2018).
397 Galon, J. & Bruni, D. Approaches to treat immune hot, altered and cold tumours with combination immunotherapies. *Nat Rev Drug Discov* **18**, 197-218, doi:10.1038/s41573-018-0007-y (2019).
398 Hamanishi, J. *et al.* The comprehensive assessment of local immune status of ovarian cancer by the clustering of multiple immune factors. *Clin. Immunol.* **141**, 338-347, doi:10.1016/j.clim.2011.08.013 (2011).
399 Bald, T. *et al.* Immune cell-poor melanomas benefit from PD-1 blockade after targeted type I IFN activation. *Cancer Discov.* **4**, 674-687, doi:10.1158/2159-8290.CD-13-0458 (2014).
400 Tumeh, P. C. *et al.* PD-1 blockade induces responses by inhibiting adaptive immune resistance. *Nature* **515**, 568-571, doi:10.1038/nature13954 (2014).
401 Karin, N. CXCR3 Ligands in Cancer and Autoimmunity, Chemoattraction of Effector T Cells, and Beyond. *Front. Immunol.* **11**, 976, doi:10.3389/fimmu.2020.00976 (2020).
402 Rogava, M. & Izar, B. CXCR3: Here to stay to enhance cancer immunotherapy? *EBioMedicine* **49**, 11-12, doi:10.1016/j.ebiom.2019.09.044 (2019).
403 Chheda, Z. S., Sharma, R. K., Jala, V. R., Luster, A. D. & Haribabu, B. Chemoattractant Receptors BLT1 and CXCR3 Regulate Antitumor Immunity by Facilitating CD8+ T Cell Migration into Tumors. *J. Immunol.* **197**, 2016-2026, doi:10.4049/jimmunol.1502376 (2016).
404 Han, X. *et al.* Role of CXCR3 signaling in response to anti-PD-1 therapy. *EBioMedicine* **48**, 169-177, doi:10.1016/j.ebiom.2019.08.067 (2019).

405 Shigeta, K. *et al.* Regorafenib combined with PD1 blockade increases CD8 T-cell infiltration by inducing CXCL10 expression in hepatocellular carcinoma. *J Immunother Cancer* **8**, doi:10.1136/jitc-2020-001435 (2020).
406 Labocha, M. K., Schutz, H. & Hayes, J. P. Which body condition index is best? *Oikos* **123**, 111-119, doi:10.1111/j.1600-0706.2013.00755.x (2014).
407 Duraiswamy, J., Freeman, G. J. & Coukos, G. Therapeutic PD-1 pathway blockade augments with other modalities of immunotherapy T-cell function to prevent immune decline in ovarian cancer. *Cancer Res.* **73**, 6900-6912, doi:10.1158/0008-5472.CAN-13-1550 (2013).
408 Smyth, M. J. *et al.* Differential tumor surveillance by natural killer (NK) and NKT cells. *J. Exp. Med.* **191**, 661-668, doi:10.1084/jem.191.4.661 (2000).
409 Kamata, T. *et al.* Blockade of programmed death-1/programmed death ligand pathway enhances the antitumor immunity of human invariant natural killer T cells. *Cancer Immunol. Immunother.* **65**, 1477-1489, doi:10.1007/s00262-016-1901-y (2016).
410 Molling, J. W. *et al.* Peripheral blood IFN-gamma-secreting Valpha24+Vbeta11+ NKT cell numbers are decreased in cancer patients independent of tumor type or tumor load. *Int. J. Cancer* **116**, 87-93, doi:10.1002/ijc.20998 (2005).
411 Molling, J. W. *et al.* Low levels of circulating invariant natural killer T cells predict poor clinical outcome in patients with head and neck squamous cell carcinoma. *J. Clin. Oncol.* **25**, 862-868, doi:10.1200/jco.2006.08.5787 (2007).
412 Lee, C. W., Bociek, G. & Faught, W. A Survey of Practice in Management of Malignant Ascites. *J. Pain Symptom Manage.* **16**, 96-101, doi:10.1016/S0885-3924(98)00037-2 (1998).
413 Kipps, E., Tan, D. S. & Kaye, S. B. Meeting the challenge of ascites in ovarian cancer: new avenues for therapy and research. *Nat. Rev. Cancer* **13**, 273-282, doi:10.1038/nrc3432 (2013).
414 Hodge, C. & Badgwell, B. D. Palliation of malignant ascites. *J. Surg. Oncol.* **120**, 67-73, doi:10.1002/jso.25453 (2019).
415 Baert, T. *et al.* The dark side of ID8-Luc2: pitfalls for luciferase tagged murine models for ovarian cancer. *Journal for immunotherapy of cancer* **3**, 57-57, doi:10.1186/s40425-015-0102-0 (2015).
416 Huang, H. *et al.* Clinical significance of ascites in epithelial ovarian cancer. *Neoplasma* **60**, 546-552, doi:10.4149/neo_2013_071 (2013).
417 Feigenberg, T. *et al.* Molecular Profiling and Clinical Outcome of High-Grade Serous Ovarian Cancer Presenting with Low- versus High-Volume Ascites. *Biomed Res Int* **2014**, 367103-367109, doi:10.1155/2014/367103 (2014).
418 Ford, C. E., Werner, B., Hacker, N. F. & Warton, K. The untapped potential of ascites in ovarian cancer research and treatment. *Br. J. Cancer* **123**, 9-16, doi:10.1038/s41416-020-0875-x (2020).
419 Wilson, A. L. *et al.* Non-Invasive Fluorescent Monitoring of Ovarian Cancer in an Immunocompetent Mouse Model. *Cancers (Basel)* **11**, 32, doi:10.3390/cancers11010032 (2018).
420 Goode, E. L. *et al.* Dose-Response Association of CD8+ Tumor-Infiltrating Lymphocytes and Survival Time in High-Grade Serous Ovarian Cancer. *JAMA Oncol* **3**, e173290, doi:10.1001/jamaoncol.2017.3290 (2017).
421 Steele, K. E. *et al.* Measuring multiple parameters of CD8+ tumor-infiltrating lymphocytes in human cancers by image analysis. *Journal for ImmunoTherapy of Cancer* **6**, 20, doi:10.1186/s40425-018-0326-x (2018).
422 Krempski, J. *et al.* Tumor-infiltrating programmed death receptor-1+ dendritic cells mediate immune suppression in ovarian cancer. *J. Immunol.* **186**, 6905-6913, doi:10.4049/jimmunol.1100274 (2011).
423 Farhood, B., Najafi, M. & Mortezaee, K. CD8+ cytotoxic T lymphocytes in cancer immunotherapy: A review. *J. Cell. Physiol.* **234**, 8509-8521, doi:10.1002/jcp.27782 (2019).
424 McEwen-Smith, R. M., Salio, M. & Cerundolo, V. The regulatory role of invariant NKT cells in tumor immunity. *Cancer Immunol Res* **3**, 425-435, doi:10.1158/2326-6066.CIR-15-0062 (2015).
425 Tiper, I. V. *et al.* VEGF Potentiates GD3-Mediated Immunosuppression by Human Ovarian Cancer Cells. *Clin. Cancer Res.* **22**, 4249-4258, doi:10.1158/1078-0432.Ccr-15-2518 (2016).
426 Li, K. *et al.* Impact of chemokine receptor CXCR3 on tumor-infiltrating lymphocyte recruitment associated with favorable prognosis in advanced gastric cancer. *Int. J. Clin. Exp. Pathol.* **8**, 14725-14732 (2015).

427 Klatte, T. *et al.* The chemokine receptor CXCR3 is an independent prognostic factor in patients with localized clear cell renal cell carcinoma. *J. Urol.* **179**, 61-66, doi:10.1016/j.juro.2007.08.148 (2008).
428 Tang, Y., Gu, Z., Fu, Y. & Wang, J. CXCR3 from chemokine receptor family correlates with immune infiltration and predicts poor survival in osteosarcoma. *Biosci. Rep.* **39**, BSR20192134, doi:10.1042/BSR20192134 (2019).
429 Ott, P. A. & Wu, C. J. Cancer Vaccines: Steering T Cells Down the Right Path to Eradicate Tumors. *Cancer Discov.* **9**, 476, doi:10.1158/2159-8290.CD-18-1357 (2019).
430 Dumauthioz, N., Labiano, S. & Romero, P. Tumor Resident Memory T Cells: New Players in Immune Surveillance and Therapy. *Front. Immunol.* **9**, 2076-2076, doi:10.3389/fimmu.2018.02076 (2018).
431 Kartikasari, A. E. R. *et al.* Therapeutic Cancer Vaccines—T Cell Responses and Epigenetic Modulation. *Front. Immunol.* **9**, doi:10.3389/fimmu.2018.03109 (2019).
432 Liu, Q., Sun, Z. & Chen, L. Memory T cells: strategies for optimizing tumor immunotherapy. *Protein & cell* **11**, 549-564, doi:10.1007/s13238-020-00707-9 (2020).
433 Parretta, E. *et al.* CD8 Cell Division Maintaining Cytotoxic Memory Occurs Predominantly in the Bone Marrow. *The Journal of Immunology* **174**, 7654, doi:10.4049/jimmunol.174.12.7654 (2005).
434 Siracusa, F. *et al.* Maintenance of CD8(+) memory T lymphocytes in the spleen but not in the bone marrow is dependent on proliferation. *Eur. J. Immunol.* **47**, 1900-1905, doi:10.1002/eji.201747063 (2017).
435 Kretschmer, L. *et al.* Differential expansion of T central memory precursor and effector subsets is regulated by division speed. *Nature Communications* **11**, 113, doi:10.1038/s41467-019-13788-w (2020).
436 Golubovskaya, V. & Wu, L. Different Subsets of T Cells, Memory, Effector Functions, and CAR-T Immunotherapy. *Cancers (Basel)* **8**, 36, doi:10.3390/cancers8030036 (2016).
437 Kinjyo, I. *et al.* Real-time tracking of cell cycle progression during CD8+ effector and memory T-cell differentiation. *Nat Commun* **6**, 6301, doi:10.1038/ncomms7301 (2015).
438 Edwards, J. *et al.* CD103 + Tumor-Resident CD8 + T Cells Are Associated with Improved Survival in Immunotherapy-Naïve Melanoma Patients and Expand Significantly During Anti-PD-1 Treatment. *Clin. Cancer Res.* **24**, 3036-3045, doi:10.1158/1078-0432.CCR-17-2257 (2018).
439 Webb, J. R., Milne, K., Watson, P., Deleeuw, R. J. & Nelson, B. H. Tumor-infiltrating lymphocytes expressing the tissue resident memory marker CD103 are associated with increased survival in high-grade serous ovarian cancer. *Clin. Cancer Res.* **20**, 434-444, doi:10.1158/1078-0432.Ccr-13-1877 (2014).
440 Komdeur, F. L. *et al.* CD103+ intraepithelial T cells in high-grade serous ovarian cancer are phenotypically diverse TCRαβ+ CD8αβ+ T cells that can be targeted for cancer immunotherapy. *Oncotarget* **7**, 75130-75144, doi:10.18632/oncotarget.12077 (2016).
441 Bösmüller, H.-C. *et al.* Combined Immunoscore of CD103 and CD3 Identifies Long-Term Survivors in High-Grade Serous Ovarian Cancer. *Int. J. Gynecol. Cancer* **26**, 671-679, doi:10.1097/IGC.0000000000000672 (2016).
442 Park, S. L., Gebhardt, T. & Mackay, L. K. Tissue-Resident Memory T Cells in Cancer Immunosurveillance. *Trends Immunol.* **40**, 735-747, doi:https://doi.org/10.1016/j.it.2019.06.002 (2019).
443 Mackay, L. K. *et al.* Cutting edge: CD69 interference with sphingosine-1-phosphate receptor function regulates peripheral T cell retention. *J. Immunol.* **194**, 2059-2063, doi:10.4049/jimmunol.1402256 (2015).
444 Schenkel, J. M. *et al.* T cell memory. Resident memory CD8 T cells trigger protective innate and adaptive immune responses. *Science* **346**, 98-101, doi:10.1126/science.1254536 (2014).
445 Kulbe, H. *et al.* The inflammatory cytokine tumor necrosis factor-alpha generates an autocrine tumor-promoting network in epithelial ovarian cancer cells. *Cancer Res.* **67**, 585-592, doi:10.1158/0008-5472.Can-06-2941 (2007).
446 Sarafi, M. N., Garcia-Zepeda, E. A., MacLean, J. A., Charo, I. F. & Luster, A. D. Murine monocyte chemoattractant protein (MCP)-5: a novel CC chemokine that is a structural and functional homologue of human MCP-1. *J. Exp. Med.* **185**, 99-109, doi:10.1084/jem.185.1.99 (1997).
447 Deshmane, S. L., Kremlev, S., Amini, S. & Sawaya, B. E. Monocyte chemoattractant protein-1 (MCP-1): an overview. *J. Interferon Cytokine Res.* **29**, 313-326, doi:10.1089/jir.2008.0027 (2009).

448 Furukawa, S. *et al.* MCP-1 Promotes Invasion and Adhesion of Human Ovarian Cancer Cells. *Anticancer Res.* **33**, 4785 (2013).
449 Fader, A. N. *et al.* CCL2 expression in primary ovarian carcinoma is correlated with chemotherapy response and survival outcomes. *Anticancer Res.* **30**, 4791-4798 (2010).
450 Wojnarowicz, P. *et al.* Overexpressing the CCL2 chemokine in an epithelial ovarian cancer cell line results in latency of in vivo tumourigenicity. *Oncogenesis* **1**, e27-e27, doi:10.1038/oncsis.2012.25 (2012).
451 Granot, Z. *et al.* Tumor entrained neutrophils inhibit seeding in the premetastatic lung. *Cancer Cell* **20**, 300-314, doi:10.1016/j.ccr.2011.08.012 (2011).
452 Woo, I. S. *et al.* Circulating stromal cell derived factor-1alpha (SDF-1alpha) is predictive of distant metastasis in gastric carcinoma. *Cancer Invest.* **26**, 256-261, doi:10.1080/07357900701684057 (2008).
453 De La Luz Sierra, M. *et al.* Differential processing of stromal-derived factor-1alpha and stromal-derived factor-1beta explains functional diversity. *Blood* **103**, 2452-2459, doi:10.1182/blood-2003-08-2857 (2004).
454 Wang, X. & Lin, Y. Tumor necrosis factor and cancer, buddies or foes? *Acta Pharmacol. Sin.* **29**, 1275-1288, doi:10.1111/j.1745-7254.2008.00889.x (2008).
455 Josephs, S. F. *et al.* Unleashing endogenous TNF-alpha as a cancer immunotherapeutic. *J. Transl. Med.* **16**, 242, doi:10.1186/s12967-018-1611-7 (2018).
456 Pelleitier, M. & Montplaisir, S. The nude mouse: a model of deficient T-cell function. *Methods Achiev. Exp. Pathol.* **7**, 149-166 (1975).
457 Butte, M. J., Keir, M. E., Phamduy, T. B., Sharpe, A. H. & Freeman, G. J. Programmed Death-1 Ligand 1 Interacts Specifically with the B7-1 Costimulatory Molecule to Inhibit T Cell Responses. *Immunity* **27**, 111-122, doi:https://doi.org/10.1016/j.immuni.2007.05.016 (2007).
458 Xiao, Y. *et al.* RGMb is a novel binding partner for PD-L2 and its engagement with PD-L2 promotes respiratory tolerance. *J. Exp. Med.* **211**, 943-959, doi:10.1084/jem.20130790 (2014).
459 Dodagatta-Marri, E. *et al.* α-PD-1 therapy elevates Treg/Th balance and increases tumor cell pSmad3 that are both targeted by α-TGFβ antibody to promote durable rejection and immunity in squamous cell carcinomas. *Journal for ImmunoTherapy of Cancer* **7**, 62, doi:10.1186/s40425-018-0493-9 (2019).
460 Chen, W. *et al.* Conversion of peripheral CD4+CD25- naive T cells to CD4+CD25+ regulatory T cells by TGF-beta induction of transcription factor Foxp3. *J. Exp. Med.* **198**, 1875-1886, doi:10.1084/jem.20030152 (2003).
461 Nakamura, K., Kitani, A. & Strober, W. Cell contact-dependent immunosuppression by CD4(+)CD25(+) regulatory T cells is mediated by cell surface-bound transforming growth factor beta. *The Journal of experimental medicine* **194**, 629-644, doi:10.1084/jem.194.5.629 (2001).
462 Wan, Y. Y. & Flavell, R. A. 'Yin-Yang' functions of transforming growth factor-beta and T regulatory cells in immune regulation. *Immunol. Rev.* **220**, 199-213, doi:10.1111/j.1600-065X.2007.00565.x (2007).
463 Gunderson, A. J. *et al.* TGFβ suppresses CD8(+) T cell expression of CXCR3 and tumor trafficking. *Nat Commun* **11**, 1749, doi:10.1038/s41467-020-15404-8 (2020).
464 Curran, M. A., Montalvo, W., Yagita, H. & Allison, J. P. PD-1 and CTLA-4 combination blockade expands infiltrating T cells and reduces regulatory T and myeloid cells within B16 melanoma tumors. *Proc. Natl. Acad. Sci. U. S. A.* **107**, 4275-4280, doi:10.1073/pnas.0915174107 (2010).
465 Nargis, T. & Chakrabarti, P. Significance of circulatory DPP4 activity in metabolic diseases. *IUBMB Life* **70**, 112-119, doi:10.1002/iub.1709 (2018).
466 Klemann, C., Wagner, L., Stephan, M. & Von Hörsten, S. Vol. 185 1-21 (2016).
467 Boonacker, E. & Van Noorden, C. J. F. The multifunctional or moonlighting protein CD26/DPPIV. *Eur. J. Cell Biol.* **82**, 53-73, doi:10.1078/0171-9335-00302 (2003).
468 Trzaskalski, N. A., Fadzeyeva, E. & Mulvihill, E. E. Dipeptidyl Peptidase-4 at the Interface Between Inflammation and Metabolism. *Clinical Medicine Insights: Endocrinology and Diabetes* **13**, 1179551420912972, doi:10.1177/1179551420912972 (2020).
469 Wronkowitz, N. *et al.* Soluble DPP4 induces inflammation and proliferation of human smooth muscle cells via protease-activated receptor 2. *Biochimica et Biophysica Acta (BBA) - Molecular Basis of Disease* **1842**, 1613-1621, doi:http://dx.doi.org/10.1016/j.bbadis.2014.06.004 (2014).
470 Kajiyama, H. *et al.* Dipeptidyl peptidase IV overexpression induces up-regulation of E-cadherin and tissue inhibitors of matrix metalloproteinases, resulting in decreased invasive potential in ovarian carcinoma cells. *Cancer Res.* **63**, 2278 (2003).

471 Domcke, S., Sinha, R., Levine, D. A., Sander, C. & Schultz, N. Evaluating cell lines as tumour models by comparison of genomic profiles. *Nature Communications* **4**, 2126, doi:10.1038/ncomms3126 (2013).
472 Beaufort, C. M. *et al.* Ovarian cancer cell line panel (OCCP): clinical importance of in vitro morphological subtypes. *PLoS One* **9**, e103988-e103988, doi:10.1371/journal.pone.0103988 (2014).
473 Varona, A. *et al.* Expression and activity profiles of DPP IV/CD26 and NEP/CD10 glycoproteins in the human renal cancer are tumor-type dependent. *BMC Cancer* **10**, 193, doi:10.1186/1471-2407-10-193 (2010).
474 Anglesio, M. S. *et al.* Type-specific cell line models for type-specific ovarian cancer research. *PLoS One* **8**, e72162, doi:10.1371/journal.pone.0072162 (2013).
475 Diaz-Jimenez, D., Petrillo, M. G., Busada, J. T., Hermoso, M. A. & Cidlowski, J. A. Glucocorticoids mobilize macrophages by transcriptionally up-regulating the exopeptidase DPP4. *J. Biol. Chem.* **295**, 3213-3227, doi:10.1074/jbc.RA119.010894 (2020).
476 Djedovic, V., Lee, Y.-Y., Kollara, A., May, T. & Brown, T. J. The Two Faces of Adjuvant Glucocorticoid Treatment in Ovarian Cancer. *Hormones and Cancer* **9**, 95-107, doi:10.1007/s12672-017-0319-0 (2018).
477 Münstedt, K., Borces, D., Bohlmann, M. K., Zygmunt, M. & von Georgi, R. Glucocorticoid administration in antiemetic therapy. *Cancer* **101**, 1696-1702, doi:https://doi.org/10.1002/cncr.20534 (2004).
478 Uematsu, T., Tanaka, H., Yamaoka, M. & Furusawa, K. Effects of oral squamous cell carcinoma-derived TGF-beta1 on CD26/DPPIV expression in T cells. *Anticancer Res.* **24**, 619-624 (2004).
479 Casrouge, A. *et al.* Lymphocytes are a major source of circulating soluble dipeptidyl peptidase 4. *Clin. Exp. Immunol.* **194**, 166-179, doi:10.1111/cei.13163 (2018).
480 Mulvihill, E. E. *et al.* Cellular Sites and Mechanisms Linking Reduction of Dipeptidyl Peptidase-4 Activity to Control of Incretin Hormone Action and Glucose Homeostasis. *Cell Metab.* **25**, 152-165, doi:10.1016/j.cmet.2016.10.007 (2017).
481 Baumeier, C. *et al.* Hepatic DPP4 DNA Methylation Associates With Fatty Liver. *Diabetes* **66**, 25-35, doi:10.2337/db15-1716 (2017).
482 Lettau, M. *et al.* Degranulation of human cytotoxic lymphocytes is a major source of proteolytically active soluble CD26/DPP4. *Cell. Mol. Life Sci.*, doi:10.1007/s00018-019-03207-0 (2019).
483 Varin, E. M. *et al.* Circulating Levels of Soluble Dipeptidyl Peptidase-4 Are Dissociated from Inflammation and Induced by Enzymatic DPP4 Inhibition. *Cell Metab.* **29**, 320-334.e325, doi:10.1016/j.cmet.2018.10.001 (2019).
484 Baggio, L. L. *et al.* Plasma levels of DPP4 activity and sDPP4 are dissociated from inflammation in mice and humans. *Nature Communications* **11**, 3766, doi:10.1038/s41467-020-17556-z (2020).
485 Toshiaki, T. *et al.* Enhancement of Antigen-Induced T-Cell Proliferation by Soluble CD26/ Dipeptidyl Peptidase IV. *Proc. Natl. Acad. Sci. U. S. A.* **91**, 3082-3086, doi:10.1073/pnas.91.8.3082 (1994).
486 Lau, T. S. *et al.* A loop of cancer-stroma-cancer interaction promotes peritoneal metastasis of ovarian cancer via TNFα-TGFα-EGFR. *Oncogene* **36**, 3576-3587, doi:10.1038/onc.2016.509 (2017).
487 Lee, S.-Y. *et al.* Soluble Dipeptidyl Peptidase-4 Induces Fibroblast Activation Through Proteinase-Activated Receptor-2. *Front. Pharmacol.* **11**, 552818-552818, doi:10.3389/fphar.2020.552818 (2020).
488 Deng, B. *et al.* Intratumor Hypoxia Promotes Immune Tolerance by Inducing Regulatory T Cells via TGF-β1 in Gastric Cancer. *PLoS One* **8**, e63777, doi:10.1371/journal.pone.0063777 (2013).
489 Price, J. D. *et al.* Effects of short-term sitagliptin treatment on immune parameters in healthy individuals, a randomized placebo-controlled study. *Clin. Exp. Immunol.* **174**, 120-128, doi:10.1111/cei.12144 (2013).
490 Martínez-Lostao, L., Anel, A. & Pardo, J. How Do Cytotoxic Lymphocytes Kill Cancer Cells? *Clin. Cancer Res.* **21**, 5047-5056, doi:10.1158/1078-0432.CCR-15-0685 (2015).
491 Tay, R. E., Richardson, E. K. & Toh, H. C. Revisiting the role of CD4+ T cells in cancer immunotherapy—new insights into old paradigms. *Cancer Gene Ther.*, doi:10.1038/s41417-020-0183-x (2020).
492 Kennedy, R. & Celis, E. Multiple roles for CD4+ T cells in anti-tumor immune responses. *Immunol. Rev.* **222**, 129-144, doi:10.1111/j.1600-065X.2008.00616.x (2008).

493 Pipkin, M. E. *et al.* Interleukin-2 and inflammation induce distinct transcriptional programs that promote the differentiation of effector cytolytic T cells. *Immunity* **32**, 79-90, doi:10.1016/j.immuni.2009.11.012 (2010).
494 Leveque, L. *et al.* Interleukin 2-mediated conversion of ovarian cancer-associated CD4+ regulatory T cells into proinflammatory interleukin 17-producing helper T cells. *J. Immunother.* **32**, 101-108, doi:10.1097/CJI.0b013e318195b59e (2009).
495 Bettelli, E., Oukka, M. & Kuchroo, V. K. TH-17 cells in the circle of immunity and autoimmunity. *Nat. Immunol.* **8**, 345-350, doi:10.1038/ni0407-345 (2007).
496 Galeano Niño, J. L. *et al.* Cytotoxic T cells swarm by homotypic chemokine signalling. *Elife* **9**, doi:10.7554/eLife.56554 (2020).
497 Vito, A., El-Sayes, N. & Mossman, K. Hypoxia-Driven Immune Escape in the Tumor Microenvironment. *Cells* **9**, doi:10.3390/cells9040992 (2020).
498 Vuillefroy de Silly, R. *et al.* Phenotypic switch of CD8(+) T cells reactivated under hypoxia toward IL-10 secreting, poorly proliferative effector cells. *Eur. J. Immunol.* **45**, 2263-2275, doi:10.1002/eji.201445284 (2015).
499 Han, Y. K. *et al.* Hypoxia induces immunogenic cell death of cancer cells by enhancing the exposure of cell surface calreticulin in an endoplasmic reticulum stress-dependent manner. *Oncol. Lett.* **18**, 6269-6274, doi:10.3892/ol.2019.10986 (2019).
500 Doedens, A. L. *et al.* Hypoxia-inducible factors enhance the effector responses of CD8+ T cells to persistent antigen. *Nat. Immunol.* **14**, 1173-1182, doi:10.1038/ni.2714 (2013).
501 Janssens, R. *et al.* Truncation of CXCL12 by CD26 reduces its CXC chemokine receptor 4- and atypical chemokine receptor 3-dependent activity on endothelial cells and lymphocytes. *Biochem. Pharmacol.* **132**, 92-101, doi:10.1016/j.bcp.2017.03.009 (2017).
502 Shioda, T. *et al.* Anti-HIV-1 and chemotactic activities of human stromal cell-derived factor 1α (SDF-1α) and SDF-1β are abolished by CD26/dipeptidyl peptidase IV-mediated cleavage. *Proceedings of the National Academy of Sciences* **95**, 6331, doi:10.1073/pnas.95.11.6331 (1998).
503 Janowski, M. Functional diversity of SDF-1 splicing variants. *Cell Adhesion & Migration* **3**, 243-249, doi:10.4161/cam.3.3.8260 (2009).
504 Marcuzzi, E., Angioni, R., Molon, B. & Calì, B. Chemokines and Chemokine Receptors: Orchestrating Tumor Metastasization. *Int. J. Mol. Sci.* **20**, 96, doi:10.3390/ijms20010096 (2018).
505 Sarvaiya, P. J., Guo, D., Ulasov, I., Gabikian, P. & Lesniak, M. S. Chemokines in tumor progression and metastasis. *Oncotarget* **4**, 2171-2185, doi:10.18632/oncotarget.1426 (2013).
506 Orimo, A. *et al.* Stromal Fibroblasts Present in Invasive Human Breast Carcinomas Promote Tumor Growth and Angiogenesis through Elevated SDF-1/CXCL12 Secretion. *Cell* **121**, 335-348, doi:10.1016/j.cell.2005.02.034 (2005).
507 Roy, I. *et al.* CXCL12 Chemokine Expression Suppresses Human Pancreatic Cancer Growth and Metastasis. *PLoS One* **9**, e90400, doi:10.1371/journal.pone.0090400 (2014).
508 Lalos, A. *et al.* Prognostic significance of CD8+ T-cells density in stage III colorectal cancer depends on SDF-1 expression. *Sci. Rep.* **11**, 775, doi:10.1038/s41598-020-80382-2 (2021).
509 Samarendra, H. *et al.* A meta-analysis of CXCL12 expression for cancer prognosis. *Br. J. Cancer* **117**, 124-135, doi:10.1038/bjc.2017.134 (2017).
510 Williams, S. A. *et al.* Multiple functions of CXCL12 in a syngeneic model of breast cancer. *Mol. Cancer* **9**, 250, doi:10.1186/1476-4598-9-250 (2010).
511 Yu, L. *et al.* Identification and expression of novel isoforms of human stromal cell-derived factor 1. *Gene* **374**, 174-179, doi:10.1016/j.gene.2006.02.001 (2006).
512 Kryczek, I. *et al.* CXCL12 and vascular endothelial growth factor synergistically induce neoangiogenesis in human ovarian cancers. *Cancer Res.* **65**, 465-472 (2005).
513 Zeng, F. *et al.* Inflammatory Markers of CRP, IL6, TNFα, and Soluble TNFR2 and the Risk of Ovarian Cancer: A Meta-analysis of Prospective Studies. *Cancer Epidemiol. Biomarkers Prev.* **25**, 1231-1239, doi:10.1158/1055-9965.Epi-16-0120 (2016).
514 Kampan, N. C. *et al.* Pre-operative sera interleukin-6 in the diagnosis of high-grade serous ovarian cancer. *Sci. Rep.* **10**, 2213, doi:10.1038/s41598-020-59009-z (2020).
515 Piura, B. *et al.* Distinct Expression and Localization of TNF System in Ovarian Carcinoma Tissues: Possible Involvement of TNF-α in Morphological Changes of Ovarian Cancerous Cells. *Anticancer Res.* **34**, 745 (2014).
516 Browning, L., Patel, M. R., Horvath, E. B., Tawara, K. & Jorcyk, C. L. IL-6 and ovarian cancer: inflammatory cytokines in promotion of metastasis. *Cancer Manag. Res.* **10**, 6685-6693, doi:10.2147/cmar.S179189 (2018).

517 Ye, L.-L., Wei, X.-S., Zhang, M., Niu, Y.-R. & Zhou, Q. The Significance of Tumor Necrosis Factor Receptor Type II in CD8+ Regulatory T Cells and CD8+ Effector T Cells. *Front. Immunol.* **9**, doi:10.3389/fimmu.2018.00583 (2018).
518 Cao, W., Chi, W. H., Wang, J., Tang, J. J. & Lu, Y. J. TNF-alpha promotes Doxorubicin-induced cell apoptosis and anti-cancer effect through downregulation of p21 in p53-deficient tumor cells. *Biochem. Biophys. Res. Commun.* **330**, 1034-1040, doi:10.1016/j.bbrc.2005.02.188 (2005).
519 Kimura, A., Naka, T. & Kishimoto, T. IL-6-dependent and -independent pathways in the development of interleukin 17-producing T helper cells. *Proc. Natl. Acad. Sci. U. S. A.* **104**, 12099-12104, doi:10.1073/pnas.0705268104 (2007).
520 Lyon, D. E. *et al.* Relationship of systemic cytokine concentrations to cognitive function over two years in women with early stage breast cancer. *J. Neuroimmunol.* **301**, 74-82, doi:10.1016/j.jneuroim.2016.11.002 (2016).
521 Qi, F. *et al.* Time-series clustering of cytokine expression after transarterial chemoembolization in patients with hepatocellular carcinoma. *Oncol. Lett.* **19**, 1175-1186, doi:10.3892/ol.2019.11209 (2020).
522 Griffiths, J. I. *et al.* Circulating immune cell phenotype dynamics reflect the strength of tumor–immune cell interactions in patients during immunotherapy. *Proceedings of the National Academy of Sciences* **117**, 16072, doi:10.1073/pnas.1918937117 (2020).
523 McAllister, S. S. & Weinberg, R. A. The tumour-induced systemic environment as a critical regulator of cancer progression and metastasis. *Nat. Cell Biol.* **16**, 717-727, doi:10.1038/ncb3015 (2014).
524 Scheen, A. J. The safety of gliptins : updated data in 2018. *Expert Opin. Drug Saf.* **17**, 387-405, doi:10.1080/14740338.2018.1444027 (2018).
525 Engel, S. S., Round, E., Golm, G. T., Kaufman, K. D. & Goldstein, B. J. Safety and tolerability of sitagliptin in type 2 diabetes: pooled analysis of 25 clinical studies. *Diabetes Ther.* **4**, 119-145, doi:10.1007/s13300-013-0024-0 (2013).
526 Elashoff, M., Matveyenko, A. V., Gier, B., Elashoff, R. & Butler, P. C. Pancreatitis, pancreatic, and thyroid cancer with glucagon-like peptide-1-based therapies. *Gastroenterology* **141**, 150-156, doi:10.1053/j.gastro.2011.02.018 (2011).
527 Dicembrini, I., Montereggi, C., Nreu, B., Mannucci, E. & Monami, M. Pancreatitis and pancreatic cancer in patientes treated with Dipeptidyl Peptidase-4 inhibitors: An extensive and updated meta-analysis of randomized controlled trials. *Diabetes Res. Clin. Pract.* **159**, 107981, doi:10.1016/j.diabres.2019.107981 (2020).
528 Spiers, L., Coupe, N. & Payne, M. Toxicities associated with checkpoint inhibitors-an overview. *Rheumatology (Oxford)* **58**, vii7-vii16, doi:10.1093/rheumatology/kez418 (2019).
529 Baraibar, I., Melero, I., Ponz-Sarvise, M. & Castanon, E. Safety and Tolerability of Immune Checkpoint Inhibitors (PD-1 and PD-L1) in Cancer. *Drug Saf.* **42**, 281-294, doi:10.1007/s40264-018-0774-8 (2019).
530 Hugo, W. *et al.* Genomic and Transcriptomic Features of Response to Anti-PD-1 Therapy in Metastatic Melanoma. *Cell* **165**, 35-44, doi:10.1016/j.cell.2016.02.065 (2016).
531 Najjar, Y. G. *et al.* Tumor cell oxidative metabolism as a barrier to PD-1 blockade immunotherapy in melanoma. *JCI insight* **4**, e124989, doi:10.1172/jci.insight.124989 (2019).
532 Scharping, N. E., Menk, A. V., Whetstone, R. D., Zeng, X. & Delgoffe, G. M. Efficacy of PD-1 Blockade Is Potentiated by Metformin-Induced Reduction of Tumor Hypoxia. *Cancer Immunol Res* **5**, 9-16, doi:10.1158/2326-6066.Cir-16-0103 (2017).
533 Ma, Y. *et al.* DPP-4 inhibitor anagliptin protects against hypoxia-induced cytotoxicity in cardiac H9C2 cells. *Artificial Cells, Nanomedicine, and Biotechnology* **47**, 3823-3831, doi:10.1080/21691401.2019.1652624 (2019).
534 Rizvi, N. A. *et al.* Cancer immunology. Mutational landscape determines sensitivity to PD-1 blockade in non-small cell lung cancer. *Science (New York, N.Y.)* **348**, 124-128, doi:10.1126/science.aaa1348 (2015).
535 Campbell, B. B. *et al.* Comprehensive Analysis of Hypermutation in Human Cancer. *Cell* **171**, 1042-1056.e1010, doi:10.1016/j.cell.2017.09.048 (2017).
536 Martin, S. D. *et al.* Low Mutation Burden in Ovarian Cancer May Limit the Utility of Neoantigen-Targeted Vaccines. *PLoS One* **11**, e0155189-e0155189, doi:10.1371/journal.pone.0155189 (2016).
537 Wakita, D. *et al.* Cisplatin Augments Antitumor T-Cell Responses Leading to a Potent Therapeutic Effect in Combination With PD-L1 Blockade. *Anticancer Res.* **39**, 1749-1760, doi:10.21873/anticanres.13281 (2019).

538 Luo, R. *et al.* Cisplatin Facilitates Radiation-Induced Abscopal Effects in Conjunction with PD-1 Checkpoint Blockade Through CXCR3/CXCL10-Mediated T-cell Recruitment. *Clin. Cancer Res.* **25**, 7243-7255, doi:10.1158/1078-0432.Ccr-19-1344 (2019).
539 Peng, J. *et al.* Chemotherapy Induces Programmed Cell Death-Ligand 1 Overexpression via the Nuclear Factor-κB to Foster an Immunosuppressive Tumor Microenvironment in Ovarian Cancer. *Cancer Res.* **75**, 5034-5045, doi:10.1158/0008-5472.CAN-14-3098 (2015).
540 O'Donnell, T. *et al.* Chemotherapy weakly contributes to predicted neoantigen expression in ovarian cancer. *BMC Cancer* **18**, 87-87, doi:10.1186/s12885-017-3825-0 (2018).
541 Martin de la Fuente, L. *et al.* PD-1/PD-L1 expression and tumor-infiltrating lymphocytes are prognostically favorable in advanced high-grade serous ovarian carcinoma. *Virchows Arch.* **477**, 83-91, doi:10.1007/s00428-020-02751-6 (2020).
542 Kim, H.-S. *et al.* Expression of programmed cell death ligand 1 and immune checkpoint markers in residual tumors after neoadjuvant chemotherapy for advanced high-grade serous ovarian cancer. *Gynecol. Oncol.* **151**, 414-421, doi:https://doi.org/10.1016/j.ygyno.2018.08.023 (2018).
543 Bazhin, A. V., von Ahn, K., Fritz, J., Werner, J. & Karakhanova, S. Interferon-α Up-Regulates the Expression of PD-L1 Molecules on Immune Cells Through STAT3 and p38 Signaling. *Front. Immunol.* **9**, doi:10.3389/fimmu.2018.02129 (2018).
544 Taube, J. M. *et al.* Colocalization of inflammatory response with B7-h1 expression in human melanocytic lesions supports an adaptive resistance mechanism of immune escape. *Sci. Transl. Med.* **4**, 127ra137-127ra137, doi:10.1126/scitranslmed.3003689 (2012).
545 Strickland, K. C. *et al.* Association and prognostic significance of BRCA1/2-mutation status with neoantigen load, number of tumor-infiltrating lymphocytes and expression of PD-1/PD-L1 in high grade serous ovarian cancer. *Oncotarget* **7**, 13587-13598, doi:10.18632/oncotarget.7277 (2016).
546 Lampert, E. J. *et al.* Combination of PARP Inhibitor Olaparib, and PD-L1 Inhibitor Durvalumab, in Recurrent Ovarian Cancer: a Proof-of-Concept Phase II Study. *Clin. Cancer Res.* **26**, 4268, doi:10.1158/1078-0432.CCR-20-0056 (2020).
547 Das, M., Zhu, C. & Kuchroo, V. K. Tim-3 and its role in regulating anti-tumor immunity. *Immunol. Rev.* **276**, 97-111, doi:10.1111/imr.12520 (2017).
548 Sakuishi, K. *et al.* Targeting Tim-3 and PD-1 pathways to reverse T cell exhaustion and restore anti-tumor immunity. *J. Exp. Med.* **207**, 2187-2194, doi:10.1084/jem.20100643 (2010).
549 Fourcade, J. *et al.* Upregulation of Tim-3 and PD-1 expression is associated with tumor antigen–specific CD8+ T cell dysfunction in melanoma patients. *J. Exp. Med.* **207**, 2175-2186, doi:10.1084/jem.20100637 (2010).
550 Sawada, M. *et al.* PD-1+ Tim3+ tumor-infiltrating CD8 T cells sustain the potential for IFN-γ production, but lose cytotoxic activity in ovarian cancer. *Int. Immunol.* **32**, 397-405, doi:10.1093/intimm/dxaa010 (2020).
551 Dang, N. H., Torimoto, Y., Deusch, K., Schlossman, S. F. & Morimoto, C. Comitogenic effect of solid-phase immobilized anti-1F7 on human CD4 T cell activation via CD3 and CD2 pathways. *The Journal of Immunology* **144**, 4092 (1990).
552 Fleischer, B. A novel pathway of human T cell activation via a 103 kD T cell activation antigen. *J. Immunol.* **138**, 1346-1350 (1987).
553 Toshiaki, T., Junichi, K., Arieh, Y., Stuart, F. S. & Chikao, M. The Costimulatory Activity of the CD26 Antigen Requires Dipeptidyl Peptidase IV Enzymatic Activity. *Proc. Natl. Acad. Sci. U. S. A.* **90**, 4586-4590, doi:10.1073/pnas.90.10.4586 (1993).
554 White, P. C., Chamberlain-Shea, H. & de la Morena, M. T. Sitagliptin treatment of patients with type 2 diabetes does not affect CD4+ T-cell activation. *J. Diabetes Complications* **24**, 209-213, doi:10.1016/j.jdiacomp.2009.09.001 (2010).
555 Cho, S. *et al.* Characterization and evaluation of pre-clinical suitability of a syngeneic orthotopic mouse ovarian cancer model. *Anticancer Res.* **33**, 1317-1324 (2013).
556 Walton, J. *et al.* CRISPR/Cas9-Mediated Trp53 and Brca2 Knockout to Generate Improved Murine Models of Ovarian High-Grade Serous Carcinoma. *Cancer Res.* **76**, 6118-6129, doi:10.1158/0008-5472.CAN-16-1272 (2016).
557 Walton, J. B. *et al.* CRISPR/Cas9-derived models of ovarian high grade serous carcinoma targeting Brca1, Pten and Nf1, and correlation with platinum sensitivity. *Sci. Rep.* **7**, 16827, doi:10.1038/s41598-017-17119-1 (2017).
558 Tudrej, P., Kujawa, K. A., Cortez, A. J. & Lisowska, K. M. Characteristics of in Vivo Model Systems for Ovarian Cancer Studies. *Diagnostics (Basel)* **9**, doi:10.3390/diagnostics9030120 (2019).

Appendix A

A.1 General solutions and buffers

2 Yeast Tryptone (2YT) media

20g Bacto-Tryptone (Thermo Scientific, #LP0042B)

10g Bacto-Yeast (Thermo Scientific, #LP0021B)

5g NaCl (Ajax, #465)

The above components were dissolved up to a total of 1L in ddH_2O. The media was sterilised and stored at room temperature.

2YT media supplemented with ampicillin 100µg/ml

Ampicillin (Sigma, #A9518) was aseptically added to sterile 2YT media to achieve a final concentration of 100µg/ml.

2YT agar plates supplemented with ampicillin 100µg/ml

10g Bacto-Tryptone (Thermo Scientific, #LP0042B)

5g Bacto-Yeast (Thermo Scientific, #LP0021B)

2.5g NaCl (Ajax, #465)

10g Agar (Thermo Scientific, #LP0011B)

The above components were dissolved up to a total of 500ml in ddH_2O. The agar mixture was sterilised and allowed to cool to ~55˚C. Prior to solidification, ampicillin was added to the agar to achieve a final concentration of 100µg/ml. The agar was aseptically poured into sterile petri dishes (~25ml per plate) and allowed to set. Plates were inverted and stored at 4˚C until use.

2YT/50% glycerol

2YT media and glycerol (Sigma, #G5516) were combined at a 1:1 vol% ratio. The solution was sterilised and stored at room temperature.

50x Tris-acetate-EDTA (TAE) buffer

242g Trizma® base (Sigma-Aldrich, #T1503)

57.1ml Glacial acetic acid (Merck Millipore, #1000560001)

18.6g EDTA disodium salt (Sigma-Aldrich, #ED2SS)

The above components were dissolved up to a total of 1L in ddH_2O. The solution was stored at room temperature.

For 1x TAE buffer, 10ml of 50x TAE buffer was added to 490ml of ddH_2O.

1% agarose gel

A 1% agarose solution was prepared by adding 1g agarose powder (USB, #US75817) per 100ml of 1x TAE buffer. The solution was heated in a microwave until all powder was dissolved. 1µl/100ml of GelRed (Biotium, #41003) was added and the solution was poured into a pre-taped gel cast with lane combs. The gel was allowed to set at room temperature for approximately 1 hour before removing tape and lane combs.

Heat-inactivated fetal bovine serum (HI-FBS)

Sterile 50ml aliquots of filtered FBS (Thermo Fisher, #16000044) were thawed and placed in a 56˚C water bath for 45 minutes, swirling every 15 minutes.

1000x Insulin-transferrin-selenium (ITS) selenite media supplement

Acidified water was prepared by adding 100µl of glacial acetic acid to 10ml sterile water. 5ml of acidified water was added to a vial of lyophilised ITS powder (Sigma, #I1884) and incubated at room temperature until completely dissolved.

For 1 x ITS in cell culture media (1µg/ml), 500µl of 1000x ITS was added to 500ml of growth medium.

Cobalt (II) chloride ($CoCl_2$)

To prepare a 100mM stock solution, 129.8mg of $CoCl_2$ powder (Sigma-Aldrich, #232696-5; M_W = 129.839g/mol) was dissolved in 10ml of sterile water and stored at room temperature. For use in hypoxic culture at 150µM, 7.5µl of stock solution was added per 5ml complete culture medium.

Radioimmunoprecipitation assay (RIPA) lysis buffer

3ml	5M NaCl (Sigma, #7136)
5ml	1M Tris pH 8.0 (Sigma, #T1503)
1ml	Triton X-100 (Sigma, #X100)
5ml	10% Sodium deoxycholate (Sigma, #D6750)
1ml	10% SDS (MP Biomedicals, #102918)

The above components were made up to 100ml with ddH_2O. The buffer was stored at 4°C protected from light. Immediately prior to protein extraction 1µl/ml of Benzonase® Nuclease (Sigma, #E1014) and if necessary, 20µl/ml of 50x protease inhibitor cocktail (Roche, #11873580001) was added to the required volume of buffer.

Sitagliptin

JANUVIA® tablets (Merck Sharp & Dohme Corp., NJ, USA) containing sitagliptin phosphate 100mg per tablet (M_W = 407.314 g/mol) were obtained from the hospital pharmacy. To prepare a 50mM stock solution, one tablet was crushed and dissolved in 4.91ml of DMSO by placing on a gentle shaker for 1 hour at room temperature. For 100µM sitagliptin**,** 1µl of 50mM stock was diluted in 499µl of assay buffer.

H-Gly-Pro-p-nitroanilide (pNA)

H-Gly-Pro-pNA lyophilised powder (Sigma, #G0513) was dissolved in methanol to prepare a 50mM stock solution. To prepare a 2mM solution, 200µl of 50mM stock H-Gly-Pro-pNA was diluted in 4.8ml of DPP4 assay buffer/6.25%MeOH.

H-Gly-Pro-amido-4-methylcoumarin (AMC)

H-Gly-Pro-AMC lyophilised powder (Sigma, #G2761) was dissolved in methanol to prepare a 50mM stock solution. To prepare a 2mM solution, 200µl of 50mM stock H-Gly-Pro-AMC was diluted in 4.8ml of DPP4 assay buffer/6.25%MeOH.

20x mouse phosphate-buffered saline

22.08g NaH_2PO_4-H_2O (Sigma, #71507)

90.8g Na_2HPO_4 (Sigma, #S7907)

350.4g NaCl (Sigma, #71376)

The above components were completely dissolved in 1L sterile water. The pH was adjusted to 7.2-7.4 and the solution was topped up to 2L with sterile water. The solution was stored at room temperature.

For 1x mouse PBS (mPBS), 50ml of 20x mouse PBS was added to 950ml of sterile water and stored at room temperature.

For mPBS/1%FBS, 500µl of HI-FBS was added to 49.5ml of 1x mPBS and stored at 4°C.

For mPBS/2%FBS, 1ml of HI-FBS was added to 49ml of 1x mPBS and stored at 4°C.

10x Ammonium-chloride-potassium (ACK) lysis buffer

86g NH_4Cl (Sigma, #A4514)

10g $KHCO_3$ (Sigma, #60339)

2ml 0.5M EDTA pH 8.0 (Sigma-Aldrich, #ED2SS)

The above components were completely dissolved in 900ml of sterile water, topped up to 1L and the pH was adjusted pH to 7.2-7.4. The solution was filtered, sterilised and stored at room temperature.

For 1x ACK lysis buffer, 100ml of 10x ACK lysis buffer was added to 900ml of sterile water.

A.2 Oligonucleotides

Table A.1. Bacterial screening primer sequences.

Primer	*Sequence 5′ – 3′*
pSIF-H1-Puro ForwardF	TGTCTTTGGATTTGGGAATCTTAT
pSIF-H1-Puro ReverseF	ATTTATTGTATCTGTGGGAGCCTC

Table A.2. shRNA template sequences.

Gene target	*Sequence 5′ – 3′*	
	Top strand	*Bottom strand*
MMP-10	GATCCATGCATCAGGCACCAATTTAT CTTCCTGTCAGAATAAATTGGTGCCT GATGCATTTTTTG	AATTCAAAAAATGCATCAGGCACCAA TTTATTCTGACAGGAAGATAAATTGG TGCCTGATGCATG
MMP-13	GATCCTCATACTACCATCCTACAAAT CTTCCTGTCAGAATTTGTAGGATGGT AGTATGATTTTTG	AATTCAAAAATCATACTACCATCCTA CAAATTCTGACAGGAAGATTTGTAGG ATGGTAGTATGAG

Table A.3. Forward and reverse sequences for primer pairs used in real-time PCR.

Gene	*Accession number*	*Primer sequence 5′ – 3′*	
		Forward	*Reverse*
18S	NR_003286.4	GTAACCCGTTGAACCCCATT	CCATCCAATCGGTAGTAGCG
HIF-1α	NM_001530	CAGCTATTTGCGTGTGAGGA	CCTCATGGTCACATGGATGA
DPP4	NM_001935	ATGCCAGGAGGAAGGAATCT	TATAGAGGGGCAGACCAGGA
MMP-1	NM_002421	GGACAACTCTCCTTTTGATGGA	CAAAGCCCCGATATCAGTAGAA
MMP-10	NM_002425	CACAGTTTGGCTCATGCCTA	TGCCATTCACATCATCTTGC
MMP-13	NM_002427	GACCCTGGAGCACTCATGTT TTGAGCTGGACTCATTGTCG	TCCTCGGAGACTGGTAATGG CTCAGTCATGGAGCTTGCTG

Table A.4. Working concentrations of DNA standards for real-time PCR.

Standard #	***Initial concentration***	***Volume DNA (µl)***	***Volume ddH_2O (µl)***	***Final concentration***
Stock	**100pg/µl**	**10**	**90**	**10pg/ul**
1	10pg/µl	10	390	250fg/µl
2	250fg/µl	20	180	25fg/µl
3	25fg/µl	20	180	2.5fg/µl
4	2.5fg/µl	20	180	0.25fg/µl
5	0.25fg/µl	20	180	0.025fg/µl
6	0.025fg/µl	20	180	0.0025fg/µl
7	0.0025fg/µl	20	180	0.00025fg/µl

A.3 Proteins

Table A.5. List of human protease targets analysed in the cell lysates and culture media of OVCAR4 cells. *(MMP array; Abcam #ab197453, Protease array; R&D Systems #ARY021).*

MMP array	***Protease Array***		
MMP-1	ADAM8	Cathepsin X/Z/P	MMP-3
MMP-2	ADAM9	DPPIV/CD26	MMP-7
MMP-3	ADAMTS1	Kallikrein 3/PSA	MMP-8
MMP-8	ADAMTS13	Kallikrein 5	MMP-9
MMP-9	Cathepsin A	Kallikrein 6	MMP-12
MMP-10	Cathepsin B	Kallikrein 7	MMP-13
MMP-13	Cathepsin C	Kallikrein 10	Neprilysin/CD10
TIMP-1	Cathepsin D	Kallikrein 11	Presenilin-1
TIMP-2	Cathepsin E	Kallikrein 13	Proprotein Convertase 9
TIMP4	Cathepsin L	MMP-1	Proteinase 3
	Cathepsin S	MMP-2	uPA/Urokinase
	Cathepsin V		

Table A.6. MMP array 10-target standard values.

Analyte	***Standard concentration (pg/ml)***							
	1	*2*	*3*	*4*	*5*	*6*	*7*	*8 (blank)*
MMP-1	100,000	33,333	11,111	3,704	1,235	412	137	0
MMP-2	50,000	16,667	5.556	1,852	617	206	69	0
MMP-3	30,000	10,000	3.333	1,111	370	123	41	0
MMP-8	20,000	6,667	2,222	741	247	82	27	0
MMP-9	30,000	10,000	3,333	1,111	370	123	41	0
MMP-10	5,000	1,667	556	185	62	21	7	0
MMP-13	20,000	6,667	2,222	741	247	82	27	0
TIMP-1	20,000	6,667	2,222	741	247	82	27	0
TIMP-2	20,000	6,667	2,222	741	247	82	27	0
TIMP-4	50,000	16,667	5,556	1,852	617	206	69	0

Table A.7. Bio-Plex Pro™ Mouse 31-plex chemokine panel normalised standard values, expected control ranges and bead regions. *(Standard Lot #64259446, Control Lot #64322209)*

Analyte	***Standard #1 concentration (pg/ml)***	***Control range (pg/ml)***	***Bead region***
BCA-1/CXCL13	9,689	253-589	28
CTACK/CCL27	418,072	9537-22251	62
ENA-78/CXCL5	64,141	906-2114	20
Eotaxin/CCL11	1,648	31-71	74
Eotaxin-2/CCL24	16,932	264-616	73
Fractalkine/CX3CL1	51,977	966-2253	25
GM-CSF	2,602	49-113	22
I-309/CCL1	2,420	35-80	26
IFN-ɣ	18,400	371-864	34
IL-1β	65,008	1202-2804	19
IL-2	6,892	127-297	36
IL-4	6.453	125-291	39
IL-6	9,486	208-486	38
IL-10	161,757	2486-5801	56
IL-16	49,310	706-1648	29
IP-10/CXCL10	72,305	981-2288	35
I-TAC/CXCL11	89,855	1200-2799	37
KC/CXCl1	26,963	565-1318	57
MCP-1/CCL2	69,943	898-2094	51
MCP-3/CCL7	1,862	25-58	46
MCP-5/CCL12	3,421	60-140	48
MDC/CCL22	2,437	33-77	52
MIP-1α/CCL3	3,138	59-137	77
MIP-1β/CCL3	46,549	680-1585	75
MIP-3α/CCL20	3,140	69-161	12
MIP-3β/CCL19	38,168	413-962	64
RANTES/CCL5	8,605	164-381	55
SCYB16/CXCL16	2,476	44-103	65
SDF-1α/CXCL12	32,172	289-673	67
TARC/CCL17	24,874	250-583	63
TNF-α	23,984	544-1269	21

A.4 Flow cytometry

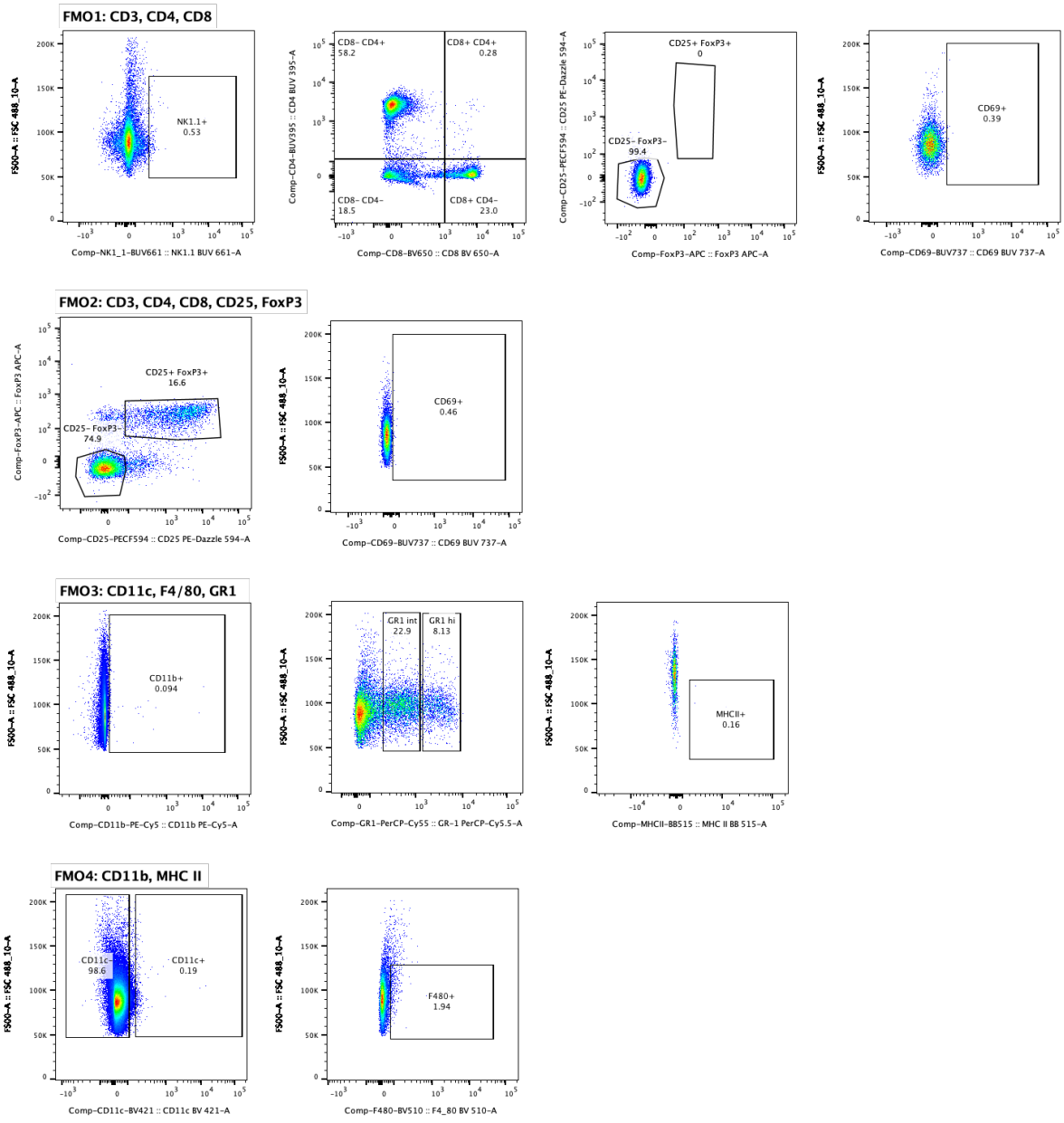

Figure A.1. FMO controls for flow cytometry. *Gates for immune cell populations in chapters 4 and 5 were set using fluorescence minus one (FMO) staining controls. (A) FMO1: CD3, CD4 and CD8 to set gates for NKT cells, Tregs and functional status (e.g., CD69). (B) FMO2: CD3, CD4, CD8, CD25, FoxP3 to set functional gates for Tregs (e.g., CD69). (C) FMO3: CD11c, F4/80 and GR1 to set gates for myeloid-derived suppressor cells (MDSCs) and macrophages. (D) FMO4: CD11b and MHC-II to set gates for MDSCs and macrophages.*

International Journal of
Molecular Sciences

MDPI

Review

Therapeutic Targeting of Collective Invasion in Ovarian Cancer

Laura Moffitt [1,2], Nazanin Karimnia [1,2], Andrew Stephens [1,2] and Maree Bilandzic [1,2,*]

[1] Hudson Institute of Medical Research, Clayton VIC 3168, Australia; lrmof1@student.monash.edu (L.M.); nazanin.karimnia@monash.edu (N.K.); andrew.n.stephens@hudson.org.au (A.S.)
[2] Department of Molecular and Translational Sciences, Monash University, Clayton VIC 3800, Australia
* Correspondence: bilandzic@hudson.org.au; Tel.: +61-385722693

Received: 26 February 2019; Accepted: 15 March 2019; Published: 22 March 2019

Abstract: Ovarian cancer is the seventh most commonly diagnosed cancer amongst women and has the highest mortality rate of all gynaecological malignancies. It is a heterogeneous disease attributed to one of three cell types found within the reproductive milieu: epithelial, stromal, and germ cell. Each histotype differs in etiology, pathogenesis, molecular biology, risk factors, and prognosis. Furthermore, the origin of ovarian cancer remains unclear, with ovarian involvement secondary to the contribution of other gynaecological tissues. Despite these complexities, the disease is often treated as a single entity, resulting in minimal improvement to survival rates since the introduction of platinum-based chemotherapy over 30 years ago. Despite concerted research efforts, ovarian cancer remains one of the most difficult cancers to detect and treat, which is in part due to the unique mode of its dissemination. Ovarian cancers tend to invade locally to neighbouring tissues by direct extension from the primary tumour, and passively to pelvic and distal organs within the peritoneal fluid or ascites as multicellular spheroids. Once at their target tissue, ovarian cancers, like most epithelial cancers including colorectal, melanoma, and breast, tend to invade as a cohesive unit in a process termed collective invasion, driven by specialized cells termed "leader cells". Emerging evidence implicates leader cells as essential drivers of collective invasion and metastasis, identifying collective invasion and leader cells as a viable target for the management of metastatic disease. However, the development of targeted therapies specifically against this process and this subset of cells is lacking. Here, we review our understanding of metastasis, collective invasion, and the role of leader cells in ovarian cancer. We will discuss emerging research into the development of novel therapies targeting collective invasion and the leader cell population.

Keywords: ovarian cancer; leader cells; metastasis; therapies; invasion

1. Ovarian Cancer: A Unique Mode of Metastasis

Whilst the molecular mechanisms driving metastasis are often similar across different tumour types, in ovarian cancer, hematogenous intravasation/extravasation comes secondary to passive peritoneal dissemination. Indeed, even the most aggressive, high-grade ovarian cancers rarely metastasize beyond the peritoneum, and this remains a poorly understood characteristic of the disease [1–4].

Local invasion of ovarian cancer cells to neighbouring tissues occurs by direct extension from the primary tumour; whereas dissemination to distal sites within the peritoneum occurs by passive movement of ovarian cancer spheres within the peritoneal fluid or ascites [5]. In the latter route, ovarian cancer cells destined for exfoliation from the primary tumour acquire a unique expression profile, where both epithelial and mesenchymal markers are co-expressed. This "cadherin switch" involves the overexpression of transcription factors including ZEB1, TWIST, and Slug and Snail

resulting in the upregulation of E-cadherin, activation of mesenchymal markers N-cadherin and Vimentin, and acquisition of an epithelial–mesenchymal transition (EMT)-like phenotype [6,7]. The remodelling of the ovarian epithelium is further dependent on integrin-mediated upregulation of matrix metalloproteinases (MMPs), which in turn facilitate the ectodomain shedding of E-cadherin, resulting in decreased cell–cell adhesion and the detachment of ovarian cancer cells from the primary tumour into the peritoneal cavity (Figure 1). Within the peritoneal cavity, ovarian cancer cells tend to form multicellular aggregates termed "spheroids" [8]. The presence of anchorage-independent spheroids complicates disease management and indicates a poor prognosis, as spheroids exhibit an increased propensity to survive chemotherapies and seed multiple distal metastases [9,10].

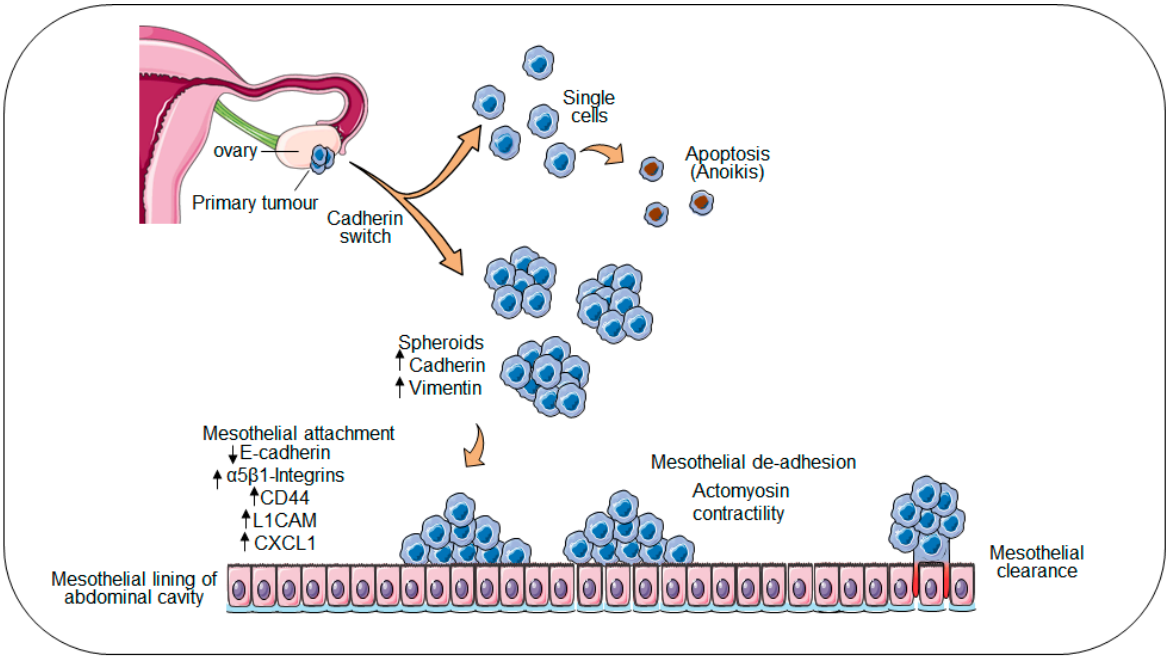

Figure 1. Metastasis model in ovarian cancer. A schematic model of ovarian cancer progression and dissemination. Ovarian cancer cells in the primary tumour acquire a unique expression profile and are exfoliated from the primary tumour site into the ascites. Ovarian cancer cells which have shed form multicellular aggregates are termed spheroids.erin. Spheres are carried passively within the peritoneum by the peritoneal fluid or ascites where they seed multiple distal metastasis by attaching to and clearing the mesothelial lining.

Whilst establishing secondary nodules, metastatic ovarian cancer cells interact with the single-cell layer of mesothelium lining the peritoneal cavity and organs, superficially attaching to and invading the underlying matrix [2,4,11]. In the period between apposition at the peritoneal lining and invasion of the underlying extracellular matrix (ECM), transcriptional "reprogramming" switches tumour cells from a proliferative to invasive physiology to facilitate degradation of the underlying matrix [12]. This process occurs universally in all ovarian cancer patients, the majority of whom are initially diagnosed with metastatic disease and persists in the >90% of patients who experience relapse following treatment. Spheroid adhesion to peritoneal surfaces is mediated directly through interactions between the cancer spheroid and receptors on the surface of the mesothelial layer. Decreased E-cadherin expression on the outer surface of the spheroid induces the expression of adhesion receptor molecules including CD44 and several integrins [13–15], priming spheroids for subsequent attachment to ECM proteins on the surface of the mesothelium [2,4,11,16]. Studies have shown that the interaction between spheroid expressed α5β1-integrin and mesothelial expressed fibronectin is essential for spheroid adhesion to the mesothelium [17,18]. Likewise, αvβ3-integrin was shown to be key to the proliferative and invasive behaviour of ovarian cancer cells [19]. In vitro

inhibition of the α3, α6, and β1 integrin subunits in ovarian cancer spheres decreased invasiveness and collagen binding. Further, the inhibition of α2β1-integrin abolished the ability of ovarian cancer spheres to disaggregate on an artificial ECM [20,21].

Studies examining CD44 blockade demonstrated a reduction in the number of secondary tumours formed, but it was not sufficient to inhibit the mesothelial adhesion of ovarian cancer cells [15]. Cell adhesion molecule L1 (L1CAM) has also been shown to modulate the adhesion of ovarian cancer spheroids to the mesothelium by interacting with mesothelial neuropilin-1 receptors (NRP-1) [22]. An L1CAM specific antibody reduced murine peritoneal metastases [23] and prolonged survival when used in conjugation with radiotherapy in animal studies [24]. Further, the fractalkine receptor (CX_3CR1) expressed by ovarian cancer cells has also been demonstrated to mediate ovarian cancer cell adhesion to mesothelium by interacting with its ligand CXCL1 present on the surface of mesothelial cells' surface [22]. siRNA-mediated downregulation of CX_3CR1 reduced the adhesion of SKOV3 cells to mesothelial LP9 cells by 50% [25]. Once ovarian tumour spheroids are attached to the mesothelium, they initiate infiltration and spread to surrounding tissue.

2. Collective Invasion and Leader Cells

Multicellular clusters of ovarian cancer cells migrate in a directed and coordinated fashion in a process called collective invasion [26]. Three key characteristics defining collective invasion are: (i) the preservation of the physical connections and cell–cell junctions to orchestrate collective movement; (ii) shared cytoskeletal dynamics, allowing groups of cells to proceed as a single unit and develop multicellular polarity; and (iii) interactions with other cells and the ECM along the migratory path [26–28]. Collective invasion is a fundamental property of many metastatic tumours in human cancers, particularly epithelial tumours [29,30] including pancreatic cancer [31], colon cancer [32], sebaceous cancer [33], melanoma [34], breast cancer [35–37], and lung cancer [38].

Despite the applicability of the basic principles governing single-cell migration to collective migration, the molecular events controlling collective invasion are far more intricate and not all cells within the cluster are invasion-competent [26]. Collective invasion is driven by "leader cells", a functionally distinct sub-population of cancer cells that direct migration, promote changes in cellular contractility, and lead the trailing "follower" cells [39]. In breast and bladder cancers, mesenchymal-like leader cells maintain distinct cellular polarity, form protrusive filopodia, and respond dynamically to environmental cues [28,37,40]. The follower population retains expression of adhesion junctional proteins and maintain a packed morphology [36,41].

During collective invasion (illustrated in Figure 2) cytoskeletal polarisation establishes a front–rear axis within the cluster. Leader cells at the front axis undergo supra-cellular cytoskeletal organization by rearranging their actin filaments, facilitating membrane protrusion and the formation of invadopodia. This process requires activation of phosphoinositide 3-kinase (PI3K) [42] and GTPase proteins, including cell division cycle 42 (Cdc24) and Ras-related C3 botulinum toxin substrate (Rac), to rearrange the cytoskeleton and induce actin expression. Concurrently, Rho signalling at the posterior side mediates actomyosin contraction, generating the force required for cellular movement [28,43]. The leader cells then enable the penetration of the basement membrane comprised of collagen I and IV, laminin, and fibronectin [44] through the expression of proteolytic enzymes including MMPs and other serine proteinases [45].

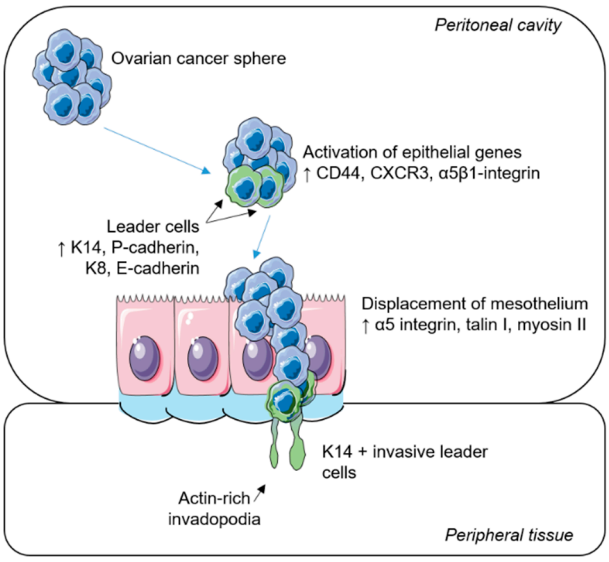

Figure 2. Collective invasion in epithelial ovarian cancer. A schematic representation of the metastatic spread of ovarian tumour cells. Ovarian cancer spheres diffuse throughout the peritoneal cavity. Upon their attachment to the mesothelial layer, epithelial genes are activated. Specialized leader cells transiently express basal epithelial and luminal epithelium markers and displace the target mesothelium via the formation of actin-rich invadopodia, where trailing cells follow to colonize surrounding tissues.

In addition to proteolytic enzymes, cancer associated fibroblasts (CAFs) are abundantly present within the tumour microenvironment (TME) and play a crucial role in mediating collective invasion. Further, CAFs induce changes including physically remodelling the TME to lay "tracks" for invading cancer cells [46]. Cancer associated fibroblasts further drive collective invasion, by mediating the heterophilic adhesion between membrane E-cadherin on the tumour cell and N-cadherin on the CAF [47]. These changes within the TME further ensure the epithelial phenotype of invading cells is retained [48].

3. Leader Cells and Progenitor-Like Properties

A unique feature of leader cells is their high degree of transcriptional plasticity, making them distinct from cells undergoing EMT and the follower cell population alike. In breast cancer, leader cells co-express multiple basal epithelial markers such as KRT14, KRT5, P63, and P-cadherin, in conjunction with markers of the luminal epithelium including KRT8, KRT18, and E-cadherin, marking them as a progenitor-like population [37]. Leader cells may also secrete immune effector molecules, influencing lymphocyte differentiation and polarizing local immune responses towards a suppressive phenotype [49]. Several studies have now demonstrated the importance of leader cells in the progression of epithelial-tumour types including breast, salivary, bladder, prostate, and lung cancers [36,38,49–51].

Several lines of evidence suggest that KRT14+ cells possess similar features to cancer stem cells (CSCs). In a bladder regeneration mouse model, KRT14+ cells exhibited increased clonogenicity and gave rise to multiple differentiated progeny; in fact, this KRT14+ cell population was an absolute requirement for the re-establishment of epithelial cell layers following damage [49]. Similarly, KRT14+ cell "stemness" was demonstrated in vivo using breast cancer mouse models [36]. In particular, KRT14+ cells were highly enriched in disseminated micro-metastases (accounting for over 50% of cells present); over time, however, the KRT14+ cell population reverted to baseline levels, in keeping with their transcriptional plasticity [36]. Other studies have also demonstrated that leader cells are enriched in response to chemotherapy and promote the acquisition of chemo-resistance over time, characteristics reflective of CSC status [37,52,53]. Together, these studies highlight the requirement of leader cells for metastasis and their potential roles as CSCs in epithelial tumours [54].

Our own studies have shown KRT14 expression is confined to the leading edge of ovarian cancer cells in both 2D and 3D format with KRT14 ablation rendering ovarian cancer cells invasion incompetent.

4. Targeting Leader Cells as a Novel Approach to Ovarian Cancer Management

Current first-line treatment methods for high grade serous ovarian cancer involve surgical debulking and adjuvant chemotherapy using platinum and taxane drugs. Unfortunately, remission is generally short-lived, and recurrence occurs in at least 90% of patients [55]. Several emerging therapies and combination strategies have shown initial promise, but as of yet, none have achieved long-term disease regression in the broader context of disease. Ultimately, repeated rounds of chemotherapies result in the emergence of chemo-resistant disease for the vast majority of patients, limiting further available treatment options.

Whilst the majority of traditional anti-cancer drugs target the proliferative behaviour of tumour cells, it is the invasive propensity of malignant cells that leads to metastasis and ultimately accounts for overall morbidity and mortality [56]. As the drivers of solid cancer migration and metastasis, inhibition of the leader cell component represents an attractive and potentially promising new approach for cancer treatment. In particular, therapies designed to eliminate leader cells in tumours are likely pivotal to achieve sustained remission for patients with ovarian cancers. However, complete definition of the transcriptional, epigenetic, and proteomic signatures of leader cells—in a variety of solid cancer types—is required before specifically targeted molecular therapies become available.

Below, we discuss existing, emergent, and potential therapeutic approaches that may be effective for targeted leader cell depletion.

5. Current Standard-of-Care in Ovarian Cancer Therapy

Amongst a plethora of ongoing clinical trials, immunotherapies (including checkpoint inhibitors and antibodies against growth factors or signalling molecules) and PARP inhibitors have proven the most widely examined for their potential to manage an otherwise terminal disease. Immune checkpoint inhibitors (e.g., Keytruda^{TM} and Avelumab^{TM}) and immune modulators that have been successful in other cancer types have shown only limited efficacy in ovarian cancer trials [57,58]. Likewise, epidermal growth factor and folate receptor targeting therapies have revealed disappointing results [59,60]. Antiangiogenic therapies have only shown a marginal increase to progression-free survival (PFS) (2–6 months) outweighed by both the high cost involved with drug administration and the toxic side-effects experienced by patients [61].

Achieving greater success are the PARP inhibitors, indicated for the treatment of ovarian cancer patients carrying BRCA mutations [62]. In ovarian cancer patients with hereditary BRCA mutations, the PARP inhibitor Olaparib^{TM} significantly increased PFS from 5.5 to 30.2 months [63]. Similarly, the PARP inhibitor Niraparib^{TM} improved PFS in all ovarian cancer patients; with the highest efficacy observed in BRCA mutation carriers (increased PFS by 15.5 months compared to the placebo [64]). Each of these inhibitors are associated with adverse haematological effects, readily managed by dose modification [64]. The impact of these drugs in non-BRCA mutated, chemo-resistant patients is the subject of ongoing clinical trials. The PARP inhibitors are now the standard of care for patients with recurrent, BRCA-mutated ovarian cancer; however, they bear costs that are up to eight times that of platinum-based care.

6. Targeting Leader Cell-Directed Processes: Collective Invasion and the Invasive Front

Metastatic disease is commonly associated with resistance to conventional treatments such as chemotherapy [65]. Fundamental to metastasis are the molecular and morphological changes associated with EMT during invasion. The transient nature of EMT and difficulties in comprehensively defining this state means that the inhibition of EMT-related processes is challenging; however, and few druggable targets have been identified [66]. By contrast, collective invasion and the processes of intra- and extravasation are a common feature of many solid cancer types including

ovarian [67,68]; and increasing evidence suggests that leader cells are pivotal drivers of these processes. Directly targeting leader cells, and the processes they regulate may thus serve as a promising approach to combat metastatic disease.

The complex nature of metastasis suggests that multiple therapeutic targets should exist for directed interventions. Indeed, ongoing research has targeted two key areas: disruption of collective invasion and the impairment of attachment and invasion-related processes at the spheroid–mesothelial interface. Clear molecular definition of the leader cell phenotype is required, however, before specifically directed molecular therapies aimed at ablation of these cells in established tumours can be developed.

7. Strategies to Inhibit Collective Invasion in Ovarian Cancers

7.1. Cytoskeletal Stability

Several studies have examined the potential of a "migrastatic" approach, using drugs broadly targeting cytoskeletal stability (e.g., actin polymerization or stabilization), cellular contractility, and ion transport to prevent the formation of invadopodia, and thus inhibit metastasis [69]. Whilst promising in vitro for the inhibition of lung, melanoma [70], and prostate cancer [71] outgrowth, the failure of anti-actin drugs to discriminate between malignant and normal cells in vivo presents an unfavourable toxicity profile [70,71]. A second class of inhibitors, targeting actin-binding proteins tropomyosin and myosin to inhibit actin assembly and function, have also been proposed as a less toxic, more suitable approach [72]. For example, the anti-tropomyosin compound TR-100 specifically disrupts the cytoskeleton of tumour cells and has been shown to effectively reduce tumour growth in melanoma and neuroblastoma mouse models [73]. Collective invasion may also be targeted by the myosin inhibitor Blebbistatin that works to decrease myosin activity in non-muscle cells. This compound has been shown to be effective at inhibiting invasion in a wide range of cancer cell lines; however, there are no published in vivo data available and its application has not been demonstrated for ovarian cancer [74].

7.2. Rho Kinase Inhibition

Targeting the specific kinases and phosphatases that regulate phosphorylation cascades involved in actin polymerisation are also a potentially useful approach [75,76]. Rho GTPases are important regulators of cytoskeletal dynamics and play a significant role in cancer cell migration and invasion [77]. Highly localised RhoA activity is observed at the leading tip of invadopodia emerging from kidney epithelial cells, associated with actin filament activation during invasion [78]. Whilst not yet demonstrated in ovarian cancer, RhoA is overexpressed in metastatic omental ovarian cancer deposits [79]. Moreover, RhoA overexpression increases ovarian cancer cell invasiveness in vitro, and nude mice implanted with RhoA overexpressing cells developed a significantly greater number of disseminated tumours [80]. Accordingly, knockdown of RhoA decreased migration and invasion in vitro and reduced ascites accumulation and peritoneal dissemination in nude mice [81].

Interestingly, a recent study reported decreased RhoA expression in lung cancer leader cells following silencing of KRT14 [82]. These cells exhibited decreased invasion and migration in vitro, strongly suggesting a key role for RhoA/Rho-associated kinase (ROCK) signalling in leader cells [82]. Accordingly, targeting of RhoA signalling by the HMG-CoA reductase inhibitor Lovastatin re-sensitized chemo-resistant ovarian cancer cell lines to doxorubicin in vitro [83]. The combination of Lovastatin with chemotherapy has yet to be tested in clinical trials.

ROCK, a downstream effector of RhoA signalling, has also been suggested as a therapeutic target for the management of metastatic disease. Following activation by RhoA, ROCK I/II phosphorylates substrates including the myosin phosphatase (MYPT1) and myosin regulatory light chain (MLC) to promote cytoskeletal rearrangement and cellular contractility [84]. The ROCK inhibitor Fasudil (HA-1077) [85] has shown promising results in vitro and in vivo in several cancer types including

brain, lung, liver, and ovarian cancers [86–89]. Tumour priming with Fasudil in pancreatic cancer mouse models and patient-derived xenografts improved response to chemotherapy at secondary sites and reduced metastatic spread [90].

In ovarian cancers, Fasudil attenuated lysophosphatidic acid (LPA)-induced ovarian cancer cell migration and invasiveness and reduced the intraperitoneal spread of cancer cells in a mouse xenograft model [91]. Similarly, the ROCK inhibitor Y27632 [92] also decreased LPA-induced invasiveness of ovarian cancer lines Caov3 and PA-1 [93]. Fasudil also enhanced sensitivity to cisplatin in A2780 ovarian cancer cells in vitro, suggesting its potential synergy with chemotherapy [94]. Whilst Fasudil has not progressed to human trials for metastatic disease, the novel ROCK I/II inhibitor AT13148 [95] is currently in phase I clinical trials for patients with advanced breast, prostate, and ovarian tumours (NCT01585701). AT13148 induced a wide range of side-effects impacting on the cardiovascular system including smooth muscle contractility, tachycardia, and high-blood pressure, which were alleviated by modifying the administered dose [96]. The effects of Rho/ROCK inhibition are likely to be cancer-type-specific; however, for example, by contrast to results in ovarian cancer cells, Y27632 increased the invasive potential of human glioma U87 and U251 cells [97] and gastric carcinoma OCUM-2MD3 cells [98]. Indeed, ROCK activation is not always oncogenic, and the specific role of ROCK is cell-type and tumour-microenvironment dependent [99].

7.3. Other Kinase Targets

Alongside established roles in proliferation and angiogenesis, Src-kinase is now gaining interest as a mediator of cellular motility and the formation of invadopodia. Src is overexpressed in several solid cancers including breast, colon, and ovarian cancer [100,101], and is essential for breast cancer invadopodia formation via downstream regulators such as cortactin and Tsk5 [102]. Cortactin is localised in breast cancer cell invadopodia, where it regulates actin stabilisation and the recruitment of ECM proteases to the invasive interface [103]. In vitro studies using the Src inhibitors dasatinib and saracatinib showed high efficacy in preventing metastasis in several cancer models including pancreatic, prostate, and ovarian cancers [104]. Unfortunately, these inhibitors did not reach their anticipated heights in clinical trials where phase II trials of Dasatinib in women with recurrent epithelial ovarian cancer or peritoneal carcinoma (NCT00671788) showed no significant increase to PFS [105].

Other multi-kinase inhibitors such as cabozantinib and sorafenib are currently being evaluated in clinical trials for the treatment of metastatic epithelial ovarian cancer; however, most have been met with limited success and exhibit significant toxicity (Table 1) [106–111]. The potential off-target effects associated with inhibition of cell contractility present a major challenge for the development of these "anti-metastatic" drugs, where effects on normal physiological processes including wound healing, cell division, and the immune cells must be minimized. Despite the development of second-generation kinase inhibitors designed to increase specificity and limit the off-target effects on normal tissue, their efficacy in vivo has yet to be demonstrated [112].

Table 1. Selected targeted drugs in clinical trials for the treatment of metastatic ovarian cancer.

Drug	Target	Clinical Trial ID	Phase	Outcome Measures	Current Status	Refs
Lovastatin	RhoA	NCT00585052	II	Tumour response rate in combination with paclitaxel for patients with relapsed ovarain cancer	Terminated due to slow accrual.	[113]
AT13148	Multi-AGC kinase	NCT01585701	I	Determine dosing and adverse events. Evaluate any response in patients with advanced-stage solid tumours including prostate, breast, and ovarian.	Completed. Preliminary data indicate tolerable on target effects.	[96,114]
Dasatinib	Src kinase	NCT00671788	II	Progression Free Survivial at 6 months and tumour response in persistent or recurrent epithelial ovarian cancer using dasatinib as a monotherapy	Completed. dasatinib has minimal activity as a single agent in ovarian cancer (PFS 2.1 months).	[105,115]
Cabozantinib	Multi-kinases	NCT00940225	II	Evaluate overall response rate and PFS in patients with advanced malignancies including melanoma, breast and ovarian cancer	Completed. Ovarian cancer patients showed the highest overall response rate (21.7%) and disease control rate was 50%. Platinum-sensitive patients achieved a longer PFS (6.9 months) than platinum-resistant patients (2.8 months).	[106,108,116]
		NCT01716715	II	Compare PFS in patients with persistent or recurrent ovarian cancer patients receiving cabozantinib or paclitaxel	Ongoing.	[117]
Sorafenib		NCT00093626	II	Assess adverse events and PFS time in patients with persistent or recurrent ovarian cancer	Completed. Significant toxicity as a monotherapy with modest anti-tumour effect (PFS 2.1 months).	[109,118]
		NCT00526799	I/II	Tolerability (Phase I) and response rate (Phase II) to treatment with sorafenib in combination with topotecan in patients with platinum-resistant or refractory-recurrent ovarian cancer	Terminated. Significant toxicity caused by sub-optimal doses of combination therapy associated with minimal clinical efficacy.	[110,119]
		NCT00390611	II	PFS over 2 years in patients with late-stage ovarian cancer receiving sorafenib in first-line treatment	Completed. Combination paclitaxel/carboplatin or paclitaxel/carboplatin/sorafenib had similar response rates and PFS (15.4 vs 16.3 months). The addition of sorafenib in first-line treatment caused increased toxicity.	[111,119]
Volociximab	α5β1-integrin	NCT00516841	II	Evaluate efficacy of volociximab monotherapy by objective response rate and tumour response in patients with platinum resistant EOC	Terminated due to insufficient clinical activity. Volociximab was well tolerated; however, there were no complete or partial responses.	[120,121]
Ketorolac	Rac1/Cdc42	NCT01670799	0 (Pilot)	Determine measurable R- and S-ketorolac in post-operative treated patients following cytoreductive ovarian cancer surgery	Ongoing.	[122]
		NCT02470299	I	Confirmation of drug specificity. Evaluation of overall survival and PFS in post-operative IV ketorolac treated ovarian cancer patients	Recruiting/ongoing. Preliminary data shows specific Rac1 and Cdc42 inhibition and potential prolonged survival in women receiving ketorolac.	[123,124]

8. Strategies to Disrupt Attachment and Invasion at the Invasive Interface

As key regulators of the metastatic cascade, leader cells define the interactions that occur between the invasive cancer deposit, ECM proteins at the target site, and the underlying healthy tissue sub-stratum tissue. During invasion, emerging cancer invadopodia comprised of leader cells must attach and degrade extracellular components including collagen IV, laminin, and proteoglycans to successfully overcome the basement membrane barrier and infiltrate peripheral tissue [125]. As previously mentioned, integrin-mediated interactions with ECM proteins on the mesothelial interface are essential for the adhesion of ovarian cancer spheroids at the site of invasion. In a xenograft mouse model of ovarian cancer, the anti-α5β1-integrin antibody Volociximab reduced tumour burden and was well tolerated in a phase I clinical trial [126]. However, in a phase II clinical

trial in women with platinum resistance and advanced epithelial ovarian cancer, volociximab was not significantly effective at preventing disease progression and was associated with adverse events (NCT00516841) [120]. Other antibodies have also been developed to target the αv-integrin family. The pan-anti-αv-integrin antibody intetumumab was shown to inhibit adhesion, migration, and invasion in breast cancer cells in vitro and reduced tumour growth and metastasis in mouse models [127]. Intetumumab treatment in stage IV melanoma patients did not significantly improve overall survival [128]. Similarly, etaracizumab (anti-αvβ3-integrin) only demonstrated a marginal increase to PFS in a phase II trial of metastatic melanoma [129]. Despite their promise in preclinical studies, anti-integrin antibody therapies have failed to demonstrate clinically meaningful improvements to PFS compared to standard treatments thus far, and have not progressed to trials in ovarian cancer patients [130].

In addition, MMPs are actively involved in the proteolytic degradation of the ECM and are commonly overexpressed in invasive cancers [131]. A key mediator of collective invasion is MT1-MMP (MMP-14), which accumulates at the invasive front of tumours and is upregulated on the surface of breast cancer invadopodia [102,132]. MT1-MMP directly degrades ECM components in addition to activating other MMPs at the tumour–stromal interface [133]. Most MMP inhibitors have limited specificity resulting in extensive off-target effects, and this class of inhibitors have been largely unsuccessful in clinical trials [45]. The monoclonal antibody DX-2400 specifically inhibits MT1-MMP and has shown promise by blocking invasion and migration in vitro. Further, in vivo DX-2400 delayed tumour growth and metastasis alone and in combination with paclitaxel in mouse breast cancer xenograft models [134]. However, this potent MT1-MMP inhibitor has yet to progress to clinical trials.

An alternative approach to directly targeting ECM proteases such as the MMPs may be to inhibit proteins involved in their intracellular trafficking or regulators of their expression. For example, multiple studies have proposed that the molecular mechanisms of inhibitors of RhoA and ROCK (described above) involve the downregulation of MMP-2 and MMP-9 which are present at the invasive front of many cancers [88,135]. Furthermore, our own preliminary studies in ovarian cancer have indicated that MMP-10 and MMP-13 may interact with the serine protease DPP4 at the cell surface, for which there are clinically available inhibitors.

9. Molecular Targets in Leader Cells

Although the targets described above are involved in the general metastatic pathway, their specific relationship to the leader cell phenotype is not completely understood. In particular, the molecular genetic phenotype of leader cells may differ between cancer types, disease location, grade or stage; thus, the identification of exclusive, cell-type-specific targets represents one of the greatest barriers for the development of directed, clinically relevant therapies.

Despite these limitations, however, new targets are emerging. Yamaguchi et al. [136] recently identified active upregulation of Rac, PI3K, and integrin β1 as specific markers of epithelial kidney leader cells that contribute to collective cell migration. Pharmacological inhibition of each of these targets individually was effective in disrupting collective cell migration. Specifically, the authors were able to demonstrate that the migration of leader cells was dependent on Rac1 activity and was likely via a downstream feedback loop involving the independent actions of PI3K and integrin β1 [136]. Rac1 and associated signalling molecules are overexpressed in epithelial ovarian cancer.

High-throughput screening and structural homology approaches identified a small molecule inhibitor, R-Ketorolac, which specifically targets Rac1 and the related protein Cdc42. In ovarian cancer cell lines, R-Ketorolac was found to decrease cell adhesion, migration, and invasion and effectively prevented Cdc42-dependent invadopodia formation [137]. In a retrospective "Phase 0" trial, ovarian cancer patients receiving ketorolac for post-operative analgesia had an increased overall survival probability compared to the placebo-treated control group, where 18% of Ketorolac-treated patients succumbed to the disease after 5 years, compared to 43% of non-treated patients [123]. The specificity and efficacy of post-operative Ketorolac in a small cohort of ovarian cancer patients

undergoing cytoreductive surgery is the subject of an ongoing clinical trial in the recruitment phase (NCT02470299).

Metastatic disease is the most significant challenge to the management of all types of cancer and accounts for more than 90% of cancer-related suffering and death. The vast majority of ovarian cancer patients are diagnosed with late-stage metastatic disease, and current treatment methods are not effective as most patients experience relapse. We anticipate future studies defining this unique subset of leader cells will facilitate the development of effective targeted therapeutics. Leader cell targeting serves as an exciting emerging area of research offering highly novel approaches to promote tumour regression and increase management options available for late-stage disease.

Acknowledgments: We thank the Victorian Government's Operational Infrastructure Support Program. L.M. is supported by the Monash University RTP Stipend, N.K. is supported by the Sue Fowler Scholarship in Ovarian Cancer, M.B. the Fielding Foundation Innovation award, A.S. is an Ovarian Cancer Research Foundation Fellow. This research received no external funding.

Conflicts of Interest: The authors declare no conflicts of interests.

References

1. Tan, D.S.; Agarwal, R.; Kaye, S.B. Mechanisms of transcoelomic metastasis in ovarian cancer. *Lancet Oncol.* **2006**, *7*, 925–934. [CrossRef]
2. Kenny, H.A.; Krausz, T.; Yamada, S.D.; Lengyel, E. Use of a novel 3D culture model to elucidate the role of mesothelial cells, fibroblasts and extra-cellular matrices on adhesion and invasion of ovarian cancer cells to the omentum. *Int. J. Cancer* **2007**, *121*, 1463–1472. [CrossRef] [PubMed]
3. Burleson, K.M.; Hansen, L.K.; Skubitz, A.P. Ovarian carcinoma spheroids disaggregate on type I collagen and invade live human mesothelial cell monolayers. *Clin. Exp. Metastasis* **2004**, *21*, 685–697. [CrossRef] [PubMed]
4. Burleson, K.M.; Boente, M.P.; Pambuccian, S.E.; Skubitz, A.P. Disaggregation and invasion of ovarian carcinoma ascites spheroids. *J. Transl. Med.* **2006**, *4*, 6. [CrossRef] [PubMed]
5. Ahmed, N.; Stenvers, K. Getting to Know Ovarian Cancer Ascites: Opportunities for Targeted Therapy-Based Translational Research. *Front. Oncol.* **2013**, *3*, 256. [CrossRef]
6. Patel Ila, S.; Madan, P.; Getsios, S.; Bertrand Monique, A.; MacCalman, C.D. Cadherin switching in ovarian cancer progression. *Int. J. Cancer* **2003**, *106*, 172–177. [CrossRef]
7. Lengyel, E. Ovarian cancer development and metastasis. *Am. J. Pathol.* **2010**, *177*, 1053. [CrossRef]
8. Elloul, S.; Silins, I.; Trope, C.G.; Benshushan, A.; Davidson, B.; Reich, R. Expression of E-cadherin transcriptional regulators in ovarian carcinoma. *Virchows Arch* **2006**, *449*, 520–528. [CrossRef]
9. Aguilar-Gallardo, C.; Rutledge, E.C.; Martinez-Arroyo, A.M.; Hidalgo, J.J.; Domingo, S.; Simon, C. Overcoming challenges of ovarian cancer stem cells: Novel therapeutic approaches. *Stem Cell Rev.* **2012**, *8*, 994–1010. [CrossRef]
10. Liao, J.; Qian, F.; Tchabo, N.; Mhawech-Fauceglia, P.; Beck, A.; Qian, Z.; Wang, X.; Huss, W.J.; Lele, S.B.; Morrison, C.D.; et al. Ovarian cancer spheroid cells with stem cell-like properties contribute to tumor generation, metastasis and chemotherapy resistance through hypoxia-resistant metabolism. *PLoS ONE* **2014**, *9*, e84941. [CrossRef]
11. Sodek, K.L.; Murphy, K.J.; Brown, T.J.; Ringuette, M.J. Cell-cell and cell-matrix dynamics in intraperitoneal cancer metastasis. *Cancer Metastasis Rev.* **2012**, *31*, 397–414. [CrossRef]
12. Yeung, T.L.; Leung, C.S.; Yip, K.P.; Au Yeung, C.L.; Wong, S.T.; Mok, S.C. Cellular and molecular processes in ovarian cancer metastasis. A Review in the Theme: Cell and Molecular Processes in Cancer Metastasis. *Am. J. Physiol. Cell Physiol.* **2015**, *309*, C444–C456. [CrossRef] [PubMed]
13. Sawada, K.; Mitra, A.K.; Radjabi, A.R.; Bhaskar, V.; Kistner, E.O.; Tretiakova, M.; Jagadeeswaran, S.; Montag, A.; Becker, A.; Kenny, H.A.; et al. Loss of E-cadherin promotes ovarian cancer metastasis via alpha 5-integrin, which is a therapeutic target. *Cancer Res.* **2008**, *68*, 2329–2339. [CrossRef] [PubMed]
14. Cannistra, S.A.; Kansas, G.S.; Niloff, J.; DeFranzo, B.; Kim, Y.; Ottensmeier, C. Binding of ovarian cancer cells to peritoneal mesothelium in vitro is partly mediated by CD44H. *Cancer Res.* **1993**, *53*, 3830–3838. [PubMed]

15. Strobel, T.; Swanson, L.; Cannistra, S.A. In vivo inhibition of CD44 limits intra-abdominal spread of a human ovarian cancer xenograft in nude mice: A novel role for CD44 in the process of peritoneal implantation. *Cancer Res.* **1997**, *57*, 1228–1232.
16. Kenny, H.A.; Chiang, C.Y.; White, E.A.; Schryver, E.M.; Habis, M.; Romero, I.L.; Ladanyi, A.; Penicka, C.V.; George, J.; Matlin, K.; et al. Mesothelial cells promote early ovarian cancer metastasis through fibronectin secretion. *J. Clin. Investig.* **2014**, *124*, 4614–4628. [CrossRef] [PubMed]
17. Casey, R.C.; Burleson, K.M.; Skubitz, K.M.; Pambuccian, S.E.; Oegema, T.R., Jr.; Ruff, L.E.; Skubitz, A.P. Beta 1-integrins regulate the formation and adhesion of ovarian carcinoma multicellular spheroids. *Am. J. Pathol.* **2001**, *159*, 2071–2080. [CrossRef]
18. Iwanicki, M.P.; Davidowitz, R.A.; Ng, M.R.; Besser, A.; Muranen, T.; Merritt, M.; Danuser, G.; Ince, T.A.; Ince, T.; Brugge, J.S. Ovarian cancer spheroids use myosin-generated force to clear the mesothelium. *Cancer Discov.* **2011**, *1*, 144. [CrossRef]
19. Landen, C.N.; Kim, T.J.; Lin, Y.G.; Merritt, W.M.; Kamat, A.A.; Han, L.Y.; Spannuth, W.A.; Nick, A.M.; Jennnings, N.B.; Kinch, M.S.; et al. Tumor-selective response to antibody-mediated targeting of alphavbeta3 integrin in ovarian cancer. *Neoplasia* **2008**, *10*, 1259–1267. [CrossRef]
20. Shield, K.; Riley, C.; Quinn, M.A.; Rice, G.E.; Ackland, M.L.; Ahmed, N. Alpha2beta1 integrin affects metastatic potential of ovarian carcinoma spheroids by supporting disaggregation and proteolysis. *J. Carcinog.* **2007**, *6*, 11. [CrossRef]
21. Symowicz, J.; Adley, B.P.; Gleason, K.J.; Johnson, J.J.; Ghosh, S.; Fishman, D.A.; Hudson, L.G.; Stack, M.S. Engagement of collagen-binding integrins promotes matrix metalloproteinase-9-dependent E-cadherin ectodomain shedding in ovarian carcinoma cells. *Cancer Res.* **2007**, *67*, 2030–2039. [CrossRef] [PubMed]
22. Stoeck, A.; Schlich, S.; Issa, Y.; Gschwend, V.; Wenger, T.; Herr, I.; Marme, A.; Bourbie, S.; Altevogt, P.; Gutwein, P. L1 on ovarian carcinoma cells is a binding partner for Neuropilin-1 on mesothelial cells. *Cancer Lett.* **2006**, *239*, 212–226. [CrossRef] [PubMed]
23. Arlt, M.; Novak-Hofer, I.; Gast, D.; Gschwend, V.; Moldenhauer, G.; Gruenberg, J.; Honer, M.; Schubiger, P.; Altevogt, P.; Krueger, A. Efficient Inhibition of Intra-Peritoneal Tumor Growth and Dissemination of Human Ovarian Carcinoma Cells in Nude Mice by Anti-L1-Cell Adhesion Molecule Monoclonal Antibody Treatment. *Cancer Res.* **2006**, *66*, 936–943. [CrossRef] [PubMed]
24. Knogler, K.; Gruenberg, J.; Zimmermann, K.; Cohrs, S.; Honer, M.; Ametamey, S.; Altevogt, P.; Fogel, M.; Schubiger, P.; Novak-Hofer, I. Copper-67 Radioimmunotherapy and Growth Inhibition by Anti-L1-Cell Adhesion Molecule Monoclonal Antibodies in a Therapy Model of Ovarian Cancer Metastasis. *Clin. Cancer Res.* **2007**, *13*, 603–611. [CrossRef] [PubMed]
25. Kim, M.; Rooper, L.; Xie, J.; Kajdacsy-Balla, A.A.; Barbolina, M.V. Fractalkine receptor CX(3)CR1 is expressed in epithelial ovarian carcinoma cells and required for motility and adhesion to peritoneal mesothelial cells. *Mol. Cancer Res.* **2012**, *10*, 11–24. [CrossRef] [PubMed]
26. Friedl, P.; Gilmour, D. Collective cell migration in morphogenesis, regeneration and cancer. *Nat. Rev. Mol. Cell Biol.* **2009**, *10*, 445–457. [CrossRef] [PubMed]
27. Montell, D.J. Morphogenetic Cell Movements: Diversity from Modular Mechanical Properties. *Science* **2008**, *322*, 1502–1505. [CrossRef]
28. Mayor, R.; Etienne-Manneville, S. The front and rear of collective cell migration. *Nat. Rev. Mol. Cell Biol.* **2016**, *17*, 97–109. [CrossRef]
29. Wang, X.; Enomoto, A.; Asai, N.; Kato, T.; Takahashi, M. Collective invasion of cancer: Perspectives from pathology and development. *Pathol. Int.* **2016**, *66*, 183–192. [CrossRef]
30. Friedl, P.; Locker, J.; Sahai, E.; Segall, J.E. Classifying collective cancer cell invasion. *Nat. Cell Biol.* **2012**, *14*, 777–783. [CrossRef]
31. Beerling, E.; Oosterom, I.; Voest, E.; Lolkema, M.; van Rheenen, J. Intravital characterization of tumor cell migration in pancreatic cancer. *Intravital* **2016**, *5*, e1261773. [CrossRef]
32. Sonoshita, M.; Itatani, Y.; Kakizaki, F.; Sakimura, K.; Terashima, T.; Katsuyama, Y.; Sakai, Y.; Taketo, M.M. Promotion of colorectal cancer invasion and metastasis through activation of NOTCH-DAB1-ABL-RHOGEF protein TRIO. *Cancer Discov.* **2015**, *5*, 198–211. [CrossRef]
33. Hesse, K.; Satzger, I.; Schacht, V.; Köther, B.; Hillen, U.; Klode, J.; Schaper, K.; Gutzmer, R. Characterisation of Prognosis and Invasion of Cutaneous Squamous Cell Carcinoma by Podoplanin and E-Cadherin Expression. *Dermatology* **2016**, *232*, 558–565. [CrossRef]

34. Hegerfeldt, Y.; Tusch, M.; Brocker, E.B.; Friedl, P. Collective cell movement in primary melanoma explants: Plasticity of cell-cell interaction, beta1-integrin function, and migration strategies. *Cancer Res.* **2002**, *62*, 2125–2130.
35. Ewald, A.J.; Huebner, R.J.; Palsdottir, H.; Lee, J.K.; Perez, M.J.; Jorgens, D.M.; Tauscher, A.N.; Cheung, K.J.; Werb, Z.; Auer, M. Mammary collective cell migration involves transient loss of epithelial features and individual cell migration within the epithelium. *J. Cell Sci.* **2012**, *125 Pt 11*, 2638–2654. [CrossRef]
36. Cheung, K.J.; Padmanaban, V.; Silvestri, V.; Schipper, K.; Cohen, J.D.; Fairchild, A.N.; Gorin, M.A.; Verdone, J.E.; Pienta, K.J.; Bader, J.S.; et al. Polyclonal breast cancer metastases arise from collective dissemination of keratin 14-expressing tumor cell clusters. *Proc. Natl. Acad. Sci. USA* **2016**, *113*, E854–E863. [CrossRef]
37. Cheung, K.J.; Gabrielson, E.; Werb, Z.; Ewald, A.J. Collective invasion in breast cancer requires a conserved basal epithelial program. *Cell* **2013**, *155*, 1639. [CrossRef]
38. Haney, S.; Konen, J.; Marcus, A.I.; Bazhenov, M. The complex ecosystem in non small cell lung cancer invasion. *PLoS Comput. Biol.* **2018**, *14*, e1006131. [CrossRef]
39. Khalil, A.A.; Friedl, P. Determinants of leader cells in collective cell migration. *Integr. Biol.* **2010**, *2*, 568–574. [CrossRef]
40. Volkmer, J.P.; Sahoo, D.; Chin, R.K.; Ho, P.L.; Tang, C.; Kurtova, A.V.; Willingham, S.B.; Pazhanisamy, S.K.; Contreras-Trujillo, H.; Storm, T.A.; et al. Three differentiation states risk-stratify bladder cancer into distinct subtypes. *Proc. Natl. Acad. Sci. USA* **2012**, *109*, 2078–2083. [CrossRef]
41. Venhuizen, J.-H.; Zegers, M.M. Making Heads or Tails of It: Cell–Cell Adhesion in Cellular and Supracellular Polarity in Collective Migration. *Cold Spring Harbor Perspect. Biol.* **2017**, *9*, a027854. [CrossRef] [PubMed]
42. Campa, C.C.; Ciraolo, E.; Ghigo, A.; Germena, G.; Hirsch, E. Crossroads of PI3K and Rac pathways. *Small Gtpases* **2015**, *6*, 71–80. [CrossRef] [PubMed]
43. Pandya, P.; Orgaz, J.L.; Sanz-Moreno, V. Actomyosin contractility and collective migration: May the force be with you. *Curr. Opin. Cell Biol.* **2017**, *48*, 87–96. [CrossRef] [PubMed]
44. Witz, C.A.; Montoya-Rodriguez, I.A.; Cho, S.; Centonze, V.E.; Bonewald, L.F.; Schenken, R.S. Composition of the Extracellular Matrix of the Peritoneum. *J. Soc. Gynecol. Investig.* **2001**, *8*, 299–304. [CrossRef]
45. Gialeli, C.; Theocharis, A.D.; Karamanos, N.K. Roles of matrix metalloproteinases in cancer progression and their pharmacological targeting. *FEBS J.* **2011**, *278*, 16–27. [CrossRef]
46. Neri, S.; Ishii, G.; Hashimoto, H.; Kuwata, T.; Nagai, K.; Date, H.; Ochiai, A. Podoplanin-expressing cancer-associated fibroblasts lead and enhance the local invasion of cancer cells in lung adenocarcinoma. *Int. J. Cancer* **2015**, *137*, 784–796. [CrossRef]
47. Labernadie, A.; Kato, T.; Brugués, A.; Serra-Picamal, X.; Derzsi, S.; Arwert, E.; Weston, A.; González-Tarragó, V.; Elosegui-Artola, A.; Albertazzi, L.; et al. A mechanically active heterotypic E-cadherin/N-cadherin adhesion enables fibroblasts to drive cancer cell invasion. *Nat. Cell Biol.* **2017**, *19*, 224–237. [CrossRef]
48. Gaggioli, C.; Hooper, S.; Hidalgo-Carcedo, C.; Grosse, R.; Marshall, J.F.; Harrington, K.; Sahai, E. Fibroblast-led collective invasion of carcinoma cells with differing roles for RhoGTPases in leading and following cells. *Nat. Cell Biol.* **2007**, *9*, 1392–1400. [CrossRef]
49. George, P.; Paraskevopoulou, V.; Vasilaki, E.; Kanaki, Z.; Paschalidis, N.; Klinakis, A. KRT14 marks a subpopulation of bladder basal cells with pivotal role in regeneration and tumorigenesis. *Nat. Commun.* **2016**, *7*, 11914.
50. Xiao-Lei, G.; Wu, J.S.; Cao, M.X.; Gao, S.Y.; Cen, X.; Jiang, Y.P.; Wang, S.S.; Tang, Y.J.; Chen, Q.M.; Liang, X.H.; et al. Cytokeratin-14 contributes to collective invasion of salivary adenoid cystic carcinoma. *PLoS ONE* **2017**, *12*, e0171341.
51. Hu, W.-Y.; Hu, D.P.; Xie, L.; Li, Y.; Majumdar, S.; Nonn, L.; Hu, H.; Shioda, T.; Prins, G.S. solation and functional interrogation of adult human prostate epithelial stem cells at single cell resolution. *Stem Cell Res.* **2017**, *23*, 1–12. [CrossRef] [PubMed]
52. Zhu, F.; Qian, W.; Zhang, H.; Liang, Y.; Wu, M.; Zhang, Y.; Zhang, X.; Gao, Q.; Li, Y. SOX2 Is a Marker for Stem-like Tumor Cells in Bladder Cancer. *Stem Cell Rep.* **2017**, *9*, 429–437. [CrossRef] [PubMed]
53. Kurtova, A.V.; Xiao, J.; Mo, Q.; Pazhanisamy, S.; Krasnow, R.; Lerner, S.P.; Chen, F.; Roh, T.T.; Lay, E.; Ho, P.L.; et al. Blocking PGE2-induced tumour repopulation abrogates bladder cancer chemoresistance. *Nature* **2015**, *517*, 209–213. [CrossRef]
54. Visvader, J.E.; Lindeman, G.J. Cancer stem cells in solid tumours: Accumulating evidence and unresolved questions. *Nat. Rev. Cancer* **2008**, *8*, 755–768. [CrossRef] [PubMed]

55. Agarwal, R.; Kaye, S.B. Ovarian cancer: Strategies for overcoming resistance to chemotherapy. *Nat. Rev. Cancer* **2003**, *3*, 502–516. [CrossRef]
56. Mehlen, P.; Puisieux, A. Metastasis: A question of life or death. *Nat. Rev. Cancer* **2006**, *6*, 449–458. [CrossRef] [PubMed]
57. Matulonis, U.A.; Barry, W.; Penson, R.T.; Konstantinopoulos, P.A.; Luo, W.; Hoffman, M.A.; Horowitz, N.S.; Farooq, S.; Dizon, D.S.; Stover, E.; et al. Phase II study of pembrolizumab (pembro) combined with pegylated liposomal doxorubicin (PLD) for recurrent platinum-resistant ovarian, fallopian tube or peritoneal cancer. *Gynecol. Oncol.* **2018**, *149*, 24. [CrossRef]
58. Disis, M.L.; Taylor, M.H.; Kelly, K.; Beck, J.T.; Gordon, M.; Moore, K.M.; Patel, M.R.; Chaves, J.; Park, H.; Mita, A.C.; et al. Efficacy and Safety of Avelumab for Patients With Recurrent or Refractory Ovarian Cancer: Phase 1b Results From the JAVELIN Solid Tumor Trial. *JAMA Oncol.* **2019**. [CrossRef]
59. Aghajanian, C.; Finkler, N.J.; Rutherford, T.; Smith, D.A.; Yi, J.; Parmar, H.; Nycum, L.R.; Sovak, M.A. OCEANS: A randomized, double-blinded, placebo-controlled phase III trial of chemotherapy with or without bevacizumab (BEV) in patients with platinum-sensitive recurrent epithelial ovarian (EOC), primary peritoneal (PPC), or fallopian tube cancer (FTC). *J. Clin. Oncol.* **2011**, *29* (Suppl. 18), LBA5007. [CrossRef]
60. Morrison, J.; Thoma, C.; Goodall, R.J.; Lyons, T.J.; Gaitskell, K.; Wiggans, A.J.; Bryant, A. Epidermal growth factor receptor blockers for the treatment of ovarian cancer. *Cochrane Database Syst. Rev.* **2018**, *10*, Cd007927. [CrossRef]
61. Monk, B.J.; Minion, L.E.; Coleman, R.L. Anti-angiogenic agents in ovarian cancer: Past, present, and future. *Ann. Oncol.* **2016**, *27* (Suppl. 1), i33–i39. [CrossRef]
62. Pal, T.; Permuth-Wey, J.; Betts, J.A.; Krischer, J.P.; Fiorica, J.; Arango, H.; LaPolla, J.; Hoffman, M.; Martino, M.A.; Wakeley, K.; et al. BRCA1 and BRCA2 mutations account for a large proportion of ovarian carcinoma cases. *Cancer* **2005**, *104*, 2807–2816. [CrossRef] [PubMed]
63. Morgan, R.D.; Clamp, A.R.; Evans, D.G.R.; Edmondson, R.J.; Jayson, G.C. PARP inhibitors in platinum-sensitive high-grade serous ovarian cancer. *Cancer Chemother. Pharmacol.* **2018**, *81*, 647–658. [CrossRef] [PubMed]
64. Mirza, M.R.; Monk, B.J.; Herrstedt, J.; Oza, A.M.; Mahner, S.; Redondo, A.; Fabbro, M.; Ledermann, J.A.; Lorusso, D.; Vergote, I.; et al. Niraparib Maintenance Therapy in Platinum-Sensitive, Recurrent Ovarian Cancer. *N. Engl. J. Med.* **2016**, *375*, 2154–2164. [CrossRef] [PubMed]
65. Lambert, A.W.; Pattabiraman, D.R.; Weinberg, R.A. Emerging Biological Principles of Metastasis. *Cell* **2017**, *168*, 670–691. [CrossRef]
66. Mittal, V. Epithelial Mesenchymal Transition in Tumor Metastasis. *Annu. Rev. Pathol. Mech. Dis.* **2018**, *13*, 395–412. [CrossRef]
67. Krakhmal, N.V.; Zavyalova, M.V.; Denisov, E.V.; Vtorushin, S.V.; Perelmuter, V.M. Cancer Invasion: Patterns and Mechanisms. *Acta Nat.* **2015**, *7*, 17–28.
68. Leong, H.S.; Robertson, A.E.; Stoletov, K.; Leith, S.J.; Chin, C.A.; Chien, A.E.; Hague, M.N.; Ablack, A.; Carmine-Simmen, K.; McPherson, V.A.; et al. Invadopodia Are Required for Cancer Cell Extravasation and Are a Therapeutic Target for Metastasis. *Cell Rep.* **2014**, *8*, 1558–1570. [CrossRef]
69. Trendowski, M. Exploiting the cytoskeletal filaments of neoplastic cells to potentiate a novel therapeutic approach. *Biochim. Biophys. Acta* **2014**, *1846*, 599–616. [CrossRef]
70. Bousquet, P.F.; Paulsen, L.A.; Fondy, C.; Lipski, K.M.; Loucy, K.J.; Fondy, T.P. Effects of cytochalasin B in culture and in vivo on murine Madison 109 lung carcinoma and on B16 melanoma. *Cancer Res.* **1990**, *50*, 1431–1439.
71. Senderowicz, A.M.; Kaur, G.; Sainz, E.; Laing, C.; Inman, W.D.; Rodriguez, J.; Crews, P.; Malspeis, L.; Grever, M.R.; Sausville, E.A.; et al. Jasplakinolide's inhibition of the growth of prostate carcinoma cells in vitro with disruption of the actin cytoskeleton. *J. Natl. Cancer Inst.* **1995**, *87*, 46–51. [CrossRef] [PubMed]
72. Jalilian, I.; Heu, C.; Cheng, H.; Freittag, H.; Desouza, M.; Stehn, J.R.; Bryce, N.S.; Whan, R.M.; Hardeman, E.C.; Fath, T.; et al. Cell elasticity is regulated by the tropomyosin isoform composition of the actin cytoskeleton. *PLoS ONE* **2015**, *10*, e0126214. [CrossRef] [PubMed]
73. Stehn, J.R.; Haass, N.K.; Bonello, T.; Desouza, M.; Kottyan, G.; Treutlein, H.; Zeng, J.; Nascimento, P.R.B.B.; Sequeira, V.B.; Butler, T.L.; et al. A Novel Class of Anticancer Compounds Targets the Actin Cytoskeleton in Tumor Cells. *Cancer Res.* **2013**, *73*, 5169. [CrossRef] [PubMed]

74. Duxbury, M.S.; Ashley, S.W.; Whang, E.E. Inhibition of pancreatic adenocarcinoma cellular invasiveness by blebbistatin: A novel myosin II inhibitor. *Biochem. Biophys. Res. Commun.* **2004**, *313*, 992–997. [CrossRef] [PubMed]
75. Hoffman, A.; Taleski, G.; Sontag, E. The protein serine/threonine phosphatases PP2A, PP1 and calcineurin: A triple threat in the regulation of the neuronal cytoskeleton. *Mol. Cell. Neurosci.* **2017**, *84*, 119–131. [CrossRef] [PubMed]
76. Gandalovicova, A.; Rosel, D.; Fernandes, M.; Vesely, P.; Heneberg, P.; Cermak, V.; Petruzelka, L.; Kumar, S.; Sanz-Moreno, V.; Brabek, J. Migrastatics-Anti-metastatic and Anti-invasion Drugs: Promises and Challenges. *Trends Cancer* **2017**, *3*, 391–406. [CrossRef] [PubMed]
77. Sadok, A.; Marshall, C.J. Rho GTPases: Masters of cell migration. *Small GTPases* **2014**, *5*, e29710. [CrossRef] [PubMed]
78. Reffay, M.; Parrini, M.; Cochet-Escartin, O.; Ladoux, B.; Buguin, A.; Coscoy, S.; Amblard, F.; Camonis, J.; Silberzan, P. Interplay of RhoA and mechanical forces in collective cell migration driven by leader cells. *Nat. Cell Biol.* **2014**, *16*, 217–223. [CrossRef] [PubMed]
79. Chen, S.; Wang, J.; Gou, W.-F.; Xiu, Y.-L.; Zheng, H.-C.; Zong, Z.-H.; Takano, Y.; Zhao, Y. The involvement of RhoA and Wnt-5a in the tumorigenesis and progression of ovarian epithelial carcinoma. *Int. J. Mol. Sci.* **2013**, *14*, 24187–24199. [CrossRef]
80. Horiuchi, A.; Kikuchi, N.; Osada, R.; Wang, C.; Hayashi, A.; Nikaido, T.; Konishi, I. Overexpression of RhoA enhances peritoneal dissemination: RhoA suppression with Lovastatin may be useful for ovarian cancer. *Cancer Sci.* **2008**, *99*, 2532–2539. [CrossRef]
81. Wang, X.; Jiang, W.; Kang, J.; Liu, Q.; Nie, M. Knockdown of RhoA expression alters ovarian cancer biological behavior in vitro and in nude mice. *Oncol. Rep.* **2015**, *34*, 891–899. [CrossRef] [PubMed]
82. Wang, X.; Han, L.; Shan, S.; Sun, Y.; Mao, Y. KRT14 promoting invasion and migration of lung cancer cells through ROCK-1 signaling pathway. *Int. J. Clin. Exp. Pathol.* **2017**, *10*, 795–803.
83. Martirosyan, A.; Clendening, J.W.; Goard, C.A.; Penn, L.Z. Lovastatin induces apoptosis of ovarian cancer cells and synergizes with doxorubicin: Potential therapeutic relevance. *BMC Cancer* **2010**, *10*, 103. [CrossRef] [PubMed]
84. Kümper, S.; Mardakheh, F.K.; McCarthy, A.; Yeo, M.; Stamp, G.W.; Paul, A.; Worboys, J.; Sadok, A.; Jørgensen, C.; Guichard, S.; et al. Rho-associated kinase (ROCK) function is essential for cell cycle progression, senescence and tumorigenesis. *eLife* **2016**, *5*, e12203. [CrossRef] [PubMed]
85. Tamura, M.; Nakao, H.; Yoshizaki, H.; Shiratsuchi, M.; Shigyo, H.; Yamada, H.; Ozawa, T.; Totsuka, J.; Hidaka, H. Development of specific Rho-kinase inhibitors and their clinical application. *BBA-Proteins Proteom.* **2005**, *1754*, 245–252. [CrossRef]
86. Deng, L.; Li, G.; Li, R.; Liu, Q.; He, Q.; Zhang, J. Rho-kinase inhibitor, fasudil, suppresses glioblastoma cell line progression in vitro and in vivo. *Cancer Biol. Ther.* **2010**, *9*, 875–884. [CrossRef] [PubMed]
87. Yang, X.; Zhang, Y.; Wang, S.; Shi, W. Effect of fasudil on growth, adhesion, invasion, and migration of 95D lung carcinoma cells in vitro. *Can. J. Physiol. Pharmacol.* **2010**, *88*, 874–879. [CrossRef]
88. Yang, X.; Di, J.; Zhang, Y.; Zhang, S.; Lu, J.; Liu, J.; Shi, W. The Rho-kinase inhibitor inhibits proliferation and metastasis of small cell lung cancer. *Biomed. Pharmacother.* **2012**, *66*, 221–227. [CrossRef]
89. Hu, K.; Wang, Z.; Tao, Y. [Suppression of hepatocellular carcinoma invasion and metastasis by Rho-kinase inhibitor Fasudil through inhibition of BTBD7-ROCK2 signaling pathway]. *Zhong Nan Da Xue Xue Bao Yi Xue Ban* **2014**, *39*, 1221–1227.
90. Vennin, C.; Chin, V.T.; Warren, S.C.; Lucas, M.C.; Herrmann, D.; Magenau, A.; Melenec, P.; Walters, S.N.; del Monte-Nieto, G.; Conway, J.R.W.; et al. Transient tissue priming via ROCK inhibition uncouples pancreatic cancer progression, sensitivity to chemotherapy, and metastasis. *Sci. Transl. Med.* **2017**, *9*, eaai8504. [CrossRef]
91. Ogata, S.; Morishige, K.I.; Sawada, K.; Hashimoto, K.; Mabuchi, S.; Kawase, C.; Ooyagi, C.; Sakata, M.; Kimura, T. Fasudil Inhibits Lysophosphatidic Acid-Induced Invasiveness of Human Ovarian Cancer Cells. *Int. J. Gynecol. Cancer* **2009**, *19*, 1473–1480. [CrossRef]
92. Uehata, M.; Ishizaki, T.; Satoh, H.; Ono, T.; Kawahara, T.; Morishita, T.; Tamakawa, H.; Yamagami, K.; Inui, J.; Maekawa, M.; et al. Calcium sensitization of smooth muscle mediated by a Rho-associated protein kinase in hypertension. *Nature* **1997**, *389*, 990. [CrossRef] [PubMed]

93. Jeong, K.J.; Park, S.Y.; Cho, K.H.; Sohn, J.S.; Lee, J.; Kim, Y.K.; Kang, J.; Park, C.G.; Han, J.W.; Lee, H.Y. The Rho/ROCK pathway for lysophosphatidic acid-induced proteolytic enzyme expression and ovarian cancer cell invasion. *Oncogene* **2012**, *31*, 4279. [CrossRef]
94. Ohta, T.; Takahashi, T.; Shibuya, T.; Amita, M.; Henmi, N.; Takahashi, K.; Kurachi, H. Inhibition of the Rho/ROCK pathway enhances the efficacy of cisplatin through the blockage of hypoxia-inducible factor-1alpha in human ovarian cancer cells. *Cancer Biol.* **2012**, *13*, 25–33. [CrossRef]
95. Yap, T.A.; Walton, M.I.; Grimshaw, K.M.; Poele, R.H.t.; Eve, P.D.; Valenti, M.R.; Brandon, A.K.d.; Martins, V.; Zetterlund, A.; Heaton, S.P.; et al. AT13148 Is a Novel, Oral Multi-AGC Kinase Inhibitor with Potent Pharmacodynamic and Antitumor Activity. *Clin. Cancer Res.* **2012**, *18*, 3912. [CrossRef]
96. Papadatos-Pastos, D.; Kumar, R.; Yap, T.A.; Ruddle, R.; Decordova, S.; Jones, P.; Halbert, G.; Garrett, M.D.; McLeod, R.; Backholer, Z.; et al. A first-in-human study of the dual ROCK I/II inhibitor, AT13148, in patients with advanced cancers. *J. Clin. Oncol.* **2015**, *33* (Suppl. 15), 2566. [CrossRef]
97. Salhia, B.; Rutten, F.; Nakada, M.; Beaudry, C.; Berens, M.; Kwan, A.; Rutka, J.T. Inhibition of Rho-Kinase Affects Astrocytoma Morphology, Motility, and Invasion through Activation of Rac1. *Cancer Res.* **2005**, *65*, 8792. [CrossRef] [PubMed]
98. Matsuoka, T.; Yashiro, M.; Kato, Y.; Shinto, O.; Kashiwagi, S.; Hirakawa, K. RhoA/ROCK signaling mediates plasticity of scirrhous gastric carcinoma motility. *Clin. Exp. Metastasis* **2011**, *28*, 627–636. [CrossRef]
99. Wei, L.; Surma, M.; Shi, S.; Lambert-Cheatham, N.; Shi, J. Novel Insights into the Roles of Rho Kinase in Cancer. *Arch. Immunol. Ther. Exp.* **2016**, *64*, 259–278. [CrossRef]
100. Mayer, E.L.; Krop, I.E. Advances in targeting SRC in the treatment of breast cancer and other solid malignancies. *Clin. Cancer Res.* **2010**, *16*, 3526–3532. [CrossRef]
101. Wiener, J.R.; Windham, T.C.; Estrella, V.C.; Parikh, N.U.; Thall, P.F.; Deavers, M.T.; Bast, R.C.; Mills, G.B.; Gallick, G.E. Activated SRC protein tyrosine kinase is overexpressed in late-stage human ovarian cancers. *Gynecol. Oncol.* **2003**, *88*, 73–79. [CrossRef] [PubMed]
102. Eckert, M.A.; Yang, J. Targeting invadopodia to block breast cancer metastasis. *Oncotarget* **2011**, *2*, 562–568. [CrossRef] [PubMed]
103. Mader, C.C.; Oser, M.; Magalhaes, M.A.O.; Bravo-Cordero, J.J.; Condeelis, J.; Koleske, A.J.; Gil-Henn, H. An EGFR–Src–Arg–Cortactin Pathway Mediates Functional Maturation of Invadopodia and Breast Cancer Cell Invasion. *Cancer Res.* **2011**, *71*, 1730. [CrossRef] [PubMed]
104. Steeg, P. Targeting metastasis. *Nat. Rev. Cancer* **2016**, *16*, 201–218. [CrossRef]
105. Schilder, R.J.; Brady, W.E.; Lankes, H.A.; Fiorica, J.V.; Shahin, M.S.; Zhou, X.C.; Mannel, R.S.; Pathak, H.B.; Hu, W.; Alpaugh, R.K.; et al. Phase II evaluation of dasatinib in the treatment of recurrent or persistent epithelial ovarian or primary peritoneal carcinoma: A Gynecologic Oncology Group study. *Gynecol. Oncol.* **2012**, *127*, 70–74. [CrossRef] [PubMed]
106. Vergote, I.B.; Smith, D.C.; Berger, R.; Kurzrock, R.; Vogelzang, N.J.; Sella, A.; Wheler, J.; Lee, Y.; Foster, P.G.; Weitzman, R.; et al. A phase 2 randomised discontinuation trial of cabozantinib in patients with ovarian carcinoma. *Eur. J. Cancer* **2017**, *83*, 229–236. [CrossRef]
107. Chekerov, R.; Hilpert, F.; Mahner, S.; El-Balat, A.; Harter, P.; de Gregorio, N.; Fridrich, C.; Markmann, S.; Potenberg, J.; Lorenz, R.; et al. Sorafenib plus topotecan versus placebo plus topotecan for platinum-resistant ovarian cancer (TRIAS): A multicentre, randomised, double-blind, placebo-controlled, phase 2 trial. *Lancet Oncol.* **2018**, *19*, 1247–1258. [CrossRef]
108. Schoffski, P.; Gordon, M.; Smith, D.C.; Kurzrock, R.; Daud, A.; Vogelzang, N.J.; Lee, Y.; Scheffold, C.; Shapiro, G.I. Phase II randomised discontinuation trial of cabozantinib in patients with advanced solid tumours. *Eur. J. Cancer* **2017**, *86*, 296–304. [CrossRef]
109. Matei, D.; Sill, M.W.; Lankes, H.A.; DeGeest, K.; Bristow, R.E.; Mutch, D.; Yamada, S.D.; Cohn, D.; Calvert, V.; Farley, J.; et al. Activity of sorafenib in recurrent ovarian cancer and primary peritoneal carcinomatosis: A gynecologic oncology group trial. *J. Clin. Oncol.* **2011**, *29*, 69–75. [CrossRef]
110. Ramasubbaiah, R.; Perkins, S.M.; Schilder, J.; Whalen, C.; Johnson, C.S.; Callahan, M.; Jones, T.; Sutton, G.; Matei, D. Sorafenib in combination with weekly topotecan in recurrent ovarian cancer, a phase I/II study of the Hoosier Oncology Group. *Gynecol. Oncol.* **2011**, *123*, 499–504. [CrossRef]

111. Hainsworth, J.D.; Thompson, D.S.; Bismayer, J.A.; Gian, V.G.; Merritt, W.M.; Whorf, R.C.; Finney, L.H.; Dudley, B.S. Paclitaxel/carboplatin with or without sorafenib in the first-line treatment of patients with stage III/IV epithelial ovarian cancer: A randomized phase II study of the Sarah Cannon Research Institute. *Cancer Med.* **2015**, *4*, 673–681. [CrossRef] [PubMed]
112. Patel, R.A.; Liu, Y.; Wang, B.; Li, R.; Sebti, S.M. Identification of novel ROCK inhibitors with anti-migratory and anti-invasive activities. *Oncogene* **2013**, *33*, 550. [CrossRef] [PubMed]
113. ClinicalTrials.gov. NCT00585052. A Phase II Study of Interaction of Lovastatin and Paclitaxel For Patients with Refractory or Relapsed Ovarian Cancer. Available online: https://clinicaltrials.gov/ct2/show/NCT00585052 (accessed on 13 December 2018).
114. ClinicalTrials.gov. NCT02943317. Study to Investigate the Safety, Pharmacokinetics, Pharmacodynamics and Preliminary Clinical Activity of Defactinib in Combination with Avelumab in Epithelial Ovarian Cancer. Available online: https://clinicaltrials.gov/ct2/show/NCT02943317 (accessed on 13 December 2018).
115. ClinicalTrials.gov. NCT00671788. A Phase II Evaluation of Dasatinib (Sprycel®, NSC #732517) in the Treatment of Persistent or Recurrent Epithelial Ovarian, Fallopian Tube, or Primary Peritoneal Carcinoma. Available online: https://clinicaltrials.gov/ct2/show/results/NCT00671788 (accessed on 13 December 2018).
116. ClinicalTrials.gov. NCT00940225. Study of Cabozantinib (XL184) in Adults with Advanced Malignancies. Available online: https://clinicaltrials.gov/ct2/show/NCT00940225 (accessed on 13 December 2018).
117. ClinicalTrials.gov. NCT01716715. Cabozantinib or Paclitaxel in Treating Patients with Persistent or Recurrent Epithelial Ovarian, Fallopian Tube, or Primary Peritoneal Cavity Cancer. Available online: https://clinicaltrials.gov/ct2/show/NCT01716715 (accessed on 13 December 2018).
118. ClinicalTrials.gov. NCT00093626. Sorafenib in Treating Patients with Persistent or Recurrent Ovarian Epithelial or Peritoneal Cancer. Available online: https://clinicaltrials.gov/ct2/show/NCT00093626 (accessed on 13 December 2018).
119. ClinicalTrials.gov. NCT00390611. Paclitaxel and Carboplatin with or without Sorafenib in the First-Line Treatment Of Patients With Ovarian Cancer. Available online: https://clinicaltrials.gov/ct2/show/NCT00390611 (accessed on 13 December 2018).
120. Bell-McGuinn, K.M.; Matthews, C.M.; Ho, S.N.; Barve, M.; Gilbert, L.; Penson, R.T.; Lengyel, E.; Palaparthy, R.; Gilder, K.; Vassos, A.; et al. A phase II, single-arm study of the anti-alpha5beta1 integrin antibody volociximab as monotherapy in patients with platinum-resistant advanced epithelial ovarian or primary peritoneal cancer. *Gynecol. Oncol.* **2011**, *121*, 273–279. [CrossRef]
121. ClinicalTrials.gov. NCT00516841: A Phase 2, Single-Arm Study of Volociximab Monotherapy in Subjects with Platinum-Resistant Advanced Epithelial Ovarian Cancer or Primary Peritoneal Cancer. Available online: https://clinicaltrials.gov/ct2/show/NCT00516841 (accessed on 25 February 2019).
122. ClinicalTrials.gov. NCT01670799. Availability & Effect of Post-OP Ketorolac on Ovarian, Fallopian Tube or Primary Peritoneal Cancer. Available online: https://clinicaltrials.gov/ct2/show/NCT01670799 (accessed on 13 December 2018).
123. Guo, Y.; Kenney, S.R.; Cook, L.S.; Adams, S.F.; Rutledge, T.; Romero, E.; Oprea, T.; Sklar, L.A.; Bedrick, E.; Wiggins, C.L.; et al. A novel pharmacologic activity of ketorolac for therapeutic benefit in ovarian cancer patients. *Clin. Cancer Res.* **2015**, *21*, 5064–5072. [CrossRef]
124. ClinicalTrials.gov. NCT02470299. Evaluation of GTPase Inhibition by Post-Operative Intravenous Ketorolac in Ovarian Cancer Patients. Available online: https://clinicaltrials.gov/ct2/show/NCT02470299 (accessed on 13 December 2018).
125. Yurchenco, P.D. Basement Membranes: Cell Scaffoldings and Signaling Platforms. *Cold Spring Harbor Perspect. Biol.* **2011**, *3*, a004911. [CrossRef]
126. Ricart, A.D.; Tolcher, A.W.; Liu, G.; Holen, K.; Schwartz, G.; Albertini, M.; Weiss, G.; Yazji, S.; Ng, C.; Wilding, G. Volociximab, a chimeric monoclonal antibody that specifically binds alpha5beta1 integrin: A phase I, pharmacokinetic, and biological correlative study. *Clin. Cancer Res.* **2008**, *14*, 7924–7929. [CrossRef]
127. Chen, Q.; Manning, C.; Millar, H.; McCabe, F.; Ferrante, C.; Sharp, C.; Shahied-Arruda, L.; Doshi, P.; Nakada, M.; Anderson, G. CNTO 95, a fully human anti αv integrin antibody, inhibits cell signaling, migration, invasion, and spontaneous metastasis of human breast cancer cells. *Off. J. Metastasis Res. Soc.* **2008**, *25*, 139–148. [CrossRef] [PubMed]

128. O'Day, S.; Pavlick, A.; Loquai, C.; Lawson, D.; Gutzmer, R.; Richards, J.; Schadendorf, D.; Thompson, J.A.; Gonzalez, R.; Trefzer, U.; et al. A randomised, phase II study of intetumumab, an anti-αv-integrin mAb, alone and with dacarbazine in stage IV melanoma. *Br. J. Cancer* **2011**, *105*, 346–352. [CrossRef]
129. Hersey, P.; Sosman, J.; O'Day, S.; Richards, J.; Bedikian, A.; Gonzalez, R.; Sharfman, W.; Weber, R.; Logan, T.; Buzoianu, M.; et al. A randomized phase 2 study of etaracizumab, a monoclonal antibody against integrin alpha(v)beta(3), + or—Dacarbazine in patients with stage IV metastatic melanoma. *Cancer* **2010**, *116*, 1526–1534. [CrossRef]
130. Kobayashi, M.; Sawada, K.; Kimura, T. Potential of Integrin Inhibitors for Treating Ovarian Cancer: A Literature Review. *Cancers* **2017**, *9*, 83. [CrossRef]
131. Deryugina, E.I.; Quigley, J.P. Matrix metalloproteinases and tumor metastasis. *Cancer Metastasis Rev.* **2006**, *25*, 9–34. [CrossRef] [PubMed]
132. Hofmann, U.B.; Eggert, A.A.O.; Blass, K.; Bröcker, E.-B.; Becker, J.C. Expression of Matrix Metalloproteinases in the Microenvironment of Spontaneous and Experimental Melanoma Metastases Reflects the Requirements for Tumor Formation. *Cancer Res.* **2003**, *63*, 8221. [PubMed]
133. Poincloux, R.; Lizárraga, F.; Chavrier, P. Matrix invasion by tumour cells: A focus on MT1-MMP trafficking to invadopodia. *J. Cell Sci.* **2009**, *122*, 3015. [CrossRef] [PubMed]
134. Devy, L.; Huang, L.; Naa, L.; Yanamandra, N.; Pieters, H.; Frans, N.; Chang, E.; Tao, Q.; Vanhove, M.; Lejeune, A.; et al. Selective Inhibition of Matrix Metalloproteinase-14 Blocks Tumor Growth, Invasion, and Angiogenesis. *Cancer Res.* **2009**, *69*, 1517. [CrossRef]
135. Yang, X.; Zheng, F.; Zhang, S.; Lu, J. Loss of RhoA expression prevents proliferation and metastasis of SPCA1 lung cancer cells in vitro. *Biomed. Pharmacother.* **2015**, *69*, 361–366. [CrossRef]
136. Yamaguchi, N.; Mizutani, T.; Kawabata, K.; Haga, H. Leader cells regulate collective cell migration via Rac activation in the downstream signaling of integrin β1 and PI3K. *Sci. Rep.* **2015**, *5*, 7656. [CrossRef]
137. Guo, Y.; Kenney, S.R.; Muller, C.Y.; Adams, S.; Rutledge, T.; Romero, E.; Murray-Krezan, C.; Prekeris, R.; Sklar, L.A.; Hudson, L.G.; et al. R-Ketorolac Targets Cdc42 and Rac1 and Alters Ovarian Cancer Cell Behaviors Critical for Invasion and Metastasis. *Mol. Cancer Ther.* **2015**, *14*, 2215. [CrossRef]

Published OnlineFirst November 15, 2017; DOI: 10.1158/1055-9965.EPI-17-0752

Research Article

Cancer Epidemiology, Biomarkers & Prevention

Autoantibodies against HSF1 and CCDC155 as Biomarkers of Early-Stage, High-Grade Serous Ovarian Cancer

Amy L. Wilson[1,2], Laura R. Moffitt[1,2], Nadine Duffield[1,2], Adam Rainczuk[1,2], Tom W. Jobling[4,5], Magdalena Plebanski[3,6], and Andrew N. Stephens[1,2,5]

Abstract

Background: Tumor-directed circulating autoantibodies (AAb) are a well-established feature of many solid tumor types, and are often observed prior to clinical disease manifestation. As such, they may provide a good indicator of early disease development. We have conducted a pilot study to identify novel AAbs as markers of early-stage high-grade serous ovarian cancers (HGSOCs).

Methods: A rare cohort of patients with early (FIGO stage Ia-c) HGSOCs for IgG, IgA, and IgM-mediated AAb reactivity using high-content protein arrays (containing 9,184 individual proteins). AAb reactivity against selected antigens was validated by ELISA in a second, independent cohort of individual patients.

Results: A total of 184 antigens were differentially detected in early-stage HGSOC patients compared with all other patient groups assessed. Among the six most highly detected "early-stage" antigens, anti-IgA AAbs against HSF1 and anti-IgG AAbs CCDC155 (KASH5; nesprin 5) were significantly elevated in patients with early-stage malignancy. Receiver operating characteristic analysis suggested that AAbs against HSF1 provided better detection of early-stage malignancy than CA125 alone. Combined measurement of anti-HSF1, anti-CCDC155, and CA125 also improved efficacy at higher sensitivity.

Conclusions: The combined measurement of anti-HSF1, anti-CCDC155, and CA125 may be useful for early-stage HGSOC detection.

Impact: This is the first study to specifically identify AAbs associated with early-stage HGSOC. The presence and high frequency of specific AAbs in early-stage cancer patients warrants a larger scale examination to define their value for early disease detection at primary diagnosis and/or recurrence. *Cancer Epidemiol Biomarkers Prev; 27(2); 183–92. ©2017 AACR.*

Introduction

High-grade serous ovarian cancers (HGSOCs) are typically diagnosed at an advanced stage, and account for approximately 90% of all ovarian cancer–related deaths (1). The combination of late-stage diagnosis and the prevalence of chemoresistant disease both contribute to an overall approximately 30% 5-year survival rate, the lowest for any gynecologic tumor type. Early diagnosis, prior to extra-ovarian spread, is associated with improved survival (2); regular longitudinal screening is therefore widely accepted as the strategy of choice to reduce ovarian cancer-related mortality. Despite intensive efforts and the identification of large numbers of potential novel biomarkers of ovarian cancer (recently reviewed; refs. 3, 4), at present only CA125 and HE4 have demonstrated clinical relevance; and neither are suitable for the detection of early-stage disease (5, 6). Large-scale trials combining CA125 with transvaginal ultrasound have also failed to deliver tangible improvements in overall survival for HGSOC patients (7). There remains an unmet clinical need to identify novel disease biomarkers for use in improved early-stage diagnosis, and to monitor disease recurrence.

The release of soluble biomarkers from early-stage, microscopic HGSOC lesions is unlikely to reach measurable concentrations circulation at a sufficiently early-stage for diagnostic purposes. However, in many solid tumor types the aberrant expression, or alterations to the function, structure, or localization of proteins, can elicit an autoimmune response (8). The presence of circulating auto-antibodies (AAbs) against tumor-associated antigens (TAAs) is well documented, and occurs prior to clinical disease manifestation and is maintained throughout progression in multiple solid cancers (reviewed in ref. 9). As potential cancer biomarkers, the measurement of AAbs has several potential advantages; AAbs are stable in circulation, can recognize cancer-specific modifications to proteins that may not be immediately evident from molecular or genetic profiles, and can effectively amplify tumor-associated signals that are otherwise below detection thresholds (9). As an early and sensitive indicator of tumor growth, AAb

[1]Department of Molecular and Translational Sciences, Monash University, Victoria, Australia. [2]Centre for Cancer Research, Hudson Institute of Medical Research, Victoria, Australia. [3]Department of Immunology and Pathology, Monash University, Melbourne, Australia. [4]Obstetrics and Gynaecology, Monash Medical Centre, Clayton, Victoria, Australia. [5]Epworth Research Institute, Epworth HealthCare, Richmond, Victoria, Australia. [6]School of Health and Biomedical Sciences, RMIT, Bundoora, Victoria, Australia.

Note: Supplementary data for this article are available at Cancer Epidemiology, Biomarkers & Prevention Online (http://cebp.aacrjournals.org/).

A.L. Wilson and L.R. Moffitt contributed equally to this article.

Corresponding Author: Andrew N. Stephens, Hudson Institute of Medical Research, 27-31 Wright St Clayton, Victoria 3168, Australia. Phone: 613-8572-2686; Fax: 613-9594-7909; E-mail: Andrew.N.Stephens@hudson.org.au

doi: 10.1158/1055-9965.EPI-17-0752

Published OnlineFirst November 15, 2017; DOI: 10.1158/1055-9965.EPI-17-0752

measurement may therefore overcome practical limitations associated with the direct measurement of soluble TAAs. Accordingly, AAb profiling has become an attractive approach to biomarker discovery for early-stage tumor detection (10).

Diverse experimental approaches have been applied for AAb identification in multiple tumor types (recently reviewed in refs. 4, 11) including phage display, cDNA expression library analyses, reversed phase, recombinant antigen and tumor lysate arrays, and various other proteomic approaches (8, 12–14). In particular, the recent development of programmable and/or commercially available, high-content antigen arrays has facilitated the rapid profiling of AAb signatures in patient sera as a mechanism to discover new biomarkers and biomarker combinations associated with ovarian cancer (12, 15–17). However, the majority of these studies have focused on the detection of AAbs in late-stage HGSOC patients. The dynamic and location-specific nature of humoral immune responses (9) makes it unlikely that these profiles will adequately reflect events occurring early in tumor progression. Moreover, most studies do not appropriately differentiate between low- and high-grade tumors (more recently described as type I or type II, respectively) which exhibit different clinical behaviors, etiologies, and underlying molecular biology (1). Unsurprisingly, no identified AAbs have yet demonstrated suitable sensitivity, specificity, or predictive power for clinical application for the detection of early-stage HGSOC.

In this pilot study, we sought to identify circulating AAbs specifically associated with early-stage HGSOCs. Plasma samples obtained from patients diagnosed with HGSOC and stratified according to FIGO stage (stage I – early, versus stage III – late) were profiled for AAb (IgG, IA, and IgM) reactivity against commercially available Protoarray antigen arrays, displaying 9,134 individual antigens. Following the identification potential early-stage AAbs, we assessed their frequency by ELISA in a second, independent sample cohort. To our knowledge, this is the first study to focus on the identification of AAbs of multiple Ig types that are specific to early-stage HGSOCs. This pilot work provides the methodology for expanded studies to identify and validate clinically relevant biomarkers of early-stage HGSOC.

Materials and Methods

Clinical specimens

EDTA-chelated plasma samples were accessed from biobanked samples, collected prospectively from women undergoing surgery for suspected gynecologic malignancies during the period 2007–2012. All clinical samples were obtained from anesthetized patients who had undergone no prior surgical treatment or neoadjuvant chemotherapy. Healthy control samples, matched for age and menopausal status, were obtained from nonanesthetized volunteers by venipuncture. Patients were excluded if they had any prior history of cancer or gynecologic disease. Women who had undergone prior tubal ligation were also excluded. Histologic assessment of tumor type, stage and grade, presurgical CA125 measurements, age, menopausal status, preexisting conditions, and any prior history of malignancy were obtained from deidentified patient medical records. Patient details immediately relevant to this study are provided in Table 1. Measurement of serum CA125 in control samples was performed in the diagnostic pathology laboratory at the Monash Medical Centre, Melbourne, Australia. Ethical approval was obtained from the Southern Health Human Research Ethics Committee (HREC certificates #06032C, #02031B) with all participants providing prior informed written consent.

Immunoglobulin isotyping arrays

Immunoglobulin (Ig) isotype titers were determined for all individual samples using Quantibody Human Ig Isotype Array 1 (#QAH-ISO-1, RayBiotech) as described by the manufacturer. Plasma samples were diluted 1:80,000 in sample diluent, and 100 μL per sample was analyzed in triplicate. A single array incubated in sample diluent alone was used to control for nonspecific binding of the detection antibody. Dried slides were stored at room temperature and protected from light until image capture and analysis.

ProtoArray protein arrays

Proteomic profiling of antibody signatures was performed using Invitrogen ProtoArray Human Protein Microarrays v5.0 (Thermo Fisher Scientific), comprising 9,184 individual recombinant human proteins spotted in duplicate. All procedures were carried out according to the manufacturer's recommendations. Arrays were probed using pooled plasma samples diluted 1:340 in wash buffer. Fluorescent detection antibodies against human IgG, IgA, and IgM were obtained from Abcam (#ab98554 goat anti-human IgA α chain-DyLight 550; #ab98544 goat anti-human IgM μ chain-DyLight 488; #ab98622 anti IgG Fc-Dylight 650), diluted to a concentration of 1 μg/mL in wash buffer prior to use. Arrays were first incubated with anti-IgG and anti-IgM antibodies simultaneously, then washed and incubated with anti-IgA. A single array incubated in wash buffer alone was used to assess nonspecific detection–antibody binding. Dried slides were stored at room temperature and protected from light until image capture and analysis.

Array image capture and analysis

Fluorescent array signals were acquired using a Fuji FLA5100 four-channel laser scanner (FujiFilm, Tokyo) using blue (473 nm excitation, custom Cy2 emission filter), green (532 nm excitation, dual Cy3/Cy5 filter), and red (635 nm excitation, dual Cy3/Cy5 filter) imaging channels. All images were acquired at 10-μm resolution, with PMT set at 1,000 V. Quantibody arrays were imaged for green fluorescence only, while cyclic imaging was used to acquire blue, green, and red fluorescence data from Protoarrays. Array alignment, feature extraction and data normalization was performed using Phoretix Array v10.2 (TotalLab Ltd). Quantibody array data were analyzed using Quantibody Q-Analyzer software (Raybiotech), with Ig quantitation performed against an 8-point standard curve specific to each antibody isotype.

Analysis of differentially detected antigens on Protoarray arrays

Protoarray data was analyzed using Qlucore Omics Explorer v3.2 (Qlucore). Raw array data were uploaded into the workspace, $\log_2$-transformed, and collapsed according to RefSeq identification number. Average intensities were used for all comparisons, with comparisons performed separately for each of the IgG, IgA, and IgM classes. Nonspecific antigens that exhibited cross-reactivity with detection antibodies alone were removed from the analysis. Data complexity was reduced by filtering to remove all variables in the dataset with $\leq$5% variance, leaving 9,037

Published OnlineFirst November 15, 2017; DOI: 10.1158/1055-9965.EPI-17-0752

variables for analysis. Principal components analysis (PCA) and hierarchical clustering were used to explore the data for differentially detected, immunoreactive antigens that best defined each sample group. Discriminating antigens displayed as heatmaps were arranged by hierarchical clustering according to detection intensity, separated by Ig class and ordered by sample type.

Antigen-specific ELISA

Immunoassays for individual antigens of interest were constructed using commercially available recombinant antigens (Supplementary Table S1), corresponding to antigens of interest identified on arrays. In each case, antigens were diluted to 4 mg/mL in binding buffer ($NaHCO_3$ 100 mmol/L, N_2CO_3 33.6 mmol/L, pH 9.6), and a 100 μL volume incubated in sealed Nunc Maxisorp 96-well microplates (Thermo Fisher Scientific) overnight at 4°C with shaking (GrantBio PMS1000i shaker, 300 rpm). Serial dilutions of purified human serum IgG, IgM and IgA (Sigma Aldrich) were incubated in parallel (range 0.5–0.178 μg/mL) for the construction of standard curves. The following morning wells were washed three times in blocking buffer (1% w/v BSA, 0.05% v/v Triton X-100, NaCl 200 mmol/L in PBS), and then a 100-μL aliquot of human plasma (diluted 1:20 in blocking buffer) added to appropriate wells in triplicate. Blocking buffer alone was used in those wells containing standards. Samples were incubated at room temperature for 1 hour with shaking, followed by 3× washes as above. To detect the binding of serum Igs to the immobilized antigens, a 100-μL aliquot of anti-IgG (3 μg/mL) and anti-IgM (5 μg/mL) cocktail in ice-cold blocking buffer was added to each well and the plate incubated at room temperature with shaking for 1 hour. Following ×3 washes as above, 100 μL of anti-IgA (5 μg/mL) in blocking buffer was added and the plate incubated for a further 1 hour. All wells were then washed five times in wash buffer, and 100-μL PBS added to each prior to measurement.

Fluorescence detection was performed using a Cytation 3 MultiMode Plate Imager (BioTek Instruments Inc.). Acquisition of fluorescence intensity corresponding to IgM (485 nm excitation, 520 nm emission), IgA (550 nm excitation, 580 nm emission), and IgG (645 nm excitation, 675 nm emission) signals was performed using a fixed probe height of 6.75 mm, acquiring 200 data-points per well, and dynamic range between 100 and 80,000 units. Standard curves were constructed using Gen5.0 software v2.05 (BioTek Instruments Inc.) and individual Ig titres for each antibody type automatically determined. All assays were performed in triplicate.

Statistical analyses

Statistical analyses of immunoassay data were carried out using GraphPad PRISM (GraphPad Software). For statistical purposes, data was log transformed to approximate normality. Significance was determined using one-way ANOVA and Bonferroni *post hoc* test, with pairwise comparisons performed using Student *t* test. For groups with significantly different variance, Welch correction was applied. Results of $P \leq 0.05$ were considered significant. ROC analysis was performed on log-transformed data using R open source software according to the method of Palmer (18), with healthy controls scaled to have a mean of zero and a variance of one. Markers were ranked according to specificity at defined sensitivity (90%, 95%, or 98%), with early-stage cancer cases ($n = 10$) compared with all controls ($n = 30$ women with no disease or benign disease). To restrict bias in marker performance, statistical fitting was not used. The R script is provided in Supplementary Data S2.

Results

Sample characteristics and antigen identification strategy

The overall strategy for autoantigen identification and validation is presented in Fig. 1A. Individual plasma samples were randomly assigned into "discovery" or "validation" groups, and antigen array experiments performed using pooled discovery group samples to provide an averaged biological measurement. We have previously established this as a cost-effective strategy for proteomic discovery studies (19). Antigens detected by protein arrays were independently confirmed by ELISA, and then retested on individual samples in the validation cohort to determine the prevalence of autoantibodies in patient's plasma.

Inclusion criteria were tightly controlled to provide age- and pathology-matched groups for investigation (Table 1). All samples were obtained from patients at first surgical presentation, prior to any chemotherapy, and were matched for age and menopausal status. Patients were excluded if they had any prior history of gynecologic disease or cancer, and were additionally excluded from control groups if they had a known predisposition (genetic or familial history) of breast or ovarian cancer. Women diagnosed with benign cystadenoma (representing ∼20% of all ovarian neoplasms, typically exhibiting simple cystic structure) or benign cystadenofibroma (representing ∼1.7% of ovarian neoplasms, and often exhibiting complex architecture and vascularization; refs. 20, 21) were included as confounding groups to reduce potential false positives. There were no significant differences in immunoglobulin (Ig) content or subtypes among the samples investigated, nor in average age of the cohort, and, as expected, CA125 was significantly elevated in both early- and late-stage cancer patients relative to all other groups (Supplementary Fig. SF1).

Antibody signatures discriminating between healthy, benign, and malignant conditions

We first assessed normalized Protoarray data using PCA to determine whether antibody signatures differentiated between samples representing (i) no disease, (ii) women with benign ovarian disease, or (iii) women with malignant disease. In addition to IgG profiling, we also assessed IgM (representing early immune response, prior to affinity maturation and class switching; ref. 22) and IgA (representing mucosal surface immunity; ref. 23) responses. Combining all differences (i.e., IgG, IgA, and IgM reactive antigens) identified between disease groups yielded a total of 1,389 antigens that discriminated between no disease, benign disease, or cancers; 96 antigens of these antigens reacted with multiple Ig types. These 1,389 antigens were further restricted by pairwise comparison to include only those showing at least a 2-fold difference ($P \leq 0.05$) between groups (Fig. 1B; Supplementary Table S3). IgM and IgG reactivity was dominant, with antigens recognized by IgA comprising only approximately 15% of the total differences observed. In contrast, we observed substantially fewer differentiating antigens in patients with benign disease; only 69 antigens were significantly different in this group compared with healthy women (Supplementary Table S3), of which approximately 90% were recognized by IgG.

Published OnlineFirst November 15, 2017; DOI: 10.1158/1055-9965.EPI-17-0752

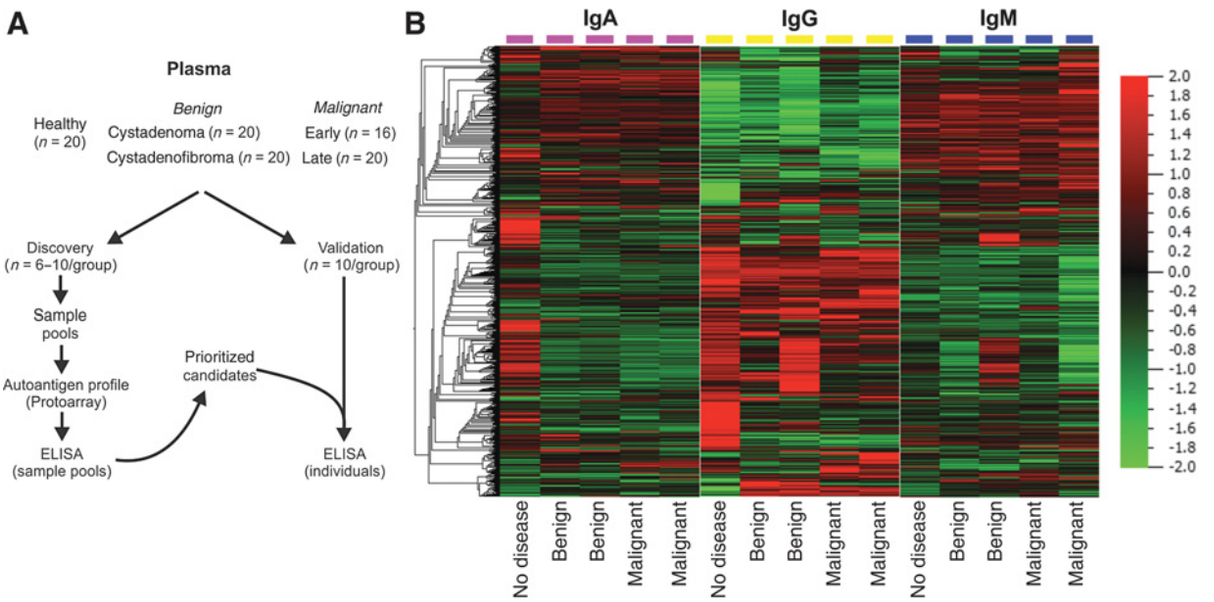

Figure 1.

A, Autoantigen discovery and validation strategy. Plasma samples were randomly divided into two cohorts ("discovery" and "validation"); all disease subgroups had $n = 10$, except for the early-stage cancer discovery group ($n = 6$). Disease sub-groups in the discovery cohort were pooled and used to probe Protoarray protein microarrays for the presence of AAbs against cross-reacting antigens. ELISA was used to validate changes in the discovery pools. Selected antigens were then re-examined by ELISA in individual patient plasma samples from the validation cohort. **B,** Identification of antigens discriminating between groups. Heatmap of antigen detection intensity differentiating between disease states. Individual genes are ordered by hierarchical clustering; samples are ordered by IgG type as indicated. Relative intensity scale is shown.

Comparing our dataset to several similar array studies (15–17, 24), we identified 40 common cancer-specific antigens (Supplementary Table S4) confirming the validity of the approach. As expected, these were largely IgG-mediated; no other studies have investigated the global contribution of IgA to ovarian cancer immune signatures. We also identified five autoantigens associated specifically with benign neoplasms (BYSL, PCBP1, MAGEB2, RAB11B, and ATG4A) that had been previously suggested as potential cancer-associated antigens (15, 16), highlighting the importance of including these confounding samples to overcome false positives in the noncancer setting.

AAb signatures discriminating between localized versus disseminated disease

The exposure, presentation, and recognition of tumor antigens is likely to vary according to tumor localization and progression (25); however, no studies have specifically explored the presence of autoimmune signatures in patients with early-stage compared with high-grade disease. Among those variables associated with malignancy, a total of 184 differences were specific to the early-stage cancer group (FIGO grade 3, stages Ia–c) with 19 antigens recognized by multiple Ig types (Supplementary Table S3). While IgG reactivity was dominant, IgA-reactive antigens were substantially more common in early-stage plasma samples than was observed for late-stage patients and comprised approximately 37% of differences detected (Fig. 2A). Among these were 17 "overlapping" antigens detected in both the early- and late-stage cancer groups (13 recognized by IgG, 4 by IgA), suggesting that while some antigens are dynamically presented or recognized, others may persist throughout disease progression (Table 2).

Enrichment for the cellular distribution of all identified antigens was assessed by Gene Ontology (GO) term, according to disease, stage, and Ig type (Fig. 2B). Cytoskeletal, nuclear, and

Table 1. Summary of sample cohort characteristics

					Discovery cohort			Validation cohort		
Group	Pathology	Grade	Stage	Menopausal status	# Patients	Median age (IQR)	Median CA125 (IQR)	# Patients	Median age (IQR)	Median CA125 (IQR)
Healthy	None	n/a	n/a	post	$n = 10$	59.5 (59–60)	9.5 (7–12.5)	$n = 10$	59.5 (56–65.5)	11.5 (8–15)
Benign A	Serous cystadenoma	n/a	n/a	post	$n = 10$	62 (57–73)	34 (11–50.5)	$n = 10$	59.5 (56–62)	18.5 (12–36)
Benign B	Serous cystadenofibroma	n/a	n/a	post	$n = 10$	70 (57.5–75)	14 (12–16)	$n = 10$	68 (62–70)	10 (9–14)
Early ($n = 6$)	Serous papillary carcinoma	3	I (a-c)	post	$n = 6$	56 (55.5–56)	130.5 (100–243)	$n = 10$	57 (53–69.5)	113.5 (28–199)
Late ($n = 10$)	Serous papillary carcinoma	3	IIIc	post	$n = 10$	59.5 (56–65)	1583.5 (681–3,093)	$n = 10$	60 (59–64.5)	1,004 (488–1,843)

Published OnlineFirst November 15, 2017; DOI: 10.1158/1055-9965.EPI-17-0752

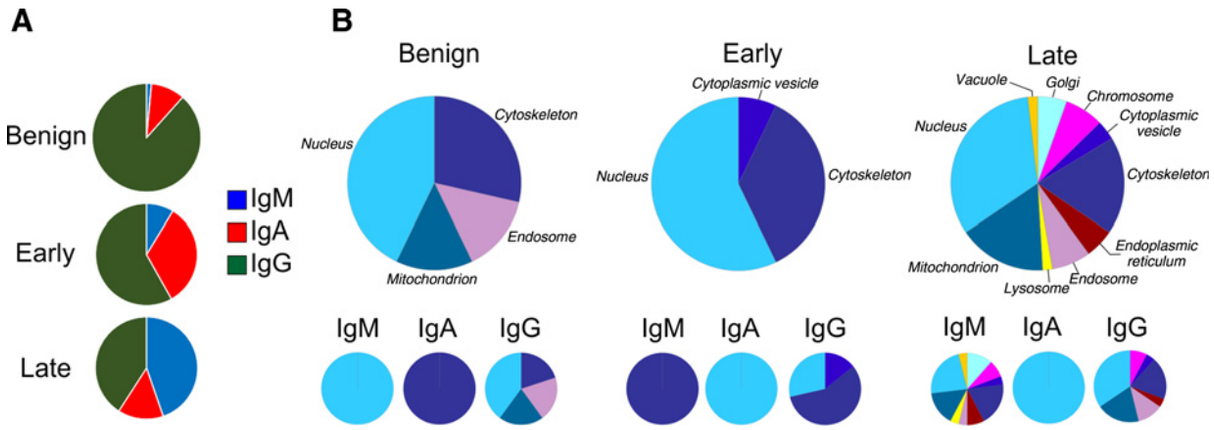

Figure 2.

Ig type and gene ontology localization of antigens associated with benign or malignant disease. **A,** Percentage of Ig type reactivity according to disease state. **B,** Antigen localization (top) and percentage of contributing antibody type (bottom) according to GO term in benign, early- or late-stage tumors.

mitochondrial antigens were over-represented in all disease states; while endosomal or cytoplasmic vesicle antigens were identified in benign or early cancer, respectively. Late-stage antigens were far more diverse in their cellular localizations (Fig. 2B), likely reflecting increased exposure of intracellular antigens in the apoptotic/necrotic cancer environment. Interestingly, cellular localization according to GO annotation differed considerably between Ig types and disease status. IgA-reactive antigens were generally nuclear in cancers, but cytoplasmic in benign disease; in contrast, IgM-reactive antigens in early-stage cancer were cytoplasmic, but were nuclear in benign disease (Fig. 2B).

Functional enrichment analysis of cancer antigens

To identify how differences in antigen recognition might reflect biological function, enrichment analysis was performed using Ingenuity Pathways Analysis (IPA) software. Differentially detected antigens (Supplementary Table S3) were uploaded and examined in benign, early-stage and late-stage specific groupings. Unsurprisingly, canonical DNA damage–induced 14-3-3 gamma signaling was significantly over-represented ($P \leq 0.001$) within the cancer antigen dataset (Supplementary Table S5). Cancer antigens in general were enriched ($P \leq 10^{-5}$) for processes involving cell cycle, gene expression, and DNA repair; cellular organization, function, and movement; and metabolic processes including lipid, amino acid, and other small-molecule biochemistry (Supplementary Table S5). When separated according to stage, both early- and late-stage antigens were enriched for cancer, organismal injury, and cell death/survival–related processes. Cell–cell signaling, cellular assembly, and inflammatory response were more highly enriched among late-stage cancer antigens; contrastingly, cell cycle, growth, and proliferation were all over-represented among the early cancer antigens (Supplementary Table S5). No significant functional enrichment was observed among benign-specific antigens, although two cancer-related

Table 2. Identified antigens common to both early- and late-stage cancers

			Early		Late	
GenBank #	**Protein name**	**Ig type**	***P***	**Fold**	***P***	**Fold**
NM_016638.1	ADP-ribosylation factor-like protein 6-interacting protein 4	IgA	0.022	2.8	0.030	2.4
BC001396.1	Chromosome 9 open reading frame 32 (C9orf32)	IgG	0.040	−2.4	0.050	−2.2
NM_001311.2	Cysteine-rich protein 1	IgG	0.004	2.3	0.003	2.8
NM_017541.2	Beta-crystallin S	IgG	0.010	3.5	0.011	3.3
NP_004084.1	EphrinB2/EFNB2 Protein	IgG	0.015	−2.9	0.027	−2.2
		IgA	0.038	2.0	n/a	n/a
NM_207009.2	Family with sequence similarity 45, member A (FAM45A), mRNA	IgG	0.038	−2.0	0.011	3.8
NM_145269.1	Protein FAM92A1	IgA	0.014	−2.3	0.018	−2.1
NM_173558.2	FYVE, RhoGEF and PH domain-containing protein 2	IgG	0.038	−2.3	0.050	−2.0
BC034146.1	Immunoglobulin kappa variable 1–5 (IGKV1-5)	IgG	0.013	−3.6	0.033	−2.2
NM_207350.1	Similar to FRG1 protein (FSHD region gene 1 protein) (MGC72104)	IgG	0.019	4.1	0.013	5.7
BC008624.1	cDNA clone MGC:18299 IMAGE:4179890, complete cds	IgG	0.044	2.7	0.044	2.7
		IgA	0.033	4.3	n/a	n/a
NM_002625.1	6-phosphofructo-2-kinase/fructose-2,6-biphosphatase 1	IgG	0.043	2.5	0.032	2.9
NP_006262.1	S100A1 Protein	IgG	0.014	−3.3	0.015	−3.2
BC000522.1	Serpin peptidase inhibitor, clade F (alpha-2 antiplasmin, pigment epithelium derived factor), member 1 (SERPINF1)	IgG	0.029	−2.4	0.042	−2.1
BC011234.1	Survival motor neuron domain containing 1 (SMNDC1)	IgG	0.040	−2.4	0.039	−2.4
NM_022827.2	Spermatogenesis associated 20 (SPATA20)	IgG	0.022	−2.2	0.042	−2.6
		IgA	0.035	−2.8	n/a	n/a
NM_004179.1	Tryptophan hydroxylase 1 (tryptophan 5-monooxygenase) (TPH1)	IgA	0.003	3.4	0.005	2.3

Published OnlineFirst November 15, 2017; DOI: 10.1158/1055-9965.EPI-17-0752

networks were identified suggesting some enrichment of functions related to cell growth, proliferation, and survival (Supplementary Table S5).

In keeping with the observed enrichment for cytoskeletal proteins, early IgM-reactive antigens were associated with biological processes related to cell morphology and movement including actin polymerization, stress fiber formation and branching, while late-stage IgM-reactive antigens were related to proliferation, immune function, and secretion (Supplementary Table S5). Early IgG-reactive antigens were associated with apoptosis, adhesion, morphogenesis, and malignancy, while late-stage IgG-reactive antigens were enriched for proliferation. In contrast, early IgA-reactive antigens were linked with cell damage, cell death, and posttranslational modification, while late-stage IgAs were enriched for processes involved in cell clustering. The data suggest that substantially different biological processes are targeted by the different Ig types, and that this process is dynamic, according to the evolution and progression of high-grade serous ovarian tumors (26).

Functional autoantibody networks according to disease stage

Network analyses were performed to identify direct relationships between the identified antigens. In both the early- and late-stage cancer groups, several causal networks strongly suggested the involvement of ERK1/2, p38MAPK, NFκB, and IFN signaling (Supplementary Table S5). Networks associated with early-stage disease were most notably involved inflammatory cytokine signaling and increased metabolic activity, while those identified in late-stage disease tended to cluster around key signaling networks (e.g., ERK1/2, NFκB). The assignment of genes to these functional networks corresponded with strong correlations (≥97% Pearson correlation) in their detection on antigen arrays.

Among the IgG-reactive cancer antigens identified, linear correlation analysis revealed two subgroupings of antigens that displayed similar patterns of detection within cancer groups (Pearson coefficient = 0.97). Collectively, these correlated antigens formed potential "linking" networks suggesting functional relationships between early- and late-stage diseases (Fig. 3A). Each of these networks were investigated further for potential functional relationships that might link antigen recognition between localized and disseminated disease (Supplementary Table S5). Linking network 1 was associated with inflammation, and was enriched for processes involving movement, growth, proliferation, and morphology. In contrast, linking network 2 was associated with metabolism and molecular transport. Enriched functions included cell movement and morphology, cell cycle, and cell–cell signaling. Genes contained within these networks were strongly discriminatory between cancer versus all other sample groups (Fig. 3B).

Validation of selected autoantigens by ELISA

To validate differences in selected antigen reactivity, we first used ELISA to confirm changes observed in the discovery pools. Antigen selection was limited to those antigens for which recombinant or purified protein, homologous to those printed on Protoarrays, could be commercially sourced. In total, we confirmed 19 of 27 antigen-specific changes by ELISA (Supplementary Table S6). Among those validated were several antigens previously identified in similar array experiments, including GMEB1, HMGA1, PFKFB1, and BC008624.1 (16, 24).

To establish the prevalence of AAbs in individual patients, the six antigens with the greatest fold difference detected between sample groups (BAG5, CCDC155, CEP72, GMEB1, HSF1, and SEC23IP) were reevaluated among individual patients ($n = 10$/group) from the "validation" cohort. The prevalence of autoantibodies against BAG5, CEP72, GMEB1, and SEC23IP was highly variable among individual patients; none of these were validated as potential biomarkers of ovarian cancer.

In contrast, two antigens (CCDC155 and HSF1) were significantly elevated in the majority of early-stage patients, in

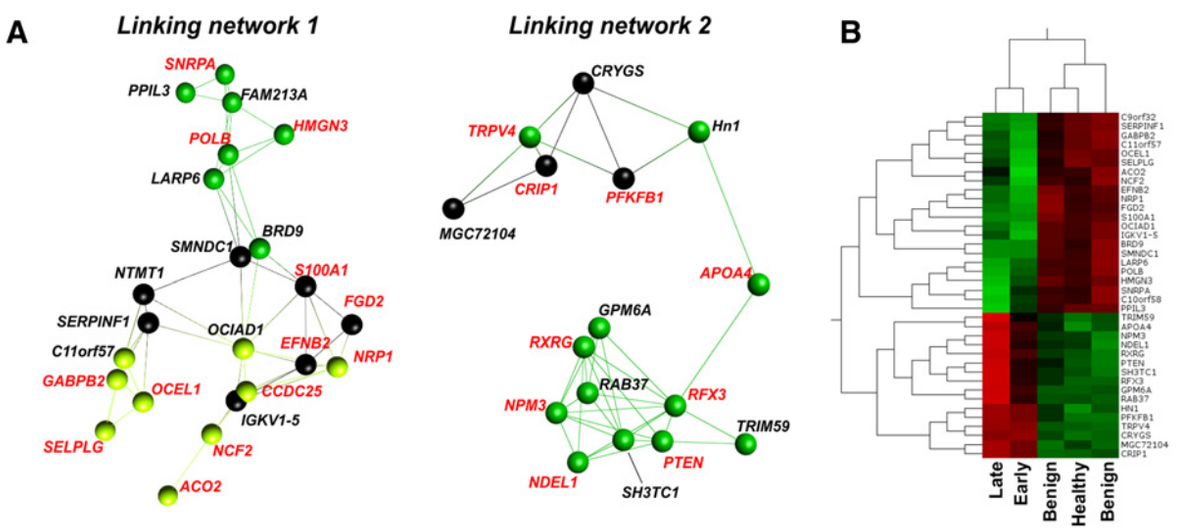

Figure 3.

Antigen reactivity networks linking early- with late-stage disease. Two strongly correlated expression networks (**A**) were identified that displayed overlapping antigen reactivity between early- and late-stage disease. Light green, early-stage; dark green, late stage; black, overlapping. **B,** Heatmap of IgG-reactive genes in linking networks 1 and 2. Genes and samples are ordered by hierarchical clustering.

Published OnlineFirst November 15, 2017; DOI: 10.1158/1055-9965.EPI-17-0752

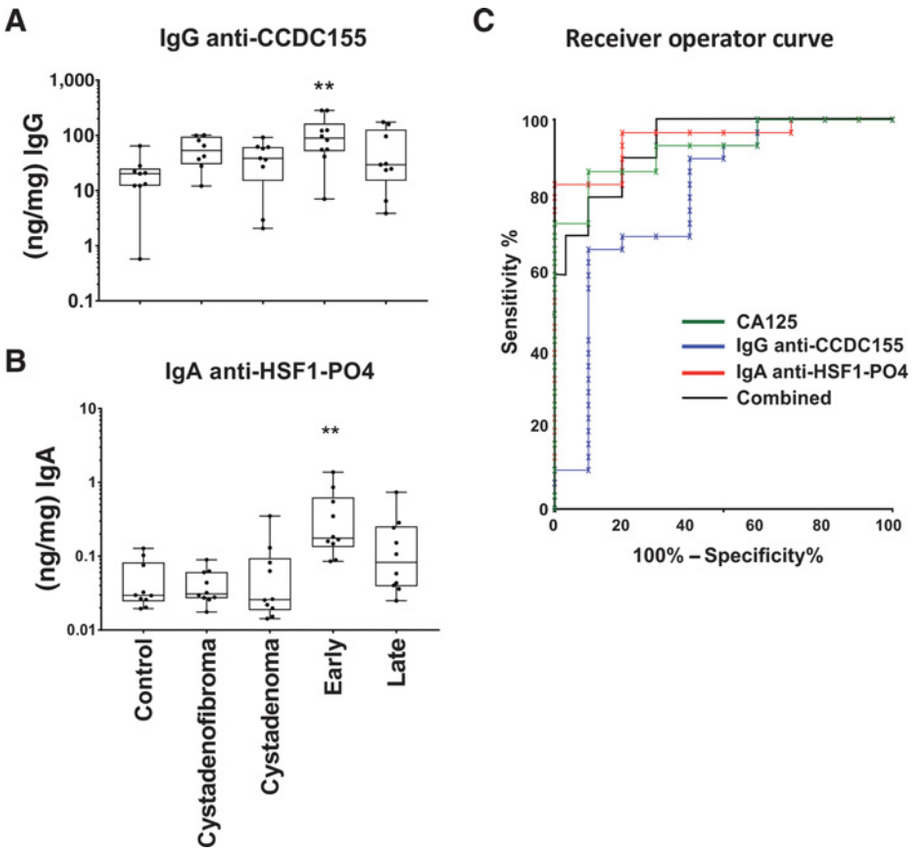

Figure 4.

Validation of autoantibodies against CCDC155 and HSF1 in the independent validation cohort by ELISA. Individual samples ($n = 10$/group) from the validation cohort were analysed for reactivity of (**A**) plasma IgG against CCDC155, or (**B**) plasma IgA against HSF1-PO4. Titres were adjusted for total IgG or IgA titre, respectively. **, $P \leq 0.01$. **C,** ROC analysis was performed on early-stage cancer samples ($n = 10$) *versus* all control and benign disease samples ($n = 30$). Calculated sensitivity/specificity for each marker and marker combination are provided in Supplementary Table S7.

agreement with data from the discovery set. IgG-specific reactivity against CCDC155 was significantly elevated ($P = 0.0013$) in patients with early-stage disease compared with healthy controls (Fig. 4A). Similarly, IgA-specific reactivity against phosphorylated HSF1 was elevated ($P = 0.0007$) in the same patient group (Fig. 4B). Interestingly, AAbs were specific for the phosphorylated form of HSF1, and did not discriminate between disease states when the nonphosphorylated variant was tested (Supplementary Table S6). There was no correlation observed between either CCDC155 or HSF1 reactivity with CA125 (Pearson coefficient).

ROC analyses were carried out to determine the potential diagnostic efficacy of each marker (Fig. 4C; Supplementary Table S7). Statistical fitting was not used due to the small size of the dataset. For the detection of early-stage disease, the best performing marker was HSF1 with sensitivity/specificity of 95%/80% (AUC 0.95) (Fig. 4C; Supplementary Table S7); this was comparatively higher that of CA125, which gave sensitivity/specificity of 95%/40% (AUC 0.93). Single measurement of anti-CCDC155 antibody performed similarly to CA125, with a sensitivity/specificity of 95%/40% (AUC 0.8). Multiple marker combinations at 95% sensitivity did not increase the overall specificity of early-stage HGSOC detection compared with HSF1 alone. However, at a sensitivity of 98% there was improved specificity using the combination of all three markers (Supplementary Table S7), suggesting a potentially additive effect of the combined measurements.

For the differentiation of all cancers from all controls, the combination of HSF1 – CA125 provided better discrimination than CA125 alone; CCDC155 did not reach significance in this comparison. Similarly, neither HSF1 nor CCDC155 reached significance for the differentiation of late-stage disease, where CA125 was clearly the best performed (sensitivity/specificity 99%/100%; Supplementary Table S7). Thus, autoantibodies against HSF1 provided better diagnostic efficacy than CA125 alone for the detection of early-stage disease patients in this small dataset, and the three-marker combination potentially provided improved diagnostic efficacy at high sensitivity for patients with early-stage HGSOCs.

Discussion

In this pilot study, we sought to determine whether AAb profiles could discriminate between early-stage HGSOCs from nonmalignant controls. We restricted our focus to high-grade (type II) epithelial tumors, as these account for approximately 90% of all ovarian cancer-related mortality (1) and therefore represent a patient group that would benefit substantially from early diagnosis. These tumors exhibit substantially different underlying molecular biology and clinical behaviors to low-grade (type I) tumors (1), and these distinct disease types are unlikely to parallel each other in terms of antigen presentation. Nevertheless, few autoantibody discovery studies have made the distinction between disease subsets.

A major limitation for studies focused on early-stage HGSOCs is their rarity of diagnosis, primarily due to their asymptomatic nature and aggressive behavior (1). Indeed, our cohort of 16 patients with FIGO stage I HGSOC was collected

Published OnlineFirst November 15, 2017; DOI: 10.1158/1055-9965.EPI-17-0752

over 6 years, and represents approximately 1% of the total number of HGSOC samples collected during that time. To maximize the potential use of these rare samples, we performed discovery experiments using pooled samples followed by independent validation in a separate cohort of individuals. This provides an efficient and cost-effective approach to biomarker discovery and validation (19), and reduces the use of precious and rare clinical material. Retrospective power analyses suggested that 10 individuals per group was sufficient to detect significant changes in this study. Moreover, the substantial overlap in identified antigens between this and other autoantigen profiling studies (8, 12, 16, 17, 24, 27, 28) suggests that this approach is suitable for the investigation of cancer autoantigens in plasma. To our knowledge, no previous studies have evaluated autoimmune signatures in patients specifically associated with early-stage HGSOCs.

Humoral immune responses are both disease-dependent and location specific; accordingly, both antigen specificity and recognition according to Ig type differed between disease states and the stage of disease dissemination. Antigens themselves were derived from multiple cellular compartments, with the greatest diversity evident for advanced-stage cancer patients. This most likely reflected an increasing level of antigen exposure at different stages of progression, with extensive inflammation contributing to increased levels of apoptotic/necrotic cell death and subsequent recognition of intracellular antigens (29). Several TAAs were also recognized across both early- and late-stage cancer patient groups and were strongly correlated in their abundance and biological functions. In keeping with the adaptive nature of humoral immunity (9), our data suggest that an antigen-specific immune response may be maintained across progressive disease stages; and that the disease-specific recognition of TAAs depends on their identity, cellular origins, and the immune-specific context of their recognition.

To provide a complete profile of circulating AAbs in ovarian cancer patients, secretory IgA- and IgM-mediated responses were examined for the first time in addition to IgG. Surprisingly, IgA AAbs were significantly more abundant in early-stage than late-stage disease, suggesting they may be useful early indicators of malignancy. Both IgA and IgM are the main humoral mediators of mucosal immunity (30–32). Local immune cells associated with mucosal surfaces in the upper female reproductive tract maintain immune surveillance and establish tolerance for sperm and the developing embryo (33), and while IgGs in the genital tract are generally derived from circulation, IgA is produced locally (34, 35). IgA-positive cells in fallopian tube mucosae increase in response to local inflammation (36, 37), and both IgA and secretory component have been found in patients with adenocarcinomas of the endocervix, endometrium, and fallopian tubes (38). As the majority of HGSOCs are suggested to evolve from serous tubal intraepithelial carcinoma (STIC) lesions in the fallopian tube (1), IgA autoantibodies may play an important role in early tumor recognition.

We identified and validated AAbs against two antigens, HSF1 and CCDC155, as potential new biomarkers of early-stage HGSOC. Heat shock transcription factor 1 (HSF1) is a master regulator of the heat shock response, and drives the transcription of multiple stress response genes. Previous work has established that IgA AAbs against HSP27, a downstream target of activated, phosphorylated HSP1, are found in women with gynecologic malignancies, particularly in women with ovarian cancer (~75%; ref. 35). Notably, HSF1 is overexpressed in a significant proportion of ovarian cancer patients (39, 40). Knockdown or knockout of HSF1 results in decreased proliferation, decreased migration, and increased apoptosis in ovarian cancer cells; and prolongs survival time in xenograft models of ovarian cancer (39, 40). The loss of HSF1 also alters ovarian cancer spheroid morphology *in vitro*, and the expression of EMT markers fibronectin, SNAIL, SLUG, and TWIST1; thus, HSF1 has been proposed as a potential anticancer therapeutic target (39, 40). Indeed, recent work has identified that a nucleoside analog Ly101-4B elicits efficient inhibition of HSF1 expression, and exerts potent anticancer activity both *in vitro* and *in vivo* (41).

Importantly, our data showed that circulating autoantibodies recognized only the phosphorylated, activated form of HSF1 (and not the inactive, nonphosphorylated form). HSF1 contains multiple phosphorylation domains, whose occupancy controls the expression of HSPs (42). Recent studies suggested that the presence of activated HSF1^{pSer326} was associated with poor prognosis and reduced overall survival in ovarian cancer patients (42). Moreover, increased levels of HSF1^{pSer326} were associated with the ALDE1^{high} stem-like population (CSCs). HSF1 knock-down decreased the overall number of ALDE1^{high} CSCs, and inhibited their ability to form spheroids *in vitro* (42). Early overexpression and/or activation of HSF1 may therefore induce an AAb response, providing a potential marker for tumor detection. Further analysis of the role of HSF1 in ovarian cancers is therefore warranted.

We also identified coiled-coil domain containing 155 (CCDC155; KASH5; Nesprin-5) as a potential cancer-associated autoantigen. CCDC155 is a member of the Klarsicht, ANC-1, and Syne Homology (KASH) family of mammalian dynein–binding proteins, that participate in mechanical connections between the nuclear envelope and actin cytoskeleton (43–45). KASH proteins play important roles in nuclear migration and positioning during cell cycle, signal transduction, and DNA repair and in the regulation of invadopodia function in tumor cells *in vitro* (46, 47). As part of the SUN1 LINC complex, CCDC155 controls the progression of meiosis in germ cells; CCDC155-deficient mice (both male and female) exhibit meiotic arrest, spindle abnormalities, and defects in homologous chromosome pairing (44, 45). CCDC155 also exhibits haplotype-dependent, allele-specific methylation (48), which is tissue-type specific; notably, several other nesprins can be found as tissue-specific variants (43). The recognition of CCDC155 as a cancer-associated antigen could therefore arise as a consequence of epigenetic changes occurring in ovarian cancer cells (49). No studies have evaluated the potential contribution of CCDC155 to ovarian cancer.

Similar to other AAb studies (e.g., refs. 16, 17), we experienced a high attrition rate when attempting to validate biomarker status using an alternative detection platform. Indeed, only 2 of 27 antigen-specific AAbs identified could be confirmed in individual patients by ELISA. Notwithstanding biological variability within the population, technical limitations also hamper efforts to identify and validate biomarkers, particularly when transferring between detection platforms. For example, the inability to validate specific markers can result from differences in sensitivity or robustness of measurement offered by different platforms or, for example, the failure to present epitopes in an appropriate conformation when moving to an ELISA format, potentially resulting in an absence of reactivity and/or nonspecific cross-reactivity (28). A further

limitation, not often highlighted, lies in the binary nature of ELISA. The single endpoint of ELISA-based testing does not account for the likelihood that circulating autoantibodies may be polyclonal in nature (50). As a consequence, the binding of multiple antibody species to a single antigen may mask *bona fide* specificity; alternately, competition for binding sites may also alter reactivity profiles. The high failure rate experienced in this and other similar studies (16, 17) may therefore reflect an inability to reliably detect and quantify specific biomarkers, rather than their absence.

Our pilot data have identified AAb signatures linked with early-stage HGSOC, and validated two autoreactive antigens (CCDC155 and HSF1) that may be useful as markers of early-stage disease. Ongoing validation studies in a larger cohort are now required to fully assess their utility as biomarkers for the detection of primary or recurrent ovarian cancer.

Disclosure of Potential Conflicts of Interest

M. Plebanski serves as the director of PX Biosolutions. No potential conflicts of interest were disclosed by the other authors.

Authors' Contributions

Conception and design: M. Plebanski, A.N. Stephens
Development of methodology: L.R. Moffitt, A.N. Stephens
Acquisition of data (provided animals, acquired and managed patients, provided facilities, etc.): A.L. Wilson, L.R. Moffitt, N. Duffield, T.W. Jobling, A.N. Stephens
Analysis and interpretation of data (e.g., statistical analysis, biostatistics, computational analysis): A.L. Wilson, L.R. Moffitt, A.N. Stephens
Writing, review, and/or revision of the manuscript: A.L. Wilson, L.R. Moffitt, A. Rainczuk, M. Plebanski, A.N. Stephens
Administrative, technical, or material support (i.e., reporting or organizing data, constructing databases): A.L. Wilson, M. Plebanski
Study supervision: A. Rainczuk, M. Plebanski, A.N. Stephens

Acknowledgments

This work was supported by the Victorian Government's Operational Infrastructure Support Program. Funding support was provided by the National Health and Medical Research Council of Australia (Project #1099375) and the Ovarian Cancer Research Foundation of Australia (https://ocrf.com.au/). M. Plebanski is the recipient of a Senior NHMRC Fellowship. Clinical samples were accessed through the OCRF-sponsored Ovarian Cancer Tissue Banking program.

We thank Ms. Rhiannon Dudley and Ms. Nicole Fairweather for their assistance with clinical sample collection and associated data management. Hudson Institute data audit #9999389.

The costs of publication of this article were defrayed in part by the payment of page charges. This article must therefore be hereby marked *advertisement* in accordance with 18 U.S.C. Section 1734 solely to indicate this fact.

Received August 15, 2017; revised October 23, 2017; accepted November 9, 2017; published OnlineFirst November 15, 2017.

References

1. Kurman RJ, Shih Ie M. The dualistic model of ovarian carcinogenesis: revisited, revised, and expanded. Am J Pathol 2016;186:733–47.
2. Siegel R, Ma J, Zou Z, Jemal A. Cancer statistics, 2014. CA Cancer J Clin 2014;64:9–29.
3. El Bairi K, Kandhro AH, Gouri A, Mahfoud W, Louanjli N, Saadani B, et al. Emerging diagnostic, prognostic and therapeutic biomarkers for ovarian cancer. Cell Oncol 2017;40:105–18.
4. Shi JX, Qin JJ, Ye H, Wang P, Wang KJ, Zhang JY. Tumor associated antigens or anti-TAA autoantibodies as biomarkers in the diagnosis of ovarian cancer: a systematic review with meta-analysis. Expert Rev Mol Diagn 2015;15:829–52.
5. Badgwell D, Bast RC Jr. Early detection of ovarian cancer. Dis Markers 2007;23:397–410.
6. Moore RG, McMeekin DS, Brown AK, DiSilvestro P, Miller MC, Allard WJ, et al. A novel multiple marker bioassay utilizing HE4 and CA125 for the prediction of ovarian cancer in patients with a pelvic mass. Gynecol Oncol 2009;112:40–6.
7. Jacobs IJ, Menon U, Ryan A, Gentry-Maharaj A, Burnell M, Kalsi JK, et al. Ovarian cancer screening and mortality in the UK Collaborative Trial of Ovarian Cancer Screening (UKCTOCS): a randomised controlled trial. Lancet 2016;387:945–56.
8. Karabudak AA, Hafner J, Shetty V, Chen S, Secord AA, Morse MA, et al. Autoantibody biomarkers identified by proteomics methods distinguish ovarian cancer from non-ovarian cancer with various CA-125 levels. J Cancer Res Clin Oncol 2013;139:1757–70.
9. Zaenker P, Gray ES, Ziman MR. Autoantibody production in cancer–the humoral immune response toward autologous antigens in cancer patients. Autoimmun Rev 2016;15:477–83.
10. Dudas SP, Chatterjee M, Tainsky MA. Usage of cancer associated autoantibodies in the detection of disease. Cancer Biomarkers 2010; 6:257–70.
11. Zhu Q, Liu M, Dai L, Ying X, Ye H, Zhou Y, et al. Using immunoproteomics to identify tumor-associated antigens (TAAs) as biomarkers in cancer immunodiagnosis. Autoimmun Rev 2013;12:1123–8.
12. Hudson ME, Pozdnyakova I, Haines K, Mor G, Snyder M. Identification of differentially expressed proteins in ovarian cancer using high-density protein microarrays. Proc Natl Acad Sci U S A 2007;104:17494–9.
13. Ehrlich JR, Tang L, Caiazzo RJ Jr, Cramer DW, Ng SK, Ng SW, et al. The "reverse capture" autoantibody microarray: an innovative approach to profiling the autoantibody response to tissue-derived native antigens. Methods Mol Biol 2008;441:175–92.
14. Chatterjee M, Mohapatra S, Ionan A, Bawa G, Ali-Fehmi R, Wang X, et al. Diagnostic markers of ovarian cancer by high-throughput antigen cloning and detection on arrays. Cancer Res 2006;66:1181–90.
15. Gnjatic S, Wheeler C, Ebner M, Ritter E, Murray A, Altorki NK, et al. Seromic analysis of antibody responses in non-small cell lung cancer patients and healthy donors using conformational protein arrays. J Immunol Methods 2009;341:50–8.
16. Anderson KS, Cramer DW, Sibani S, Wallstrom G, Wong J, Park J, et al. Autoantibody signature for the serologic detection of ovarian cancer. J Proteome Res 2015;14:578–86.
17. Katchman BA, Chowell D, Wallstrom G, Vitonis AF, LaBaer J, Cramer DW, et al. Autoantibody biomarkers for the detection of serous ovarian cancer. Gynecol Oncol 2017;146:129–36.
18. Palmer C, Duan X, Hawley S, Scholler N, Thorpe JD, Sahota RA, et al. Systematic evaluation of candidate blood markers for detecting ovarian cancer. PLoS One 2008;3:e2633.
19. Rainczuk A, Condina M, Pelzing M, Dolman S, Rao J, Fairweather N, et al. The utility of isotope-coded protein labeling for prioritization of proteins found in ovarian cancer patient urine. J Proteome Res 2013;12:4074–88.
20. Cho SM, Byun JY, Rha SE, Jung SE, Park GS, Kim BK, et al. CT and MRI findings of cystadenofibromas of the ovary. Eur Radiol 2004;14:798–804.
21. Alcazar JL, Errasti T, Minguez JA, Galan MJ, Garcia-Manero M, Ceamanos C. Sonographic features of ovarian cystadenofibromas: spectrum of findings. J Ultrasound Med 2001;20:915–9.
22. Hoyer BF, Radbruch A. Protective and pathogenic memory plasma cells. Immunol Lett 2017;189:10–2.
23. Heineke MH, van Egmond M. Immunoglobulin A: magic bullet or Trojan horse? Eur J Clin Invest 2017;47:184–92.
24. Gunawardana CG, Memari N, Diamandis EP. Identifying novel autoantibody signatures in ovarian cancer using high-density protein microarrays. Clin Biochem 2009;42:426–9.
25. Dunn GP, Old LJ, Schreiber RD. The immunobiology of cancer immunosurveillance and immunoediting. Immunity 2004;21:137–48.

Published OnlineFirst November 15, 2017; DOI: 10.1158/1055-9965.EPI-17-0752

26. Zhang L, Conejo-Garcia JR, Katsaros D, Gimotty PA, Massobrio M, Regnani G, et al. Intratumoral T cells, recurrence, and survival in epithelial ovarian cancer. N Engl J Med 2003;348:203–13.
27. Ali-Fehmi R, Chatterjee M, Ionan A, Levin NK, Arabi H, Bandyopadhyay S, et al. Analysis of the expression of human tumor antigens in ovarian cancer tissues. Cancer Biomark 2010;6:33–48.
28. Murphy MA, O'Connell DJ, O'Kane SL, O'Brien JK, O'Toole S, Martin C, et al. Epitope presentation is an important determinant of the utility of antigens identified from protein arrays in the development of autoantibody diagnostic assays. J Proteomics 2012;75:4668–75.
29. Kourtzelis I, Rafail S. The dual role of complement in cancer and its implication in anti-tumor therapy. Ann Transl Med 2016;4:265.
30. Brandtzaeg P. Mucosal immunity in the female genital tract. J Reprod Immunol 1997;36:23–50.
31. Kutteh WH, Hatch KD, Blackwell RE, Mestecky J. Secretory immune system of the female reproductive tract: I. Immunoglobulin and secretory component-containing cells. Obstet Gynecol 1988;71:56–60.
32. Kutteh WH, Mestecky J. Secretory immunity in the female reproductive tract. Am J Reprod Immunol 1994;31:40–6.
33. Lee SK, Kim CJ, Kim DJ, Kang JH. Immune cells in the female reproductive tract. Immune Netw 2015;15:16–26.
34. Wang Y, Ben K, Cao X, Wang Y. Transport of anti-sperm monoclonal IgA and IgG into murine male and female genital tracts from blood. Effect of sex hormones. J Immunol 1996;156:1014–9.
35. Korneeva I, Bongiovanni AM, Girotra M, Caputo TA, Witkin SS. IgA antibodies to the 27-kDa heat-shock protein in the genital tracts of women with gynecologic cancers. Int J Cancer 2000;87:824–8.
36. Kutteh WH, Blackwell RE, Gore H, Kutteh CC, Carr BR, Mestecky J. Secretory immune system of the female reproductive tract. II. Local immune system in normal and infected fallopian tube. Fertil Steril 1990;54:51–5.
37. Arraztoa JA, Rocha A, Varela-Nallar L, Velasquez L, Toro V, Cardenas H, et al. IgA in the lumen of the human oviduct is not related to the menstrual cycle but increases during local inflammation. Fertil Steril 2002;77:633–4.
38. Lee YS, Raju GC. Expression of IgA and secretory component in the normal and in adenocarcinomas of Fallopian tube, endometrium and endocervix. Histopathology 1988;13:67–78.
39. Powell CD, Paullin TR, Aoisa C, Menzie CJ, Ubaldini A, Westerheide SD. The heat shock transcription factor HSF1 induces ovarian cancer epithelial-mesenchymal transition in a 3D spheroid growth model. PLoS One 2016;11:e0168389.
40. Chen YF, Wang SY, Yang YH, Zheng J, Liu T, Wang L. Targeting HSF1 leads to an antitumor effect in human epithelial ovarian cancer. Int J Mol Med 2017;39:1564–70.
41. Chen YF, Dong Z, Xia Y, Tang J, Peng L, Wang S, et al. Nucleoside analog inhibits microRNA-214 through targeting heat-shock factor 1 in human epithelial ovarian cancer. Cancer Sci 2013;104:1683–9.
42. Yasuda K, Hirohashi Y, Mariya T, Murai A, Tabuchi Y, Kuroda T, et al. Phosphorylation of HSF1 at serine 326 residue is related to the maintenance of gynecologic cancer stem cells through expression of HSP27. Oncotarget 2017;8:31540–53.
43. Autore F, Shanahan CM, Zhang Q. Identification and validation of putative nesprin variants. Methods Mol Biol 2016;1411:211–20.
44. Luo Y, Lee IW, Jo YJ, Namgoong S, Kim NH. Depletion of the LINC complex disrupts cytoskeleton dynamics and meiotic resumption in mouse oocytes. Sci Rep 2016;6:20408.
45. Horn HF, Kim DI, Wright GD, Wong ES, Stewart CL, Burke B, et al. A mammalian KASH domain protein coupling meiotic chromosomes to the cytoskeleton. J Cell Biol 2013;202:1023–39.
46. Esra Demircioglu F, Cruz VE, Schwartz TU. Purification and structural analysis of SUN and KASH domain proteins. Methods Enzymol 2016;569:63–78.
47. Revach OY, Weiner A, Rechav K, Sabanay I, Livne A, Geiger B. Mechanical interplay between invadopodia and the nucleus in cultured cancer cells. Sci Rep 2015;5:9466.
48. Do C, Lang CF, Lin J, Darbary H, Krupska I, Gaba A, et al. Mechanisms and disease associations of haplotype-dependent allele-specific DNA methylation. Am J Hum Genet 2016;98:934–55.
49. Saleh MH, Wang L, Goldberg MS. Improving cancer immunotherapy with DNA methyltransferase inhibitors. Cancer Immunol Immunother 2016;65:787–96.
50. Kijanka G, Murphy D. Protein arrays as tools for serum autoantibody marker discovery in cancer. J Proteomics 2009;72:936–44.

cancers

MDPI

Article

DPP4 Inhibitor Sitagliptin Enhances Lymphocyte Recruitment and Prolongs Survival in a Syngeneic Ovarian Cancer Mouse Model

Amy L. Wilson [1,2,3], Laura R. Moffitt [1,2], Kirsty L. Wilson [4], Maree Bilandzic [1,2], Mark D. Wright [3], Mark D. Gorrell [5], Martin K. Oehler [6], Magdalena Plebanski [4,*] and Andrew N. Stephens [1,2,*]

1 Centre for Cancer Research, Hudson Institute of Medical Research, Clayton 3168, Australia; amy.wilson@hudson.org.au (A.L.W.); laura.moffitt@monash.edu (L.R.M.); maree.bilandzic@hudson.org.au (M.B.)
2 Department of Molecular and Translational Sciences, Monash Health, Clayton 3168, Australia
3 Department of Immunology and Pathology, Monash University, Clayton 3800, Australia; mark.wright@monash.edu
4 School of Health and Biomedical Sciences, RMIT University, Bundoora 3083, Australia; kirsty.wilson2@rmit.edu.au
5 Centenary Institute, Faculty of Medicine and Health, University of Sydney, Camperdown 2006, Australia; m.gorrell@centenary.org.au
6 Department of Gynaecological Oncology, Royal Adelaide Hospital, Adelaide 5000, Australia; martin.oehler@adelaide.edu.au
* Correspondence: magdalena.plebanski@rmit.edu.au (M.P.); Andrew.n.stephens@hudson.org.au (A.N.S.)

Simple Summary: The role of immunity in the development and progression of epithelial ovarian cancer (EOC) is well established. Poor T-cell infiltration is associated with mortality in EOC patients, and recent evidence has suggested that the enzyme DPP4 plays a role in this process. The aim of our study was to evaluate the potential of the clinically-approved DPP4-inhibitor sitagliptin to improve immune responses in mice with EOC. We showed that sitagliptin improved CD8+ T-cell responses in an EOC mouse model, consequently reducing metastatic burden and prolonging survival. These data provide a rationale for the use of DPP4-inhibitors as a second-line treatment for EOC.

Abstract: Immunity plays a key role in epithelial ovarian cancer (EOC) progression with a well-documented correlation between patient survival and high intratumoral CD8+ to T regulatory cell (Treg) ratios. We previously identified dysregulated DPP4 activity in EOCs as a potentially immune-disruptive influence contributing to a reduction in CXCR3-mediated T-cell infiltration in solid tumours. We therefore hypothesized that inhibition of DPP4 activity by sitagliptin, an FDA-approved inhibitor, would improve T-cell infiltration and function in a syngeneic ID8 mouse model of EOC. Daily oral sitagliptin at 50 mg/kg was provided to mice with established primary EOCs. Sitagliptin treatment decreased metastatic tumour burden and significantly increased overall survival and was associated with significant changes to the immune landscape. Sitagliptin increased overall CXCR3-mediated CD8+ T-cell trafficking to the tumour and enhanced the activation and proliferation of CD8+ T-cells in tumour tissue and the peritoneal cavity. Substantial reductions in suppressive cytokines, including CCL2, CCL17, CCL22 and IL-10, were also noted and were associated with reduced CD4+ CD25+ Foxp3+ Treg recruitment in the tumour. Combination therapy with paclitaxel, however, typical of standard-of-care for patients in palliative care, abolished CXCR3-specific T-cell recruitment stimulated by sitagliptin. Our data suggest that sitagliptin may be suitable as an adjunct therapy for patients between chemotherapy cycles as a novel approach to enhance immunity, optimise T-cell-mediated function and improve overall survival.

Keywords: sitagliptin; ovarian cancer; DPP4; ID8; syngeneic; immune; T-cell

Citation: Wilson, A.L.; Moffitt, L.R.; Wilson, K.L.; Bilandzic, M.; Wright, M.D.; Gorrell, M.D.; Oehler, M.K.; Plebanski, M.; Stephens, A.N. DPP4 Inhibitor Sitagliptin Enhances Lymphocyte Recruitment and Prolongs Survival in a Syngeneic Ovarian Cancer Mouse Model. *Cancers* **2021**, *13*, 487. https://doi.org/10.3390/cancers13030487

Academic Editors: Oscar J. Cordero and Armand Bensussan
Received: 11 December 2020
Accepted: 19 January 2021
Published: 27 January 2021

1. Introduction

Epithelial ovarian cancer (EOC) is the most lethal gynaecological malignancy and the sixth-leading cause of cancer-related deaths in females [1]. Standard treatments for ovarian cancer involve highly invasive surgery and concurrent platinum (carboplatin and cisplatin) and taxane (paclitaxel) chemotherapies, to which the majority of patients initially respond favourably [2]. However, disease recurrence and acquired chemoresistance is almost universal, limiting therapeutic options and accounting for the disproportionally high mortality rate of EOC [3]. Novel therapeutic strategies for EOC include endocrine therapy, which has thus far shown reasonable therapeutic responses [4] and immunotherapies. However, their further development for the treatment of EOC is urgently required to improve survival rates.

Whilst substantial evidence supports an important and complex role for immunity in the development and progression of EOC [5], immunotherapy currently lacks efficacy for EOC due to immune evasion and subsequent poor lymphocyte infiltration and dysfunction [6]. Tumour-infiltrating lymphocytes (TILs) including cytotoxic CD8+ T effector (Teff) cells are recruited to the ovarian tumour by expression of chemokines such as CXCL10 in a CXCR3-mediated manner and facilitate antitumour immune responses by producing interferon (IFN)-γ and by releasing the content of cytolytic granules for the direct elimination of cancer cells [7]. By contrast, T regulatory cells (Tregs) impair antitumour immunity by secreting cytokines such as TGF-ß and IL-10 and by inhibiting the production and activity of proinflammatory cytokines [8]. Accordingly, a high ratio of Treg to Teff cells is a strong predictor of poor prognosis in ovarian cancer patients [9]. Whilst active immunosuppression within the ovarian tumour microenvironment thus promotes tumour progression, its targeted disruption holds significant potential to improve immunotherapeutic efficacy for EOC treatment.

Dysregulation of the type II transmembrane glycoprotein dipeptidyl peptidase 4 (DPP4) has been implicated in several cancer types including urothelial carcinoma [10], papillary thyroid carcinoma [11], metastatic prostate cancer [12] and epithelial ovarian cancer [13]. DPP4 can enzymatically truncate proteins containing either L-proline or L-alanine at the penultimate position, and for this reason plays a major role in glucose metabolism where it regulates glucagon-like peptide-1 (GLP1) and gastric inhibitory protein (GIP) [14]. Accordingly, several DPP4 inhibitors such as sitagliptin are approved for the management of type 2 diabetes, as DPP4 inhibition in this context prolongs the half-life of GLP1 and GIP, increasing endogenous insulin secretion [15]. Other DPP4 substrates include neuropeptide Y, substance P and chemokines such as CXCL9, CXCL10, CXCL11 and CXCL12 [16–18]. In particular, DPP4 plays an important role in the regulation of CXCL10 function and associated T cell recruitment in patients with hepatitis C virus (HCV) [19]. Previous work has demonstrated preserved bioactive CXCL10 in healthy individuals receiving the clinically approved DPP4 inhibitor sitagliptin, thereby establishing its role in CXCL10 post-translational modification [20]. Furthermore, mice bearing melanoma and colorectal tumours treated with sitagliptin showed improved naturally occurring antitumour immune responses via preservation of bioactive CXCL10, a chemokine that is essential for lymphocyte chemotaxis [21].

DPP4 overexpression has been established in EOC [13,18]. However the use of DPP4 inhibitors as a novel immunotherapy for this disease has not yet been shown. In the current study, we sought to determine whether DPP4 inhibition using sitagliptin enhances lymphocyte tumour infiltration in a syngeneic mouse model of EOC [22] to abrogate tumour-mediated immune suppression and promote antitumour immunity. In the current study, we demonstrated delayed tumour metastasis and increased survival with associated increases in CD8+ T-cell activation, proliferation and CXCR3-mediated T-cell recruitment to ovarian tumour tissue. Overall, our findings provide proof of principle evidence for the repurposing of DPP4 inhibitors as a novel ovarian cancer immunotherapy.

2. Methods

2.1. Cell Culture

The ID8 mouse epithelial ovarian cancer cell line (a gift from Dr. Kathy Roby, Kansas University Medical Center) was maintained in DMEM (Gibco, Palo Alto, CA, USA) containing 4% fetal bovine serum (FBS), 1% penicillin/streptomycin (PS) and 1x insulin-transferrin-selenium (ITS). *pROSA*-iRFP720 ID8 cells were generated and maintained as previously described [22].

2.2. Animal Experiments

Female 8-week-old C57BL/6 mice were obtained from Monash Animal Services (Melbourne, VIC, Australia) and housed in a specific-pathogen-free (SPF) facility. All animal protocols were approved by the Alfred Medical Research and Education Precinct (AMREP) animal ethics committee, Melbourne, Australia (approval #E/1682/2016/M). Treatment and care of the animals were in accordance with institutional guidelines and with the Australian code for the care and use of animals for scientific purposes.

Mice were supplemented with an SF-AIN-93M rodent diet to reduce intrinsic autofluorescence. Mice (n = 5/group) were divided into four treatment groups (untreated, sitagliptin, paclitaxel, sitagliptin-paclitaxel combination) and three time points (early-stage disease, metastatic disease, survival) (Supplementary Figure S1). For treatments, mice were given food containing 50 mg/kg/day equivalent sitagliptin (Januvia®, Merck, Kenilworth, NJ, USA) (plus 25 mg/kg and 100 mg/kg for optimisation studies) from week two post-tumour implantation. For combination treatment studies, mice receiving sitagliptin were also administered two doses of intraperitoneal paclitaxel (15 mg/kg) (Pfizer Inc., New York, NY, USA) at week three and four post-tumour implantation. Mice were monitored weekly for weight and circumference, and humane endpoints were determined by a body abdominal circumference of > 100 mm and general wellbeing (lack of responsiveness, hunched posture, piloerection, eyes squinted). Once endpoint was reached, mice were humanely sacrificed by CO_2 asphyxiation. Blood was processed for serum for cytokine analysis, and red blood cells were lysed for leukocyte analysis by flow cytometry. Brachial and inguinal lymph nodes, spleen and peritoneal washes were harvested for flow cytometry, and ovarian tumour and metastatic tumour tissue were either formalin-fixed and embedded in paraffin for immunofluorescence or preserved in optical cutting temperature (O.C.T.) compound for DPP4 in situ enzyme activity assays.

2.3. Intrabursal Implantation of ID8 pROSA-iRFP720 Tumours

Tumours were established by ovarian intrabursal (IB) implantation of *pROSA*-iRFP720 ID8 cells as described previously [22,23]. Mice were anaesthetised in an induction chamber using 3% isofluorane in 1L/min oxygen and then maintained at 2% isofluorane in 0.3 L/min oxygen using a rodent facemask. An incision was made at the mid-dorsal region of the skin and the peritoneal membrane was excised at the latero-dorsal point above the location of the right ovary. The ovarian fat pad was externalised and stabilised with a serrefine clamp. 1×10^6 *pROSA*-iRFP720 ID8 cells were loaded into a Hamilton microliter syringe (Sigma-Aldrich, St. Louis, MO, USA) and injected underneath the ovarian bursa using a dissecting microscope for guidance. The skin was closed using Michel suture clips. Mice were monitored for recovery, and suture clips were removed seven days postsurgery.

2.4. In Vivo Fluorescence Imaging

In vivo near-infrared fluorescence imaging was performed weekly using an IVIS Lumina III in Vivo Imaging System as described previously [22]. Briefly, *pROSA*-iRFP720 ID8 tumour-bearing mice were anesthetised using isofluorane in oxygen and were imaged at field of view (FOV) C with brightfield and X-ray set on auto-exposure. iRFP720 fluorescence was detected using the spectral unmixing iRFP filter set (excitation 620 nm, 640 nm, 660 nm, 680 nm; emission 710 nm), at an exposure time of 5 s. Spectral unmixing of iRFP720 signal from intrinsic autofluorescence was performed by subtracting $680_{ex}/710_{em}$

fluorescence values from the other channels using an established custom spectral unmixing algorithm. All quantitative fluorescence measurements and analyses were performed using the Living Image software (v 4.5.1, PerkinElmer, Waltham, MA, USA).

2.5. Measurement of Plasma DPP4 Enzyme Activity

DPP4 enzyme activity in mouse serum was measured using H-Gly-Pro-pNA (Sigma-Aldrich, MO, USA) as previously described [18] Human recombinant DPP4 (Abcam, Cambridge, England) was used as a positive control for DPP4 enzyme activity, and recombinant DPP4 treated with 1µM sitagliptin (Januvia®) was used as a control for enzyme inhibition. A standard curve was constructed using pNA (Sigma-Aldrich, MO, USA) ranging from 1.56 mM–50 mM. All measurements were carried out in duplicate. Absorbance at 405 nm and 570 nm was measured every 5 min for 3 h at 37 °C using a Cytation 3 MultiMode Plate Imager (BioTek® Instruments Inc., Winooski, VT, USA). Absorbance values at 405nm were subtracted from readings at 570 nm to account for potential optical interference. Standard curves were constructed using Gen5.0 software v2.05 (BioTek Instruments Inc., Winooski, VT, USA).

2.6. In Situ Staining of DPP4 Activity

For evaluation of in situ DPP4 activity, 10 µm frozen cryosections from ovarian tumours were air dried and incubated with 1.5 mM glycyl-prolyl-4-methoxy-β-naphthylamide and 2.5 mM Fast Blue BB Salt in assay buffer (50 mM Tris, 150 mM NaCl, 0.05% Tween 20 at pH 7.6) for 30 min at 37 °C [24]. Sections were washed with assay buffer, nuclei were stained using Harris haematoxylin (Sigma-Aldrich, MO, USA) and slides were mounted with water. Slides were immediately imaged with a Nikon Eclipse 50i microscope (Nikon, Tokyo, Japan) using a 10× and 20× objective, and captured with a Nikon DS-Fi1 camera (Nikon, Tokyo, Japan). Ovarian tumour and liver sections treated with 1 µM sitagliptin (Januvia®) served as negative controls, and liver sections served as positive controls. Images were analysed using ImageJ v1.0 (National Institute of Health, Rockville, MD, USA) for percentage of area and integrated density.

2.7. Flow Cytometry

Leukocytes from lymph nodes, blood, spleen and peritoneal cavity wash were collected and isolated as described [25], and analysed by flow cytometry. Antimouse CD16/CD32 antibody (1:50, BD Biosciences, clone #2.4G2) was used to block nonspecific binding. Zombie Aqua™ fixable viability dye (BioLegend, San Diego, CA, USA) was used to distinguish live and dead cells. The following fluorochrome-conjugated antibodies were used: CD3e-AF700 (1:200, BD Biosciences, clone #500A2), CD4-BUV395 (1:100, BD Biosciences, clone #RM4-5), CD8a-PerCP (1:100, BioLegend, clone #53-6.7), CD25-PE-CF594 (1:100, BD Biosciences, #PC-61), FoxP3-APC (1:50, eBioscience, clone #FJK-16S), CD11b-APC (1:200, BioLegend, clone #MI/71), CD11c-BV421 (1:50, BD Biosciences, clone #HL3), GR1-PerCP Cy5.5 (1:200, BD Biosciences, clone #RB6-8C5), F4/80-BV711 (1:100, BioLegend, clone #BM8), CD69-APC/Cy7 (1:100, BD Biosciences, clone #HI-2F3), Ki67-BV786 (1:100, BD Biosciences, clone #B56), CCR4-BV421 (1:100, Biolegend, clone #2G12), and CXCR3-BV605 (1:100, BioLegend, clone #CXCR3-173). Single stained beads were used to set compensation controls, and fluorescence minus one (FMO) controls were used to define population gates (Supplementary Figure S2). FMO1: CD3, CD4, CD8; FMO2: CD3, CD4, CD8, CD25, FoxP3; FMO3: CD11c, F4/80, GR1. Data were acquired using a BD LSRFortessa X-20 (BD Biosciences, Franklin Lakes, NJ, USA), and was analysed using FlowJo software v10.5.0 (LCC, Ashland, OR, USA).

2.8. Tissue Immunofluorescent Staining

Immunofluorescent staining was performed on 4µm formalin-fixed, paraffin-embedded tumour tissue microarrays (TMAs), constructed by Monash Health, Clayton, Australia. Following deparaffinisation, antigen retrieval was performed by boiling slides in sodium cit-

rate buffer, and permeabilisation was performed using 0.25% *v/v* Triton X-100. Nonspecific antibody binding was blocked with 6% normal serum in TBS/0.25% Triton X-100, and primary antibodies were applied and incubated overnight at 4 °C. Fluorochrome-conjugated antibodies used were: CD3-AlexaFluor®647 (30 µg/mL, BD Biosciences, clone #17A2), CD4-eFluor660 (10 µg/mL, eBioscience, clone #4SM95), CD8a-eFluor615 (20 µg/mL, eBioscience, clone #53-6-7), CD69-AlexaFluor®488 (30 µg/mL, BioLegend, clone #H1-2F3) and CXCR3 (5 µg/mL, GeneTex, Irvine, CA, USA) plus goat antirabbit IgG H + L-AlexaFluor®488 secondary antibody (Abcam, Cambridge, UK). Sudan Black B (Sigma-Aldrich, MO, USA) (0.3% in 70% ethanol) was used to reduce intrinsic autofluorescence. Nuclei were stained with DAPI (ThermoFisher Scientific, Walsham, MA, USA) prior to mounting with DPX (Sigma-Aldrich, MO, USA). Fluorescence images were captured using the VS120 Virtual Slide Microscope (Olympus Corporation, Shinjuku City, Tokyo, Japan) by the Monash Health Translation Precinct (MHTP) Histology Facility, Clayton, Australia. Images were processed using the Olyvia software v2.9.1 (Olympus Corporation, Japan) and analysed using the ImageJ v1.0 software (National Institute of Health, Bethesda, MD, USA) for colocalisation of CD4+CXCR3+, CD8+CXCR3+, and CD3+CD8+CD69+ (percentage of area).

2.9. Chemokine Luminex Assay

Quantitation of 31 cytokines in mouse serum was determined using a Bio-Plex Pro™ Mouse Chemokine Panel 31-Plex (Bio-Rad, Hercules, CA, USA) as described [26]. The assay was performed using mouse serum diluted at 1:5 in sample diluent, data acquisition was performed using the Bio-Plex 200 reader (Bio-Rad, CA, USA) and was analysed using a two-group comparison of fold-change on the Qlucore Omics Explorer v3.5 software (Qlucore AB, Lund, Sweden).

2.10. Statistical Analysis

All statistical analyses were performed using GraphPad Prism v8.0.2 (GraphPad Software Inc., San Diego, CA, USA) unless otherwise stated. A two-way ANOVA was used to analyse statistical significance between groups for DPP4 activity and analysis of small intestine-associated tumour nodules. A two-way ANOVA and Sidak multiple comparisons test were used to analyse statistical significance between groups for flow cytometry immune populations. A log-rank (Mantel-Cox) test was used to analyse statistical significance between groups for the Kaplan-Meier survival curve, with approximate 95% confidence intervals calculated for the sample medians. A two-group comparison was used to analyse statistical significance between cytokines using the Qlucore Omics Explorer v3.5 software (Qlucore AB, Lund, Sweden). Data are presented as mean ±SD unless otherwise stated, and $p < 0.05$ was considered statistically significant.

3. Results

3.1. Sitagliptin Alters DPP4 Activity and Localisation in Tumour Tissue

To establish the optimal concentration of sitagliptin required to inhibit systemic and tumour-localised DPP4 activity, mice bearing ovarian tumours were treated with 25, 50 or 100 mg/kg/day (oral, in food) sitagliptin for two weeks. DPP4 protein expression and activity were measured in serum and in ovarian tumour tissue. 50 mg/kg/day was the minimum concentration required to significantly reduce DPP4 specific activity in circulation two weeks following treatment initiation, with an approximate 58% reduction (Figure 1A). Total DPP4 inhibition was not reached at any of the concentrations examined. Interestingly, we observed that total soluble DPP4 (sDPP4) protein increased following sitagliptin treatment (Figure 1B) with no accompanying change in enzyme activity (Figure 1C). This supports previous data demonstrating the upregulation of sDPP4 levels following enzyme inhibition in diabetic mice [27].

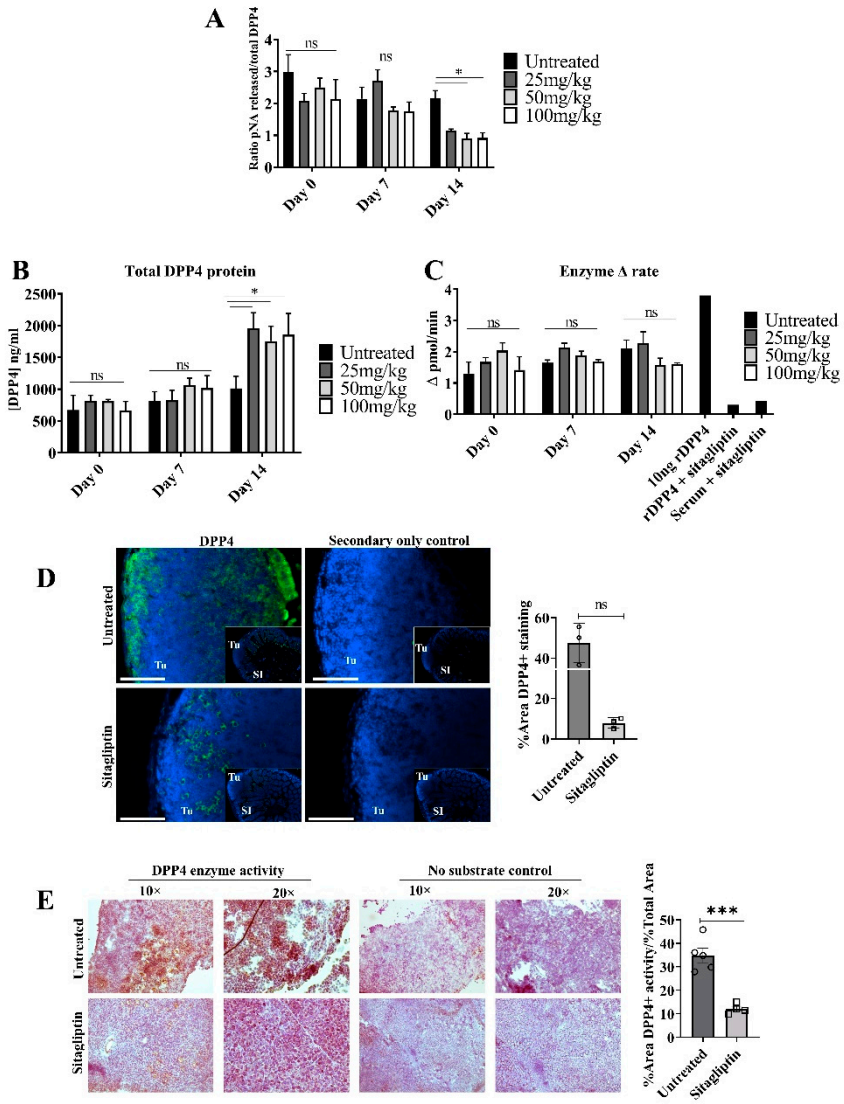

Figure 1. Circulating soluble and tumour-specific DPP4 expression and enzyme activity in mice treated with sitagliptin. ID8 iRFP+ epithelial ovarian tumours were intrabursally implanted into C57BL/6 mice and were allowed to develop for two weeks. Mice received daily oral sitagliptin treatment (25, 50 and 100 mg/kg) and circulating DPP4 protein expression and enzyme activity was measured. (**A**) Specific DPP4 activity in serum from mice treated with 25, 50, 100 mg/kg/day of sitagliptin at days 0, 7 and 14 following treatment. Specific DPP4 activity was determined by calculating the ratio of DPP4 enzyme activity (pmol/mL) to total protein concentration (ng/mL). (**B**) DPP4 protein concentration (ng/mL) was determined using a mouse anti-DPP4 ELISA kit. (**C**) Soluble DPP4 enzyme activity was determined by measuring the amount of p-nitronaniline (pNA) cleaved by DPP4 from the substrate H-Gly-Pro-pNA. (**D**) Representative fluorescent images of small intestine-associated metastases from mice bearing ID8 pROSA-iRFP720 tumours, treated with or without 50 mg/kg/day sitagliptin. DPP4 staining is shown in green and nuclei are stained with DAPI (blue). SI = small intestine; Tu = tumour. Scale bar represents 100 µm. Images were acquired using the Cytation 3 imaging Multi-Mode Reader (BioTek, VT, USA) and were processed using the Gen5™ software v2.05 (BioTek, VT, USA). Bar graph shows the percentage of DPP4-positive staining in metastatic small intestine-associated metastases (n = 3). (**E**) Tumour in situ DPP4 activity in mice bearing ID8 *pROSA*-iRFP720 tumours treated with 50mg/kg/day sitagliptin. In situ DPP4 activity was detected using Gly-Pro 4-methoxy-β-naphthylamide as a substrate, and nuclei were stained with haematoxylin. The bar graph indicates quantitated in situ DPP4 activity (n = 5). Data are presented as mean ± SD. ns = no significance; * = $p < 0.05$; *** = $p < 0.001$.

We also evaluated the effect of sitagliptin on DPP4 expression and activity in tumour tissues in situ. Unlike sDPP4 in circulation, there was a decreasing trend in DPP4 abundance in tumour tissue two weeks following the commencement of sitagliptin treatment (Figure 1D). Unexpectedly, DPP4 localization was also altered; in untreated tumours, DPP4 staining was largely associated with the periphery of tumour mass, whilst in sitagliptin-treated mice, peripheral localization was absent and DPP4 staining was localised inside the tumour mass (Figure 1D). In situ DPP4 enzyme activity was also substantially reduced in sitagliptin-treated mice, in agreement with reduced local abundance (Figure 1E).

3.2. Sitagliptin Reduces Overall Tumour Burden and Prolongs Survival

Using our validated ID8 iRFP720 syngeneic ovarian cancer model [22], we evaluated the effect of sitagliptin treatment on ovarian cancer progression and overall survival. Mice with primary ID8 *pROSA*-iRFP720 ovarian tumours were treated with 50 mg/kg/day of oral sitagliptin, commencing two weeks post-implant, until experimental endpoint. Whilst sitagliptin treatment did not alter primary tumour volume (Figure 2A–C), there was a significant reduction in visible metastatic deposits compared to untreated controls (Figure 2D,E). Consistent with progression in this model, untreated mice developed extensive, disseminated metastatic deposits throughout the peritoneum, macroscopic tumour deposits on the liver, signs of anaemia (pale liver and extremities) and an accumulation of ascites fluid at eight weeks post-implant. By contrast, sitagliptin-treated mice had significantly fewer visible metastatic nodules and did not display signs of anaemia (Figure 2D,E). Overall, reducing DPP4 activity with sitagliptin reduced metastatic tumour burden in vivo.

The impact of daily sitagliptin treatment on overall survival was also assessed. Mice received daily oral sitagliptin until they became moribund due to ascites fluid accumulation. Sitagliptin treated mice had a median survival of 138 days (95% CI = 90–152), compared to 108 days (95% CI = 88–127) in the untreated controls (Figure 2F). The experiment overall was terminated at day 152, with a single sitagliptin-treated animal euthanised before reaching humane endpoint. Thus, daily oral sitagliptin significantly improved overall survival of mice (n = 5/group) with ID8 *pROSA*-iRFP720 epithelial tumours (p = 0.0269).

3.3. Sitagliptin Alters the Immune Landscape During Early-Stage Disease

To investigate the effect of sitagliptin on lymphocyte populations during early stage tumour dissemination [22], lymphocyte populations in the spleen, lymph nodes, blood and peritoneal tumour environment were assessed four weeks post-implant (two weeks post-sitagliptin initiation). At this stage, sitagliptin induced a significant increase splenic in CD3+ T cells, while CD3+ T cells remained unchanged in other tissues examined (Figure 3A). T cell lineage was altered, however, with decreased proportions of CD4+CD25-FoxP3- T cells observed in the lymph nodes, peritoneal cavity and spleen (Figure 3B). The %CD8+ T cell in blood also increased (Figure 3C), with a reciprocal decrease in %Tregs (Figure 3D). As a consequence, the overall CD8+ T cell/Treg ratio in circulation was increased (Figure 3E), consistent with clinical data associating these changes with a favourable prognosis [28]. A concomitant decrease in myeloid-derived suppressor cell (MDSC) proportions was also observed (Supplementary Figure S3A).

Cytokine analysis also revealed treatment-specific changes in serum, largely involving cytokines with immunosuppressive properties (Figure 3F). CCR4 ligands CCL22 and CCL17, each involved in Treg recruitment into the tumour microenvironment (TME) [29], were comparatively decreased in mice treated with sitagliptin (Figure 3F) and were consistent with the observed decrease in Treg abundance (Figure 3D). Decreased abundance of IL-10, IL-16 and CCL2 (Figure 3F), each with immune suppressive properties [30,31], were also noted. By contrast, the DPP4 substrate CXCL12 increased in mice receiving sitagliptin treatment (Figure 3F), consistent with several in vivo studies [32,33]. Abundance increases in the B cell and eosinophil chemotactic ligands CXCL13 and CCL11, respectively, (Figure 3F) were also observed. Taken together, these data show that sitagliptin (i) increased CD8+ T cell/Treg ratios and (ii) reduced the expression of immunosuppressive cytokines, thereby

altering the entire circulating immune landscape during the early dissemination stages of ovarian cancer.

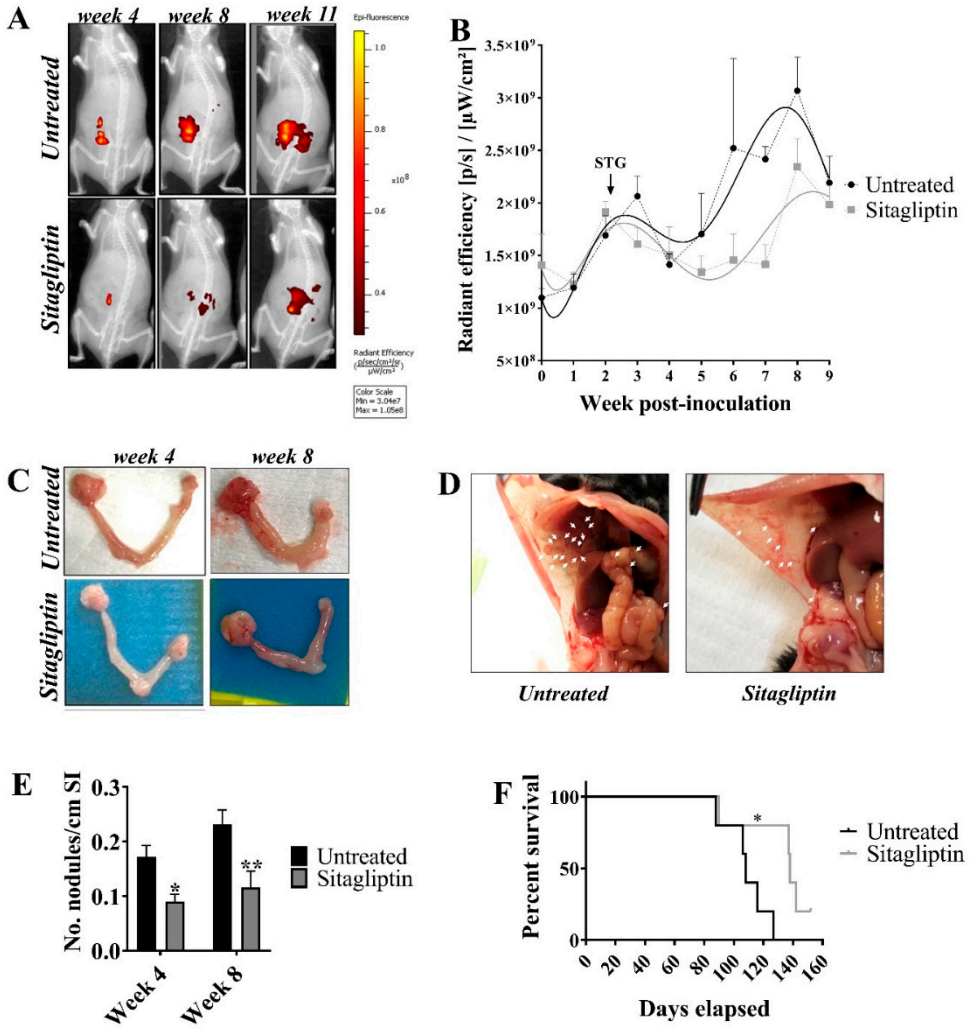

Figure 2. Tumour burden and metastatic spread in ID8 pROSA-iRFP720 tumour-bearing mice following sitagliptin treatment. (**A**) ID8 *pROSA*-iRFP720 cells were implanted into the ovarian bursa and iRFP720 fluorescence was measured using the IVIS Lumina III In Vivo Imaging System (Perkin Elmer, Waltham, MA, USA). Mice were imaged at FOV C (n = 5–15/group) and iRFP720 fluorescence was detected using the iRFP filter set at an exposure time of 5 s. iRFP signal was isolated using a custom spectral unmixing algorithm. Representative images of iRFP fluorescence are shown. (**B**) Quantitative region of interest (ROI) analysis of iRFP total radiant efficiency [p/s]/[µW/cm^2] over time. (**C**) Representative images of ovaries from untreated mice or mice receiving sitagliptin at weeks 4 and 8 post tumour inoculation. ID8 *pROSA*-iRFP720 tumours are shown on the right and nontumour bearing ovaries are shown on the left. (**D**) The proportion of macroscopic tumour nodules on the small intestine/length (cm). (**E**) Representative images of tumour nodules on the peritoneal wall from untreated mice and mice receiving sitagliptin treatment. (**F**) The Kaplan-Meier curve and log-rank test of overall survival analysis for ID8 *pROSA*-iRFP720 tumour-bearing mice. Data are presented as mean ± SD (upper SD for iRFP720 fluorescence). * = $p < 0.05$; ** = $p < 0.01$.

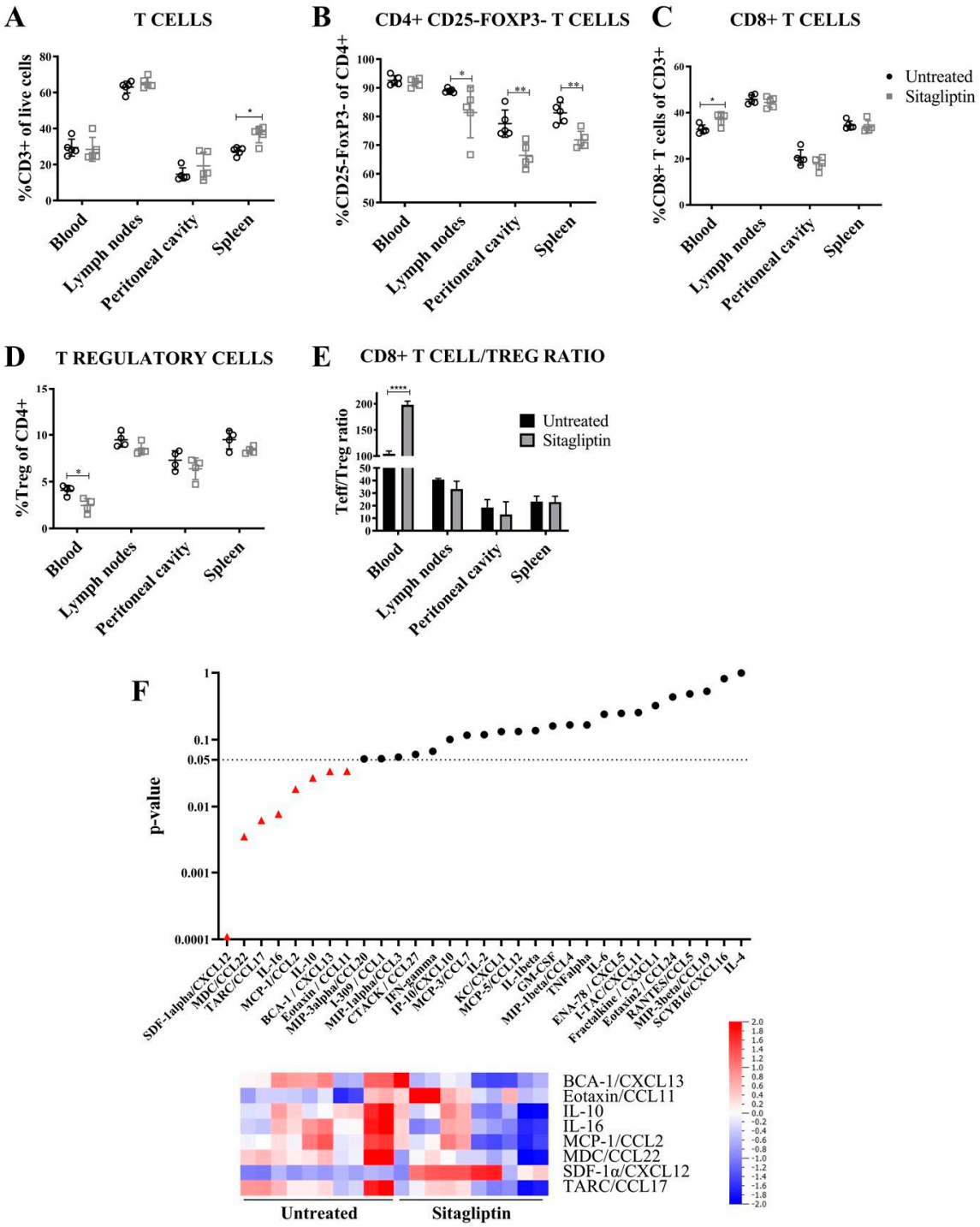

Figure 3. Gross lymphocyte populations and circulating cytokines in mice treated with sitagliptin. Leukocytes were isolated from the blood, lymph nodes, peritoneal cavity and spleen of ID8 *pROSA*-iRFP720-bearing mice at week four post-inoculation and examined using a BD LSRFortessa X-20 (BD Biosciences). (**A**) Percentage of CD3+ T cells of live cells. (**B**) Percentage of CD4+ T cells (CD3+CD4+CD25-FoxP3-) of CD4+ cells. (**C**) Percentage of CD8+ T cells (CD3+CD8+) of CD3+ cells. (**D**) Percentage of T regulatory cells (CD3+CD4+CD25+FoxP3+) of CD4+ cells. (**E**) CD8+ T cell/T regulatory cell ratio. Data are presented as mean ± SD, $n = 5$. * = $p < 0.05$; ** = $p < 0.01$; **** = $p < 0.0001$. (**F**) Cytokines significantly altered in the serum of mice receiving sitagliptin examined at week four post tumour inoculation. The heat map represents cytokines with significant changes between the untreated and sitagliptin-treated mice (individual mice shown). Blue indicates the lowest value while red indicates the highest value. Data analysed using Qlucore Omics Explorer v3.5 (Qlucore AB, Lund, Sweden).

3.4. Sitagliptin Induces Activation and Proliferation of Peripheral and Intra-Tumoral CD8+ T Cells

Functional CD8+ T-cell status was next assessed using flow cytometry to detect the activation and proliferation markers CD69 and Ki67, respectively. There was a significant increase in the percentage of CD69+ peritoneal CD8+ T-cells in sitagliptin treated mice (Figure 4A), in addition to an increased CD69+CD8+ T cell/Treg ratio in the lymphoid organs (Figure 4A). Blood and peritoneal ratios were not examined due to insufficient CD69+ Treg numbers. Immunofluorescence staining of tumour tissue confirmed that CD69+CD8+ T cells were increased in abundance in situ and localised to the primary tumour at this early stage (Figure 4B). Sitagliptin also altered proliferation, with a substantial increase in Ki67+CD4+ and Ki67+CD8+ T cells (both Teff and Tregs) in the spleen and peritoneal cavity. Sitagliptin also increased the %Ki67+CD4+ T cells in lymph nodes (Figure 4C). As a consequence, the ratio of proliferating Ki67+CD8+ T cell/Tregs in the peritoneal microenvironment increased (Figure 4C). Together, these data indicate that sitagliptin improved lymphocyte activation, proliferation and in situ accumulation in tumour tissues. These changes resulted in a beneficial increase in Teff/Treg ratios and are likely to positively influence anti-tumour immunity.

3.5. Enhanced CXCR3-Mediated Recruitment of CD8+ T Cells Is Abrogated by Paclitaxel

Previous work demonstrated that CXCL10, an established DPP4 substrate, mediates T-cell migration and recruitment to tumour tissue in vivo [34,35]. Moreover, reduction of DPP4 activity using sitagliptin can protect the biological activity of CXCL10 to enhance T-cell recruitment into tumours and improve overall survival [21]. We therefore examined CXCR3 expression on T cells as surrogate marker of CXCL10-mediated trafficking, as well as CCR4, a key mediator of Th2 and Treg recruitment [36].

Consistent with its primary role in CD8+ Teff recruitment [37], we observed no change in CXCR3+CD4+T cells following sitagliptin treatment (Figure 5A). However, the percentage of CXCR3+CD8+ T cells in the peritoneal cavity was significantly increased, with a concomitant decrease in spleen (Figure 5B) suggesting directed trafficking between these compartments. This trend was also consistent with absolute CXCR3+CD8+ lymphocyte counts (Supplementary Figure S3B). There was no change in percentage of CCR4+CD4+ T cells (Figure 5C), suggesting that the increased lymphocyte trafficking induced by sitagliptin was CXCR3-dependent. Consistent with these changes, immunofluorescence staining confirmed the increased CD8+ and CXCR3+ T cell abundance and colocalisation in sitagliptin-treated tumour tissue; whilst there was no significant change in CD4/CXCR3 colocalisation (Figure 4D). This trend was also retained throughout disease progression (Supplementary Figure S3C), demonstrating a sustained shift in CXCR3+ mediated CD8+ lymphocyte migration and retention in both the peripheral and intratumoral microenvironment.

To evaluate the relevance of sitagliptin-mediated lymphocyte trafficking to improve disease management in a clinical context, mice receiving sitagliptin were coadministered paclitaxel at one and two-weeks post-initiation of sitagliptin treatment. Paclitaxel was chosen as a representative second line therapy typically used for patients who have experienced disease relapse [38] when sitagliptin would likely be administered in a clinical context. Mice that received combination therapy exhibited decreased splenic percent CXCR3+CD8+ T cells (Figure 6A), as previously observed for sitagliptin alone. Unlike single therapy, however, the sitagliptin-paclitaxel combination did not induce a concomitant increase in peritoneal CXCR3+CD8+ T cells (Figure 6A). Furthermore, combination therapy also decreased percent CXCR3+CD4+ T cells in the spleen (Figure 6B). These results were recapitulated within the primary ovarian TME, where sitagliptin alone increased intra-tumoral CD8+/CXCR3+ expression and colocalisation but combination therapy did not (Figure 6D). Similar to sitagliptin-alone data, combination therapy did not alter CCR4-mediated migration (Figure 6C). Interestingly, paclitaxel-mediated inhibition of CXCR3+ T-cell recruitment to tumour tissue was temporary. Two weeks following final paclitaxel administration, the sitagliptin-mediated increase in CD8+/CXCR3+ expression and colocalisation in tu-

mour tissue was restored (Supplementary Figure S3C). Our data demonstrate that daily administration of sitagliptin increased the recruitment and retention of CD8+ T cells into the tumour microenvironment. Furthermore, whilst active paclitaxel therapy temporarily inhibited CXCR3-mediated CD8+ T cell migration to tumour tissue, the effect was transient and could be reversed.

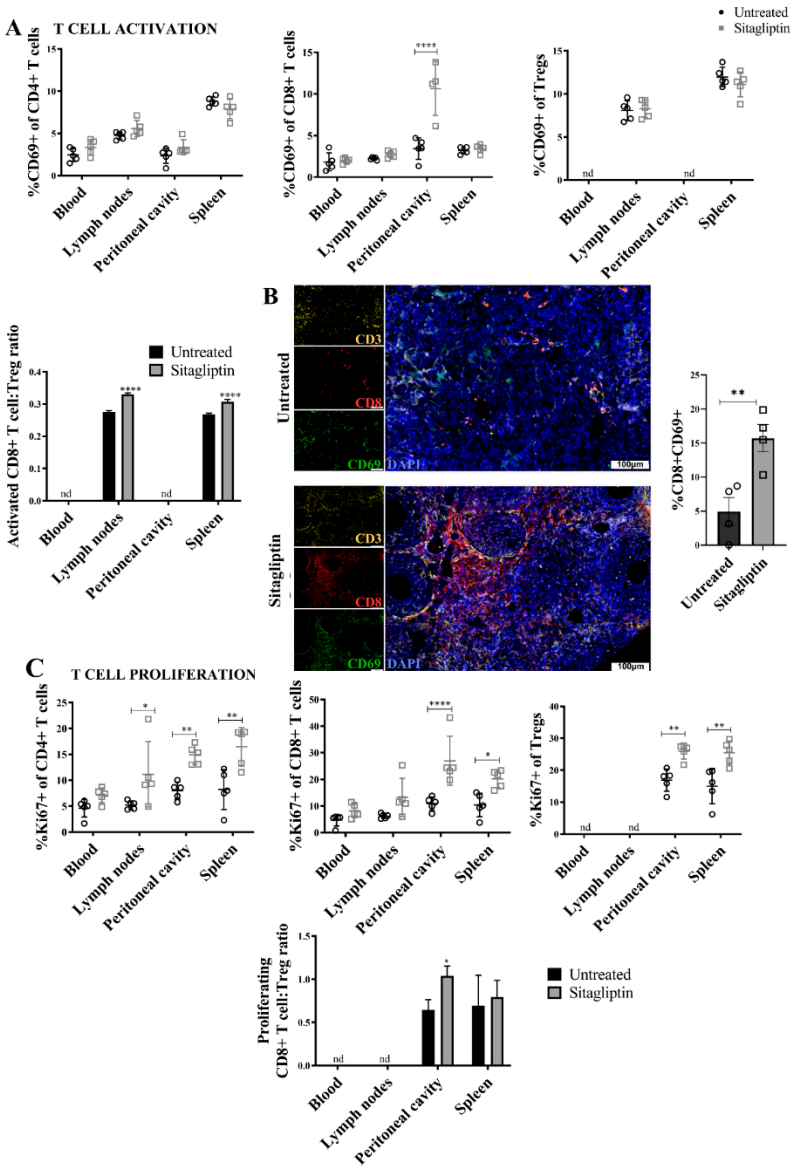

Figure 4. Lymphocyte activation and proliferation in ID8 tumour-bearing mice treated with sitagliptin. Leukocytes were isolated from the blood, lymph nodes, peritoneal cavity and spleen of ID8 *pROSA*-iRFP720-bearing mice at week four post-inoculation and examined using a BD LSRFortessa X-20 (BD Biosciences). (**A**) Percentage of activated (CD69+) CD4+ T cells, CD8+ T cells, and T regulatory cells of the corresponding parent population, and ratio of CD69+ CD8+ T cells to CD69+ Tregs in each of the compartments examined. (**B**) Representative images of ovarian tumour sections stained with CD3 (yellow), CD8 (red) and CD69 (green) at week four post tumour inoculation. Nuclei were stained with DAPI (blue). Bar graph shows the percentage area of ovarian tumour sections stained with CD8+CD69+. Images were acquired using the VS120 Virtual Slide Microscope (Olympus Corporation, Japan) and processed using the Olyvia software v2.9.1 (Olympus Corporation, Japan). Data were analysed by calculating the percentage area of CD8+CD69+ colocalisation of total tissue area using a consistent binary threshold in ImageJ v1.0 (National Institute of Health, MD, USA). (**C**) Percentage of proliferating (Ki67+) CD4+ T cells, CD8+ T cells, and T regulatory cells of the corresponding parent population, and ratio of Ki67+ CD8+ T cells to Ki67+ Tregs in each of the compartments examined. Flow cytometry data are presented as mean ± SD, $n = 5$. * = $p < 0.05$; ** = $p < 0.01$; **** = $p < 0.0001$.

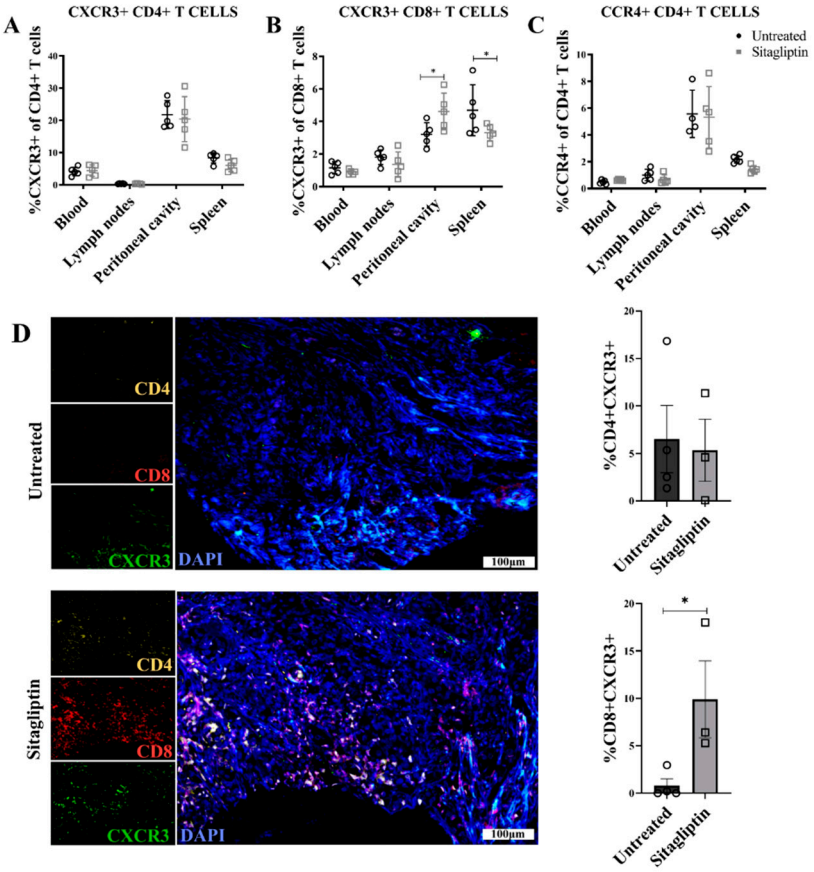

Figure 5. Chemokine receptor expression in ID8 tumour-bearing mice treated with sitagliptin. Leukocytes were isolated from the blood, lymph nodes, peritoneal cavity and spleen of ID8 *pROSA*-iRFP720-bearing mice at week four post-inoculation and examined using a BD LSRFortessa X-20 (BD Biosciences). Percentage of (**A**) CXCR3+ CD4+ T cells, (**B**) CD8+ T cells, and (**C**) CCR4+ CD4+ T cells of the corresponding parent population. (**D**) Representative images of ovarian tumour sections stained with CD4 (yellow), CD8 (red) and CXCR3 (green) at four weeks post tumour inoculation. Nuclei were stained with DAPI (blue). Bar graphs show the percentage area of ovarian tumour sections stained with (i) CD4+CXCR3+ and (ii) CD8+CXCR3+. Images were acquired using the VS120 Virtual Slide Microscope (Olympus Corporation, Japan) and processed using the Olyvia software v2.9.1 (Olympus Corporation, Japan). Data were analysed by calculating the percentage area of CD4+CXCR3 or CD8+CXCR3+ colocalisation of total tissue area using a consistent binary threshold in ImageJ v1.0 (National Institute of Health, MD, USA). * = $p < 0.05$.

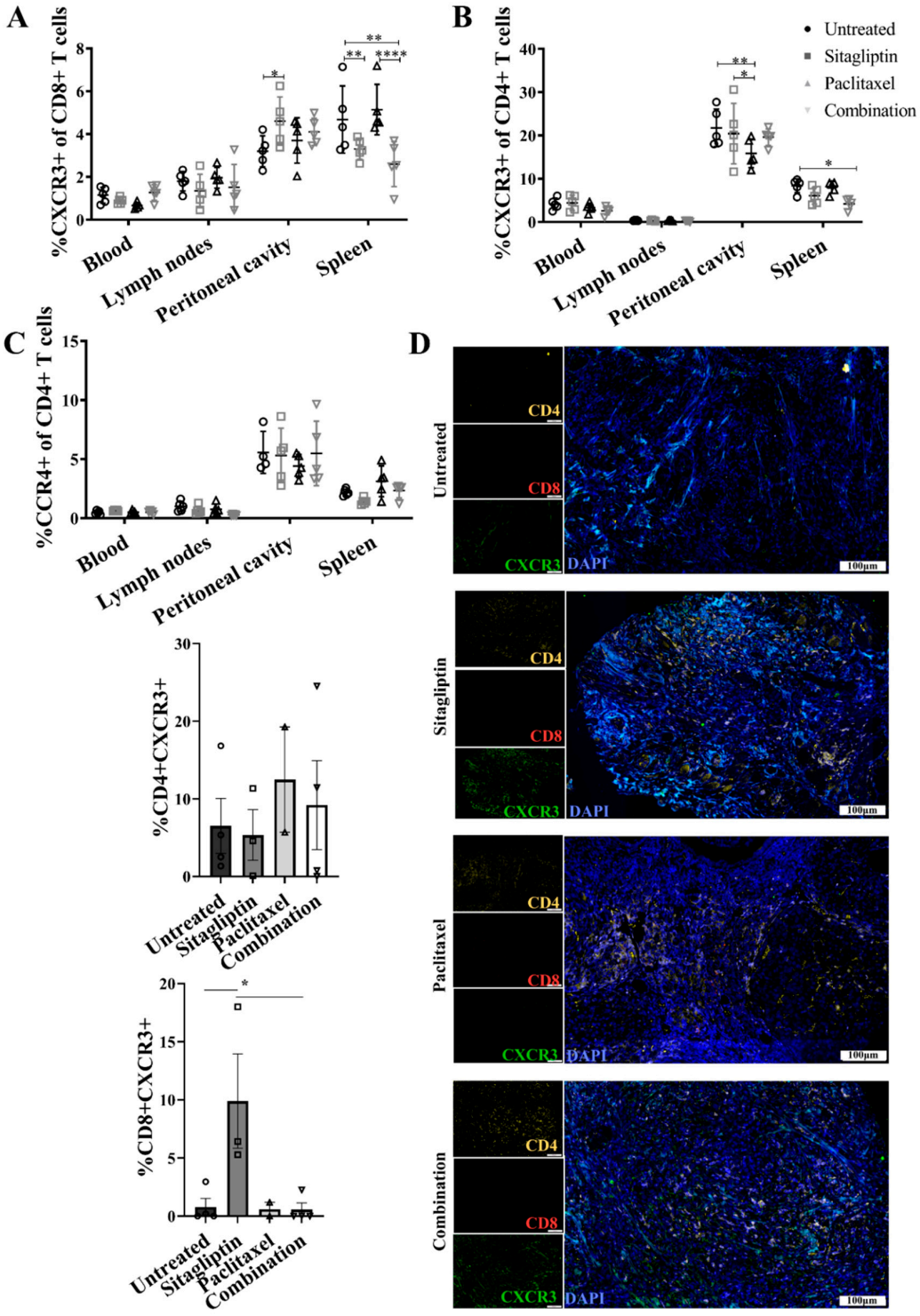

Figure 6. Chemokine receptor expression in ID8 tumour-bearing mice treated with sitagliptin and paclitaxel. Leukocytes were isolated from the blood, lymph nodes, peritoneal cavity and spleen of ID8 *pROSA*-iRFP720-bearing mice at week four post-inoculation and examined using a BD LSRFortessa X-20 (BD Biosciences). Percentage of (**A**) CXCR3+ CD8+ T cells, (**B**) CXCR3+ CD4+ T cells, and (**C**) CCR4+ CD4+ T cells of the corresponding parent population. (**D**) Representative images of ovarian tumour sections stained with CD4 (yellow), CD8 (red) and CXCR3 (green) at four weeks post tumour inoculation. Nuclei were stained with DAPI (blue). Bar graphs show the percentage area of ovarian tumour sections stained with (i) CD4+CXCR3+ and (ii) CD8+CXCR3. Images were acquired using the VS120 Virtual Slide Microscope (Olympus Corporation, Japan) and processed using the Olyvia software v2.9.1 (Olympus Corporation, Japan). Data were analysed by calculating the percentage area of CD4+CXCR3 or CD8+CXCR3+ colocalisation of total tissue area using a consistent binary threshold in ImageJ v1.0 (National Institute of Health, MD, USA). * = $p < 0.05$; ** = $p < 0.01$; **** = $p < 0.0001$.

4. Discussion

The role of the immune system in the development and progression of ovarian cancer is well established [39], and overexpression of the enzyme DPP4 has been noted in several cancer types [1,11]) including ovarian cancer [13,40]. However, the role of DPP4 in various malignancies remains controversial. Recent work demonstrated that DPP4 inhibition can delay tumour progression in other malignancies [21,41]. However, the role of DPP4 and its potential as a therapeutic target in ovarian cancer has not been established. We provide the first evidence that sitagliptin can alter the tumour immune microenvironment in ovarian cancer in a prognostically desirable manner and may have utility as an adjunct to existing ovarian cancer therapies or emerging immunotherapies.

Our data demonstrate that sitagliptin delays tumour progression and extends survival of mice with ovarian tumours in vivo. The number and extent of metastases, particularly to the peritoneal wall, in mice receiving daily sitagliptin treatment was considerably reduced compared to controls. Similarly, previous studies have shown that DPP4 silencing or treatment with sitagliptin significantly reduced thyroid tumour growth in vivo [11]. Rats treated with sitagliptin had decreased precancerous lesions and reactive oxygen species in a colon cancer in vivo model [12], and DPP4 inhibition with sitagliptin suppressed tumour growth in a 4T1 syngeneic model of breast cancer [42]. Moreover, DPP4 inhibition with vildagliptin was also found to significantly reduce liver metastatic foci and metastatic index in a high fat diet-induced model of hepatocellular carcinoma [41]. It should also be considered that DPP4 is an adhesion molecule and can bind to fibronectin [43], which may influence metastasis. It is, therefore, essential to examine the effects of sitagliptin in an immune-deficient model to determine whether our observations are lymphocyte-dependent. It would also be interesting to examine epithelial-to-mesenchymal transition (EMT) in this context.

Surprisingly, whilst overall specific DPP4 activity decreased in serum, we observed that sitagliptin induced an overall increase in sDPP4 abundance, potentially due to increased sheddase expression subsequently releasing DPP4 from the cell surface [44]. Similar findings have been observed in HCC cell lines [45], and diabetic mice treated with the selective DPP4 inhibitor MK-0626 similarly exhibited a ~4-fold increase in circulating DPP4 [27]. Activated T-lymphocytes also display elevated secretion of sDPP4 and are a major source of sDPP4 in serum [46]. The relative contribution of DPP4 activity from each of these biological sources is unclear, however, with recent studies suggesting that circulating sDPP4 derived from multiple biological sources may contribute to different, nonoverlapping biological roles [47,48]. By contrast to serum, where only an ~50% decrease in specific activity was detected, we observed an almost complete abrogation of tumour-specific DPP4 abundance and activity following sitagliptin treatment. Similar tissue-specific effects have also been reported in liver and adipose tissue from animals treated with MK-0626 [27] Whilst the expression of DPP4 is ubiquitous and complex and can be influenced in a disease-specific manner [35,49], the mechanisms underlying tissue specific effects of sitagliptin remain unclear. However, our data do suggest that measurement of sDPP4 in serum is unlikely to provide a robust measurement to monitor the tumour-specific effects of sitagliptin in vivo.

We also identified increased expression of the CXCL10 receptor, CXCR3, on CD8+ T cells in the peritoneal cavity, and increased CXCR3+ expression in ovarian tumour sections following sitagliptin treatment. These data are consistent with previous work demonstrating preservation of full-length CXCL10 in the tumour microenvironment following DPP4 inhibition [21]. Furthermore, our group previously provided the first evidence for N-terminally cleaved antagonistic CXCL10 in malignant high-grade serous ovarian tumour samples but not benign ovarian disease and suggested that this was responsible for reduced lymphocyte infiltration in these tumours [35]. Whilst our study does not directly test a role for altered post-translational modification of CXCL10, the similarity in our results to the mechanisms described in da Silva et al. [21] strongly suggest the observed effects arise directly from CXCR3-mediated lymphocyte migration. By contrast to sitagliptin alone, the decreased splenic %CXCR3+CD8+ T cells in the combination group was not accompa-

nied by increased peritoneal and ovarian TME CXCR3+CD8+ T cells. This may suggest that for mice receiving combination therapy, CXCR3+CD8+ T cells are migrating out of the spleen but not reaching their peripheral site. Paclitaxel targets tubulin and stabilises the microtubule polymer to prevent its disassembly, and microtubules play an essential role in directional cell migration initiated in response to chemokines [50]. Impairment of microtubule dynamics by paclitaxel may thus disrupt the migration of CXCR3+ T cells in response to the sitagliptin-mediated increased in bioactive CXCL10 [21], preventing their migration from spleen to their target site. However, the effect was reversible suggesting sitagliptin may provide clinical benefit through enhanced immune activation in patients not on active paclitaxel therapy. These results highlight the importance of timing optimisation when examining the efficacy of combined therapy in vivo and in clinical trials.

5. Conclusions

To summarise, we provided proof-of-concept evidence that the clinically approved drug sitagliptin can improve antitumour immunity in a syngeneic ovarian cancer mouse model, consequently reducing metastatic burden and prolonging survival. From a therapeutic perspective, our results provide a strategy to improve immune responses in ovarian cancer and establish a rationale for the use of DPP4 inhibitors as a rapidly translatable second-line treatment for this disease.

Supplementary Materials: The following are available online at https://www.mdpi.com/2072-6694/13/3/487/s1, Figure S1: Flow chart and timeline of study design, Figure S2: Flow cytometry gating strategy, Figure S3: MDSC percentages, CXCR3+ CD8+ lymphocyte absolute counts and intratumoral chemokine receptor expression in mice treated with sitagliptin +/− paclitaxel. Leukocytes were isolated from the blood, lymph nodes, peritoneal cavity and spleen of ID8 *pROSA*-iRFP720-bearing mice at week 4 post-inoculation.

Author Contributions: Conceptualization, M.D.G., M.K.O., A.N.S. and M.P.; methodology, A.L.W., L.R.M., K.L.W., A.N.S. and M.P.; validation, A.L.W.; formal analysis, A.L.W., M.D.W., A.N.S. and M.P.; investigation, A.L.W., L.R.M. and A.N.S.; resources, M.P. and A.N.S.; data curation, A.L.W.; writing—original draft preparation, A.L.W.; writing—review and editing, A.L.W., L.R.M., K.L.W., M.B., M.D.W., M.D.G., M.K.O., M.P. and A.N.S.; visualization, A.L.W.; supervision, K.L.W., M.B., M.D.W., M.P. and A.N.S.; project administration, M.P. and A.N.S.; funding acquisition, M.P. and A.N.S. All authors have read and agreed to the published version of the manuscript.

Funding: This work was supported by Australian National Medical Research Council (NHMRC) grant #1099375 and the Victorian Government's Operational Infrastructure Support Program. MP is supported by an NHMRC Senior Fellowship. A.N.S., M.B. and A.L.W. are supported by a fellowship from the Ovarian Cancer Research Foundation (OCRF.com.au). M.D.G. is supported by NHMRC project grant #1105238.

Institutional Review Board Statement: The study was conducted according to the guidelines of the Declaration of Helsinki, and approved by the Ethics Committee of Monash University (ethics number #E/1051/2016/M).

Informed Consent Statement: Not applicable.

Data Availability Statement: The data presented in this study are available in this article and supplementary material.

Acknowledgments: The authors would like to thank the Monash Animal Research Platform (MARP/MICU), Katharina Haigh for training in the intrabursal procedure, M. Madondo for codevelopment of flow-cytometry panels for immune infiltrate analysis, and Angela Vais for her assistance with immunofluorescent staining. We acknowledge the facilities, scientific and technical assistance of FlowCore, Monash Micro Imaging and Monash Histology Platform of Monash University and Monash Health Translation Precinct (internal audit #11178223).

Conflicts of Interest: The authors declare no conflict of interest. The funders had no role in the design of the study; in the collection, analyses, or interpretation of data; in the writing of the manuscript, or in the decision to publish the results

References

1. Wei, W.; Li, N.; Sun, Y.; Li, B.; Xu, L.; Wu, L. Clinical outcome and prognostic factors of patients with early-stage epithelial ovarian cancer. *Oncotarget* **2017**, *8*, 23862–23870. [CrossRef] [PubMed]
2. Ozols, R.F.; Bundy, B.N.; Greer, B.E.; Fowler, J.M.; Clarke-Pearson, D.; Burger, R.A.; Mannel, R.S.; DeGeest, K.; Hartenbach, E.M.; Baergen, R.; et al. Phase III trial of carboplatin and paclitaxel compared with cisplatin and paclitaxel in patients with optimally resected stage III ovarian cancer: A Gynecologic Oncology Group study. *J. Clin. Oncol.* **2003**, *21*, 3194–3200. [CrossRef] [PubMed]
3. Davidson, B.; Trope, C.G. Ovarian cancer: Diagnostic, biological and prognostic aspects. *Womens Health* **2014**, *10*, 519–533. [CrossRef] [PubMed]
4. Paleari, L.; Gandini, S.; Provinciali, N.; Puntoni, M.; Colombo, N.; DeCensi, A. Clinical benefit and risk of death with endocrine therapy in ovarian cancer: A comprehensive review and meta-analysis. *Gynecol. Oncol.* **2017**, *146*, 504–513. [CrossRef]
5. Wilson, A.L.; Plebanski, M.; Stephens, A.N. New Trends in Anti-Cancer Therapy: Combining Conventional Chemotherapeutics with Novel Immunomodulators. *Curr. Med. Chem.* **2018**, *25*, 4758–4784. [CrossRef]
6. Curiel, T.J.; Coukos, G.; Zou, L.; Alvarez, X.; Cheng, P.; Mottram, P.; Evdemon-Hogan, M.; Conejo-Garcia, J.R.; Zhang, L.; Burow, M.; et al. Specific recruitment of regulatory T cells in ovarian carcinoma fosters immune privilege and predicts reduced survival. *Nat. Med.* **2004**, *10*, 942–949. [CrossRef]
7. Zhang, L.; Conejo-Garcia, J.R.; Katsaros, D.; Gimotty, P.A.; Massobrio, M.; Regnani, G.; Makrigiannakis, A.; Gray, H.; Schlienger, K.; Liebman, M.N.; et al. Intratumoral T cells, recurrence, and survival in epithelial ovarian cancer. *N. Engl. J. Med.* **2003**, *348*, 203–213. [CrossRef]
8. Woo, E.Y.; Chu, C.S.; Goletz, T.J.; Schlienger, K.; Yeh, H.; Coukos, G.; Rubin, S.C.; Kaiser, L.R.; June, C.H. Regulatory CD4(+)CD25(+) T cells in tumors from patients with early-stage non-small cell lung cancer and late-stage ovarian cancer. *Cancer Res.* **2001**, *61*, 4766–4772.
9. Giuntoli, R.L., 2nd; Webb, T.J.; Zoso, A.; Rogers, O.; Diaz-Montes, T.P.; Bristow, R.E.; Oelke, M. Ovarian cancer-associated ascites demonstrates altered immune environment: Implications for antitumor immunity. *Anticancer Res.* **2009**, *29*, 2875–2884.
10. Liang, P.I.; Yeh, B.W.; Li, W.M.; Chan, T.C.; Chang, I.W.; Huang, C.N.; Li, C.C.; Ke, H.L.; Yeh, H.C.; Wu, W.J.; et al. DPP4/CD26 overexpression in urothelial carcinoma confers an independent prognostic impact and correlates with intrinsic biological aggressiveness. *Oncotarget* **2017**, *8*, 2995–3008. [CrossRef]
11. Lee, J.J.; Wang, T.Y.; Liu, C.L.; Chien, M.N.; Chen, M.J.; Hsu, Y.C.; Leung, C.H.; Cheng, S.P. Dipeptidyl Peptidase IV as a Prognostic Marker and Therapeutic Target in Papillary Thyroid Carcinoma. *J. Clin. Endocrinol. Metab.* **2017**, *102*, 2930–2940. [CrossRef] [PubMed]
12. Nazarian, A.; Lawlor, K.; Yi, S.S.; Philip, J.; Ghosh, M.; Yaneva, M.; Villanueva, J.; Saghatelian, A.; Assel, M.; Vickers, A.J.; et al. Inhibition of circulating dipeptidyl peptidase 4 activity in patients with metastatic prostate cancer. *Mol. Cell. Proteomics* **2014**, *13*, 3082–3096. [CrossRef] [PubMed]
13. Zhang, M.; Xu, L.; Wang, X.; Sun, B.; Ding, J. Expression levels of seprase/FAPalpha and DPPIV/CD26 in epithelial ovarian carcinoma. *Oncol. Lett.* **2015**, *10*, 34–42. [CrossRef] [PubMed]
14. Ou, X.; O'Leary, H.A.; Broxmeyer, H.E. Implications of DPP4 modification of proteins that regulate stem/progenitor and more mature cell types. *Blood* **2013**, *122*, 161–169. [CrossRef]
15. Sesti, G.; Avogaro, A.; Belcastro, S.; Bonora, B.M.; Croci, M.; Daniele, G.; Dauriz, M.; Dotta, F.; Formichi, C.; Frontoni, S.; et al. Ten years of experience with DPP-4 inhibitors for the treatment of type 2 diabetes mellitus. *Acta Diabetol.* **2019**, *56*, 605–617. [CrossRef]
16. Klemann, C.; Wagner, L.; Stephan, M.; von Horsten, S. Cut to the chase: A review of CD26/dipeptidyl peptidase-4's (DPP4) entanglement in the immune system. *Clin. Exp. Immunol.* **2016**, *185*, 1–21. [CrossRef]
17. Rainczuk, A.; Rao, J.; Gathercole, J.; Stephens, A.N. The emerging role of CXC chemokines in epithelial ovarian cancer. *Reproduction* **2012**, *144*, 303–317. [CrossRef]
18. Zhang, H.; Maqsudi, S.; Rainczuk, A.; Duffield, N.; Lawrence, J.; Keane, F.M.; Justa-Schuch, D.; Geiss-Friedlander, R.; Gorrell, M.D.; Stephens, A.N. Identification of novel dipeptidyl peptidase 9 substrates by two-dimensional differential in-gel electrophoresis. *FEBS J.* **2015**, *282*, 3737–3757. [CrossRef]
19. Casrouge, A.; Decalf, J.; Ahloulay, M.; Lababidi, C.; Mansour, H.; Vallet-Pichard, A.; Mallet, V.; Mottez, E.; Mapes, J.; Fontanet, A.; et al. Evidence for an antagonist form of the chemokine CXCL10 in patients chronically infected with HCV. *J. Clin. Investig.* **2011**, *121*, 308–317. [CrossRef]
20. Decalf, J.; Tarbell, K.V.; Casrouge, A.; Price, J.D.; Linder, G.; Mottez, E.; Sultanik, P.; Mallet, V.; Pol, S.; Duffy, D.; et al. Inhibition of DPP4 activity in humans establishes its in vivo role in CXCL10 post-translational modification: Prospective placebo-controlled clinical studies. *EMBO Mol. Med.* **2016**, *8*, 679–683. [CrossRef]
21. Barreira da Silva, R.; Laird, M.E.; Yatim, N.; Fiette, L.; Ingersoll, M.A.; Albert, M.L. Dipeptidylpeptidase 4 inhibition enhances lymphocyte trafficking, improving both naturally occurring tumor immunity and immunotherapy. *Nat. Immunol.* **2015**, *16*, 850–858. [CrossRef] [PubMed]
22. Wilson, A.L.; Wilson, K.L.; Bilandzic, M.; Moffitt, L.R.; Makanji, M.; Gorrell, M.D.; Oehler, M.K.; Rainczuk, A.; Stephens, A.N.; Plebanski, M. Non-Invasive Fluorescent Monitoring of Ovarian Cancer in an Immunocompetent Mouse Model. *Cancers* **2018**, *11*, 32. [CrossRef] [PubMed]
23. Nunez-Cruz, S.; Connolly, D.C.; Scholler, N. An orthotopic model of serous ovarian cancer in immunocompetent mice for in vivo tumor imaging and monitoring of tumor immune responses. *J. Vis. Exp.* **2010**. [CrossRef] [PubMed]

24. Luippold, G.; Mark, M.; Klein, T.; Amann, K.; Daniel, C. Differences in kidney-specific DPP-4 inhibition by linagliptin and sitagliptin. *Diabetes Res. Clin. Pract.* **2018**, *143*, 199–203. [CrossRef] [PubMed]
25. Coquery, C.M.; Loo, W.; Buszko, M.; Lannigan, J.; Erickson, L.D. Optimized protocol for the isolation of spleen-resident murine neutrophils. *Cytometry A* **2012**, *81*, 806–814. [CrossRef]
26. Manglani, M.; Rua, R.; Hendricksen, A.; Braunschweig, D.; Gao, Q.; Tan, W.; Houser, B.; McGavern, D.B.; Oh, K. Method to quantify cytokines and chemokines in mouse brain tissue using Bio-Plex multiplex immunoassays. *Methods* **2019**, *158*, 22–26. [CrossRef]
27. Varin, E.M.; Mulvihill, E.E.; Beaudry, J.L.; Pujadas, G.; Fuchs, S.; Tanti, J.F.; Fazio, S.; Kaur, K.; Cao, X.; Baggio, L.L.; et al. Circulating Levels of Soluble Dipeptidyl Peptidase-4 Are Dissociated from Inflammation and Induced by Enzymatic DPP4 Inhibition. *Cell Metab.* **2019**, *29*, 320–334.e325. [CrossRef]
28. Sato, E.; Olson, S.H.; Ahn, J.; Bundy, B.; Nishikawa, H.; Qian, F.; Jungbluth, A.A.; Frosina, D.; Gnjatic, S.; Ambrosone, C.; et al. Intraepithelial CD8+ tumor-infiltrating lymphocytes and a high CD8+/regulatory T cell ratio are associated with favorable prognosis in ovarian cancer. *Proc. Natl. Acad. Sci. USA* **2005**, *102*, 18538–18543. [CrossRef]
29. Chang, D.K.; Peterson, E.; Sun, J.; Goudie, C.; Drapkin, R.I.; Liu, J.F.; Matulonis, U.; Zhu, Q.; Marasco, W.A. Anti-CCR4 monoclonal antibody enhances antitumor immunity by modulating tumor-infiltrating Tregs in an ovarian cancer xenograft humanized mouse model. *Oncoimmunology* **2016**, *5*, e1090075. [CrossRef]
30. Draghiciu, O.; Lubbers, J.; Nijman, H.W.; Daemen, T. Myeloid derived suppressor cells-An overview of combat strategies to increase immunotherapy efficacy. *Oncoimmunology* **2015**, *4*, e954829. [CrossRef]
31. Kovacs, E. The serum levels of IL-12 and IL-16 in cancer patients. Relation to the tumour stage and previous therapy. *Biomed. Pharmacother.* **2001**, *55*, 111–116. [CrossRef]
32. Focosi, D.; Kast, R.E.; Metelli, M.R.; Benedetti, E.; Galimberti, S.; Papineschi, F.; Petrini, M. Enhancement of hematopoietic stem cell engraftment by inhibition of CXCL12 proteolysis with sitagliptin, an oral dipeptidyl-peptidase IV inhibitor: A report in a case of delayed graft failure. *Leuk. Res.* **2009**, *33*, 178–181. [CrossRef] [PubMed]
33. Papazafiropoulou, A.K.; Papanas, N.; Trikkalinou, A.; Fousteris, E.; Melidonis, A. The Oral Dipeptidyl-Peptidase-4 Inhibitor Sitagliptin Increases Circulating Levels Of Stromal-Derived Factor-1 Alpha. *Exp. Clin. Endocrinol. Diabetes* **2018**, *126*, 367–370. [CrossRef] [PubMed]
34. Lambeir, A.M.; Durinx, C.; Scharpe, S.; De Meester, I. Dipeptidyl-peptidase IV from bench to bedside: An update on structural properties, functions, and clinical aspects of the enzyme DPP IV. *Crit. Rev. Clin. Lab. Sci.* **2003**, *40*, 209–294. [CrossRef]
35. Rainczuk, A.; Rao, J.R.; Gathercole, J.L.; Fairweather, N.J.; Chu, S.; Masadah, R.; Jobling, T.W.; Deb-Choudhury, S.; Dyer, J.; Stephens, A.N. Evidence for the antagonistic form of CXC-motif chemokine CXCL10 in serous epithelial ovarian tumours. *Int. J. Cancer* **2014**, *134*, 530–541. [CrossRef]
36. Halim, L.; Romano, M.; McGregor, R.; Correa, I.; Pavlidis, P.; Grageda, N.; Hoong, S.J.; Yuksel, M.; Jassem, W.; Hannen, R.F.; et al. An Atlas of Human Regulatory T Helper-like Cells Reveals Features of Th2-like Tregs that Support a Tumorigenic Environment. *Cell Rep.* **2017**, *20*, 757–770. [CrossRef]
37. Zsiros, E.; Duttagupta, P.; Dangaj, D.; Li, H.; Frank, R.; Garrabrant, T.; Hagemann, I.S.; Levine, B.L.; June, C.H.; Zhang, L.; et al. The Ovarian Cancer Chemokine Landscape Is Conducive to Homing of Vaccine-Primed and CD3/CD28-Costimulated T Cells Prepared for Adoptive Therapy. *Clin. Cancer Res.* **2015**, *21*, 2840–2850. [CrossRef]
38. Buda, A.; Floriani, I.; Rossi, R.; Colombo, N.; Torri, V.; Conte, P.F.; Fossati, R.; Ravaioli, A.; Mangioni, C. Randomised controlled trial comparing single agent paclitaxel vs epidoxorubicin plus paclitaxel in patients with advanced ovarian cancer in early progression after platinum-based chemotherapy: An Italian Collaborative Study from the Mario Negri Institute, Milan, G.O.N.O. (Gruppo Oncologico Nord Ovest) group and I.O.R. (Istituto Oncologico Romagnolo) group. *Br. J. Cancer* **2004**, *90*, 2112–2117. [CrossRef]
39. Kandalaft, L.E.; Powell, D.J., Jr.; Singh, N.; Coukos, G. Immunotherapy for ovarian cancer: What's next? *J. Clin. Oncol.* **2011**, *29*, 925–933. [CrossRef]
40. Shao, S.; Wang, C.; Tian, J.; Zhang, H.; Wang, S.; Du, Y. Diagnostic and prognostic significance of serum CD26 level in Asian women with high-grade serous ovarian carcinoma. *Future Oncol.* **2019**, *15*, 1863–1871. [CrossRef]
41. Qin, C.J.; Zhao, L.H.; Zhou, X.; Zhang, H.L.; Wen, W.; Tang, L.; Zeng, M.; Wang, M.D.; Fu, G.B.; Huang, S.; et al. Inhibition of dipeptidyl peptidase IV prevents high fat diet-induced liver cancer angiogenesis by downregulating chemokine ligand 2. *Cancer Lett.* **2018**, *420*, 26–37. [CrossRef] [PubMed]
42. Choi, H.J.; Kim, J.Y.; Lim, S.C.; Kim, G.; Yun, H.J.; Choi, H.S. Dipeptidyl peptidase 4 promotes epithelial cell transformation and breast tumourigenesis via induction of PIN1 gene expression. *Br. J. Pharmacol.* **2015**, *172*, 5096–5109. [CrossRef]
43. Piazza, G.A.; Callanan, H.M.; Mowery, J.; Hixson, D.C. Evidence for a role of dipeptidyl peptidase IV in fibronectin-mediated interactions of hepatocytes with extracellular matrix. *Biochem. J.* **1989**, *262*, 327–334. [CrossRef] [PubMed]
44. Röhrborn, D.; Eckel, J.; Sell, H. Shedding of dipeptidyl peptidase 4 is mediated by metalloproteases and up-regulated by hypoxia in human adipocytes and smooth muscle cells. *FEBS Lett.* **2014**, *588*, 3870–3877. [CrossRef]
45. Fasolato, S.; Trevellin, E.; Ruvoletto, M.; Granzotto, M.; Zanus, G.; Boscaro, E.; Babetto, E.; Terrin, L.; Battocchio, M.A.; Ciscato, F.; et al. SerpinB3 induces dipeptidyl-peptidase IV/CD26 expression and its metabolic effects in hepatocellular carcinoma. *Life Sci.* **2018**, *200*, 134–141. [CrossRef] [PubMed]

46. Casrouge, A.; Sauer, A.V.; Barreira da Silva, R.; Tejera-Alhambra, M.; Sanchez-Ramon, S.; Icare, B.; Cancrini, C.; Ingersoll, M.A.; Aiuti, A.; Albert, M.L. Lymphocytes are a major source of circulating soluble dipeptidyl peptidase 4. *Clin. Exp. Immunol.* **2018**, *194*, 166–179. [CrossRef]
47. Lettau, M.; Dietz, M.; Vollmers, S.; Armbrust, F.; Peters, C.; Dang, T.M.; Chitadze, G.; Kabelitz, D.; Janssen, O. Degranulation of human cytotoxic lymphocytes is a major source of proteolytically active soluble CD26/DPP4. *Cell Mol Life Sci.* **2020**, *77*, 751–764. [CrossRef]
48. Nargis, T.; Kumar, K.; Ghosh, A.R.; Sharma, A.; Rudra, D.; Sen, D.; Chakrabarti, S.; Mukhopadhyay, S.; Ganguly, D.; Chakrabarti, P. KLK5 induces shedding of DPP4 from circulatory Th17 cells in type 2 diabetes. *Mol. Metab.* **2017**, *6*, 1529–1539. [CrossRef]
49. Javidroozi, M.; Zucker, S.; Chen, W.T. Plasma seprase and DPP4 levels as markers of disease and prognosis in cancer. *Dis. Markers* **2012**, *32*, 309–320. [CrossRef]
50. Etienne-Manneville, S. Microtubules in cell migration. *Annu. Rev. Cell Dev. Biol.* **2013**, *29*, 471–499. [CrossRef]

cancers

MDPI

Article

Non-Invasive Fluorescent Monitoring of Ovarian Cancer in an Immunocompetent Mouse Model

Amy L. Wilson [1,2,3], Kirsty L. Wilson [3,4], Maree Bilandzic [1,2], Laura R. Moffitt [1,2], Ming Makanji [1,2], Mark D. Gorrell [5], Martin K. Oehler [6,7], Adam Rainczuk [1,2,8], Andrew N. Stephens [1,2,*] and Magdalena Plebanski [4,*]

1 Hudson Institute of Medical Research, Clayton 3168, Australia; Amy.Wilson@monash.edu.au (A.L.W.) Maree.Bilandzic@Hudson.org.au (M.B.); Laura.Moffitt@monash.edu.au (L.R.M.); Ming.Makanji@Hudson.org.au (M.M.); Adam.Rainczuk@Hudson.org.au (A.R.)
2 Department of Molecular and Translational Sciences, Monash University, Clayton 3168, Australia
3 Department of Immunology and Pathology, Monash University, Clayton 3168, Australia; Kirsty.Wilson@monash.edu.au
4 School of Health and Biomedical Sciences, RMIT University, Bundoora 3083, Australia
5 Centenary Institute, The University of Sydney, Sydney 2006, Australia; m.gorrell@centenary.org.au
6 Department of Gynaecological Oncology, Royal Adelaide Hospital, Adelaide 5000, Australia; martin.oehler@adelaide.edu.au
7 Robinson Institute, University of Adelaide, Adelaide 5000, Australia
8 Bruker Biosciences Pty Ltd., Preston 3072, Australia
* Correspondence: Andrew.n.stephens@hudson.org.au (A.N.S.); magdalena.plebanski@rmit.edu.au (M.P.); Tel.: +61-3-8572-2686 (A.N.S.); +61-3-9925-7263 (M.P.)

Received: 26 November 2018; Accepted: 23 December 2018; Published: 31 December 2018

Abstract: Ovarian cancers (OCs) are the most lethal gynaecological malignancy, with high levels of relapse and acquired chemo-resistance. Whilst the tumour–immune nexus controls both cancer progression and regression, the lack of an appropriate system to accurately model tumour stage and immune status has hampered the validation of clinically relevant immunotherapies and therapeutic vaccines to date. To address this need, we stably integrated the near-infrared phytochrome iRFP720 at the *ROSA26* genomic locus of ID8 mouse OC cells. Intrabursal ovarian implantation into C57BL/6 mice, followed by regular, non-invasive fluorescence imaging, permitted the direct visualization of tumour mass and distribution over the course of progression. Four distinct phases of tumour growth and dissemination were detectable over time that closely mimicked clinical OC progression. Progression-related changes in immune cells also paralleled typical immune profiles observed in human OCs. Specifically, we observed changes in both the CD8+ T cell effector (Teff):regulatory (Treg) ratio, as well as the dendritic cell (DC)-to-myeloid derived suppressor cell (MDSC) ratio over time across multiple immune cell compartments and in peritoneal ascites. Importantly, iRFP720 expression had no detectible influence over immune profiles. This new model permits non-invasive, longitudinal tumour monitoring whilst preserving host–tumour immune interactions, and allows for the pre-clinical assessment of immune profiles throughout disease progression as well as the direct visualization of therapeutic responses. This simple fluorescence-based approach provides a useful new tool for the validation of novel immuno-therapeutics against OC.

Keywords: iRFP; iRFP720; ovarian cancer; ID8; syngeneic; immune; T cell; tumour

1. Introduction

Ovarian cancer (OC) is the most lethal gynaecological malignancies, typically characterised by asymptomatic progression, diagnosis at an advanced stage, and a high rate of recurrence [1].

The majority of OC patients ultimately develop platinum-resistant disease, limiting therapeutic options and underlying the very high mortality rate from this disease. Therapeutic vaccines based on antigenic protein epitopes, DNA or pulsed dendritic cells (DCs) offer one promising approach to stimulating immune activation in vivo [2,3]. Vaccination has proven successful in other gynaecological tumour types (e.g., cervical cancers), and numerous antigenic targets (e.g., cancer–testis antigen sperm protein 17 (SP17) [4]) have been suggested in OC. However, immunotherapy trials in OC (e.g., immune checkpoint inhibitors, and therapeutic vaccines) have failed in inducing the clinically robust and durable responses achieved for other tumour types (reviewed in [5]). There remains a clear need for improved therapies that can regress disease against the background of chemo-resistance and immune suppression endemic to these cancer types.

The lack of effective immune-targeted OC therapies to date suggests that improved pre-clinical in vivo models are required to model therapeutic response and accurately assess efficacy. Orthotopic patient-derived xenograft (PDX) models necessarily lack the key tumour–immune interactions that drive tumour growth and progression [6], whilst no available genetically engineered mouse models (GEMMs) accurately recapitulate all features of human disease (reviewed in [7,8]). Syngeneic models (including ID8 [9], MOSE-L [10], STOSE [11]) offer an excellent alternative for the study of OC as they are generally well characterised in vitro, readily amenable to ex vivo genetic manipulation, and facilitate the reliable, rapid development of tumours following implant. Of these, the ID8 model is the most extensively studied in the context of cancer biology and tumour–host immune interaction [12,13], making it the model of choice for analyses of antigenic determinants in vivo [4]. The limitations of this model, however, include slow development, uncertainty around the molecular mechanisms driving their malignant potential [14], and an inability to accurately monitor real-time tumour progression in the context of human disease [15].

Tumour–immune interactions are dynamic, changing over time and in response to therapy [16]. OC models must therefore replicate the complex tumour microenvironment, permit quantitative detection and analysis of low-volume tumours, allow for high-fidelity monitoring of tumour progression over time, and permit correlations between tumour growth, spread and changes in immune response. Bioluminescence imaging using luciferin injection into mice bearing ID8 *luc+* cells has previously been used to image ID8 tumours during progression [17]. However, luciferin injection is invasive and can initiate an inflammatory response, and only provides qualitative information regarding tumour progression [18]. Alternatives such as green fluorescent proteins (GFPs) are widely used in vitro for diverse applications, but their in vivo application is unfavourable due to extensive tissue absorption and autofluorescence [19,20]. The more recent development of near-infrared fluorescent proteins (iRFPs) for non-invasive deep tissue imaging could potentially overcome these drawbacks [21]. Tissue absorption in the near-infrared spectrum is minimal, and the relatively low level of autofluorescence and light scatter by mammalian tissues at these wavelengths make iRFPs desirable for deep tissue imaging [21]. Near-infrared fluorescent proteins have been used to track the progression of prostate cancer [21], brain tumours [22], lung adenocarcinoma [23], glioblastoma, osteosarcoma, and melanoma [24], but have not been applied in the context of OC.

In this study, we have developed and characterized a new ID8 tumour model, utilizing a near infra-red fluorescent protein (iRFP720 [21]) stably integrated into the *ROSA26* locus of ID8 cells to non-invasively monitor and directly stage tumour progression in mice. This approach permits real-time imaging of tumour progression and evaluation of response to therapy and particularly stage-specific therapeutic vaccines, enabling the direct analysis of immune-mediated tumour regression in vivo.

2. Results

2.1. Generation of Clonal ID8 Cells Expressing Genomically Integrated iRFP720

The pROSA26-puro-iRFP720 vector (Figure 1) was constructed to constitutively express iRFP720 from a cytomegalovirus (CMV) promoter, puromycin and ampicillin selection markers, and flanking

homology arms corresponding to upstream and downstream regions of the *ROSA26* locus. Successful genomic integration transfers both CMV-iRFP720 and PGK-puro cassettes, conferring puromycin resistance and stable expression of iRFP720. ID8 cells were co-transfected with pROSA-puro-iRFP720 and plentiCRISPRv1 vectors, containing either ROSA26-sgRNA2 or ROSA26-sgRNA4 [25]. Following single cell sorting for iRFP720+ cells, clonal expansion and fluorescence microscopy were used to confirm iRFP+ status (Figure 2A,B). Individual clones were then screened by PCR for genomic integration of iRFP720 into *ROSA26* (Figure 2C,D). Screening primers were directed against: (i) an endogenous ROSA26 region upstream of the incorporation; (ii) an endogenous ROSA26 region between the left and right arms; and (iii) a region specific to the iRFP720 sequence (as depicted in Figure 2C). This approach differentiates between homo- and heterogeneous clones. Heterozygous incorporation of iRFP720 into the *ROSA26* locus was confirmed in 40% of clones (Figure 2D); no clones homozygous for iRFP720 integration were detected. A single iRFP+ clone was selected for all subsequent studies.

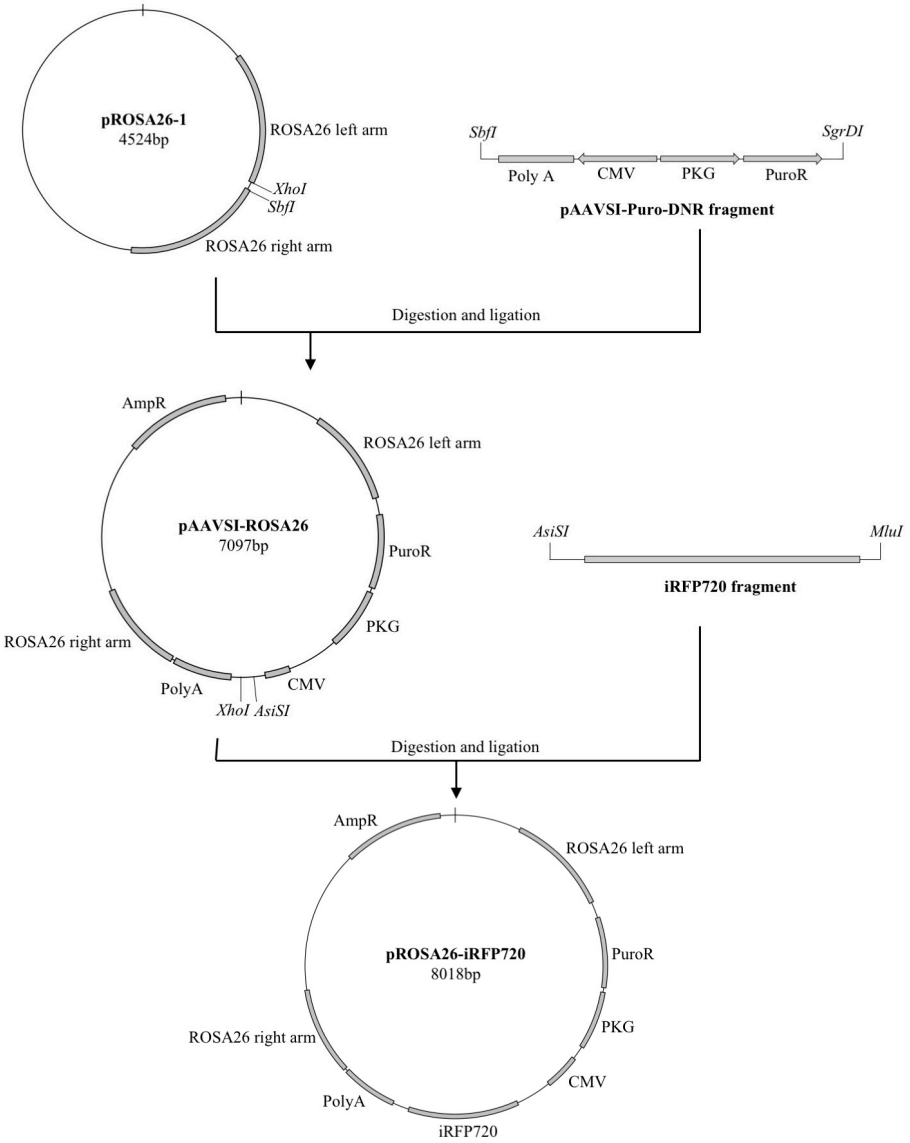

Figure 1. Strategy for pROSA-puro-iRFP720 vector generation and genomic screening. Schematic representation of the overall cloning strategy for the generation of the pROSA-puro-iRFP720 vector. A fragment from the pAAVS1-puro-DNR plasmid was PCR-amplified, digested with SbfI and SgrDI and ligated into an SbfI/XhoI-digested pROS A26-1 plasmid. An iRFP720 fragment from piRFP720-N1 was PCR-amplified, digested with AsiSI and MluI and ligated into the AsiSI/MluI-digested pAAVSI-ROSA26 vector.

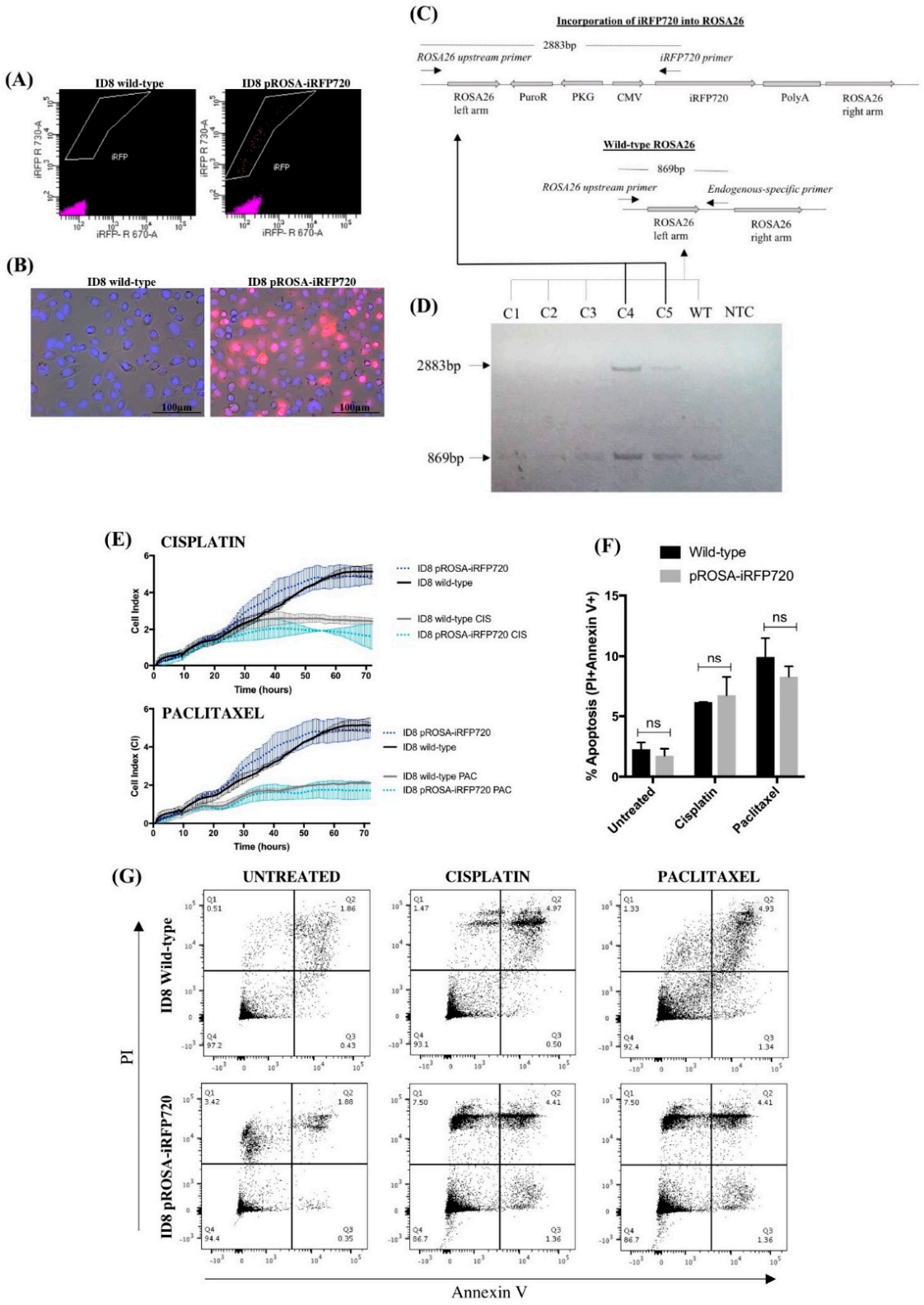

Figure 2. iRFP720 fluorescence and characterisation of pROSA-iRFP720-expressing ID8 cells. (**A**) Fluorescence-activated cell sorting (FACS) enrichment of iRFP720-expressing ID8 cells. iRFP720-positive single cells ([R]730/45 vs. [R]670/30) were sorted into a 96-well plate using the FACSAria Fusion cell sorter (BD Biosciences, San Jose, CA, USA), and single clones were expanded and

screened. (**B**) iRFP720 fluorescence was observed using the Cytation 3 imaging Multi-Mode Reader equipped with a Cy5.5 filterset (BioTek Instruments Inc., Winooski, VT, USA). Hoechst 33342 was used to visualise the nucleus ($377_{ex}/447_{em}$). (**C**) Schematic diagram representing the genomic screening strategy used for identifying iRFP720 incorporation into the *ROSA26* locus. (**D**) Genomic DNA isolated from pROSA-puro-iRFP720-transfected single-cell ID8 clones was PCR-amplified using a *ROSA26* upstream F primer, an endogenous *ROSA26*-specific R primer and an iRFP720-specific R primer, and PCR products were separated with a 1.2% agarose gel. Wild-type *ROSA26* gives an 869bp product and successful iRFP720 incorporation gives a 2883bp product. C1–5: clones 1–5; WT: wild-type ID8; NTC: no-template control. (**E**) Proliferation was assessed by electrode impedance using xCELLigence real-time cell analysis. Cells (8×10^3/well) were treated with cisplatin (10 μg/mL) or paclitaxel (20 nM) after 8 h, and proliferation was analysed for further 64 h. (**F**) Wild-type and pROSA-iRFP720 ID8 (3×10^5 cells/well) were cultured for 24 h, and then incubated for further 24 h in the presence of cisplatin (10 μg/mL) or paclitaxel (20 nM). Apoptosis was determined by Alexa Fluor®647 annexin V and PI staining on the BD LSRFortessa X-20 (BD Biosciences) flow cytometer. (**G**) Representative images of the apoptosis analysis. Data are presented as mean ± SD, $n = 3$.

2.2. Expression of iRFP720 Does Not Alter ID8 Cell Growth Characteristics or Chemo-Sensitivity In Vitro

Following genomic incorporation of iRFP720 into ID8 cells, we assessed both their proliferative capacity and response to chemotherapy compared to wild-type ID8 cells in vitro. Using xCELLigence real-time cell analysis (RTCA), we observed no significant difference in the adhesive or proliferative capacity of pROSA-iRFP720 ID8 cells compared to wild-type ID8 cells over 72 h (Figure 2E). Similarly, there was no significant difference in cell index (CI) between wild-type or iRFP+ ID8 cells following treatment with cisplatin (10 μg/mL) or paclitaxel (20 nM) (Figure 2E). We also assessed apoptosis 24 h post-chemotherapy by Annexin V and propidium iodide staining. Again, pROSA-iRFP720 ID8 cells displayed no apparent difference in apoptotic cell death following cisplatin or paclitaxel treatment compared to wild-type (Figure 2F,G). These data demonstrate that the genomic incorporation and subsequent constitutive expression of iRFP720 had no influence over ID8 cell growth, proliferation, chemo-sensitivity or apoptosis in vitro.

2.3. Non-Invasive Detection and Imaging of iRFP720 Fluorescence In Vivo

To determine the minimum cell titre for detection of iRFP720+ ID8 cells in vivo, cells were injected intrabursally (from 6.25×10^4 to 1×10^6 cells/ovary) and mice were imaged using an IVIS Lumina III Imaging System. A minimum titre of 0.5×10^6 cells was required for detection of iRFP+ ID8 cells following implant, with robust detection at 1×10^6 cells (data not shown). We therefore used 1×10^6 cells for all subsequent intrabursal implant experiments.

Mice implanted with 1×10^6 iRFP720+ ID8 cells were monitored over a period of 10 weeks (humane endpoint). All mice were fed a low-fluorescence chow diet to minimize potential autofluorescence; and a spectral unmixing algorithm was created for imaging, to assist in visualization of iRFP+ signal (see Section 4.9). Fluorescence associated with implanted cancer cells was clearly detected immediately following implant, and increased over time corresponding to the growth of iRFP+ tumours (Figure 3A).

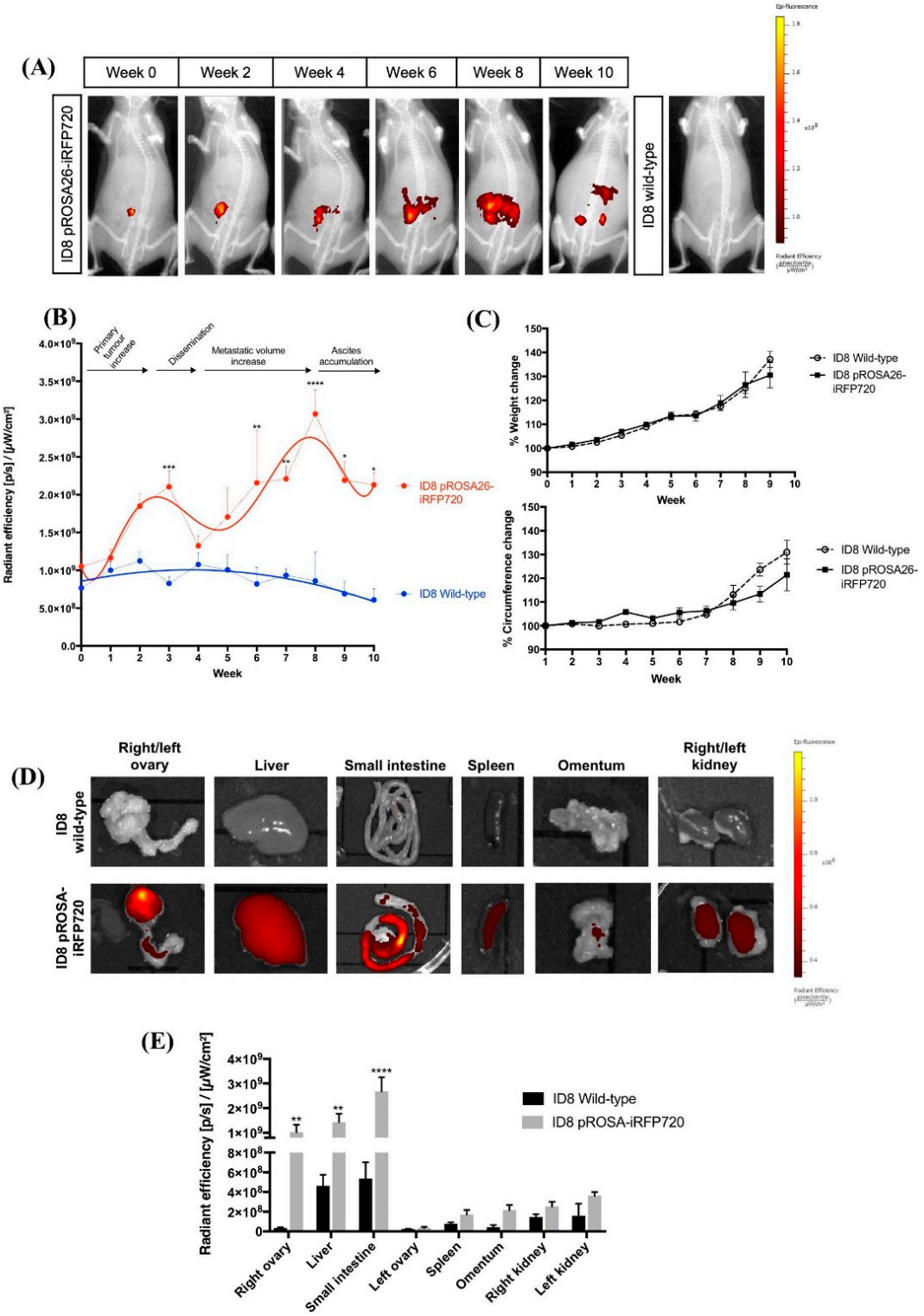

Figure 3. In vivo tracking of iRFP720 fluorescence in real time. (**A**) pROSA-iRFP720 or wild-type ID8 cells (1×10^6 cells/mouse) were implanted into the ovarian bursa and iRFP720 fluorescence was measured using the IVIS Lumina III In Vivo Imaging System (Perkin Elmer, MA, USA). Mice were imaged at field of view (FOV) C (n = 4–16) and iRFP720 fluorescence was detected using the iRFP filter set at an exposure time of 5 s. The iRFP signal was isolated using a custom spectral unmixing algorithm. Representative images are shown. (**B**) Quantitative region of interest (ROI) analysis of iRFP

total radiant efficiency (p/s)/(μW/cm^2) over time. (**C**) Average weight and circumference of mice over time following tumour implantation (n = 4–16). (**D**) Representative images of iRFP720 fluorescence in excised organs post-mortem at the humane endpoint. (**E**) Quantitative ROI analysis of excised organs indicating iRFP total radiant efficiency (p/s)/ (μW/cm^2) (n = 4,5). *, $p < 0.05$; **, $p < 0.01$; ***, $p < 0.001$; ****, $p < 0.0001$.

2.4. iRFP720 Fluorescence Corresponds with Discrete Tumour Progression Stages In Vivo

To evaluate whether iRFP720 could be used to monitor tumour growth over time, mice implanted with iRFP720+ ID8 were imaged weekly for fluorescence. At 2-week intervals (and at the endpoint), mice were culled and an autopsy was performed to assess primary tumour size, localization and number of metastatic nodules. Weight and abdominal girth, the most commonly used surrogate parameters of tumour progression, were also measured and correlated with iRFP fluorescence and macroscopic tumour deposition.

Both the intensity and distribution of iRFP fluorescence increased over time in iRFP+ ID8 mice compared to those in non-fluorescent controls (Figure 3A,B), and displayed a biphasic pattern with two distinct fluorescence peak and trough events (Figure 3B). Correlation of these fluorescent events with tumour growth and spread at autopsy allowed us to define four distinct stages in ID8 tumour progression. At fluorescence peak event 1 (3 weeks post-implant), mice had small primary tumours that remained confined to the implant site, with some peritoneal adhesions but no evidence of capsule disruption or dissemination of cancer cells. Accordingly, this was defined as a Stage I tumour. Immediately following stage I, fluorescence decreased; in addition to primary tumours and extensive local adhesions to the peritoneal wall, at this time we observed disruption of the ovarian capsule and the first evidence of micro-metastases (observed by iRFP fluorescence) within the peritoneum. This initial decrease event was therefore defined as the transition to Stage II. Fluorescence then steadily increased to reach a second maxima after 8 weeks by which point mice had developed large primary tumours, extensive peritoneal adhesions and multiple metastatic nodules throughout the peritoneal cavity involving the peritoneum, small intestine, liver, kidneys and omentum. This second fluorescence maxima was defined as Stage III and was again followed by a decline in fluorescence corresponding to the development of peritoneal ascites. At the endpoint, mice had developed large primary tumours, extensively disseminated secondary tumours, and accumulated peritoneal ascites. By contrast to fluorescence measurements, weight gain proceeded in a linear fashion over time whilst abdominal circumference only evidenced an increase from ~week 7 onwards (Figure 3C).

Tumour tissues at the endpoint were also evaluated for iRFP fluorescence ex vivo, and immuno-stained for common markers of serous cancers including pan-cytokeratin (pan-CK), programmed death-ligand 1 (PD-L1), p53 and Wilms tumour protein (WT1). Consistent with previous studies [26], tumour deposition at the endpoint was present on intestines, peritoneum, liver and stomach; and iRFP720 fluorescence was evident in all tumour deposits (Figure 3D). The expression of all tumour markers was similar between wild-type and pROSA-iRFP720 ID8 tumour tissues (Figure 4A–E), indicating that iRFP720 expression did not alter their abundance.

Real-time monitoring using iRFP was thus able to define discrete tumour stages that corresponded closely to the clinical progression of OC. Moreover, fluorescence measurements permitted the detection of tumour progression at a significantly earlier time-point than the commonly used measurements of weight and abdominal girth. Taken together, our data indicate that iRFP fluorescence is suitable for non-invasive monitoring of stage-specific tumour progression in vivo.

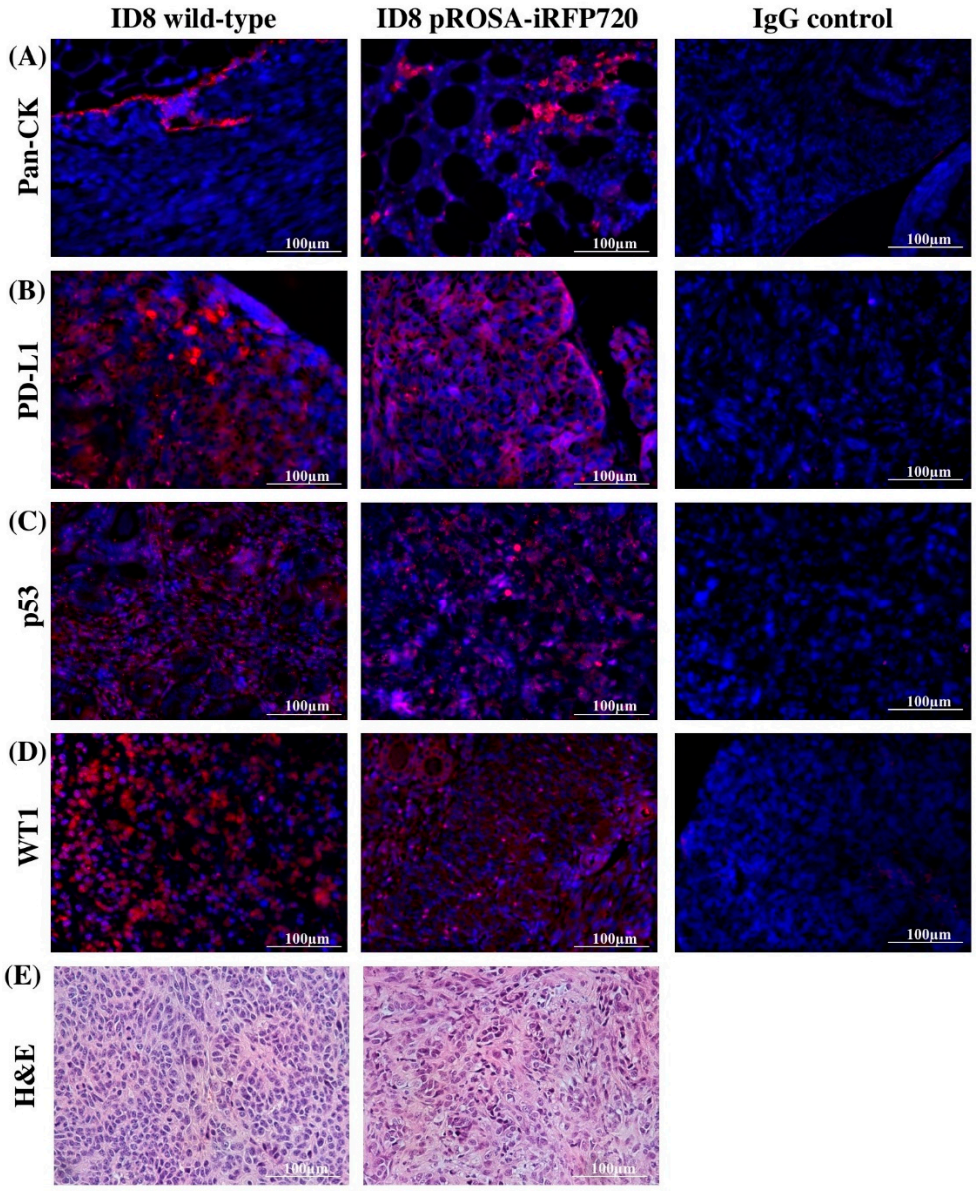

Figure 4. Expression of serous tumour markers by immunofluorescence. Representative fluorescent images of pROSA-iRFP720 and wild-type ID8 ovarian tumour sections stained with (**A**) pan-cytokeratin (pan-CK), (**B**) PD-L1, (**C**) p53 and (**D**) Wilms Tumour protein 1 (WT1). Images were acquired using the Cytation 3 imaging Multi-Mode Reader (BioTek) and were processed using the Gen5™ software v 2.05 (BioTek). Staining appears red against nuclei stained with DAPI (blue). (**E**) Wild-type and pROSA-iRFP720 ID8 ovarian tumour sections stained with hematoxylin and eosin (H&E).

2.5. The Presence of Anti-iRFP720 Antibodies Does Not Impact Tumour Progression

Expression of a foreign protein can stimulate an autoimmune response [27], to potentially alter tumour progression or overall survival [17]. ELISA was used to test for the presence of circulating IgG against the iRFP720 protein. Only 2/14 mice (14%) had a detectible titre (~1 µg/mL) of anti-iRFP720 IgG (Figure 5), and there was no discernible effect on disease progression in either of these animals or for iRFP+ ID8 tumour mice generally compared to that in wild-type cells. This is consistent with findings for mice implanted with ID8-*luc* cells [17]. Thus, iRFP720 was only weakly immunogenic in C57BL/6 mice and its expression did not alter tumour progression in vivo.

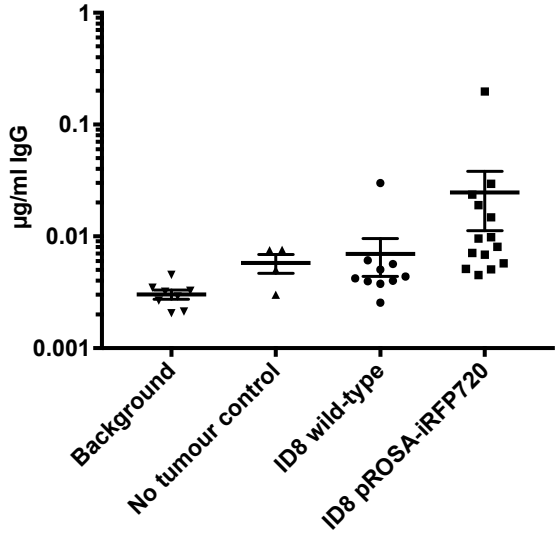

Figure 5. Circulating endogenous iRFP720-specific IgG antibodies in mice bearing pROSA-iRFP720 ID8 tumours. Serum iRFP720-specific IgG antibodies (µg/mL) in the sera of pROSA-iRFP720 ID8 and wild-type ID8 tumour-bearing mice at the endpoint (n = 4–14). Bars represent ± SD.

2.6. iRFP720 Expression Does Not Alter the Tumour Immune Microenvironment In Vivo

To achieve utility as a model for tumour immune studies, we performed extensive leukocyte profiling to establish a baseline for tumour–immune interactions and further confirm the equivalence of iRFP720 ID8 mice to wild-type ones. Mice were culled at weeks 4 and 8 post-inoculation, corresponding to early dissemination (stage 2) or advanced disease (stage 3), and leukocyte populations present in blood, peritoneal fluid and lymphoid organs (nodes, spleen) were evaluated by flow cytometry. No significant changes between iRFP+ vs. wild-type mice were identified in any of the macrophage, MDSC, DC or multiple T-cell populations examined (Figure 6). Between "early" (stage II) and "late" (stage III) tumour dissemination, we observed that percentages of total CD3+ T cells in all tissues examined were largely unchanged over time. However, a significant increase in Treg cells (CD3+CD4+CD25+FoxP3+) occurred in all tissues tested (Figure 6B), and a corresponding decrease in Teff cells (CD3+CD8+) in lymph nodes (Figure 6C) led to an overall decrease in the Teff:Treg ratio in the blood and peritoneum (Figure 6D). Macrophages (CD3-CD11b+F4/80+MHCII+) residing in the peritoneal cavity and lymphoid organs also decreased over time (Figure 6E), as did MDSCs (CD3−CD11c−D11b+GR1+) in blood and lymphoid tissues; but in the peritoneal cavity, there was an ~3-fold increase in MDSCs (Figure 6F). The percentage of DCs (CD3−GR1−CD11c+) decreased in lymphoid organs, but were unchanged in the blood or peritoneum (Figure 6G). These data are largely consistent with the well-characterised immune profile of human OCs [28], and demonstrate that iRFP expression did not influence the overall immune profile. Thus, our data show that iRFP720 ID8 cells are a suitable model for ongoing studies of tumour–immune interactions in OC.

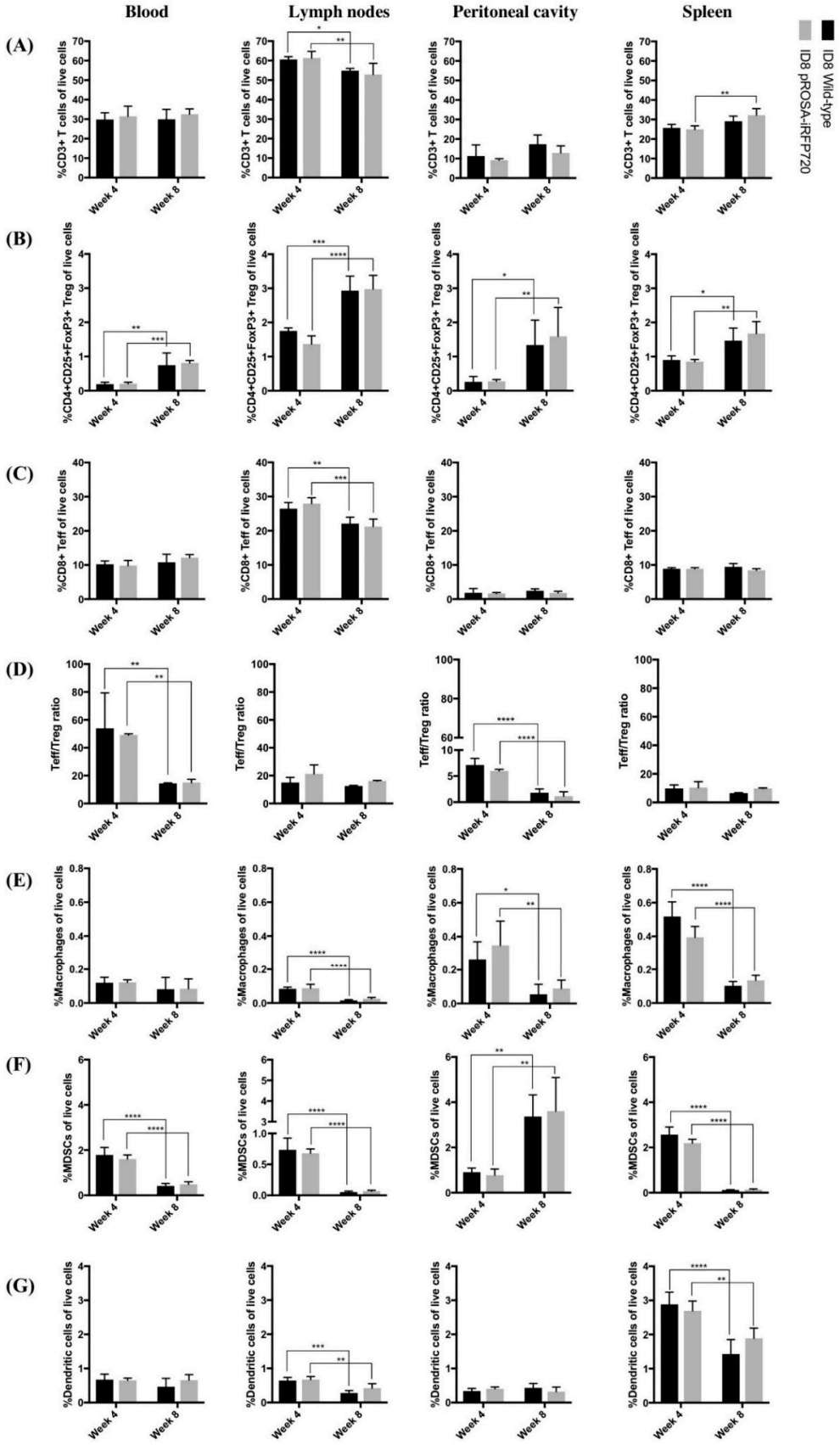

Figure 6. Changes in immune populations over time in mice bearing pROSA-iRFP720 ID8 tumours. Percentages of (**A**) total CD3+ T cells, (**B**) T regulatory cells (CD3+CD4+CD25+FoxP3+), (**C**) CD8+ T effector

cells (CD3+CD8+) of live cells; (**D**) Teff/Treg ratios; percentages of (**E**) macrophages (CD3−CD11b+F4/80+MHCII+), (**F**) myeloid-derived suppressor cells (MDSCs) (CD3–CD11c−CD11b+GR1+) and (**G**) dendritic cells (CD3−GR1−CD11c+) of live cells in the blood, lymph nodes, peritoneal cavity and spleen of pROSA-iRFP720 and wild-type ID8 tumour bearing mice at 4 weeks and 8 weeks post-inoculation. Data are presented as mean ± SD, n = 4,5. *, $p < 0.05$; **, $p < 0.01$; ***, $p < 0.001$; ****, $p < 0.0001$.

3. Discussion

Immune-mediated therapies have been successful in many solid tumour types, and several checkpoint inhibitors and therapeutic vaccines are now FDA-approved for cancer-related indications [29–32]. However, none has been successful in clinical trials for OC to date. The majority of pre-clinical models rely on xenografted tissue explants; these models do not recapitulate either the immune-mediated drivers of tumour progression or the complexity of the anti-tumour immune response [33,34]. Moreover, dynamic changes in the tumour microenvironment drive, and in turn are driven by immune-mediated events over time and according to tumour progression [16,35]. It is therefore crucial to develop an appropriate pre-clinical model that permits the evaluation of tumour dynamics, allows for direct correlation with tumour stage, and operates in the context of an immune-competent microenvironment. Such a model is essential to appropriately assess and validate immune-directed therapies for successful translation in OC.

We have demonstrated that the near-infrared fluorescent protein iRFP720, a bacterial phytochrome with far-red spectral emission [21], can be stably integrated into the genome of ID8 OC cells and can be used to non-invasively track tumour progression over time. iRFPs have been used for deep tissue imaging in several systems [22–24,36], but have never been applied in the context of OC. Integration of a constitutively expressed iRFP720 at the *ROSA26* genomic locus [37] had no discernible consequences for cell growth in vitro, nor did it induce any significant changes in either cellular or humoral immune responses in vivo. Moreover, low-titre anti-iRFP antibodies could only be detected in 2/14 mice with advanced disease; and iRFP expression had no discernible impact on tumour growth, progression or survival time in any animals. Whilst other fluorescent proteins (e.g.,enhanced green fluorescent protein) can induce an autoantibody response with subsequent effects on tumour growth [38], our data are similar to a previous report utilizing randomly integrated *Renilla spp.* luciferase in ID8 cells where no significant immune response was detected [17]. Moreover, CRISPR-mediated integration of the iRFP cassette at the "safe harbour" *ROSA26* locus, extensively validated for GEMM construction [37], was utilized to ensure minimal potential for genomic disruption. Our data demonstrate that iRFP fluorescence is an effective tool for monitoring tumour-specific changes in vivo, has low immunogenicity and does not exert any major alterations to cellular phenotype.

Fluorescence imaging allowed us to define four distinct stages of tumour progression in the ID8 model, which closely mimic the progression of human OCs [39]. Discrete fluorescence events were directly correlated with primary tumour growth (Stage I), early dissemination (Stage II), advanced dissemination (Stage III) and the accumulation of ascites fluid. Importantly, these events were identified simply and non-invasively permitting the direct monitoring of tumour growth. Fluorescence monitoring was far superior to the standard surrogate measurement of abdominal girth, where changes did not become evident until week 7, at which point mice had already progressed to stage III disease. Unlike luciferase-based imaging, which can induce inflammation and permits only qualitative assessment of tumour presence/absence [18,19], fluorescence monitoring does not require an endogenous substrate and can be assessed quantitatively. The ability to make repeated measurements during progression, monitor response to therapy and directly correlate changes according to tumour stage adds a powerful new dimension to the ID8 OC model.

Immune-mediated destruction of OC is a multi-faceted process, requiring the co-ordination of multiple cell types, their activation status and the complex interplay to balance immune active vs. suppressive phenotypes. OC is generally characterised by a decreased tumour-infiltrating CD8+/T regulatory cell ratio, accumulation of MDSCs), and a high MDSC-to-DC ratio [40–44]. The consequent

accumulation of MDSCs and increased ratios of infiltrating T-regulatory to T-effector (Treg:Teff) or ascites-associated MDSC:DCs are thus independent prognostic predictors for OC patients [41,44]. Each of these features was paralleled by the ID8-iRFP720 model, and accumulated progressively from early metastatic to late metastatic disease. This demonstrates not only the suitability of the ID8-iRFP720 model for the stage-specific analysis of immune cell changes, but also the potential to monitor complex changes beyond simple alterations in cell numbers. For example, the Teff cell generation, tumour trafficking and infiltration, activation status, avidity for tumour antigens, longevity and differentiation state are all highly variable and expected to alter throughout the course of disease. By staging and monitoring these events longitudinally throughout progression, the ID8-iRFP720 model has the potential to unparalleled depth for the investigation of tumour–immune interplay over time.

There is increasing interest in the development of therapeutic vaccines for OC treatment, aimed at inducing or altering specific aspects of immunity to promote immune-mediated tumour regression [2,45–47]. For example, vaccination of mice with irradiated mouse ovarian surface epithelial cells (MOSEC) expressing Hsp70 [48] induced a significant CD8+ T cell response, via enhanced antigen-specific T cell priming. Encapsulation of OC antigens in microparticles also increased CD4+ and CD8+ T cell populations in the ID8 model following immunisation [49]. In phase I clinical trials, immunization with a p53 peptide-based vaccine increased CD4+ and CD8+ T cells and improved progression-free survival rates in patients who developed p53-reactive T cells [50]. Nevertheless, no vaccine or targeted immune therapies indicated for OC have been successfully translated to the clinic to date. Our new ID8-iRFP720 model allows for the pre-clinical assessment of immune profiles in response not only to disease, but also to treatment, and can provide a direct, parallel visualization of tumour regression in response to therapy. This is an essential component of vaccine-based studies, where precise knowledge of timing for required vaccine prime/boost or the efficacy of specific adjuvants would be highly beneficial. Moreover, the efficacy of vaccination over time, ability to modulate specific immune populations, and direct determination of recurrence and influence of re-challenge following treatment can all be assessed. This will be crucial for the ongoing development of vaccine-based therapies that can translate successfully for OC treatment.

4. Materials and Methods

4.1. Plasmids

pROSA26-1 (#21714) [51], piRFP720-N1 (#45461) [21] and plentiCRISPRv1 (#49535) were purchased from Addgene (Watertown, MA, USA). pAAVS1-puro-DNR CRISPR vector (#GE100024) [52] was purchased from Origene (Rockville, MD, USA). All plasmids were transformed into competent *Escherichia coli STBL3*^{TM} cells (ThermoFisher Scientific, Franklin, MA, USA) and stored as glycerol stocks at −80 °C. *ROSA26* sequence guide strands were adapted from Quadros and colleagues [25] for cloning into lentiCRISPRv1 [52]. Guide strands used were ROSA26-sgRNA2 F: 5′-CACCGGTGTGTGGGCGTTGTCCTGC-3′; ROSA26-sgRNA2 R: 5′-AAACGCAGGACAACGCCCACACACC-3′; ROSA26-sgRNA4 F: 5′-CACCGATGTCTTTAATCTACCTCGA-3′; and ROSA26-sgRNA4 R: 5′-AAACTCGAGGTAGATTAAAGACATC-3′.

4.2. pROSA-puro-iRFP720 Vector Generation

pROSA26-1 was digested with *SbfI/XhoI* (NEB, Ipswich, MA, USA) to release a 4434 bp product. Digest products were separated by electrophoresis in a 1.2% agarose gel, excised and purified (Promega, Madison WI, USA). A QuikChange II XL Site-Directed Mutagenesis Kit (Agilent Technologies, Santa Clara, CA, USA) was used to introduce an *SbfI* restriction site at position 6849 (downstream from the polyA term site), and an *SgrDI* restriction site at position 4320 (3′ end of the puromycin resistance cassette) of the pAAVS1-puro-DNR vector. pAAVS1-puro-DNR was digested with *SbfI/SgrDI* (ThermoFisher Scientific) and ligated with the

4434bp *SbfI/XhoI* pROSA26-1 fragment to form the pAAVS1-ROSA26 vector. pAAVS1-ROSA26 was digested with *SgfI/MluI* (NEB) to release a 7054bp product which was purified by electrophoresis as above. A complete iRFP720 cassette was amplified by PCR from piRFP720-N1 using a Q5 high-fidelity polymerase and primers iRFP720-AsiSI F: 5′-TTTTGCGATCGCCACCATGGCG-3′ and iRFP720-MluI R: 5′-TTTTACGCGTGCCGCTCACTCTTCCA-3′. The amplified iRFP720 fragment was *AsiSI/MluI*-digested to release a 964bp product, which was ligated into pAAVS1-ROSA26 to generate the final pROSA-puro-iRFP720 vector (8018bp). The pROSA-puro-iRFP720 vector and accompanying ROSA26-sgRNA constructs for genomic integration are available from Ximbio (https://ximbio.com/search?q=pROSA&tab=products).

4.3. ID8 Cell Transfection and Cell Sorting

The ID8 mouse epithelial OC cell line (a gift from Dr. Kathy Roby, Kansas University Medical Center, Kansas City, KA, USA) was maintained in Gibco DMEM (ThermoFisher Scientific) containing 4% fetal bovine serum (FBS) with 1% insulin-transferrin-selenite (ITS) and 1% penicillin/streptomycin (PS). ID8 cells were grown to 70–80% confluence and then co-transfected with pROSA-puro-iRFP720 and plentiCRISPRv1 ROSA26-sgRNA2 or ROSA26-sgRNA4 using Lipofectamine 2000 (Invitrogen, CA, USA), using 3.5 μg of DNA in total. Transfected ID8 cells were maintained in puromycin selection for two weeks and then sorted by flow cytometry for single iRFP720+ clones ([R]730/45 vs. [R]670/30) using the FACSAria Fusion cell sorter (BD Biosciences, San Jose, CA, USA). Clones were maintained under selective pressure in DMEM/FBS/ITS/PS until outgrowth was evident.

4.4. Genomic Screening

Genomic DNA was isolated from iRFP720+ single-cell clones using the ISOLATE II Genomic DNA Kit (Bioline, Memphis, TN, USA) as described by the manufacturer. DNA was PCR-amplified using the following primers: *ROSA26* upstream F: 5′-GGCGTGTTTTGGTTGGCGTAAG-3′ (targeted to a genomic region upstream of the *ROSA26* left arm); *ROSA26* downstream R: 5′-ACCAGGTTAGCCTTTAAGCCTGC-3′ (targeted to an endogenous region between the *ROSA26* left and right arms); and iRFP720 R: 5′-TCGTCGCAGGTCAAGAGGTCA-3′. The ROSA26 upstream F and ROSA26 downstream R primers amplify an 869 bp band if the endogenous ROSA26 sequence has been retained, and the ROSA26 upstream F and iRFP720 R primers amplify a 2883 bp product upon successful incorporation of iRFP720 into *ROSA26.*

4.5. xCELLigence Assay

xCELLigence real-time cell analysis (ACEA Biosciences, San Diego, CA, USA) was used to assess adhesion and proliferation of wild-type and pROSA-iRFP720 ID8 cells as described previously [53]. Briefly, cells were cultured to 70–80% confluence and serum-starved overnight for cell-cycle synchronization. Cells were harvested with trypsin/EDTA, seeded into an E-Plate®96 plate (ACEA Biosciences) at a concentration of 8×10^3 cells/well, and allowed to adhere and proliferate for 8 h. After 8 h, cells were treated with cisplatin (10 μg/mL) or paclitaxel (20 nM) for further 64 h. Data are represented as CI, where CI = electrical impedance at timepoint *n*.

4.6. Apoptosis Assay

Annexin V and propidium iodide (PI) staining was used to assess apoptosis by flow cytometry. Wild-type and pROSA-iRFP720 ID8 cells were seeded into a 6-well plate at a concentration of 3×10^5 cells/well and were allowed to adhere overnight. Cells were treated with cisplatin (10 μg/mL) or paclitaxel (20 nM) and collected after 24 h by trypsinisation. Cells were stained with Alexa Fluor ®647 Annexin V (BioLegend, San Diego, CA, USA) and propidium iodide (ThermoFisher Scientific) in annexin V binding buffer (10 mM HEPES, 140 mM NaCl, 2.5 mM $CaCl_2$) for 15 min and analysed using the BD LSRFortessa™ X-20 (BD Biosciences). Unstained and single-stained cells were used to set compensation and gates.

4.7. Mice

Female 8-week-old C57BL/6 mice were obtained from Monash Animal Services (Clayton, VIC, Australia) and housed in a specific-pathogen-free (SPF) facility. All animal protocols were approved by the Alfred Medical Research and Education Precinct (AMREP) animal ethics committee, Melbourne, Australia (approval #E/1682/2016/M). Treatment and care of the animals were in accordance with institutional guidelines and with the Australian code for the care and use of animals for scientific purposes.

4.8. Intrabursal Implantation of ID8 pROSA-iRFP720 Tumours

Tumours were established by ovarian intrabursal (IB) implantation of ID8 cells as described previously [54]. Mice were anesthetised in an induction chamber using 3% isofluorane in 2 L/min oxygen and then maintained at 2% isofluorane in 1 L/min oxygen using a rodent facemask. An incision was made at the mid-dorsal region of the skin and the peritoneal membrane was excised at the latero-dorsal point above the location of the right ovary. The ovarian fat pad was externalised and stabilised with a serrefine clamp. Either 1×10^6 wild-type or pROSA-iRFP720 ID8 cells were loaded into a Hamilton microliter syringe (Sigma-Aldrich, St Louis, MO, USA) and injected underneath the ovarian bursa using a dissecting microscope for guidance. The skin was closed using Michel suture clips. Mice were monitored for recovery, and suture clips were removed 7 days post-surgery. Mice were fed an SF-AIN-93M rodent diet to reduce intrinsic autofluorescence. Mice were monitored weekly for weight and circumference, and humane endpoints were determined by a body abdominal circumference of >100 mm and general wellbeing (lack of responsiveness, hunched posture, ruffled fur, and eyes squinted). Once the endpoint was reached, mice were humanely sacrificed by CO_2 asphyxiation, and blood and tissues were harvested for fluorescence imaging, ELISA, flow cytometry, and formalin fixed for immunofluorescence.

4.9. In Vivo Fluorescence Imaging

In vivo near-infrared fluorescence imaging was performed weekly using an IVIS Lumina III In Vivo Imaging System (PerkinElmer, Boston, MA, USA). Wild-type or pROSA-iRFP720 ID8 tumour-bearing mice were anesthetised using 3% isofluorane in 2 L/min oxygen, a small patch of abdominal fur shaved, and placed into the IVIS Lumina under 2% isofluorane in 1 L/min oxygen. Mice were imaged at field of view (FOV) C with a brightfield and X-ray set on auto-exposure, and iRFP720 fluorescence was detected using the spectral unmixing iRFP filter set (excitation: 620 nm, 640 nm, 660 nm, and 680 nm; emission: 710 nm), at an exposure time of 5 s. Spectral unmixing of iRFP720 signal from intrinsic autofluorescence was performed by subtracting $680_{ex}/710_{em}$ fluorescence values from the other channels, and a custom spectral unmixing algorithm was created using known iRFP720 fluorescence from a pROSA-iRFP720 ID8 mouse vs. autofluorescence in a wild-type ID8 mouse. For culled animals, the ovaries, omentum, liver, kidneys, small intestine and spleen were excised post-mortem and imaged using the IVIS Lumina. All quantitative fluorescence measurements and analyses were performed using the Living Image software (v 4.5.1, PerkinElmer).

4.10. Tissue Immunofluorescent Staining

Immunofluorescent staining was performed on 4 µm formalin-fixed, paraffin-embedded ovarian tumour sections. After deparaffinization, antigen retrieval was performed by boiling slides in sodium citrate buffer, and permeabilization was performed for nuclear antigens only using 0.25% v/v Triton X-100. Non-specific antibody binding was blocked with 5% BSA in PBS, and primary antibodies were applied and incubated overnight at 4 °C. Primary antibodies used were rabbit anti-wide-spectrum cytokeratin (#ab9377, 1:100, Abcam, Cambridge, UK), rabbit anti-Wilms tumor protein-1 (#ab89901, 1:100, Abcam), goat anti-PD-L1 (#AF1019, 1:125, R&D Systems, Minneapolis, MN, USA) and rabbit anti-p53 (#ab31333, 1:100, Abcam). Alexa Fluor®594 or 647-conjugated goat anti-rabbit or donkey

anti-goat secondary antibodies (1:1000, Abcam) were applied at 1:1000 for 1 h, and slides were mounted using ProLong™ Gold Antifade Mountant with DAPI (ThermoFisher Scientific). Fluorescence images were captured using the Cytation 3 imaging Multi-Mode Reader (BioTek) and processed using the Gen5™ software v 2.05 (BioTek).

4.11. Enzyme-linked Immunosorbent Assay

The presence of iRFP720-specific IgG antibodies in sera was assessed by ELISA as described [55]. iRFP720 protein was purified from *E. coli* cells using a Ni-NTA Fast Start kit (Qiagen, Hilden, Germany). Standards were mouse IgG (Sigma-Aldrich, MO, USA) from 0.5 μg/mL to 0.00781 μg/mL. All measurements were carried out in triplicate. The detection antibody was an Alexa-594-conjugated anti-mouse IgG (5 μg/mL, Abcam). Fluorescence was measured using a Cytation 3 MultiMode Plate Imager (BioTek), with fluorescence (590 nm excitation, 617 nm emission) acquired using a fixed probe height of 6.75 mm, 200 data-points per well and dynamic range 100–80,000 units. Standard curves were constructed using Gen5.0 software v 2.05 (BioTek). A positive IgG serum titre was defined as a reading of ≥2 standard deviations above the mean for mice implanted with wild-type ID8 cells.

4.12. Flow Cytometry

Leukocytes from lymph nodes, blood, spleen and peritoneal cavity wash were collected and isolated as described [56], and analysed by flow cytometry. Anti-mouse CD16/CD32 antibody (1:50, BD Biosciences, clone #2.4G2) was used to block non-specific binding. The following fluorochrome-conjugated antibodies were used: CD3e-AF700 (1:200, BD Biosciences, clone #500A2), CD4-BUV395 (1:100, BD Biosciences, clone #RM4-5), CD8a-PerCP (1:100, BioLegend, clone #53-6.7), CD25-PE-CF594 (1:100, BD Biosciences, #PC-61), FoxP3-APC (1:50, eBioscience, clone #FJK-16S), CD11b-APC (1:200, BioLegend, clone #MI/71), CD11c-BV421 (1:50, BD Bioscience, clone #HL3), GR1-PerCP Cy5.5 (1:200, BD Biosciences, clone #RB6-8C5), F4/80-BV711 (1:100, BioLegend, clone #BM8) and MHCII-APC/Cy7 (1:500, BioLegend, clone #M5/114.15.2). Single-stained beads were used to set compensation controls, and fluorescence-minus-one (FMO) controls were used to define population gates. Data were acquired using a BD LSRFortessa X-20 (BD Biosciences), and were analysed using FlowJo software v10.5.0 (BD Biosciences).

4.13. Statistical Analysis

Graphs and statistical analyses were performed using GraphPad Prism v 7.0b (GraphPad Software Inc., La Jolla, CA, USA). A two-way ANOVA and Sidak multiple comparisons test were used to analyse statistical significance between groups for apoptosis, iRFP720 fluorescence post-mortem, and immune populations. A two-way ANOVA and Tukey post-hoc test was used to analyse statistical significance between groups for proliferation, iRFP720 fluorescence, weight and circumference over time. A non-parametric one-way ANOVA and Tukey post-hoc test was used for the IgG assay. Data are presented as mean ± SD and $p < 0.05$ was considered statistically significant.

5. Conclusions

Our data demonstrate that the pROSA-iRFP720 ID8 model is a suitable tool for non-invasive, longitudinal tumour monitoring in vivo, and provides the first simple fluorescence model for real-time discrimination between distinct stages of ovarian tumour progression. All specific features of host–tumour immune interactions that parallel human clinical progression are preserved in this system, providing a tool for the accurate preclinical development, evaluation and testing of novel vaccine and immune-based therapies for OC. By directly assessing tumour regression, recurrence and response to therapies at an early stage, it will be possible to accurately determine therapeutic scheduling and optimize combination therapies to achieve clinically relevant and robust outcomes for OC treatment.

Author Contributions: Conceptualization, A.L.W., A.R., A.N.S. and M.P.; data curation, A.L.W., M.B., L.R.M., M.M., A.N.S. and M.P.; formal analysis, K.L.W., M.B., A.N.S. and M.P.; funding acquisition, M.D.G., M.K.O., A.N.S. and M.P.; investigation, A.L.W., L.R.M., M.M. and A.N.S.; methodology, K.L.W. and A.R.; supervision, A.N.S. and M.P.; writing of the original draft, A.L.W., K.L.W., M.B., L.R.M., A.N.S. and M.P.; writing of review and editing, A.L.W., K.L.W., M.B., L.R.M., M.M., M.D.G., M.K.O., A.R., A.N.S. and M.P.

Funding: This work was supported by NHMRC grant #1099375, and the Victorian Government's Operational Infrastructure Support Program. M.P. is supported by an NHMRC Senior Fellowship. A.S. is supported by a fellowship from the Ovarian Cancer Research Foundation (OCRF.com.au).

Acknowledgments: The authors would like to thank the Monash Animal Research Platform (MARP/MICU), Katharina Haigh for training in the intrabursal procedure, and M Madondo for co-development of flow-cytometry panels for immune infiltrate analysis. We acknowledge the facilities, scientific and technical assistance of FlowCore, Monash Micro Imaging and MHTP Medical Genomics of Monash University and Monash Health Translation Precinct (internal audit #11178223).

Conflicts of Interest: The authors declare no conflicts of interest.

References

1. Jelovac, D.; Armstrong, D.K. Recent progress in the diagnosis and treatment of ovarian cancer. *CA Cancer J. Clin.* **2011**, *61*, 183–203. [CrossRef] [PubMed]
2. Odunsi, K.; Matsuzaki, J.; James, S.R.; Mhawech-Fauceglia, P.; Tsuji, T.; Miller, A.; Zhang, W.; Akers, S.N.; Griffiths, E.A.; Miliotto, A.; et al. Epigenetic potentiation of NY-ESO-1 vaccine therapy in human ovarian cancer. *Cancer Immunol. Res.* **2014**, *2*, 37–49. [CrossRef] [PubMed]
3. Kandalaft, L.E.; Chiang, C.L.; Tanyi, J.; Motz, G.; Balint, K.; Mick, R.; Coukos, G. A Phase I vaccine trial using dendritic cells pulsed with autologous oxidized lysate for recurrent ovarian cancer. *J. Transl. Med.* **2013**, *11*, 149. [CrossRef] [PubMed]
4. Gao, Q.; Xiang, S.D.; Wilson, K.; Madondo, M.; Stephens, A.N.; Plebanski, M.; Gao, Q. Sperm Protein 17 Expression by Murine Epithelial Ovarian Cancer Cells and Its Impact on Tumor Progression. *Cancers* **2018**, *10*, 276. [CrossRef] [PubMed]
5. Wilson, A.L.; Plebanski, M.; Stephens, A.N. New trends in anti-cancer therapy: Combining conventional chemotherapeutics with novel immunomodulators. *Curr. Med. Chem.* **2018**, *25*, 4758–4784. [CrossRef] [PubMed]
6. Scott, C.L.; Mackay, H.J.; Haluska, P., Jr. Patient-derived xenograft models in gynecologic malignancies. In *American Society of Clinical Oncology Educational Book, American Society of Clinical Oncology, Annual Meeting, Chicago, IL, USA, 30 May–3 June 2014*; American Society of Clinical Oncology: Alexandria, VA, USA, 2014; pp. e258–e266.
7. McCloskey, C.W.; Rodriguez, G.M.; Galpin, K.J.C.; Vanderhyden, B.C. Ovarian Cancer Immunotherapy: Preclinical Models and Emerging Therapeutics. *Cancers* **2018**, *10*, 244. [CrossRef] [PubMed]
8. Russo, A.; Czarnecki, A.A.; Dean, M.; Modi, D.A.; Lantvit, D.D.; Hardy, L.; Baligod, S.; Davis, D.A.; Wei, J.-J.; Burdette, J.E. PTEN loss in the fallopian tube induces hyperplasia and ovarian tumor formation. *Oncogene* **2018**, *37*, 1976–1990. [CrossRef] [PubMed]
9. Roby, K.F.; Taylor, C.C.; Sweetwood, J.P.; Cheng, Y.; Pace, J.L.; Tawfik, O.; Persons, D.L.; Smith, P.G.; Terranova, P.F.; Roby, K.F. Development of a syngeneic mouse model for events related to ovarian cancer. *Carcinogenesis* **2000**, *21*, 585–591. [CrossRef]
10. Roberts, P.C.; Mottillo, E.P.; Baxa, A.C.; Heng, H.H.Q.; Doyon-Reale, N.; Gregoire, L.; Lancaster, W.D.; Rabah, R.; Schmelz, E.M. Sequential molecular and cellular events during neoplastic progression: A mouse syngeneic ovarian cancer model. *Neoplasia (New York, NY)* **2005**, *7*, 944–956. [CrossRef]
11. McCloskey, C.W.; Goldberg, R.L.; Carter, L.E.; Gamwell, L.F.; Al-Hujaily, E.M.; Collins, O.; Macdonald, E.A.; Garson, K.; Daneshmand, M.; Carmona, E.; et al. A new spontaneously transformed syngeneic model of high-grade serous ovarian cancer with a tumor-initiating cell population. *Front. Oncol.* **2014**, *4*, 53. [CrossRef]
12. Guo, Z.; Wang, X.; Cheng, D.; Xia, Z.; Luan, M.; Zhang, S. PD-1 blockade and OX40 triggering synergistically protects against tumor growth in a murine model of ovarian cancer. *PLoS ONE* **2014**, *9*, e89350. [CrossRef] [PubMed]

13. Duraiswamy, J.; Freeman, G.J.; Coukos, G. Therapeutic PD-1 pathway blockade augments with other modalities of immunotherapy T-cell function to prevent immune decline in ovarian cancer. *Cancer Res.* **2013**, *73*, 6900–6912. [CrossRef] [PubMed]
14. Walton, J.; Blagih, J.; Ennis, D.; Leung, E.; Dowson, S.; Farquharson, M.; Tookman, L.A.; Orange, C.; Athineos, D.; Mason, S.; et al. CRISPR/Cas9-Mediated Trp53 and Brca2 Knockout to Generate Improved Murine Models of Ovarian High-Grade Serous Carcinoma. *Cancer Res.* **2016**, *76*, 6118–6129. [CrossRef]
15. Javadi, S.; Ganeshan, D.M.; Qayyum, A.; Iyer, R.B.; Bhosale, P. Ovarian Cancer, the Revised FIGO Staging System, and the Role of Imaging. *AJR* **2016**, *206*, 1351–1360. [CrossRef] [PubMed]
16. Dunn, G.P.; Old, L.J.; Schreiber, R.D. The Immunobiology of Cancer Immunosurveillance and Immunoediting. *Immunity* **2004**, *21*, 137–148. [CrossRef] [PubMed]
17. Liao, J.B.; Ovenell, K.J.; Curtis, E.E.M.; Cecil, D.L.; Koehnlein, M.R.; Rastetter, L.R.; Gad, E.A.; Disis, M.L.; Liao, J.B. Preservation of tumor-host immune interactions with luciferase-tagged imaging in a murine model of ovarian cancer. *J. Immunother. Cancer* **2015**, *3*, 16. [CrossRef] [PubMed]
18. Klerk, C.P.W.; Overmeer, R.M.; Niers, T.M.H.; Versteeg, H.H.; Richel, D.J.; Buckle, T.; Van Noorden, C.J.F.; van Tellingen, O.; Klerk, C.P.W. Validity of bioluminescence measurements for noninvasive in vivo imaging of tumor load in small animals. *BioTechniques* **2007**, *43*, S7–S13, S30. [CrossRef]
19. Iglesias, P.; Costoya, J.A. A novel BRET-based genetically encoded biosensor for functional imaging of hypoxia. *Biosens. Bioelectron.* **2009**, *24*, 3126–3130. [CrossRef]
20. Morvova, M., Jr.; Jeczko, P.; Sikurova, L. Gender differences in the fluorescence of human skin in young healthy adults. *Skin Res. Technol.* **2018**, *24*, 599–605. [CrossRef]
21. Shcherbakova, D.M.; Verkhusha, V.V. Near-infrared fluorescent proteins for multicolor in vivo imaging. *Nat. Methods* **2013**, *10*, 751–754. [CrossRef]
22. Yu, D.; Gustafson, W.C.; Han, C.; Lafaye, C.; Noirclerc-Savoye, M.; Ge, W.-P.; Thayer, D.A.; Huang, H.; Kornberg, T.B.; Royant, A.; et al. An improved monomeric infrared fluorescent protein for neuronal and tumour brain imaging. *Nat. Commun.* **2014**, *5*, 3626. [CrossRef] [PubMed]
23. Lai, C.-W.; Chen, H.-L.; Yen, C.-C.; Wang, J.-L.; Yang, S.-H.; Chen, C.-M. Using Dual Fluorescence Reporting Genes to Establish an In Vivo Imaging Model of Orthotopic Lung Adenocarcinoma in Mice. *Mol. Imaging Biol.* **2016**, *18*, 849–859. [CrossRef] [PubMed]
24. Jiguet-Jiglaire, C.; Cayol, M.; Mathieu, S.; Jeanneau, C.; Bouvier-Labit, C.; Ouafik, L.h.; El-Battari, A. Noninvasive near-infrared fluorescent protein-based imaging of tumor progression and metastases in deep organs and intraosseous tissues. *J. Biomed. Opt.* **2014**, *19*, 16019. [CrossRef] [PubMed]
25. Quadros, R.M.; Harms, D.W.; Ohtsuka, M.; Gurumurthy, C.B. Insertion of sequences at the original provirus integration site of mouseROSA26 locus using the CRISPR/Cas9 system. *FEBS Open Bio* **2015**, *5*, 191–197. [CrossRef] [PubMed]
26. Cho, S.; Sun, Y.; Soisson, A.P.; Dodson, M.K.; Peterson, C.M.; Jarboe, E.A.; Kennedy, A.M.; Janát-Amsbury, M.M.; Cho, S. Characterization and evaluation of pre-clinical suitability of a syngeneic orthotopic mouse ovarian cancer model. *Anticancer Res.* **2013**, *33*, 1317–1324. [PubMed]
27. Pfau, J.C.; Brown, J.M.; Holian, A. Silica-exposed mice generate autoantibodies to apoptotic cells. *Toxicology* **2004**, *195*, 167–176. [CrossRef] [PubMed]
28. Cai, D.L.; Jin, L.-P. Immune Cell Population in Ovarian Tumor Microenvironment. *J. Cancer* **2017**, *8*, 2915–2923. [CrossRef]
29. Cheever, M.A.; Higano, C.S. PROVENGE (Sipuleucel-T) in Prostate Cancer: The First FDA-Approved Therapeutic Cancer Vaccine. *Clin. Cancer Res.* **2011**, *17*, 3520–3526. [CrossRef]
30. Hodi, F.S.; O'Day, S.J.; McDermott, D.F.; Weber, R.W.; Sosman, J.A.; Haanen, J.B.; Gonzalez, R.; Robert, C.; Schadendorf, D.; Hassel, J.C.; et al. Improved Survival with Ipilimumab in Patients with Metastatic Melanoma. *N. Engl. J. Med.* **2010**, *363*, 711–723. [CrossRef]
31. Robert, C.; Ribas, A.; Wolchok, J.D.; Hodi, F.S.; Hamid, O.; Kefford, R.; Weber, J.S.; Joshua, A.M.; Hwu, W.-J.; Gangadhar, T.C.; et al. Anti-programmed-death-receptor-1 treatment with pembrolizumab in ipilimumab-refractory advanced melanoma: A randomised dose-comparison cohort of a phase 1 trial. *Lancet* **2014**, *384*, 1109–1117. [CrossRef]
32. Brahmer, J.R.; Tykodi, S.S.; Chow, L.Q.M.; Hwu, W.-J.; Topalian, S.L.; Hwu, P.; Drake, C.G.; Camacho, L.H.; Kauh, J.; Odunsi, K.; et al. Safety and activity of anti-PD-L1 antibody in patients with advanced cancer. *N. Engl. J. Med.* **2012**, *366*, 2455–2465. [CrossRef] [PubMed]

33. Voskoglou-Nomikos, T.; Pater, J.L.; Seymour, L. Clinical predictive value of the in vitro cell line, human xenograft, and mouse allograft preclinical cancer models. *Clin. Cancer Res.* **2003**, *9*, 4227–4239. [PubMed]
34. Morgan, R.A. Human Tumor Xenografts: The Good, the Bad, and the Ugly. *Mol. Ther.* **2012**, *20*, 882–884. [CrossRef]
35. Drakes, M.L.; Stiff, P.J. Regulation of Ovarian Cancer Prognosis by Immune Cells in the Tumor Microenvironment. *Cancers* **2018**, *10*, 302. [CrossRef] [PubMed]
36. Lu, Y.; Darne, C.D.; Tan, I.-C.; Wu, G.; Wilganowski, N.; Robinson, H.; Azhdarinia, A.; Zhu, B.; Rasmussen, J.C.; Sevick-Muraca, E.M. In vivo imaging of orthotopic prostate cancer with far-red gene reporter fluorescence tomography and in vivo and ex vivo validation. *J. Biomed. Opt.* **2013**, *18*, 101305. [CrossRef]
37. Casola, S. *Mouse Models for miRNA Expression: The ROSA26 Locus, in MicroRNAs and the Immune System*; Springer: Berlin, Germany, 2010; pp. 145–163.
38. Castano, A.P.; Liu, Q.; Hamblin, M.R. A green fluorescent protein-expressing murine tumour but not its wild-type counterpart is cured by photodynamic therapy. *Br. J. Cancer* **2006**, *94*, 391–397. [CrossRef] [PubMed]
39. Jayson, G.C.; Kohn, E.C.; Kitchener, H.C.; Ledermann, J.A. Ovarian cancer. *Lancet* **2014**, *384*, 1376–1388. [CrossRef]
40. Odunsi, K. Immunotherapy in ovarian cancer. *Ann. Oncol.* **2017**, *28*, viii1–viii7. [CrossRef]
41. Santegoets, S.J.A.M.; de Groot, A.F.; Dijkgraaf, E.M.; Simões, A.M.C.; van der Noord, V.E.; van Ham, J.J.; Welters, M.J.P.; Kroep, J.R.; van der Burg, S.H. The blood mMDSC to DC ratio is a sensitive and easy to assess independent predictive factor for epithelial ovarian cancer survival. *Oncoimmunology* **2018**, *7*, e1465166. [CrossRef]
42. Charbonneau, B.; Goode, E.L.; Kalli, K.R.; Knutson, K.L.; Derycke, M.S. The immune system in the pathogenesis of ovarian cancer. *Crit. Rev. Immunol.* **2013**, *33*, 137–164. [CrossRef]
43. Preston, C.C.; Goode, E.L.; Hartmann, L.C.; Kalli, K.R.; Knutson, K.L. Immunity and immune suppression in human ovarian cancer. *Immunotherapy* **2011**, *3*, 539–556. [CrossRef] [PubMed]
44. Preston, C.C.; Maurer, M.J.; Oberg, A.L.; Visscher, D.W.; Kalli, K.R.; Hartmann, L.C.; Goode, E.L.; Knutson, K.L.; Preston, C.C. The Ratios of CD8+ T Cells to CD4+CD25+ FOXP3+ and FOXP3- T Cells Correlate with Poor Clinical Outcome in Human Serous Ovarian Cancer. *PLoS ONE* **2013**, *8*, e80063. [CrossRef] [PubMed]
45. Berinstein, N.L.; Karkada, M.; Morse, M.A.; Nemunaitis, J.J.; Chatta, G.; Kaufman, H.; Odunsi, K.; Nigam, R.; Sammatur, L.; MacDonald, L.D.; et al. First-in-man application of a novel therapeutic cancer vaccine formulation with the capacity to induce multi-functional T cell responses in ovarian, breast and prostate cancer patients. *J. Transl. Med.* **2012**, *10*, 156. [CrossRef] [PubMed]
46. Oh, J.; Barve, M.; Matthews, C.M.; Koon, E.C.; Heffernan, T.P.; Fine, B.; Grosen, E.; Bergman, M.K.; Fleming, E.L.; DeMars, L.R.; et al. Phase II study of Vigil®DNA engineered immunotherapy as maintenance in advanced stage ovarian cancer. *Gynecol. Oncol.* **2016**, *143*, 504–510. [CrossRef] [PubMed]
47. Khan, A.N.H.; Kolomeyevskaya, N.; Singel, K.L.; Grimm, M.J.; Moysich, K.B.; Daudi, S.; Grzankowski, K.S.; Lele, S.; Ylagan, L.; Webster, G.A.; et al. Targeting myeloid cells in the tumor microenvironment enhances vaccine efficacy in murine epithelial ovarian cancer. *Oncotarget* **2015**, *6*, 11310–11326. [CrossRef] [PubMed]
48. Chang, C.-L. Cancer immunotherapy using irradiated tumor cells secreting heat shock protein 70. *Cancer Res.* **2007**, *67*, 10047–10057. [CrossRef] [PubMed]
49. Tawde, S.A.; Chablani, L.; Akalkotkar, A.; D'Souza, C.; Chiriva-Internati, M.; Selvaraj, P.; D'Souza, M.J.; Tawde, S.A. Formulation and evaluation of oral microparticulate ovarian cancer vaccines. *Vaccine* **2012**, *30*, 5675–5681. [CrossRef]
50. Schuler, P.J.; Harasymczuk, M.; Visus, C.; Deleo, A.; Trivedi, S.; Lei, Y.; Argiris, A.; Gooding, W.; Butterfield, L.H.; Whiteside, T.L.; et al. Phase I dendritic cell p53 peptide vaccine for head and neck cancer. *Clin. Cancer Res.* **2014**, *20*, 2433–2444. [CrossRef]
51. Soriano, P. Generalized lacZ expression with the ROSA26 Cre reporter strain. *Nat. Genet.* **1999**, *21*, 70–71. [CrossRef]
52. Sanjana, N.E.; Shalem, O.; Zhang, F. Improved vectors and genome-wide libraries for CRISPR screening. *Nat. Methods* **2014**, *11*, 783–784. [CrossRef]

53. Bilandzic, M.; Stenvers, K.L. Assessment of ovarian cancer spheroid attachment and invasion of mesothelial cells in real time. *J. Vis. Exp.* **2014**, *87*, 51655. [CrossRef] [PubMed]
54. Nunez-Cruz, S.; Connolly, D.C.; Scholler, N. An orthotopic model of serous ovarian cancer in immunocompetent mice for in vivo tumor imaging and monitoring of tumor immune responses. *J. Vis. Exp.* **2010**, *45*, 2146. [CrossRef] [PubMed]
55. Wilson, A.L.; Moffitt, L.R.; Duffield, N.; Rainczuk, A.; Jobling, T.W.; Plebanski, M.; Stephens, A.N. Autoantibodies against HSF1 and CCDC155 as biomarkers of early-Stage, high-Grade serous ovarian cancer. *Cancer Epidemiol. Biomark. Prev.* **2018**, *27*, 183–192. [CrossRef] [PubMed]
56. Coquery, C.M.; Loo, W.; Buszko, M.; Lannigan, J.; Erickson, L.D. Optimized protocol for the isolation of spleen-resident murine neutrophils. *Cytom. Part A* **2012**, *81A*, 806–814. [CrossRef] [PubMed]